Università degli Studi di Ferrara

UCA Universidad de Cádiz

INTERNATIONAL DOCTORAL COURSE IN
"EARTH AND MARINE SCIENCES (EMAS)"

CYCLE XXXII

COORDINATOR Prof. COLTORTI MASSIMO

3D rheological modelling in the Aegean Region and its importance for the seismotectonics of the area

Scientific/Disciplinary Sector (SDS) GEO/03

Candidate
Dott. Massimiliano Maggini

Supervisor
Prof. Riccardo Caputo

Years 2016/2019

To my family and

to my flower

Acknowledgements

To complete such a long, fascinating, though at times scientifically and emotionally demanding experience, as my Ph.D. has been, it would have not been possible without the constant help of many people around me that I would like to sincerely thank here.

First of all, I have to start with my supervisor, Professor Riccardo Caputo. Not only he was always available for scientific discussions and useful suggestions, but he also showed me the way research and teamwork should be carried on. His profound love and interest for Earth Sciences, together with his strong work ethic, have really indicated me how to face, from time to time, the new problems that came up during this research.

I would like to thank the University of Patras and the staff of the Department of Geology for showing me the tectonic and geological environment of the Aegean Region. I also want to thank the University of Cambridge and the personnel at the Bullard Laboratories for hosting me there and giving me so many tips and advices on both purely scientific and not-strictly scientific, though inherent to the academic world, topics.

Dr. Ganas, Dr. Kassaras and Dr. Karastathis are greatly acknowledged for providing me with the seismological data on relocated seismic events in the Aegean Region. Prof. Xypolias, Prof. Zeilinger and Prof. Schettino are also deeply thanked for their useful suggestions and helpful comments about my thesis.

A special thank also goes to my family, for constantly and lovingly supporting me through the course of this Ph.D and offering a solid base on which I could always rely, no matter what!

A particularly profound and heart-felt thank goes to Margherita, for always standing by my side and sustaining me during the bad and good times of this experience, that we both shared. Her strength, patience and perserverance have really represented to me a solid anchor, an example and a motivation to pursue my goals.

Also thanked are all my friends, the old and the new ones met during the course of these three years, for brightening my time here, especially in the long and hard days.

Finally, I would like to sincerely thank the University of Ferrara, the University of Cadiz and the MIUR for giving me the opportunity to live this challenging experience and financially supporting it.

Extended abstract

The main topic of this Ph.D. research is the thermo-rheological modelling of the broader Aegean Region, for the purpose of seismotectonic characterization and with the final aim of improving the seismic hazard assessment. The concept behind this project resides in the link between rheological parameters obtained from the modelling and the properties of the corresponding rocks in terms of seismogenic behaviour. In particular, applying the principle that brittle deformation is associated to potential seismogenesis, the modelled depth of the brittle-ductile transition (BDT) has been adopted as a constraint for determining the bottom depth of the seismogenic layer. For the purpose of the modelling two dominant deformation mechanisms have been considered, namely the frictional sliding and the power-law (dislocation) creep representing, respectively, the brittle behaviour and the ductile one (§2.1). Parallel to the reconstruction of the rheological profiles, the corresponding geothermal gradients have been carefully estimated, in order to properly evaluate and take into account the influence of thermal properties on the rheological behaviour (§2.3). Literature data have been searched for and collected, in order to define the proper range of values for the majority of the input parameters (heat flow, strain rate, power-law and thermal ones) in the rheological constitutive equations. Additional geodynamic and geological considerations have been taken into account for determining the values of parameters such as the friction coefficient, the pore fluid pressure ratio and the one indicating the tectonic regime (§3.1).

Before focusing on the reconstruction of the strength envelopes for the study area, a detailed sensitivity analysis on the variability and uncertainties of the input parameters and their influence on the main thermo-rheological modelled properties (BDT depth, strength and temperature) has been carried out (ch. 4). The results of the sensitivity tests indicate that thermal-related parameters such as activation energy, surface heat flow and thermal conductivity are the most influential ones for the BDT properties (depth and strength in particular). The joint analysis of the uncertainties confirmed that, after a careful selection of the ranges of values for the input parameters, reliable rheological profiles can be obtained, together with the estimation of the variations associated to the main rheological indicators (BDT depth, strength and temperature).

Dedicated and specific scripts have been developed in a Matlab environment for the purposes of the thermo-rheological modelling (§3.2.3). The latter has been carried out in three different and consequential stages. Firstly, 1D strength envelopes have been realized for specific test sites in the Aegean Region and have also been compared with the depth distribution of relocated seismicity, in order to test the precision and reliability of the correspondence between the BDT depth and the cutoff depth of seismicity (§5.1). In a second phase, 2D rheological pseudo-sections have been reconstructed (through interpolation) along several transects in the study area,

belonging to different geodynamic settings (§5.2). Such a modelling stage allowed determining and observing the lateral variations in the thermo-rheological properties across some of the different sectors of the Aegean Region. Particular care has been devoted to the western Hellenic subduction zone and the comparison between continental and oceanic subduction settings, through the realization of WSW-ENE trending transects, north (continental) and south (oceanic) of the Kefallinia Transform Fault. The results highlighted the following differences between the two domains: i) a slightly shallower BDT in the western sectors of the northern transects (~30-33 km) with respect to the southern ones (~40 km); ii) a relatively deeper BDT (~20-25 km) for the northern transects when compared with the southern ones (~15 km), in the eastern sectors of the investigated area; iii) the occurrence of a thick, deeper brittle layer below the shallowest BDT, in the central-eastern sectors of the northern transects.

The third and last stage of the modelling consisted in the reconstruction of a complete 3D thermo-rheological model for the whole study area (§5.3). Such a model also takes into account the large-scale characteristics of the litho-stratigraphic layering, the geometry of the Hellenic subduction zone and the thermal perturbation associated to the cold downgoing oceanic slab. The 3D reconstruction, in particular for the BDT depth, allows observing its regional variations over the entire study area. At this regard, some large-scale characteristics can be identified: firstly, taking as a reference the subduction zone, the BDT is much shallower (between 10 and 20 km and always in the upper plate) in the internal sectors (back-arc region, Aegean Sea and continental Greece) with respect to the external areas, where the transition lies at ca 40 km in the oceanic lithosphere of the lower plate, and at ca 35 km in the continental sectors (Apulia, Cyrenaica).

Secondly, the strength and temperature at the BDT are generally well correlated with the BDT depth, meaning that strength values lesser than 100 MPa characterize the internal sectors, while values up to 1 GPa are associated to the BDTs occurring within the oceanic lithosphere. Similarly, BDT temperatures are limited to ca 200-300 °C for the shallow BDTs in continental Greece and in the Aegean Sea, while greater values around 600-650 °C are attained in the external sectors.

In terms of interpretation and explanation of the thermo-rheological results, both the 1D envelopes, the 2D transects and the 3D model suggest that the main control on the BDT depth (and consequently also on the associated strength and temperature) is exerted by the surface heat flow distribution and more in general by the corresponding geothermal gradient. A secondary role is also locally played by the lithological layering and, to a minor extent, by the strain rate values distribution.

The results of the modelling, in particular in terms of BDT depth and strength, have been successively applied, mainly to the fields of seismotectonics and geodynamics. The BDT depth has been used as a constraint for defining the width of the major seismogenic sources in the Aegean Region, and by applying several empirical relationships, estimates of the maximum

expected magnitudes for each source have been obtained (§6.1). The improved knowledge on the depth of the BDT has also allowed to better characterize the seismically deforming volumes, and for some selected seismic zones, a new calculation of the seismic strain rates has been performed (§6.2). Finally, by integrating along depth the values of the strength, as defined by the strength envelopes, estimates of the total strength for both the upper and the lower plate have been obtained (§6.3).

To conclude, this project focused on the rheological characterization of the Aegean Region, being the first to propose a complete 3D model of the BDT depth and the associated strength and temperature values, for the investigated area. This research has also demonstrated how the rheological properties can effectively be linked to the seismogenic processes, for the purposes of the improvement in the seismotectonic characterization and, finally, in the seismic hazard assessment.

Riassunto esteso

Questo progetto di dottorato è stato dedicato alla modellazione termo-reologica nella Regione Egea, al fine ultimo di migliorare la caratterizzazione sismotettonica e la valutazione del rischio sismico nell'area di studio. Il concetto alla base di questa ricerca è rappresentato dalla relazione tra i parametri reologici ottenuti dalla modellazione e le proprietà delle rocce corrispondenti, in termini di comportamento sismogenico. In particolar modo, tenendo in considerazione il principio teorico secondo il quale solo la deformazione fragile è potenzialmente associabile alla sismogenesi, la profondità modellata della transizione fragile-duttile (BDT) è stata usata come vincolo per determinare la profondità della base del *layer* sismogenico.

Ai fini della modellazione reologica due meccanismi principali di deformazione sono stati selezionati: rispettivamente, lo scorrimento frizionale per il comportamento fragile ed il creep secondo la legge di potenza (*dislocation power-law creep*) per quello duttile (§2.1). Parallelamente alla ricostruzione dei profili reologici anche i corrispondenti gradienti geotermici sono stati calcolati, in modo tale da poter valutare e tenere in considerazione in maniera appropriata l'influenza delle proprietà termiche sul comportamento reologico (§2.3). Per quanto riguarda la definizione degli intervalli dei valori, per la maggior parte dei parametri di input presenti nelle equazioni costitutive sono stati considerati e raccolti principalmente dati di letteratura. Ulteriori osservazioni geologiche e geodinamiche sono state utilizzate per determinare i valori dei parametri frizionali, quali coefficiente d'attrito, pressione dei fluidi e regime tettonico (§3.1).

Ancor prima della ricostruzione dei profili reologici è stata effettuata una dettagliata analisi di sensibilità della variabilità e delle incertezze dei parameteri di input e della loro influenza sulle principali proprietà termo-reologiche modellate (cap. 4). I risultati dei tests di sensibilità indicano che i parametri termici, come l'energia di attivazione, il flusso di calore in superficie e la conducibilità termica, sono i più influenti per quanto riguarda le proprietà della BDT (ed in particolare la sua profondità e resistenza associata). L'analisi congiunta delle incertezze ha inoltre confermato che un'attenta selezione dei valori dei parametri di input, con i rispettivi errori, permette la ricostruzione di profili reologici precisi ed affidabili, nonché la stima delle variazioni associate ai principali indicatori reologici (profondità della BDT, resistenza e temperatura).

Il software Matlab è stato poi utilizzato per implementare degli specifici codici appositamente destinati alla modellazione reologica (§3.2.3). Quest'ultima è stata realizzata in tre fasi tra loro consequenziali. Innanzitutto, sono stati prodotti i profili reologici 1D per degli specifici test sites nella Regione Egea e sono poi stati confrontati con la distribuzione di profondità della sismicità rilocalizzata, al fine di testare la precisione e l'affidabilità della corrispondenza tra la profondità della BDT e il limite in profondità della sismicità stessa (§5.1).

In una seconda fase, sono state ricostruite (attraverso l'interpolazione) delle pseudo-sezioni 2D lungo dei transetti selezionati nell'area di studio, riconducibili a differenti assetti geodinamici (§5.2). Tale fase di modellazione ha permesso di determinare ed osservare le variazioni laterali nelle proprietà termo-reologiche attraverso differenti settori della Regione Egea. Una particolare attenzione è stata rivolta al confronto tra assetti di subduzione oceanica e continentale, attraverso la realizzazione di transetti orientati WSW-ENE, a nord (continentale) ed a sud (oceanica) della faglia trasforme di Cefalonia. I risultati hanno evidenziato le seguenti differenze tra i due domini: i) una BDT leggermente più superficiale nei settori occidentali dei transetti a nord (~30-33 km) rispetto ai transetti a sud (~40 km); ii) per i settori orientali, una BDT relativamente più profonda lungo i transetti a nord (~20-25 km) rispetto a quelli a sud (~15 km); iii) la presenza di uno spesso e profondo secondo strato fragile al di sotto della BDT più superficiale, esclusivamente nei settori centro-orientali dei transetti a nord.

La terza ed ultima fase della modellazione è consistita nella ricostruzione di un modello termo-reologico 3D completo per tutta la Regione Egea (§5.3). Tale modello prende in considerazione le caratteristiche a larga scala della stratificazione lito-meccanica, la geometria della zona di subduzione Ellenica e la perturbazione termica associata alla presenza in profondità dello slab oceanico. La ricostruzione in 3D ha permesso di osservare la variazioni regionali nell'intera area di studio, con particolare riferimento alla profondità della BDT. Per quanto riguarda la profondità di quest'ultima, possono essere identificate alcune caratteristiche principali: innanzitutto, prendendo come riferimento la zona di subduzione, la BDT è molto più superficiale (~10-20 km e sempre nella placca di tetto) nei settori interni (zona di retroarco, mar Egeo e Grecia continentale) rispetto alle aree esterne, dove la transizione si trova a ca 40 km nella litosfera oceanica della placca di letto, ed a ca 35 km nei settori continentali (e.g. Apulia, Cirenaica). In secondo luogo, la resistenza e la temperatura alla BDT sono generalmente ben correlate con la profondità della BDT stessa, cosicché valori di resistenza minori di 100 MPa caratterizzano i settori interni, mentre valori fino a ca 1 GPa sono associati alle BDT nella litosfera oceanica. Similmente, le temperature alla BDT non superano i 200-300 °C nella Grecia continentale e nel mar Egeo, mentre valori maggiori di ca 650 °C vengono raggiunti nei settori esterni.

Per quanto riguarda l'interpretazione dei risultati termo-reologici, i modelli realizzati suggeriscono un controllo sulla profondità della BDT esercitato principalmente dalla distribuzione del flusso di calore in superficie e più in generale dal corrispondente gradiente geotermico. Un ruolo secondario è invece attribuito a fattori ulteriori, quali la stratificazione litologica e lo *strain rate*, in particolar modo in corrispondenza di area caratterizzate da una deformazione fortemente concentrata lungo le zone di taglio principali (ad esempio il rift di Corinto, la faglia trasforme di Cefalonia e il North Aegean Trough).

I risultati della modellazione, in particolare in termini di profondità della BDT e resistenza associata, sono stati successivamente applicati in ambito sismotettonico e geodinamico. La profondità della BDT è stata utilizzata come vincolo per definire la larghezza delle maggiori sorgenti sismogeniche nella Regione Egea e, applicando differenti relazioni empiriche, sono state quindi fornite delle stime delle magnitudo massime attese per ogni sorgente (§6.1). Le nuove informazioni sulla profondità della BDT hanno inoltre permesso di migliorare la caratterizzazione dei volumi a deformazione sismica, cosicché per alcune zone sismiche selezionate sono stati realizzati dei nuovi calcoli degli *strain rates* sismici (§6.2). Infine, integrando i valori di resistenza, definiti dagli inviluppi, lungo la profondità, sono state ottenute delle stime della resistenza totale, sia per la placca superiore che per quella inferiore (§6.3).

In conclusione, questo progetto è stato incentrato sulla caratterizzazione reologica della Regione Egea, per la quale è stato il primo a proporre un modello 3D completo della profondità della BDT e della resistenza e temperatura ad essa associate. Questa ricerca ha inoltre dimostrato che le proprietà reologiche possono essere collegate efficacemente ai processi sismogenici, e fungere quindi da validi strumenti per migliorare la caratterizzazione sismotettonica ed, in ultimo, la valutazione della pericolosità sismica.

Εκτεταμένη περίληψη

Το κύριο θέμα αυτής της Διδακτορικής διατριβής είναι η έρευνα των θερμο-ρεολογικών χαρακτηριστικών του φλοιού στην ευρύτερη περιφέρεια του Αιγαίου και η μοντελοποίησή τους. Ο σκοπός αυτή ςτη ςεργασίας είναι ο χαρακτηρισμός της σεισμοτεκτονικής με τελικό στόχο τη βελτίωση της εκτίμησης του σεισμικού κινδύνου της περιοχής. Η ιδέα πίσω από αυτή τη διατριβή έγκειται στη σχέση μεταξύ των ρεολογικών παραμέτρων που προκύπτουν από τη μοντελοποίηση των ιδιοτήτων των πετρωμάτων και της σεισμογόνου συμπεριφοράς τους. Συγκεκριμένα, εφαρμόζοντας την αρχή ότι η εύθραυστη παραμόρφωση συνδέεται με πιθανή σεισμογένεση, το μοντέλο βάθους της εύθραυστης-εύπλαστης μετάβασης (BDT) έχει υιοθετηθεί στην βιβλιογραφία ως το όριο για τον προσδιορισμό του βάθους της σχιστόσφαιρας. Για το σκοπό της μοντελοποίησης αυτής έχουν ληφθεί υπόψη δύο μηχανισμοί δεσπόζουσας παραμόρφωσης, η ολίσθηση τριβής και ο νόμος του κλιμακωτού (power-law) ερπυσμού που αντιπροσωπεύει, αντίστοιχα, το όριο μεταξύ της εύθραυστης και της όλκιμης συμπεριφοράς (§2.1). Παράλληλα με την αναπαράσταση των ρεολογικών προφίλ, εκτιμήθηκαν προσεκτικά οι αντίστοιχες γεωθερμικές βαθμίδες, προκειμένου να αξιολογηθεί και να ληφθεί υπόψη η επίδραση των θερμικών ιδιοτήτων στη ρεολογική συμπεριφορά (§2.3). Τα δεδομένα της βιβλιογραφίας έχουν αναζητηθεί και συλλεχθεί για να καθορίσουν τις τιμές για τις περισσότερες παραμέτρους εισόδου στα μοντέλα που χρησιμοποιήθηκαν (ροή θερμότητας, ταχύτητα παραμόρφωσης, κλιμακωτών παραμέτρων και θερμική ισχύ) στις αντίστοιχες θεωρητικές ρεολογικές εξισώσεις. Για τον προσδιορισμό των τιμών των παραμέτρων όπως ο συντελεστής τριβής, ο λόγος πίεσης υγρού πόρων και ο δείκτης του τεκτονικού καθεστώτος (§3.1) ελήφθησαν υπόψη γεωδυναμικές και γεωλογικές εκτιμήσεις.

Πριν επικεντρωθούμε στην αναπαράσταση των ορίων αντοχής στην περιοχή μελέτης, έγινε λεπτομερής ανάλυση της ευαισθησίας και των ασαφειών των παραμέτρων εισόδου και της μεταβλητότητάς τους καθώς και η επίδραση τους στις κύριες θερμο-ρεολογικές ιδιότητες (βάθος BDT, αντοχή και θερμοκρασία) (κεφάλαιο 4). Τα αποτελέσματα των δοκιμών ευαισθησίας υποδεικνύουν ότι οι παράμετροι που σχετίζονται με τη θερμοκρασία, όπως η ενέργεια ενεργοποίησης, η θερμική ροή στην επιφάνεια και η θερμική αγωγιμότητα είναι οι πλέον σημαντικές για τις ιδιότητες του BDT (ειδικότερα για το βάθος του BDT και την αντοχή). Η ανάλυση των αβεβαιοτήτων έδειξε ότι μετά από προσεκτική επιλογή του εύρους των τιμών για τις παραμέτρους εισόδου, μπορούν να συναχθούν αξιόπιστα ρεολογικά προφίλ, μαζί με την εκτίμηση των παραλλαγών που σχετίζονται με τους κύριους ρεολογικούς δείκτες (βάθος BDT, αντοχή και θερμοκρασία).

Για τους σκοπούς της θερμο-ρεολογικής μοντελοποίησης τα ειδικά σενάρια έχουν αναπτυχθεί σε περιβάλλον Matlab (§3.2.3). Τα σενάρια στην Matlab διεξήχθησαν σε τρία διαφορετικά και επακόλουθα στάδια. Το πρώτο, προσομοιάζει σε 1D τα όρια αντοχής για συγκεκριμένες περιοχές δοκιμών στην περιοχή του Αιγαίου και αυτή ηπροσομοίωση έχει συγκριθεί με την αναθεωρημένη κατανομή σεισμικότητας με το βάθος, προκειμένου να εκτιμηθεί η ακρίβεια και η αξιοπιστία της αντιστοιχίας μεταξύ του βάθους BDT και του βάθους της σεισμικότητας (§5.1). Το δεύτερο στάδιο, έχουν παραχθεί σε 2D ψευδο-ρεολογικές τομές (μέσω παρεμβολής) κατά μήκος διαφόρων τομών στην περιοχή μελέτης. Οι τομές αυτές ανήκουν σε διαφορετικές γεωδυναμικές επαρχίες (§5.2). Αυτή η μοντελοποίηση επέτρεψε τον προσδιορισμό και την παρατήρηση των πλευρικών μεταβολών στις θερμο-ρεολογικές ιδιότητες σε ορισμένες από τις διαφορετικές γεωδυναμικές επαρχίες της περιοχής του Αιγαίου. Ιδιαίτερη προσοχή έχει δοθεί στο δυτικό τμήμα της Ελληνικής δίαυλου και στη σύγκριση μεταξύ ηπειρωτικών και ωκεάνιων τμημάτων του φλοιού, μέσω της σύνθεσης τομών ΔΝΔ-ΑΒΑ διεύθυνσης στα βόρεια (για τον ηπειρωτικό φλοιό) και στα νότια (για τον ωκεάνιο φλοιό) σε σχέση με το ρήγμα μετασχηματισμού της Κεφαλονιάς. Τα αποτελέσματα υπογράμμισαν τις ακόλουθες διαφορές μεταξύ των δύο τομέων: i) μια ελαφρώς ρηχότερη BDT στα δυτικά στην βόρεια τομή (~ 30-33 km) σε σχέση με την νότια τομή όπου το βάθος του BDT αυξάνεται (~ 40 km). ii) Μια σχετικά βαθύτερη BDT (~ 20-25 χλμ.) στην βόρεια τομή σε σχέση με την νότια τομή όπου το βάθος είναι ~ 15 χλμ., στα ανατολικά. iii) Την εμφάνιση ενός παχύτερου, βαθύτερου εύθραυστου στρώματος κάτω από το ρηχότερο BDT, στα κεντρικά-ανατολικά τμήματα των βόρειων τομών.

Το τρίτο και τελευταίο στάδιο της μοντελοποίησης περιέλαβε την ανακατασκευή ενός τρισδιάστατου θερμο-ρεολογικού μοντέλου για ολόκληρη την περιοχή μελέτης (§5.3). Ένα τέτοιο μοντέλο έλαβε επίσης υπόψη τα μεγάλης κλίμακας χαρακτηριστικά της λιθοστρωματογραφικής διάρθρωσης, τη γεωμετρία της Ελληνικής Διαύλου και τη θερμική διαταραχή που συνδέεται με την καταβυθιζόμενη "ψυχρή" ωκεάνια πλάκα. Η 3D ανασυγκρότηση, ιδιαίτερα για το βάθος BDT, επιτρέπει την παρατήρηση των περιφερειακών παραλλαγών της BDT στην περιοχή μελέτης. Από την άποψη αυτή, μπορούν να εντοπιστούν ορισμένα μεγάλης κλίμακας χαρακτηριστικά. (1) Λαμβάνοντας ως σημείο αναφοράς τη ζώνη καταβύθισης, το βάθος της BDT είναι πολύ ρηχότερο, μεταξύ 10 και 20 km στην άνω πλάκα, στους εσωτερικούς τομείς (περιοχή πίσω από το τόξο, όπως στο Αιγαίο και την ηπειρωτική Ελλάδα). Στις εξωτερικές περιοχές, το βάθος της BDT βρίσκεται στα περίπου 40 χλμ. στην ωκεάνια λιθόσφαιρα της καταβυθιζόμενης πλάκας και στα 35 χλμ περίπου στους ηπειρωτικούς τομείς (Απουλία, Κυρηναϊκή). (2) Η αντοχή και η θερμοκρασία στη BDT είναι γενικά καλά συσχετισμένες με το βάθος του. Οι τιμές αντοχής στην BDT είναι μικρότερες από 100 MPa στον εσωτερικό τομέα, ενώ στην ωκεάνια λιθόσφαιρα οι τιμές φθάνουν το 1 GPa. Οι θερμοκρασίες της BDT περιορίζονται σε περίπου 200-300 ° C για τις ρηχές BDTs στην ηπειρωτική Ελλάδα και στο Αιγαίο, ενώ οι τιμές είναι υψηλότερες γύρω στους 600-650 ° C στους εξωτερικούς τομείς.

Από την άποψη της ερμηνείας και της εξήγησης των θερμο-ρεολογικών αποτελεσμάτων, τόσο οι 1D προσομοιώσεις, οι 2D τομές αλλά και το 3D μοντέλο υποδηλώνουν ότι ο κύριος έλεγχος του βάθους της BDT (και συνεπώς και στη σχετική αντοχή και θερμοκρασία) αντιστοιχίζεται με την επιφανειακή τιμή της κατανομής της θερμικής ροής και γενικότερα με την αντίστοιχη γεωθερμική βαθμίδα. Ένας δευτερεύων ρόλος αποδίδεται τοπικά στην λιθολογική στρωμάτωση και, σε μικρότερο βαθμό, στις τιμές του ρυθμού παραμόρφωσης σε κάθε περιοχή.

Τα αποτελέσματα της μοντελοποίησης, ειδικότερα όσον αφορά το βάθος και την αντοχή του BDT, εφαρμόστηκαν διαδοχικά κυρίως στα πεδία της σεισμοτεκτονικής και της γεωδυναμικής. Το βάθος του BDT χρησιμοποιήθηκε ως περιορισμός για τον καθορισμό του πλάτους των μεγάλων σεισμογόνων πηγών στην περιοχή του Αιγαίου εφαρμόζοντας διάφορες εμπειρικές σχέσεις, ελήφθησαν εκτιμήσεις των μέγιστων αναμενόμενων σεισμικών μεγεθών για κάθε πηγή (§6.1). Οι βελτιωμένες γνώσεις σχετικά με το βάθος του BDT επέτρεψαν επίσης τον καλύτερο χαρακτηρισμό του όγκου των σεισμικών πηγών και για ορισμένες επιλεγμένες σεισμικές ζώνες έγινε ένας νέος υπολογισμός των σεισμικών ρυθμών καταπόνησης (§6.2). Τέλος, με την ενσωμάτωση κατά μήκος του βάθους, οι τιμές της αντοχής, όπως ορίζονται από τα περιβλήματα αντοχής, έχουν εκτιμηθεί για την συνολική ισχύ τόσο για την ανώτερη όσο και για την κατώτερη πλάκα (§6.3).

Συμπερασματικά, η διατριβή επικεντρώθηκε στο ρεολογικό χαρακτηρισμό της περιφέρειας του Αιγαίου, και είναι η πρώτη που προτείνει ένα πλήρες τρισδιάστατο μοντέλο βάθους της BDT και τις σχετικές τιμές αντοχής και θερμοκρασίας. Αυτή η έρευνα έχει επίσης καταδείξει πώς οι ρεολογικές ιδιότητες μπορούν να συνδεθούν αποτελεσματικά με τις διεργασίες σεισμογένεσης, για την βελτιστοποίηση του χαρακτηρισμού της σεισμοτεκτονικής και την εκτίμηση του σεισμικού κινδύνου.

Contents

List of figures

Chapter 1: Introduction

1.1 The question posed

The relationship between rheology, seismogenesis and seismotectonics has been a central and debated topic among the geological and geophysical scientific communities since the seventies, with the pioneering works of Sibson (1974; 1975; 1977) paving the way for the development of such an intriguing theme. Almost contemporarily, the Aegean Region became a preferential study area for trying to link plate kinematics concepts (Caputo *et al.*, 1970) with geodynamic long-term and seismic short-term processes, while the debate was being propelled and fed by classic literature works, such as those of McKenzie (McKenzie, 1972; 1978), Le Pichon, Angelier (*e.g.* Le Pichon and Angelier, 1979) and Mercier (Mercier *et al.* 1976; 1979a).

Since then several studies have investigated the seismological, rheological and seismotectonic features of the Aegean Region. Nonetheless, possibly because of the difficulty in recording and obtaining high-quality seismic data and subsurface structure reconstructions, at least until recent years, only a limited number of works have dealt with the topic of relating the rheological stratification of the Aegean Region with its seismicity distribution. Furthermore, no one has studied such relationship with the final aim of applying the results for the improvement of the seismotectonic knowledge and characterization of the main seismogenic sources in the broader Aegean Region (Caputo and Pavlides, 2013).

The questions risen here, then, and to which this study aims to contribute finding some answers are: i) whether a detailed rheological modelling, compared with good quality seismic data is able to explain the seismological behaviour of the various mechanical layers that make up the lithosphere(s) of the Aegean Region and ii) whether the results of such a rheological modelling, and in particular the depth of the brittle-ductile transition (hereinafter BDT) and its associated strength, can effectively help constraining the geometrical and mechanical characteristics of the main seismogenic sources affecting the region.

In other words, with this study I wanted to test the potentialities of rheological modelling for its application to seismotectonic issues and also its capability of reproducing the spatial extent of the brittle and ductile deformations and reconciling the former with the seismological behaviour, in an area characterized by a very intense seismic activity, as it is the Aegean Region.

1.2 Major goals of the research

The objectives of this study are manifold and not just restrained to a single field. Indeed the philosophy of and the disciplines behind this research naturally imply to obtain results and set the focus firstly on rheology and only subsequently on the applications of rheological modelling results to the fields of seismotectonics, active tectonics and geophysics of the solid Earth.

The first objective is to assess the validity of rheological strength profiles and their sensitivity to input parameter variations. To do so, I firstly performed tests on each single input parameter in order to quantify the effects of varying their values on the resulting rheological profiles. Successively a statistical analysis on BDT depth, strength and temperature for selected test sites has been carried out, with the final aim of determining and assessing also the combined effects obtained on strength envelopes when varying simultaneously more than one parameter.

With regard to the strength envelopes, I also wanted to test whether classical brittle-ductile rheological profiles could represent enough precise indicators for the depth distribution of brittle and ductile layers within the lithosphere of the Aegean Region. The objective in this sense was to understand whether brittle deforming layers were also effectively the loci of potential seismogenic processes. To do so, the obtained rheological profiles have been compared with the depth distribution of well-located seismicity. In other words, a secondary scope of this work was to check and eventually confirm the similarity between BDT and seismic-aseismic transition, with special emphasis and testing always on the Aegean Region.

This research also aimed at highlighting the potential differences in the rheological behaviour of the several tectonic domains and geodynamic settings that characterize the Aegean Region. At this regard, a particular focus was set on the rheological differences between continental collision and oceanic subduction settings. An intermediate step and scope is the realization (and the analysis) of 2D rheological transects across and along some of the main structures of the Aegean Region (*e.g.* Hellenides fold-and-thrust belt, Hellenic Arc). In this case I tried to detect potential lateral variations of the main rheological properties of the crust and to assess whether such variations may be related or caused by the geometry, distribution, evolution and kinematics of the main tectonic and/or geological features investigated along the transects.

The final objective for the rheological modelling section is the realization of a 3D model of the Aegean lithosphere in terms of rheological behaviour. In particular, this study aims at defining the depth of the brittle-ductile transition and its relationship with the bottom of the seismogenic layer. Additional scopes are those regarding the determinations of the strength values at the BDT depth for the whole Aegean Region and the total integrated strength, which can be correlated with the elastic thickness of the lithosphere.

With regard to the identification of the BDT depth, the primary objective is to precisely locate the shallowest BDT, which usually corresponds to the (upper) crustal rheological transition

and tends to represent the downdip seismogenic boundary of the most frequent upper crustal seismicity of the Aegean Region. However, a further aim is also represented by the determination of potential deeper brittle layers with their corresponding thickness and BDTs depths, especially where the geothermal gradient is relatively low and/or along the Hellenic subduction zone where deeper lower crustal/upper mantle seismicity could occur.

As regards the application of the rheological modelling results to the field of the seismotectonics, the main objective is represented by the determination of the seismogenic layer thickness and the analysis of its lateral variations over the whole Aegean Region. The focus is also set on the identification of possibly seismogenic layers below the shallowest crustal one and hence on the determination of their thickness and associated seismogenic potential.

The use of BDT depth and strength values in the seismotectonic field is also aimed at better constraining geometrical, kinematic and mechanical properties of the main seismogenic sources (both individual, *i.e.* relatively well known active and possibly capable faults, and composite ones). In particular, the BDT depths can help constraining the maximum width of the investigated sources and then, by applying empirical relationships between width-length and moment magnitude (*e.g.* Wells and Coppersmith, 1994), can also give insights on the maximum expected magnitudes for such sources. To this point, the final objective is always represented by the improvement in the knowledge of the kinematic and geometric characteristics of the main seismogenic faults and sources, which, in turn, aims at better defining the seismic hazard for the investigated area and hence at better mitigating the seismic risk. Furthermore, information on the strength of the faults obtained from rheological modelling allows defining the resistance of such structures and hence could help determining the boundaries for speculations on *e.g.* potential earthquake recurrence times or the stress field and stress state, especially for faults and areas where historical seismicity is scarce.

An additional secondary objective in the application of the BDT depths and rheological results is the improvement in the calculations of the seismic strain rates for the Aegean Region. To this point indeed, the knowledge of the BDT depth and therefore of the thickness of the brittle and potentially seismogenic layer may help refining the analysis and the assessment of the seismic deformation, by better defining the volume within which seismogenic behaviour predominates and takes place (*e.g.* Kostrov, 1974).

To sum up, the present research aims, as concerns the rheological modelling, at firstly defining the rheological properties of the lithosphere in the Aegean Region and in particular at determining the depth of the BDT, the (crustal) strength and the associated thermal regime. Secondly, using and applying the results of the rheological modelling, this study is devoted to contribute to our knowledge improvement on the seismotectonics of the area, with the final scope being the seismic hazard risk reduction.

1.3 Applied investigation methods

This study has been conducted mainly through numerical rheological modelling. In particular all the models and the elaborations have been realized using specifically developed Matlab scripts, which allow to obtain both 1D strength envelopes, 2D transects and a comprehensive 3D model. For the realization of the strength envelopes two main rheological behaviours have been considered, namely the frictional sliding for the brittle deformation and the power-law creep for the ductile one, following the classical approach by *e.g.* Sibson (1977; 1983), Ranalli and Murphy (1987), Ranalli (1995). The thermo-rheological properties of the lithosphere(s) in the Aegean Region have been investigated by mainly analysing the values, uncertainties and variations of the following parameters: BDT depth, strength expressed in terms of critical differential stress and temperature (both latter parameters at the BDT and along the whole considered lithospheric column, as vertical variations of the geothermal gradient).

The choice of the input parameters values for the reconstruction of the rheological model has been based mainly on the collection of various sources of literature data and also on geological, tectonic and geodynamic considerations, some of which have been also confirmed and supported by field observations (*e.g.* tectonic regime, lithologies selection). The results of the 1D and 2D models have been also compared with the depth distribution of well-located seismicity in order to evaluate their goodness and reliability. Such calibrated test sites have then been used as reference and control points for the reconstruction of the 3D model.

Finally, in the application of the rheological results to the seismotectonic and geodynamic fields, investigating methods based on the application of rheologically-determined geometrical and mechanical constraints and empirical relationships have been adopted. In particular, the BDT depth has been used for determining the geometrical characteristics (primarily the seismogenic layer thickness and width of the faults) of the main seismogenic sources affecting the Aegean Region, especially for what concerns their termination at depth.

Empirical relationships such as those of Wells and Coppersmith (1994) and Pavlides and Caputo (2004) have then been applied for estimating parameters such as the maximum expected magnitudes for the investigated seismogenic sources. In the calculations of the seismic strain rates, instead, the BDT depth has been used as a constraint for the volumetric dimensions of the seismically-deforming blocks, within which Kostrov's formula (1974) has been applied in order to estimate the deformation rates.

1.4 Research work flow

In this section I will briefly describe the workflow followed during the three-years research project, which is reflected in the way this work has been organized and it is presented here. In a

first stage, all the available literature data for the input parameters values have been collected and stored into a GIS software, where they have been georeferenced in order to be easily accessible and ready to be used for the whole area. At the same time, specifically designed Matlab codes have been developed and implemented in order to run all the different calculations for both 1D, 2D and 3D rheological models.

Several test sites have been selected for modelling the corresponding 1D strength envelopes, which have been carefully calibrated by comparing them with the seismicity data. As a successive step several 2D rheological transects have been realized in different tectonic settings of the Aegean Region, *i.e.* in the continental collisional setting, as well as in the oceanic subduction one and in the back-arc extending realm. The comparison between the mechanical, lithological and seismological characteristics of such transects has allowed to assess the relative weight of the geodynamic setting on the resulting rheological properties of the lithosphere, and specifically on the lateral variations of the main thermo-rheological parameters along the investigated transects. Both the 1D test sites and the 2D transects have successively been used as references for the reconstruction of the 3D rheological model of the whole study area.

One of the Matlab scripts allows to create both the 3D map of the BDT depth, the one of the BDT strength and the one displaying the total integrated strength. The results of the 3D model, and in particular the depth of the BDT, have been used as constraints for determining the thickness of the seismogenic layer in the Aegean Region and defining the maximum possible width of the major seismogenic sources. In this way, and adopting the above-mentioned empirical relationships, potential estimates of the maximum expected magnitude for some selected sources have been obtained.

The BDT depth map found a further application in the calculation of the seismic strain rates for the Aegean Region, as it allows to better define the vertical dimension of the seismogenic volumes, within which the (seismic) deformation rates have been calculated. Finally, the results on the total integrated strength have represented a useful tool for assessing the long-term lithospheric-scale deformation in the study area and trying to relate the observed kinematics with the geodynamic processes occurring in the Aegean Region.

What follows now is a comprehensive review of the study area extent, kinematic and geodynamic framework, structural evolution and active tectonics. Subsequently, in Chapter 2 I will briefly recall the theoretical principles of the rheological modelling, focusing in particular on the brittle and ductile deformation styles and their associated rheological behaviours. Chapter 3 shows the main datasets and methods used for the modelling, while Chapter 4 focuses on the main outcomes of a sensitivity analysis that has been realized for the input rheological parameters in selected test sites. Then, in Chapter 5 the obtained results are presented with particular emphasis on the BDT depth, strength and temperature variations for the 1D test sites, along the 2D transects and within the 3D model, for the whole study area. The application of the above-mentioned

modelling constraints into the fields of seismotectonics and geodynamics and the obtained results are then shown in Chapter 6. Finally, in Chapter 7, the conclusive remarks are presented together with the potential future developments for this study.

1.5 Study area extent

The study area has a squared shape on a Mercator projection and comprises the whole broader Aegean Region including the southern sector of the Balkan peninsula, continental and insular Greece as well as western Anatolia (fig. 1.1).

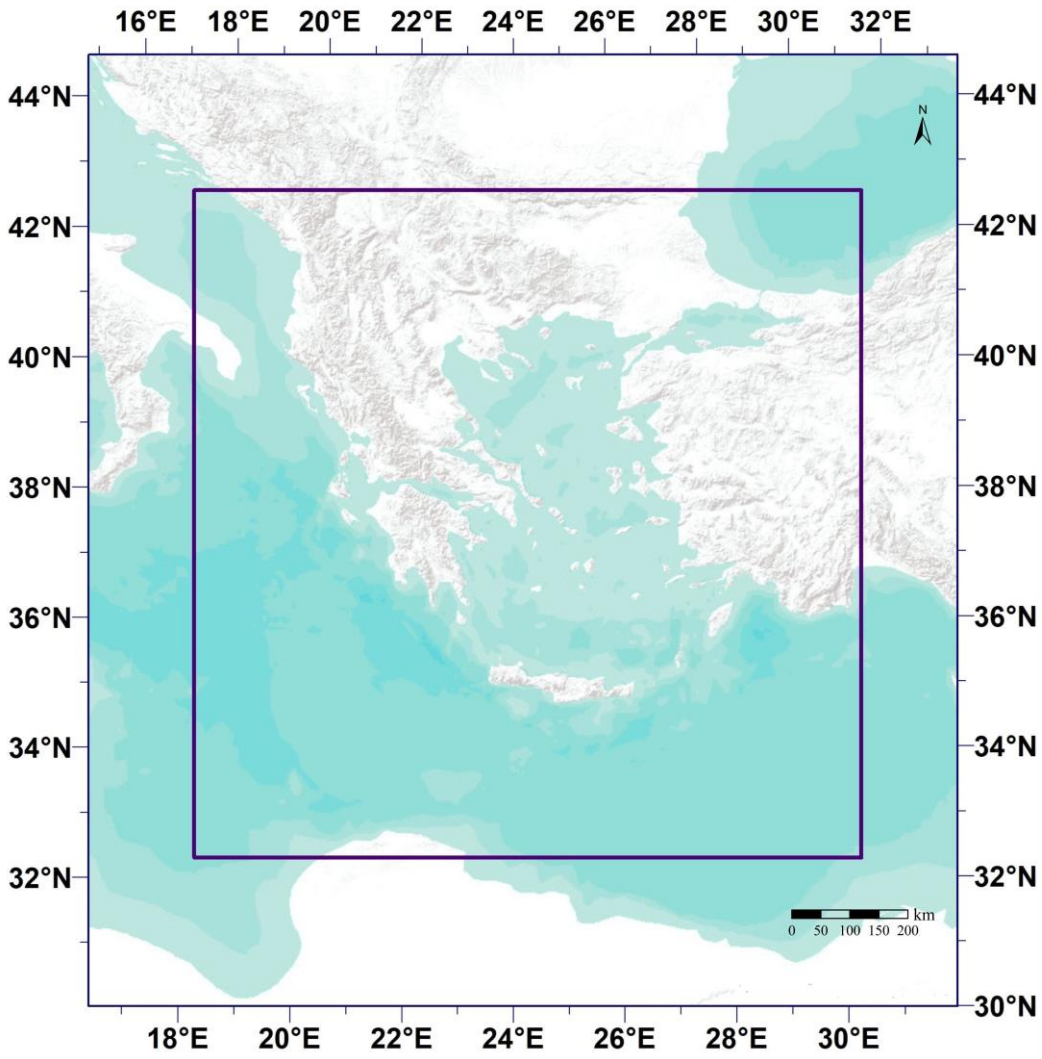

Fig. 1.1 - Topographic and bathymetric map of the Central-Eastern Mediterranean Region. The blue solid line depicts the extent of the study area.

At the western side the area extends to the southern Adriatic and Ionian Seas reaching the Salento area (Southern Italy); to the south it includes the Central-Eastern Mediterranean Sea and a coastal sector of Cyrenaica, Libya; to the east it reaches the longitude of Antalya, Turkey and to the north the latitude of Sofia, Bulgaria.

The total extent of the study area is ca. 1,322,500 km^2, resulting from a squared region having a side length (so equal both in the north-south and in the east-west direction) of 1150 km. For the sake of simplicity in all the elaborations I used the Greek Grid coordinate system, which is adapted from the Mercator projection specifically for the Aegean Region. Using such a coordinate system, the north, east, south and west boundaries coordinates are respectively (in m) 4,750,000; 1,100,000; 3,600,000; -50000.

1.6 Kinematic and geodynamic framework

From a geological point of view, the Aegean Region represents one of the most tectonically and seismically active areas all over the world (fig. 1.2).

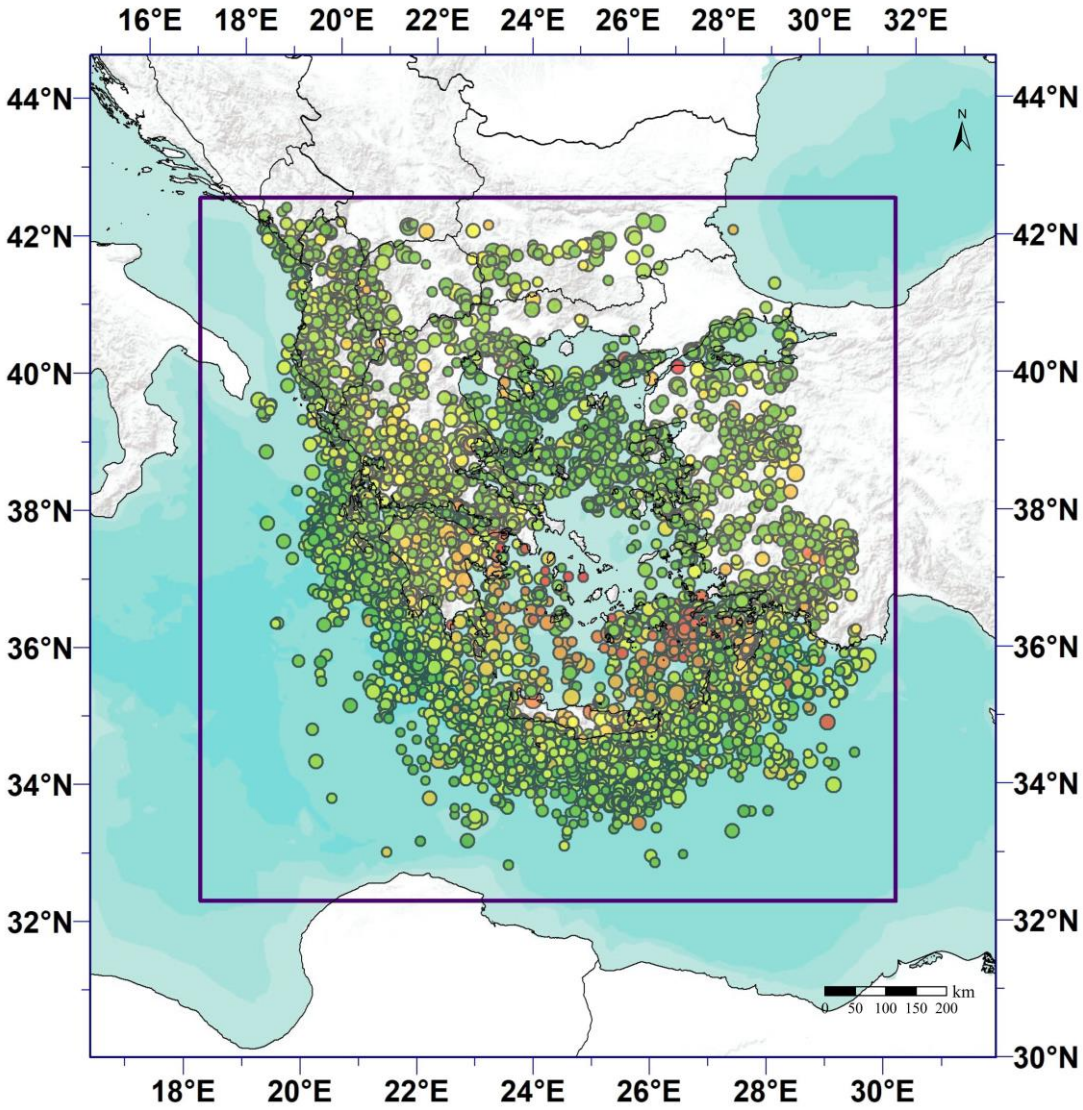

Fig. 1.2 – Seismicity of the Aegean Region in the period 1900-2009 (catalogue from Makropoulos et al.*, 2012). The circles are color coded according to the depth (green-shallow; red-deep), while the dimension is proportional to the magnitude.*

Almost the entire study area could be ideally included in the deformational belt which acts as a rather diffuse plate boundary between Africa and Eurasia (*e.g.* Dewey and Sengor, 1979; McKenzie and Jackson 1983; Jackson and McKenzie, 1988; England and Jackson, 1989; Jackson, 1994). More in detail, several different sub-areas could be identified, spanning from continental collision to oceanic subduction, passive margin, back-arc basin and core complexes settings.

From a kinematic point of view the entire region is dominated by the interplay of two main features, being: i) the overall north-south directed Africa-Eurasia convergence and ii) the westward motion of the Anatolian microplate (or block). Within this geodynamic framework a variety of tectonic settings occurs, including both E-W and N-S compression, as well as extension with transpressive, transtensional and transfer zones linking the compressional and the extensional domains.

The main geological features that result from such a complex stress field in the Aegean Region (and may locally influence it) are the Kefallinia Transform Fault (KTF), the Hellenic subduction Zone (HSZ), the Corinth Rift, the North Aegean Trough (NAT) and the western termination of the North Anatolian Fault Zone (fig. 1.3).

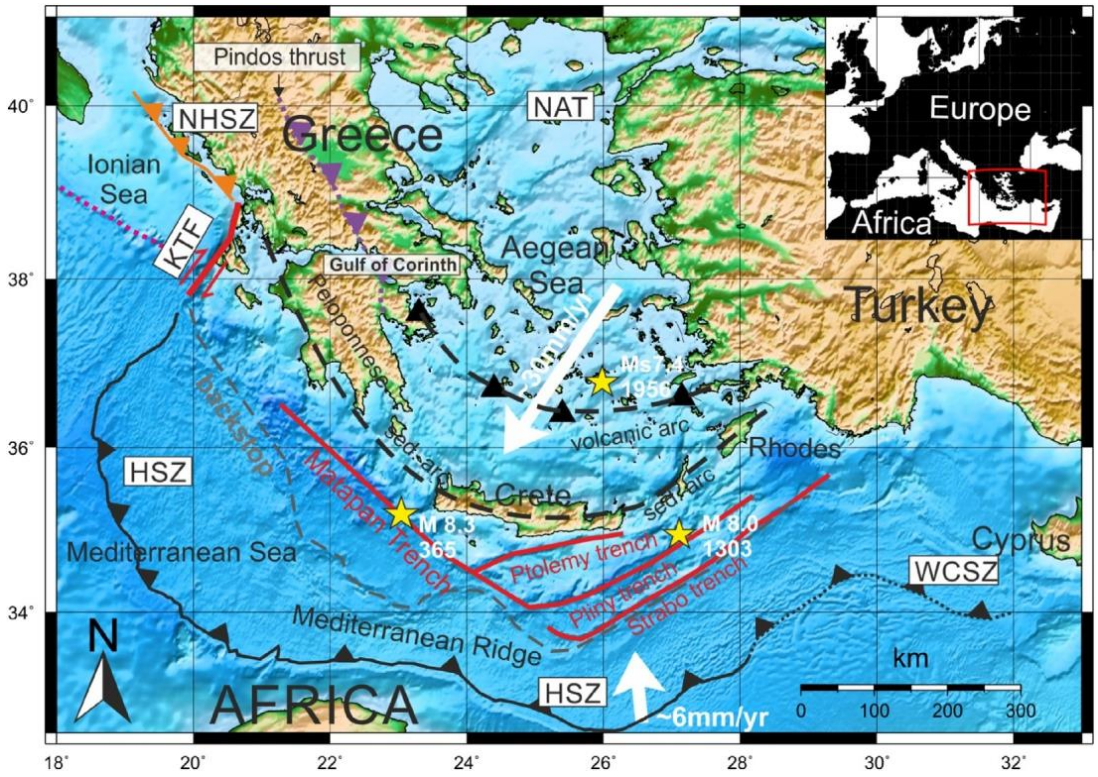

Fig. 1.3 – Kinematic and geodynamic setting of the Aegean Region (from Bocchini et al., 2018). The solid black line with triangles indicates the current position of the active deformation front of the Hellenic subduction zone (HSZ), where oceanic subduction is occurring. The orange line with triangles represents the boundary of the continental collision between Apulia (lower plate) and Eurasia (Hellenides). White arrows and associated values indicate the average geodetic velocity vectors of the Aegean microplate and Northern Africa with respect to Eurasia. The black dashed line in the Aegean Sea locates the volcanic arc.

What follows is a brief recall on the geological and tectonic evolution of the Aegean Region; then, I will focus more in detail on the stress field characteristics across the Aegean Region and on the main resulting geological features, especially on those mentioned above.

1.7 Structural and tectonic evolution

The geological evolution and history of the Aegean Region starts and it is fundamentally linked with the closure of the Neo-Tethyan ocean and the accretion of the different interposed continental terranes to the southern Eurasian margin, up to the final collisional stages between the African northern (once) passive margin and the Eurasia (and the Aegean microplate) itself (see *e.g.* Mountrakis, 2006; van Hinsbergen *et al.*, 2005) (fig. 1.4).

Fig. 1.4 – Evolution of the African-Eurasian (Aegean microplate) active margin since Triassic to present times (from Papanikolaou, 2013).

Such an evolution must therefore be reconstructed since Early Mesozoic times. Different models have been proposed to explain the tectono-stratigraphic and palaeogeographic evolution of the Aegean Region. Such models share common traits, but often disagree, especially as regards the sense of vergence of the subduction processes during peculiar times and the mechanism for the emplacement of the ophiolites outcropping in different areas across the Balkan, Aegean and Anatolian regions. The commonly referred to models are those proposed by Jacobshagen (1986), Doutsos *et al.* (1993), van Hinsbergen *et al.* (2005), Mountrakis (2006) and Papanikoulaou (2013).

In the following, I will describe the tectonic evolution of the Aegean Region trying to take into account, as far as possible, the principal evolutionary models, also considering that many of

those arguments are still being debated. The geological evolution of the destructive plate margin between Eurasia and Africa in the Aegean Region is mainly characterized by the spatial and temporal alternation of oceanic lithosphere subduction and continental terranes collision. Given these features, and the fact that a great part of the region around the active margin is nowadays characterized by continental lithosphere, the boundary appears more like a large distributed high strain rate zone, where intense deformation is diffuse over hundreds of kilometres rather than being localized along a thin and well detectable margin. This is also in agreement with the spatial distribution of seismicity (*e.g.* Makropoulos and Burton, 1984; Papazachos, 1990), which, even though with varying density and rates, is spread all over the Aegean Region (fig. 1.2).

The bulk of the deformation takes the form of shallow brittle seismic faulting in the upper crust of the back-arc Aegean Region and along the Hellenides, even though ductile deformation has also played a significant role in the tectonic evolution of both thrust belts and exhumation-related structures (*e.g.* Xypolias and Doutsos, 2000; Xypolias *et al.*, 2012). Currently, within the Hellenic subduction zone additional processes, such as aseismic creep and deep intra-slab seismicity, contribute to the overall deformation, even though their extent and effective role are still a matter of debate (see *e.g.* Jackson and McKenzie, 1988; Shaw and Jackson, 2010; Laigle *et al.*, 2004; Ganas and Parsons, 2009; Halpaap *et al.*, 2018). From a tectono-stratigraphic point of view the Hellenides and the broader Aegean Region in general are the result of a mainly northward-northeastward directed emplacement and stacking of tectonic nappes (or terranes) which nowadays correspond at the surface to different geological domains, sometimes referred to as isopic zones (Aubouin, 1959) (fig. 1.5).

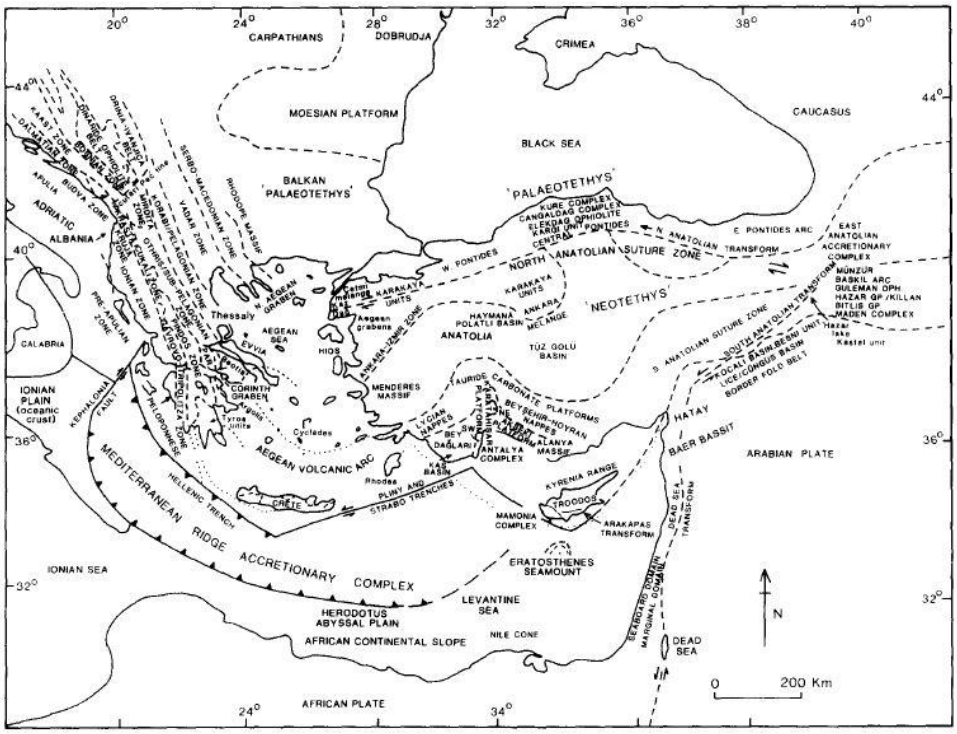

Fig. 1.5 – Isopic zones (or terranes) of the Aegean Region (from Robertson et al.*, 1991).*

Such isopic zones are all internally characterized by their own typical facies association and a laterally more or less homogenous stratigraphic succession. Furthermore, the tectono-stratigraphic domains in the Aegean realm have also been linked to similar zones belonging to the Anatolia microplate. The structural evolution of the latter is thought to be the result of an eastward continuation of the orogenic processes that led to the formation of both Internal (Mesozoic) and External (Tertiary) Hellenides. Their counterparts within the Anatolia peninsula are, respectively, the Pontides and the Taurides belts (*e.g.* Sengor and Yilmaz, 1981; Robertson and Dixon, 1984; Mountrakis, 1986).

The oldest and structurally uppermost nappes are those corresponding to the Srednogorie block, Serbo-Macedonian Massif and Rhodope block. The latter is a terrane of possibly continental Cimmerian origin which is thought to correspond to the terranes north of the Pontides suture in the northern Anatolian region (see *e.g.* Mountrakis, 2006). The Srednogorie terrane has a similar continental origin and at present day covers the area north of Rhodope, extending from eastern FYROM to central Bulgaria. Finally, the Serbo-Macedonian massif corresponds to an elongated region spanning from Serbia (to the north) to the Chalkidiki peninsula (to the south) and it is characterized by crystalline basement units within which granitoids plutons have intruded (fig. 1.6).

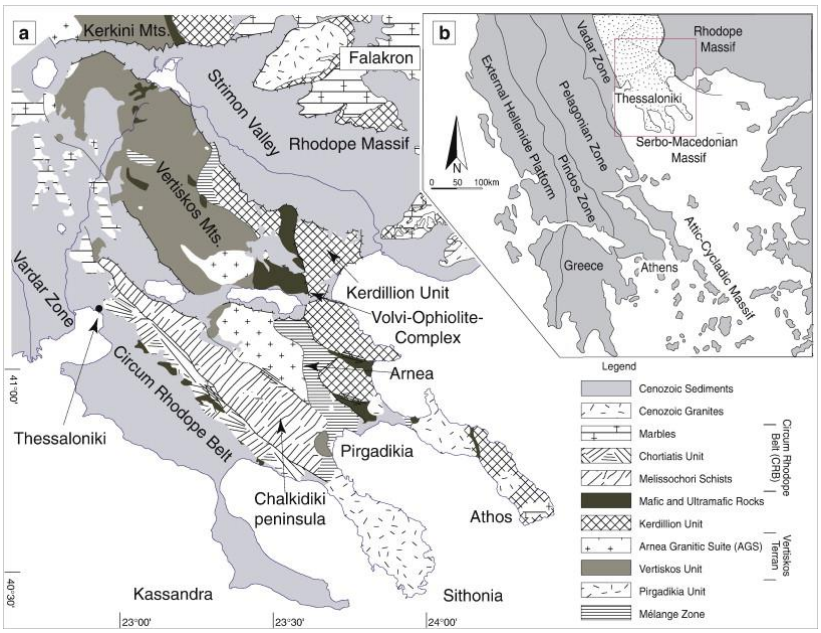

Fig. 1.6 – Schematic geological map of the Serbo-Macedonian Massif in the Chalkidiki and Central Macedonia regions, showing the distribution of the granitic intrusions (from Himmerkus et al., 2009).

These old terranes represent the suture zone to the north with the Moesian platform, which can be considered as an extension of the Eurasian continent. In this view, the top of the Hellenides (in this case referred to as Internal Hellenides) as on orogen can effectively be traced along the Mesozoic suture zone which represents the transition to the actual Eurasian plate margin. The

emplacement of the abovementioned blocks occurred in Jurassic and Cretaceous times in a time span going from ~185 to ~100 Ma (Ring *et al.*, 2010; Mposkos and Kostopoulos, 2001).

Tectonically underlying the Rhodope block and lying to the southwest with respect to it, is the Vardar unit representing the remnants of an oceanic basin which separated the Rhodope microcontinent from the Pelagonian one (on which I will focus later).

The Vardar zone therefore comprises deep basinal units together with ophiolitic slices on whose emplacement polarity and mechanism no clear and shared view has been reached yet in the scientific community (see *e.g.* Mountrakis, 2006; Doutsos *et al.*, 1993; 2006).

Similar to the Rhodope block, also the Vardar unit can be related in terms of origin, palaeogeography, facies association and tectonic transport to its counterpart in the Anatolian microplate, which is referred to as Izmir unit. The arc-shaped linking region also comprises the area around Thessaloniki, the southern part of the Chalkidiki peninsula and possibly the island of Chios, while the islands of the northern Aegean Sea such as Thassos, Samothraki, Limnos and (partially) Lesbos are generally considered to belong to the Rhodope-Circum Rhodope terranes (see *e.g.* Papanikolaou, 2013).

The Pelagonian unit is the one that structurally lies just below the Vardar oceanic one. Pelagonia is considered to be a microcontinent characterized by a carbonate platform (whose products are now mainly metamorphosed) overlying a metamorphic crystalline basement, mainly made up of gneisses and (blue-facies) schists. The Pelagonian block is thought to have been amalgamated to the Vardar zone (and therefore to the growing Hellenic orogen and finally to Eurasia) between 125 and 85 Ma, even though its tectonic evolution and transport history are not always shared by the whole scientific community, especially in terms of underthrusting/subduction polarities at its margins and the timing of the metamorphism.

The counterpart of the Pelagonian block in the Anatolian region is generally thought to be represented by the Menderes Massif block (see *e.g.* Robertson *et al.*, 1991). This is a highly extensional basin mainly characterized by E-W trending active normal faults and by an almost N-S direction of extension. Actually, the Pelagonian-Menderes block cannot be laterally traced in a continuous manner from the Aegean Region to the Anatolian one since the interposed Aegean Sea is characterized by the occurrence of the Cycladic Blueschist Unit resulting from the development of the Cycladic core complex due, in turn, to the very intense and long-lasting (mainly ductile) extension that took place in the central back-arc Aegean Region since at least Early Miocene times (*e.g.* Gautier *et al.*, 1993).

Underlying the Pelagonian block are the remnants of the Pindos Oceanic Unit and the contact among the two isopic zones marks the suture between the continental Pelagonian lithosphere and the partially obducted Pindos oceanic lithosphere, belonging to the Neo-Tethys oceanic branch. The Pindos Unit mainly consists of flysch deposits, pelagic limestones, radiolarites and possibly oceanic suites, testified by the occurrence in different outcrops of the associated ophiolites. The

age of such oceanic crust is in the range 80-65 Ma (*e.g.* Keay, 1998) while the transitional and clastic units are generally younger (55 to 30 Ma).

According to Ring *et al.* (2010), the Cyladic Blueschist complex can be considered as part of the Pindos Unit, even though its final evolutionary stage differs from the latter. Indeed, the Cyclades islands region has been directly involved in, and affected by, the strong lithospheric stretching characterizing the central Aegean, which finally led to the exhumation of the Cycladic core complex. The Pindos Unit is spatially separated from and not in direct contact with the structurally overlying Pelagonian block in northwestern continental Greece, because a piggyback-type foredeep basin developed there from middle Eocene to middle Miocene times (*e.g.* Doutsos *et al.*, 1994). Such a basin is usually referred to as the MesoHellenic Trough, as it substantially separates the Internal Hellenides (Rhodope, Vardar and Pelagonian zones) from the External Hellenides (Pindos, Gavrovo-Tripolitza and Ionian zones); its infill is of post-orogenic origin (in this view it has been also considered as a molasse basin) mainly consisting of conglomerates, sandstones and shales. The geometry of the basin, the position of the depocentres and the thickness of the sedimentary infill were also tectonically controlled by folds and faults on both flanks of the basin, which is elongated in a NW-SE direction, parallel to the other isopic zones of the Hellenic orogen in continental Greece.

Tectonically underlying the Pindos Oceanic Unit is the Gavrovo-Tripolitza zone. This nappe is mainly characterized by lithological units related to neritic sedimentation in carbonate platform environments. Accordingly, the Gavrovo-Tripolitza unit represents an almost completely different realm from the Pindos Oceanic Unit, with its crust and lithosphere being instead of continental, though stretched in a passive margin setting, nature. The Gavrovo name is usually attributed to the corresponding zone in northern Greece (north of the Corinth and Patras Gulfs) while the Tripolitza name is referred to the region in southern Greece, mainly Peloponnesus, even though by an evolutionary, tectonic and geological point of view the two platforms can effectively be considered as a single nappe and isopic zone. The Gavrovo-Tripolitza lithological column also includes an Eocene-Oligocene flysch (Jacobshagen, 1986), while the platform units have a Triassic to Eocene age. In terms of tectonic evolution and transport, the Gavrovo-Tripolitza nappe started to underthrust the Pindos Oceanic Unit at ~35 Ma (*e.g.* Thomson *et al.*, 1998; Ring *et al.*, 2010 and references therein). Some fragments of the Gavrovo-Tripolitza units are also exposed in the island of Crete, were they appear to be partially metamorphosed, even though not to a high degree, similarly to what observed in southern Peloponnesus.

The nappe structurally lying below the Gavrovo-Tripolitza and being to the southwest with respect to it is the Ionian (or Ionian/Mani taking into account its southern sector) isopic zone. From a palaeogeographic point of view, this zone corresponds to a transitional and deep basinal environment, whose representative lithostratigraphic column is made up of a Carboniferous to Triassic basement over which sedimentation of pelagic limestones and flysch occurred until late

Eocene times (*e.g.* Aubouin, 1959; Papanikolaou, 1986). The Ionian/Mani basin should actually be distinguished from, for example, the Pindos basin, since the latter is also characterized by radiolarites sedimentation, volcanic products and, above all, by clear evidences of oceanic crust formation, while the former does not show any sign of this very deep sedimentation or oceanic lithosphere development and can be therefore termed as an epicontinental basin (*e.g.* Papanikolaou, 2013), associated to the formation of a passive margin.

From a chronological point of view, the Ionian basin Unit has started to be involved in the folding and thrusting process during Late Oligocene and it is largely outcropping at present in Western Greece. In late Miocene (Royden and Papanikolaou, 2011), the Ionian Zone was finally emplaced over the more external Paxos Unit (or Pre-Apulian Platform, see *e.g.* Jolivet and Brun, 2010). This latter unit represents a structural high with respect to the basinal Ionian unit and is characterized by neritic carbonate platform sedimentation followed by flysch deposition occurred until Late Miocene (see *e.g.* Burchfiel *et al.*, 2018).

The latest stages of Miocene correspond to a crucial period for the onset of the current kinematics and tectonic setting of the Aegean Region, in particular for the Western Hellenic subduction zone. Indeed, the Late Miocene marks the initial time of oceanic lithosphere subduction resumption south of the Kefallinia Transform Fault, where the Ionian Sea oceanic lithosphere is currently subducting below the Hellenides fold-and-thrust belt (and more in general below the Aegean microplate) at ~35 mm/a (*e.g.* Royden and Papanikolaou, 2011).

The actual and current convergence rate between Africa (in this case the Ionian Sea oceanic lithosphere) and Eurasia is around 5-10 mm/a (*e.g.* McClusky *et al.*, 2000; McQuarrie *et al.*, 2003 Reilinger *et al.*, 2006), therefore the observed and above-mentioned value of the subduction rate has to result also from the contribution due to the SW directed motion of the Aegean microplate and the associated Hellenic trench retreat, which is estimated to be around 20-25 mm/a (*e.g.* Jolivet and Brun, 2010).

North of the Kefallinia Transform Fault, thrusting has been propagating westwards involving the Pre-Apulian platform and towards the continental crust of the Apulian foreland since late Miocene. As a consequence, continental collision is currently occurring, with a much lower convergence rate with respect to the oceanic subduction setting, being indeed around 5-10 mm/a. Such a decrease in convergence rate from south to north across the Kefallinia Transform Fault can be mainly attributed to the different nature of the downgoing lithosphere, being respectively oceanic to the south (Ionian Sea) and continental to the north (Apulian platform) (fig 1.7).

In particular, the positive buoyancy of the colliding continental lithospheres in the north prevents the Apulian microplate from rapidly sinking below the Hellenides, but rather slows down the convergence process. The result of this differential convergence rate from north to south is,

from a kinematic point of view, the creation of a SW-NE directed dextral shear motion between the continental collision region to the north and the oceanic subduction zone to the south.

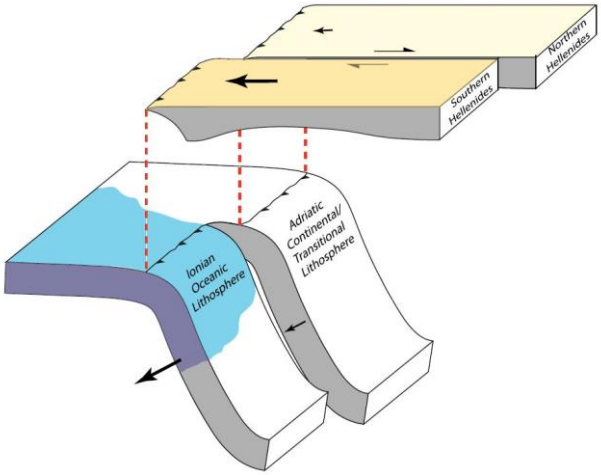

Fig. 1.7 – Cartoon showing the development of the KTF due to fast subduction beneath the Southern Hellenides vs *slow collision in the Northern Hellenides (from Royden and Papanikolaou, 2011).*

The KTF, developed as a consequence of this dextral shear motion, has accommodated a total offset of ca. 100-120 km (Royden and Papanikolaou, 2011) since the late Miocene (6-8 Ma). The dextral strike-slip motion is actually accompanied by a minor thrust component (rake around 170°-175°) and the KTF is currently moving with a mean rate of 25 mm/a (*e.g.* Hollenstein *et al.*, 2008). From a tectonic and geodynamic point of view, the KTF represents a lateral steep ramp of the Hellenic subduction zone and may be possibly interpreted as a STEP (Subduction-Transform Edge Propagator, *sensu* Govers and Wortel, 2005) fault (fig. 1.8).

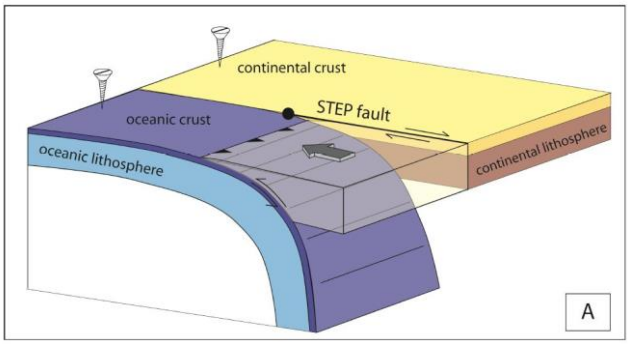

Fig. 1.8 – Simplified representation of a STEP fault, from Gallais et al.*, 2013.*

1.8 Active tectonics and seismotectonic characterization

The KTF is characterized by an intense seismic activity, with moderate-strong magnitude earthquake sequences occurring with a high frequency (*e.g.* M_w = 6.2 Lefkada 2003; M_w = 6.0 Kefallinia 2014; M_w = 6.5 Lefkada 2015). The dextral shear motion affecting the region is also accommodated by secondary strands, as it is testified, for instance, by the 2008 M_w = 6.4 Achaia

earthquake (also referred to also as Movri or Andravida earthquake) which occurred in northwestern Peloponnesus, southeast of the KTF, and exhibited a similar dextral strike-slip motion, indicating the possible lithospheric-scale nature of the shear zone.

As regards the current tectonic activity, one of the most prominent features in the Aegean Region is the Corinth Rift (fig. 1.9). Such an extensional large-scale structure is elongated in a WNW-ESE direction (total length around 110-115 km) and has a maximum width of *ca.* 30 km. The Corinth Rift is characterized by WNW-ESE trending normal faults, which produce an almost N-S extension, responsible for the formation of a (semi) graben, whose depocentre is 900 m below sea level (see *e.g.* Sorel *et al.*, 2000). The development of the Corinth Rift began in Pliocene-Pleistocene (Armijo *et al.*, 1996) and is still currently active at slip rates up to 15-18 mm/a in the western segment and down to 5 mm/a towards the eastern termination (*e.g.* Birillis *et al.*, 1991; Clarke *et al.*, 1998). Even though normal faults border both sides of the Corinth Gulf, the most active ones are considered to be the north-dipping faults on the southern side, as recent and historical seismicity would suggest (*e.g.* Heliki 1861 earthquake, Aigion 1995).

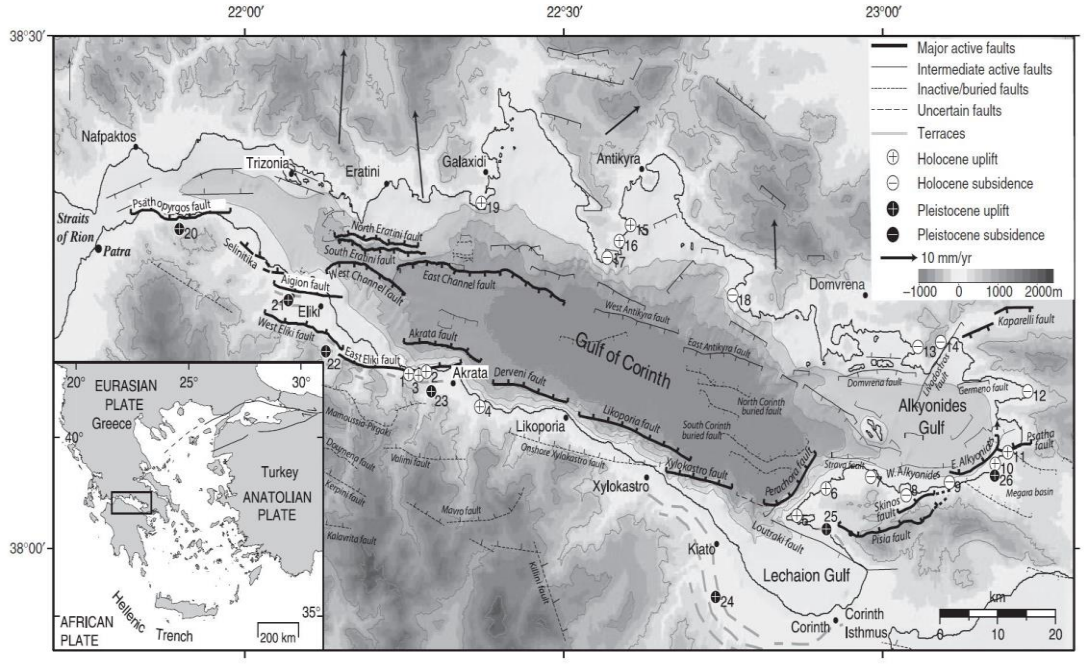

Fig. 1.9 – Main faults and structures of the Corinth Rift area (from Bell et al., *2009).*

Such faults take the name of respectively, from west to east, Psathopyrgos, west Heliki, Aigion, east Heliki, Xylokastro and Perachora (GreDaSS, Caputo and Pavlides, 2013); they are characterized by slip rates in the order of 1-10 mm/a (*e.g.* Armijo *et al.*, 1996; Koukouvelas *et al.*, 2005; Roberts *et al.*, 2009) and maximum expected magnitudes in the range 6.5-6.6. Some active and potentially seismogenic normal faults also lie on the northern side of the Corinth Rift, dipping to the south. This is the case, for example, of the Delfi Fault and the Kaparelli Fault, which is also considered the causative fault of the March 4th 1981 M_s = 6.4 Corinth Rift

earthquake. A debated point is the relative activity and the associated potential seismogenic behaviour of the older north-dipping faults, south of the Corinth Gulf, such as the Mamousia Fault (see fig. 1.9) or the Kenchreai Fault (just south of Corinth, out of map in figure 1.9). Such faults are nowadays in an elevated and inland position with respect to the main frontal faults that lie in the Gulf or just close to it, and possibly take up a minor component of the total extension which is accommodated by the whole Corinth Rift. Nonetheless some authors (*e.g.* Copley *et al.*, 2018) have provided evidences of Holocene slip on the Kenchreai Fault, possibly indicating that those older faults, even though less active than the most recent ones, should not be overlooked in terms of their current tectonic and kinematic significance and above all for seismic hazard assessment purposes.

In continental Greece, extension takes place since Early Pleistocene with a mean N-S direction (see *e.g.* Mercier *et al.*, 1976, 1989; Caputo and Pavlides, 1993; Mountrakis, 2006), even though local rotations of the stress tensor induce a more NW-SE oriented extension in northwestern Macedonia and SSW-NNE oriented in the region around Evia. The major extensional tectonic structures in continental central Greece (beyond the Corinth Rift) are the Sperchios Rift, the Evia rift and the Thessaly basin (1.10).

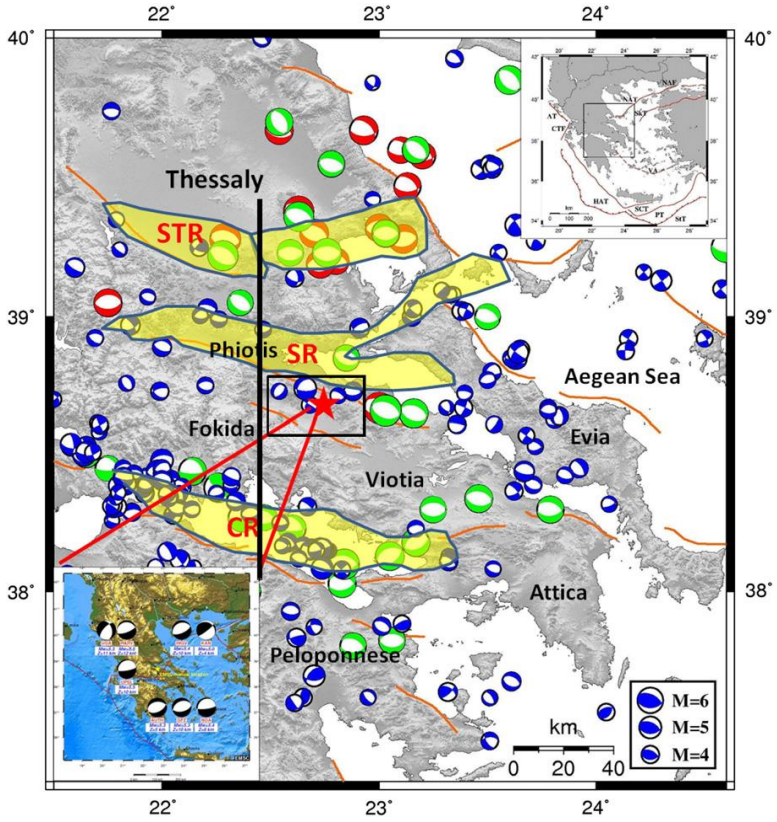

Fig. 1.10 – Main extensional basins in Central continental Greece (yellow-shaded areas). CR: Corinth Rift; SR: Sperchios Rift; STR: Southern Thessaly Rift (from Ganas et al.*, 2014).*

All these structures are characterized by more than one active seismogenic fault, as it is documented by the historical seismicity. Indeed, significant events occurred, for example, in 1954

in southern Thessaly, like the Sophades earthquake (M 6.7-7) reactivating the Ekkara fault system (Papastamatiou and Mouyaris, 1986; Palyvos *et al.*, 2010), the July 1980 Volos sequence (mainshock M_w 6.5; Papazachos *et al.*, 1983) associated to the Volos and Nea Anchialos faults bounding to the north the Almyros basin (*e.g.* Caputo, 1996) and the 1894 Atalanti event (M 6.8, Ganas *et al.*, 1998; Pantosti *et al.*, 2001), on the southern side of the Evia rift (Lokris Composite Source; Caputo and Pavlides, 2013).

A unifying feature for the majority of the seismicity occurring in the extensional tectonic setting of central Greece is that seismogenesis, both in terms of mainshock nucleation depth and aftershocks depth distribution, is limited to approximately the first 15 km (Kementzetzidou, 1996; Hatzfeld *et al.*, 1999, 2000). Such a characteristic suggests a potential rheological control in terms of BDT depth on the maximum possible depth of the seismogenic process. Accordingly, in the frame of this work, the determination of the rheological layering in these regions by independent rheological modelling could help confirming this hypothesis.

The most important active structures in northern Greece are mainly extensional, even though towards the east a secondary dextral strike-slip component becomes more significant. In Western Macedonia and in the westernmost sector of Central Macedonia the main active tectonic features are the Aliakmonas Fault System, the Ptolemaida basin with its associated fault systems of Amyndeo and Komanos, the Florina basin and the South and North Almopia faults (fig. 1.11).

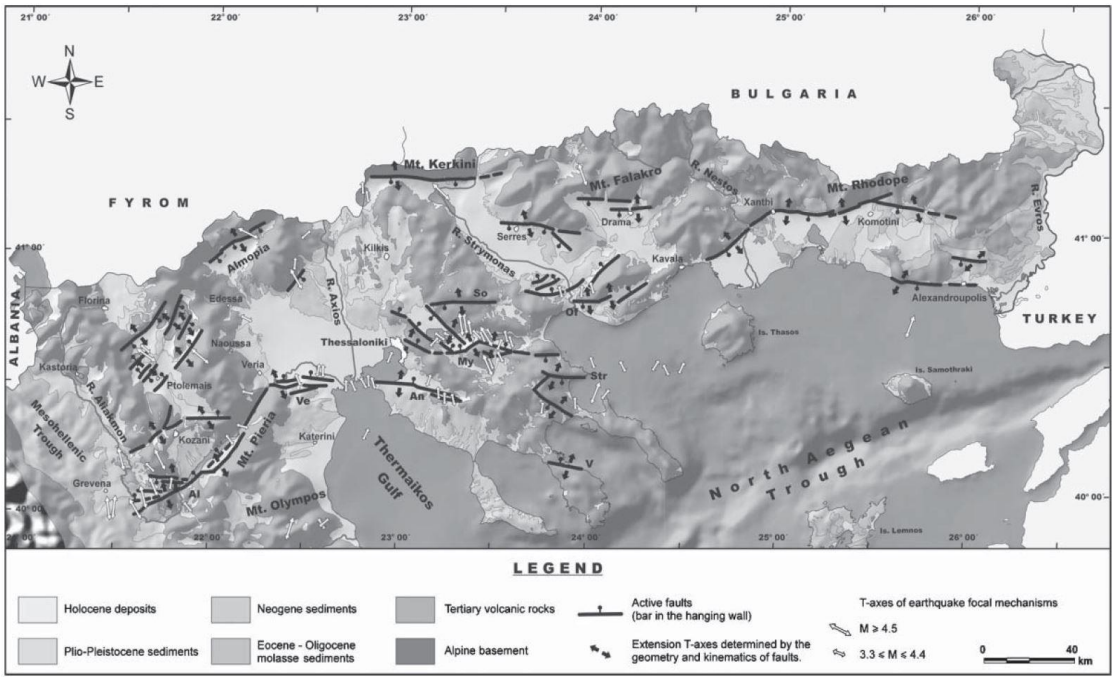

Fig. 1.11 – Main active faults in northern Greece (from Mountrakis, 2006).

All these structures are ca. SW-NE trending and are characterized by multiple segments or single faults either dipping NW or SE, but in any case with an almost pure dip-slip normal kinematics. The associated slip rates are all comprised between 0.1 and 0.6 mm/a while the

expected M_{max} values are in the range 6.3-6.9 (GreDaSS; Caputo and Pavlides, 2013). Historical and recent seismicity is also associated with some of these fault systems. In particular, two of the faults, namely the Palaeochori and the Rymnio ones, which constitute the Aliakmonas fault system, have been referred to as the causative structures of the 1995 M_s 6.6 Kozani-Grevena earthquake (*e.g.* Pavlides *et al.*, 1995; Doutsos and Koukouvelas, 1998; Rigo *et al.*, 2004; Resor *et al.*, 2005).

More in general the seismicity cutoff depth in Western and Central Macedonia is slightly greater (15-18 km) compared to the eastern Corinth Rift area (12-15 km). This evidence, together with the lower slip rates observed for faults in the former area, may result into lower seismic strain rates, on which I will focus in a dedicated chapter. To this point, it is sufficient to recall that the slightly different maximum depth of seismogenesis may be due to minor but still effective rheological changes and above all thermal regime variations.

In the eastern portion of Central Macedonia and in Eastern Macedonia and Thrace regions the main active fault systems show an E-W to WNW-ESE trend. In particular, the region around Thessaloniki is dominated by normal faulting on mostly WNW-ESE oriented structures, among which the most important ones belong to the Mygdonia basin fault system. The mean slip rates for the associated structures are in the range 0.1-0.7 mm/a. Recent and active faults, with opposite dip directions, have been recognized on both sides of the basin, even though the longest and more active structures border the southern side of the basin, dipping north. Here the Gerakarou Fault has been identified (Mercier *et al.*, 1979b; Chatzipetros *et al.*, 2004; Tranos *et al.*, 2003) as the causative structure for the M_w 6.5 1978 Thessaloniki earthquake.

In the eastern Chalkidiki peninsula, WNW-ESE dip-slip normal trending faults are also predominant and the main tectonic structures, from north to south, can be identified in the Stratoni-Varvara, the Gomati, the Singitikos and the Vourvourou faults. Maximum expected magnitudes for this roughly parallel set of structures are comprised between 6.0 (for the single fault segments) and 7.0 (in case of reactivation of the entire composite sources). The rake for such structures vary between 260° and 300°, while the available slip rates fall in the range 0.3-1.1 mm/a (GreDaSS; Caputo and Pavlides, 2013).

Moving into eastern Macedonia and Thrace the main tectonic structure is represented by the Thrace Fault Zone consisting of some major segments (Kavala, Xanthi, Iasmos and Komotini; Mountrakis and Tranos, 2004). Such a fault zone exhibits quite a dramatic and evident fault scarp, which runs in an average E-W direction for over 130 km, with marked changes in strike from one segment to another and is locally bounded by orthogonal minor relay zones. The maximum expected magnitudes are in the order of 6.4-6-7 for the single fault segments and up to 7.1 for the whole structure with a slip rate in the range 0.2-0.5 mm/a (GreDaSS; Caputo and Pavlides, 2013); due to the scarcity of historical and recent seismicity data, both latter values represent estimates

obtained from empirical relationships. The rake varies between 200° and 290°, thus indicating a possible minor dextral component in addition to the prevailing dip-slip motion.

Such a kinematic feature is shared with the other major active structures located offshore in the northern Aegean Sea and may be mainly attributed to the presence and influence of the North-Anatolian Fault Zone (hereinafter NAFZ) propagating into the Aegean Sea and merging with the North Aegean Trough (hereinafter NAT; *e.g.* Koukouvelas and Aydin, 2002). Indeed, the northern Aegean Sea is effectively characterized by fault and structures that exhibit a transtensional kinematics, as a result of the stress perturbation induced by the dextral shear motion associated with the NAFZ. These structures roughly correspond to the composite seismogenic sources reported in GreDaSS (Caputo and Pavlides, 2013) of North Aegean Basin, South Chalkidiki Offshore, North NAT, South NAT (fig. 1.12).

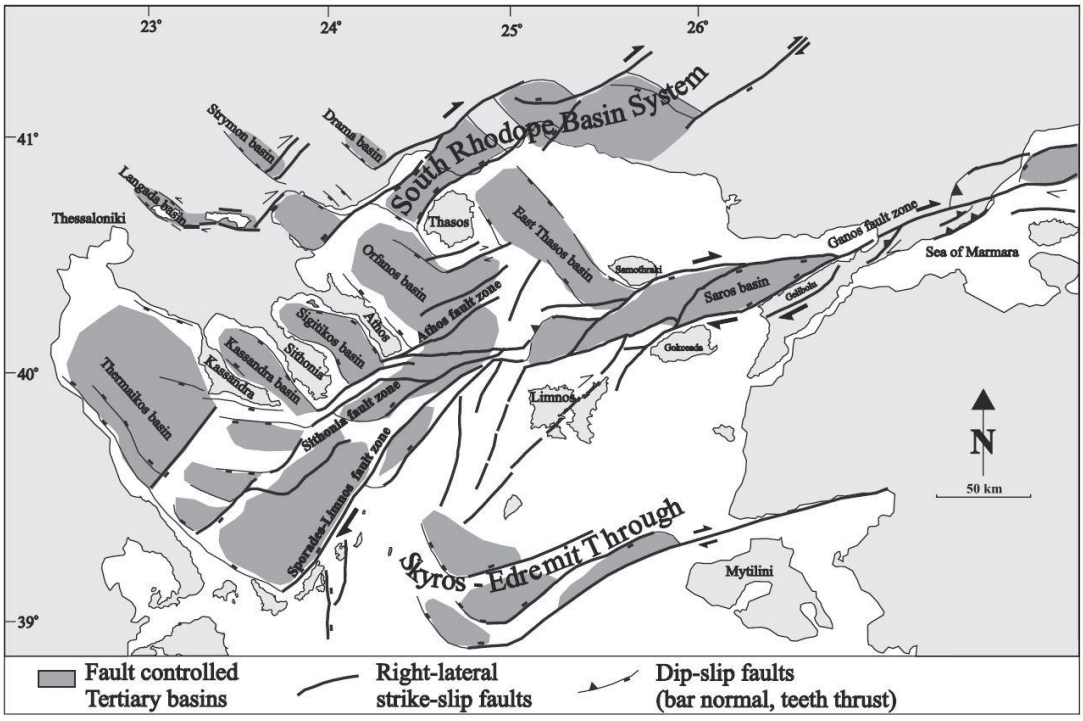

Fig. 1.12 – Principal basins and active fault systems bordering the North Aegean Trough (from Koukouvelas and Aydin, 2002).

Most of these faults are characterized by a predominant dextral strike-slip kinematics, with a secondary though signficant extensional component, as indicated by seismological evidences, marine geophysics studies and tectonic considerations (*e.g.* Mascle and Martin, 1990; Pavlides and Caputo, 1994; Koukouvelas and Aydin, 2002; Kiratzi and Louvari, 2003; McNeill *et al.,* 2004; Chatzipetros *et al.*, 2013). The rake angles for these faults are indeed comprised between 180° and 250°, while the slip rates fall in the range 1-4 mm/a, indicating and confirming the very high strain rates characterizing this zone, as obtained from geodetic measurements (*e.g.* Kreemer *et al.*, 2014). In addition, moderate to strong magnitude seismicity occurs with high frequency, as documented by recent earthquakes along the NAT, such as the 2014 M_w 6.8-6.9 Samothraki

earthquake (*e.g.* Kiratzi *et al.*, 2016; Evangelidis, 2015) and the 2003 M_w 5.7 Gulf of Saros event (Karabulut *et al.*, 2006). Moreover, the maximum expected magnitudes for these tectonic structures are actually as high as 7.5, making it an important case for the need of a robust determination of the exact potential magnitudes, to which rheological modelling could help provide some constraints.

In the northwestern sector of the study area, corresponding roughly to the Greek regions of Epirus and the westernmost part of Western Macedonia and to the Albanian-FYROM regions, the tectonic and kinematic framework is slightly more complex. Here, indeed, a locally and at small wavelength varying stress field resulted into the development of structures showing different orientations, going from NE-SW (*e.g.* Konitsa Fault in Epirus, or Elbasan-Dibra faults in Albania) to N-S (Ohrid Graben and associated faults in Albania) and finally to NW-SE in the westernmost sector (fig. 1.13).

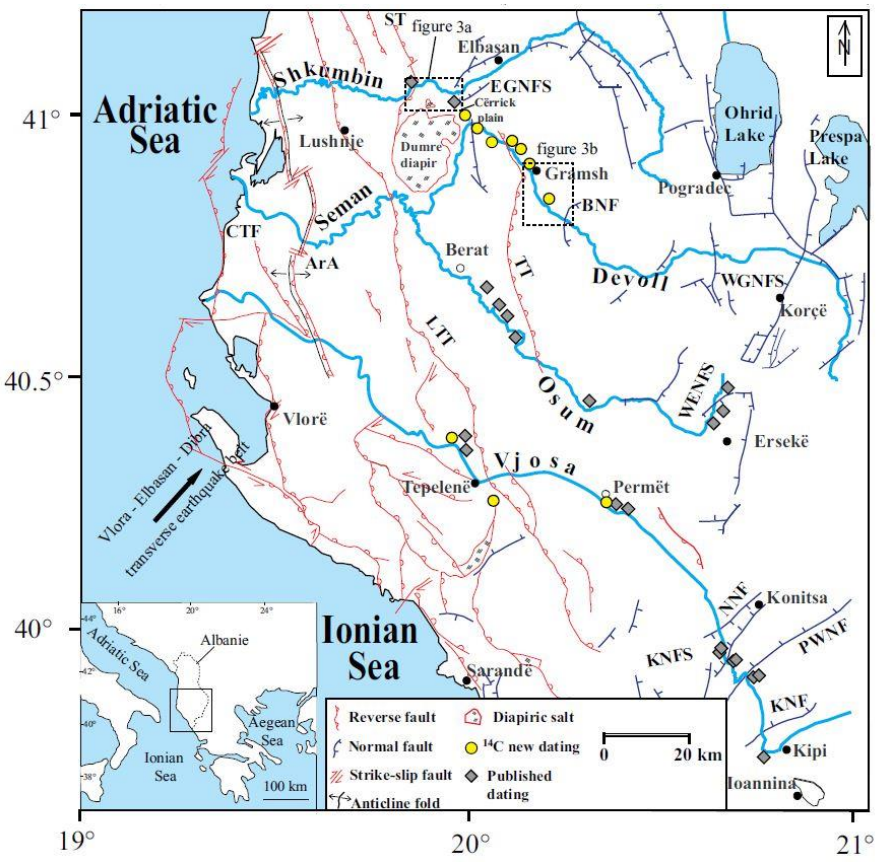

Fig. 1.13 –Main tectonic lineaments of northwestern Greece and southern Albania. KNF: Kipi Normal Fault; PWNF: Papingo West Normal Fault; KNFS: Konitsa Normal Fault System; NNF: Nerotrivi Normal Fault; LTT: Lushnje - Tepelene Thrust; TT: Tomorrica Thrust; WENFS; West Herseke Normal Fault System; WGNFS: West Graben Normal Fault System; CTF: Coastal Thrust Fault; EGNFS: Elbasan Graben Normal Fault System; BNF: Bulcar Normal Fault; ST: Shkumbin Thrust (from Guzman et al., *2013).*

This latter area is actually characterized by a swap between σ_1 (maximum stress axis) and σ_3 (minimum stress axis), as the former becomes sub-horizontal in the coastal and pre-coastal sectors of Albania and Epirus, leading to a prevalent compressional tectonics and the development of

ENE dipping imbricate thrusts. In some areas of central Epirus (*e.g.* around Ioannina), deeper seismicity in the middle lower crust is indeed attributed to the reactivation of such thrusts, while shallower clusters of seismic events are likely associated to a local E-W extension on N-S trending shallow normal faults, according to the available seismological data and the calculated focal mechanisms (*e.g.* Hatzfeld *et al.*, 1995; Tselentis *et al.*, 2006; Kassaras *et al.*, 2016). Such a different origin of the seismicity as a function of depth would also imply a vertical (in addition to the areal one) change in the stress field and in particular a further deep swap between σ_1 and σ_3. An additional element that contributes to the tectonic complexity of this investigated sector is the presence of ca. WSW-ENE trending, mainly strike slip, transfer faults and shear zones, such as the Kerkyra, Lushnje and Shkodra ones (GreDaSS; Caputo and Pavlides, 2013), which dissect and offset (with respect to each other) the coastal thrusts and interrupt their continuity along strike (fig. 1.14, see, for instance, the map view on the Corfu island).

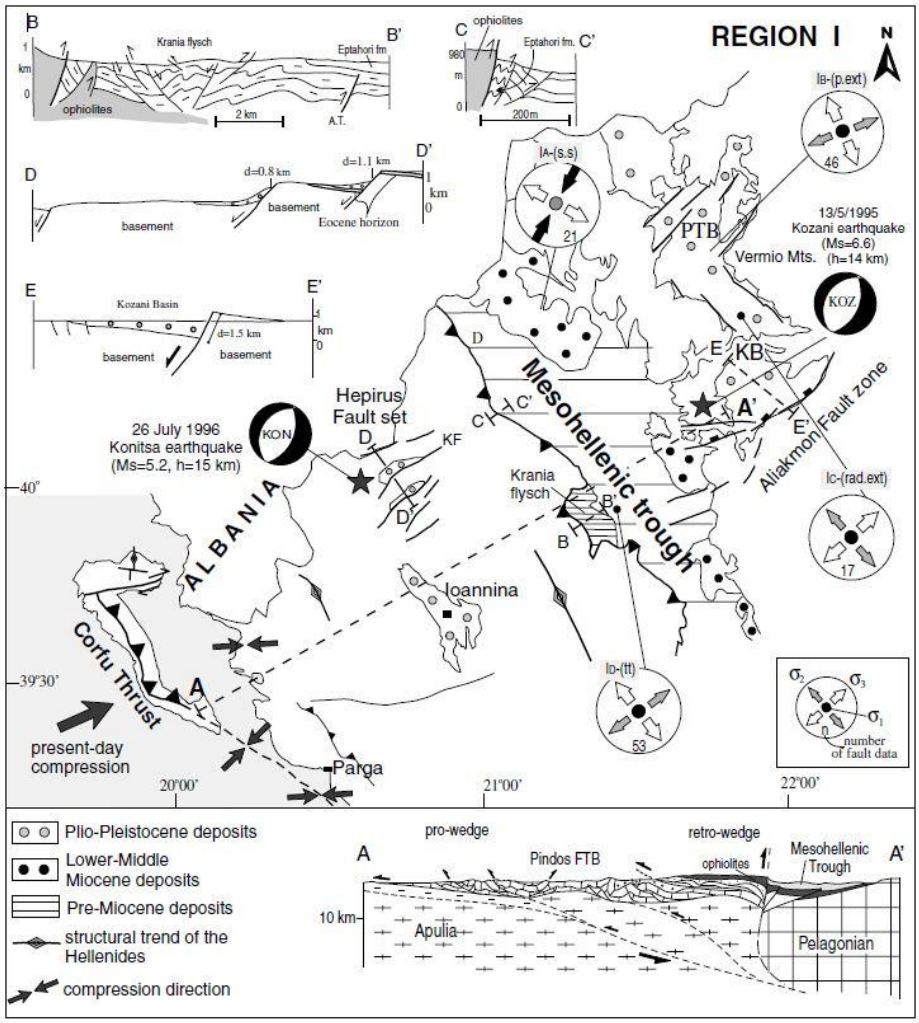

Fig. 1.14 – Structural and tectono-stratigraphic map of western Greece and Corfu island. Note the thrust in Corfu being crosscut by the ESE-WNW trending dextral strike-slip fault (from Kokkalas et al.*, 2006).*

From a seismogenic point of view, the internal active structures of these regions have been associated with moderate-to-strong magnitude events. Among these, one of the faults showing the greatest seismogenic potential is the Dibra fault zone, which is characterized by transtensional kinematics on a SW-NE trending and SE-dipping structure (*e.g.* Sulstarova *et al.*, 2000). The Dibra fault zone is deemed to be the responsible for the 1967 M 6.6 earthquake (Sulstarova and Kociaj, 1980) and it is associated with a maximum expected magnitude of 6.8 (GreDaSS), as it is part of a greater seismogenic belt also referred to as the Vlora-Elbasani-Dibra transversal fault zone.

The Konitsa Fault in northwestern Greece is instead characterized by normal kinematics on a SW-NE trending structure, with a slip rate in the range 0.1-0.4 mm/a. Here moderate seismicity has been recorded in recent times (M_s 5.7; Papanastassiou, 2001), and seismic events with maximum magnitudes up to 6.1 may also occur.

The transfer shear zones across the Albanian coastal region, namely the abovementioned Lushnje and Shkodra transfer faults, exhibit a prevalent dextral strike-slip motion with a possible minimal dip-slip extensional component. Their associated maximum expected magnitudes are respectively 6.9 and 7.1 (GreDaSS; Caputo and Pavlides, 2013).

As regards the E-W trending Kerkyra Fault, it is characterized by a dextral transpressional kinematics, especially along the western and central sectors, corresponding to the Makrades Fault and the Spartylas Fault. The composite source is associated with slip rates in the range 0.4-0.6 mm/a and a maximum expected magnitude of 6.7. However, for most of these WSW-ENE trending transfer fault zones, few seismological data and scarce historical seismicity are available and therefore the relative estimates present some degree of speculation and large uncertainties.

The active thrusts offshore Paxos, Corfu, Karaburuni, Durresi and Montenegro are all associated to maximum expected magnitudes in the range 7.1-7.3, with an almost pure contractional kinematics (GreDaSS; Caputo and Pavlides, 2013).

As already mentioned, the available historical seismicity data are quite scarce, with the only recent relevant exception represented by the 1979 M = 6.9 Montenegro earthquake. However, even if the slip rates are not known, with a proposed estimate only for the Paxos Thrust (0.5-0.8 mm/a), these structures are certainly potentially active and could be associated to moderate-high seismic hazard. Also in this case, the constraining of the BDT depth-seismogenic layer on the basis of the rheological modelling could help improving their seismotectonic characterization and contribute to a better and more realistic seismic hazard assessment.

Southeast of Corfu, a similar compressional tectonic setting is observed around the island of Paxos. Here lies indeed the Paxos Thrust, which exhibits a NNW-SSE strike with a rake indicating almost pure compression. This tectonic structure is associated with some strong historical earthquakes (e.g. 1743, 1786, 1444), with estimated magnitudes in the range 6.8-7.1 (Papazachos and Papazachou, 1997; Ambraseys, 2009), even though uncertainties especially in the location of

the events are quite high. In any case, the considerable seismogenic potential also for this fault requires a better seismotectonic characterization to which rheological modelling could contribute.

In the inland region to the east and southeast of Paxos Island the tectonic setting is quite complex, with the co-occurrence of E-W to WNW-ESE trending normal faults, both south dipping (*e.g.* Arta) and north dipping (*e.g.* Trichonida), and NNW-SSE trending left-lateral strike slip faults along the Amphilochia fault zone (*e.g.* Vassilakis *et al.*, 2011) (fig. 1.15). The latter seismogenic source, which dips to the ENE, also exhibits, actually, a minor normal dip-slip kinematics component.

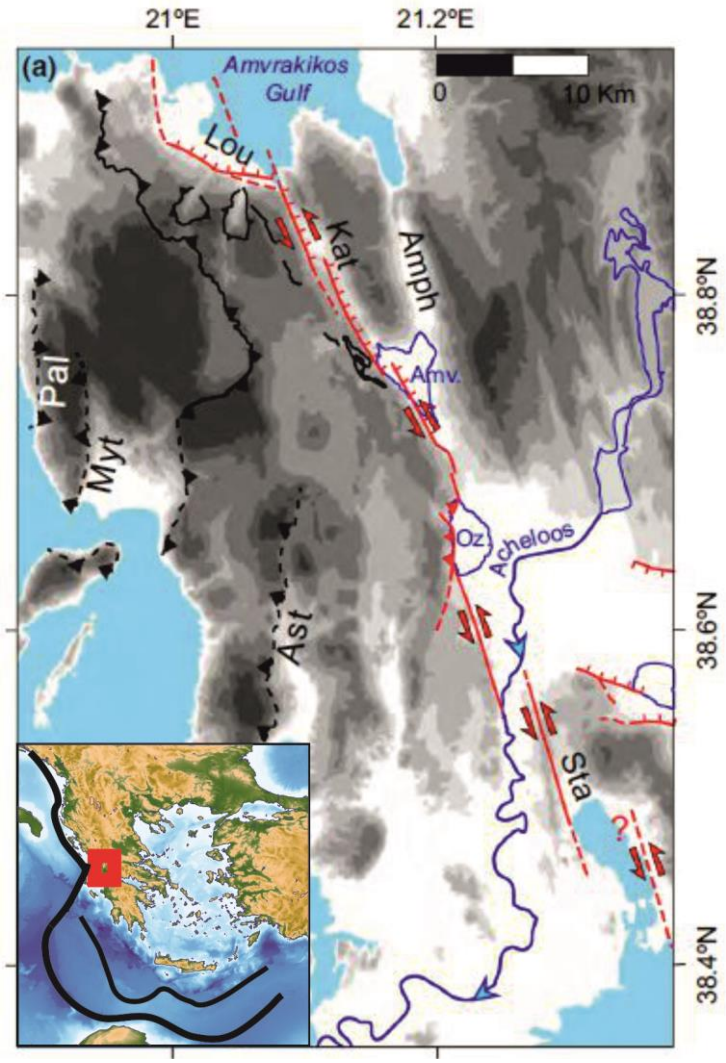

Fig. 1.15 – Amphilochia (or Katouna-Stamna) fault system in the Aitoloacharnania region (modified from Perouse et al.*, 2017).*

This fault zone, also referred to as Katouna-Stamna fault system (Perouse *et al.*, 2017), is characterized by high slip rates in the range 4-10 mm/a, even though a considerable portion of the motion is thought to be accommodated aseismically also because of the lack of historical seismicity and of a clear morphological expression (see Perouse *et al.*, 2017). Nonetheless, some deep microseismicity down to a depth of 20 km has been recorded in the Amphilochia region

(Hatzfeld *et al.*, 1995), suggesting that seismic nucleation and rupture may actually occur along the fault zone, whose dimensions would also imply a high seismogenic potential. As regards the Trichonida fault zone, recent seismicity of moderate magnitude (M_w ~6, 1975; Kiratzi *et al.*, 2008) has been recorded on NW-SE auxiliary structures with respect to the main, almost E-W trending, fault segment. The relocated seismicity is almost completely confined within the first 15 km (*e.g.* Kiratzi *et al.*, 2008; Kassaras *et al.*, 2014), suggesting a similar depth extent of the seismogenic layer in the volume of the Trichonida composite source, whose maximum expected magnitude according to GreDaSS is ~6.7.

Moving to the south of Corfu and Paxos thrusts, the Kefallinia Transform Fault zone, whose dextral strike-slip motion dominates the kinematics of the corresponding Ionian Islands region, is entered. A brief summary on its major geodynamic significance, separating continental collision and oceanic subduction domains, and on its geological and tectonic evolution has already been presented above (§1.7). Accordingly, at this stage, I aim to focus more specifically on its kinematic behavior and internal segmentation. In particular, two main segments can be distinguished, the Lefkada northern one and the Kefallinia southern one (fig. 1.16).

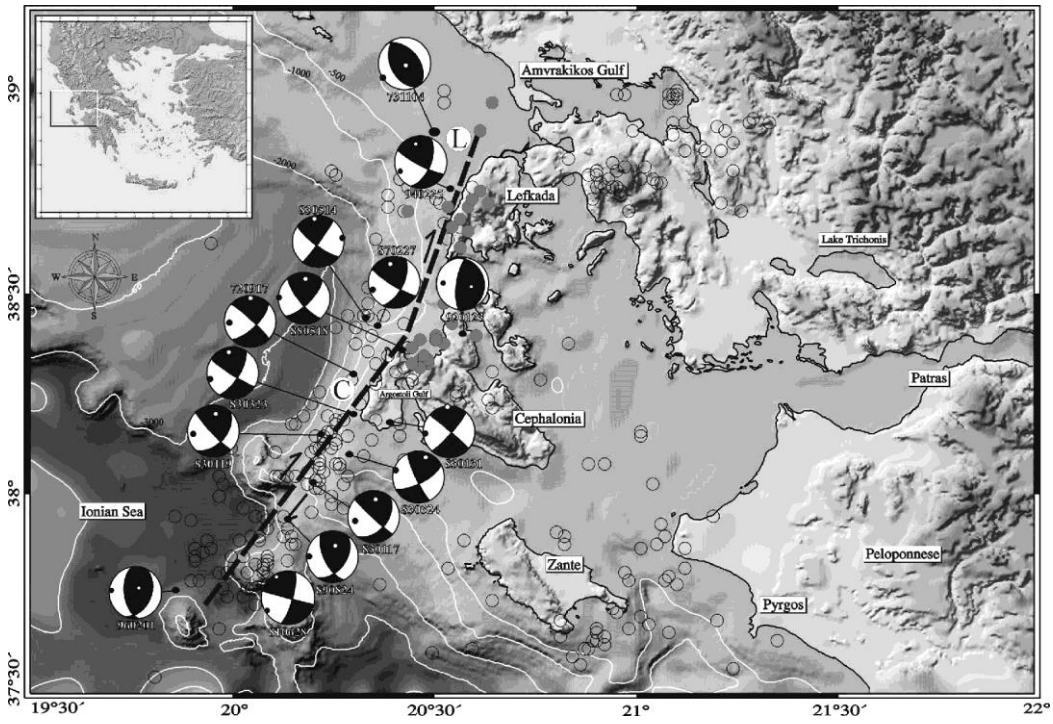

Fig. 1.16 – Structure and geometry of the Kefallinia Transform Fault, with the two slightly different trending segments indicated by letters L and C, corresponding respectively to the Lefkada segment and the Kefallinia one (from Louvari et al.*, 1999).*

The former is characterized by a slightly more NNE-SSW direction (azimuth ~15°) with respect to the latter, following instead a more NE-SW trend (azimuth ~38°); in terms of maximum expected magnitude, the Lefkada segment is associated with values around 6.8 (Louvari *et al.*, 1999) while for the Kefallinia one the maximum expected magnitude in case of co-rupture of its three main sub-segments would be ~7.2 (GreDaSS). Finally, as regards the slip rates, the Lefkada

segment is characterized by values around 10 mm/a, being therefore slower than the Kefallinia one, associated to rates up to 25 mm/a (*e.g.* Papadimitriou, 2002).

Further east-southeast the main structure encountered is the Zakynthos Fault, which is characterized by mainly compressional dip-slip kinematics on a NNW-SSE trending and ENE dipping fault plane (fig. 1.17).

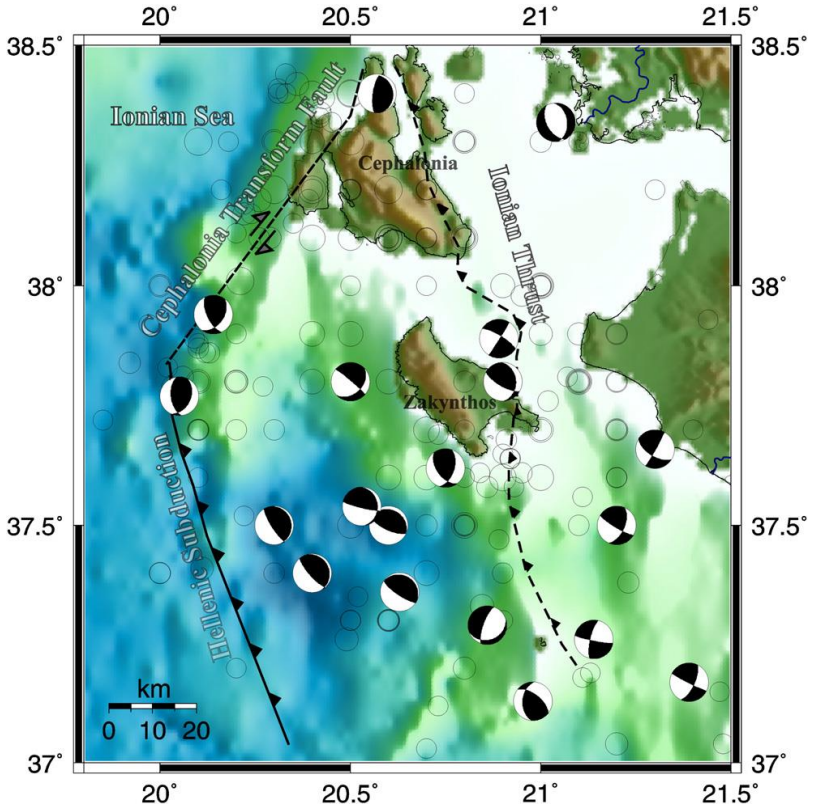

Fig. 1.17 – Traces of the main compressional structures in the region around Zakynthos and focal mechanisms indicating NNW-SSE trending seismogenic sources characterized by dip-slip thrust kinematics (from Serpetsidaki et al.*, 2010).*

As regards the seismic behavior properties, here the bottom of the seismogenic layer lies in the crust at around 20-25 km (*e.g.* Serpetsidaki *et al.*, 2010) and moderate-to-strong magnitude seismic events have been recorded in historical and recent times (in particular, it is worth recalling the 1959 earthquake with an M_w ~6.8 according to Kiratzi and Louvari, 2003). Slip rates along the fault are around 10 mm/a (*e.g.* Papadimitriou *et al.*, 2006) while maximum expected magnitudes fall in the range 6.8-7.0.

An even greater seismogenic source lies to the southeast, offshore western Pelopennesus and it is referred to as Sfakteria Fault in GreDaSS (fig. 1.18). This is deemed to be the causative fault of the M 7.5 1886 earthquake (*e.g.* Papazachos *et al.*, 2000), and such a magnitude is also considered as the maximum expected one. This structure, differently from the ones just described above, seems not to be influenced anymore by the strike-slip lithospheric-scale shear zone of the Kefallinia Transform Fault, and therefore exhibits an almost pure dip-slip reverse kinematics. Close to Sfakteria Fault, but to the southeast of it, lies another active fault, called Theganoussa

Fault, probably the causative structure of the M_w 6.7-6.9 2008 Methoni earthquake (*e.g.* Roumelioti *et al.*, 2009; Howell *et al.*, 2017).

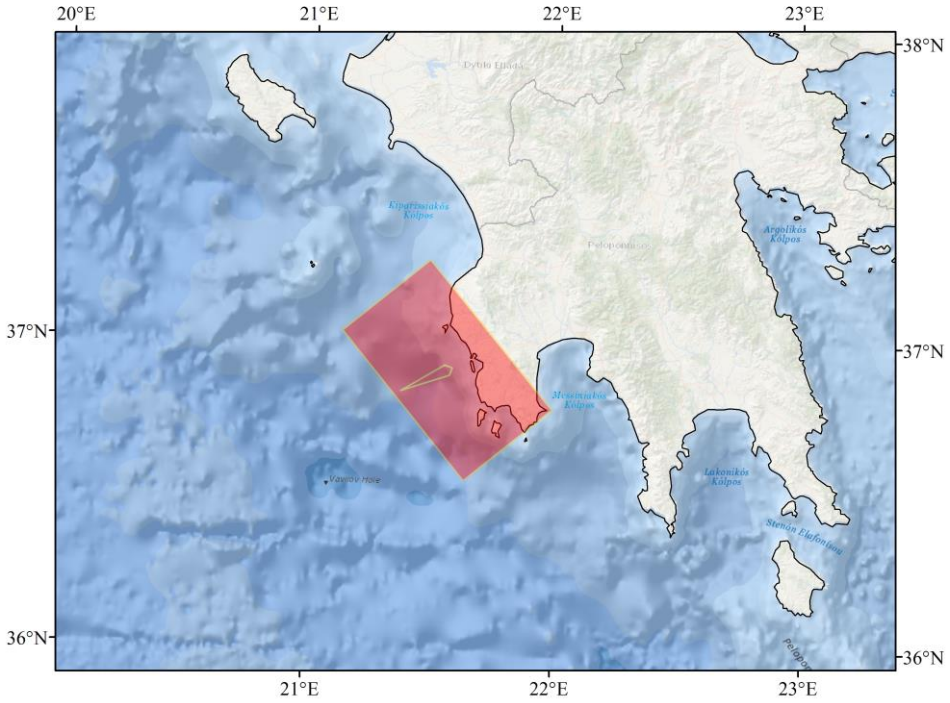

Fig. 1.18 – Surface projection of the Skafteria fault, as taken from GreDaSS (Caputo and Pavlides, 2013). The fault dips to the NE and the arrow represents the motion of hanging-wall relative to the footwall, thus indicating the thrust kinematics.

In terms of seismogenic potential, the 2008 earthquake and associated sequence probably resulted from an almost total rupture of the source and therefore represents a worst-case scenario and can be considered as indicative for the maximum expected magnitude along such a fault. Here too, the prevalent kinematics is pure dip-slip in a reverse fashion, while the seismogenic layer base could be as deep as 30 km.

In the internal and southern Peloponnesus region the kinematic and tectonic setting is dominated by ca. NNW-SSE trending normal faults (with some exceptions), whose activity causes a prevalent WSW-ENE extension orthogonal to the trend of the orogenic belt of the Hellenides. The main structures on land correspond to the Kalamata Fault and the Sparta Fault, while offshore additional seismogenic sources are present in the Messinian, Lakonikos and Argolikos Gulfs (fig. 1.19).

The Kalamata Fault follows a slightly different trend than the regional one, being more NNE-SSW oriented and dipping to the WNW. This structure is characterized by slip rates in the range 0.1-1 mm/a and an almost pure dip-slip normal kinematics. Relatively recent seismicity occurred on the Kalamata Fault, with the M_s 6.2 1986 earthquake (*e.g.* Papazachos et al., 1988) being the main event even though smaller than the maximum expected one, having a potential magnitude of ~6.7 (GreDaSS).

The Sparta Fault, localized further east with respect to the Kalamata one, dips to the ENE and exhibits a NNW-SSE trend. Even though no recent relevant seismicity has been recorded in this zone, the Sparta Fault is considered to have been active in historical times, producing devastating earthquakes and originating a quite evident morphological scarp (*e.g.* Benedetti *et al.*, 2002; Papanikolaou *et al.*, 2013). In terms of slip rates, the fault is associated with values in the range 1-2 mm/a, while the maximum expected magnitude is around 7.0.

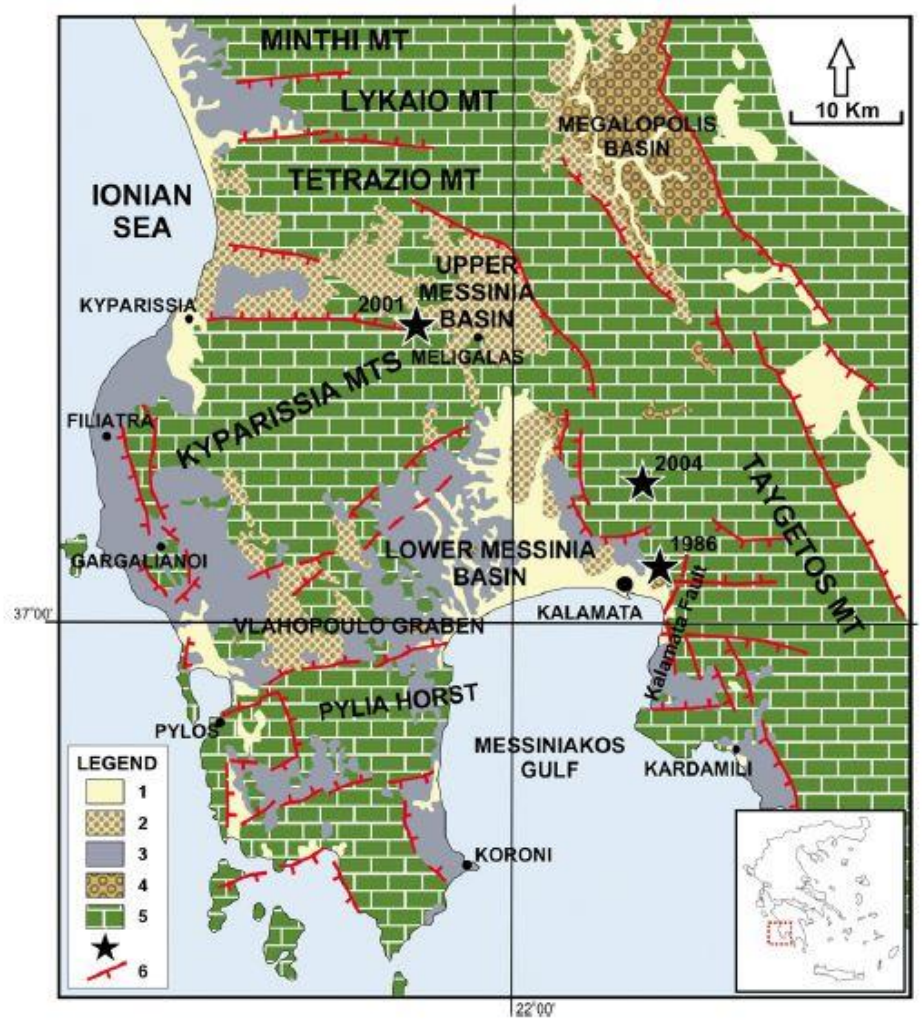

Fig. 1.19 – Simplified geological and structural map of the southern Peloponnesus, showing the main active tectonic lineaments. Colours legend: 1- Holocene deposits; 2 – Neogene-Quaternary continental deposits; 3 – Neogene-Quaternary marine deposits; 4 – lacustrine deposits; 5 – Pre-Neogene basement (from Kassaras et al., *2014).*

Having completed a brief summary on the main seismogenic sources in continental Greece together with the ones along the North Aegean Trough and in the offshore western area, a description of the active structures affecting the highly extended and thinned regions of the central, eastern and southern Aegean comes next, together with a presentation of the tectonic framework of Crete island.

The central-northern Aegean Sea is mainly characterized by SW-NE trending dextral strike slip to transtensional fault zones (fig. 1.20), similarly to the tectonic setting of the North Aegean Trough, further north. An additional element here is represented by the occurrence of more WSW-ENE trending structures especially in the eastern sectors, close to the Turkish coastline, as for example in the Edremit region or in the Lesvos island zone, which are associated with a prevailing dip-slip normal kinematics and a minor strike-slip component.

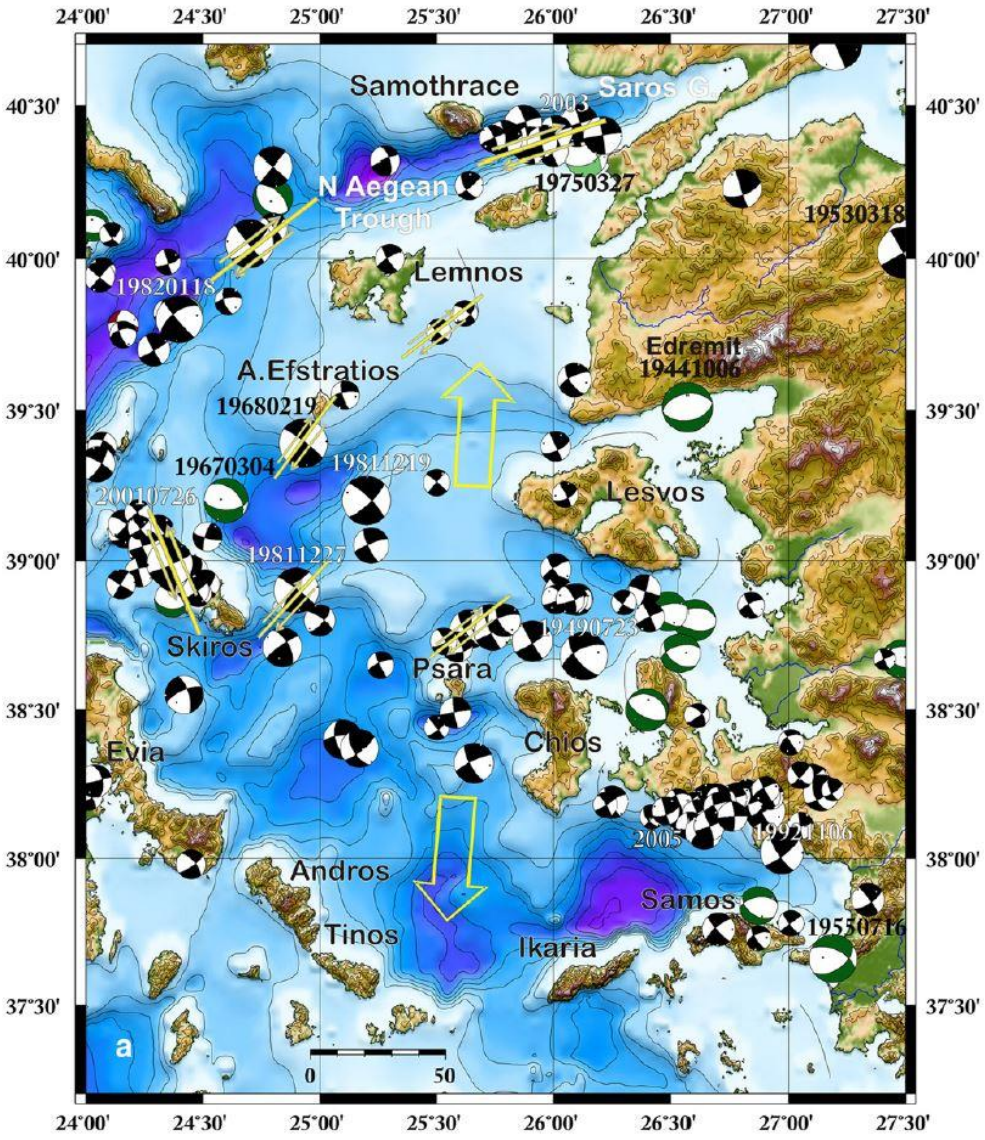

Fig. 1.20 – Main active faults of the central and northern Aegean Sea. Also shown are the representative focal mechanisms (modified from Chatzipetros et al.*, 2013).*

One of the main SW-NE trending faults is the Agios Efstratios one, which is mainly located offshore, outcropping solely in the corresponding island and it is characterized by an almost pure dextral strike-slip kinematics (*e.g.* Pavlides and Tranos, 1991). This structure is the causative fault of the 1968 Agios Efstratios earthquake, with surface waves magnitude M_s estimates comprised between 7.0 and 7.2 (*e.g.* North, 1977; Taymaz *et al.*, 1991). A comparable maximum expected

magnitude of 7.2 is indicated for this source in GreDaSS, while the slip rate for the fault falls around the value of 5 mm/a (e.g. Papadimitriou and Sykes, 2001).

Further west of Agios Efstratios, a relevant seismogenic source is represented by the Skyros Fault. Also in this case, most of the fault lies offshore, but differently from the previous one, this structure is NW-SE trending and exhibits a sinistral strike-slip kinematics. Slip rates are in the order of 1-1.5 mm/a and recent seismicity occurred in this area, with the 2003 M_w 6.4-6.5 earthquake (*e.g.* Benetatos *et al.*, 2002; Ganas *et al.*, 2005) being the reference event, even though smaller than the maximum expected one, having M_w around 7.1. Further east, around the island of Lesvos, normal faulting predominates over transcurrence, which also occurs but as a minor component of the regional tectonics. The strikes of the main seismogenic sources affecting the area vary from ca. 70° to ca. 130°, roughly associated with a N-S extension. In June 2017 a M_w 6.3 earthquake struck just south of Lesvos, and the seismological data analysis indicated prevalent NNE-SSW extension, with the events being as deep as ~15 km (*e.g.* Kiratzi, 2018). However, the maximum expected magnitudes in the area could be as high as 6.7 (GreDaSS) and the slip rates are in the range 0.5-1.5 mm/a.

In the central Aegean Sea around the islands of Chios, Psara, Ikaria and Samos, the main seismogenic sources are WSW-ENE to E-W trending normal faults, also exhibiting a minor dextral strike-slip kinematics component. The slip rates in these regions are not very high, being always comprised between 0.1 and 3 mm/a, while maximum expected magnitudes are in the range 6.7-7.0. Even though this region (and especially the area around Ikaria) is traditionally considered as an area of low seismicity rates, several moderate-to-strong magnitude events have been recorded, in particular around Chios.

Indeed, both seismogenic sources offshore the northern and the southern coastline (dipping respectively to the north and to the south) have been associated with historical relevant events (1881 M_w 6.5; 1949 M_w 6.7; see *e.g.* Altinok *et al.,* 2005), therefore indicating that a precise and careful seismic hazard assessment, to which rheological modelling could contribute through the definition of the brittle and potentially seismogenic layers, is necessary also for these regions of the central Aegean Sea.

Furthermore, additional minor sources occur there and are represented by NW-SE trending left-lateral strike-slip faults, whose slip rates are even lower, falling in the range 0.1-1.0 mm/a and the relative maximum expected magnitudes are smaller than 7.0 (GreDaSS). These sources are mainly located to the west of the above-mentioned islands, in an area where the prevailing stress field of the Aegean Sea, generally characterized by N-S extension and SW-NE oriented dextral strike-slip motion, becomes more complex and NW-SE sinistral strike-slip on faults orthogonal to the main normal and dextral ones is also observed.

Further east, in the confining Anatolian region, the main seisemogenic sources correspond to E-W trending normal faults bounding extensional basins and grabens like the Kucuk Menderes

and the Buyuk Menderes (see *e.g*. Bozkurt, 2001 for a review on the neotectonics of Western Anatolia) (fig. 1.21).

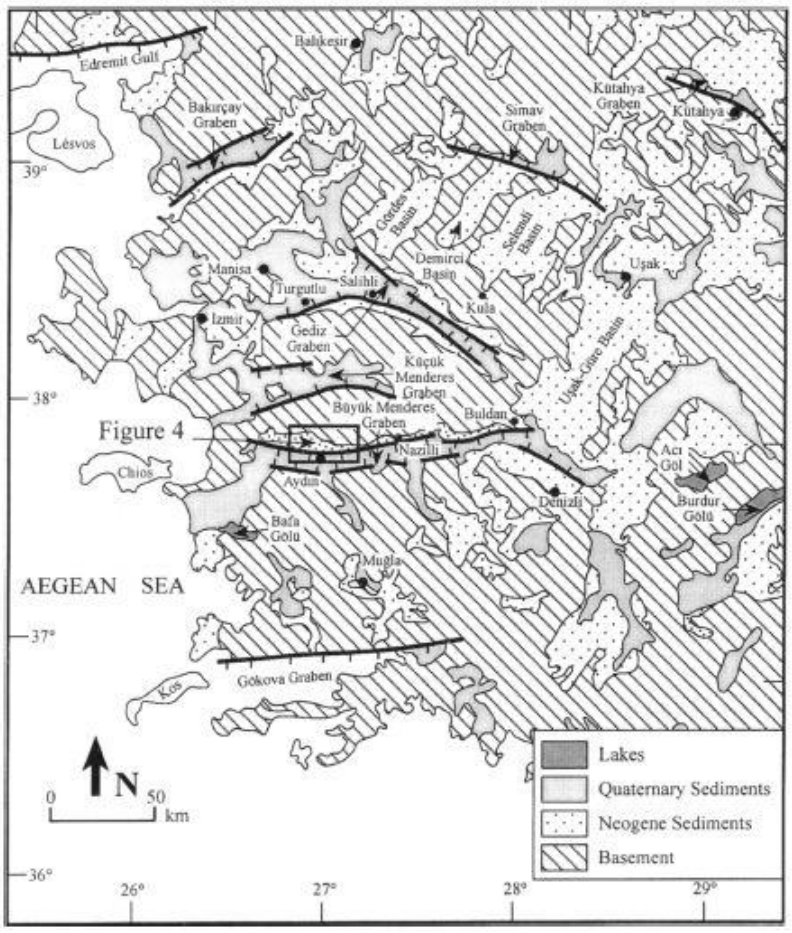

Fig. 1.21 – Main active normal faults in western Anatolia (from Bozkurt, 2000).

These structures have been associated with relevant historical earthquakes, like the 1899 one, which has an estimated magnitude in the range 6.7-6.9 (*e.g*. Pavlides and Caputo, 2004; Ocakoglu *et al*., 2013) and produced long and evident traces of surface ruptures in the Buyuk Menderes graben. Given the magnitude of potential maximum earthquakes occurring on these structures (M_{max} ~7) and the quite high slip rates along them, being around 4.2 mm/a (*e.g*. Paradisopoulou *et al*., 2010), the probability that these potential earthquakes would also affect the Greek eastern Aegean Region is considerable and therefore a seismotectonic characterization in terms of maximum depth of seismogenesis would be needed also in this case.

Moving south, towards the Cyclades Islands and the sourthern Aegean Sea region, a general lack of renowned seismogenic sources is observed. Such a feature is mainly due to the fact that this region is moving coherently to the SW with almost complete absence of internal deformation (*e.g*. Hollenstein *et al*., 2008) as it is proved by the very low geodetic strain rates for this area. At the same time, the central-southern Aegean region behaving as a rigid block also implies the lack

of seismic deformation and therefore the region is considered as seismically quiet, without the presence of relevant active faults.

When moving further south into the southernmost Aegean Sea and especially in its eastern sector, however, the tectonic and kinematic settings change and some seismicity at times even of strong magnitude, though not very frequent, is recorded together with internal deformation. One of the main seismogenic sources in this area is represented by the Amorgos Fault, which is indicated as the most likely causative source of the M_w 7.1 – M_s 7.4 1956 Amorgos earthquake (*e.g.* Papadopoulos and Pavlides, 1992; Stiros *et al.*, 1994). Such a structure follows a SW-NE trend, dips to the southeast and exhibits a prevalent dip-slip normal kinematics with a minor dextral slip component (fig. 1.22).

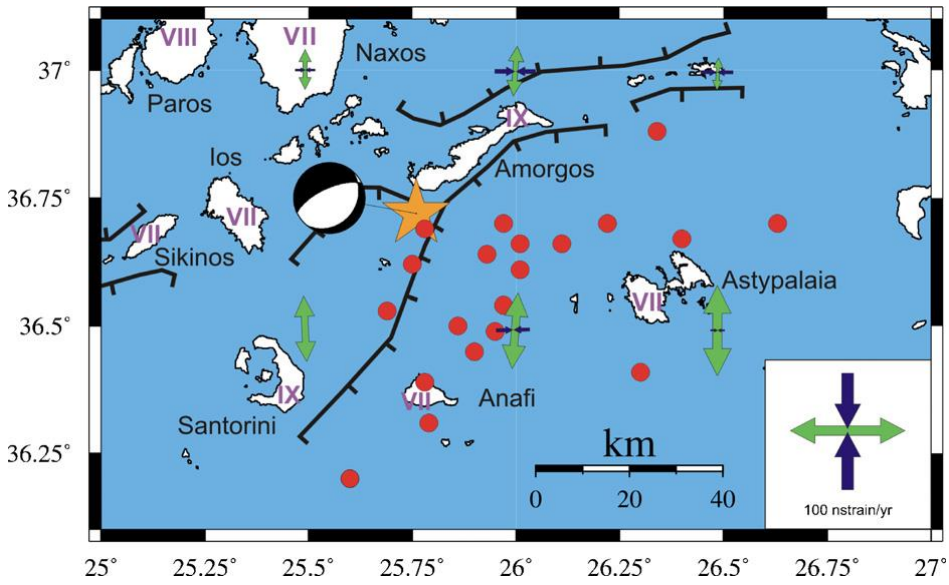

Fig. 1.22 – Main active faults around Amorgos (from Konstantinou, 2010).

The slip rates ranges around 2.4 mm/a (Paradisopoulou et al., 2010) and the expected M_{max} for the individual source corresponds to the 1956 earthquake magnitude. This fault, in any case, represents one of the most hazardous seismogenic sources in the Aegean Region in terms of potential occurrence of associated catastrophic phenomena like marine landslides and primary or induced tsunamis and therefore requires a detailed seismotectonic characterization, especially as regards the depth of seismogenesis and faulting processes.

Further east, close to the island of Kos and the city of Bodrum on the Turkish coastline, the main seismogenic sources are represented by WSW-ENE trending normal faults, which are referred to as Kos Fault and Ula-Oren composite source in GreDaSS (fig. 1.23). This region belongs to the extensional structure of the Govoka graben (*e.g.* Dewey and Sengor, 1979) and hosted a recent M_w 6.6 earthquake on July 2017 (see *e.g.* Karasozen *et al.*, 2018). The earthquake actually occurred on a north-dipping, almost E-W trending structure and also caused a local tsunami.

As regards the slip rates on the south dipping Gokova fault zone, Tiryakioglu *et al.* (2018) suggest a value around 0.2 mm/a, while the maximum expected magnitudes are in the order of 7.0-7.2 according to the GreDaSS.

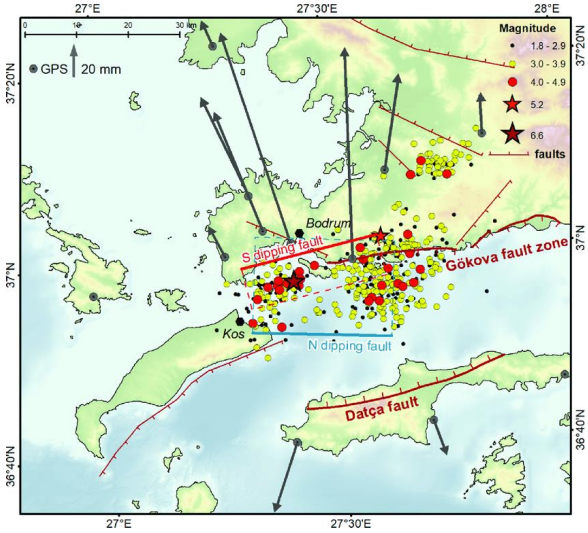

Fig. 1.23 –Active faults bordering the Gokova graben. Also shown are the seismicity from the recent 2017 Kos-Bodrum (mainshock M_w 6.6) seismic sequence and the displacement vectors following the mainshock (from Papadopoulos et al.*, 2019).*

In the Cretan Sea the major seismogenic sources correspond to E-W trending structures dipping both to the north and to the south. Such faults in some cases define marine basins and grabens, as it is the Christiana basin (fig. 1.24). This region has hosted some moderate magnitude seismicity in recent times (M_w 5.3 on January 2012; Kiratzi, 2013), which is thought to have been caused by N-S striking, mainly dextral strike-slip faults, which are also present in GreDaSS as mainly transtensional kinematics structures. The E-W striking faults are instead considered to behave as normal faults with almost pure or prevalent dip-slip kinematics.

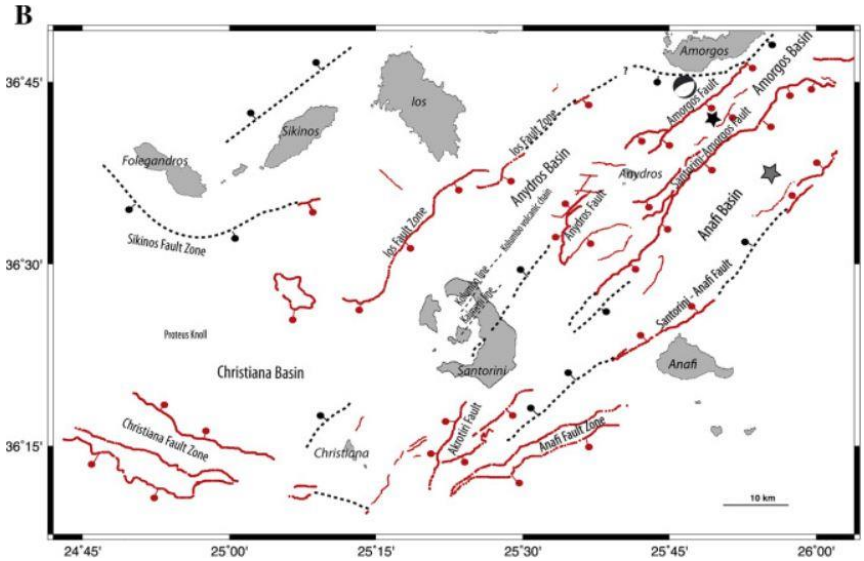

Fig. 1.24 – Main tetctonic lineaments around the Christiana basin and Santorini island (from Hooft et al.*, 2017).*

Even though such structures and this region in general are not associated with many large magnitude earthquakes in historical times and slip rates are quite low, being comprised in the range 0.1-1 mm/a, their seismogenic potential should not be overlooked, as maximum expected magnitudes are as high as 7.1. Also in this case, given the paucity of available seismological and geological data for this region, an improved seismotectonic characterization aided by rheological modelling could help defining the extent of the seismogenic layer, which is right now considered to extend down to depth of ca. 13-15 km.

The island of Crete is also characterized by the presence of both E-W and N-S to NE-SW trending structures (fig. 1.25). The great majority of them exhibits a dip-slip normal kinematics and the onset of the currently active extensional stage on these faults can be traced back to Middle Pleistocene times (*e.g.* Caputo *et al.*, 2010). Many of these structures can be easily identified on land since their relative fault planes tend to put into contact footwall resistant lithologies, belonging either to the metamorphic exposed basement or to carbonate platforms and pelagic sequences, with mainly unconsolidated sediments and Holocene deposits in the hanging-wall. Some other structures lie instead mainly offshore but can be recognized through the analysis of bathymetric relief maps, as their activity has left sharp scars on the sea bottom, so that they have sometimes been termed (even if improperly) as trenches.

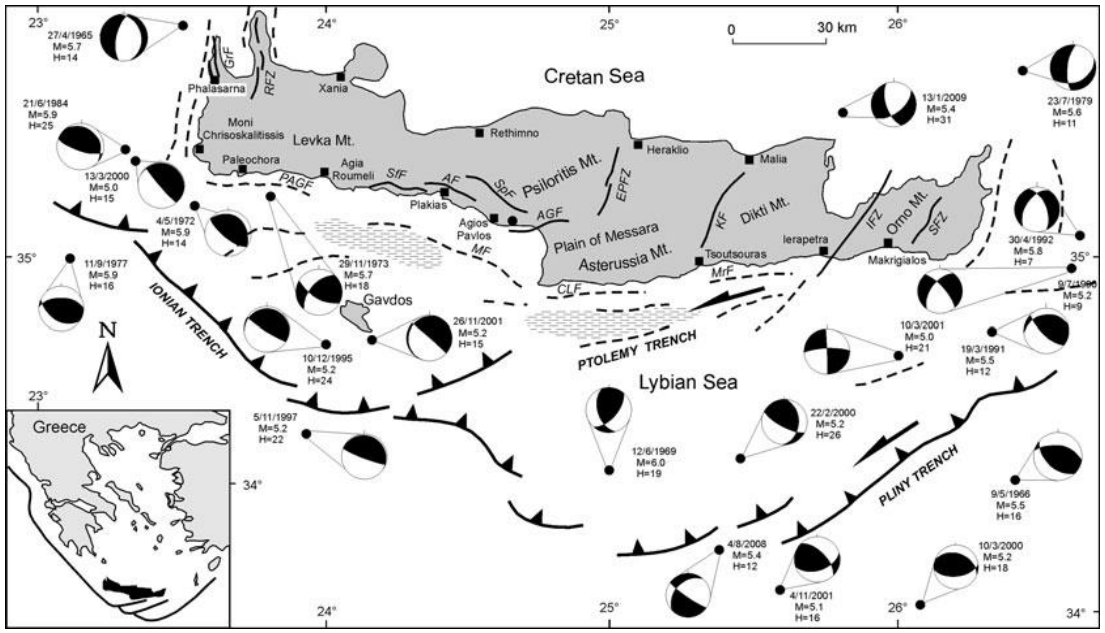

Fig. 1.25 – Active faults onshore and offshore Crete. Also shown are several representative focal mechanisms (from Caputo et al.*, 2010).*

The main E-W trending sources are the Palaeochora-Tympaki, the Agia Galini and the Ptolemy Trench, with the latter being characterized by a considerable sinistral strike-slip kinematics component. Their relative slip rates are respectively comprised between 0.6-4.5 mm/a,

0.1-1 mm/a and 0.5-2 mm/a, while the maximum expected magnitudes fall in the range 6.5-7.0 (GreDaSS).

The main orthogonal structures following the SSW-NNE trend are, from W to E, the Gramvousa, Rodopos, Psiloritis and Ierapetra faults. All of them are associated with slip rates in the range 0.1-2 mm/a, with the highest values characterizing the Ierapetra structure. In terms of seismogenic potential, these faults, showing also a smaller length than the E-W trending ones, are deemed to be able of generating relatively smaller events (with respect to the orthogonal ones), which could have maximum expected magnitudes not greater than 6.5.

East of Crete in the offshore region close to the islands of Kasos and Karpathos, the seismogenic sources mostly follow two main trends, *i.e.* SSW-NNE and WSW-ENE. The latter group of sources (*e.g.* North Kasos, Stakida and Karpathos 3 in GreDaSS) is characterized by a kinematic component of sinistral strike-slip in addition to the dip-slip normal motion, which prevails along the SSW-NNE trending structures. The associated slip rates are in the range 0.1-1 mm/a for the WSW-ENE trending structures, with maximum expected magnitudes not greater than 6.6, while the SSW-NNE oriented sources, displaying longer length, may be able to generate earthquakes with maximum magnitudes up to 6.9 and are characterized by higher slip rates, comprised between 0.5 and 3 mm/a (GreDaSS).

The island of Rhodes is particularly affected by the occurrence of strong earthquakes along the plate interface in the subduction zone (or along other parallel reverse faults), which occurs to the offshore south-eastern region with respect to the island. Such earthquakes may reach magnitudes greater than 7.5 and also cause considerable damages and associated catastrophic phenomena such as large tsunamis (see *e.g.* Kontogianni *et al.*, 2002; Howell *et al.*, 2015).

Finally, west of Crete, in the area around the islands of Kythira and Antikythira, the main shallow seismogenic sources are ca. SE-NW oriented and exhibit a prevalent normal dip-slip kinematics, together with a minor dextral strike-slip component (*e.g.* Lyberis *et al.*, 1982). These faults are characterized by slip rates in the range 0.1-1.0 mm/a and maximum expected magnitudes comprised between 6.7 and 6.9. The Kythira area, however, is also affected by intermediate depth (~60-70 km) seismicity probably related to both the activity along the Wadati-Benioff plane and the internal deformation of the downgoing African slab. A recent relevant intermediate depth event struck the area in January 2006 (M_w 6.7, Konstantinou *et al.*, 2006, 2009) and has been attributed to the arc-parallel compression, which results into reverse slip on structures orthogonal to the Hellenic subduction zone, occurring within the downgoing plate.

To sum up, the current tectonic framework of the Aegean region mainly results from the interaction of three different processes: i) the Africa-Eurasia convergence–related collision and subduction along the Hellenic subduction zone; ii) the post-orogenetic extension in the back-arc region corresponding to a great part of the Aegean Region, also due to the slab sinking and retreat; iii) the propagation into the Aegean Region of the dextral strike-slip motion occurring along the

North Anatolian Fault and the North Aegean Trough, resulting from the westward extrusion of the Anatolian plate.

Given such a complexity, the seismogenic sources all over the Aegean Region exhibit all kind of kinematics, from reverse and transpressional along and externally of the Hellenic subduction zone, to normal dip-slip in the back-arc region and especially in continental Greece and finally to transtensional along the North Aegean Trough and almost pure strike-slip in the Kefallinia Transform Fault area. It has also been shown and remarked the great variability of strain rates and slip rates on specific fault zones across the whole study area, with the greatest values focusing along the Hellenic arc and in Corinth Rift region (with strain rates locally over 500 nanostrain/a and slip rates up to 10-15 mm/a), while other areas such as the central Aegean Sea are almost not internally deforming at all. These different deformational behaviours across the Aegean Region could possibly be related also to rheological variations, which this work aims to highlight.

Moreover, the varying rheological and deformational properties across the Aegean Region also result into different seismic and seismogenic behaviours, with drastic changes from one region to another, especially in terms of maximum depth of seismogenesis and maximum expected magnitudes, which however, except for earthquakes occurring along the Wadati-Benioff plane of the Hellenic subduction zone, never exceed values of 7.5-7.6. In conclusion, the rheological modelling of the Aegean Region could help improving its seismotectonic characterization and contribute to a better and more detailed seismic hazard assessment.

Chapter 2: Theoretical principles

2.1 Rheological behaviours

2.1.1 *Rheological modelling: a brief introduction*

Rheology, in the fields of geology and geophysics, is concerned with the study of the deformation of rocks under stress. By a semantical point of view, the term rheology comes from the Greek language and literally means "study of what flows". Geologists however, have expanded the concept and therefore rheology can be considered as the discipline studying the link between every type of rocks deformation (brittle failure, plastic creep, semi-brittle fracture, etc.) and the stresses that have caused them. In other words, rheology is concerned with describing the stress-strain relationships.

Rheological profiles, also termed strength envelopes, have been used, first qualitatively and then quantitatively, since the seventies to distinguish rock layers deforming in a brittle fashion from those undergoing ductile processes (Sibson, 1977; Goetze and Evans, 1979) (fig. 2.1).

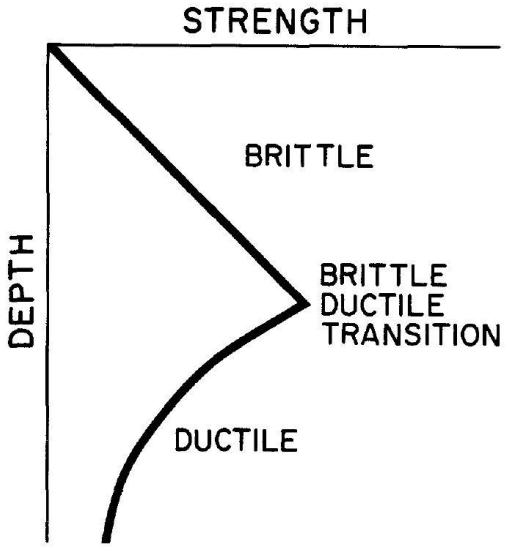

Fig. 2.1 – Schematic representation of a strength envelope, indicating the brittle and ductile deformation domains (from Scholz, 1988).

At the same time, the bulk rheology of rocks has been also associated to the potential of the corresponding layers to behave in a seismic manner. The distinction between brittle and ductile deformation, even though partially oversimplifying the problem, can effectively still represent a first tool to determine whether rocks may in principle store and successively release seismic

(elastic) energy through coseismic very fast slip or rather slowly deform in aseismic fashion, giving rise to a gamut of ductile processes (*e.g.* power-law long-term creep, pressure-solution creep, slow-slip etc.). In other words, the brittle-ductile transition (hereinafter BDT) can represent, as a first approximation, the seismic-aseismic boundary (*e.g.* Scholz, 1989; Williams, 1996) (fig. 2.2).

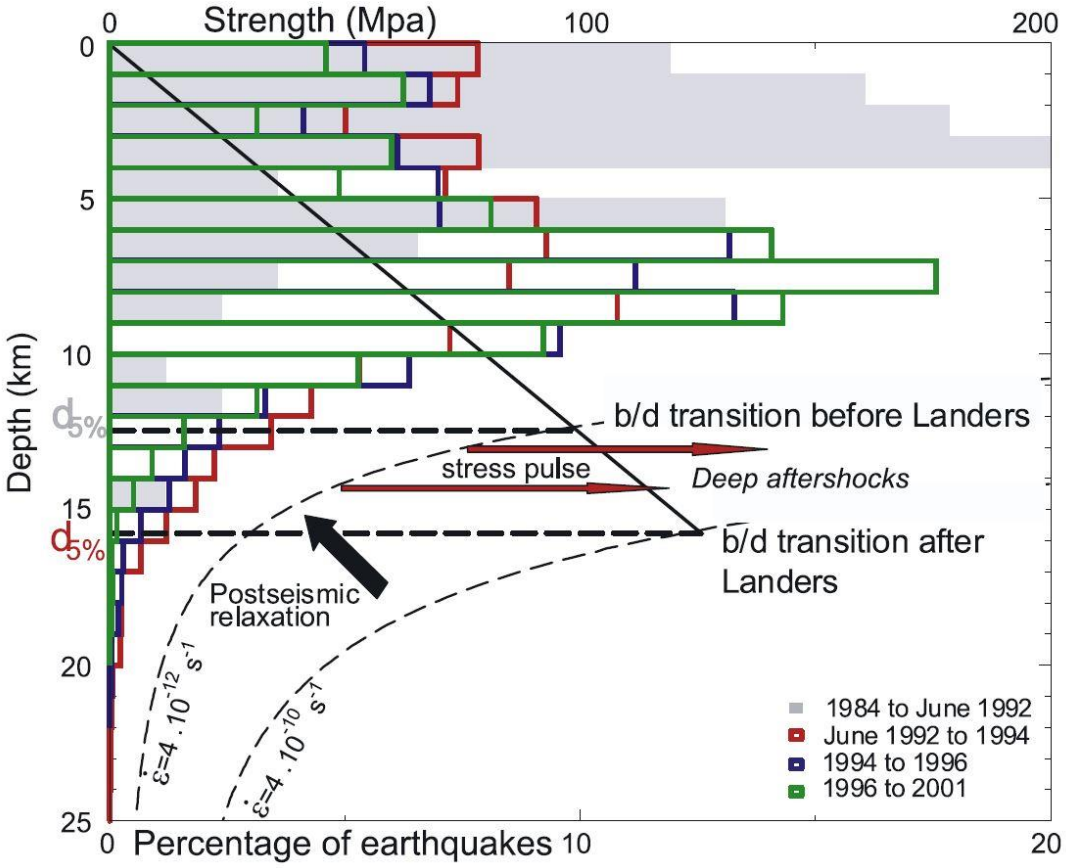

Fig. 2.2 – Correlation of the BDT (in the figure indicated as b/d) with the seismic-aseismic transition, as defined by the maximum depth of occurrence of seismicity. The figure also shows the BDT deepening as a result of the strain rate increase following the 1992 Landers earthquake and the associated increase of the seismogenic layer thickness (from Rolandone et al., 2004).

Furthermore, rheological profiles also provide the values of the shear strength of the rocks at the depth of the BDT and all along the investigated vertical column. This means that the use of strength envelopes can help retrieving information on the mechanical resistance and the critical stress that can be supported by the rocks in the analyzed column/volume.

The rheological profiles in the classic literature (*e.g.* Goetze and Evans, 1979; Brace and Kohlstedt, 1980; Sibson, 1977; Scholz, 1988) represent the value of the shear strength, usually visualized on the abscissa, as a function of depth (on the ordinate) (fig. 2.3). The resulting strength always corresponds to the minimum between the brittle and the ductile one. The brittle rheology is typically associated with the frictional sliding behaviour, where shear strength, expressed in terms of differential stress, is a function of pressure (and therefore depth) while being independent of strain rate and temperature. On the contrary, the ductile strength is usually related to

temperature-dependent behaviours, such as the power-law creep, where the strength is also affected by the strain rate, but has a negligible dependence on pressure.

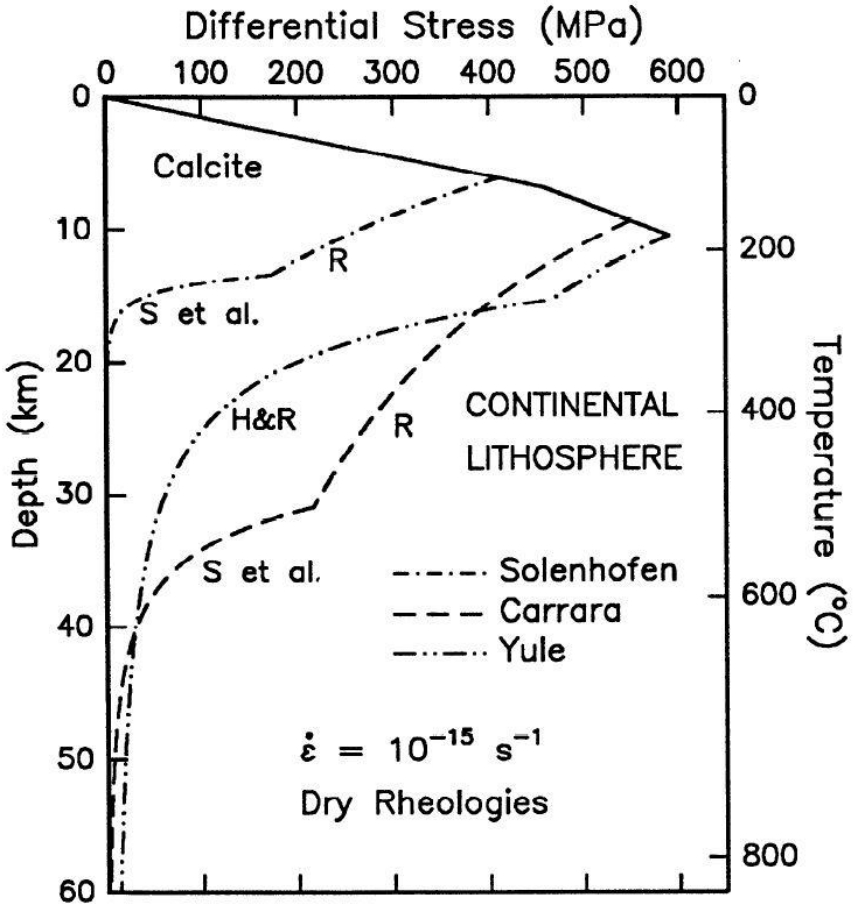

Fig. 2.3 – Typical strength envelopes of the continental lithosphere for different lithologies and a constant strain rate (Kohlstedt et al., 1995).

Brittle and ductile behaviours and their relative constitutive equations will be thoroughly described in detail in the dedicated sections below (§2.1.2; §2.1.3). Intermediate rheologies, such as semi-brittle behaviour, brittle-fracture (Zang *et al.*, 2007) and frictional-viscous behaviour (Bos and Spiers, 2002) may effectively help describing the rheological characteristics of the region around the BDT and will be therefore examined in depth too, in a dedicated section (§2.1.4). However, it should be already pointed out that the use of these intermediate behaviours may at the same time introduce major uncertainties and potential errors, mainly due to the paucity of experimental data and the difficulty in extrapolating those data from the laboratory conditions, at which they have been obtained, to real deep Earth conditions.

Major focus will be also set on the temperature depth profile (fig. 2.4). Indeed, the reconstruction of the most likely distribution of temperature at depth, *i.e.* the geothermal gradient, is of primary relevance in order to obtain reliable strength envelopes. Such a strong connection is mainly related to the exponential dependence of ductile strength on temperature in the power-law

creep equation (see following sections for a detailed analysis). Accordingly, the right choice of the most likely and representative geothermal gradient equation is fundamental to the aim of this reasearch, especially in relationship with the peculiar tectonic settings of the study area, which clearly require different equations (*e.g.* oceanic subduction and continental collision settings).

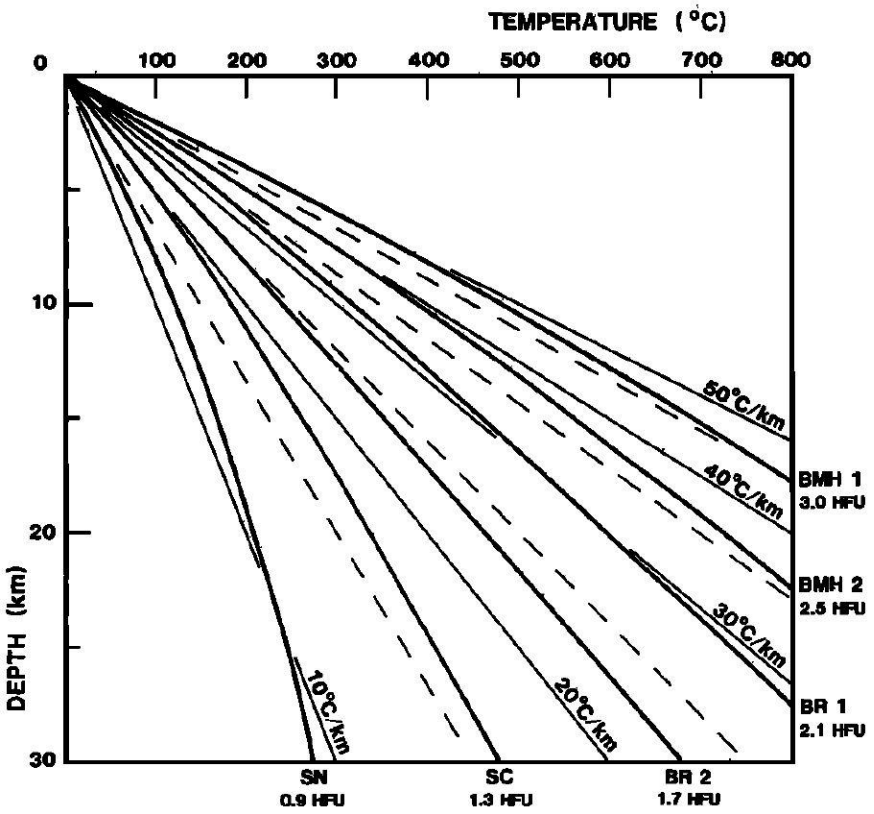

Fig. 2.4 – Examples of temperature-depth profiles and comparison between linear geotherms (thin solid and dashed lines) and conductive ones, for several thermal provinces of US (as proposed by Lachenbruch and Sass, 1977). Each province is associated with its own representative heat flow value, here expressed in Heat Flow Units (1 HFU = 41.8 mW/m^2) (from Sibson, 1984).

Noticeable roles are therefore played also by the parameters in those equations, such as thermal conductivity and radiogenic heat production rate (*e.g.* Lachenbruch and Sass, 1977), whose relative relevance, weight and range of potential values will be discussed in dedicated sections (§2.3; §3.1.6).

2.1.2 *Brittle deformation and frictional sliding*

Brittle deformation follows the principle that rocks fail when a critical applied stress value is attained, which corresponds to the strength of the rocks. If the stress overcomes the strength value, failure occurs and permanent deformation is stored in the rock volume. On the contrary, if the applied stress is not sufficient to cause brittle failure the rocks could in principle (if applied stresses are removed) return almost instantaneously to their undeformed status.

At this regard, brittle deformation can be linked to elastic behaviour, where indeed the application of stress is followed by instantaneous strain and once the stress is removed the deformed body returns immediately to its undeformed status (fig. 2.5).

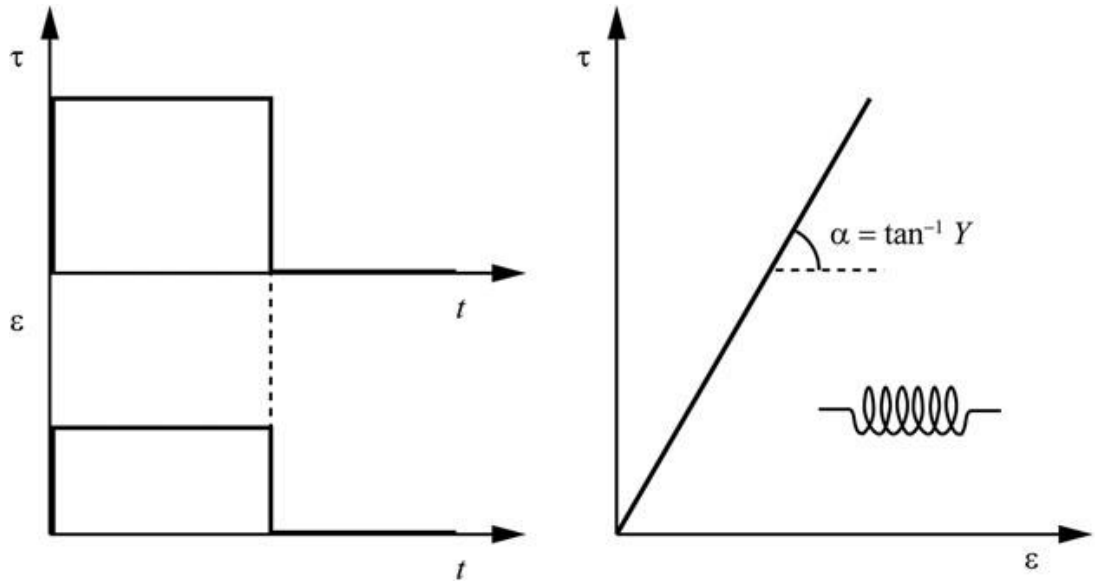

Fig. 2.5 – The left figure shows the instantaneous complete recovery of deformation, once the applied stress load is removed. On the right, the spring model with the linear correlation between stress and strain is displayed (from Schettino, 2014).

The elastic behaviour is conceptually represented by a spring, which is able to take on deformation by elongation or shortening (it depends on the direction and sense of the applied stress vector) and come back to its original length once the applied force (and hence stress) is removed. In mathematical terms, the elastic behaviour of a spring is described by the following equation, also called Hooke's law:

$$\sigma = E \cdot \varepsilon \qquad [2.1]$$

where σ represents the applied stress [Pa], ε the strain (which is adimensional) and E is the elastic modulus (in this case the Young's modulus, expressed in Pa). As it can be observed from the above equation, the elastic behaviour is characterized by a linear correlation between stress and strain.

The (one-dimensional) strain, which can be expressed as a percentage, is defined as the ratio of the difference between final length and initial one to the initial length. The above equation states that given a certain fixed amount of deformation, the greater is Young's modulus, the greater will be the stress that has to be applied in order to cause deformation. In other words, the Young's modulus describes how easy is for a given body to behave in an elastic manner (if the applied stress is fixed, the greater is the Young's modulus, the smaller is the resulting

deformation). In the tensor notation the generalized Hooke's law for an isotropic body reads as follows:

$$\sigma_{ij} = \lambda \cdot \theta \cdot \delta_{ij} + 2\mu\varepsilon_{ij} \qquad [2.2]$$

where λ and μ are the Lamé's parameters, θ is the dilatation and δ_{ij} is the Kronecker delta. λ does not have any simple physical meaning while μ represents the shear modulus (or rigidity modulus), *i.e.* the coefficient, expressed in Pa, corresponding to the ratio between shear stress and shear strain. The shear modulus μ has many applications in the fields of rheology and seismology as it is used, *e.g.*, in the calculation of the tectonic parameter for the frictional sliding constitutive law (as it will be shown in detail later) and also in the equation of the seismic moment.

However, if the applied force reaches a threshold corresponding to the yield stress or the ultimate stress, in case of plastic and brittle behaviours, respectively, the spring will start failing and a permanent deformation with respect to its initial shape will be observed. In the former case, the spring will deform ductilely, in the latter case the spring (*viz.* the rock volume) will break.

The elastic-brittle mechanism of deformation is also typically associated to the fault behaviour in relationship with the seismic cycle. At this regard, the fault is considered to behave elastically during the interseismic stage, when the application of tectonic stress leads to the storage of elastic strain within the fault volume. If a stress rate persists long enough to approach the fault strength and finally overcome it, rupture propagation and co-seismic slip along the fault surface occur, thus causing a discontinuous permanent deformation. Such a fault behaviour during the earthquake cycle has generally been termed as stick-slip behaviour (*e.g.* Brace and Byerlee, 1966; Sibson, 1977; Savage, 1983).

Overall, brittle deformation corresponds to a rapid failure of the considered rock volume, usually associated with crack opening and slip along preferential surfaces. The latter represent weak zones where deformation tends to concentrate, obeying to the simple law that deformation occurs where the strength is minimum and a lesser stress is required to obtain the same amount of deformation (*i.e.* strain). However, not all these surfaces present the same rheological and mechanical properties and therefore the corresponding brittle deformation mechanisms should be distinguished. In particular, a clear distinction has to be made between intact-rock surfaces and reactivated ones (*e.g.* Sibson, 1985) (fig. 2.6). The former ones are characterized by a considerable cohesion, which cannot be overlooked and discarded.

Accordingly, following the Navier-Coulomb rupture criterion, the relationship between shear stress and normal stress for failure along a newly formed surface reads as follows:

$$\tau = C + \sigma \cdot \tan\varphi \qquad [2.3]$$

where τ is the shear stress [Pa], C is the cohesion [Pa], σ is the normal stress and φ the angle between the direction of the applied stress vector and the considered surface, or the angle of internal friction of the constitutive material. For re-activated surfaces, however, the cohesion term is almost nil and therefore the failure criterion takes the following form (from Ranalli, 1995):

$$\tau = \mu_0 \cdot \sigma \qquad [2.4]$$

where μ_0 represents the coefficient of friction.The equation [2.4] follows the concepts behind Amontons' laws of friction, even though it differentiates from the latter by taking into account stresses rather than forces.

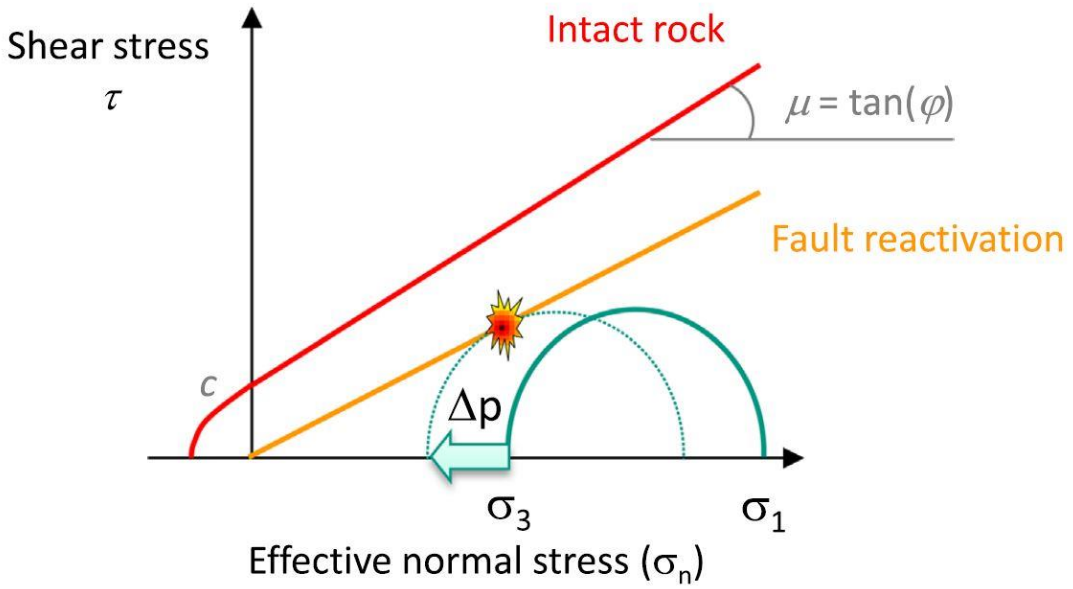

Fig. 2.6 – Comparison of an intact rock surface failure envelope and a reactivated fault, following the Mohr-Coulomb theory (from Gaucher et al., 2015).

Since the late sixties there have been several studies regarding the values of the friction coefficient for sliding of rocks along weak surfaces in a defined volume, starting from the seminal reviewing works of Byerlee (1968, 1978). He proposed, on the basis of original and literature experimental results, an empirical version of the Navier-Coulomb criterion, which reads as follows:

$$\tau = 0.85 \cdot \sigma_n \qquad \text{for } \sigma_n \leq 200 \text{ MPa} \qquad [2.5]$$

$$\tau = 0.5 + 0.6 \cdot \sigma_n \qquad \text{for } \sigma_n > 200 \text{ MPa} \qquad [2.6]$$

where τ is the shear stress required for sliding along the considered surface, and σ_n is the applied normal stress. From such empirical relationships, it follows that in natural conditions the friction coefficient varies between 0.6 and 0.85 for most rocks, since the so-called Byerlee's law is valid independently of lithology and of other important ambient parameters, such as temperature, strain rate and grain size. However, even if in principle Byerlee's law can help retrieving a first insight on the shear brittle strength of the considered rocks, recent studies on the friction coefficient have shown that its lower boundary can be noticeably smaller than 0.6 (*e.g.* Di Toro *et al.*, 2004; Carpenter *et al.*, 2011; Collettini *et al.*, 2019). A detailed description and analysis of the friction coefficient potential values along fault shear zones will be given later in a dedicated section in chapter 3 (§3.1.7).

In terms of geological record and structures, brittle deformation is typically associated to faults, fractures and fault rocks. In particular, following the classification of Sibson (1977), the products of brittle deformation in the fault zone are the so-called cataclasites (fig. 2.7).

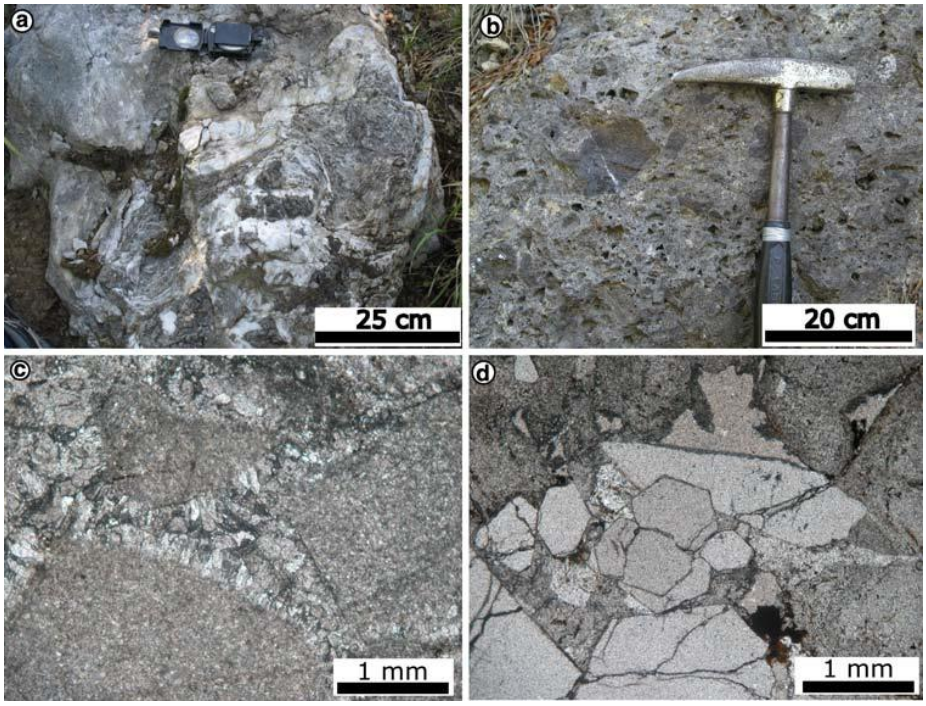

Fig. 2.7 – Different examples of fault zone cataclasites in Tuscany, Italy (from Liotta et al., 2010).

Such rocks may present different degrees of comminution and wearing with respect to the parental rocks (*e.g.* proto- and ultra-cataclasites), which can also give insights on the time evolution and the onset of activity of the considered structure (mainly faults).

A particular case is represented by the pseudotachylites, which are amorphous rocks typical of the fault core zone and whose genesis derives from the rapid cooling of the melt produced by the shear heating due to to the very rapid co-seismic slip along the fault plane. Accordingly, such rocks, if present and recognized within the fault/shear zone, can help identifying the depth extent of the brittle deforming layer. On the other hand, pseudotachylites are sometimes embedded

between mylonitic rocks, which are in turn the product of ductile deformation. The interbedded occurrence of these two typologies of fault/shear zone rocks may thus indicate the alternating occurrence of brittle and ductile prevailing deformation mechanisms, thus locally leading to a broad brittle-ductile transition zone.

The presence of pseudotachylites in an otherwise mylonitic matrix may be also interpreted as an indication of temporary deepening of the brittle-ductile transition during and just after the co-seismic stage. Such a deepening may be ultimately attributed to the instantaneous surge of the strain rate (even up to 10 orders of magnitude) during the fast slip episodes, since the strain rate, as it will be shown later in the dedicated section (§2.1.3) for the ductile deformation, greatly affects the ductile strength. Indeed, as a general rule, an increase in strain rate results in an increase of ductile strength and a consequent downward shift of the brittle-ductile transition.

From a rheological modelling point of view, the brittle deformation is usually associated to the frictional sliding mechanism (*e.g.* Sibson, 1977; Scholz, 1988; Ranalli, 1995), whose constitutive law reads as follows:

$$(\sigma_1 - \sigma_3) = \alpha \cdot \rho \cdot g \cdot z \cdot (1 - \lambda) \qquad [2.7]$$

where $(\sigma_1 - \sigma_3)$ is the shear strength expressed in terms of differential stress [Pa], α is the tectonic parameter, ρ is the average density [kg·m^{-3}] of the considered rock volume down to a depth equal to z [m], g is the gravity force acceleration [m·s^{-2}] and finally λ is the pore fluid pressure ratio. I will discuss later the role, weight, significance and variability of each of these parameters in dedicated sections in chapters 3 and 4 (§3.1.8, §3.1.9 and §4.2.1).

What can be observed at first sight is that the frictional strength is (almost) linearly correlated with (lithostatic) pressure ($\rho \cdot g \cdot z$), while it is totally independent of temperature, strain rate and grain size. The frictional sliding equation is somewhat similar to Amontons' and Byerlee's laws for slip re-activation on pre-existing surfaces. In this case, however, the coefficient multiplying the normal stress (*viz.* lithostatic pressure) does not only depend on the friction coefficient itself (which is nonetheless included in the equation for the calculation of the tectonic parameter, as it will be shown later), but it also takes into account the pore fluid pressure and the shape of the stress ellipsoid in the considered volume. Moreover, since (lithostatic) pressure increases with depth, it follows that the frictional strength is almost nil towards the surface while it tends to progressively increase at depth.

The lithospheric layers that usually display a brittle behaviour are, at least in part, the sedimentary cover, the upper crust and in some peculiar cases either the lower crust and/or the uppermost mantle. Strength profiles representing real setting conditions with a brittle layer extending from the topographic surface down to the upper mantle are quite rare, as it will be shown and explained in the section dedicated to the strength envelopes description (§2.2).

2.1.3 *Ductile deformation and power-law creep*

The term ductility refers to a rheological behaviour characterized by permanent and irreversible deformation, though differently from brittle behaviour, no loss of continuity or cohesion in the deforming material is observed (see also Schettino, 2014). From a strict rheological point of view, the ductile deformation can be associated to the plastic behaviour. The latter is characterized by no deformation at all until a yield strength is attained and beyond which the material starts deforming in a viscous manner (fig. 2.8).

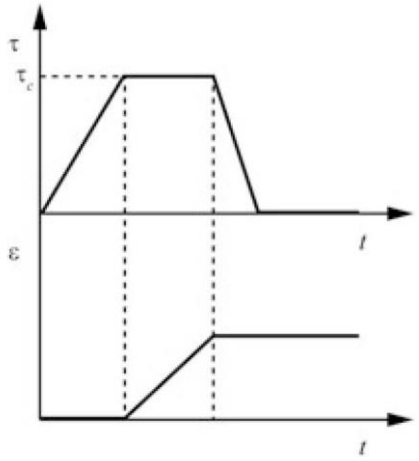

Fig. 2.8 – Representation of the plastic behaviour, in terms of stress and strain vs time graphs. Note how deformation only starts when a critical (yield) stress is attained, and the strain is not recovered after the stress removal (from Schettino, 2014).

The viscous rheology for a perfectly Newtonian fluid is expressed in mathematical terms by the following equation:

$$\tau = 2\eta \cdot \dot{\gamma} \qquad [2.8]$$

where η is a coefficient describing the viscosity of the material and is expressed in Pa·s, and $\dot{\gamma}$ is the shear strain rate. As can be deduced from the above equation, a perfectly Newtonian viscous fluid is characterized by a linear relationship between shear stress and (shear) strain rate, represented by a straight line in a stress-strain rate plot (fig. 2.9), whose coefficient corresponds to the viscosity. In a certain way the viscous behaviour can be regarded as an extreme case of plastic behaviour with yield strength being nil.

For most rocks deforming in a ductile way at depth, non-Newtonian behaviours have actually been observed and are considered to represent more realistically the corresponding deformation mechanisms. Deviations from ideal plastic behaviour are also related to the concepts of strain hardening and strain softening, which are also observed in nature: in the first case an increase of the stress is required to keep deforming the material once the yield stress has been attained, while

in the second case even if the stress applied is partially removed the material will continue to ductilely deform anyway. Ductile deformation in the crust and upper mantle layers is usually modelled with non-Newtonian rheologies where the strain rate is related to the stress elevated to some power (typically comprised between 3 and 5). I will return and focus on this so-called power-law creep rheology shortly.

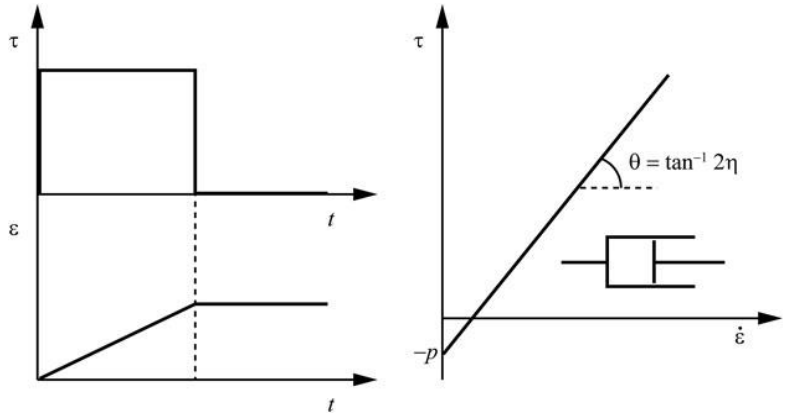

Fig. 2.9 – On the left, stress and strain vs time graphs for the Newtonian rheology are displayed. On the right, the linear correlation between stress and strain rate together with the dashpot model are shown (from Schettino, 2014).

When dealing with deformation styles at crustal and lithospheric scales, however, what should be never overlooked but rather carefully taken into account is the time-scale at which observations on the corresponding rheological behaviours are made. Indeed, if the very short co-seismic stage is considered, the lower crust and upper mantle will behave in an elastic manner as the seismic waves will propagate through them; at the same time scale, the fault zone in the upper crust will exhibit a brittle failure deformation mechanism. On the contrary, if a much longer time scale is considered, such as the interseismic period, the lower crust and upper mantle will deform in a ductile way, while the upper crust will be storing elastic deformation. Finally, if observations are made on an even longer time scale in the order of hundreds of Ma, the whole lithosphere will appear to behave in a ductile manner, even though with remarkably high viscosity values (say greater than 10^{21}–10^{22} Pa·s).

For the scope of this work, being the rheological modelling aimed at seismotectonic applications, the ductile deformation has been modelled as a power-law creep. Such a choice is in agreement with the concepts exposed above and also finds wide acceptance and application in most of the dedicated literature (*e.g.* Brace and Kohlstedt, 1980; Sibson, 1983; Ranalli, 1995; Burov and Diament, 1995; Cloetingh and Burov, 1996). The corresponding constitutive equation reads as follows:

$$(\sigma_1 - \sigma_3) = (\frac{\dot{\varepsilon}}{A})^{\frac{1}{n}} \cdot e^{\frac{E}{R \cdot n \cdot T(z)}} \qquad [2.9]$$

where $(\sigma_1 - \sigma_3)$ is the differential stress, $\dot{\varepsilon}$ is the strain rate, A is the so-called power-law parameter [$Pa^{-n} \cdot s^{-1}$], n is the power-law exponent, E is the thermal activation energy [$J \cdot mol^{-1}$], R is the gas constant (value equal to 8.31447 $J \cdot mol^{-1} \cdot K^{-1}$) and $T(z)$ is the temperature at depth z [K]. Equation [2.9] is only valid for the crustal layers (which are the main target of this research) and the upper lithospheric mantle, while at greater depth, in the mantle, activation enthalpy (which depends on pressure) should also be considered (see *e.g.* Ranalli, 1995). If equation [2.9], which is sometimes referred to also as *Dorn's law*, is inverted for the strain rate the following equation is obtained:

$$\dot{\varepsilon} = A(\sigma_1 - \sigma_3)^n e^{\frac{-E}{R \cdot T(z)}} \qquad [2.10]$$

From the latter equation it is evident the dependence of the deformation on the shear stress elevated to the power n and it is similarly clear why such ductile deformation mechanism is called power-law creep. Another outstanding point for this rheological behaviour is the strong influence exerted by the temperature on the resulting ductile strength. Indeed, as it can be noted from equation [2.9], the temperature (as a function of depth) appears in the exponent of the exponential function, thus playing a major role on the determination of the ductile properties of the investigated material.

The variation of temperature with depth, *i.e.* the vertical geothermal gradient, is therefore a crucial parameter for the ductile behaviour modelling. Given its primary importance, the equation for the geothermal gradient and the role played by each of the parameters in such equation will be discussed and analyzed in a dedicated section (§2.3). At this stage it is sufficient to underline that low temperatures at depth result in a greater ductile strength, while elevated geothermal gradients are generally associated with lower values of the ductile strength.

Differently from the frictional sliding mechanism, the power-law creep does not significantly depend on pressure (and in any case the potential dependence is not well known, thus generally ignored, also taking into account that its inclusion would not substantially affect the resulting ductile strength, see also the discussion in Ranalli, 1995), while it is clearly affected by the values of the strain rate. On the contrary, similarly to the brittle deformation, power-law creep is not affected by the grain size of the material, since the microphysical mechanism through which the ductile deformation (or flow) occurs, which is called dislocation creep, does not show any strong dependence on the material grains dimension, but rather it is generally grain-size insensitive.

The dislocation creep is generally considered as the main and prevalent deformation mechanism for the macroscopic ductile behaviour in the crustal layers and upper (lithosperhic) mantle. However, some additional processes and mechanisms may contribute to the overall

deformation or sometimes, under peculiar conditions, even replace the dislocation creep as main ductile deformation mechanism.

Such alternative processes include diffusion creep, Peierls mechanism, Harper-Dorn creep, Nabarro-Herring, Coble, (see *e.g.* the review from Artemieva, 2011) dissolution-precipitation and pressure-solution creep (see *e.g.* Rutter, 1976; Sleep and Blanpied, 1992; Gratier *et al.*, 2013) (fig. 2.10).

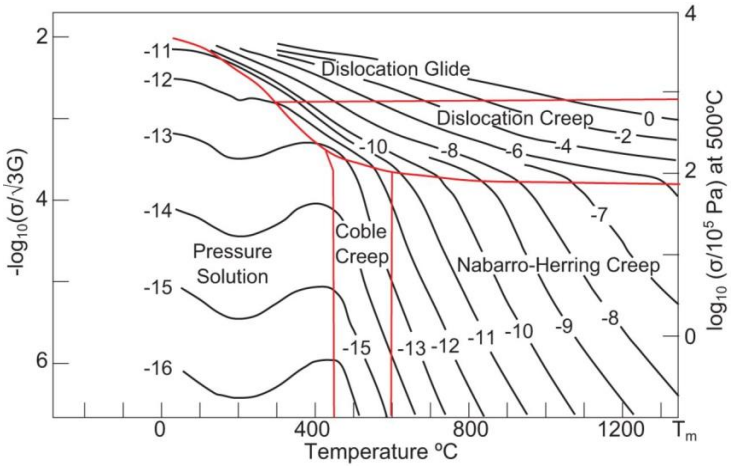

Fig. 2.10 –Predominance of each ductile deformation mechanism for calcite, as a function of temperature, stress and strain (from Mariani et al., 2015).

I am now going to briefly present the characteristics of each of these deformation processes. Diffusion creep consists in the process of atoms diffusion through the vacancies, which are point defects, within the crystallographic structure (fig. 2.11).

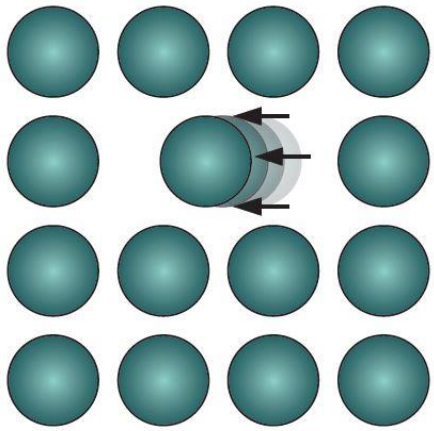

Fig. 2.11 – Schematic example of a point defect (vacancy) movement through which diffusion creep occurs (from Fossen, 2010).

It is particularly efficient at low temperatures and stresses, and the strain rate tends to increase with the grain size decrease, thus being strongly grain-size sensitive, differently from the dislocation creep. Moreover, it differentiates from the dislocation mechanism because the atomic diffusion is characterized by a linear relationship between strain rate and stress (Newtonian creep)

and no lattice preferred orientation and consequent anisotropy are induced. Finally, the diffusion creep may be divided into two main groups in terms of process characteristics, one being dominated by grain boundary diffusion (Coble creep) and the other by matrix diffusion (Nabarro-Herring creep) (see the review from Artemieva, 2011 and references therein for the details).

Dislocation creep is first of all a mechanism where the deformation occurs by glide and/or climb movements of linear defects (*i.e.* the dislocations themselves) within the crystal lattice (*e.g.* Fossen, 2010) (fig. 2.12). As already mentioned, the dislocation (or power-law) creep is characterized by a power law relationship between the applied stress and the resulting strain rate, while it is almost not dependent on grain size. Other distinctive features of the dislocation creep are the strong sensitivity to the presence of water (whose occurrence, even in trace amounts, drastically reduces the resulting strength of the "wet" rocks) and the tendency to produce lattice-preferred orientations and remarkable anisotropic deformation in general.

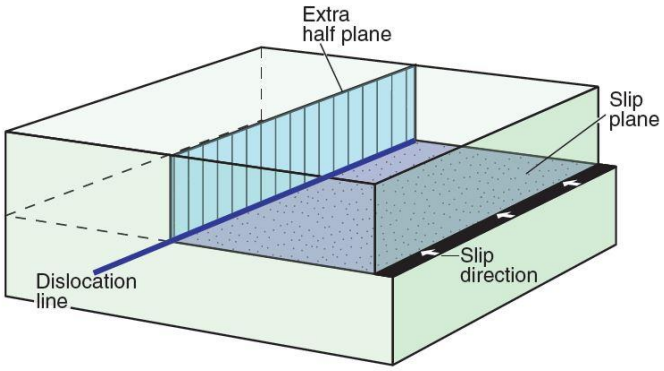

Fig. 2.12 – Schematic representation of linear defects and dislocation processes in the crystallographic structure (from Fossen, 2010).

Furthermore, such deformation mechanism is considered to be highly effective at depths and pressure-temperature conditions compatible with the lower crust and the upper (lithospheric) mantle layers (*e.g.* see the review by Burgmann and Dresen, 2008; Karato, 1989). Accordingly, since the seventies several experimental studies and reviews on the ductile deformation and flow laws of representative lithologies such as quartzites, pyroxenites and olivines have been conducted (*e.g.* Carter *et al.*, 1964; Tullis *et al.*, 1973; Heard, 1976; Kirby and Kronenberg, 1987; Tsenn and Carter, 1987; Kohlstedt *et al.*, 1995; Hirth *et al.*, 2001). Dislocation in the form of power-law creep is therefore commonly used and presented as the main process responsible for ductile deformation in crustal- and lithospheric-scale rheological models, where its constitutive equation or very similar forms are generally applied (*e.g.* Sibson, 1977; Goetze and Evans, 1979; Brace and Kohlstedt, 1980; Ranalli and Murphy, 1987; Ranalli, 1995; Afonso and Ranalli, 2004; Hauksson and Meier, 2019).

At very high stresses another deformation mechanism, the so-called Peierls creep, becomes relevant. Such a creep is characterized by an exponential relationship between strain rate and

stress and by the lack of the need for thermal activation in the dislocation glide phenomenon. Indeed, the Peierls mechanism is associated with relatively low temperature and therefore may be suited especially for describing the ductile deformation processes occurring in cold cratonic settings.

Finally, the pressure-solution creep, also termed dissolution precipitation creep, is characterized by dissolution of rock materials and particles at high normal stress, then transport in a fluid phase and final precipitation when the normal stress decreases (Gratier *et al*., 2013). Such a deformation mechanism is usually associated with macroscopic ductile deformation in the upper crust, in particular along major shear and fault zones at plate boundaries or orogenic front regions, and it is spatially and temporally alternated with a brittle deformation mechanism, especially within the brittle-ductile transition zone.

Dissolution precipitation creep has also been proposed as a potential deformation mechanism acting along the subduction channel (*e.g*. Wassman and Stockhert, 2013; Audet and Burgmann, 2014; Fagereng and den Hartog, 2016), possibly in concomitance with the dissolution creep mechanism. The main effect of considering the dissolution precipitation creep would be a significant reduction of the differential stresses that can be supported within the subduction channel zone. However, the main experimental and empirical relationships rigorously describing the dissolution precipitation creep are only available for single mineral phases (*e.g*. quartz; Niemeijer *et al*., 2002), while the above-mentioned deformation mechanism most likely involves polyphase aggregates and rocks (see also discussion in Wassman and Stockhert, 2013). Accordingly, dissolution precipitation creep equations have not been included in the modelling and the weakening effect has been mostly reproduced through an increase of the pore fluid pressure around the subduction zone (see sections §2.2 and §3.1.9).

As already mentioned, in the classical works on rheological profiles and modelling, where the simplified approach is applied, the dislocation creep is usually selected as the main representative deformation mechanism for the ductile behaviour. The reason for this is twofold: firstly, the dislocation creep is effectively the predominant process in the crustal and upper mantle layers at most temperature and pressure conditions as observed in different settings. Secondly, with respect to all the others ductile deformation mechanisms, a greater variety of tests and laboratory experiments have been carried out on several different lithologies and rock samples for determining the values of the power-law creep parameters in different thermophysical conditions (see references above). Such a relative abundance of experimental results allows to apply the relevant equation to many different geological and tectonic settings, even though some approximations and possible errors should be always considered during modelling (see Chapters 3 and 4).

In terms of geological and structural records, the ductile deformation is mainly associated to rocks classified by Sibson (1977) as mylonites (fig. 2.13). Such rocks are the products of ductile

processes such as recrystallization, pressure-solution creep, and more in general of an internal redistribution and re-organization of the atomic structures and crystal lattices of the forming minerals. Similarly to brittle processes, the products of the ductile deformation present different grades of mylonitization, ranging from proto-mylonites to ultra-mylonites, according to their (increasing) time of exposure to such plastic strain.

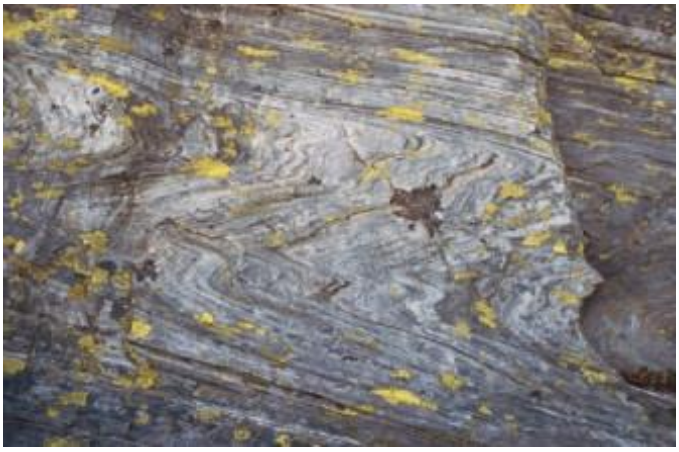

Fig. 2.13 – Folded mylonites in a ductilely deforming shear zone (from Fossen, 2010)

As a general trend, higher grades of mylonitization are progressively expected at greater depths, as a result of the downwards decreasing ductile strength due to the increase of temperature with depth (in "normal" unperturbed geothermal gradient conditions). However, it could also happen that, especially in strongly extensional tectonic settings such as *e.g.* metamorphic core complexes or continental rifts, the results of the long-lasting ductile deformation on the rock structure, foliation, texture etc. are overprinted by rapidly occurring brittle processes. Such brittle overprints become predominant once the rocks are progressively exhumed towards the surface due to the ongoing extension, consequent thinning and final denudation from the overlying rocks, mostly related to the activity of low-angle normal faults.

Indeed, even though the rocks exhumation is not accompanied by a fast temperature values decrease, at the same a much more rapid confining pressure reduction occurs. Accordingly, the latter plays a major role and causes a remarkable brittle strength decrease, which ultimately leads to the final embrittlement.

Also the opposite process, with brittle layers becoming exposed to higher temperatures and thus starting to deform in a ductile manner, may potentially occur, *e.g.* as a result of delamination of the lowermost crust/upper mantle layers with the consequent upwards shift of the asthenosphere and the local increase of the geothermal gradient. In this case, however, in order for us to observe at the surface the superposition of ductile processes and structures on the brittle deformation, the considered rocks should make their way back through the upper crust to the Earth surface. This, in turn, necessarily implies an upwards crossing of the brittle-ductile

transition, thus leading to a final re-overprint of brittle and frictional processes on the considered rock volumes.

Generally speaking, from a structural point of view, the principal crustal-scale features related to ductile deformation correspond to shear zones, whose widths are some order of magnitude greater than those of the slip surfaces occurring within the brittle, seismogenic layer (fig. 2.14). Such ductilely deforming shear zones still represent weakness regions where deformation is concentrated and partially localized, even though the localization is much less evident and efficient with respect to brittle fault zones. Moreover, the greater width of the shear zones in the *plastosphere* (*sensu* Scholz, 1988) with respect to fault zones in the *schizosphere*, implies that the strain in the former is not as much concentrated as in the latter.

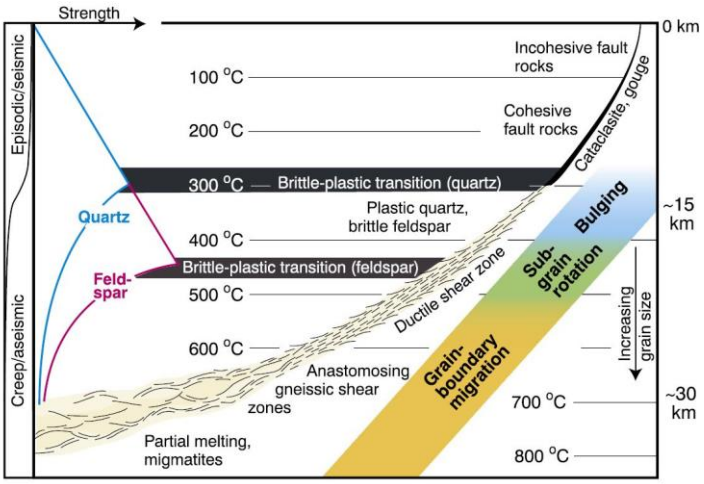

Fig. 2.14 – Variation of a fault/shear zone thickness as a function of depth, temperature and rheological behaviour (from Fossen and Cavalcante, 2017).

As a consequence, the strain rates in the ductile shear zones are generally lower than those along the corresponding slip surfaces in the brittle layer. I shall return on this issue in Chapter 3 (section §3.1.2).

2.1.4 *Semi-brittle deformation*

Semi-brittle behaviour, to which I will refer also as *intermediate behaviour*, mainly characterizes the region around the brittle-ductile transition (fig. 2.15).

Such intermediate rheology shares some common traits with both brittle and ductile deformation and also shows some peculiar features of its own. Before entering a more detailed description, it is worth pointing out that even though some advances have been made in the last decades (*e.g.* Handy *et al.*, 1999; Bos and Spiers, 2002; Zang *et al.*, 2007; Pec *et al.,* 2012) regarding experimental and laboratory tests on semi-brittle behaviours, their use and application in the context of rheological modelling is still affected by some caveats and drawbacks, on which I will focus later in this section.

The semi-brittle behaviour has long been theorized as the necessary and natural link between the brittle and the ductile deformation styles, *e.g.* in the synoptic conceptual model of a fault zone and shear zone by Sibson (1983) and later modified by Scholz (1988). From a seismogenic point of view, which also has relevant implications for seismotectonic applications, the intermediate behaviour zone is considered as a peculiar layer where no earthquake could nucleate, but where seismic rupture originated in the overlying brittle seismogenic layer could potentially propagate through (Scholz, 1989). Such a characteristic implies that the base of the semi-brittle layer could represent the effective bottom of the seismically slipping surfaces, at least during the co-seismic and short post-seismic stages when the rapid increase of the strain rate leads to a temporary deepening of the *schizosphere* (figure 2.2; *e.g.* Rolandone *et al.*, 2004; Beeler *et al.*, 2018).

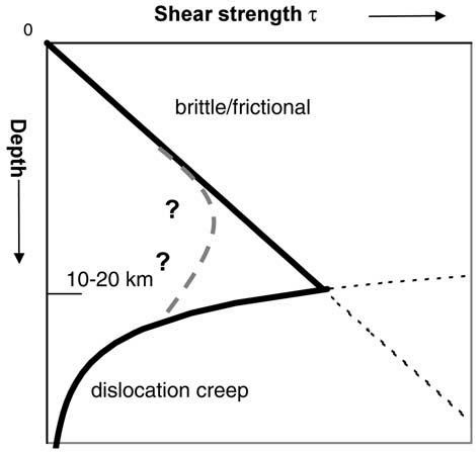

Fig. 2.15 – Qualitative representation of an alternative strength envelope where the transition zone is dominated by semi-brittle deformation, indicated by the dashed grey curve (from Bos and Spiers, 2002).

Due to such behaviour with regard to the seismic rupture propagation, I prefer to refer to the intermediate rheology as semi-brittle rather than semi-ductile. Such a rheological behaviour, similarly to the brittle-frictional one, is still characterized to some degree by localized deformation and dependence on lithostatic and pore fluid pressure. At the same time, however, it shows peculiar features of the ductile deformation, such as being strain rate and temperature dependent and grain-size sensitive.

The mechanisms through which semi-brittle deformation occurs may be multiple and several authors refer to them with different names. Pec *et al.* (2012) also adopt the definition of semi-brittle flow; Handy *et al.* (1999) and Bos and Spiers (2002) have termed the intermediate rheological behaviour as frictional-viscous flow, while Zang *et al.* (2007) refer to it as high-pressure brittle fracture; finally, in the classic works from Sibson (1984) or Scholz (1988) (see also the review by Fagereng and Toy, 2011), the dissolution-precipitation creep is indicated as one of the potentially contributing deformation mechanisms of the transitional rheological regime.

All these different names, however, can be approximately reconducted to a similar intermediate rheology, which shows in any case some particular characteristics. First of all, the

transition from brittle to ductile behaviour rather than occurring at a precise point and being limited to some metres in vertical extent, becomes much more spread over some kilometres, thus effectively defining a thick transitional layer. From a graphical point of view, the transition does not correspond anymore to an apex determined by the intersection of the frictional sliding straight-line with power-law creep curve, but rather, a smooth and vertically extended curve characterizes the transitional region. A second common point, which is also strictly related to the first one, is that the maximum peak strength, if intermediate rheology is considered, is markedly lower than that at the BDT depth as obtained by the classical two-behaviours strength envelopes (fig. 2.16).

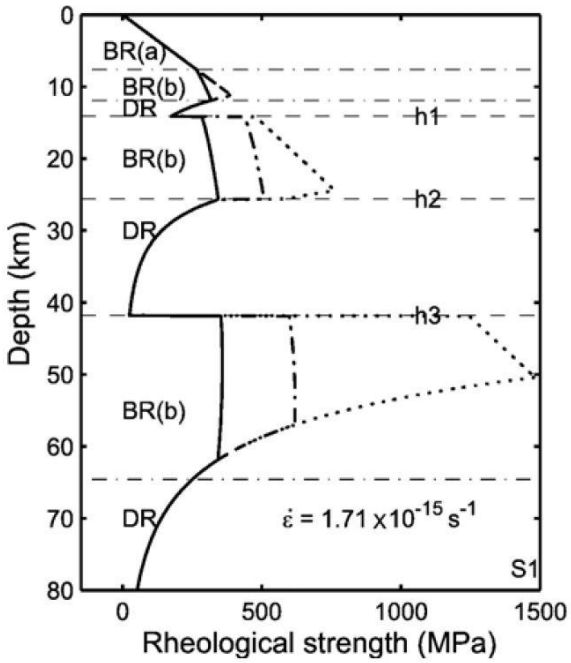

Fig. 2.16 – Differences between strength envelope taking into account semi-brittle deformation (BR(b)), indicated by the solid curve and the classic one (dotted curve). Note the deeper BDT(s) along the solid curve and the decrease in maximum strength values (from Zang et al., 2007).

Such a decrease of the peak strength allows to contain the maximum strength values into an acceptable and more realistic range (say around 1 GPa and not much more than that, as it would instead occur at the simplified, two-curves BDT). This better adherence to the natural expected values of peak shear strength represents one of the major advantages of realizing rheological models including the semi-brittle behaviour.

A further peculiarity of the intermediate rheological behaviour consists in the position of the maximum peak shear strength, which does not coincide with the depth of the transition to the ductile behaviour. Indeed, such a transition could occur deeper than the strength peak, differently from the purely brittle rheology where the BDT is always associated to the maximum peak shear strength. In the present research, Zang *et al*. (2007) equation is selected as representative of semi-brittle rheology. As above mentioned, the Authors refer to such a behaviour as high-pressure brittle fracture, since the mechanism becomes effective only at mid-lower crustal depth, when

pressure attains very high values such that further deformation mechanisms may be promoted other than simple frictional sliding processes. Zang *et al.*'s empirical equation reads as follows:

$$\sigma_1 - \sigma_3 = B_0 \left[1 + K \left(\frac{\sigma_c}{B_0}\right)^n\right] \left[1 + \alpha \left(\log \frac{T}{T_0}\right)^\beta\right] \left[1 + \gamma \log \left(\frac{\dot{\varepsilon}}{\dot{\varepsilon}_0}\right)\right] \qquad [2.11]$$

where B_0, K, n, α, β and γ are all empirical fracture parameters that vary with the selected lithology (corresponding values are reported in table 2.1).

	B_0	K	n	α	β	γ
	MPa	/	/	/	/	
Granite	34.1	4.57	0.52	-1.128	1.732	0.035
Gabbro	36.1	3.18	0.55	-2.536	2.340	0.035
Basalt	48.5	2.98	0.51	-2.536	2.340	0.035
Peridotite	28.3	3.35	0.68	-1.875	1.310	0.035

Table 2.1 *– Values of the parameters in the empirical equation by Zang et al., 2007.*

$(\sigma_1 - \sigma_3)$ represents the brittle fracture strength, σ_c is the confining pressure, T_0 is the reference temperature and $\dot{\varepsilon}_0$ is the reference strain rate for the specific size of the sample. Unfortunately, all the empirical parameters values are only available for a limited number of lithologies, on which tests have been carried out. Such lithologies correspond to granite, gabbro, basalt and peridotite. Clearly, the absence of other typical lithologies representative of, above all, the continental crust (such as limestone, quartzite, granodiorite, diorite etc.) limits the applicability of Zang's equation to natural geological settings and this problem represents the first major drawback in using such a rheology for modelling purposes.

Moreover, a further issue is raised by the need to extrapolate the experimental results obtained using a limited range of values for the boundary and ambient conditions (*e.g.* temperature, pressure, strain rate) to natural conditions.

The frictional-viscous flow behaviour from Bos and Spiers (2002) also presents characteristics of both brittle frictional (normal pressure dependence) and ductile creep (strain rate sensitivity) deformation mechanisms (fig. 2.17).

They propose a microphysical model for the rheological behaviour around the BDT region and tentatively validate it on the basis of a comparison with mechanical data on faults characterized by kaolinite gouge. Their results are robust and indicate a substantial decrease in strength around the BDT, which might be obtained applying an apparent friction coefficient value comprised between 0.25 and 0.35. The drawback, in this case, is related to the fact that such results have only been tested and therefore are only valid for phyllosilicates-bearing faults. Accordingly, the frictional-viscous flow constitutive equation cannot be applied for large-scale

models where no detailed information on every fault zone is available and cannot be considered as representative of long-term rheological behaviour of the whole crust.

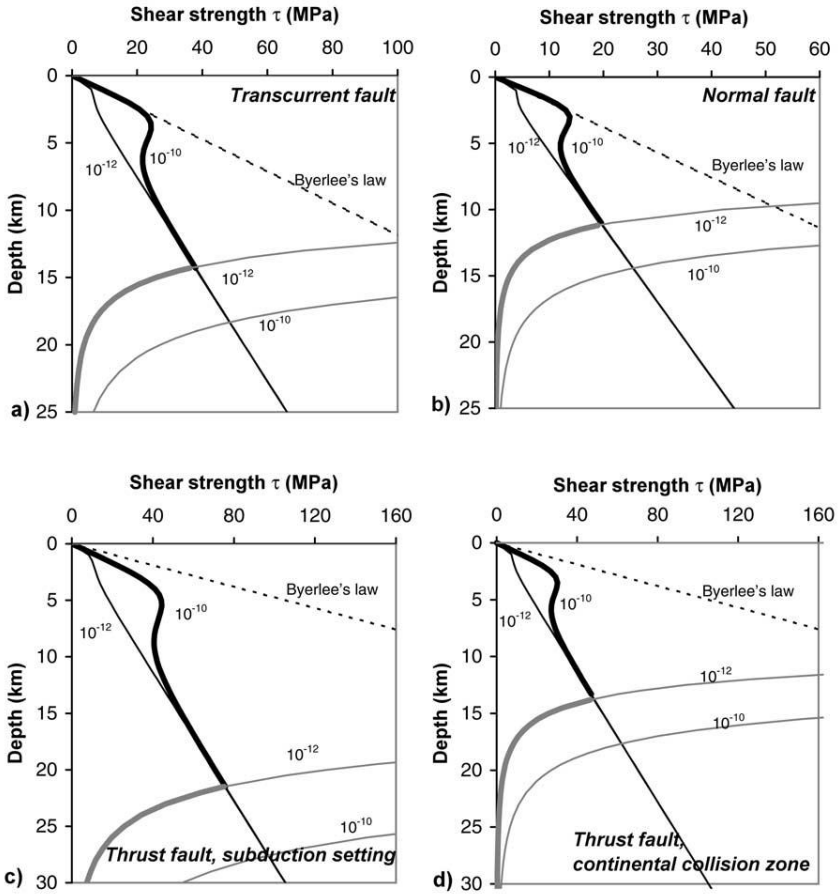

Fig. 2.17 – Comparison between frictional-viscous (FV) behaviour and classic strength envelopes, for different tectonic settings. Note that the thick black solid line representing the FV behaviour is characterized by initial linearity similarly to the frictional sliding mechanism and then by a strength decrease resembling ductile weakening (from Bos and Spiers, 2002).

Given these premises, Zang's equation could be preferentially used since, notwithstanding its limitations, it still provides a larger sample of values for different lithologies. Accordingly, the high pressure brittle fracture rheology can be applied in the rheological modelling even though with some necessary caution and with the only objective of providing more accurate estimates of the strength values around the BDT.

In many cases, however, its application strongly contrasts with the peculiar geological setting of the investigated regions and therefore, even though the equation has been implemented in the computer code (see §3.2.2), the obtained results could introduce errors and bias, especially when applied to other research fields such as seismotectonics and earthquake geology. Consequently, the models produced by including Zang *et al.*'s rheology have not been take into account in the final analyses and applications of the modelling results.

2.2 Strength envelopes

Rheological profiles or strength envelopes were first introduced as a tool for determining the critical strength within the lithosphere in the pioneering works by Goetze and Evans (1979) and Brace and Kohlstedt (1980). Goetze and Evans proposed the use of strength *versus* depth profiles in order to better visualize and analyze the stress and temperature conditions in the bending lithosphere; they also pointed out the great influence that geothermal gradient has on the resulting strength and rheology. Brace and Kohlstedt (1980) defined the boundaries for the range of supported stresses in the lithosphere, using as a constraint the laboratory results and as a tool the strength envelopes first introduced by Goetze and Evans (1979).

Since then, rheological profiles have found application in a wide variety of tectonic, structural, seismological and geodynamic issues. They range from crustal maximum strength and depth for brittle faulting (*e.g.* Sibson, 1982; 1984) and lithospheric integrated strength estimations (*e.g.* Burov, 2011; Tesauro *et al.*, 2013), lithospheric equivalent or effective elastic thickness calculations (*e.g.* Burov and Diament, 1995; Watts and Burov, 2003) and thermomechanical modelling of lithospheric structure (Cloetingh and Burov; 1996) to local-scale investigations on the structural setting and deformation style in peculiar tectonic regions (*e.g.* Lamontagne and Ranalli, 1996; Boncio *et al.*, 2007; Pauselli *et al.*, 2010) and global-scale studies on the correspondence between rheology and seismic behaviour of rocks (Chen and Molnar, 1983; Chen *et al.*, 2013; Maggi *et al.*, 2000; Jackson *et al.*, 2008).

The use of rheological profiles with the final aim of applying them to seismotectonics and earthquake geology investigations, which is the main objective of this research, has been particularly important and central in the classical works of Sibson (1977; 1984) and Scholz (1988, 1989). They both tried to relate the rheological stratification in the crust with the spatial occurrence (or absence) of seismogenic processes (fig. 2.18).

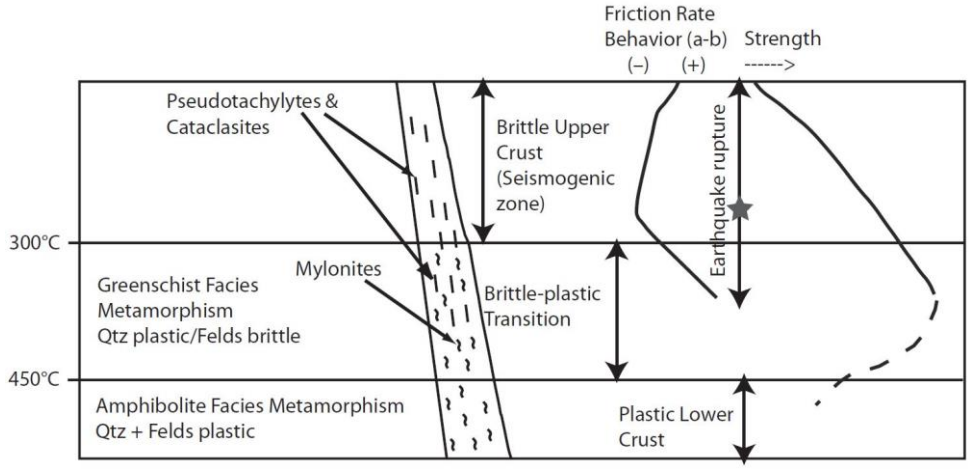

Fig. 2.18 – Schematic representation of a fault zone, relating the rheological behavior with the seismogenic process. A qualitative corresponding strength envelope is also shown (from Allen and Shaw, 2011).

Sibson (*e.g.* 1977; 1983; 1984) focused on the effect that the different deformation styles have on the resulting geological record. In particular, he reconstructed the architecture of fault/shear zone, resulting from the combination of long-term brittle and ductile processes and short-term co-seismic phenomena, as the formation of typical rocks like pseudotachylytes. Their presence is usually considered as a clear evidence that at least one seismogenic process has occurred in the past within the corresponding rock volume.

The core of Scholz's work (1988; 1989) is instead the relationship between rheological properties of the crustal layers and their ability to generate or propagate/arrest a seismic rupture, with particular emphasis on the physical-mechanical aspects of the process. Following the work of Tse and Rice (1986), Scholz (1988) recognized that rocks exhibiting the so-called velocity-weakening mechanism are suitable for earthquake nucleation and rupture propagation while velocity-strengthening results into halting of the seismic rupture process (fig. 2.19).

In his works (Scholz, 1988; 1989), he pointed out that the velocity-weakening/velocity-strengthening transition does not exactly coincide with the brittle-ductile transition, though it could be reasonably approximated to it.

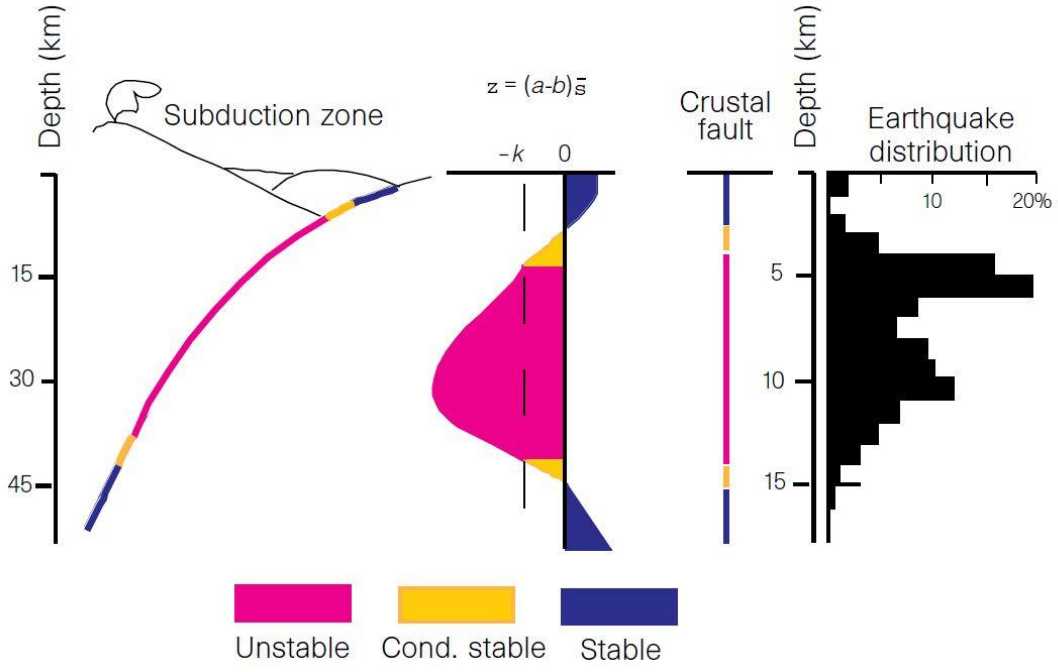

Fig. 2.19 – Correlation between earthquakes depth distribution and frictional stability/unstability fields (from Scholz, 1998).

The conceptual model developed by Scholz (1988; 1989), together with the studies by Dieterich (1978; 1979) and Tse and Rice (1986) on the generation of earthquakes as a function of crustal instabilities related to depth-dependent and varying frictional properties, helped defining

a rigorous physical and mathematical representation of the earthquake process, expressed by the rate- and state-variable friction law (see the review by Scholz, 1998).

His conceptual representation of the rheology of a fault zone distinguishes the brittle layer deforming by frictional and quasi-elastic mechanisms (that he calls *schizosphere*) from the ductile and fully-plastic deforming *plastosphere*. In the former, velocity-weakening is observed and earthquake nucleation is allowed, while in the latter velocity-strengthening characteristics prevail, thus halting the seismic rupture.

The transition zone between the two is characterized by the so-called *conditionally stable behaviour* (I will come back in §5.1.2 to a more detailed description of the bulk rheology of the rocks and its relationships with the physical phenomenon of the seismogenesis) and, even though earthquake nucleation cannot occur within this layer, the downward propagation of a seismic rupture initiated in the *schizosphere* may eventually reach the base of the transition region.

The strength envelopes typically applied to the tectonic, geodynamic and seismotectonic fields are obtained by using the simplified approach, which only considers purely brittle-frictional and fully ductile behaviours. The semi-brittle intermediate rheologies are commonly not considered because of their limited applicability and also due to the increased possible errors and bias that their use would introduce, for the reasons discussed in section §2.1.4.

Such a simplified approach still allows to obtain reliable profiles, in terms of vertical strength distribution in the various lithospheric layers and for the depth of the rheological transitions, thus helping to reconstruct the depth extent of both brittle (potentially seismogenic) and ductile (creep-deforming) layers. The simplified approach has gained particularly wide acceptance with the works of Ranalli (*e.g.* Ranalli and Murphy, 1987; Ranalli, 1995).

He applied the tool of rheological profiles in a variety of fields, ranging from the lithospheric structure and its total strength, the distribution of load-bearing layers within the lithosphere (*e.g.* Ranalli and Murphy, 1987; Afonso and Ranalli, 2004), to the determination of the seismogenic layer thickness through a comparison between crustal rheological layering and the depth of seismicity (*e.g.* Ranalli, 1995).

Moreover, the use of rheological profiles and modelling has been applied in many different tectonic settings (*e.g.* Lamontagne and Ranalli, 1996; Fernandez and Ranalli, 1997; Boncio, 2008; Pauselli *et al.*, 2010; Huet *et al.*, 2011), going from cratonic shields to accretionay wedges, fold-and-thrusts belts and extensional basins, proving that strength envelopes may represent a powerful and useful tool within the various tectonic frameworks, provided that enough data for structural, layering, lithological and thermal modelling are available.

With the simplified approach the strength envelope is realized by taking into account the frictional sliding mechanism for the brittle deformation (eq. 2.7) and power-law creep (eq. 2.9) for the ductile one. In the most simple and typical profile, the predominant behaviour (which for any depth is always the one having the smaller strength value) is the brittle frictional one at

shallow depths. The strength then tends to increase following a straight line, whose slope is determined by the parameters in the frictional sliding equation (eq. 2.7) such as friction coefficient, pore fluid pressure ratio and the tectonic parameter (fig. 2.20).

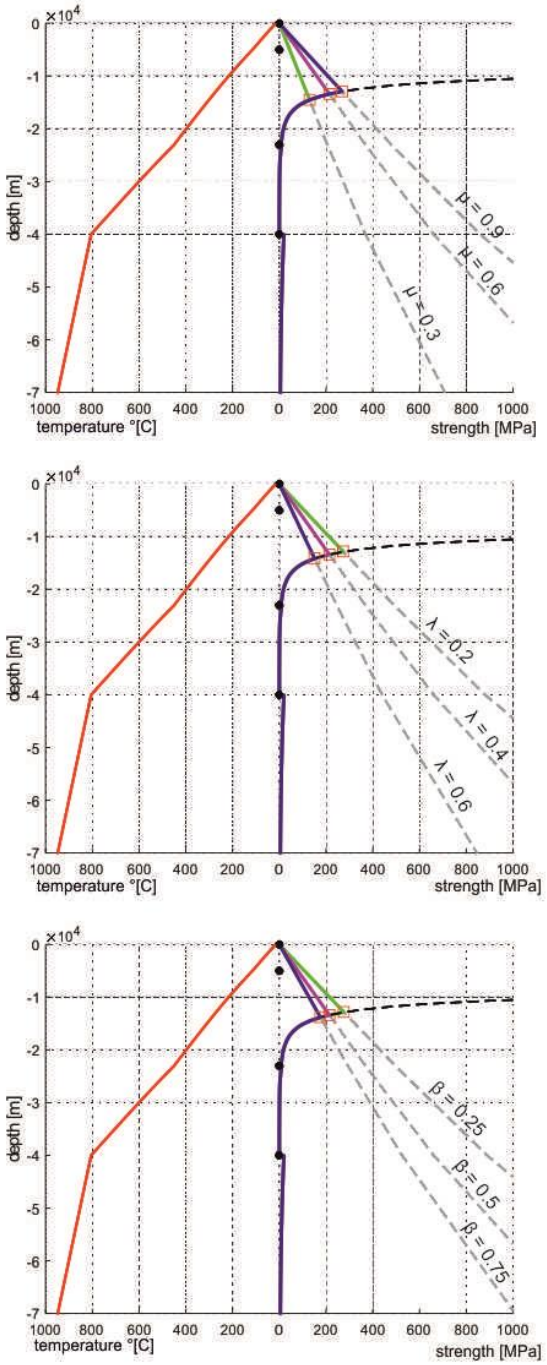

Fig. 2.20 – Variations in the strength envelopes resulting from different input values for, respectively, friction coefficient (μ), pore fluid pressure ratio (λ) and tectonic regime parameter (β).

At a certain depth, mainly depending on the geothermal gradient, the selected lithologies and the strain rate, the lowest strength value becomes the one associated to the ductile creep, which starts being effective and predominant below the brittle-ductile transition where ductile deformation takes place. The brittle-ductile transition (BDT) also corresponds to the depth at

which the maximum (or peak) shear strength is attained along the rheological profile, as long as a simple envelope with a single BDT is taken into account as represented in figure 2.22b. Indeed, at depths greater than the BDT, the shape of the envelope is always determined by the curve of the power-law creep, whose strength tends to exponentially decrease with increasing depth, due to the associated increasing temperature (the latter, unless other external perturbation factors are introduced, always increases with depth).

At even greater depths, the rock strength becomes negligible, as the rocks tend to behave like a fluid and offer a very low shear resistance. The rate of strength exponential decrease, and as a consequence the depth at which the strength becomes almost nil, mainly depend on the geothermal gradient (the higher the temperature at depth, the faster is the strength decrease and the shallower the negligible strength depth).

The area under the curve defined by the strength envelope (both the brittle and the ductile part) graphically represents the total strength of the considered lithospheric column (fig. 2.21).

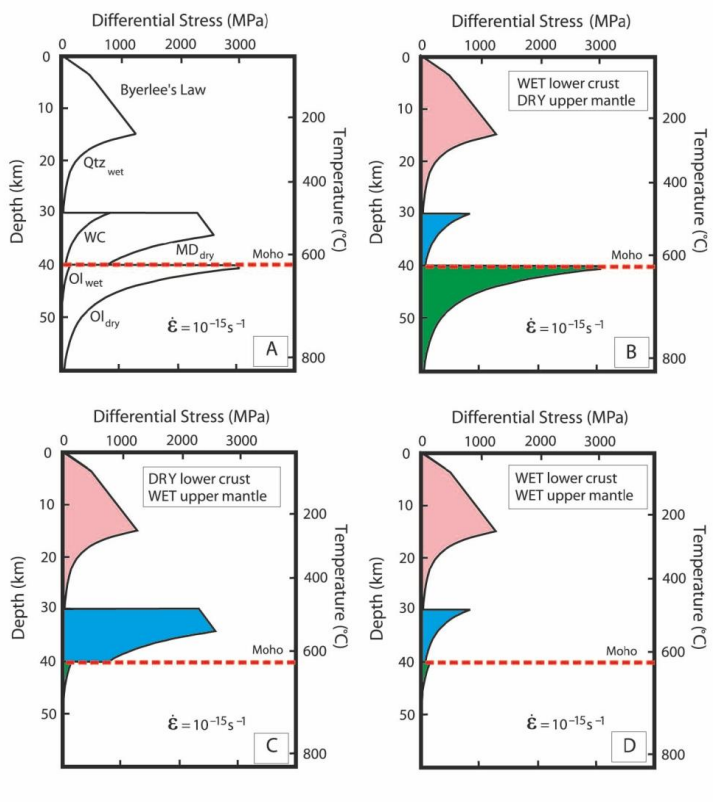

Fig. 2.21 – Different examples of the specific contribution of each layer to the total lithospheric strength. The pink, cyan and green colored areas under the strength envelopes respectively represent the total strength of upper crust, lower crust and upper mantle (from Jackson, 2002).

In order to calculate the value of such total strength, which is measured in $N \cdot m^{-1}$, the shear strength is integrated over depth *z*, down to the maximum depth at which the strength approaches the zero value. Such integrated strength is a useful indicator of the total long-term resistance of

the lithosphere to tectonic or non-tectonic loads and can also be correlated with the thickness of the elastic lithosphere (see *e.g.* Watts and Burov, 2003).

A higher value of total strength is clearly correlated with a greater ability to support long-term stress and a thicker (equivalent) elastic layer, while low integrated strength values may result in permanent deformation of the bulk of the lithosphere, which will behave and flow as a highly viscous fluid in the long-term. The highest values of total strength result from the combination of several different factors, among which the most important ones correspond to a very low geothermal gradient, a compressional tectonic setting, low pore fluid pressure, high friction coefficient and the occurrence of vertically extended crustal layers mainly characterized by mafic lithologies.

According to the vertical distribution of brittle and ductile layers several types of strength envelopes can be recognized (fig. 2.22).

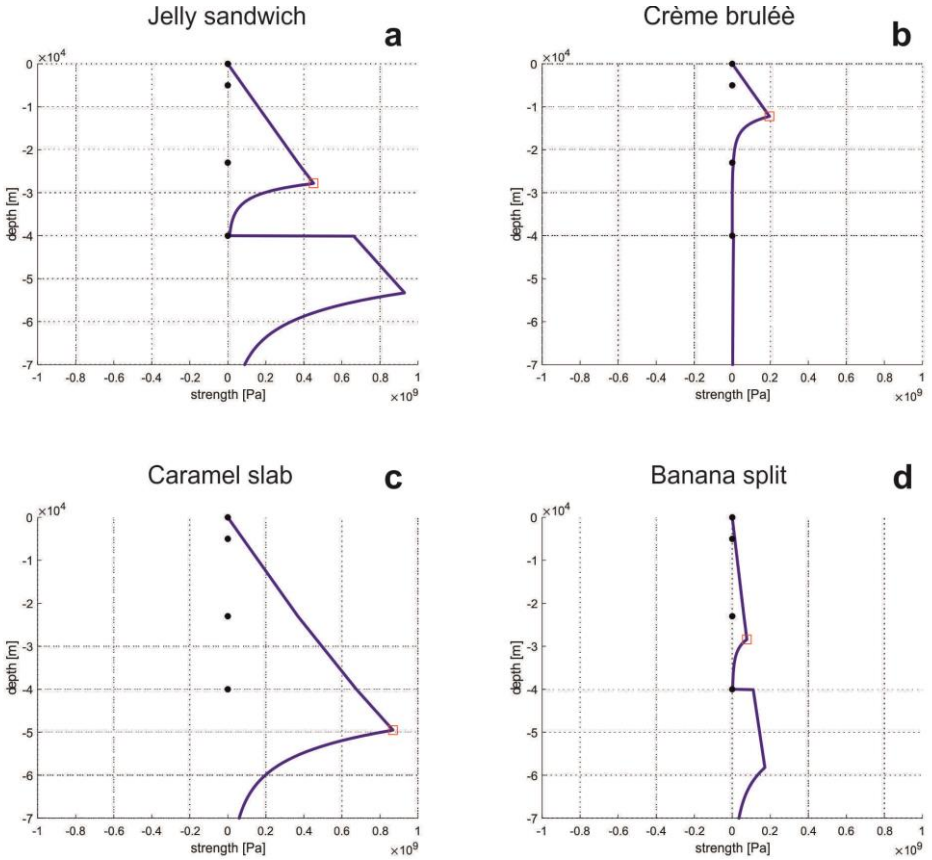

Fig. 2.22 – The different typologies of strength envelopes typically associated to peculiar geodynamic and tectono-thermal settings (see the discussion in the text for details). The red squares indicate the position of the shallowest BDT in each rheological profile.

In the literature, they are typically referred to with peculiar names recalling their main characteristics, so that their acknowledgement and classification can be easily kept in mind.

The so-called *jelly sandwich* model indicates the occurrence of a ductile layer, usually in the lower crust, embedded between two brittle layers, the upper one corresponding to the upper crust and the lower one to the upper mantle. In this view, the upper crust and mantle would represent

the high-strength layers (the "sandwich"), being able to support long-term tectonic or non-tectonic applied stress and in the short-term hosting seismogenic nucleation and propagation. On the contrary, the lower crust would correspond to the "jelly", and would therefore lead to distributed ductile deformation, without being able to sustain high stress values.

The *jelly sandwich* strength envelope (figure 2.22a) has long been associated with the typical continental crust rheological layering (*e.g.* Ranalli and Murphy, 1987; Ranalli, 1995; Chen *et al.*, 2012), even though more recently some authors have questioned its validity for all continental settings and have suggested that it may be appropriate only for describing peculiar settings (Jackson, 2002; Afonso and Ranalli, 2004; Jackson *et al.*, 2008). In particular, its applicability may depend on the tectonic and geological evolution of the considered continental crust and also on its composition (more mafic lithologies in the lower crust may lead to a brittle and resistant layer extending through the entire crust and possibly propagating into the uppermost mantle).

Another relevant factor may be represented by the presence of fluids in the crustal layers and the grade of metamorphism for the lower crust and upper mantle rocks. Indeed, wet lithologies are much less resistant than dry ones and may lead to ductile behaviour if enough fluids are present.

Jackson *et al* (2008) and Maggi *et al* (2000), however, argued that at least for the continental crust beneath Himalaya, the lower crust of Eurasia would be in dry conditions rather than wet (as it is instead usually assumed for many continental settings) and the seismicity occurring at depths as great as 80 km should actually be localized at the base of the lower crust rather than in the uppermost mantle.

The high strength of the lower crust at great depths could therefore make it able to behave in a brittle manner, accumulating elastic energy and finally releasing it through seismicity. Such a high strength and resistance could also be justified by the high-grade of metamorphism of the rocks at those depths, corresponding to (dry) granulite facies and, going into even greater depths, attaining conditions for transformation into eclogite facies.

The resulting rheological profile would therefore be characterized by high brittle strength in the crustal layers and by a weak and ductilely deforming upper mantle. Accordingly, almost the whole lithospheric strength and the ability to support long-term stresses would reside in the upper layers (namely the upper and the lower crust), while the remaining lower part of the selected lithospheric column would only behave in a ductile way, offering no resistance to tectonic and non-tectonic loading. From this point of view, the *jelly sandwich* and the rheological model proposed by Jackson and co-workers (Maggi *et al.*, 2000; Jackson *et al.*, 2008) can be considered as the two opposite end-members in terms of long-term behaviour of the lower crust and upper mantle, being respectively ductile and brittle in the former, while corresponding to a brittle and a ductile layer in the latter.

Chen *et al* (2012) propose a very similar strength envelope for the Himalayan area, with the major difference, with respect Jackson *et al.*'s one (2008), being the extent of the brittle, resistant and potentially seismogenic layer, which in this case would also involve the uppermost mantle. Such a model is referred to by Chen and co-workers (2012) as *caramel slab* (figure 2.22c) and, in their view, it is typically associated with uppermost mantle seismicity, mainly attributable to low geothermal gradients. Indeed, the entire crust would be at temperatures below 350 °C and the uppermost mantle below 700 °C, thus not attaining conditions for ductile flow (dislocation creep) to be effective and predominant as deformation mechanism.

On the contrary, when the considered lithosphere is much warmer, the strength is only expected to reside in the uppermost crustal layer corresponding to the upper crust. Such a model is termed *crème brulée* (figure 2.22b) and it is usually associated to very high geothermal gradients and possibly highly extensional tectonic settings. The brittle and seismogenic layer is therefore only limited to the first 10-15 km of the considered lithospheric column and in particular of the upper crust.

Finally, a further model is the so-called *banana split* one (*e.g.* Burgmann and Dresen, 2008), where the shape of the rheological profile could be similar to the jelly sandwich one (figure 2.22d), though the peculiar feature is represented by the very low absolute values of the strength, being up to 2-10 times smaller than in the other models. The reason for such a decrease is related to the high importance that is attributed in this model to the weak and highly deforming regions in the lithosphere, where the bulk of the total deformation is expected to focus on. In this view, taking into account the low resistance of such shear, fault and weakness zones, the resulting strength only attains values around 100-200 MPa, and additional deformation mechanisms likely play major roles.

In particular, the diffusion creep, which is highly grain-size sensitive, is considered to be much more efficient than dislocation creep as regards the ductile behaviour. Such a choice comes from the consideration that comminution and abrasion processes occurring along major fault and shear zones lead to a sensible grain-size reduction of the involved rocks, thus fostering diffusion over dislocation creep.

Given the possible occurrence of all the above-mentioned different typologies of rheological profiles, in my view it may result simplistic and possibly misleading to try defining a single reference envelope valid and representative for the whole continental crust all around the world. Rather, the most appropriate rheological profile for any investigated region should be carefully selected on the basis of the tectonic setting, the geological evolution and a regionally-averaged geothermal gradient. Accordingly, the resulting profile may locally look similar to the *jelly sandwich* model as well as the *crème bruléè* or the *caramel slab*, without the need to assign *a priori* features of the strength envelope, which are not reflected by the natural occurring rheological properties of the considered region. Time and space variations of the typical

continental crust strength envelope are therefore expected and likely even needed to explain the different observed long- and short-term behaviours, in terms of stress accumulation and strength values, as suggested in Afonso and Ranalli (2004).

In the study area investigated during this Ph.D. research, corresponding to the broader Aegean Region, several different tectonic settings are juxtaposed and therefore various typologies of rheological profiles are expected to occur. As a first large-scale observation, the western continental Greece and whole southwestern sector, comprising both continental collision and oceanic subduction settings, are characterized by a low geothermal gradient and therefore potential brittle layers are expected also at considerable depths, for instance in the mantle: in this case, *jelly sandwich* models, especially for the continental collision zone, may be the most appropriate and likely to represent the rheological conditions of the region. On the contrary, the very high geothermal gradient occurring in the back-arc region of the Aegean Sea and northeastern Greece may result in very low strength values even at intermediate-shallow depths, leading to *crème brulée*-style rheological profiles.

2.3 Geothermal gradient

The knowledge or the estimation of temperature distribution at depth is fundamental for any rheological modelling study, as it greatly affects the resulting rheological behaviour, especially the ductile one, and as a consequence also influences the depth extent of brittlely and ductilely deforming layers. Given these premises, a considerable effort has been devoted to the reconstruction of the geotherms, both in continental and oceanic settings and also to considering the thermal perturbation induced by a cold subducting plate, as occurs along the Hellenic Arc.

As a general rule, a strong geothermal gradient leads to high temperatures at depth, which result into a shallow transition to the ductile behaviour, while on the contrary low geothermal gradients are typically associated with deep BDTs (fig. 2.23). The proxy information that is usually taken into account for estimating, at a first approximation, the thermal distribution and temperature values at depth is the surface heat flow. Since this parameter greatly affects the resulting geothermal gradient (and as a consequence the related strength envelope), a particular care has been dedicated to its description and to the selection of its values for the Aegean Region, which is also dealt with in a dedicated section (§3.1.1). An additional parameter that has to be considered (even though with lesser emphasis, since its relevance and influence on the geothermal gradient is minor with respect to the heat flow), especially for the continental crust, is the radiogenic heat production rate.

In the following, there is a description of the main characteristics of, and differences between, the geothermal gradients in the oceanic and in the continental crust, as both are present in the investigated area and are associated with different thermal properties and processes. One of the

main differences is related to the fact that the geothermal gradient in the continental crust strongly depends on the selected lithology for the various layers, while in the oceanic crust the thermal state mostly derives from the age of the plate itself.

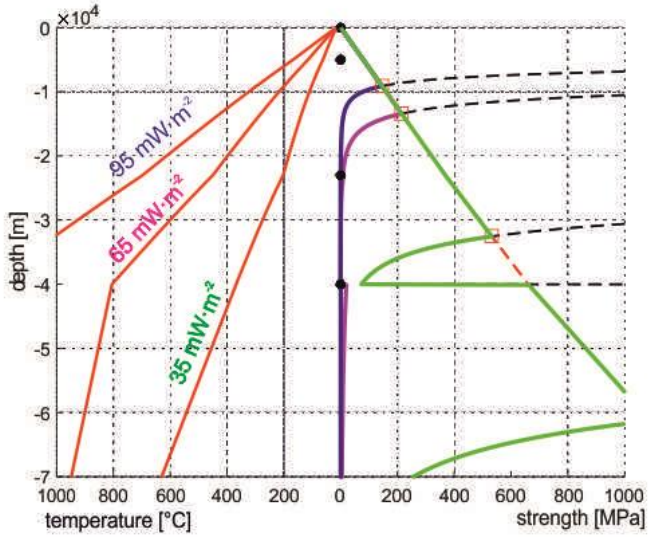

Fig. 2.23 – Effect of surface heat flow values variability on the resulting strength envelopes. Note how a lower heat flow is associated to a thickening of the uppermost brittle layer and may also lead to the occurrence of a deeper one.

Another differentiating factor is represented by the radiogenic heat production, which plays a much bigger role for the determination of the geothermal gradient in the continental crust rather than in the oceanic one.

The geotherm of the oceanic lithosphere is strictly dependent on its cooling age and tends to decrease with time until it reaches a steady-state equilibrium, as indicated by several models (*e.g.* McKenzie *et al.*, 2005) (fig. 2.24).

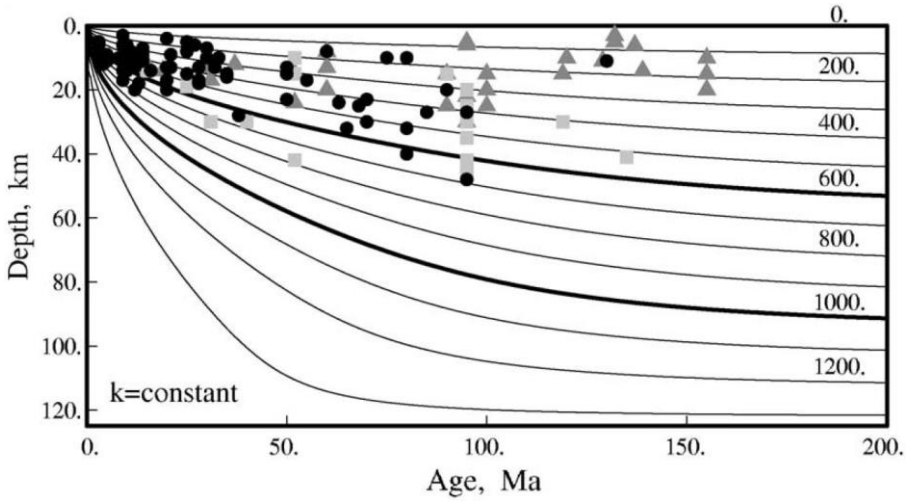

Fig. 2.24 – Isotherms depth variation as a function of the oceanic crust formation age. Values on the right are in °C. The triangle, square and circle symbols indicate, respectively, outer rises normal earthquakes, outer rises thrust ones and intraplate ones (from McKenzie et al., 2005).

On the contrary, the temperature at depth in the continental lithosphere is not just a function of the terrane/platform/plate formation age, but it also strongly depends on the tectonic evolution and, above all, on the occurrence of radioactive elements in the crust, which is clearly related to the lithological composition (see, for instance, Chapman, 1986; Beardsmore and Cull, 2001 among others).

Continental lithosphere usually requires the distinction into different thermorheological layers (here represented by sedimentary cover, upper crust, lower crust, lithospheric mantle), where additional factors (other than the tectonothermal age) could play an important role (Chapman, 1986; Beardsmore and Cull, 2001 among others). This is the case of the occurrence of radioactive elements and their spatial distribution (especially in the crust), as well as the presence of hot igneous intrusions or peculiar structural/tectonic settings (anticlinal structures or rapidly subsiding basins with an aggrading sediment infill having the effect of thermal blanketing) (see, for example, Mareschal and Jaupart, 2013; Lucazeau and Le Douaran, 1985). All these possible phenomena and features should be properly considered for a correct and rigorous thermal modelling. Accordingly, the geothermal gradient in the continental lithosphere is the result of the contributions of a greater number of factors and consequently it could show remarkable heterogeneities and lateral variability (fig. 2.25).

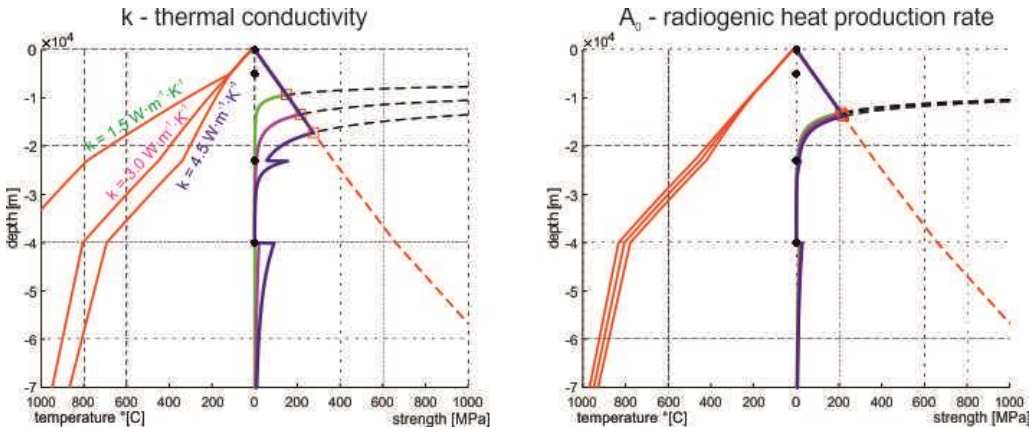

Fig. 2.25 – Variability of continental geotherms (in red) as a function of thermal conductivity (left) and radiogenic heat production rate (right). The resulting different strength envelopes are also shown. Note how a 50% variability with respect to a central reference value for k *is reflected into substantially different geotherms, while similar variations in* A_0 *do not produce significant effects on the geothermal gradients.*

The equation for the calculation of the temperature at depth is the steady-state 1D conductive law, first proposed by Lachenbruch (1968) and then adopted by Cermak (1982):

$$T(z) = T_0 + \frac{(q_0 - A_0 \cdot D) \cdot z}{k} + \frac{A_0 \cdot D^2 (1 - e^{-z/D})}{k} \qquad [2.12]$$

where $T(z)$ is the temperature [K] at depth z, T_0 is the temperature at the top of the considered layer, q_0 is the surface heat flow density [W/m^2], A_0 is the radioactive surface heat production [W/m^3], D is an exponential decay constant, which is also called characteristic depth and has the dimensions of a length [m], and k is the thermal conductivity [W/m·K]. Such an equation takes into account the radiogenic heat production, which is an exclusive feature of the continental lithosphere and it is therefore suited to the thermal modelling of such settings.

In the case of the oceanic lithosphere the contribution of the radiogenic heat production is negligible and therefore the third addend of equation [2.12] is discarded and the resulting simplified equation is:

$$T(z) = T_0 + \frac{q_0}{k} \cdot z \qquad [2.13]$$

The differences in thermal modelling for oceanic and continental lithosphere is also obviously reflected into the resulting strength envelopes. For example, the typical oceanic profile only exhibits a single BDT usually occurring in the upper mantle, with the whole, thin oceanic crust behaving in a brittle fashion. On the contrary, more than one reference profile exists for the continental lithosphere. In all of them, however, at least the shallowest BDT occurs in the crust, and the upper mantle could behave in a brittle or ductile manner mainly as a function of the thermal gradient.

When the shallowest BDT occurs in the upper continental crust, the lower crust is supposed to be weaker and (at least partially) ductilely deforming, while a second deeper brittle layer could sometimes occur in the upper mantle if temperature conditions for peridotite flow at depth are not met. In case of a higher geothermal gradient, only one BDT is observed within the upper crust, while the remaining part of the lithospheric column deforms by ductile processes.

As above-mentioned, the main parameters controlling the geothermal gradient are the surface heat flow, thermal conductivity and radiogenic heat production. Their listed order also reflects the respective relevance and influence on the temperatures at depth and, as a consequence, on the resulting strength envelopes. Their relative importance and the effects that their corresponding variations induce on the 1D rheological profiles have also been tested with a sensitivity analysis, whose results will be presented later (see Chapter 4).

Surface heat flow q_0 is probably the most important factor to consider for thermorheological modelling, and the reason for that is twofold: on one hand, its effective weight on the ductile strength is paramount (Sibson, 1982) and on the other hand, it is possibly the most readily available datum measurable on the Earth surface, acting as a good proxy for estimating deep thermal conditions (Ranalli, 1995). As a general rule, the surface heat flow can be viewed as an

indicator of the tectonothermal and geological history (together with the geodynamic setting) of a given area.

Nevertheless, caution should be paid when treating heat flow data, as they should be thoroughly analyzed and interpreted within their specific geological frame and scale of observation. Indeed, the site specific information recorded at the surface about heat flow does not always correspond to an accurate estimate, or better say proxy, of the actual thermal gradient at depth for the same spot, as surface recordings may be affected by very localized and shallow heat sources, such as hydrothermal vents, fracture-related conduits for deeper high-temperature fluids or even the occurrence of shallow magma chambers, sills and laccoliths (*e.g.* Sibson, 1982).

In all these cases, the surface values may be not really representative of, and strictly linked to, the thermal gradient at depths beyond the main local heat source and this should be carefully kept in mind (see Beardsmore and Cull, 2001 for a thorough review on the possible errors and bias related to heat flow measurements and estimates). In other cases, a high surface heat flow may be representative of a wide and deep heat source, even though the surface value may still lead to an overestimation of the deep thermal conditions as the surface heat flow will tend to manifest and exit the Earth surface through narrow fracture zones and preferential pathways, consequently focusing on these specific spots and locally increasing their value from the depth-averaged one.

Finally, one should also take into account that whenever site specific measurements are not available and interpolated maps are used to derive the surface heat flow, the scale and the informatic tool used for the map interpolation, together with the degree of spike-like peaks filtering and/or smoothing, play important roles on the resulting heat flow values at the regional scale. Moreover, also the possible bias related to the fact that heat flow measurements are more commonly recorded by technicians and scientists where manifest surface evidence of thermal anomalies are observed (which tend to coincide with very localized heat sources, especially in case of hydrothermal and volcanic settings) should be taken into account.

Notwithstanding all these possible complications, heat flow maps still remain one of the most readily available data providing a crucial source of information for thermal (and hence rheological) modelling. In general, high heat flow values increase the thermal gradient and thus decrease the ductile strength, which also leads to a remarkable shallowing of the BDT depth (Sibson, 1984).

The thermal conductivity k is the coefficient linking the thermal gradient ($\Delta T/\mathrm{d}z$) with the surface heat flow q_0, where the relationship is expressed by Fourier's law for the thermal conduction.

Since the main focus of this research is the lithospheric rheology modelling, only conduction has been considered here as the unique truly effective process of heat transfer, while convection

and diffusion start being efficient only in the astenospheric layer (see for example Ranalli, 1995; Turcotte and Schubert, 2014). Fourier's law states that

$$q_0 = -k \cdot \frac{\Delta T}{dz} \qquad [2.14]$$

where the sign "minus" is introduced to represent the fact that heat transfer is directed from the inner portion of the Earth to the surface, as the heat exchange always occurs from the hotter body to the cooler one. Accordingly, by a physical point of view, the thermal conductivity represents an estimate of how "easily" and efficiently heat is transferred to the surface, given a certain thermal gradient.

It has been proven that thermal conductivity is a function of temperature and density of the surrounding rocks (*e.g.* Birch and Clark, 1940), even though such a dependence can be disregarded for thermorheological modelling aims (see Beardsmore and Cull, 2001 among others). Basically, thermal conductivity influences the BDT depth and shear strength values in such a way that, for example, a high k value means that heat is efficiently transferred to the surface and therefore a relatively low thermal gradient is required to fit the surface heat flow (which in principle should be measured at the site of interest). This would result in generally cooler and hence stronger rocks and a consequently deeper BDT.

The radiogenic heat production in a given rock volume is one of the primary sources of heat, especially for the continental, felsic upper crust. Radiogenic heat is the product of the decay of unstable isotopes of some specific elements (Th, U, K among others). Such elements are in general highly incompatible and therefore a differentiated, mostly felsic, continental crust is markedly enriched with them. Such a genetic process for the distribution of the radioactive elements also explains why the mantle, and to a lesser extent the lower crust, being depleted in these unstable isotopes, are characterized by noticeably lower levels of radiogenic heat production.

The radiogenic heat production depth distribution was first described by Lachenbruch (1968), whose equation states that

$$A(z) = A_0 \cdot e^{-z/D} \qquad [2.15]$$

where D is the so-called characteristic depth, that somehow describes how rapidly the radiogenic production decreases going towards greater depths. In most cases, the commonly assumed value is ~8.5 km ±1.5 km (after Pollack and Chapman, 1977). Clearly, A_0 is a function of the bulk lithology and it is also affected by the possible presence of shallow felsic intrusions, whose melt can deliver further amounts of unstable isotopes into the upper crust.

Given certain surface heat flow and thermal conductivity values, a relatively high value of A_0 means that a considerable portion of the total heat transferred to the Earth surface is produced locally (and at shallow depths) by radioactive decay processes and therefore even a relatively high value of q_0 does not necessarily imply a high geothermal gradient. In other words, at a fixed depth, for example the Conrad discontinuity, in case of high A_0 value a lower temperature is expected with respect to the case of a low A_0 value.

Chapter 3: Data and methods

3.1 Input rheological parameters values

3.1.1 Heat Flow

As largely discussed in Chapter 2, temperature exerts a major control on the rheological behaviour of rocks. The surface heat flow density (measured in $mW \cdot m^{-2}$) is usually considered a readily available proxy for estimating the geothermal gradient and, together with thermal conductivity ($W \cdot m^{-1} \cdot K^{-1}$), allows to estimate the temperature at any given depth. Accordingly, a good estimate of heat flow values for the Aegean Region is crucial to the purpose of this research, and a particular care has been devoted to the implementation of a heat flow map covering the entire study area. For the Aegean Region four different literature sources of heat flow data have been collected: Fytikas and Kolios (1979), Taktikos (2001), Hurter and Haenel (2002), Cloetingh *et al*. (2010) (fig 3.1).

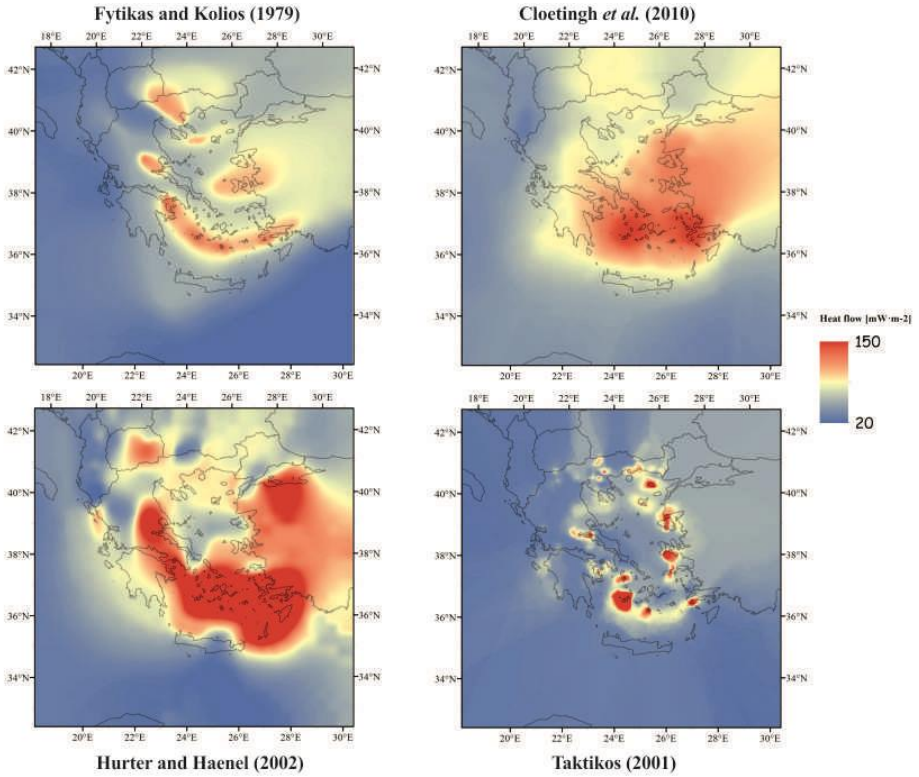

Fig. 3.1 – The various sources used for the realization of the final heat flow map of the investigated area. Note the different degree of smoothing in Cloetingh et al. (2010) with respect to, for instance, Fytikas and Kolios' map (1979). All the maps have been scaled with the same palette and the same minimum-maximum values in order to facilitate their comparison, even though maxima and minima are different for each of them (see text for more details).

The first two (Fytikas and Kolios, 1979; Taktikos, 2001) are only focused on the heat flow distribution over Greece and the broader Aegean Region, while the last two are from European projects and therefore also embrace the western Anatolian area.

Fytikas and Kolios (1979) produced a map with isolines of heat flow obtained from the re-elaboration of previously published data (from Jongsma 1974, Erickson 1970, Hsu *et al.*, 1975) combined with their own measurements. Taktikos' map (2001) has been realized for the IGME (Institute of Geology and Mineral Exploration, Thessaloniki), and it is therefore mostly based on measurements provided by Greek public services (*e.g.* Public Petroleum corporation, Department of Hydrogeology, Department of Energy Resources-Geothermal Energy section of IGME etc.). Since such a work was promoted by the Greek IGME, it is only intended for Greece and therefore it only covers areas inside the national borders. Given that the total area of the map is markedly smaller than those from other works here taken into account (*e.g.* Hurter and Haenel, 2002; Cloetingh *et al.*, 2010), it results in a higher degree of resolution and detail, therefore depicting short-wavelength features, including (small) local peaks and lows.

On the contrary, the maps published by Hurter and Haenel (2002), and Cloetingh *et al.* (2010) (with original data coming from Haenel *et al.*, 1988; Hurtig *et al.*, 1992; Hurter and Haenel, 2002) cover the whole European region and, as a consequence, they are more representative of the long-wavelength features of the heat flow distribution all over the Aegean and the western Anatolian Regions. Overlapping and exploiting the information from these two types of heat flow maps allows to properly take into account both the local features and variations as well as the large-scale trends of the heat flow over the broader Aegean Region.

The collection of heat flow data has then been extended to the western Anatolia area (partially covered by Hurter and Haenel, 2002; Cloetingh *et al.*, 2010) in order to obtain a more complete and extended view of the heat flow distribution in the study area. Two maps, respectively from Tezcan and Turgay (1989) and Akin *et al.* (2014), have been considered for the western Turkey area.

All the maps have been loaded in a GIS environment as rasters, and then properly geo-referenced. As a following step, the contour lines have been vectorialized as *shape* files locally completing the interpolation by connecting separate segments. The vectorialized contours for the entire investigated region have been then used for producing a new raster containing the numerical information and representing the distribution of the heat flow. The *Topo to Raster* tool has been applied selecting a cell size of 10x10 km. All rasters have been produced and georeferenced in the Greek Grid coordinate system. As a last step the arithmetic mean between all the heat flow rasters has been calculated on the basis of the Cell Statistics tool.

The final extent of this averaged heat flow map is 1150×1150 km in the Greek Grid coordinate system, with the cell size of 10×10 km. This final output evidences the presence of an high heat flow arcuate-shaped belt in the central Aegean reaching maximum values around the

islands of Milos to the west (~180 $mW \cdot m^{-2}$) and Nisyros to the east (160 $mW \cdot m^{-2}$). The western Anatolia region is characterized by moderate to high values, while the lowest values (around 25-30 $mW \cdot m^{-2}$) are observed in the northwestern sector of the study area (Albania, Epirus, Ionian Sea and western Peloponnesus).

Some of the maps presented above, and in particular the ones specifically focused on the Aegean Region from Taktikos (2001) and Fytikas and Kolios (1979; herein after FK79), actually show some very elevated peaks of high heat flow values which are to be attributed to measurements close to geothermal/hydrothermal vents or volcanic cones. Such measurements, at least to some extent, are biased with respect to the larger area/region where the measurement site belongs, because the vents or cones represent preferential pathways for the heat to escape. In this way, too concentrated measurements with respect to the actual areal distribution of the heat flow are collected and some corrections should be taken into account when working with these data.

In order to correct for such a bias I applied a Gaussian filter to the maps of Taktikos (2001) and FK79. Such a filtering allows to cut out both the minimum and the maximum peaks values, so that a much more smoothed map is obtained. The filtering and smoothing technique is carried out by analyzing each cell and and the nine cells around it in order to apply the filter. For the implementation of the filtering procedure the specific Surfer GIS software from Golden Software has been used, as it allows to easily perform such raster smoothing techniques. Different degrees of smoothing can be obtained by applying the Gaussian filtering multiple times. Indeed, the repetition of the filtering technique allows to further reduce the magnitude of the extreme peaks and their difference with respect to the average values, so that the final outcome resembles the initial intent of discarding the biased extreme values. In this way a more equilibrated map with the peaks being diminished in absolute values and the highs and lows in the heat flow being spread over larger areas, as they are more likely to effectively be, is finally obtained.

In order to take into account both the short- and the long-wavelength variations of the heat flow, the maps by FK79, Hurter and Haenel (2002; hereinafter HH02) and Cloetingh *et al.* (2010; hereinafter Cl10) have all been considered for realizing a synthesis map. To do so, some different averaged and weighted maps have been produced. In one of such maps all the different values from the various sources of data have been considered and a simple arithmetic mean has been calculated. In other rasters instead, a specific and different weight has been associated to each source, usually taking into account the fact that the FK79 one is specifically designated for and focused on the Aegean Region and therefore has been assigned a higher weighting factor than the others.

The weighting factors are then simply used as multipliers for each value from the different sources of data and thus a weighted average is performed in order to obtain the final map. In particular, maps resulting from a 50% FK79, 25% HH02 and 25% Cl10, as well as 67% FK79, 33% Cl10 and 75% FK79, 25 % Cl10 have been produced. The latter, since it takes into account

the most authoritative sources for the surface heat flow distribution in the Aegean Region and also assign a greater weight to the values of the FK79 specifically designated map, has been selected as the representative one for the subsequent modeling (fig. 3.2).

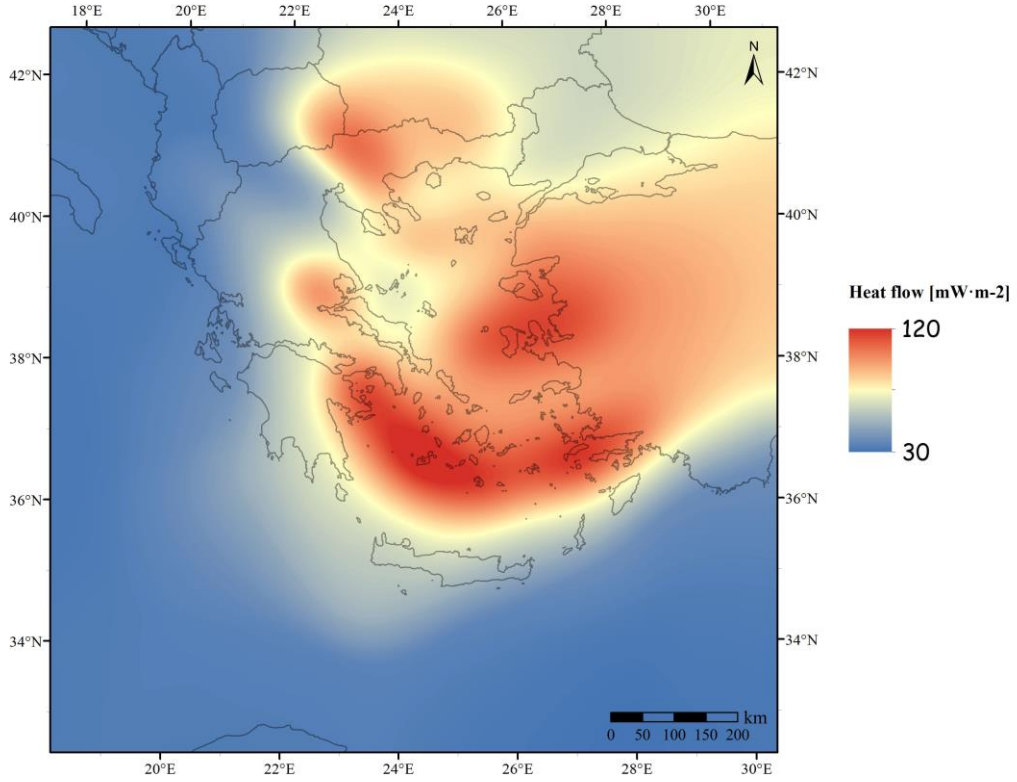

Fig. 3.2 – Surface heat flow map adopted for the reconstruction of the reference rheological model of the Aegean Region, resulting from the weighted average of Fytikas and Kolios, 1079 (75%) and Cloetingh et al., 2010 (25%).

Accordingly, the corresponding areal layer of the heat flow, in the form of a raster, has been produced and then transformed into an ASCII file in order to be used and implemented in the Matlab code. Nonetheless, if one would like to include any other sources of data, the relative rasters could be easily realized and the code readily updated.

3.1.2 Strain rate

The strain rate ($\dot{\varepsilon}$), *i.e.* the velocity at which volumes of rocks are deforming, plays a crucial role in the determination of the BDT depth. The strain rate, which is defined as the total deformation of a body during a finite amount of time (and it is accordingly expressed in terms of s^{-1}), is directly involved in the calculation of the ductile strength and consequently it affects the depth of occurrence of the BDT.

However, its weight on the BDT position is markedly lower than that of the heat flow (as it will be discussed later in Chapter 4). Nevertheless, the role played by the strain rate has to be carefully taken into account as well, especially in crustal weakness regions, (*e.g.* fault zones)

where deformation tends to be highly concentrated over relatively limited volumes, therefore leading to high values.

Since the strain rate appears in the numerator of the equation relating the ductile strength with the temperature (depending, on its turn, on the depth), an increase in the strain rate leads to an increase of the ductile strength, given a certain depth. This, in turn, affects the BDT depth, which tends to increase since, looking by a simple graphical point of view, the intersection between the brittle strength and the ductile strength curves occurs at greater depths. To sum up, it can be said that the strain rate is positively correlated with the BDT depth.

By a mathematical point of view, the strain rate is described by a 3×3 tensor. However, on the assumption that the vertical (*z*) dimension in our model is (at least) one order of magnitude smaller than the horizontal dimensions (*x, y*) of the study area, the strain rate can be approximately described by a 2×2 tensor, where the *z* vertical dimension is neglected (see *e.g*. Jackson and McKenzie, 1988). The horizontal strain rate tensor components are

$$\begin{vmatrix} \dot{\varepsilon}_{xx} & \dot{\varepsilon}_{xy} \\ \dot{\varepsilon}_{yx} & \dot{\varepsilon}_{yy} \end{vmatrix}.$$

Since the strain rate tensor is a symmetric tensor, it can be diagonalized. The diagonalized tensor is an equivalent form of the original tensor, where the off-diagonal components are null and the directions of the two eigenvalues $\dot{\varepsilon}_1$ and $\dot{\varepsilon}_2$ are perpendicular to each other. The reference system of the original and the diagonalized tensors are different but there exist some quantities (invariants), which remain constant for a given tensor, independently from the reference system.

The diagonalized (or reduced) tensor, whose components are termed principal strain rates (with the principal axes orientations corresponding to those of the eigenvectors), can be obtained by solving for the roots of a second grade equation having as a variable the quantity λ which has to be subtracted to the original values of the components of the tensor. The equation is obtained by equalizing to zero the determinant of the tensor

$$\begin{vmatrix} \dot{\varepsilon}_{xx} - \lambda & \dot{\varepsilon}_{xy} \\ \dot{\varepsilon}_{yx} & \dot{\varepsilon}_{yy} - \lambda \end{vmatrix}$$

The eigenvalues $\dot{\varepsilon}_1$ and $\dot{\varepsilon}_2$ of the diagonalized tensor correspond to the solutions of this equation, while the direction of the principal axes is given by the following equation

$$\varphi = -\frac{1}{2}\arctan\left(\frac{\dot{\varepsilon}_{xy}}{\dot{\varepsilon}_{xx}-\dot{\varepsilon}_{yy}}\right) \qquad [3.1]$$

where φ is the azimuth (angle to the geographic north) of the eigenvector corresponding to the greatest eigenvalue. The convention is that a positive eigenvalue corresponds to an elongation while negative values represent contractions.

For the purpose of this work, corresponding to the determination of the BDT depth in the broader Aegean Region, several different datasets of strain rate values have been taken into account, even though the final input values come from a single source, for areal coverage and coherence all over the study area reasons. I focused particularly on the two following datasets: the first one is from Hollenstein *et al.* (2008), while the second one is from Kreemer *et al.* (2014). Both working groups provide data comprising geographical coordinates and relative $\dot{\varepsilon}_1$, $\dot{\varepsilon}_2$ and azimuth angle, while only Kreemer *et al.* (2014) also furnish the values of the components of the original non-diagonalized tensor, *i.e.* $\dot{\varepsilon}_{xx}$, $\dot{\varepsilon}_{yy}$, $\dot{\varepsilon}_{xy}$.

Hollenstein *et al.* (2008) use GPS data from 1993 to 2003 to derive a velocity field, which is then converted into a strain rate field using the method of collocation of Kahle *et al.* (2000). GPS measurements in Kreemer *et al.* (2014) cover a time span from 1996 to 2013; in this case, the GPS-derived velocity field is converted into a strain rate field applying the method of Haines and Holt (1993). In both cases, the original data of strain rate values are used to obtain the second invariant of the strain rate tensor, which represents the 'magnitude' of the total strain rate of a certain deforming region. The second invariant is defined as

$$\dot{E}^{II} = \sqrt{\dot{\varepsilon}_1^2 + \dot{\varepsilon}_2^2} \qquad [3.2]$$

or alternatively

$$\dot{E}^{II} = \sqrt{\dot{\varepsilon}_{xx}^2 + \dot{\varepsilon}_{yy}^2 + 2\dot{\varepsilon}_{xy}^2} \qquad [3.3]$$

When using the second invariant as representative of the strain rate of a certain region without considering the orientation of the axes, the important assumption that all the structures (in the crust) accommodating the deformation are favourably oriented relative to the axes directions is made.

The two datasets provide strain rate values in terms of nanostrain/year, which have then been transformed in s^{-1}. Successively, the second invariant has been calculated using the first of the two above-mentioned definitions (reduced tensor components). In the case of Kreemer *et al.* (2014) data, since some regions (*e.g.* southern Aegean) that actually have almost not been deforming in recent times have been attributed values equal to zero, in order to be able to calculate the ductile strength in any case, the points with the second invariant equal to zero have been

modified and assigned a conventional value of 0.05 nanostrain/year, that is half of the lowest value of the second invariant for any other point in the study area.

The datasets have then been imported in a GIS environment where, using a triangulation interpolation method, the two corresponding rasters (with 10×10 km cell dimensions) of strain rate second invariant values have been realized. The data from Hollenstein *et al.* (2008) are regularly spaced over a mesh of 0.5°×0.5° while strain rate values in Kreemer *et al.* (2014) are given every 0.1°×0.1°. Given the higher resolution and the greater areal coverage, Kreemer *et al.*'s (2014) values have been preferred over Hollenstein *et al.*'s (2008) ones and have been therefore adopted in all the following calculations for the modelling (figs. 3.3 and 3.4).

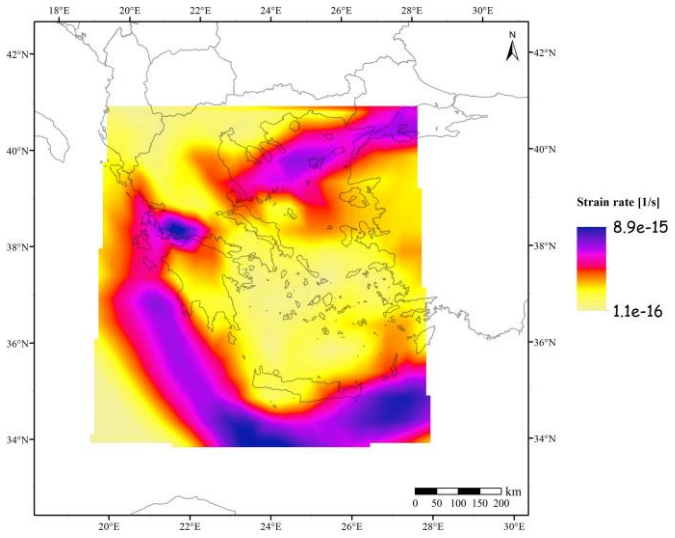

Fig. 3.3 – Strain rate map obtained by interpolating (triangulation) the geodetic data by Hollenstein et al. (2008).

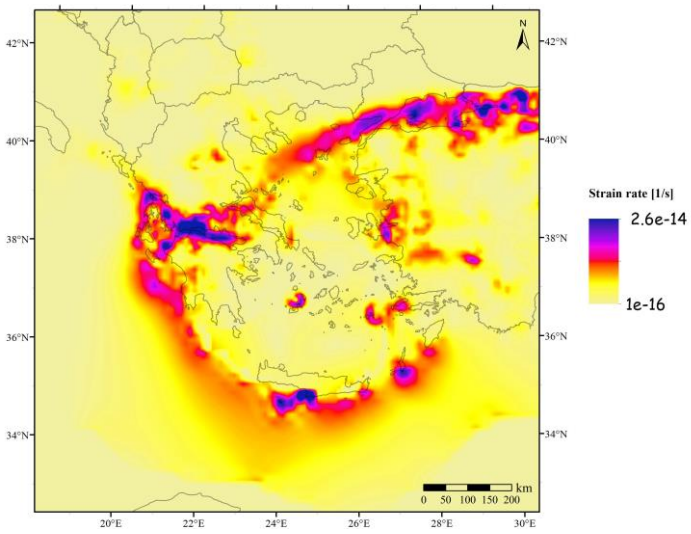

Fig. 3.4 – Strain rate map obtained by interpolating (triangulation) the geodetic data by Kreemer et al. (2014) and then adopted in the reference model. Note the higher maximum values with respect to figure 3.3

Additional datasets and works on the geodetic strain rates for the Aegean Region have also been considered, in order to compare the values and verify whether they would show a good agreement and could therefore be adopted as effectively representative values. More specifically the works of Floyd *et al.* (2010), Kahle *et al.* (1998), Chousianitis *et al.* (2015) and England *et al.* (2016) have also been taken into account (fig. 3.5).

Floyd *et al.* (2010) used both survey-mode and continuous GPS measurements from 1991 to 2009 to derive a geodetic strain rate field for the Aegean Region. Their final results indicate that relatively high strain rates (greater than 120 nanostrain/year) are only attained in the region around the Corinth Rift. Kahle *et al.* (1998) focused more on the Aegean Sea region and used data from the period 1988-1996. They obtained higher deformation rates than Floyd *et al.* (2010), with the maximum values of the strain rate field attaining ca. 170 nanostrain/year along the North Aegean Trough.

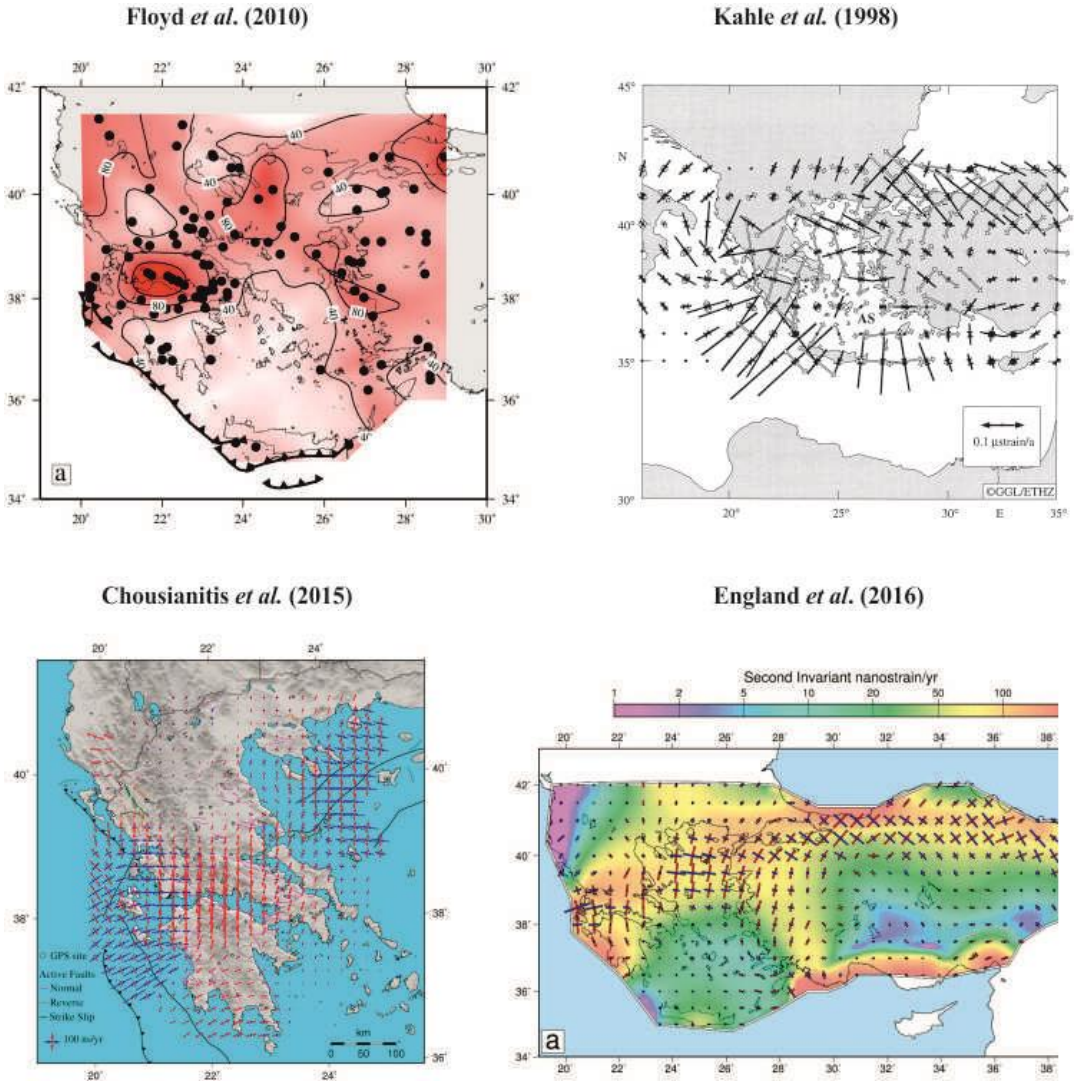

Fig. 3.5 – Strain rate maps from (clockwise): Floyd et al. (2010); Kahle et al. (1998); England et al. (2016); Chousianitis et al. (2015).

Chousianitis *et al.* (2015) also used continuous GPS observations to derive a velocity field and a deformation pattern for the Aegean Region. They found out that the maximum strain rate values characterize the western Corinth rift, with values up to 226 nanostrain/year. Finally, England *et al.* (2016) based their calculations and analysis on measurements from 346 GPS sites, in order to minimize the errors. Their geodetically derived strain rates attain maximum values of ca. 150 nanostrain/year and are in fair agreement with the results of their rheological model of lithosphere deformation, which indicates maximum strain rates in the order of 100 nanostrain/year in the regions of the Corinth Rift/Ionian Islands and along the North Aegean Trough.

As shown above, some variability and differences between the data provided by different research groups for the strain rate values of the Aegean Region do actually exist, but the main features are quite well defined and highlighted in each of the above-mentioned works, even though different calculations methods are applied. The values of Kreemer *et al.* (2014) nicely depict such main features in terms of strain rate values distribution over the study area, and fit quite well the range of values provided by the other works, thus confirming their reliability for being adopted into further calculations, as it has been done here for the rheological modelling.

3.1.3 Crustal thickness of the upper plate and LAB depth

As already pointed out in the section dedicated to the description of the geodynamic framework of the Aegean Region (Chapter 1), the study area is characterized by the presence of the Hellenic subduction zone, along which the lower subducting Nubian/African plate and the upper overriding Aegean/Eurasian plate converge. The geometry of the plate interface, *i.e.* the slab top, has been obtained by merging the data and models from Bocchini *et al.* (2018) and Halpaap *et al.* (2018), both based on tomographic velocities reconstructions and relocated seismicity (fig. 3.6). The work by Bocchini *et al* (2018) deals with the Hellenic subduction zone reconstruction for the whole Aegean Region (fig. 3.6a), while Halpaap *et al.* (2018) are more focused on the Western Hellenic subduction zone geometry (fig. 3.6b). The two plates above and below the subduction interface present different crustal structure, whose peculiarities have been implemented in the Matlab script for the rheological modelling. Accordingly, I will describe the crustal characteristics of each plate (both in terms of structure/thicknesses and lithologies) in separated sections. The current one is focused on the crustal structure of the upper Aegean plate.

In order to determine the crustal thicknesses of the upper plate for the realization of the simplified geological model to be implemented in the Matlab code, I first took into account all the available literature data on the depth of the Moho discontinuity, as a starting point. Indeed, quite a good number of geophysical surveys investigating the crustal structure of the Aegean Region are available. Moreover, the information retrieved on the depth of the Moho discontinuity is generally much more reliable and precise than that relative to the Conrad or any other internal

crustal discontinuity and therefore I preferred to base the reconstruction of the crustal model on the Moho position.

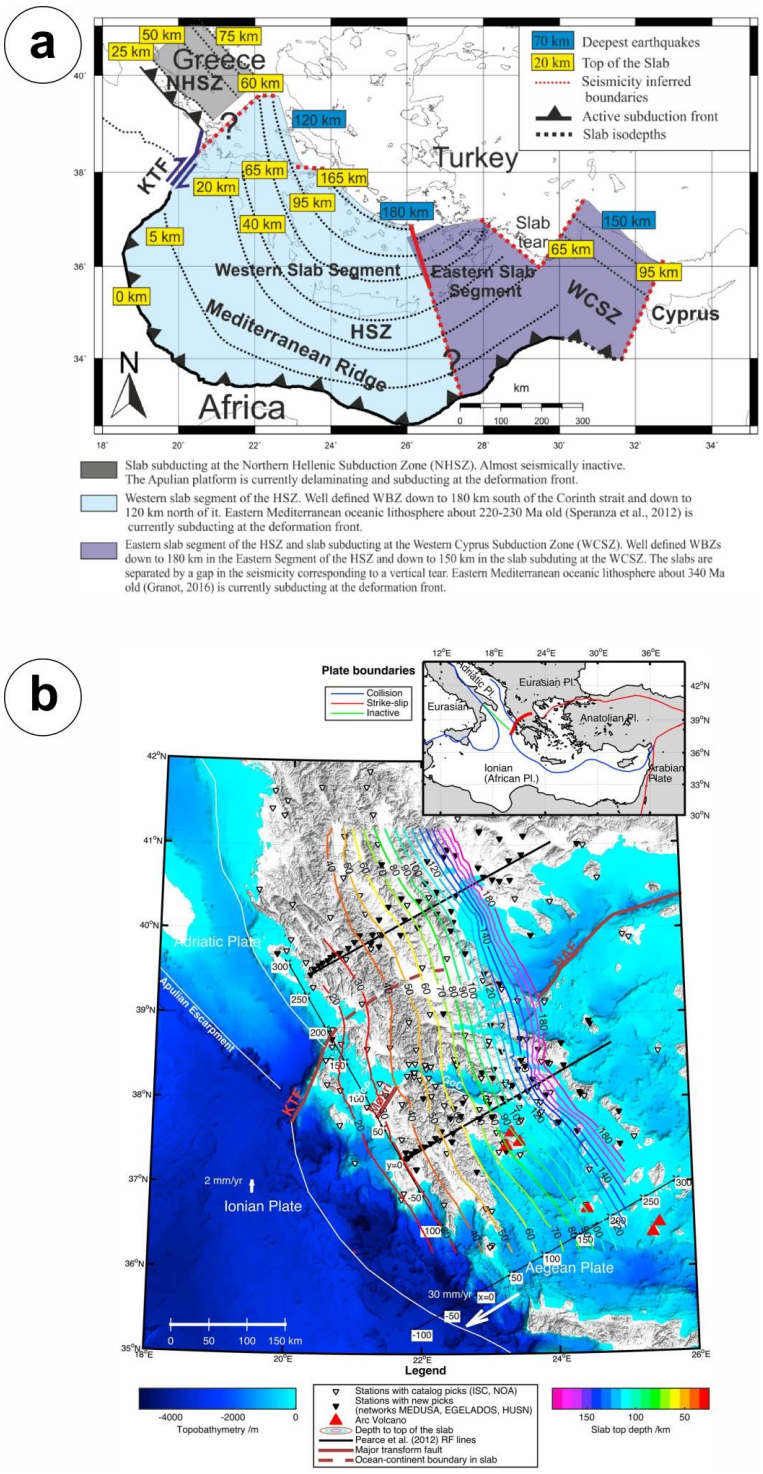

Fig. 3.6 – Slab top depth and Hellenic subduction zone geometry according to: a) Bocchini et al. (2018); b) Halpaap et al. (2018).

In order to get a comprehensive view on the crustal structure and Moho depth of the Aegean Region, literature works and data obtained applying as many different geophysical methods and techniques as available, ranging from seismic tomographies, reflection, refraction and receiver

functions to gravity data inversion, have been considered (Makris *et al.*, 2013; Grigoriadis *et al.*, 2016; Sodoudi *et al.*, 2006; Zelt *et al.*, 2005; Tiberi *et al.*, 2001, Tirel *et al.*, 2004).

The work by Makris *et al.* (2013) is based on gravimetric measurements inversions constrained by seismic reflection and refraction data. Since it provides a Moho depth map (fig. 3.7) and also a sediments thickness one (fig. 3.8) for the whole broader Aegean Region, which result from the conjunct use of different geophysical data and inversion techniques, it can be considered as a reliable and useful source of data.

Accordingly, I relied primarily on Makris *et al.* (2013) work for determining the crustal structure in the study area, and in particular for defining the depth of the Moho along the Hellenides, in the rest of continental Greece and in the back-arc Aegean Sea region.

The Hellenides fold-and-thrust belt is characterized by a crustal thickening due to the presence of a crustal root beneath the mountain belt itself, related to the nappe stacking that led to the orogenesis. As a consequence, the Moho depth along the Hellenides, according to Makris *et al.* (2013) reaches a depth of ca. 40 km. On the contrary, the remaining sectors of continental Greece and the back-arc region corresponding to the Aegean Sea are associated with very a shallow Moho, being respectively around 30 and 20 km deep, with minimum values also as low as ca. 16 km in the central-southern Aegean Sea (fig. 3.6).

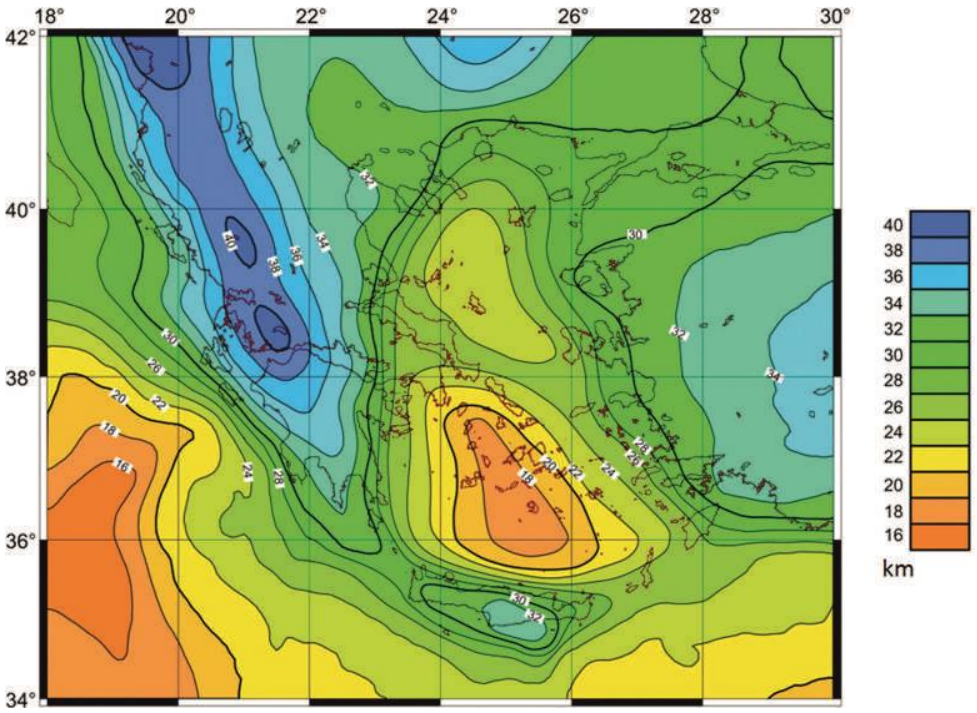

Fig. 3.7 – Moho depth in the Aegean Region (from Makris et al., 2013).

Here the Miocene to present extensional stage has led to diffuse normal faulting and locally to the development of metamorphic core-complexes (*e.g.* the Cycladic core complex in the central-southern Aegean Sea) and low-angle normal faults, which all together contributed to a

considerable crustal thinning, as indicated by both gravity and seismic data in the work of Makris *et al.* (2013).

Sodoudi *et al.* (2006) used teleseismic P and S waves receiver functions in order to image the depth of the Moho in the Aegean Region. They found out fairly consistent values with the ones of Makris *et al.* (2013), with maxima of ca. 40 km along the Hellenides and minima of ca. 20 km in the southern Aegean.

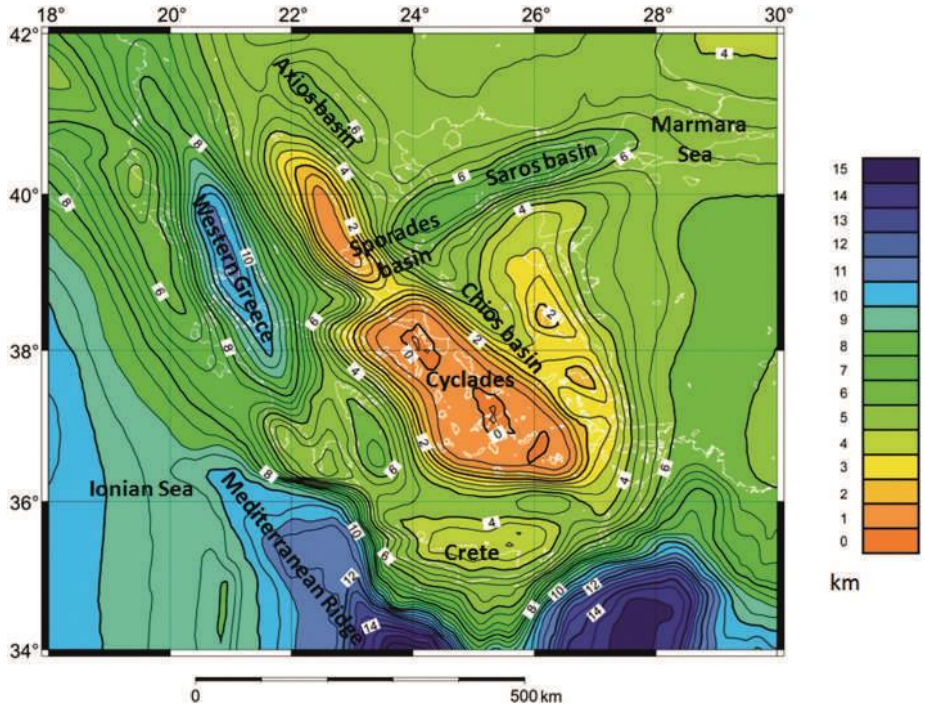

Fig. 3.8 – Thickness of the sedimentary cover in the Aegean Region (from Makris et al., 2013).

Grigoriadis *et al.* (2016), Tirel *et al.* (2004) and Tiberi *et al.* (2001) modelled the Moho topography through the use of gravity data inversions. The former provided results for the whole Aegean Region, with values going from ca. 45 km in the western continental Greece and Corinth Rift regions to slightly less than 20 km in the southern Aegean and Cretan Seas. On the contrary, the last two focused on specific areas, being respectively the Aegean and Cretan Seas regions (average values ~25 km and minima of ca. 22 km in the Cretan Sea) and the Corinth Rift region (maximum values around 40 km in the western Corinth Rift and minimum values of ca. 25 in the eastern sector).

Finally, also Zelt *et al.* (2005) concentrated on the Moho topography and crustal structure around the Corinth Gulf area, with maximum values around 40 km in the western sector (and an average Moho depth of ca. 37 km beneath the Hellenides) and down to 25 km moving eastwards, but they used seismic refraction and reflection traveltimes in order to depict the crustal structure on the basis of the obtained velocity models.

The work of Sodoudi *et al.* (2006) has been also taken into account for what concerns the estimation of the lithosphere-asthenosphere boundary (hereinafter LAB) depths of both the

Aegean and the African plate. The LAB depth furnish information on the thickness of the corresponding plate and therefore represents a relevant parameter, especially with regard to the features of the thermal gradient in the mantle and of the total lithospheric strength. Indeed, a very deep LAB usually implies a low geothermal gradient in the lithospheric mantle and is also typically associated with high values of integrated lithospheric strength.

Sodoudi *et al.* (2006), using the S waves receiver functions, estimated a LAB depth and an equivalent lithospheric thickness of ca. 150 km for the Aegean plate below continental Greece (fig. 3.9).

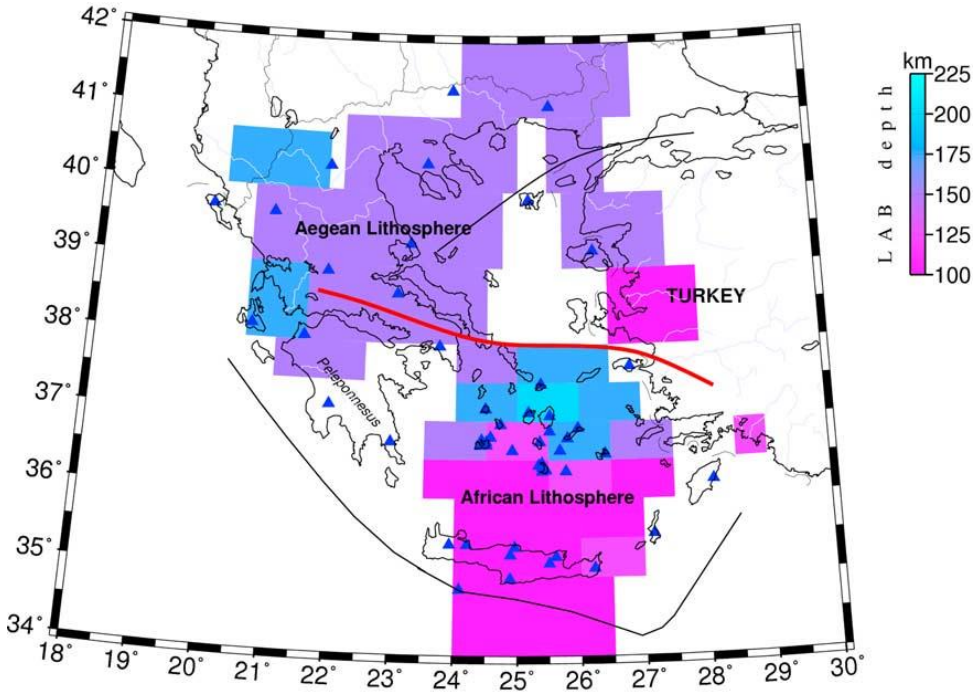

Fig. 3.9 – LAB depth for the Aegean plate, estimated from S receiver functions (from Sodoudi et al., 2006).

For determining the thickness of the lithosphere in our model, the values proposed by Gung *et al.* (2003) have also been considered. They used shear waves velocities in order to estimate the depth of the LAB and obtained depths around 100 km for the Aegean Region. Such a value lies in between and it is consistent with the ones proposed by Sodoudi et al. (2006) for the Aegean block and the African plate, also keeping in mind that Gung *et al.* (2003) did not differentiate between and did not indicate specific different values for the two plates.

A further source of data that has been considered for the thickness of the lithosphere in the study area is the model by Artemieva *et al.* (2006), where different geophysical techniques, methods and surveys (seismics, magnetotellurics, electromagnetics and thermal and gravity intepretations) have been merged and integrated in order to obtain a lithospheric structure model of the whole European continent and neighbouring regions. Their results indicate a varying thickness of the lithosphere in the broader Aegean Region, anyway always comprised between

100 ±25 km and 150 ±25 km (the maximum values are attained along the Hellenides fold-and-thrust belt).

However, both Artemieva *et al.* (2006) and Gung *et al.* (2003) works are realized at a very large scale (respectively, continental and global) and therefore may lack some resolution and precision in defining the depth of the LAB and its lateral variations. Accordingly, in order to determine the thickness of the lithosphere for the purpose of this work, a greater weight and consideration has been assigned to the values proposed by Sodoudi *et al.* (2006), since their work is specifically set for, and focused on, the Aegean Region, while the other works have just been taken into account as a confirmation and general indication, given their larger scale with lesser precision nature.

Once identified the depth of the LAB and above all of the Moho, which represents the base of the crust, I proceeded to determine the thickness of the internal mechanical-rheological layers which make up the crust, namely the sedimentary cover, the upper crust and lower crust. From now on I will refer to the combination of upper and lower crust as the crystalline crust, in order to distinguish it from the general term 'crust' which usually includes also the sedimentary layer. The thickness of the latter, which results from the difference between the depths of the bathymetry/topography (data from Becker *et al.*, 2009) and the depth to the crystalline basement (*i.e.* the contact between the sedimentary cover and the crystalline crust) has also been defined mainly following the data and the relative map proposed by Makris *et al.* (2013).

Their results indicate considerable thickness of the sedimentary cover in correspondence of the Hellenides fold-and-thrust belt from the Epirus to the Peloponnesus, with maximum values around 11 km. The greatest thicknesses in the whole broader Aegean Region are actually encountered around the Mediterranean Ridge, where the fast development of the rapidly growing accretionary prism has led to a sedimentary cover as thick as 15 km. A further region with noticeable thickness of the sedimentary layer is the area around the North Aegean Trough, where values up to ca. 7 km are attained. On the contrary, in the central Aegean Sea regions, where the Cycladic core complex development since Miocene times has led to the exhumation and direct outcropping of the crystalline basement (*i.e.* the upper crust lithologies), the sedimentary cover is absent and consequently its thickness is locally equal to zero or close to it.

For what concerns the subdivision of the crystalline crust into upper and lower one, no regional-scale and reliable information on the depth of the Conrad transition, which is generally considered as the discontinuity surface between the two layers, is available for the Aegean Region. Moreover the Conrad discontinuity: i) is not as easily detectable and laterally continuous as the Moho surface and ii) is not unanimously considered by the scientific community as the effective transition between upper crust and lower crust layers, since its physical meaning is not always clear and may therefore be related to other variations rather than lithological ones.

Accordingly, the depth of the upper-to-lower crust transition and consequently the thicknesses of the two crustal layers (fig 3.10) have been assigned following the global-scale estimates of the lower crust-to-crystalline total crust thickness ratio proposed by Rudnick and Fountain (1995) and Rudnick and Gao (2003). Such a ratio is in the order of 0.4-0.45; accordingly the thickness of the crystalline crustal layers has been calculated following these steps: i) firstly, the thickness of the crystalline crust has been obtained as the difference between the Moho depth and the depth to the crystalline basement; ii) secondly, using the above-mentioned ratio, the thickness of the lower crust has been derived and iii) thirdly, the thickness of the upper crust has been calculated by subtracting the lower crust thickness to the total crystalline crustal one.

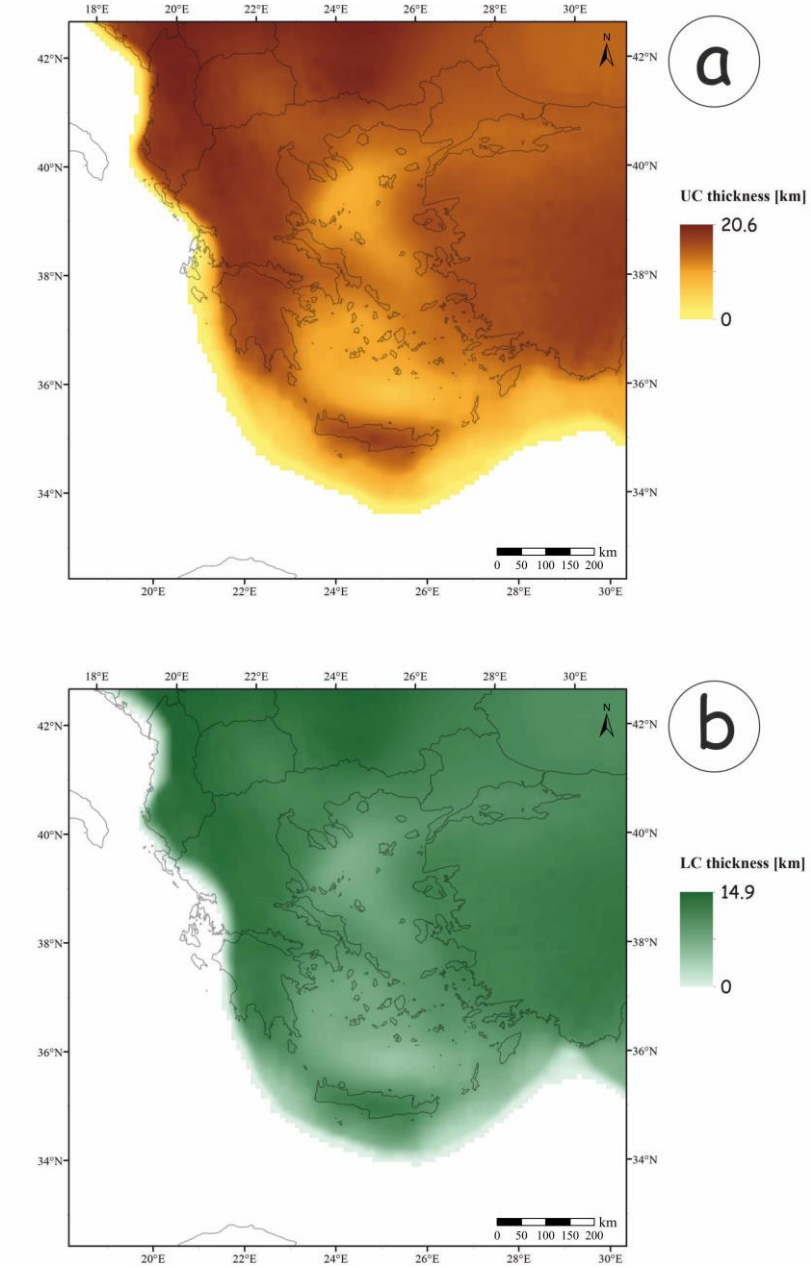

Fig. 3.10 – a) Upper crust thickness for the upper overriding plate; b) lower crust thickness.

As a consequence of the method applied to determine the thicknesses of the upper and the lower crust, the geographical distribution of the maximum and minimum values results from the combination and the interplay of the Moho depth and the thickness of the sedimentary cover. Accordingly, the maxima are located along the Albanides and the northern Hellenides in the Epirus region, with thicknesses attaining values of ca. 20 km and 15 km, respectively for the upper and the lower crust. The minimum values correspond instead to the back-arc regions of the southern Aegean and Cretan Seas, where thicknesses as low as 6.6 km (upper crust) and 4.8 km (lower crust) are observed. It is worth reminding that all the procedure described just above for the calculations of the upper and lower crust thicknesses, is only valid for the sectors of the study area (which are actually the great majority of it) where continental crust occurs. Oceanic crust thicknesses determination will be dealt with in section 3.1.5.

3.1.4 Lithologies of the upper plate

For the determination of the lithotypes, representative of the various layers making up the considered lithospheric column mechanical stratification, different factors had to be taken into account. First of all, the choice of the lithologies is limited by the availability of the rheological characterization in terms of precise parameters values for the different lithologies. Secondly, geological, structural and geodynamic evolution models have been considered in order to reconstruct the possible composition of the various layers (sedimentary cover, upper crust, lower crust, upper mantle). Finally, further considerations on the local and peculiar geological setting together with the structural fabric of the different isopic zones and tectonic regions have been evaluated, so that a final choice consistent with the outcropping rocks and the geological history of each region could be made. As regards the sedimentary cover of the upper plate, the main considered and more appropriate lithologies, among those available, useful for describing almost the entire Aegean Region are the metasediments (sandstones, silts, etc.), limestones and marbles. In order not to make the mechanical vertical stratification unnecessarily complex, a single layer for the sedimentary cover has been designed and implemented in the model. Accordingly, and since in most of the broader Aegean Region the sedimentary cover is made up of a combination of siliciclastic sediments and carbonate ones, a rheological synthesis of the parameters of the two above-mentioned lithologies has been performed.

In such a way a sort of intermediate rheology, representative of a mixed marine-terrigenous deposition environment, has been created and adopted for the whole study area. Considering the relative thicknesses (see *e.g.* Smith and Morton-Moores, 1974), a relatively greater weight has been assigned to the terrigenous sediments (metasediments) with respect to the carbonate ones. The reasons for such a choice are twofold: first of all in many tectonic and isopic zones of the Aegean Region the main sedimentary layers are siliciclastic and at times have also been

metamorphosed and therefore the metasediments lithotype, overall, better represent the sedimentary cover rather than the carbonate ones. Secondly, even where both tpyes of sedimentary deposits are present, the thickness of the terrigenous ones, being usually related to turbidites and gravity-driven mass deposits, could notoriously be very considerable and possibly greater than the carbonate one, thus leading to a prevalent siliciclastic composition.

For the upper crust lithology of the overriding (upper) plate, a dry quartzitic lithology has been selected as the most appropriate one. This choice has been, first of all, partly motivated by similar literature works making such a selection, as the typical composition of the continental (upper crust) is deemed to be quite felsic and thus comparable to that of the quartzite. The "dry" factor preferred over the "wet" version is related to the fact that the upper crust, even when lying over the subduction zone, is actually quite far from the regions of dewatering and fluid circulation related to the slab dehydration phenomena. In fact several interposed layers, such as the lower crust and the upper mantle of the upper plate and possibly also an asthenospheric wedge, occur between the upper crust and the downgoing slab, thus hindering the upwards percolation of fluids and water up to the shallowest layers.

The second reason for selecting the quartzite dry as the lithology of the upper crust is directly related to the nature of the outcropping rocks in many sectors of the Aegean Region, which effectively display the occurrence of arenaceous and low-grade metamorphic rocks, such as schists, phyllites, quartzarenites, sandstones, etc. Taking into account the two above-mentioned factors, as well as the available rocks in terms of rheological characterization and parameterization, and also considering that in general the upper crust is richer in sialic elements than in mafic ones, the quartzite dry lithology has been deemed to be the most suited one for representing an average composition of the shallowest crustal basement layer in the Aegean Region. Clearly, the selection of the quartzite for the whole thickness of the upper crust is a simplification of the actual internal stratification of the layer, mainly justified by the large scale of the investigation and the broad study area selected for this research. Indeed, at a more local scale interleaved beds of metasedimentary and metagranitoids rocks may be distinguished in the crystalline basement of regions such as Peloponnesus (Phyllite-Quartzite series), Crete (Plattenkalk series; *e.g*. Bonneau, 1973) and Cyclades (see *e.g*. Xypolias and Doutsos, 2000; Robertson, 2008; Zulauf *et al*., 2008; 2015). However, the quartzitic lithology, when zooming out and adopting a wider perspective corresponding to the whole study area, can effectively represent a good approximation of the average composition of the upper crust, for most of the Aegean Region.

An exception is represented by the upper crust composition of the region around Thessaloniki, Chalkidiki peninsula, part of the Thrace region and Samothraki island. Here the upper crust is deemed to be better represented by (dry) granite and granodiorite lithologies, as a result of the granitic and granodioritic intrusions occurred in Triassic, Jurassic and Tertiary times

(*e.g.* Papadopoulos and Kilias, 1985; Lips *et al.*, 2000; Himmerkus *et al.*, 2009). The resulting distribution of quartzite, granodiorite and granite lithologies used for representing the upper crust of the upper plate for the whole study area is shown in fig. 3.11.

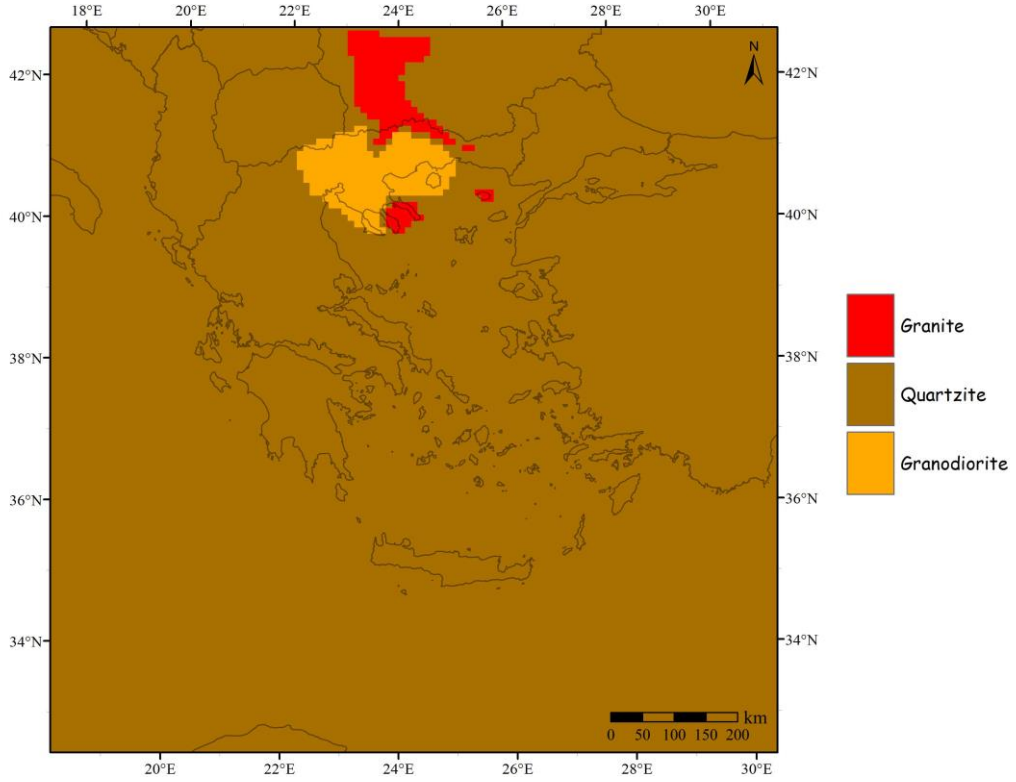

Fig. 3.11 – Upper crust lithologies for the upper plate.

A diorite (wet) type of lithology has been selected for the lower crust following the work of Tesauro (2009), who considered such lithology as representative for the Aegean Region due to its good fit with geophysical properties (such as seismic velocities and density) obtained from different kinds of analyses (seismic tomographies, gravimetric inversions, etc). I also took into account the work from Huet *et al.* (2011) which also proposed, among other models, a (quartz-) dioritic lower crust for the crust around the Cyclades Islands. For the Northern Greece area, corresponding to the Rhodope and Serbo-Macedonian massifs isopic zones, a granulite lithology for the lower crust has been instead selected, following the work of Tesauro (2009). The high-grade metamorphic nature of the crust under the Rhodope zone is also underlined in dedicated literature, *e.g.* in Barr *et al.* (1999).

As regards the lithology of the upper mantle layer, the peridotite wet lithotype has been chosen and selected as the most suited one. The composition of the mantle is generally accepted to be mostly corresponding to olivines and pyroxenes, in the form of and proportions of the peridotite lithology, and therefore the same choice was made for the model in this work. As regards the content of fluids (and water in particular) different opinions and lines of reasoning exist, even though fluid occurrence in the mantle, although at times in trace quantities, is indicated

in the majority of the dedicated literature works (*e.g.* Hirth and Kohlstedt, 1996; Karato, 2003; Peslier *et al.*, 2010).

Accordingly, the wet version of the peridotite, which is slightly less resistant than the dry one, in terms of rheological and mechanical behaviour, has been chosen for this work.

3.1.5 Crustal structure and lithologies of the lower plate

No real subdivision into different crystalline crustal layer has been applied for the regions characterized by oceanic crust, namely the area external to the Mediterranean Ridge and the downgoing Hellenic slab at depth. Indeed, by a compositional (and also rheological) point of view, the thin oceanic crust is almost entirely made up along its vertical extension (*viz.* thickness) of the same mafic lithology, for which only the texture changes, going from basalts at the shallowest levels to diabases and gabbros at greater depths. In any case, also considering the availability of the rheologically characterized and parameterized mafic lithologies, a single lithology corresponding to diabase has been assigned to the oceanic crust and therefore no distinction between upper and lower crust was neither needed nor justified, also considering the relatively limited vertical extent of the oceanic crust itself.

Taking into account the Mesozoic age of formation of the Ionian/Nubian oceanic crust and the classic models correlating thermal contraction, progressive cooling, distance from the spreading centres, age and thickness (see *e.g.* McKenzie *et al.*, 2005), a value of 8 km for the total thickness of the Ionian/Nubian oceanic crust has been selected. Such a value is consistent with the estimation on the average thickness of the oceanic crust sufficiently far away from the mid-ocean ridges, with the crust being formed under normal conditions in the spreading centers (see *e.g.* models from White *et al.*, 1992; McKenzie *et al.*, 2005). Such a thickness, however, is only representative for the portions of the oceanic plate that have not been directly involved in the subduction process yet and therefore have also not entered the subduction shear zone and channel yet. On the contrary, the thickness of the oceanic crust in the downgoing slab is progressively reduced from the initial value of 8 km due to the mechanical, thermal and chemical erosion that takes place together with shearing and possibly with the delamination of the lowermost portions of the crust.

Above the oceanic crustal layer in the subducting plate also a sedimentary cover is clearly present, whose maximum thickness in the outer portions of the Ionian/Nubian plate with respect to the Mediterranean Ridge has been fixed to 7 km. Such a value is in agreement with the data, models and estimations for the thickness of the sedimentary (mainly pelagic) deposits above a very old oceanic crust such as the Ionian/Nubian one (*e.g.* Truffert *et al.*, 1993). The rate of consumption of the sedimentary layer in the lower plate is much faster than that of the (crystalline) oceanic crust, mainly because of: i) the softer mechanical-rheological nature of the sedimentary

deposits, which fosters their progressive tectonic slicing and thinning as the subduction phenomena proceed; ii) their relative position at the interface between the two converging plates, which promotes their mechanical erosion, especially within the subduction channel and iii) finally, their high content in fluids (water) that, under the progressively higher pressures to which they are subjected in the subduction process, leads to compaction by dewatering and further decrease of the vertical extent of the layer.

The thinning of the sedimentary cover as the slab reaches greater and greater depths is therefore quite rapid and the zero thickness is already attained in correspondence of the vertical projection of the coastal areas of Crete and southwestern Peloponnesus, at horizontal distances of ca. 200 km from the surface trace of the current active front of the subduction zone in the Mediterranean Sea (fig. 3.12a). Once the sedimentary layer is completely eroded, the consumption process begins to take place within the oceanic crustal layer, starting from the uppermost levels, though at a considerably slower rate than for sediments (fig. 3.12b).

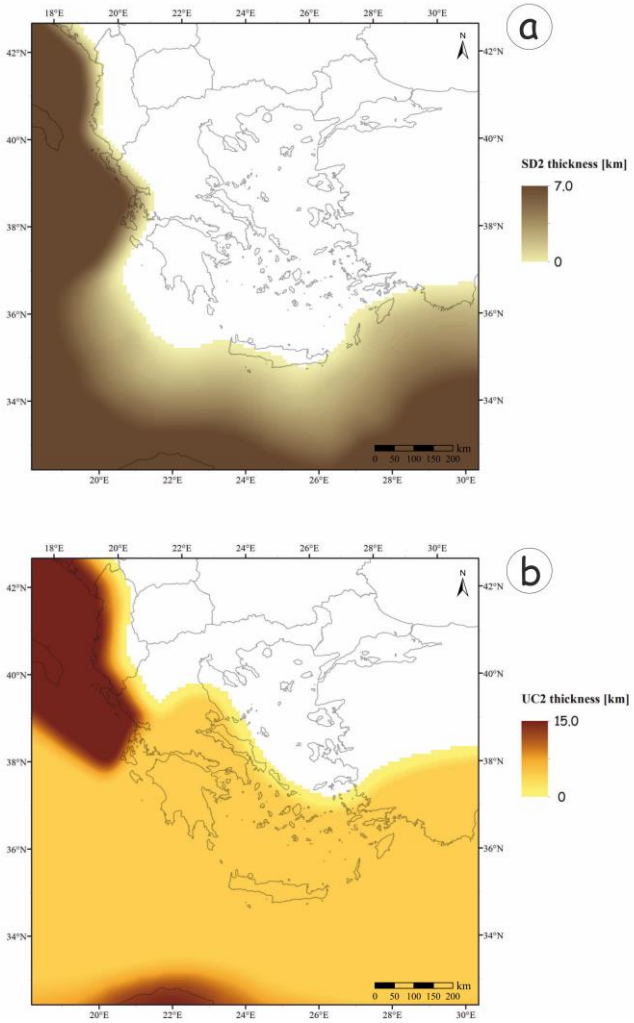

Fig. 3.12 – a) Thickness of the sedimentary layer for the lower plate; b) Upper crust thickness of the lower plate. The areas in brown correspond to continental crust with quartzitic composition.

As a result, the total elision of the oceanic crust is only reached at considerable depths following the downgoing slab, in correspondence of (vertical projection) northern-central Aegean Sea just north of the islands of Evia, Andros and Leros, at a horizontal distance of ca. 600 km from the Hellenic subduction zone front.

An average granulite has been selected as the representative lithology for the lower crust of the lower plate in the continental areas, following the work by Amato *et al.* (2014,) which suggest such a lithology for the Apulia region, on the basis of seismic velocities retrieved from teleseismic receiver functions studies. They also indicate that the Moho depth for Apulia is ~32 km (in any case comprised between 28 and 32 km) and therefore, considering a sedimentary cover thickness of ~7 km, an original pre-collision total crustal thickness for the continental lower plate of ~25 km has been selected.

Successively a geological model for the transition from continental to oceanic crust (and lithosphere) along the southern passive margin of Apulia has been realized. On the northeastern margin of Apulia the plate boundary (*i.e.* the active deformation front represented by the frontal external and active thrusts in the Ionian – south- and Adriatic – north – sea) has been identified by following the thrust-regime seismogenic sources in GreDaSS (Caputo *et al.*, 2012) and the work of Bocchini *et al.* (2018), for the segment around Corfu.

As already mentioned above, a negative gradient of progressive thickness decrease for the layers of the lower plate crust was imaged and applied. In this way, a total consumption of the downgoing plate (continental) crust is attained, as a result of wearing and shearing along the main decollement/underthrusting/subduction shear zone and chemical/mineralogical weakening reactions phenomena due to increasing temperature and pressure conditions with depth. The first process is considered to be predominant in terms of efficiency in eroding the downgoing crust. Accordingly, the direction of consumption of the layers is top-to-bottom (*i.e.* sedimentary cover first, followed by upper crust once sediments are fully scraped off and lastly lower crust).

The gradient of downgoing sedimentary cover and crust consumption rate is higher for the continental crust than for the oceanic one (fig. 3.12). This is mainly related to the steepness of the plate interface (greater for the continental collision zone than for the oceanic subduction region) and consequently to the degree of efficiency in scraping off the layer(s) below as the overriding plate acts as a bulldozer-like indenter. An additional reason for the longer transport and conservation of subducting oceanic crust along the slab with respect to continental one is the different mineralogical composition between the two.

Indeed, the oceanic crust is mainly characterized by a mafic composition (usually basalts, gabbros and diabase) which makes it, as a first order, markedly denser and heavier than the felsic-intermediate continental crust. Such a physical property helps the oceanic crust to subduct and sink together with the peridotitic lithospheric mantle. On the contrary, the low-density continental crust is hindered in its descent and sinking process and tends to be delaminated from the

downgoing lithospheric mantle and finally to be underthrusted and accreted to the crust of the overriding plate (in a similar manner to what shown by Burchfiel *et al.*, 2018). The peculiar mineralogical composition of the oceanic (mainly pyroxens, amphiboles and olivines) and continental (feldspars and quartz) crusts is also responsible for differences in the mechanical behaviour and in the reactions to thermal perturbations (and weakening phenomena) between the two.

In fact, the mafic minerals which make up the bulk of the oceanic crust have been shown in experimental works (*e.g.* Chopra and Paterson, 1981; Ranalli, 1995; Scholz, 1989; Kirby and Kronenberg, 1987) to need higher temperatures for the onset of plastic ductility and also higher temperatures of the solidus for the phase change to melt, with respect to continental crust typical minerals. This, in turn, translates into a lower probability of preservation of the continental crust along the downgoing slab. Such crust is indeed subjected to higher mechanical wearing and erosion and less able to sustain high temperature and pressure conditions occurring at depth. All these properties suggest to apply a higher consumption rate to the continental crust with respect to the oceanic one (along the downgoing slab).

As concerns the selection of the most appropriate lithologies, since Apulia is often considered as a promontory of the African/Nubian plate (*e.g.* Amato *et al.*, 2014, and references therein), for its upper and lower crust layers, lithologies consistent with a shield/craton nature have been chosen. Accordingly, the upper crust is represented by a (dry) quartzite while the lower crust, as previously mentioned, corresponds to a (felsic) granulite (Craig *et al.*, 2011; McGuire and Stern, 1993).

Finally, with regard to the determination of the lower African plate LAB depth, estimations proposed by Sodoudi *et al.* (2006) have been primarily taken in to account. Their estimated thickness of the oceanic African plate, based on S waves receiver functions analysis, is around 60-65 km. Such values result from the calculation of the plate thickness obtained by taking into account the geometry of the subducting slab, *i.e.* its dip angle, the depth of the Wadati-Benioff plane (the top of the plate) and that of the LAB (the bottom of the plate). The latter has been imaged and placed at a depth of ca. 100 km below Crete and down to 225 km beneath the volcanic Hellenic arc, thus leading to the above-mentioned reduced estimates of the lithospheric thickness corresponding to values in the range of 60-70 km, typical of the oceanic lithosphere.

3.1.6 Power-law creep and geothermal gradient parameters

The parameters of the power-law creep, representing the rheological behaviour associated to ductile deformation, are the so-called power-law parameter (A), power-law exponent (n) and the thermal activation energy (E). They are associated to the selected lithology for each lithospheric layer and therefore their values for the rheological modelling in this work are strictly related to

the choice of the lithotypes. Once the lithology for each layer has been assigned, the Matlab code automatically recalls the value of the parameters associated to that specific lithology.

The values of the power-law creep parameters have been obtained from experimental studies and laboratory analyses mainly conducted in the '80s on samples taken from selected lithologies, usually corresponding to the most common lithotypes and minerals encountered both in the continental and in the oceanic crust (*e.g.* granite, quartzite, limestone, dunite). The majority of the original works were focused on the determination of experimental flow laws for a single (or a few) selected lithology (*e.g.* Carter *et al.*, 1981; Chopra and Paterson, 1981; 1984; Shelton and Tullis, 1981; Hansen and Carter, 1982). In the end of the '80s and at the beginning of the '90s many reviews and synthesis papers were also published (*e.g.* Kirby and Kronenberg, 1987; Carter and Tsenn, 1987; Ranalli and Murphy, 1987; Ranalli, 1995; Karato and Wu, 1993). All these sources of data have been taken into account in this study, in order to determine the values of the power-law parameters commonly associated to each available lithology.

Similar to the power-law creep ones, also the values of the geothermal gradient parameters, namely the thermal conductivity (k) and the radiogenic heat production rate (A_0), are always associated to, and depending on, the selected lithology. Their values mainly result from experimental works and synthesis studies, such as those from *e.g.* Birch and Clark (1940), Roy *et al.* (1981), Drury (1986) and Vilà *et al.* (2010). In table 3.1 the selected values (of both power-law and geothermal gradient parameters) for the lithologies used in this work are shown and in the caption the corresponding source from the literature is indicated.

	A	***n***	***E***	***k***	***A₀***
	$MPa^{-n} \cdot s^{-1}$	/	J/mol	W/m·K	W/m^3
mixed-sediments	$2.0 \cdot 10^{-4}$ *(1,2)*	2.74 *(1,2)*	$1.95 \cdot 10^{5}$ *(1,2)*	3.1 *(2,3)*	$1.56 \cdot 10^{-6}$ *(4)*
quartzite dry	$6.7 \cdot 10^{-6}$ *(5)*	2.4 *(5)*	$1.56 \cdot 10^{5}$ *(5)*	4.2 *(6)*	$1.84 \cdot 10^{-6}$ *(4)*
granite dry	$1.8 \cdot 10^{-9}$ *(5)*	3.2 *(5)*	$1.23 \cdot 10^{5}$ *(5)*	3 *(3)*	$2.43 \cdot 10^{-6}$ *(4)*
granodiorite	$1.3 \cdot 10^{-3}$ *(5)*	2.4 *(5)*	$2.19 \cdot 10^{5}$ *(5)*	2.65 *(3)*	$1.88 \cdot 10^{-6}$ *(4)*
granulite	$8 \cdot 10^{-3}$ *(5)*	3.1 *(5)*	$2.43 \cdot 10^{5}$ *(5)*	2.1 *(7)*	$4.5 \cdot 10^{-7}$ *(7)*
diorite wet	$3.2 \cdot 10^{-2}$ *(9)*	2.4 *(9)*	$2.12 \cdot 10^{5}$ *(9)*	3.2 *(8)*	$8.62 \cdot 10^{-7}$ *(4)*
diabase wet	$2.0 \cdot 10^{-4}$ *(10)*	3.4 *(10)*	$2.60 \cdot 10^{5}$ *(10)*	2.64 *(3)*	$3.45 \cdot 10^{-7}$ *(4)*
dunite wet	$2.0 \cdot 10^{3}$ *(11)*	4.0 *(11)*	$4.71 \cdot 10^{5}$ *(11)*	/	/

Table 3.1 *– Values of the power-law creep and geothermal gradient parameters for the lithologies used in this study. The original source of the values is indicated by the number in parenthesis: 1 – Schmid et al. (1977); 2 – Doser and Kanamori (1986); 3 – Cermak and Rybach (1982); 4 - Vilà et al. (2010); 5 - Ranalli (1995); 6 - Roy et al. (1981); 7 – Afonso and Ranalli (2004); 8 – Turcotte and Schubert (2014); 9 – Carter and Tsenn (1987); 10 – Shelton and Tullis (1981); 11 – Chopra and Paterson (1981).*

3.1.7 Friction coefficient

The standard friction coefficient value that has been selected for and used in the frictional sliding equation is 0.6, in agreement with and following Byerlee's law (Byerlee 1968, 1978). In

correspondence of the surface projection of the major seismogenic sources, a lower friction coefficient in the range 0.4-0.5 has been assigned, representing in such a way a first areal variation of the parameter values distribution (fig. 3.13).

A vertical variation could also be taken into account by tentatively varying the friction coefficient values as a function of the lithology in the corresponding litho-mechanical layer. In general, lower friction coefficient values should been assigned to those layers characterized by weak and more easily deformable lithologies. In this way, for example, the sedimentary cover, represented by lithologies such as clays and soft sediments, can be associated with a lower friction coefficient value, with respect to a granitic or quartz-rich upper crust.

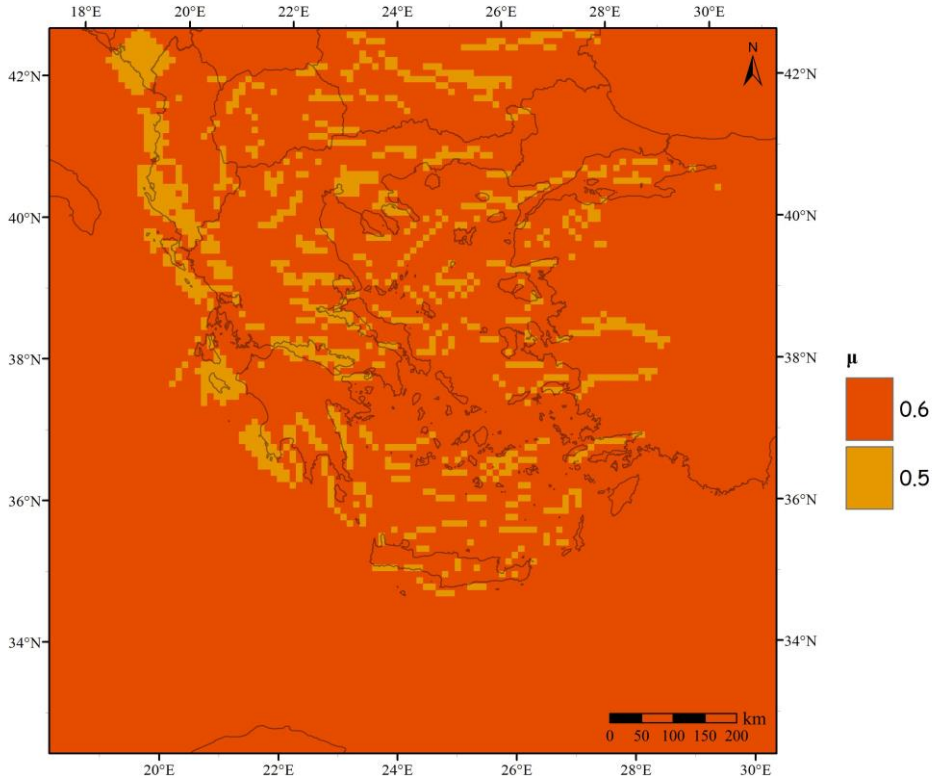

Fig. 3.13 – Map showing the variation of the friction coefficient over the study area, following the areal distribution of the main fault zones.

Such a weakening effect by clay minerals, serpentinites and talc has been proposed has an explanation to the weak mechanical behaviour of some faults, and also to explain their potential misorientation with respect to the current stress field (see for a review Collettini *et al.*, 2019). The friction coefficient values for the above-mentioned weak minerals, especially when foliation is developed and therefore the phyllosilicates and micae foliae can act as preferential slip surface, could be as low as 0.2-0.3. Another possible cause for the decrease of the friction coefficient values is the fault lubrication related to the physical-chemical reactions leading to the creation of silica gel during the coseismic stage (Di Toro *et al.*, 2004; 2011).

Yet, it must be underlined that especially for high and medium angle normal faults, which characterize a large portion of the Aegean Region and the study area, it has been proved that

friction coefficients effectively follow Byerlee's rule (Byerlee, 1978) and therefore values in the range 0.5-0.8 are more representative of their mechanical and rheological behaviour. Nonetheless, given all the above premises, I have also tested the results of an alternative rheological model of the Aegean Region, with friction coefficient values for the surface projection of the seismogenic sources corresponding to 0.2.

However, such a model is not considered to be realistic for the Aegean Region, since: i) as already mentioned, the geometrical and mechanical features of the main seismogenic sources in this region are more consistent with friction coefficients in the range 0.5-0.8; ii) the very low values of friction coefficient are typically associated to the development of pervasive foliation and the occurrence of interconnected crystals of minerals such as quartzitic micae, serpentinites and gypsum along the fault core zone, while the majority of the faults in the Aegean Region are at least partially characterized by carbonate formations, especially in the upper portions, thus excluding the possibility to find such well-developed microstructures and minerals association throughout the entire fault zone, from the surface to the bottom of the seismogenic layer.

These peculiar features of the main fault zones in the Aegean Region would rule out the very low values of friction coefficients, say 0.2-0.4, with only some limited exceptions (one could be represented by the hypothesized north-dipping, low angle normal fault lying on the southern side of the Corinth Rift, against which the main known active sources, corresponding to high angle normal faults, would terminate). Accordingly, the model realized with friction coefficient values in the range 0.5-0.8 remains the preferred one and will be used for further applications.

Only some exceptions represented by specific fault zones with peculiar characteristics occur and have been assigned a lower value of 0.4. The main factor leading to the selection and assignment of such a lower value is the repeated shearing activity along such fault zones, indicated by high slip rates and small earthquake recurrence time intervals.

Indeed, the prolonged and frequent seismic (but also aseismic) activity on a fault/shear zone fosters weakening phenomena, such as mechanical wearing and comminution, and also promotes microstructural and chemical/mineralogical ones, with the development of weaker mineralogical phases, pervasive foliation and chemically-aggressive circulating fluids.

The combined effects of all these above-mentioned weakening phenomena and processes finally lead to a decrease of the mechanical strength of the fault/shear zone and, thus, to lower values for the associated friction coefficients.

3.1.8 Tectonic parameter

The parameter α in the frictional sliding equation is usually referred to as the tectonic one. Actually, it results from the interplay of the friction coefficient μ, which has been treated in its

own section, and the parameter β, which substantially represents the stress ratio. The relationship between α, β and μ is expressed by the following equations:

$$\alpha = \frac{\mathrm{R} - 1}{1 + \beta \cdot (\mathrm{R} - 1)} \qquad [3.4]$$

$$\mathrm{R} = \left(\sqrt{1 + \mu^2} - \mu\right)^{-2} \qquad [3.5]$$

The stress ratio β is a useful indicator of the stress ellipsoid shape and is generally adopted as a proxy for the corresponding tectonic regime. It results from the following expression, relating the three axes of the reduced stress tensor:

$$\beta = \frac{\sigma_2 - \sigma_3}{\sigma_1 - \sigma_3} \qquad [3.6]$$

where the convention which states that $\sigma_1 > \sigma_2 > \sigma_3$ is followed. In a purely Andersonian regime (*i.e.*, $\sigma_z = 0$ at the surface), one-directional horizontal compression implies $\sigma_z = \sigma_3 = 0$ and $\sigma_2 = \sigma_3$, therefore resulting in $\beta = 0$. Conversely, for an ideal strike-slip regime, where σ_1 and σ_3 are equal in magnitude but opposite in sign, it is $\sigma_z = \sigma_2 = 0$ and therefore $\beta = 0.5$. Finally, a one-directional tensile regime is characterized by $\sigma_z = \sigma_1 = 0$ and $\sigma_2 = \sigma_1$, thus leading to $\beta = 1$.

Given these general rules and premises, here I will focus on the β parameter and its variations across the Aegean Region. A representative map of the β value for the whole study area has been produced, based on both literature data and, above all, tectonic, geodynamic and seismotectonic considerations on the geological framework of the broader Aegean Region (fig 3.14).

I will now proceed with a very short and quick recall on the large-scale tectonic setting and features of the study area. The tectonic setting of the Aegean Region has been extensively studied since the pioneering works of *e.g.* Aubouin (1959), McKenzie (1972, 1978), Mercier (1976) and Le Pichon and Angelier (1979). Even though no complete agreement is shared for some geodynamic details, the general tectonic framework is nowadays quite well known and widely accepted. Briefly, the Aegean Region is characterized by compression in the external outer portion of the Hellenic arc (Hellenic subduction zone and, to the northwest, Ionian collision), where subduction and continental collision are still currently active.

On the contrary, the back-arc regions in the Aegean and Cretan Seas and in continental Greece are mostly characterized by post-orogenic extension. Additionally, strike-slip tectonics occurs along major crustal faults, *i.e.* on the Kefallinia Transform Fault and on the Aegean propagation of the North Anatolian Fault, referred to as the North Aegean Trough. In addition to such large-scale features, in order to select the proper values of the β parameter at a higher resolution, I also took into account the tectonics, kinematics, slip and rake directions of the seismogenic sources in the GreDaSS database (Caputo *et al.*, 2012; Caputo and Pavlides, 2013).

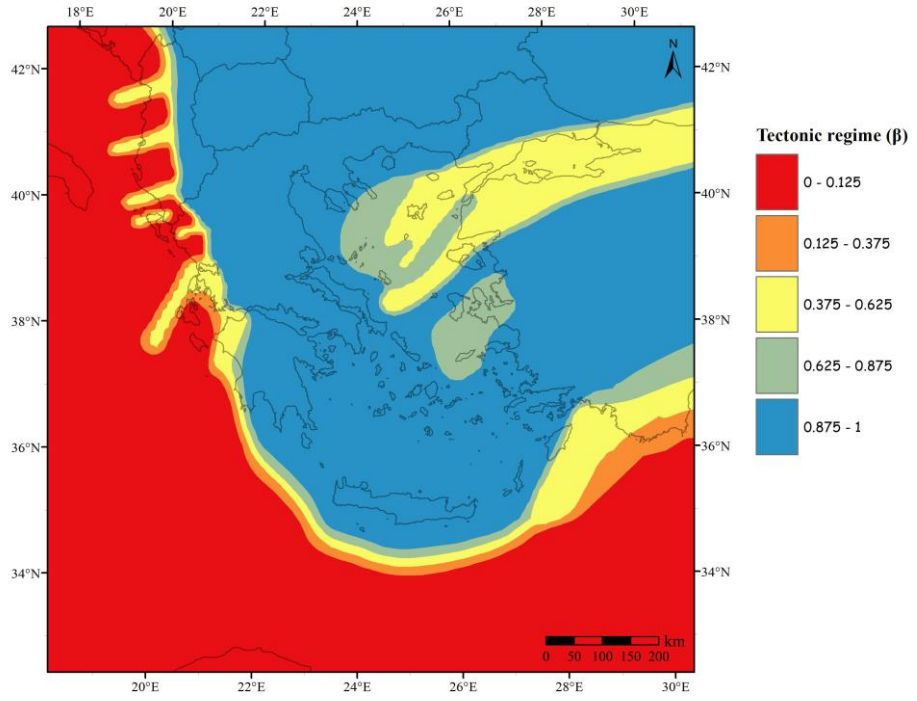

Fig. 3.14 – Tectonic regimes characterizing the Aegean Region. 0 corresponds to pure compression, 0.5 to a transcurrent regime and 1 to an extensional one.

The result of such considerations can be observed in fig 3.13 and can be shortly described as follows. The area external to the Hellenic subduction zone has been associated with a β value of 0, *i.e.* is deemed to be characterized by compressional tectonics. A value of β=1 has instead been assigned to almost the whole back-arc region in the Aegean Sea and also to the majority of continental Greece. All these areas are indeed associated with extensional tectonics and kinematics, following a still currently ongoing phase of quite rapid stretching, initiated diachronously in Miocene-Pliocene times, and which has resulted from the sinking and roll-back of the Hellenic slab and from the gravitational collapse of the Hellenides fold-and-thrust belt.

A few exceptions are represented by the areas characterized by prevailing strike-slip tectonics, *i.e.* the Kefallinia Transform Fault and the northern Aegean Sea region, in particular along the North Aegean Trough. The latter area has been associated with a β value equal to 0.5, thus indicating pure transcurrent kinematics, while the former region around Kefallinia and Lefkada islands has been assigned a β value of 0.4. Such a value is obtained by taking into account

also the minor compressional tectonics and thrust-kinematic component observed along the Kefallinia Transform Fault.

Additional zones characterized by prevalent strike-slip tectonics are the WSW-ENE trending transfer faults orthogonal to the Ionian/Apulian collisional front, which correspond to structures such as the Lushnje, Qeparo and the Corfu transfer faults (Caputo and Pavlides, 2013). Such structures are generally associated with a β value of 0.4, because of the minor dip-slip component that characterizes their kinematics.

In order to smooth out the gradients between the values of β for the different zones of prevailing compressional, transcurrent and extensional tectonic regime, some transitional buffer zones have been introduced at the corresponding contact areas. The creation of such buffer zones is also consistent and compatible with the potential effective deviations of the stress field, whose tensor is expected to vary in such a way that, at least in areally limited sectors, intermediate values of the stress ratio should occur between the end-members (β = 0, equal to uniaxial compression and β = 1, corresponding to uniaxial extension).

3.1.9 Pore fluid pressure

The λ_e parameter in the frictional sliding equation stands for the pore fluid factor, *i.e.* the ratio between the pore fluid pressure and the lithostatic pressure. It is sometimes referred to as Skempton's coefficient and in the rheological modelling literature it is generally assumed to be in the range 0.37-0.4. The exact value actually depends on the average density selected for the crustal rocks, which determines the overburden pressure. Such a density is commonly between 2600 and 2700 kg/m^3 and its variations within this interval are reflected into the above-mentioned range of assumed hydrostatic pressure values of λ_e (*e.g.* Ranalli, 1995).

The variations in the pore fluid pressure may produce a relevant effect on the resulting rheological features of the investigated rock volume, especially as regards the strength of the rocks, expressed in terms of differential stress and consequently also on the depth of the brittle-ductile transition. Indeed, as it is well-known from classic literature works (*e.g.* Sibson, 1974; 1977), the increase of fluid pressure causes a decrease in the effective strength and conditions for brittle failure are much more easily met (with reference to the Coulomb-Mohr circle, the latter is shifted towards the left and the failure envelope is reached at lower strength values).

The physical explanation for the pressure-related decrease of the effective strength lies in the fact that the fluid under pressure in the pore spaces and cracks distributed within the rock volume tends to exert a sort of outwards-directed push, which acts as an opposing force with respect to the overburden, lithostathic pressure. Accordingly, the final result on the strength of the rocks is that a lower force and traction is necessary to bring the rock volume to failure, since

the overburden pressure compacting and strengthening effect is almost completely counterbalanced and finally cancelled by the increasing fluid pressure.

Generally speaking, in dry conditions the pore fluid pressure (and its ratio with the confining pressure) is nil, while in hydrostatic conditions, considering common crustal rocks densities, it typically varies in the range 0.35-0.45 (see for example Sibson, 1984; Ranalli, 1995). However, in peculiar geodynamic and tectono-stratigraphic conditions within the uppermost crust, for example within accretionary wedges, suprahydrostatic conditions (λ_e > 0.5) affecting large sedimentary volumes are much more likely to occur. In such a geological setting, poorly consolidated ocean-bottom sediments enter the subduction zone while still being highly permeated by circulating fluids. As the subduction process advances, these sediments undergo progressive compaction due to the rapid increase of the stress genetic component caused by gravity (Caputo, 2005). This leads to considerable pore reduction and fluid pressure increase due to a poor water seepage, thus locally increasing the Skempton coefficient, sometimes even up to unity. However, in deeper crustal conditions, *i.e.* in crystalline rocks, such extreme hydraulic conditions are rare and the coefficient could be reasonably assumed to be nearly hydrostatic.

Nevertheless, slightly suprahydrostatic conditions could be also caused by a rapid temperature change leading to thermal expansion of the fluids and the consequent pressure increase, or directly by a magma-related fluid injection, as it could occur in volcanotectonic settings or in correspondence with mantle plumes. In such peculiar environments, even supralithostatic conditions (λ_e > 1) could also locally occur, generating, for example, laccoliths and horizontal sills (*e.g.* Gressier *et al.*, 2010).

For the bulk of the Aegean Region, a hydrostatic value of the fluid pressure has been assumed and therefore a λ_e value equal to 0.4 has been selected in the preferred model (see Chapter 5). However, geological/geodynamic considerations and numerical modelling (*e.g.* Kufner *et al.*, 2014) suggest that supra-hydrostatic and even supra-lithostatic conditions could occur in the accretionary wedge along the Hellenic subduction zone. Accordingly, some alternative models (with respect to the preferred one), where I allowed the λ_e parameter to vary and attain values closer to 1 in the region comprised between the Hellenic trenches and the outer active deformation front, have also been tested (fig. 3.15).

Indeed, in correspondence of the Hellenic trench, the accretionary wedge reaches its maximum thickness and water-rich sediments are expected to undergo compaction phenomena, thus leading to a remarkable build-up of the fluid pressure (*e.g.* Saffer and Tobin, 2011). Clearly, the pore fluid pressure is maximum (*i.e.* λ_e ~1) where the accretionary wedge thickness attains its greatest values and tends to progressively decrease to hydrostatic values moving towards the back-arc region.

Finally, in the portion of the lower African/Ionian plate, which has not been involved in the subduction process yet, the λ_e parameter is also assumed to be equal to 0.4. Several models for

the λ_e layer have been realized, where different gradients of pore fluid pressure decrease in the back-arc region are applied, in order: i) to verify the possible influence of such fluid pressure variations on the resulting rheology, with particular care for the BDT depth and strength and ii) to explore all the possible ranges of reasonable and potential values that the λ_e parameter can assume, especially in the absence of direct information and measurements.

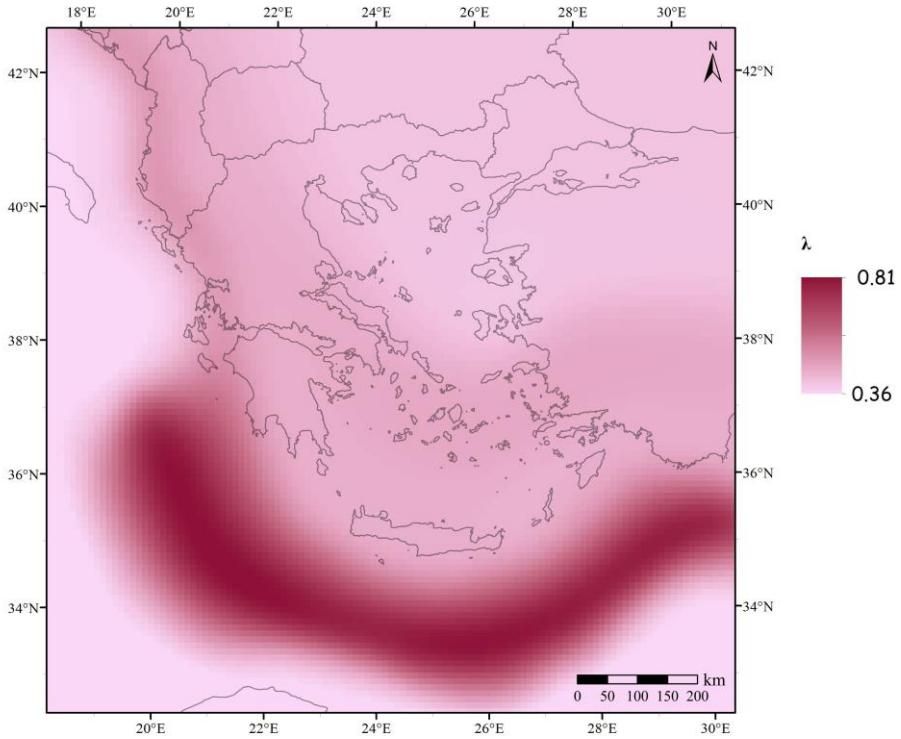

Fig. 3.15 – Potential pore fluid pressure ratio values across the study area. The distribution shown here has been adopted in an alternative model (see Chapter 5 for more details), where suprahydrostatic conditions (λ~0.8) characterize the Mediterranean Ridge accretionary wedge.

However, it should be reminded that since no specific data exist for the pore pressure and fluid flow in the back-arc Aegean Region, the assumption of λ_e being equal to 0.4 (as it is in the preferred model) may still represent a reasonable simplification, also because of the opportunity that such a choice allows in terms of direct comparison with other areas characterized by hydrostatic pore pressure.

3.2 Methods

3.2.1 1nput layers construction

The stage of scientific information gathering, for the purposes of the modelling, has been carried out mainly by first collecting the data from different sources, as it has just been shown in the previous paragraphs, with the values selection for each parameter. In a second phase, all the

collected data have been stored in a GIS (Geographic Informative System) software, so that they could be easily viewed together and compared.

If the collected data were in the form of geographically unreferenced images, they have been first of all geolocalized and georeferenced. Furthermore, if any data were needed in the vectorial format, at least in a first elaboration stage, a manual digitalization has been performed. For instance, the values of the heat flow parameter have been produced by initially georeferencing input images and raster and then by digitalizing the contour lines of iso-heat flow, identified in the previously georeferenced images. At the end of those processes a final raster obtained by interpolating the redrawn contour lines has been produced. Such a procedure has been followed for many other parameters, like crustal layers thicknesses, strain rates and pore fluid pressure ratio.

In other cases, instead, for parameters such as the tectonic regime and the friction coefficient, polygons identifying areas with internal constant values have been realized and digitalized, leaving empty spaces between polygons, where the transition buffer zones are created. Subsequently a transformation from polygons to raster, based on the selected parameter values that have been stored in a dedicated field of the attribute table of the polygon feature class, has been performed. During this stage the buffer zones have been automatically attributed intermediate values, resulting from an interpolation that took into account the corresponding values of the bordering polygons. In this way, a smoother shift from the values of one polygon to the closest one has been obtained, with the buffer zone representing the gradual transition. Clearly, the degree of smoothing and the rate of such a transition depend on how large is the initial gap left, which could be directly set to the desired measure, according to the needs and purposes of the user.

Other parameters, such as the lithologies of the various crustal layers, can only assume precise values because they are represented by discrete functions rather than continuous ones, as it is, instead, the case for the previously described parameters. The discrete values are therefore assigned by simply correlating each starting polygon with a unique and precise value, without leaving any blank space in between and then by simply transforming the polygon into a raster, without any further interpolation. In this way, the values of some specific rheological and thermal parameters, which are typically dependent only on the lithology (power-law parameter and exponent, activation energy, thermal conductivity and radiogenic heat production rate), are directly recalled into the Matlab script and the modelling procedure by simply identifying the corresponding lithology through the dedicated raster layer.

Indeed, for such rheological and thermal parameters, an Excel table with the corresponding values, ordinated according to the lithology, has been prepared, so that the only variable introduced in the script for the rheological model is the lithology itself, which is identified through a specific number that allows to automatically recall all the related parameters values. The

numbers corresponding to each lithology have been grouped according to the different mechanical layers to which they belong.

In particular, the numbers from 1 to 39 identify lithologies belonging to the layers of the upper plate (UP) and from 51 to 89 to the ones of the lower (subducting) plate (LP), with the ranges 1-9 (UP) and 51-59 (LP) corresponding to the sedimentary cover, 10-19 (UP) and 60-69 (LP) to the upper crust, 20-29 (UP) and 70-79 (LP) to the lower crust (LP), 30-39 (UP) and 80-89 (LP) to the upper mantle. Finally, the numbers in the range 40-49 correspond to the potentially interposed asthenospheric layer between the two lithospheric plates and the numbers 91 and 92 respectively to the air and water (oceans and seas) layers. The relative number of each lithology is then shown in the table 3.2.

.

Lithology	**Number**
Mixed-sediments – *Upper plate*	5
Granite Dry – *Upper plate*	11
Quartzite Dry – *Upper plate*	13
Granodiorite – *Upper plate*	15
Diorite Wet – *Upper plate*	26
Dunite Wet – Upper *plate*	32
Mixed-sediments – *Lower plate*	55
Quartzite Dry – *Lower plate*	63
Granulite – *Lower plate*	71
Diabase Wet – *Lower plate*	75
Dunite Wet – *Lower plate*	82
Air	91
Water	92

Table 3.2 *– Lithologies of the various layers in the upper and lower plates adopted for the rheological modelling, with the corresponding number used for indicating them in the Matlab script.*

All the parameters needed for the rheological modelling and in particular for the Matlab script (see the section below for a thorough description) have then been associated with corresponding areal layers. Such layers are effectively represented by georeferenced rasters produced via a GIS software as described above. All the rasters share a common reference system, corresponding to the Greek Grid (projected coordinates in metres) and are also characterized by the same planar dimensions, being 1100 km long on each side of the square-shaped study area. The rasters, in Greek Grid coordinates, extend from -50000 m in the west to 1100000 m in the east and from 3600000 m at the southern border to 4750000 m at the northern one.

All the rasters are subdivided into 115 cells on each direction, for a total number of 13225 pixels. The cell size is 10 km on each side, and represents a good compromise between the achievement of an adequate lateral resolution in the modelling outputs, compatible with the detail of the input parameters spatial information, and the need for an acceptable calculation time, in the frame of quality production-employed time economics. Nonetheless, the cell size could be varied

and halved to 5000 m in order to obtain a higher resolution and the time needed for running all the calculations would still be compatible with an effective modelling in terms of required temporal and effort costs.

The areal layers into the raster format can then be saved with the corresponding specific function either as ASCII or Excel files, in order for the information to be stored in a much more accessible format, without losing the geographical reference. Such ASCII files are then loaded into the Matlab code, where they are quickly read by the script and used as initial inputs for all the calculations in the modelling procedure. Since a very important requisite for the layers is the equal areal extension for all of them, if the relative geographical information for some pixels is missing, they are labelled with either negative or positive out of scale values rather than with the NoData or NotANumber labels, in order to avoid any potential failure or error of the code itself, during its calculations.

3.2.2 Subduction zone thermal model

A particular care has been devoted to the reconstruction of the temperature profiles in correspondence of the Hellenic subduction zone, for the purposes of thermo-rheological modelling. The thermal model here described has then been implemented in the dedicated Matlab script for the modelling (see next section §3.2.3). The thermal perturbation attributable to the downgoing cold oceanic lithosphere has been taken into account in this work by considering and using as a model the one proposed by Turcotte and Schubert (2014) (fig. 3.16). In such a model, one important variable is the initial temperature (and the associated undisturbed geothermal gradient) in the oceanic undergoing plate. This parameter has thus been assigned a value consistent with the age of the oceanic crust, following the model for the relationship between age and temperature in an oceanic plate proposed by McKenzie *et al*. (2005).

The oceanic crust of the subducting African plate (sometimes also referred to as Ionian oceanic lithosphere, *e.g*. Royden and Papanikolaou, 2011) is possibly as old as 200-230 Ma. The relative heat flow data combined with the thermal parameters of the dunite/peridotite lithology for such an old lithosphere provide a temperature at the base of the crust (*i.e*. at the Moho) of ca. 140 °C. Such a value is consistent and compatible with the one predicted by McKenzie's model, which is indeed around 150 °C, for such an old (and cold) lithosphere. For the continental subducting lithosphere along the northwestern coast, the boundary temperature at the Moho is around 295 °C. Such a temperature has been obtained by taking into account the crustal structure in the region offshore northwestern Greece, corresponding to the Apulian platform, which is characterized by a Moho depth of ca. 33 km, and also by considering the local heat flow values, which are relatively low (around 30 $mW \cdot m^{-2}$).

When dealing with the thermal modelling for the subduction zone of both oceanic and continental lithosphere I also took into account mechanical processes that may lead into further perturbations of the original undisturbed geotherm. In particular, the process of progressive thinning and final elision of the downgoing crust, through either mechanical erosion (see section §3.1.5 for details and discussion on the topic) or accretion and underplating to the overriding plate, may result into higher temperature of the top of the lower plate lithosphere, at the contact with the upper plate, *i.e.* at the Wadati-Benioff plane, with respect to an undisturbed situation where the downgoing crust is completely preserved. Such an increase in temperature is mainly due to higher values that lower crustal layers have, with respect to the shallowest (eroded) portions, and it is therefore dependent on the percentage of elided downgoing crust.

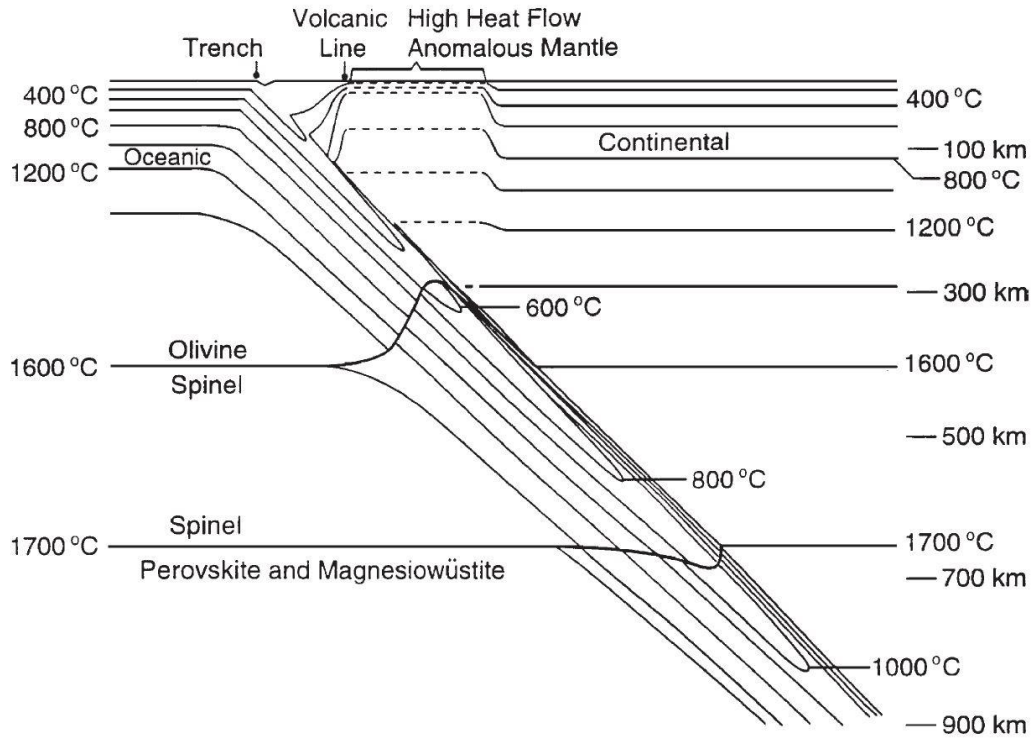

Fig. 3.16 – Subduction zone isotherms according to the model of Turcotte and Schubert (2014).

In order to calculate and take into account the 'elision factor', representative thicknesses of the oceanic and continental lithospheres in the study area have been selected, being respectively 15 and 33 km. Following this concept, the temperature at the Wadati-Benioff plane increases almost linearly as the elision progresses at gradually greater depths. The velocity of this increase mainly depends on how quickly the subducting crust in consumed. Indeed, a more rapid consumption and elision of the continental crust has been assumed with respect to the oceanic one, since the former is associated with lower densities and higher temperatures and it is therefore weaker and positively buoyant, thus leading to easier erosion and/or accretion to the overriding plate with delamination of the heavier and more mafic mantle.

When the soon-to-be-subducted plate has not entered the process yet, the temperature at the top of the plate is assumed to be equal to Ts, *i.e.* surface temperature, with a value of 15 °C. On the contrary, when a total consumption ('elision') has occurred, the theoretical temperature (from which to start the effective temperature calculations by also considering radiogenic heat production, thermal conductivity and the thermal perturbation effect related to the slab subduction) at the Wadati-Benioff plane (corresponding to the top of the lower plate) is given, respectively, for continental and oceanic crust by Ts = + 297 °C and Ts =+ 141 °C. Such temperatures are those expected at the corresponding Moho depth of respectively 33 and 15 km, for regionally representative continental and oceanic crusts.

Moreover, since, as it has been already mentioned, a linear relationship between temperature rise and 'elision' factor increase with depth has been assumed, the theoretical temperatures at mid-crustal depths of respectively 16.5 km and 7.5 km for continental and oceanic crusts, correspond to values of Ts + 148.5 °C and Ts + 70.5 °C. The thermal model has been implemented in order to take into account also the peculiarities of the transitional tectonic and crustal domains, between oceanic and continental. In particular, along the passive margins regions, where a transitional and thinned continental crust is present, but thinning is not related at all to subduction processes, the theoretical temperature at the top of the lower plate is kept constant and equal to Ts.

As a secondary effect, the subduction process also induces perturbations in the geothermal gradient of the upper plate even at great distances from the trench, in what could be called a "wider" back-arc region. In the Aegean Region, for example, McKenzie (1978) suggested that the surface heat flow in the back-arc area has been almost doubled from pre-subduction average values of ca. 44 $mW \cdot m^{-2}$ to the current 88 $mW \cdot m^{-2}$. Such an estimate of the undisturbed pre-subduction heat flow value has been questioned by other researchers, such as Stiros (1991), who argued that the amount of stretching in the Aegean is not as high as suggested by McKenzie (1978) and therefore the crustal thinning could not justify the post-orogenetic Miocene to present extension-related thermal heating of the upper Aegean plate crust. As a consequence, the heat flow should have been higher than 44 $mW \cdot m^{-2}$ even before the onset of the subduction and the following extension, due to local anomalies and possibly flow along major inherited shear zones.

In any case, it is has been long recognized that the subduction process affects to some extent the geothermal gradient by mainly: i) causing the release of water and fluids from the downgoing slab into the overlying upper mantle wedge, which results into melt formation, rising to the surface and general increase of temperature at depth and also at the surface especially along the volcanic arc; ii) sinking and retreating, which promote extension in the upper plate resulting into crustal thinning and isotherms upwards rising and iii) creating a volcanic arc, which implies ponding of magma at depth and heat flow increase due to surface manifestations. The shape of the isotherms in the back-arc region in this work model can therefore be effectively attributed to the processes

mentioned above, with closer isotherms towards the surface, especially in the volcanic arc region, indicating a very high geothermal gradient.

As a result, the temperature of a representative Moho at around 25-35 km could increase from a pre-subduction average value of ca 600 °C (see *e.g.* Soto *et al.*, 2008) to even 900-1000 °C (*e.g.* Currie and Hyndman, 2006) in the back-arc region, after the subduction process has affected the temperatures at depth and modified the geothermal gradient also in the upper plate. At this point, it may be helpful to recall that the geothermal gradient in the crust is calculated by taking into account the specific radiogenic heat production and thermal conductivity of each layer and therefore strongly depends, in addition to the surface heat flow, on the lithological vertical stratification. Accordingly, the close isotherms in the crustal sectors of the back-arc region above the subduction zone could also be possibly related to high thermal conductivity values that characterize the crustal layers.

On the contrary, the gradient in the upper mantle only depends on the depth of the lithosphere-asthenosphere boundary, while it is almost independent from the selected lithology, also because an irrelevant radiogenic heat production occurs in the mantle. The temperature at the lithosphere-asthenosphere boundary (hereinafter LAB) is typically assumed to be ~1330 °C and therefore a LAB lying at around 100 km, with the Moho occurring at around 30 km and having a high temperature of ca. 900 °C (which is the situation that occurs in some specific zones of the back-arc Aegean Region), would imply a relatively low geothermal gradient within the mantle layer. Accordingly, such a low gradient is reflected in much more largely spaced isotherms below the Moho, with respect to those lying within the crustal layers, as occurs in the model produced with this work for the back-arc Aegean Region.

If the Moho temperature or the LAB depth varies laterally, a corresponding change in the isotherm distribution is observed and therefore lateral temperature gradients other than the vertical one could characterize the mantle layer. Such a pattern would not be in disagreement with conduction being the main heat transfer mechanism acting in the lithosphere (and therefore also in the mantle). Indeed, conduction does not imply a homogeneous distribution of temperature in all the directions throughout the layer within which occurs, differently from the convection mechanism.

The latter typically characterizes the asthenosphere below the mantle, and its onset actually represents one of the distinctive features that help identifying the LAB. Convection requires almost homogeneous temperature distribution and therefore the geothermal gradient in the asthenosphere is almost null, which graphically, in a typical temperature (on abscissa) *vs* depth (on ordinate) chart, results into a nearly vertical line, while in the mantle the geotherm, though being quite steep, is still indicating temperature rising with increasing depth.

The effect of the thermal perturbation on the upper plate, which corresponds to a local cooling of the previous undisturbed geothermal gradient, does not propagate throughout the entire

upper plate, unless the Wadati-Benioff plane is quite shallow. In this work the thermal model has been designed in such a way that the thermal perturbation effect on the upper plate (cooling) extends upwards for ca. 20 km, from a Wadati-Benioff plane depth of 70 km, and the heating effect propagate downwards for ca. 15 km.

For example, if the Benioff plane lies deeper, say at around 90 km, the upwards perturbation extends for ca. 30 km and the downwards one for about 20 km. With a shallower Benioff plane at ca. 25 km of depth, the thermal perturbation effect would propagate for about 10 km upwards and for ca. 5-6 km downwards (fig. 3.17).

Clearly, the edge case where the Wadati-Benioff plane is at the surface or at the sea bottom actually implies that no subduction or collision has occurred and therefore no upper plate is present and no thermal perturbation is generated at all, thus leading to a simple and undisturbed geothermal gradient. On the other side, the opposite edge case is represented by a very deep-lying Wadati-Benioff plane: where it is deeper than 140-150 km (which is generally the depth limit assumed for all the model calculations in this work) no sensible effect is observed on the geothermal gradient of the upper plate.

Indeed, below that depth, an asthenospheric wedge is present between the upper plate and the lower one, as the overriding plate LAB lies at maximum at ca. 150 km, so that the potential thermal cooling effect on the overlying layers, due to the subduction process, eventually takes place in the asthenosphere and does not propagate through the lithosphere of the upper plate.

The absolute intensity of the thermal cooling related to the slab subduction mainly depends on the thermal properties of the slab itself, and in the particular case of the oceanic lithosphere, on the formation age of its crust. Accordingly, in the case of the old Ionian/African oceanic crust, the cooling effect on the upper plate is considerable, due to the very old nature of the subducting plate, but in the case of subduction of younger oceanic lithosphere the thermal perturbation effect can be reduced, with respect to the one used in this model, by simply applying a reduction coefficient.

The decrease of the cooling and heating effects away from the slab is modelled through the use of two specular mathematical functions. Such functions are respectively the *s-* and *z-function*, as found in the Matlab environment, within which the script returning the thermal model has been implemented. The rate of the cooling and heating effects decrease mainly depends on the ability to transfer the heat across the rocks of the overlying (hotter) layers to the underlying (cooler) ones, with respect to the subduction interface.

Such properties, since conduction is assumed to be the most effective heat transfer process in the lithosphere and almost the only one acting there, are primarily described by the thermal conductivities of the rocks surrounding the downgoing slab, at least at shallow and intermediate depths where no asthenospheric wedge occurs between the slab and the overriding plate.

Some additional processes, such as thermal advection and convection could partially contribute to the heat transfer only in the case where interconnected fracture zones have developed around the slab and fluids able to circulate in those conduits and convey the heat are present.

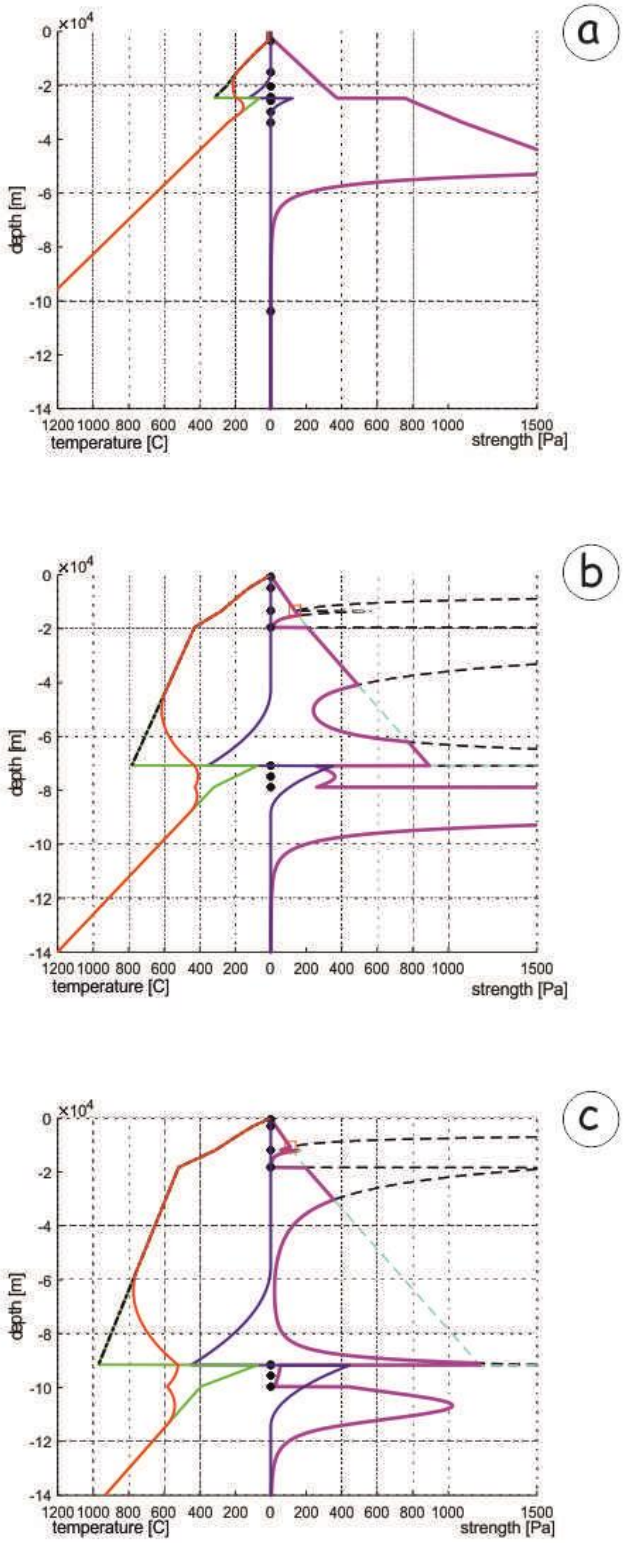

Fig. 3.17 – Geothermal gradients and extent of the thermal perturbation in the Hellenic subduction zone, for increasing depths of the slab top: a – 25 km; b – 70 km; c – 90 km. See figure 3.18 for the colors legend.

However, even though the release of fluids may effectively characterize the subduction zone, the presence of opened and interconnected fractures seems to be unlikely, given the great pressures at those depths and the prevailing compressional regime. Accordingly, the thermal conductivities of the slab confining rocks are effectively the parameters controlling the rate and the distance at which the thermal perturbation propagates.

More specifically, a high thermal conductivity is generally translated into a considerable and efficient capability of transferring the heat and therefore, in the corresponding rocks, it is associated with great propagation rate and distances of the thermal perturbation originated from the slab. On the other hand, a low thermal conductivity denotes opposite thermal behaviours and properties, thus leading to more locally confined thermal cooling/heating effects and to a slower propagation of those perturbations.

As regards the distribution of the total thermal perturbation effect on the upper plate and the lower plate, a simple 50% percent of the total intensity has been assigned to each plate, since no clear evidence for a prevailing cooling of the upper plate rather than a heating of the lower one or viceversa has been found out. However, also in this case, the Matlab script which reproduces the thermal subduction model has been implemented in such a way that the balance between the cooling/heating effects can be easily changed by varying the respective coefficients, as long as information and data on the their different relative weights become available. The thermal model is thus designed to be adaptable to each possible tectonic setting. Indeed, as it has just been shown above, it can be easily modified to be representative of both an oceanic plate, a subduction zone, a collisional one, and an extending back-arc region, according to the geological contexts and the desired purposes. Finally, in terms of initial setup strategy, especially as regards the lithological stratification and the thermal boundary conditions, the subduction zone model developed with this research is similar and comparable to those proposed in other works, such as the ones from Gerya et al., 2002, Gerya and Meilick, 2011, which also consider the general case of rheological modelling in subduction zones and along active margins. In particular, the shape of the isotherms in the subduction zone and in its surroundings presents a good agreement in the different models, thus representing a confirmation of the plausibility and reliability of the model here proposed.

3.2.3 Matlab code

In order to realize the rheological model of the Aegean Region, I produced and implemented a series of Matlab ® scripts (or codes) which are designed to obtain 1D rheological profiles, as well as a complete 3D model. Then, a specific implemented code is also able to produce pseudo 2D transects having any desired starting and ending points. An additional code has been developed in order to quickly visualize the strength envelope for a precise selected point, starting

from the 3D model. I will now describe thoroughly how the code works and the philosophy followed for implementing the script.

I will begin with the 1D code, which has been termed "RheolMod1D"; the concept at the very base of the script is that the values of the most important variables for describing the rock rheology, *i.e.* strength and temperature, are calculated every 100 m ("step") down to the desired bottom depth of the model, which could be, for instance, even the base of the mantle. Both the brittle and the ductile strength are calculated for the whole vertical extension of the selected rheological profile, and additionally also the strengths corresponding to alternative behaviours, such as the Zang's rheology, the frictional-viscous one (see *e.g.* Bos and Spiers, 2002) or the pressure-solution, could be obtained, compared with the others and finally visualized.

The actual strength of rocks at each depth is always given by the smallest value of strength among those provided by the considered behaviours. The vertical column is subdivided into different litho-mechanical layers corresponding to the sedimentary cover, the upper crust, the lower crust and the upper mantle. I also took into account the possibility of modelling a lower plate made up of four additional layers, in the case where the selected point of the rheological profile belongs to a subduction or collision zone. The lower plate layers obviously lie below the upper plate ones and in the case that no subduction or collision occurs in the selected zone their thickness could be simply set equal to zero.

For each layer the desired and most suitable lithology can be selected among the available ones, and the selection automatically defines the corresponding values of the associated rheological parameters, which depend only on the lithological properties. Such parameters are, in particular, those related to the power-law creep behaviour (activation energy, power-law creep parameter and exponent), the average density, the thermal conductivity and finally the internal radiogenic heat production rate. These parameters values are stored in dedicated Excel tables, which are then loaded and recalled into the Matlab script. Other parameters, such as the friction coefficient, the pore fluid pressure ratio, heat flow and strain rate can be directly evaluated and their values set up by the user.

Once all the required parameters of the constitutive equations have been assigned their numerical value, the code performs the calculations for the desired depth step, which has been set up as equal to 100 m. This choice represents a good compromise between the need for a good vertical resolution and the computational speed in order for the code running not to be too much time-consuming. However, the step dimension could be easily decreased by the user if a greater vertical detail is required and the scale of the modelling is restrained to a few kms. On the other hand, if a very deep rheological profile is needed, the user could set up a greater step value which will result in a resolution decrease but at the same an acceptable total time for the elaboration will be obtained.

The determination of the BDT depth is based on a comparison, at each step, between the frictional behaviour strength and the power-law creep one. At the surface and at very shallow depths the ductile strength is always associated with high values because of the low temperatures and therefore the effective deformation behaviour corresponds to the frictional one. However, at greater depths the difference between the two strengths tends to shrink because of the temperature increase and consequent power-law creep strength decrease, until at some depth the two strengths become (almost) equal. If at the next step the ductile strength is effectively lower than the brittle one, the code is designed to identify that precise depth as the one corresponding to the brittle-ductile transition.

Once all the calculations are performed, the script also produces a figure (3.18), which displays the different rheological behaviours strengths as a function of depth, together with the BDT depth, the resulting strength envelope and the depths of the interfaces between the various lithological layers. Furthermore, in parallel to the strength envelope also the temperature profile *vs* depth is shown in the figure, so that a quick account on the thermal state and its influence on the resulting rheological profile can be visually obtained. Actually, also the continuation of each strength *vs* depth curve is shown as a dashed line, so that a rapid insight on the difference between the relative strengths of the various rheological behaviours can be visually gained.

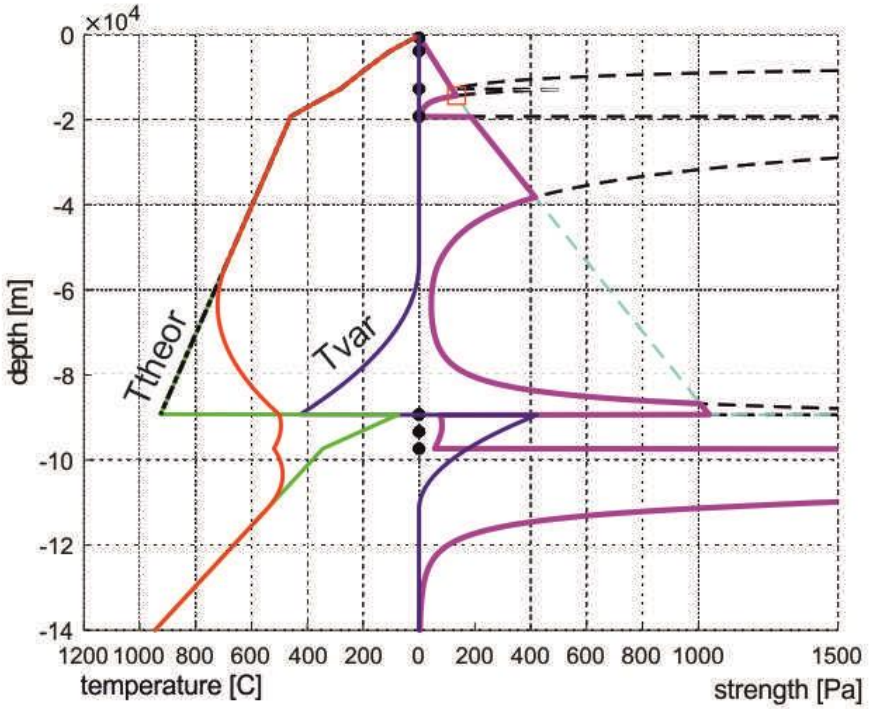

Fig. 3.18 – Figure obtained from the 1D Matlab code. On the right, the strength envelope (solid magenta) is shown together with the theoretical curves for the brittle (dashed cyan) and ductile behaviours (dashed black). The thin red square indicates the position of the BDT. The resulting geothermal gradient is displayed on the left (solid red). Tvar (solid blue) corresponds to the temperature variation induced by the slab cooling effect during the subduction process, while Ttheor (dash-dotted black) represents the theoretical temperature if no perturbation were introduced.

As for the temperature profile, the output figure (fig. 3.18) allows to show the thermal perturbation (which is indicated in the code as Tvar, *i.e.* 'temperature variation') caused by the subduction process and also the hypotethical undisturbed profile, which would represent the thermal state at depth if no subduction or any other perturbating process/phenomenon occurred (see previous section §3.2.2 for the thorough description and discussion on the subduction zone thermal model and principles behind it).

In this way, by comparing the two curves, it can be easily estimated at a first view the effect (and weight) of the subduction-induced temperature variation on the geothermal gradient. For instance, it can be assessed whether a change in the effective temperature gradient at depth is the result of: i) a change in the slope of the undisturbed gradient; ii) fluctuations in the magnitude of the 'Tvar' factor or iii) a combination of the former two cases.

The code producing the 3D model is actually made up of two different scripts, each one having its own specific functions. The first one is called "RheolMod3D_saver" and should be run before the other script, termed "RheolMod3D_producer". The "RheolMod3D_saver" contains all the parameters values necessary for running the producer code; all the information is stored as ASCII files, which can be directly extracted from GIS environments and therefore maintain their georeferencing data. Given the 3D nature of the model produced, in this case the input parameters are first recalled and then saved as 2D layers with a specific (pre-determined by the user) areal extension.

Also for these codes, the user can increase or decrease the dimension of the investigated area (and as a consequence of the total volume) according to the final aim and scale of the modelling. One important constraint is represented by the fact that all the areal layers must have the same dimensions and therefore sufficient geographical coverage is needed for each parameter in terms of available data. Once that all the layers are imported as ASCII files and recalled in the saver code, the latter proceeds to their saving as Matlab variables files '.mat'.

The producer code "RheolMod3D_producer" is then used to load the '.mat' files and run all the calculations. The elaborations are made through a couple of nested loops, which represents the latitude and longitude extensions of the modelling. Clearly, within those two loops the vertical iterative process of rheological (strength and BDT depth) and thermal (temperature) parameters calculations is maintained as in the 1D code, and a final 3D model, with vertically-developed information for each pixel within the selected input area (defined by the pre-set maximum and minimum latitude and longitude), is obtained.

The final outputs of the 3D script are again ASCII files containing information on the BDT depth, strength and temperature, which could be easily loaded in a GIS environment and georeferenced in order to be analyzed. Moreover, many of the variables regarding in particular the thermal model and the rheological transitions, which are calculated during the script

elaborations, are then stored as '.mat' files in order to be used in other codes or for any other required purpose.

Furthermore, a 3D figure representing the model results in terms of BDT depth or associated strength and temperatures is displayed at the end of the code running, so that a first view and assessment on the obtained results can be easily gained. A further tool is given by the possibility of plotting on the same figure also any other desired surface (*e.g.* the Moho or the Conrad discontinuities), so that a rapid comparison and check of any potential control of the selected surfaces on the BDT depth can be performed. The figure itself can be rotated in order to be observed from any possible point of view, so that different details and properties of the displayed surface and/or parameter can be highlighted.

In addition to the 3D figure, also ASCII files containing information on the BDT depth, strength and temperatures are produced so that they can be uploaded in a GIS software, georeferenced and displayed both as 2D surfaces and as 3D figures. Furthermore, additional outputs are represented by ASCII files indicating the total integrated strength, the strength of the brittle layers with respect to the ductile ones and the strength of the upper plate with respect to the lower one in the cases where collision or subduction occur.

A very light and quick additional 1D code termed “Figure1D_from3D” allows to select a specific point (better say the pixel to which the selected point belongs) from the 3D model, whose producing script must have been run just before. For the selected pixel the corresponding strength envelope it is thus quickly shown in the typical strength *vs*. depth graph, together with the geothermal gradient and the lithological stratification.

The code "m3D2section" has instead been implemented in order to realize a rheological transect with any desired orientation and length. In this way 2D information on the main thermo-rheological parameters can be obtained and realizing close transects could help identifying, for instance, the spatial correlation between input parameters and the resulting rheological characteristics.

Moreover, directional trends in BDT depths, strengths and temperatures can be noticed and analyzed and an alternative 3D view can be gained by realizing intersecting transects. This script also allows to select the thickness of the buffer zone orthogonal to the transect direction, within which all the analyzed parameter values are projected onto the transect itself, so that a swath-like pseudo 2D section of thermo-rheological properties is obtained. The sampling frequence along the transect is around 5 km, as pixels (which have dimensions of 10×10 km) are selected and projected onto the profile from both sides with respect to the transect itself.

Also this script produces as outputs a series of ASCII files containing the information for all the projected pixels along the transect, going from the resulting thermo-rheological parameters to the input ones describing the litho-mechanical stratification, so that they could be uploaded in GIS environments and easily interpreted and analyzed.

In particular, the files regarding the BDT depth, strength and temperature, record not only the areal variation of such parameters, but also their values along the vertical dimension, with a sampling frequency equal to that of the model calculations in the script, *i.e.* 100 m. Such a good vertical resolution in terms of available information allows to create quite accurate pseudo 2D-sections potentially down to depths of 150 km (or in any case down to the bottom depth of the calculations).

Additionally, in a separate figure all the exploited strength envelopes are juxtaposed and plotted in correspondence of their projection on the section trace, providing the general picture, at a first glance, of the rheological layering (fig. 3.19).

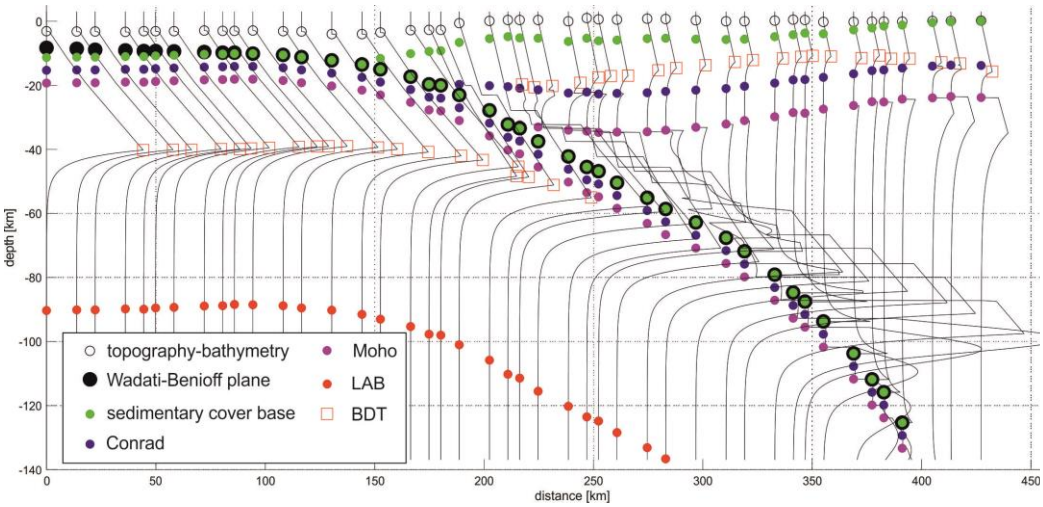

Fig. 3.19 – Rheological layering along a hypothetical 2D pseudo-section in an oceanic subduction setting, as depicted by the 1D strength envelopes. Lateral variations, both for lithological and rheological layering, can be observed following the markers in the figure (see the legend for explanation).

As concerns the semi-brittle behaviour, both the 1D, the (pseudo) 2D and the 3D codes offer the possibility to take into account Zang's (Zang *et al.*, 2007) rheology. In particular, such a rheological behaviour and its corresponding strength can be compared with the traditional brittle and ductile ones and all the relative rheological transitions depths can be determined. Regardless of the associated strengths, the deepest between the BDT and the ZDT (Zang-ductile transition) can be selected so that, if desired, the most cautious choice can be made for defining the thickness of the seismogenic layer, according to the purposes of the seismic hazard assessment.

Chapter 4: Sensitivity analysis

4.1 Aims and workflow

In this chapter I am going to present the methods that have been followed in order to test the validity of rheological profiles and their sensitivity to variations in the input parameters, with particular emphasis on the resulting BDT (brittle-ductile transition) depth and corresponding strength and temperature. For this purpose two test-sites from the Aegean Region have been selected, one in an extensional tectonic setting and the other in a strike-slip regime, and the corresponding "reference" rheological profiles have been carefully realized on the basis of literature data and specific geological constraints. The reference envelopes have been then compared with a set of different profiles, realized by varying the input parameters of the constitutive equations of the brittle and ductile behaviours within reasonable ranges.

Firstly, tests were performed by changing the value of only one input parameter per time, with the aim of quantifying and comparing its influence on the BDT properties. The parameters exerting the greatest control are the activation energy, the power-law exponent and the surface heat flow (through its influence on the geothermal gradient), for the creep behaviour. As regards the brittle behaviour parameters, the friction coefficient and the pore fluid pressure could play a significant role, especially in determining the maximum strength.

In a second phase, I simultaneously varied all the input parameters in order to take into account the possible synergistic effects on the resulting rheological profiles and to verify the likelihood and consistency of the reference models. For the statistical approach, one hundred thousand random combinations of the analyzed parameters have been generated. The particular care spent on selecting the value of each parameter for the rheological modelling purposes is reflected in the results of the statistical analyses, which show a good agreement with the reference profiles and allow to estimate the overall uncertainties.

Finally, the obtained strength envelopes have been compared with the accurately relocated depth distribution of recent seismic sequences that affected the two test areas. In both cases, the depth corresponding to the 95% of the total released energy nicely fits the BDT depth obtained from the rheological modelling, therefore confirming that this parameter could represent a reasonable and reliable approximation of the seismogenic layer thickness.

In the following sections of this chapter, firstly, the influence of each parameter in determining both the BDT depth and the maximum strength of the schizosphere is analyzed. Secondly, two case studies from the Aegean Region (fig. 4.1) are presented and modelled.

They are representative of a tensile and a mainly transcurrent tectonic regime, both typical of this Mediterranean area. Thirdly, several sensitivity tests are systematically applied to both

case studies in order to quantitatively analyze the resulting uncertainties associated with each parameter.

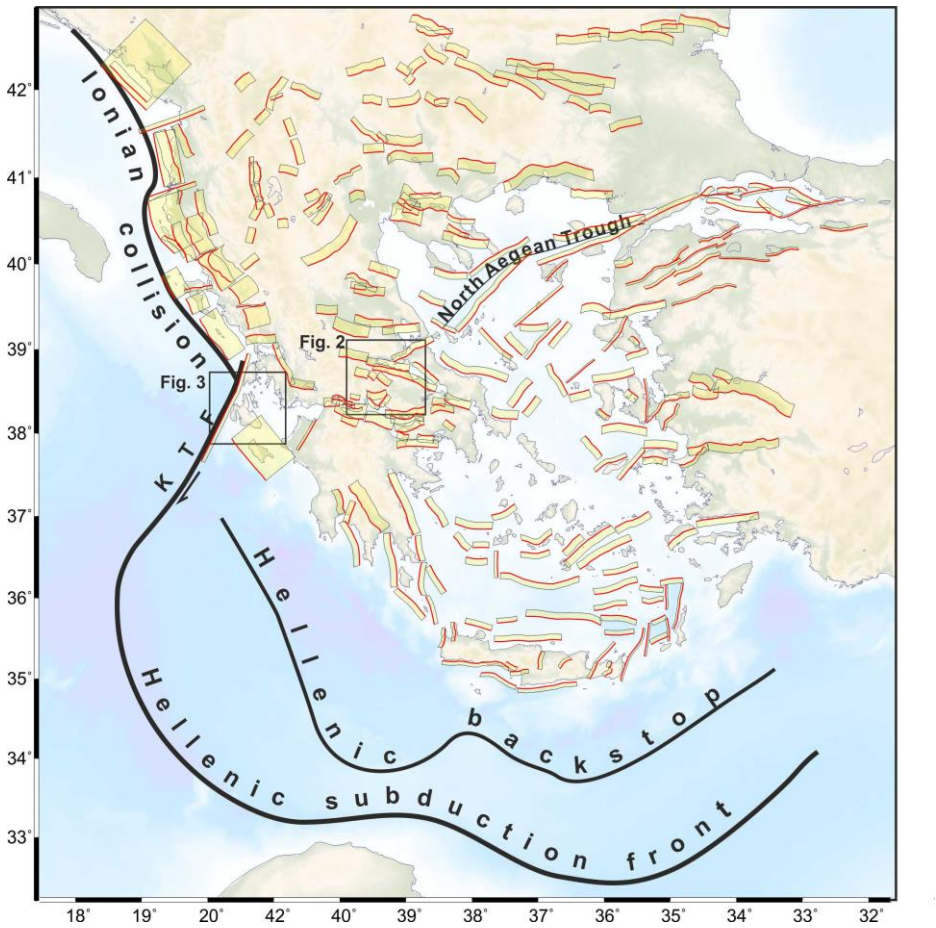

Fig. 4.1 – Synthetic geodynamic map of the broader Aegean Region. KTF: Kefallinia Transform Fault. Major active tectonic structures (composite seismogenic sources) are from GreDaSS (Caputo and Pavlides, 2013). The boxes bounded by solid black lines indicate the locations of the two test sites.

Finally, the results of the analyses (including the cumulative uncertainties) are compared with the depth distribution of the seismic activity recorded in correspondence of the selected case studies.

4.2 Parameters uncertainties and variations

4.2.1 Frictional sliding parameters

Rock density

Assuming as a reasonable approximation that gravity acceleration is constant within the depth range of the brittle behaviour, as concerns the confining pressure, only rock density has some motivation to be tested. This parameter primarily depends on the lithological composition of the overlying rocks. Density is actually dependent on temperature (an increase in temperature

results in a density decrease because of thermal expansion), while also a progressively increasing confining pressure may cause a compaction process within the intergranular structure of rocks, thus decreasing the volume of pores and leading to an overall increase of rock density.

Density is considered to vary primarily with the lithological composition along a vertical profile: in other words, density is assumed to change at the boundary between one major crustal layer and the next one. However, minor lithological-compositional vertical variations could occur even within a single layer, due to temperature- and compaction-induced changes. Moreover, possible sources of error and/or uncertainty, such as laboratory measurements, should be taken into account. Accordingly, a possible variability up to ±10% with respect to a reference density, for each crustal layer, has been considered. In general, an increase of density possibly causes an increase of the peak strength but also a decrease of the BDT depth.

Tectonic parameter α

The parameter α takes into account both the effect of the various tectonic regimes (β) and the one of the friction coefficient (μ). In this regard, it may be appropriate to analyze the two factors separately, as they may actually vary independently and could exert a different influence on the resulting shear strength.

The tectonic regime (and the associated prevailing type of faulting), which is described by equation [3.6] (section §3.1.8), affects the frictional sliding strength in such a way that a lesser amount of stress is required to attain the critical slip conditions for a normal fault (extensional regime) with respect to a reverse fault (compressive regime). Indeed, according also to the classical theory of Sibson (1974; 1977), the shear strength in a tensile regime is markedly lower than that associated with the compressional regime, with the strike-slip regime's one having intermediate values.

The friction coefficient μ for most common crustal rocks has been investigated since the 1950s and earlier (see the classic reviews of Byerlee, 1968; 1978). He observed that the maximum friction coefficient linearly correlates the normal stress to the shear strength, independent of rock types; the statistical fit is quite good and also suggests a progressive decrease of μ from ~0.85 to 0.6 beyond 200 MPa of normal stress. Taking into account i) common crustal densities, ii) fluid pressures and iii) the tectonic regime, the change in frictional behaviour observed in the laboratory should generally occur between 5 and 15 km.

On the other hand, the experimental data collected by Byerlee (1978) also indicate that, in case of thick fault gouges, the friction coefficient could be quite lower, as it has been later documented for some faults in different geological settings, especially where clay and phyllosilicate minerals occur with a lubricating effect (*e.g.* Ikari *et al.*, 2011; Middleton and Copley, 2014). Evidences for low friction coefficient have been found both for lithospheric, strike-slip structures such as the San Andreas Fault (*e.g.* Lachenbruch and Sass, 1980; Zoback *et al.*, 1987; Carpenter *et al.*, 2011; Lockner *et al.*, 2011) and for smaller-scale, dip-slip normal faults

(*e.g.* Collettini and Holdsworth, 2004; Chiaraluce *et al.*, 2007; Numelin *et al.*, 2007; Abers, 2009; Haines *et al.*, 2014), as well as in subduction settings (*e.g.* Remitti *et al.*, 2015).

In crustal rheological modelling a value of 0.70-0.75 is commonly considered (*e.g.* Ranalli and Murphy, 1987; Ranalli, 1995; among many others). However, since the reasonings and conclusions by Byerlee were based on observations on intact samples, this value may be more suited for cratonic and (almost) tectonically stable regions, while in strongly deformed and highly deforming settings, pervasively characterized by mechanical discontinuities of recent formation and affected by continuous weakening processes, a smaller yield shear stress, together with a lower value of the friction coefficient, is expected, at least for optimally oriented faults (with respect to the active stress field).

In general, the larger are i) the fault surface, ii) the cumulative slip and iii) the number of seismic events that reactivated a fault, the smoother will be the rupture surface and the sliding path and the richer in fine-grained elements is the cataclastic zone. Accordingly, an older and/or more active fault could be considered mechanically weaker than the surrounding intact rocks and hence, in the frame of rheological modelling, crustal rocks containing major faults could be reasonably characterized by a lower friction coefficient (see also section §3.1.7).

In summary, the tectonic parameter α is proportional to μ and a decrease of the friction coefficient decreases its value and vice versa. For example, assuming a very low friction coefficient, say $\mu = 0.2$, α is equal to 0.49 and 0.32 (for $\beta = 0$ and $\beta = 1$, respectively), while for $\mu = 0.8$ (the usual upper bound for the friction coefficient of most crustal rocks; Ranalli, 1995) α would be 3.33 and 0.77 (for $\beta = 0$ and $\beta = 1$, respectively).

Pore fluid pressure

The role of the pore fluid pressure is included in equation [2.7] via the Skempton coefficient (λ_e). In dry conditions, the pore fluid pressure (and its ratio with the confining pressure) is nil, while in hydrostatic conditions, considering common crustal rock densities, it usually varies in the range 0.35-0.45 (see, for example, Sibson, 1984; Ranalli, 1995). However, as already discussed in section §3.1.9, in peculiar geodynamic and tectono-stratigraphic conditions within the uppermost crust, for example within accretionary wedges, suprahydrostatic conditions ($\lambda_e > 0.5$) affecting large sedimentary volumes are much more likely to occur.

From a mechanical point of view, an increase of the pore fluid pressure leads to a decrease of the effective stress, which in general promotes failure. This diminishes the peak shear strength and thus it slightly deepens the transition depth from brittle to ductile behaviour.

4.2.2 Ductile creep parameters

The ductile behaviour is represented by the power-law creep equation [2.9], which implies a strong dependence of the shear strength on the temperature as a function of depth, i.e. on the

thermal gradient. When dealing with the power-law creep behaviour, it should be also emphasized the paramount importance of the selected lithology. Unlike the frictional behaviour, where just the density parameter is lithology-dependent, most parameters used to describe the ductile behaviour can markedly vary from one lithotype to another.

The three parameters A, n, and E are referred to as, respectively, "power-law parameter", "power-law exponent" and "activation energy" (see also section §3.1.6). The values proposed for several lithologies have been commonly obtained by fitting the experimental data (among others, Shelton and Tullis, 1981; Hansen and Carter, 1982; Kirby, 1985) to the power-law equation, based on a least-squares regression approach. The experiments, mostly conducted in the 1980s, were carried out at temperatures between ~400 and ~1000 °C, with a confining pressure of ~1 GPa and strain rates between 10^{-4} and 10^{-8} s^{-1}. Such setting conditions pose severe questions about the possibility to extrapolate the observed data to real geological conditions. This observation has a primary relevance for strain rates, which may be even 10 orders of magnitude smaller than the experimental values.

In order to analyze the role of the uncertainties associated with these three parameters and caused by both experimental results and by their inference at typical crustal strain rates, here at the least a ±10% of uncertainty is considered, relative to the accepted values provided in the literature. For example, considering a dry quartzite rock, variations of the power law parameter *A* show a negligible effect on the BDT depth and shear strength. The power-law exponent *n* exerts a higher weight than *A*, as expected for simple mathematical reasons. An increase (decrease) of *n* causes a shallowing (deepening) of the BDT in the order of 2-3 km and a decrease (increase) in peak strength of some tens of MPa.

From a physical point of view, the activation energy *E* represents an estimate of the amount of energy necessary to initiate the dislocation glide creep phenomena. An increase in *E* leads to an increase in strength, as intuitively much more energy (*viz.* stress) has to be stored and applied on that volume to allow deformation begin. Its variability plays a major role on the BDT depth determination and on the resulting strength. For example, a +10% variation could cause a BDT deepening of some kilometres and a strength increase in the order of 105 Pa. Depending on the upper crustal thickness, such a variation may also locally imply the shift of the transition to the lower crust below the Conrad discontinuity surface. In this case, the BDT depth would become a function of the rheological parameters of the lower crust rather than of those of the upper crust.

4.2.3 Strain rate

The rate at which deformation takes place is among the most influencing factors when dealing with the rheological modelling, as it is of remarkable importance for the ductile behaviour, where the dependence of the strength on the strain rate is explicitly indicated in the governing equation [2.9] (see also sections §2.1.3 and §3.1.2).

The strain rate is considered to be representative of the long-term ductile deformation velocity and values in the order of 10^{-15} s^{-1} are commonly selected in the literature (see Sibson, 1982; Ranalli, 1995 among others). A greater strain rate causes general strengthening associated with a BDT deepening and a peak strength increase. This is a direct effect of inhibiting the ductile deformation (rocks are more viscous), thus fostering brittle failure propagation at greater depths. As regards the related uncertainties, variations in the order of ±10%, which do not induce substantial changes in both BDT depth (say, few hundreds meters) and shear strength (say, few MPa), have been considered.

On the other hand, lateral variations of ± one order of magnitude, depending on the resolution of the interpolation, are normally documented by geodetic investigations carried out at the regional scale and represented by smoothly variable maps (Hollenstein *et al.*, 2008; Floyd *et al.*, 2010; Devoti *et al.*, 2011; Kreemer *et al.*, 2014; Mastrolembo and Caporali, 2017). Estimates of strain rates from geodetic measurements, if deprived of any non-tectonic disturbance or coseismic slip effect, are considered to be representative of the long-term, interseismic deformation rates and rheological behaviours at depth in the crust and in the upper mantle (see Burgmann and Dresen, 2008, for a review). More recently, Doglioni *et al.* (2015) have also used space geodesy to estimate strain rate values below the BDT.

Accordingly, I used literature data from GPS measurements to select the proper values for the strain rate entering the power-law creep equation, which once again is representative of the rheological behaviour of the ductilely deforming lower portion of the crust. At this regard however, it must be also considered that in highly deforming regions like in several Mediterranean sectors where major faults affect the whole crust, ductile shear zones may be possibly characterized by much higher strain rates than geodetically averaged. As a consequence, the BDT depth would locally experience a deepening up to few kilometres and a strength increase of some tens of MPa. In order to maintain the shear zone active and keep concentrating the deformation, in such crustal volumes a sort of compensation there must occur between rock weakening phenomena, caused by grain comminution, and the formation of a fabric (for example, S-C structures) and rock strengthening due to the locally higher strain rate.

Other variations of the strain rate also certainly occur during the seismic cycle. For example, even if during the interseismic period the bulk of the deformation could be characterized by a low strain rate, say 10^{-15} s^{-1}, during the seismic and immediate post-seismic stage a strain rate increase of even 10 orders of magnitude can be temporarily experienced, at least by the uppermost portion of the plastosphere, in correspondence of the deepest tip of the reactivated fault zone (*e.g.* Scholz, 1989).

Due to the transient nature of such phenomenon, it should be properly taken into account, especially when applying rheology studies to the investigation of short-term seismogenic processes or specific active faults mechanics. However, since I am primarily interested in the

long-term rheology and its relationship with the thickness of the seismogenic layer during the longer interseismic period, the possible time-dependent variations of the strain rate related to the very short-term seismic transient have been disregarded in the present study. The reason for this choice lies in the fact that, when the seismic cycle is close to its end and a seismic sequence occurs, the depth of the BDT effectively corresponds to the one stabilized during the interseismic period.

In this view, it is sensible to consider the interseismic BDT depth as a constraint for the thickness of the seismogenic layer and to compare the rheological transition with the depth distribution of the seismic events, especially at the start of the sequence and possibly with the mainshock. In other words, the long-term build-up of the elastic deformation during the interseismic period is conceptually linked to the short-term, rapid release of seismic energy and deformation during the co-seismic stage through the rheological constraint imposed by the depth of the BDT, which corresponds to the bottom of the seismogenic layer when the seismic sequence gets started.

Seismological evidences (*e.g*. Rolandone *et al*., 2004) and mechanical-rheological modelling (Beeler *et al*., 2018) have proved that the embrittlement caused by the increase of the strain rate after a major seismic event may result in a deepening of BDT, with respect to the interseismic period depth, in the range of 1-3 km. Accordingly, afthershocks are often recorded at depths slightly greater than those of the mainshock and of the background seismicity during relative seismic quiescience periods. In order to take into account for such an effect, when comparing the depth distribution of complete seismic sequences, including multiple aftershocks, with the depth of the interseismic BDT, a 90-95% threshold, with respect to the maximum depth of the recorded seismicity, is generally selected for the comparison. Such a procedure, which has now become a standard in these rheological and seismological analyses, has also been followed in this work, as it will be shown later in a dedicated section.

4.2.4 Thermal gradient parameters

Variation of temperature with depth is a crucial issue in the reconstruction of rheological profiles, as the thermal gradient represents the primary factor controlling the ductile shear strength and consequently the depth of the BDT (*e.g*. Sibson, 1984; Doser and Kanamori, 1986). The 1D equation from Çermak (1982) has been used here for modelling the temperature distribution over depth, considering the relation between surface heat flow, depth and radiogenic heat production, as first proposed by Lachenbruch (1968). Accordingly, the aforementiond thermal gradient could be calculated following equation [2.12]. Given the importance of the temperature gradient on the resulting strength envelopes, each parameter of the thermal equation has been tested individually as all of them, even though with different weights, could have a deep impact on the rheological modelling.

In general, as already mentioned in Chapter 2 (see section §2.3), high heat flow values increase the thermal gradient and thus decrease the ductile strength, which also leads to a remarkable shallowing of the BDT depth (Sibson, 1984). As regards the influence of q_0 on the thermal gradient, a ±10% uncertainty implies, for example at 15 km or at a typical Moho depth, a variation of the temperature of ±20-35 and ±80-85 °C, respectively. Such a difference could therefore lead to a shallowing/deepening of the BDT of some kilometres and a peak strength decrease/increase of few tens of MPa.

In principles, thermal conductivity affects the BDT depth and shear strength values in such a way that, for example, a high *k* value means that heat is efficiently transferred to the surface and therefore a relatively low thermal gradient is required to fit the surface heat flow (which in principle should be measured at the site of interest). This would result in generally cooler and hence stronger rocks and a consequently deeper BDT. After having realized several tests with different thermal conductivities and geothermal gradients, I observed that a variation of ±10% of *k* could induce a temperature difference, for example at 15 km or in correspondence of the Moho, of ca. ±10-30 and ±25-40 °C, respectively.

For what concerns the radiogenic heat production rate (see discussion in Chapter 2, section 2.3 for its role and physical meaning for the continental crust geotherm), the introduction of higher A_0 values in the rheological modelling causes a BDT deepening and a ductile strength increase, though induced variations are minimal, if uncertainties of ±10% are considered.

4.3 Case studies from the Aegean Region

As above mentioned, two case studies of rheological profiles are here proposed and used as starting points for the quantitative sensitivity analyses carried out in the following sections. They are both from the Aegean Region and represent two Andersonian regimes (tensile and transcurrent, respectively) that largely pervade this area of the Mediterranean realm (fig. 4.1). Indeed, almost the totality of the seismogenic faults in the internal Aegean domain (with respect to the Hellenic subduction arc) is characterized either by pure normal and strike-slip kinematics or by a combination of the two (see for reference the GreDaSS database from Caputo *et al.*, 2012).

Active thrusting is limited to the central and western sectors of the Hellenic subduction zone and to the regions external with respect to it. In the following, the parametric selection is firstly discussed to provide the preferred models, assumed as the 'reference' in the subsequent sensitivity tests.

4.3.1 Kallidromo area

The first selected case study is from the Kallidromo area, Central Greece, along the southern border of the Sperchios Basin (fig. 4.2a) located in the eastern sector of the External Hellenides

fold-and-thrust belt. The tectonostratigraphic and geological evolution of the area has undergone some major deformation phases, which could be synthetically described as follows: a) the mostly Cenozoic nappe stacking caused by the Alpide orogeny (Brunn, 1956; Aubouin, 1959; van Hinsbergen *et al.*, 2005; Mountrakis, 2006); b) the mainly Pliocene NE-SW trending post-orogenic collapse (Mercier, 1976; Mercier *et al.*, 1987; Caputo and Pavlides, 1993; Doutsos *et al.*, 1994) or gravitational spreading (Le Pichon and Angelier, 1979), causing the thinning of the previously thickened crust and c) the general rearrengement of the stress field within the Aegean domain (Mercier *et al.*, 1979; 1989; Angelier *et al.*, 1982; among others), which started in Middle Pleistocene and still characterizes the whole region.

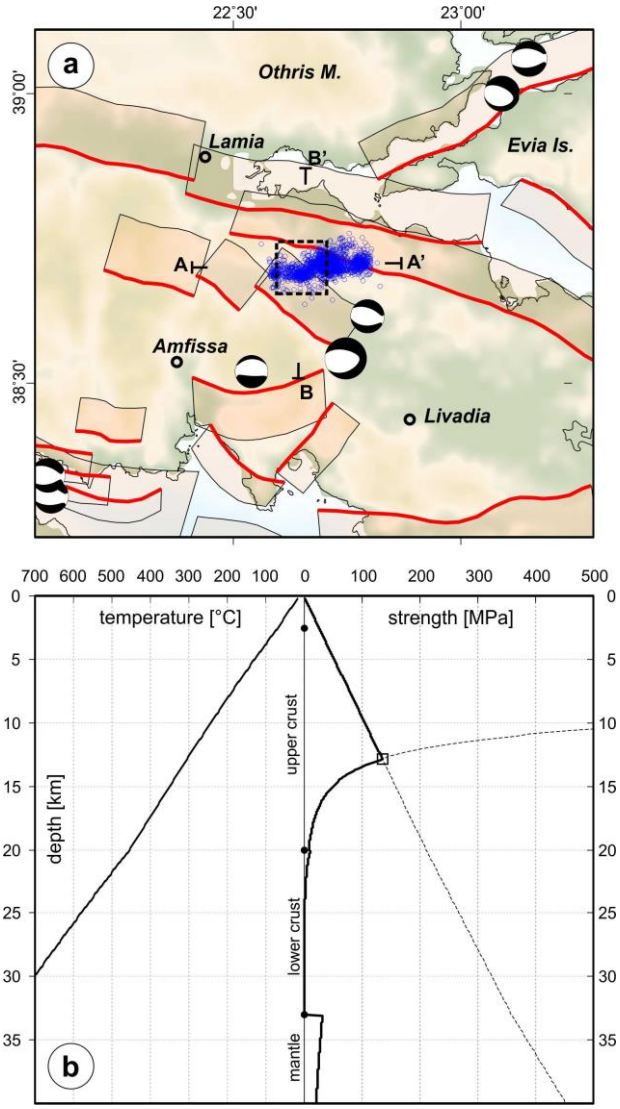

Fig. 4.2 – a) location map of the Kallidromon case study. Major active tectonic structures (composite seismogenic sources) are from GreDaSS (Caputo and Pavlides, 2013) and focal mechanisms (M>5.0) are from CMT (Ekstrom et al., 2012) catalogue. Blue circles represent the 2013 seismic sequence relocated by Ganas et al. (2014). The dashed box represents the test site rheologically modelled in this study. b) thermal gradient (left) and strength profile (right) of the test site.

Such a tectonic phase is characterized by ca. N-S crustal stretching and has generated new, mainly E-W trending, horst and grabens structures, with the latter being filled up with Neogene-

Quaternary sedimentary successions locally as thick as 1.5 km. Accordingly, taking into account the long-term (since Pliocene) stretching and thinning, possibly involving also the upper crust, and considering that the locally outcropping sedimentary portion of the Sub-Pelagonian (Othrys) transitional/oceanic sequence has a thickness of ~1 km (Smith and Morton Moores, 1974), a reasonable value for the complete sedimentary layer thickness is ~2.5 km.

The total crustal thickness can be retrieved from the regional estimates of the Moho depth. From gravity data (Tiberi *et al*., 2001) and tomographic inversion (Zelt *et al*., 2005), the Moho depth in the Kallidromo massif is 31-32 and 33-34 km, respectively. Makris *et al*. (2013), using gravity data constrained by seismic profiles, proposed a value of 32-33 km. I thus selected 32.5 km as the most likely value to represent the Moho depth at this test site. No data are available to discriminate upper and lower crust for the investigated area but, on a global scale, a thickness ratio of lower to crystalline total crust of ca. 0.4-0.45 has been proposed (*e.g*., Rudnick and Fountain, 1995; Rudnick and Gao, 2003). Applying this approach to the Kallidromo area and considering an average topography of 0.5 km (as obtained from SRTM30), the assumed thicknesses for the upper and lower crust are 17.5 and 13 km, respectively.

Based on the geodynamics of the broader area and the local geological conditions and considering also the availability of laboratory tested rocks, the most reasonable lithologies representative of the three upper layers (*viz*. sedimentary cover, upper and lower crust) for the rheological modelling are metasediments, dry quartzite and wet diorite, respectively. I also took into account two deep seismic soundings performed slightly north of the Kallidromo test site, in the Evoikos Gulf, by Makris *et al*. (2001), in order to verify whether the lithological choices were compatible with the detected seismic velocities at depth.

Such a procedure, which consists in deriving the most appropriate lithologies from the seismic velocities using the compilations by Christensen and Mooney (1995), has already been successfully applied in studies based on rheological profiles and modelling realization, *e.g*. in Boncio *et al*. (2007). Clearly, the use of seismic velocities data is subjected to their availability for the investigated region or eventually to their possible extrapolation from close and similar geological-tectonic settings. Accordingly, considering the comparable geological and tectonic framework of the investigated area in Makris *et al.* (2001) with respect to Kallidromo test site, such a methodological approach has been adopted here.

However, for the Kefallinia test site no similar deep seismic soundings are available and therefore, also considering the different tectonic setting, the above-mentioned procedure could have not been applied in this case, as it will be shown later. The values proposed for the upper crust layer by Makris *et al* (2001) are in the range 5.9-6.3 km/s and are therefore compatible with a quartzite lithology, having a typical seismic velocity of ~5.9-6 km/s at depths around 10 km. As regards the lower crust layer, the deep seismic soundings suggest values in the range 6.5-6.8 km/s,

also consistent with the choice of a diorite lithology for such a layer, showing characteristic velocities of ~6.5 km/s at 20 km of depth, according to Christensen and Mooney (1995).

Dry quartzite and wet diorite also correspond to the lithologies proposed for this region in a previous work by Tesauro (2009) and they also seem to be consistent with the present and recent tectonic and geodynamic scenario, where the effects of dehydration of the underlying Nubian slab may be responsible for the presence of water in the overlying mantle wedge and in the lower crust of the overriding Aegean plate, while the uprising of water from the deep mantle wedge did not likely pervade the upper crust.

For the upper mantle (which, however, does not affect directly the modelling of the brittle-ductile transition) a wet dunite lithology has been selected. The corresponding values of power-law exponent n, power-law parameter A and activation energy E (equations [2.9] - [2.10]) for the above lithologies are provided by Brace and Kohlstedt (1980), Chopra and Paterson (1981), Doser and Kanamori (1986), Carter and Tsenn (1987), Ranalli (1995), Afonso and Ranalli (2004), while the values of density ρ, thermal conductivity k and radiogenic heat production A_0 are taken from Çermak and Rybach (1982), Doser and Kanamori (1986), Olhoeft and Johnson (1989), Vilà *et al.* (2010), Turcotte and Schubert (2014), Marotta *et al.* (2015). All values are reported in Table 4.1.

On the basis of the S-waves receiver functions technique, the base of the Aegean lithosphere in the study area is taken to be ~150 km deep (Artemieva *et al.*, 2006; Sodoudi *et al.*, 2006). I would like to stress however, that the depth of the lithosphere-asthenosphere boundary (LAB) basically influences the geothermal gradient in the lithospheric mantle, but for the Kallidromo case study it does not affect the estimate of the BDT depth, which in any case occurs within the (upper) crust.

Based on the analysis of the geodetic velocity field, the present-day strain rate interpolated for the broader Kallidromo area ranges between $3 \cdot 10^{-15}$ and $6.5 \cdot 10^{-15}$ s^{-1} (Hollenstein *et al.*, 2008; Floyd *et al.*, 2010; Kreemer *et al.*, 2014; England *et al.*, 2016). Following the discussion of section §4.2 and considering that the Kallidromo area is affected by major crustal faults, in order to take into account the actual concentration of strain, the upper bound of the above-mentioned strain rate range ($6.5 \cdot 10^{-15}$ s^{-1}) has been selected.

As previously discussed, a value of 0.70-0.75 for the friction coefficient μ is commonly assumed in rheological modelling. However, taking into account that major crustal faults affect the Kallidromo area (e.g. Tithorea Fault-GRCS434; Caputo and Pavlides, 2013) since at least Middle Pleistocene, with a cumulative slip in the order of some hundreds meters, for the purpose of the present study a slightly lower friction coefficient (0.60) has been assumed as the preferred value. As far as in the Kallidromo region the tectonic regime is purely tensile, β is unity and the α parameter could be readily calculated from equations [3.4] and [3.5]. As a consequence, it takes a value of 0.68.

As concerns the pore fluid pressure, hydrostatic conditions could be reasonably assumed in the study area as far as there are no particular reasons for supra- or sub-hydrostatic conditions to occur within the crust of the Kallidromo area. Consequently and assuming common density values, the Skempton coefficient λ_e is conventionally posed equal to 0.4.

As regards the surface heat flow, the works of Cloetingh *et al.* (2010), Fytikas and Kolios (1979), Hurter and Haenel (2002) and Taktikos (2001) have been considered. The latter two have been discarded for this study, since Hurter and Haenel (2002) show a systematic anomalously high heat flow with respect to all the other studies likely due to some bias in the interpolation. As for the map proposed by Taktikos (2001), it is characterized by the presence of some single spike-like markedly high values probably suffering i) from the scattered geographical distribution of the source data, ii) a possible bias due to a concentration of measurements at (hot) spring sites and iii) a likely unsuitable interpolation method. Thus, only the values proposed by Fytikas and Kolios (1979) and Cloetingh *et al.* (2010) have been averaged, assigning a greater weight (ratio of 2:1) to the former, due to their focus on the Aegean Region. In summary, the inferred surface heat flow value for the study area is 75 mW/m2.

Based on the above constraints, estimates and assumptions providing the preferred parametric model (Table 4.1), the local rheological profile has been reconstructed, using a purposely developed Matlab® code. The results for the Kallidromo test site show the occurrence of the BDT at a depth of 12.3 km, where the temperature is 303 °C and the corresponding shear strength is 136 MPa (fig. 4.2b). The strength envelope shows the predominance of the frictional sliding behaviour for the sedimentary layer and the higher portion of the upper crust. Here the brittle-ductile transition occurs and the ductile creep characterizes all the remaining layers (lower portion of the upper crust, lower crust and upper mantle) as the prevailing deformation mechanism. Such an envelope implies that the strength at the BDT corresponds to the maximum shear strength along the entire profile. The reason for this characteristic are that i) no other brittle layer is encountered along the profile and ii) the creep strength tends to uninterruptedly diminish from the BDT to greater depths due to increasing temperature.

4.3.2 Kefallinia area

The second case study corresponds to the area of the Kefallinia island (fig. 4.3a), which is the major of the Ionian islands (western Greece). From a tectonic point of view, this region is dominated by the presence of the Kefallinia Transform Fault (KTF), which exhibits prevailing dextral strike-slip kinematics with a slight inverse component and can be subdivided into a (southern) Kefallinia, NE-trending and a (northern) Lefkada, NNE-trending segment, both steeply (~65°) ESE dipping (Scordilis *et al.*, 1985; Louvari *et al.*, 1999). The KTF separates the External Hellenides accretionary wedge still evolving along the Hellenic Arc from the Adriatic/Apulian

block representing the foreland. This crustal-scale shear zone is characterized by ~20 mm/a of cumulative slip rate (Serpelloni *et al.*, 2005; Ganas *et al.*, 2016).

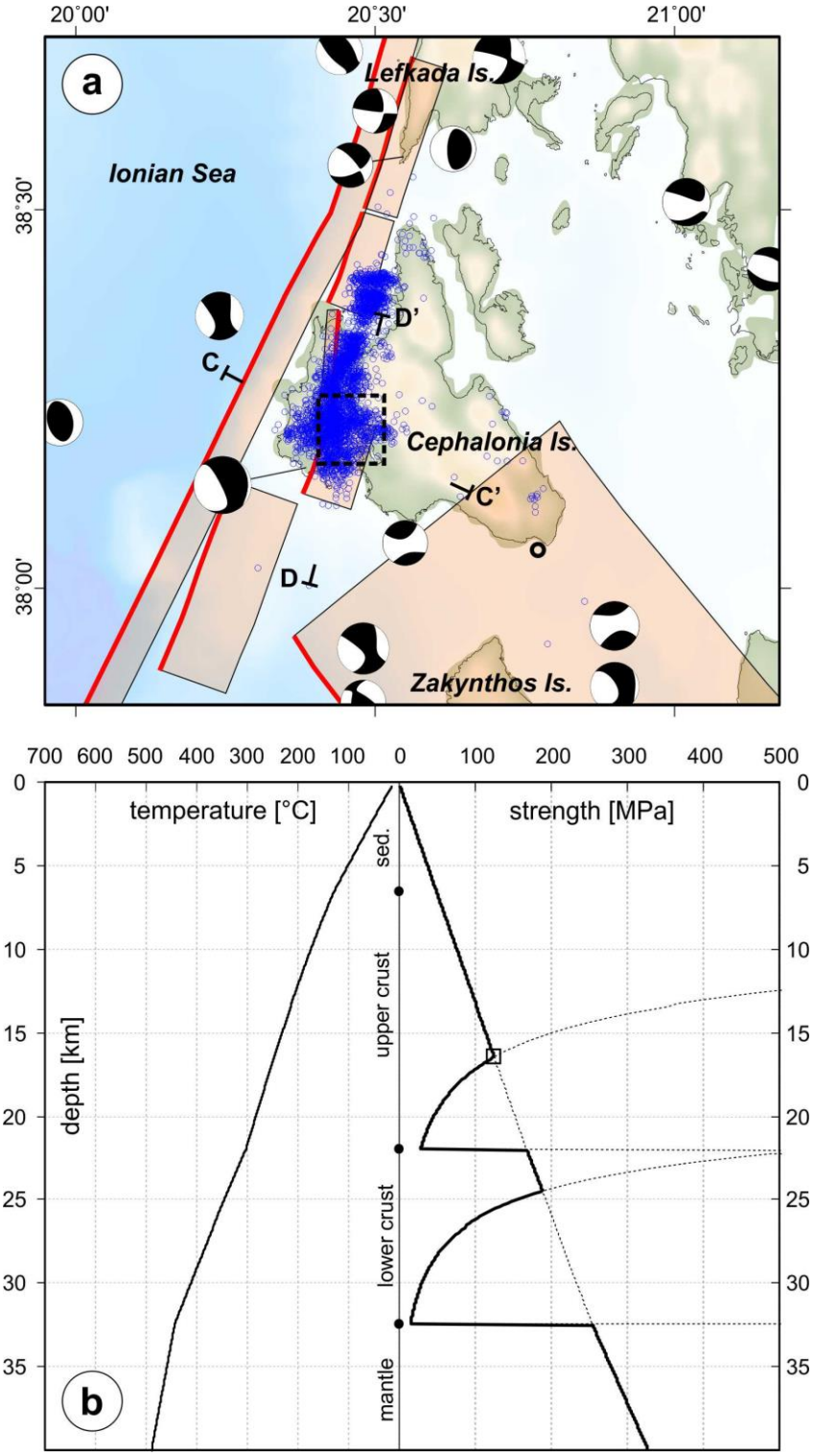

Fig. 4.3 – a) location map of the Kefallinia Island case study. Major active tectonic structures (composite seismogenic sources) are from GreDaSS (Caputo and Pavlides, 2013) and Ganas et al. (2016), and focal mechanisms (M>5.0) are from CMT catalogue. Blue circles represent the 2014 seismic sequence relocated by Karastathis et al. (2015). The dashed box represents the test site rheologically modelled in this study. b) thermal gradient (left) and strength profile (right) of the test site.

The KTF accommodates the markedly different convergence rates characterizing on the southern side the Hellenic trench (where the Ionian/Nubian oceanic lithosphere is subducting at ~35 mm/a beneath the Aegean microplate), and, on the northern side, the continental collision between Adria/Apulia and the Dinarides/Albanides orogens, where the relative motion (i.e. convergence) is noticeably slower (~5-10 mm/a) (Royden and Papanikolaou, 2011).

Given the complexity of the kinematic frame and the tectonic setting, strikingly different geological and tectonostratigraphic crustal domains are juxtaposed on the two sides of the KTF. In order to avoid averaging and approximations of the parameters used for the rheological modelling, the area selected for this second test site corresponds to the rock volume containing the January/February 2014 seismic sequence, 10 km east of the KTF (Karastathis *et al.*, 2015). It thus geologically belongs to the Aegean microplate. In terms of tectonostratigraphic domain, the region is part of the Paxos Zone, where Smith and Morton Moores (1974) indicate the occurrence of a sedimentary cover (mainly consisting of marls, sandstones, limestones, cherts, dolomites and anhydrites) up to 3.5-4 km-thick. However, taking into the account the close presence of the Mediterranean ridge accretionary prism, the overall thickness of the sedimentary layer is likey to be larger, say ca. 6.5 km, as also suggested by Makris *et al.* (2013). The latter value has been accordingly assumed as more representative for this site.

The estimates of the Moho depth are provided by several authors (Sodoudi *et al.*, 2006; Raykova and Nikolova, 2007; Makris *et al.*, 2013; Grigoriadis *et al.*, 2016) using different methods, like P- and S-waves receiver functions, surface waves tomography, gravity data or gravity constrained by seismic profiles. Likely due to the different methodological approaches and original datasets, they provide a quite wide range of values for this site, going from ~27 to ~40 km. It should be also noted that the proximity to the downgoing, transitional/oceanic, Ionian/Nubian lithosphere, whose exact geometry may be modelled and considered differently in the inversions, could strongly interfere with the estimates of the overriding (Aegean plate) Moho depth. For the purpose of the rheological modelling, an average Moho depth of 32.5 km has been thus assumed.

Then, the thicknesses of the upper and lower crust have been assigned following the same approach described for the Kallidromo test site. The resulting values are, respectively, 15.5 and 10.5 km. As concerns the lithologies representative of the sedimentary cover, the upper and the lower crusts, and the upper mantle, carbonate (given the prevailing nature of the tectonically piled up sedimentary rocks), wet quartzite, wet diorite and wet dunite have been respectively selected. The choice of a wet lithology also for the upper crust is justified by the very close occurrence of the subduction zone, and by the lithospheric-scale nature of the KTF, which is expected to be connected at depth to the lower crust and to the Benioff zone, therefore facilitating the rise of fluids. The corresponding values of A, n, E, ρ, k and A_0 for the aforementioned lithologies are listed in Table 4.1.

The thickness of the lithosphere is taken from Sodoudi (2005) to be ~180 km, on the basis of the S receiver functions estimation technique.For the strain rate of the Kefallinia test site, the different interpolations provided by several authors (Hollenstein *et al.*, 2008; Floyd *et al.*, 2010; Kreemer *et al.*, 2014; England *et al.*, 2016), based on the analysis of geodetic data, indicate values ranging between $2 \cdot 10^{-15}$ and $7 \cdot 10^{-15}$ s^{-1}. Similarly to the Kallidromo case study, the upper bound value of $7 \cdot 10^{-15}$ s^{-1} has been selected.

For what concerns the coefficient of friction μ, it has been taken into account that the KTF system contains major crustal faults characterized by high slip rates. It is therefore reasonable to assume 'smooth' fault zones and for the purpose of the rheological modelling this could be expressed by a lower μ (0.5). As above mentioned, the Kefallinia test site is affected by a transpressional tectonic regime for which a certainly more appropriate stress ratio β of ~0.4 has been assumed. As a consequence, the calculated α parameter takes a value of 0.98.

As regards the pore fluid pressure and considering that the investigated crustal volume belongs to the accretionary wedge being obliquely affected by the KTF, a slightly suprahydrostatic value of $\lambda e = 0.7$ has been considered. The Kefallinia area is located far away from the Hellenic volcanic arc, it is characterized by a recently thickened crust and, as expected, the surface heat flow is quite low. Following the same approach of the other test site, the local heat flow value is ~42 mW/m^2. Based on the above constraints, estimates and assumptions providing the preferred parametric model (Table 4.1), the local rheological profile for the Kefallinia test area yields a BDT depth of 16.4 km, where the temperature is 246 °C and the corresponding shear strength is ~125 MPa (fig. 4.3b).

Differently from the Kallidromo test site, here two additional brittle layers occur (respectively, in the uppermost portion of the lower crust and in the upper mantle) at depths greater than the first BDT. The brittle layer in the lower crust has a reduced thickness of ~2 km, while the one in the mantle reaches a greater thickness of ~25 km. Consequently, the maximum value of the shear strength (~500 MPa) is attained at the lowermost brittle-ductile transition, in the mantle.

4.4 Methodological approach

As above mentioned, the principal aim of this work is to assess and analyze the sensitivity of rheological profiles to the several input parameters. In other words, variability in the resulting BDT depth, the corresponding temperature and peak shear strength is here investigated quantitatively, by changing the values of the input parameters. Such a procedure is carried out by obtaining numerous rheological profiles, using a dedicated Matlab® code. For each rheological profile, a single parameter is varied at time with respect to the reference models described earlier, so that its influence on the resulting rheological modelling can be properly evaluated.

Each rheological parameter is varied within the uncertainties provided by the authors that carried out the laboratory experiments, or considering the constraints provided by a careful geological, tectonic and evolutionary analysis of the selected lithospheric volumes. If the uncertainty cannot be defined, the variation is assumed to be ±10% with respect to the preferred value.

Such a variation value has been chosen as I considered it to be comparable with the variations of the parameters whose uncertainties had already been defined. Variations equal to ±5% and ±15% of the preferred value of the corresponding parameter have also been tested, but no relevant impact on the sensitivity results has been found out, with respect to selecting a fixed ±10% variation for each parameter. Accordingly, I decided, for simplicity sake and coherence with the already fixed parameters variations, to select and apply the ±10% uncertainty threshold for all the parameters.

The Matlab® code produces strength envelopes through an iteration process, from average topography or sea level to the LAB (lithosphere-astenosphere boundary) depth, with each loop representing a vertical step of 100 m (see also section §3.2.3). Finer griddings with nodes every 50 m and 20 m have also been tested but I verified that, in spite of an augmentend elaboration time, no sensible improvement in the resolution and reliability of the results was obtained. The assumed vertical step then represents a reasonable compromise between the need for precise, high-resolution profiles and computer running time. The yield strength envelopes can be easily represented and visualized by means of simple cartesian graphs, where the critical stress (expressed as differential stress) is on the abscissa axis, while the corresponding depth is on the ordinate axis (fig. 4.2b and 4.3b). The 1D lithospheric column is subdivided into four lithologically uniform layers, namely the sedimentary cover, the upper crust, the lower crust and the upper mantle.

Only the purely brittle and ductile behaviours (*i.e.* frictional sliding and power-law creep equations, respectively) are here taken into account, given the aforementioned shortcomings and drawbacks of using the empirical equations proposed for the intermediate behaviour (Bos and Spiers, 2002; Wei and Zang, 2006; Zang *et al.*, 2007). The purposely developed Matlab code, for each vertical step, calculates the values of three following variables: temperature at depth, brittle frictional strength and power-law creep strength.

Calculations are always 1D, both for the constitutive rheological equations and for the geothermal gradient, where thermal conductivity is therefore assumed to vary only along the vertical direction. The code also compares the values of the strength for the two rheological behaviours so that the lesser between the two is always determined and BDT depth, along with its corresponding strength and temperature, is finally recorded.

The first assumption here is that the active deformation mechanism (between frictional sliding and ductile creep) is always the one requiring less stress to be applied in order to initiate

the deformation process. It follows that, whenever ductile strength (and viceversa) becomes smaller than frictional one, the prevailing deformation mechanism switches from stick-slip, potentially seismogenic behaviour to slow, continuous and distributed creep.

A second assumption is related to the modelled vertical stratification of the lithosphere: all the layers are considered to be internally characterized by homogenous lithological properties and moreover, since the modelling is one-dimensional, no potential lateral variations and volume effects are considered. However, it is noteworthy to highlight that the selected test sites lie in such geological domains that are likely to be characterized by lateral continuity in the lithological (and consequently in the rheological) properties, at least in the proximity of the test sites.

Accordingly, I do not expect to overlook any relevant areal or volumetric effect on the local-scale 1D modelling. In case of occurence of a ductile layer embedded within two brittle layers (for example upper crust and lower crust layers), the BDT has been selected in correspondence of the shallower brittle-to-ductile transition, provided that a sufficient thickness of the ductile layer is interposed.

Such mechanical conditions during coseismic rupture propagation should guarantee a sufficient decoupling between the two brittle bodies and hence making independent their seismogenic potential. The latter issue is crucial in seismotectonic investigations to which rheological profile modelling could provide a reasonable base and a strong constraint relative to the maximum width of the seismic rupture (as a function of the dip angle) and therefore also to the possible maximum expected magnitude for a crustal fault (obviously assuming the length is known). At this regard, Beeler *et al.* (2018) have recently proposed a possible coseismic deepening of the BDT of about 10% of the 'interseismic' depth, while Rolandone *et al.* (2004) documented an immediate 2-3 km deepening of the seismic-aseismic transition after the Landers earthquake followed by a time-dependent shallowing in the subsequent years.

However, the theoretical approach followed in the former paper and the seismotectonic setting characterizing the latter case strongly differ from the selected test sites of this study as far as the investigated faults here are inclined and not vertical, the maximum expected magnitude is certainly smaller (and hence the coseismic slip is comparably shorter), while slip- and strain rate are both more diffuse within the investigated crustal volumes than the only 100 m-thick shear zone assumed by Beeler *et al.* (2018). Based on these differences, a more reasonable criterion for selecting the shallower rheological transition is verified when the interposed ductile layer is at least of 500 m.

Moreover, as far as in the selected crustal conditions the BDT always occurs within the upper crust, with only few exceptions in the Kefallinia test site, in this reasearch are described and discussed only the sensitivity tests that have been performed in a systematic way for all relevant parameters characterizing this lithospheric layer (the upper crust), keeping fixed all the lithological and thermo-rheological parameters of the other modelled layers.

4.5 Results and discussion

4.5.1 Single parameter effects

As previously mentioned, in a first investigation phase only one parameter is changed at time. Accordingly, the *reference model* of each case study is adopted to fix the other parameters during the calculation of the several rheological profiles (see Table 4.1). The results of all sensitivity tests on single parameters are synthetized in Table 4.2 and Table 4.3 for, respectively, the Kallidromo and Kefallinia test sites, where the BDT depths and relative peak strengths and temperatures are reported, together with the tested range of each parameter.

Kallidromo area

As concerns the effects of the single-parameter variations on the BDT depth, the most influencing ones belong to the constitutive equation of the power-law creep deformation mechanism. The most influencing parameter is the activation energy, causing the strongest BDT depth variation (±2.3 km), while the uncertainty on the exponent n also induces a +0.8/-0.9 km change. Such effects are likely due to the high reference value (10^5 J/mol) and the exponential role in equation [2.9], respectively. These effects are reflected on the numerical results even if only a ±10% uncertainty range is considered. However, also the surface heat flow and the thermal conductivity, which determine the geothermal gradient, induce BDT changes of about 1 km (up to 1.4 km).

		Kallidromo site				**Kefallinia site**			
		SD	**UC**	**LC**	**UM**	**SD**	**UC**	**LC**	**UM**
		Metasediments	Quartzite Dry	Diorite Wet	Dunite Wet	Metasediments	Quartzite Wet	Diorite Wet	Dunite Wet
thick.	km	2.5	17.5	13.0	117.0	6.5	15.5	10.5	147.5
α	/								
β	/	1.0				0.4			
μ	/	0.6				0.5			
λ_e	/	0.4				0.7			
Q_0	mW/m^2	75				42			
$\dot{\varepsilon}$	s^{-1}	$6.5 \cdot 10^{-15}$				$7.0 \cdot 10^{-15}$			
ρ	kg/m^3	2650	2650	2840	3350	2650	2650	2840	3350
A	MPa$^{-n} \cdot$ s^{-1}	$5.0 \cdot 10^{-6}$	$6.7 \cdot 10^{-6}$	$3.2 \cdot 10^{-2}$	$2.0 \cdot 10^{3}$	$5.0 \cdot 10^{-6}$	$3.2 \cdot 10^{-4}$	$3.2 \cdot 10^{-2}$	$2.0 \cdot 10^{3}$
n	/	3	2.4	2.4	4	3	2.3	2.4	4
E	J/mol	$1.9 \cdot 10^{5}$	$1.56 \cdot 10^{5}$	$2.12 \cdot 10^{5}$	$4.71 \cdot 10^{5}$	$1.9 \cdot 10^{5}$	$1.54 \cdot 10^{5}$	$2.12 \cdot 10^{5}$	$4.71 \cdot 10^{5}$
k	W/m·K	3.3	3	2.91	/	3.3	3	2.91	/
A_0	W/m^3	$1.84 \cdot 10^{-6}$	$1.84 \cdot 10^{-6}$	$8.62 \cdot 10^{-7}$	/	$1.84 \cdot 10^{-6}$	$1.84 \cdot 10^{-6}$	$8.62 \cdot 10^{-7}$	/

Table 4.1 *- 'Preferred' values used for determining the rheological behaviour of the sedimentary cover (SD), upper crust (UC), lower crust (LC) and upper mantle (UM) in the two case studies. See text for discussion. The corresponding strength envelopes have been taken as reference models during the sensitivity analyses (see figures 4.2 and 4.3).*

As discussed in a previous section, this is in line with the weight exerted by the thermal properties on the depth distribution and layering of brittle versus ductile behaviours. As concerns the remaining tested parameters, and especially those used for describing the brittle behaviour, none of them seems to have a relevant influence on the BDT depth, inducing variations in the calculated values of only few hundred meters (maximum 0.4 km).

As regards the peak shear strength (*i.e.* the strength at the BDT depth), a major role is played by the choice of the parameters describing the frictional sliding behaviour, and particularly by the friction coefficient, which may induce a strength variation of 25 MPa if a lower (μ = 0.4) than standard value is assumed. Similar changes (-20/+18 MPa) are caused by ±0.1 variation of the pore fluid factor, while the tested ranges of ρ, $\acute{\varepsilon}$ and β have a limited effect, by inducing less than 10 MPa differences in peak shear strength. The relevance of friction and fluid pressure on the resulting peak strength is actually an expected feature, since these factors directly affect the capability of rocks to build up and sustain a certain amount of stress. However, also the parameters governing the 'thermal-ductile' behaviour of rocks (E, q_0, n and k) could induce comparable variations of several MPa, from ±9 and up to +24/-25 MPa (*e.g.* activation energy).

A further property I focused on in order to assess the relative importance of all the constitutive parameters for the thermorheological modelling is the temperature at the BDT depth, which can also give insights on the mineralogical and mechanical characteristics of the typical rocks at the corresponding depths. Once again, the most influencing parameter is the activation energy, whose ±10% 'uncertainty' relative to the reference value leads to temperature changes of almost 50 °C. However, since the activation energy and to a lesser extent the power-law exponent, though affecting the ductile creep strength, are not directly controlling the geothermal gradient, their influence on the temperature is simply due to the vertical shift of the BDT itself. Perhaps quite unexpectedly, the tested uncertainties of the other "thermal" parameters (namely, the heat flow, the thermal conductivity and the radiogenic heat production) only cause very slight changes of the BDT temperature, in the order of a few degrees. Also for these parameters, the apparent lack of influence is likely due to the fact that, even though the geothermal gradient is substantially modified, at the same time also the BDT depth is shifted, and the combined effect ultimately acts to produce an almost zero net variation of the BDT temperature. None of the other parameters produces significant temperature variations at the BDT within the tested ranges.

Kefallinia area

The Kefallinia test site is characterized by a deeper BDT with respect to Kallidromo (16.4 *vs* 12.3 km), though exhibiting a comparable peak shear strength (125 *vs* 136 MPa). This is likely due to the different lithologies and, above all, fluid pressure conditions at depth.

Analogous to the Kallidromo case study, the most relevant BDT depth variations are obtained when testing the uncertainties on the activation energy that induce a +4.3/-4.0 km changes. Also the heat flow tested range induces a sensible BDT depth variation (-1.8/+2.4 km). On the other

hand, n and k, among the other creep parameters, and μ and λ_e, among the parameters describing the brittle behaviour, have a limited influence (in the range -1.3 and +1.4 km, but with opposite roles). The effects of the other parameters is instead negligible.

As concerns the peak shear strength, the greatest weights are exerted by the Skempton coefficient (-36/+66 MPa) and by the friction coefficient (+38/-41 MPa). In particular, pore fluid pressure could locally attain markedly variable values within an accretionary wedge setting (*e.g.* Suppe, 2014), such as that of Kefallinia, and consequently it plays a major role in defining the stress tensor distribution at depth and the total strength of rocks. On the other hand, also the friction coefficient could be characterized by possible vertical (and lateral) variations due to the presence of asperities and irregularities along the fault surface of a major and well developed structure such as the Kefallinia Transform Fault; this effect should be carefully taken into account in computing the value of peak shear strength when modelling the rheology of crustal volumes containing major shear zones. Similarly to the Kallidromo case study and likely for the same reasons, also in terms of peak strength, the tested range of the activation energy causes important differences in the calculated strength values (+32/-31 MPa). Although to a lesser extent, also the uncertainty on the heat flow and secondarily on the power-law exponent and β factor could induce less than ±20 and *ca.* ±10 MPa variations of the BDT peak strength, respectively.

The BDT temperature variations are mostly influenced by the activation energy parameter, similarly to what observed in the Kallidromo area. In this case, the maximum variations are in the order of ±43 °C. Among the other parameters, only the friction and Skempton coefficients and n could induce up to ±10-15 °C of temperature change within the tested range of values, while the effect of the remaining ones is negligible.

4.5.2 Combined effects

I also analyzed the combined effects on the BDT depth and the associated values of strength and temperature by simultaneously varying all tested parameters. In order to achieve this goal, a statistical approach was followed. Firstly, a set of 10k values for each tested parameter has been randomly generated. All the distributions have been generated by considering the preferred value of the reference model (Table 4.1) as the mean value, with the extremes of the uncertainty range, reported in Tables 4.2 and 4.3, as the values delimiting the 95% confidence interval of the randomly generated distributions. For the sake of simplicity, a Gaussian normal distribution has been generally assumed, with the only exceptions of the friction coefficient (for both test sites), the Skempton coefficient λ_e for Kefallinia and the tectonic regime factor β for Kallidromo, which are better represented by skewed normal distributions (due to the asymmetric ranges), or by a truncated normal distribution in the case of β for Kallidromo.

	Kallidromo										
tested parameters	**reference model**	**tested range**	**BDT [km]**	**δ [km]**	**δ/BDT [%]**	**$\Delta\sigma_{BDT}$ [MPa]**	**δ [MPa]**	**$\delta/\Delta\sigma_{BDT}$ [%]**	**T_{BDT} [°C]**	**δ [°C]**	**δ/T_{BDT} [%]**
β	1	0.9	12.2	-0.1	-0.8	144	8	5.9	301	-2	-0.7
		1	12.3	0.0	0.0	136	0	0.0	303	0	0.0
μ	0.6	0.4	12.7	-0.4	-3.3	111	-25	-18.4	312	9	3.0
		0.75	12.1	0.2	1.6	147	11	8.1	299	-4	-1.3
ρ	2650 [kg·m^{-3}]	2385	12.4	-0.1	-0.8	126	-10	-7.4	305	2	0.7
		2915	12.2	0.1	0.8	145	9	6.6	301	-2	-0.7
λ_e	0.4	0.3	12.0	0.3	2.4	154	18	13.2	297	-6	-2.0
		0.5	12.6	-0.3	-2.4	116	-20	-14.7	310	7	2.3
$\dot{\varepsilon}$	6.5·10^{-15} [s^{-1}]	4.0·10^{-15}	11.9	0.4	3.3	131	-5	-3.7	295	-8	-2.6
		9.0·10^{-15}	12.5	-0.2	-1.6	138	2	1.5	307	4	1.3
A	6.70·10^{-6} [MPa^{-n}·s^{-1}]	6.03·10^{-6}	12.4	-0.1	-0.8	137	1	0.7	305	2	0.7
		7.37·10^{-6}	12.2	0.1	0.8	134	-2	-1.5	301	-2	-0.7
n	2.4	2.16	13.2	-0.9	-7.3	145	9	6.6	322	19	6.3
		2.64	11.5	0.8	6.5	127	-9	-6.6	286	-17	-5.6
E	1.56·10^{5} [J·mol^{-1}]	1.40·10^{5}	10.0	2.3	18.7	111	-25	-18.4	254	-49	-16.2
		1.72·10^{5}	14.6	-2.3	-18.7	160	24	17.6	352	49	16.2
q_0	75 [mW·m^{-2}]	67.5	13.7	-1.4	-11.4	150	14	10.3	298	-5	-1.7
		82.5	11.1	1.2	9.8	123	-13	-9.6	306	3	1.0
k	3.0 [W·m^{-1}·K^{-1}]	2.7	11.3	1.0	8.1	125	-11	-8.1	305	2	0.7
		3.3	13.2	-0.9	-7.3	145	9	6.6	299	-4	-1.3
A_0	1.84·10^{-6} [W·m^{-3}]	1.66·10^{-6}	12.2	0.1	0.8	134	-2	-1.5	303	0	0.0
		2.02·10^{-6}	12.4	-0.1	-0.8	137	1	0.7	303	0	0.0
reference model			**12.3**			**136**			**303**		

***Table 4.2**: Ranges of the tested parameters for the Kallidromo test site.*

	Kefallinia										
tested parameters	**reference model**	**tested range**	**BDT [km]**	**δ [km]**	**δ/BDT [%]**	**$\Delta\sigma_{BDT}$ [MPa]**	**δ [MPa]**	**δ/$\Delta\sigma_{BDT}$ [%8**	**T_{BDT} [°C]**	**δ [°C]**	**δ/T_{BDT} [%]**
β	0.4	0.3	16.1	-0.3	-1.8	136	11	8.8	243	-3	-1.2
		0.5	16.6	0.2	1.2	115	-10	-8.0	248	2	0.8
μ	0.5	0.3	17.7	1.3	7.9	84	-41	-32.8	260	14	5.7
		0.75	15.5	-0.9	-5.5	163	38	30.4	237	-9	-3.7
ρ	2650 [kg·m^{-3}]	2385	16.6	0.2	1.2	118	-7	-5.6	248	2	0.8
		2915	16.2	-0.2	-1.2	130	5	4.0	244	-2	-0.8
λ_e	0.7	0.5	15.1	-1.3	-7.9	191	66	52.8	232	-14	-5.7
		0.8	17.5	1.1	6.7	89	-36	-28.8	258	12	4.9
$\acute{\varepsilon}$	$7.0\cdot10^{-15}$ [s^{-1}]	$4.5\cdot10^{-15}$	15.9	-0.5	-3.0	121	-4	-3.2	241	-5	-2.0
		$9.5\cdot10^{-15}$	16.8	0.4	2.4	128	3	2.4	250	4	1.6
A	$3.20\cdot10^{-4}$ [MPa^{-n}·s^{-1}]	$2.88\cdot10^{-4}$	16.5	0.1	0.6	125	0	0.0	247	1	0.4
		$3.52\cdot10^{-4}$	16.3	-0.1	-0.6	124	-1	-0.8	245	-1	-0.4
n	2.3	2.07	17.8	1.4	8.5	135	10	8.0	261	15	6.1
		2.53	15.2	-1.2	-7.3	115	-10	-8.0	234	-12	-4.9
E	$1.54\cdot10^{5}$ [J·mol^{-1}]	$1.39\cdot10^{5}$	12.4	-4.0	-24.4	94	-31	-24.8	203	-43	-17.5
		$1.69\cdot10^{5}$	20.7	4.3	26.2	157	32	25.6	289	43	17.5
q_0	42 [mW·m^{-2}]	37.8	18.8	2.4	14.6	143	18	14.4	242	-4	-1.6
		46.2	14.6	-1.8	-11.0	111	-14	-11.2	250	4	1.6
k	3.0 [W·m^{-1}·K^{-1}]	2.7	15.4	-1.0	-6.1	117	-8	-6.4	248	2	0.8
		3.3	17.3	0.9	5.5	131	6	4.8	244	-2	-0.8
A_0	$1.84\cdot10^{-6}$ [W·m^{-3}]	$1.66\cdot10^{-6}$	16.2	-0.2	-1.2	123	-2	-1.6	246	0	0.0
		$2.02\cdot10^{-6}$	16.6	0.2	1.2	126	1	0.8	246	0	0.0
reference model			**16.4**			**125**			**246**		

***Table 4.3**: Ranges of the tested parameters for the Kefallinia test site*

Secondly, assuming that the variability of each parameter is basically independent from the others, the above sets (of 10000 values each) have been randomly combined for calculating as many rheological profiles for each case study. The results for Kallidromo and Kefallinia test sites are represented in fig 4.4 and 4.5, respectively, as probability density functions graphs of the three main descriptive indicators (namely, the BDT depth, strength and temperature). Histograms are built considering bins of 0.5 km, 5 MPa and 5 °C, for the BDT depth, its strength and temperature, respectively. In order to verify the robustness of the statistical results, for each analyzed indicator, the procedure has been applied to ten 10k populations and as many curves are plotted in fig. 4.4 and 4.5. The light gray thick line represents the average of the ten datasets (*viz.* 100k random combinations), which confirms the stability of the outcomes.

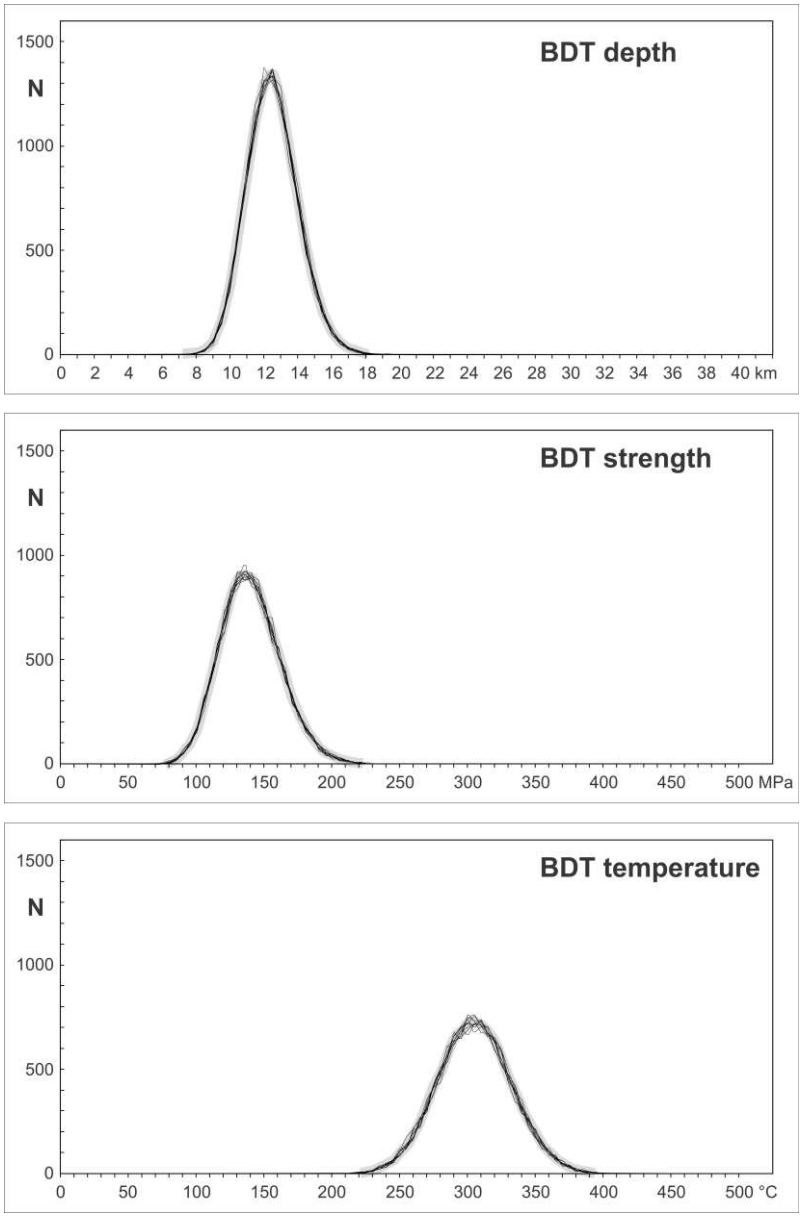

Fig. 4.4 – Frequency distributions of the 100000 random combinations from the Kallidromo test site for the BDT depth (a), BDT strength (b), and BDT temperature.

It is noteworthy that the Kallidromo distribution for the BDT depth (fig. 4.4a) follows a quasi-normal geometry, slightly positively skewed. For each of the ten plots the mode, expressed in terms of the most populated depth class having a dimension of 0.5 km, has been selected and the ten values averaged, showing that it basically coincides with the BDT depth obtained from the reference model (bin 12.0-12.5 km *versus* 12.3 km). The standard deviation for the BDT depth over the whole 10 populations of 10k parametric combinations are quite limited, being *ca.* ±1.5 km, thus indicating that all the values are focused around the mean and occur in the upper crust layer.

The frequency distribution of the strength at the BDT depth (fig. 4.4b) is slightly more positively skewed than the BDT depth (quasi-normal) distribution. For this parameter, the most frequent class corresponds to 130-135 MPa, in good agreement with the reference model value (136 MPa). The slightly longer tail on the greater values may be due to the effect of the β factor, whose assumed distribution is obviously truncated at 1 (the reference model value) and results in slightly greater strengths for all the other values of the distribution. The standard deviation is up to ~22 MPa, mostly because of the uncertainties in the pore fluid pressure, the friction coefficient and the above-mentioned tectonic regime factor β.

Also, as regards the BDT temperature distribution (fig.4.4c), this resembles a normal one, with the peak in the bin 295-300 °C, being compatible with the typical values for the onset of plasticity of quartz, typically placed at 300 ±50 °C (*e.g.* Scholz, 1989). The mean value of the 100k-combinations is ~303 °C (standard deviation of almost 27 °C), perfectly coinciding with that obtained from the reference model (303 °C).

For the Kefallinia test site, the BDT depth frequency distribution basically follows a quasi-normal shape (fig. 4.5a), though the deeper tail in the upper crust is slightly truncated due to the lithological stratification (upper/lower crust boundary), while a minor cluster occurs around bin 26.0-26.5 km-depth (*i.e.* in the lower crustal layer). However, as far as this cluster represents less than 4% of the total random combinations, it could be considered statistically meaningless and therefore the distribution should be not effectively considered as bimodal. The calculated average values of the 10k most populated classes falls in the bin 16.0-16.5 km and the 100k-combinations mean is 16.5 km (while the standard deviation is 3.1 km), in perfect agreement with the reference model value of 16.4 km.

The distribution of the peak strength is instead clearly unimodal, with a roughly normal distribution, even though with a sensible positive skewness (fig. 4.5b). This difference could be possibly, but not exclusively, related to the few BDTs occurring in the lower crust, since the strength is not solely dependent on the depth, as it is instead the case for the BDT temperature. The average of the most populated classes for the 10 datasets falls in the bin 115-120 MPa, with a 100k-combinations mean of 136 MPa (standard deviation of ca. 43 MPa), in reasonable agreement with the value obtained on the basis of the reference model (125 MPa).

As previously mentioned, the temperature is directly dependent on the depth. As expected, the overall distribution of the BDT temperatures obtained for the Kefallinia test site closely resembles that of the BDT depth, showing a secondary and statistically negligible peak around bin 340-345 °C (fig. 4.5c), representing less than 4% of the results.

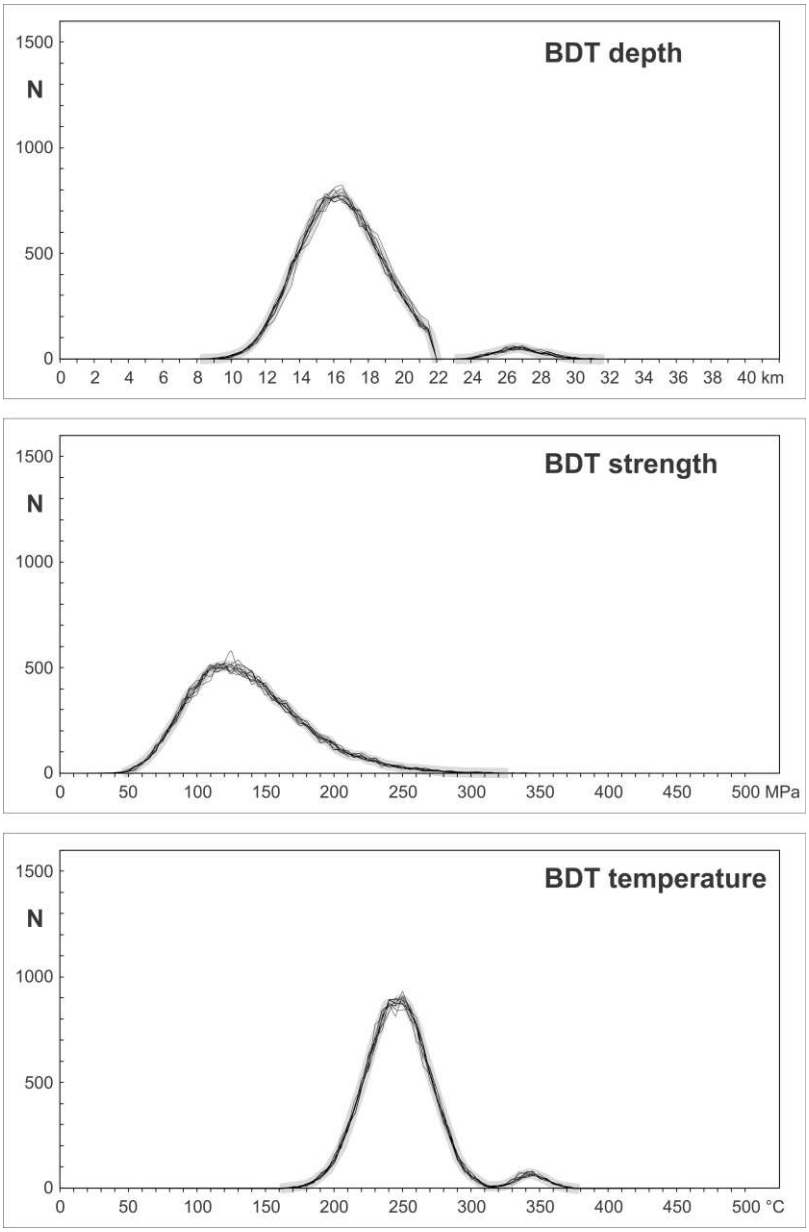

Fig. 4.5 – Frequency distributions of the 100000 random combinations from the Kefallinia island test site for the BDT depth (a), BDT strength (b), and BDT temperature.

The mean value of the 100k-combinations and the associated standard deviation are respectively 247 and 29 °C, while the most populated class is the range 245-250 °C. All statistical indexes are in good agreement with the temperature value obtained on the basis of the reference model (246 °C). The lower BDT temperature with respect to the Kallidromo test site (ca. 300 °C), even though the BDT is deeper in the Kefallinia area, is a likely consequence of the very low geothermal gradient characterizing the Ionian region with respect to Central Greece, the former

belonging to a thick active accretionary wedge, the latter being close to the Aegean realm, which is undergoing crustal extension at least since the Pliocene.

The respective dependences of BDT depth, strength and temperature for both test sites considering all the ten 10000 combinations have also been tested, by analysing their distributions as a function of each other. In fig. 4.6 and fig. 4.7 the BDT depth-BDT strength, BDT depth-BDT temperature and BDT strength-BDT temperature distributions are shown for, respectively, the Kallidromo and the Kefallinia test site.

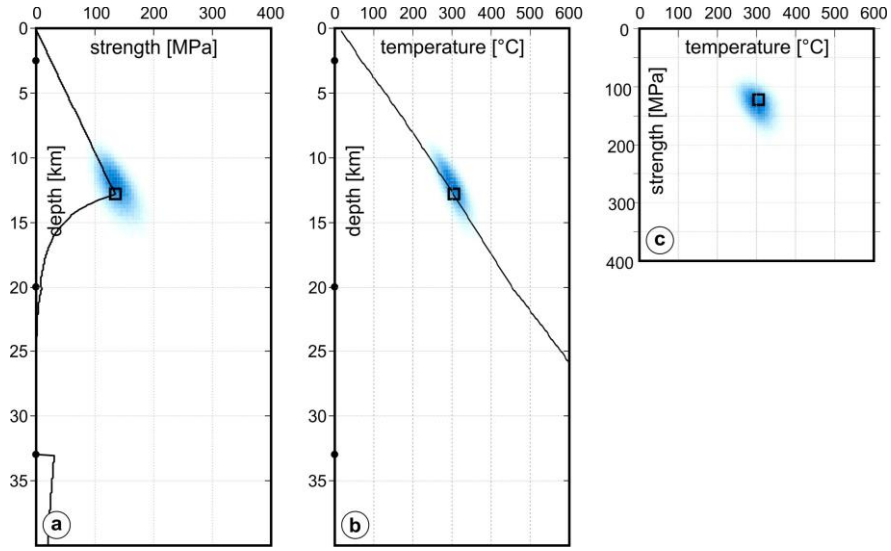

Fig. 4.6 – Distribution of the numerical results obtained from the 100000 random combinations for the Kallidromo test site in the planes strength-depth (a), temperature-depth (b), and temperature-strength (c), showing the clustering of the numerical results. Black squares indicate the output of the reference model.

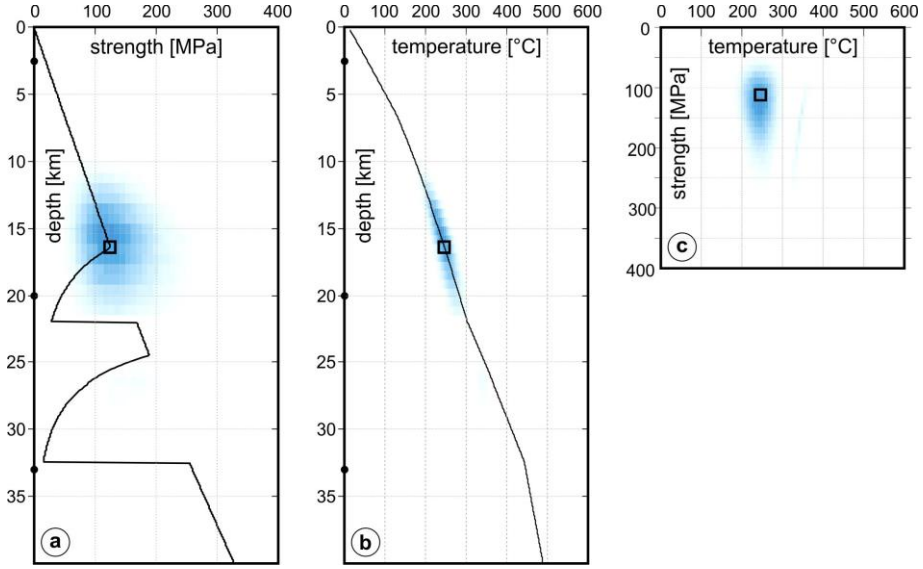

Fig. 4.7 – Distribution of the numerical results obtained from the 100000 random combinations for the Kefallinia Island test site in the planes strength-depth (a), temperature-depth (b), and temperature-strength (c), showing the clustering of the numerical results. Black squares indicate the output of the reference model.

From these figures it can observed that dispersions around the preferred model values of BDT depth, strength and temperature are smaller for the Kallidromo test site, with respect to the Kefallinia one. As a first interpretation, it may be reasonably affirmed that this is due to the higher geothermal gradient and the BDTs all occurring in the upper crustal layer for the Kallidromo test site, thus limiting also the spread for the values of the BDT strength and temperature. It can be also noted, from both fig. 4.6 and fig. 4.7, that the BDT depth-BDT temperature graphs are the ones showing the greatest correlation. This is intuitively attributed to the direct proportionality between temperature and depth (temperature, as a general rule, always increases with depth), which instead does not characterize the BDT depth-BDT strength and BDT strength-BDT temperature relationships.

4.5.3 Comparison with seismicity

In order to further verify the reliability of the rheological modelling and the analysis of the uncertainties for both test sites, the BDT depths have been compared with the seismicity of the two areas. For this purpose, I considered the distribution at depth of relocated events from two recent seismic sequences, occurred in August 2013 and during January 2014 in the Kallidromo area and Kefallinia island, respectively.

As already mentioned, the brittle-ductile transition could be considered as a reasonable approximation of the maximum depth at which seismogenesis occurs. More precisely, no major earthquake is expected to nucleate below the BDT, even though coseismic rupture during strong events may propagate below the transition (e.g., Scholz, 1988). In exhumed crustal shear zones the presence of pseudotachylites have been documented to be embedded within a mylonitc fabric matrix; the former clearly documents large amounts of coseismic frictional sliding (and heat production high enough to induce local melting), while the latter is typical of a distributed (*viz.* ductile) rock deformation (Sibson, 1980; Koch and Masch, 1992; Passchier, 1982; Lin *et al.*, 2005). Bearing in mind the possibility that the rupture propagation on major crustal faults during strong events could extend somehow deeper, the BDT depth as inferred from rheological modelling could nevertheless represent a crucial information to constrain the width of the seismogenic faults, especially in case their deep structure and geometry are still debated.

It is noteworthy that the aftershocks spatial distribution commonly highlights and focuses on the boundaries of the main patch ruptured during the mainshock and, if the rupture reached the bottom of the seismogenic layer, some of the subsequent foci will be located below the long-term BDT. This last phenomenon, i.e. the temporary deepening of the maximum depth of earthquake nucleation, is, however, independently expected to occur, due to the very rapid increase of the strain rate from the long-term rate to the coseismic velocities at depth, which causes a transient embrittlement of otherwise ductilely deforming regions.

Based on local velocity structure models and relocation procedures of the hypocentres (such as HypoDD) (Waldhauser and Ellsworth, 2000), detailed seismological and tectonic analyses have been carried out for the Kallidromo and Kefallinia areas affected by two recent seismic sequences sequences (Ganas *et al.*, 2014; Karastathis *et al.*, 2015; Sokos *et al.*, 2015; Sakkas and Lakios, 2015). The use of precisely relocated seismicity arises from the need to compare the modelling results with an independent data source, namely the hypocentral distribution, with appropriate accuracy and resolution.

The 2013 Kallidromo sequence occurred on a secondary fault antithetic to the main fault of the Tithorea seismogenic source (GRCS434; Caputo and Pavlides, 2013), which represents one of the major normal faults characterizing the Sperchios rift area. The magnitude of the mainshock was 5.4 and though the maximum depth reached by some of the aftershocks (from Ganas *et al.*, 2014; 90 days period from the mainshock of 7 August 2013) is up to 15 km (fig. 4.8), it is common practice in this kind of analyses to consider the depth including the 95% of the events, which in this case corresponds to 12.6 km.

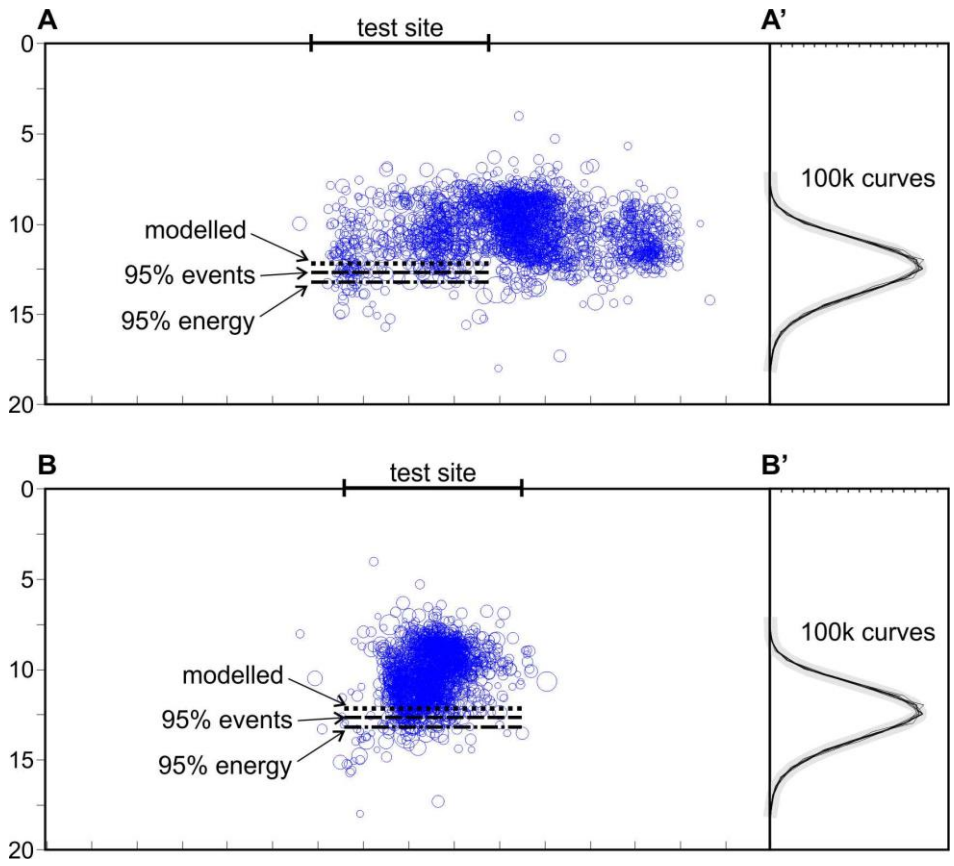

Fig. 4.8 – Hypocentral distribution in the Kallidromo test sites showing the good fit with the results of the rheological modelling. The traces of the profiles are represented in fig. 4.2. On the right column is shown the statistical distribution of hundred thousand random combinations discussed in the text (see also fig. 4.4).

If instead the empirical relationships between magnitude and energy (e.g. Kanamori, 1983) are applied, the 95% of the energy is contained within the first 13.2 km. Both values are in

reasonable agreement with the results from the rheological modelling, based either on the preferred values (12.3 km; Table 4.2) and on the most likely depth according to the statistical analysis (12.3 km; fig. 4.4).

As concerns the 2014 Kefallinia sequence, it was characterized by two mainshocks of similar magnitude (M_W 6 and 5.9) occurred on the 26th of January and 3rd of February, respectively (*e.g.* Papadopoulos *et al.*, 2014; Karastathis *et al.*, 2015; Sokos *et al.*, 2015). The causative faults are represented by antithetic (westward steeply dipping) and subvertical splay structures (Briole *et al.*, 2015), belonging to the crustal-lithospheric boundary represented by the Kefallinia Transform Fault, which separates the External Hellenides from the Apulian Foreland. According to the distribution of the relocated hypocentres (from Karastathis *et al.*, 2015; time period from 26 January to 15 May), the maximum locally recorded depth is about 18 km, while the 95% of the events occurred within the first 13.4 km (fig. 4.9).

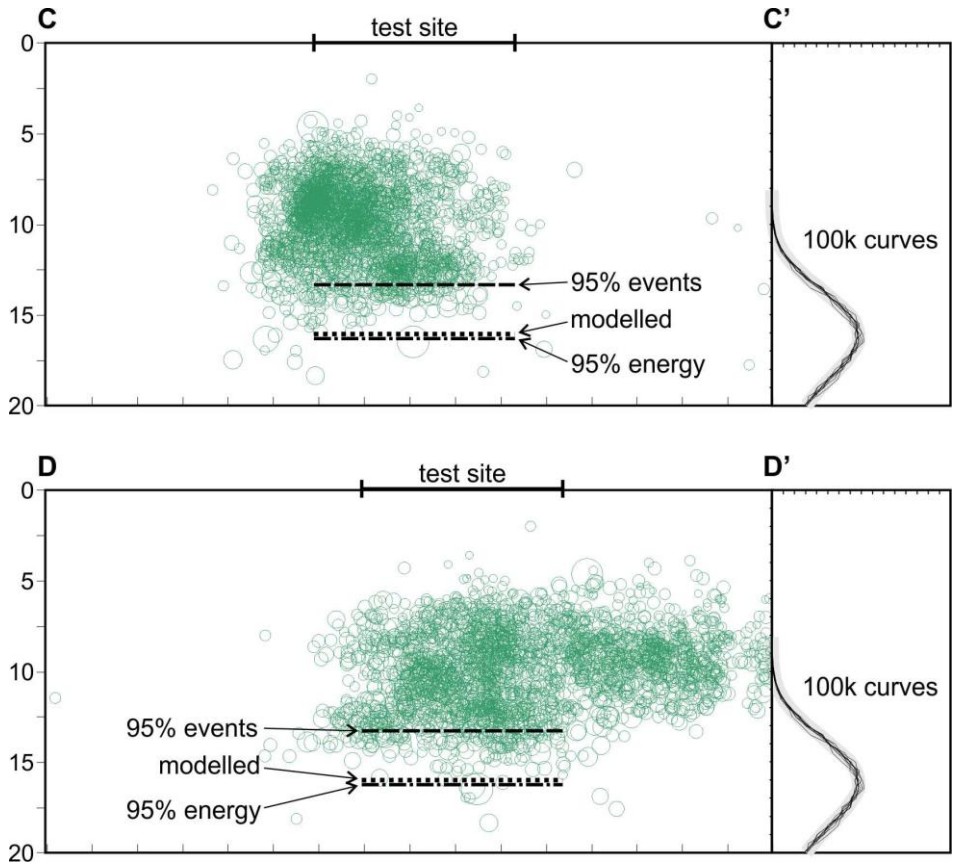

Fig. 4.9 – Hypocentral distribution in the Kefallinia Island test site, showing the good fit with the results of the rheological modelling. The traces of the profiles are represented in fig. 4.3. On the right column is shown the statistical distribution of hundred thousand random combinations discussed in the text (see also fig. 4.5).

However, if the energy distribution is taken into account, the 95% has been released above 16.3 km, being in perfect agreement with the BDT depth calculated on the basis of the rheological modelling (16.4 km; Table 4.3 and fig. 4.5).

Chapter 5: Results and discussion

5.1 1D test sites and comparison with seismicity

5.1.1 Outline and brief summary

In this chapter I am going to present the results of the rheological modelling performed in this work. First, I will focus on the 1D rheological profiles realized for selected test sites, highlighting the different features of the strength envelopes in the various geodynamic settings and also their relationships with the geothermal gradient and the litho-mechanical stratification. Secondly, I will present the two-dimensional features and variations of the rheological properties along specific 2D transects, realized in different geodynamic and geologic settings of the Aegean Region (continental collision, oceanic subduction, back-arc region, Hellenides fold-and-thrust belt).

Thirdly and lastly, I will show the 3D outcomes of the rheological model that has been realized for the Aegean Region through the use of a dedicated Matlab script. The results, in this case, will be presented in the form of 3D maps, in order to underline the three-dimensional variations of the main thermo-rheological parameters (*i.e.* BDT depth, strength and temperature) all over the study area. Furthermore, in order to validate the results obtained with the 1D, 2D and 3D rheological modelling for the Aegean Region, a detailed comparison with the seismicity depth distribution in the study area has been carried out.

I will now proceed with only a quick recall on the relationship between rheology and seismogenesis, as the topic has already been treated in the previous chapters, and then all the seismicity data used for the comparison will be presented. After that, the results will be shown and discussed, by comparing them to the seismicity depth distribution and also by considering the consistency of the rheological model outcomes with the geodynamic, geologic and tectonic features of the Aegean Region.

5.1.2 Rheology and seismogenesis: a brief recall

The BDT region has been associated with the bottom depth of the seismogenic layer since the early works of Sibson (1977; 1984). In this view, the brittle layers are the potentially seismogenic ones, being able to store elastic energy to be finally released through rapid co-seismic slip during earthquakes. On the contrary, the ductile regions undergo continuous and diffuse plastic deformation, which prevents the accumulation of elastic strain, thus not leading to any stress build-up.

With the work of Scholz (1988; 1989), it was proposed that the interseismic BDT could represent the maximum depth for earthquake nucleation, while seismic rupture propagation could possibly extend some kilometres below the transitional zone, in a region where intermediate rheological behaviours are dominant. Furthermore, Tse and Rice (1986) demonstrated that precise seismic-aseismic transition, even though being similar and usually comparable to the rheological brittle-ductile transition, is actually determined by the velocity weakening-velocity strengthening behaviour of the considered rocks.

As later clarified by Scholz (*e.g.* 1988), earthquake can nucleate only in the unstable field (fig. 5.1) corresponding to a velocity-weakening regime (*i.e.* when high-velocity slip causes dynamic strength decrease), where the parameter (a-b) from the rate- and state-variable friction law (the so-called Dieterich-Ruina law, see *e.g.* Dieterich 1979) is negative. Seismic rupture propagation is instead rapidly halted in the stable field, where the rocks behaviour is velocity-strengthening (*i.e.* the strength quickly increases as the velocity of slip rises and therefore the applied stress is no longer sufficient to overcome strength and sustain slip propagation) and the (a-b) factor is positive. Finally, there exist an intermediate field, called conditionally-stable, where earthquakes cannot nucleate but can potentially propagate through.

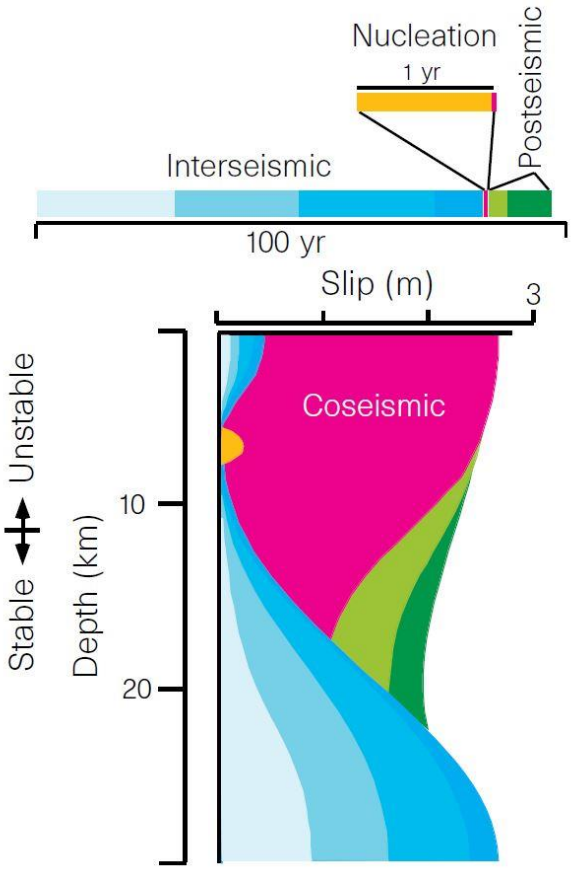

Fig. 5.1 – Depth vs slip diagram in relationship with the seismic cycle. The figure shows how the nucleation of a seismic event is confined in the unstable field, while the rupture propagation and the coseismic slip may occur also into the conditionally stable field (from Scholz, 1998).

This said, the long-term, interseismic brittle-ductile transition still remains a valid and relatively simpler proxy for the bottom depth of the seismogenic layer, especially for determining the maximum potential depth of mainshocks at the start of seismic sequences, when the vertical extent of the brittle layer roughly coincides with that of the seismogenic one.

Seismicity data

I will now present the seismological data that have been used to compare the rheological layering and the seismicity depth distribution, especially for the 1D test sites and 2D transects. For such a purpose, the fundamental feature of the considered seismological data is their precision in terms of localization, especially as regards the hypocentral depth. However, depth, rather than latitude and longitude, is the most difficult parameter to be constrained when reading and inverting seismic stations recordings and seismological data in general, in order to precisely localize the considered seismic event.

As a result, routinely recorded raw seismic data, in the absence of applied relocalization techniques, may result into estimates of the hypocentral depths having uncertainties even greater than 10 km. Accordingly, such variations do not allow to use unrelocalized seismic events depths as a validation tool for assessing the goodness of the modelled rheological layering, as no sensible comparison can be made, for instance, between brittle-ductile transition and the bottom of the potential seismogenic layer, simply because the latter is not well defined and identifiable. Given these premises, in order to properly compare the results of the rheological modelling with the seismicity depth distribution, only relocated earthquake data have been taken into account.

The majority of such considered data have been relocated using techniques such as the Hypoinverse algorithm (Klein, 1989), the HypoDD algorithm (Waldhauser and Ellsworth, 2000) or by applying a local velocity model, together with an error minimization procedure (*e.g.* Kissling *et al.*, 1994; Papadimitriou *et al.*, 2010). The Hypo DD algorithm, in particular, allows to remarkably improve the initial localization, on the basis of a double difference technique, with which every earthquake is associated with another, better located one, and its final localization is thus adjusted and determined.

In addition to the relocated seismicity, also the seismic events and sequences recorded with local networks and purposely deployed ones have been taken into account. Indeed, the use of local seismic networks is usually correlated with a specific geometry of the network, which is developed with the final aim of obtaining the maximum possible azimuthal coverage, thus recording high-quality seismic data. Moreover, with local-scale and purposely deployed networks, also locally determined velocity models for the crustal layers are typically used and therefore better estimations of the hypocentral depths can be obtained.

The use of relocated or local seismic network recorded seismicity allows therefore to minimize the hypocentral depth errors to values even lower than 1 km, according to the applied procedure

and the precision of the seismic stations of the local network (see *e.g.* Karastathis *et al.*, 2015). Such values represent a remarkable improvement with respect, for instance, to the typical error associated to the hypocentral depth for events recorded with the standard procedure by the HUSN (Hellenic Unified Seismic Network), which is, in average, around 4-5 km (D'Alessandro *et al.*, 2011).

Accordingly, relocated seismicity and data coming from local, specifically-designed, seismic networks are the only ones used in this work for comparison between rheological layering (in particular for the extent of the brittle layers) and the depth distribution of seismicity. Other sources of data, like global, national or regional seismic catalogs such as, for instance, the ones from ISC (International Seismological Centre), NOA (National Observatory of Athens) and AUTH (Aristotelian University of Thessaloniki), which do not provide enough hypocentral precision with the standard location procedure, will be therefore used only for statistical purposes and as indicators of the total rate of seismicity.

I will now briefly describe all the seismic catalogs, with their relative main features, that have been taken into account for this study. The NOA database covers a time span that goes from 1964 to the present day (in this work the most recent seismicity is actually from December 2017); its geographical coverage includes the entire broader Aegean Region and it is therefore a valuable source of information for the whole study area, even though in terms of hypocentral depth precision errors may be up and over 10 km.

The AUTH catalog collects the recordings of the seismic network operated by the university itself, and has therefore a better azimuthal coverage for northern-eastern Greece with respect to the western area. Also in this case, however, hypocentral depth precision is not sufficient for directly comparing the depth distribution of seismicity with the results of the rheological modelling. Finally, the ISC catalog is based on recordings from globally spaced seismic stations and it is therefore quite precise in terms of geographical localization of the seismic events.

In particular, I took into account the catalog of revised events by Engdahl *et al.* (1998), which however, even though representing an improvement with respect to standard localizations, may still present events with an associated hypocentral depth uncertainty up to 10 km. Additional regional networks and catalogs, such as those from the National Kapodistrian University of Athens (NKUA) and the Seismological Laboratory of the University of Patras (UPSL), have been also taken into account for the statistical analysis on the seismicity rates. Furthermore, in order to gain a more detailed picture of the seismicity features in the easternmost region of the study area, corresponding to western Anatolia, the seismic catalog from the Turkish KOERI University has also been considered. I also collected different literature data sources for the moment tensors in the Aegean Region. Focal mechanisms indeed, when available, represent a useful and independent tool to get a first glimpse on the tectonic style of deformation and stress field of the investigated area. Moreover, moment tensors are necessary and will be used for further applications of the rheological modelling results to seismotectonic fields, such as the calculation of the seismic strain rates, on which I will

focus later on in a dedicated section. Accordingly, several different focal mechanisms catalogs have been considered and analyzed.

Also in this case, both local catalogs (NOA, NKUA, AUTH, UPSL, with a total time coverage of ~25 years, from 1995 to present date) and global ones (CMT Harvard, from 1976 to present date) have been taken into account, in order to obtain a list of moment tensors as much complete as possible in terms of seismic moment and magnitude values. The CMT Harvard catalogue (fig. 5.2) has a lesser number of total recorded events than the local catalogues, though, with respect to the latter, it better allows for comparison with studies from different regions all over the world, as it is usually and almost everywhere the most used source for moment tensors in seismotectonics studies. Indeed, CMT Harvard focal mechanisms are generally deemed to be the most reliable ones and are also used as a reference for comparing moment tensors calculated by different agencies and/or universities and for assessing their goodness and precision.

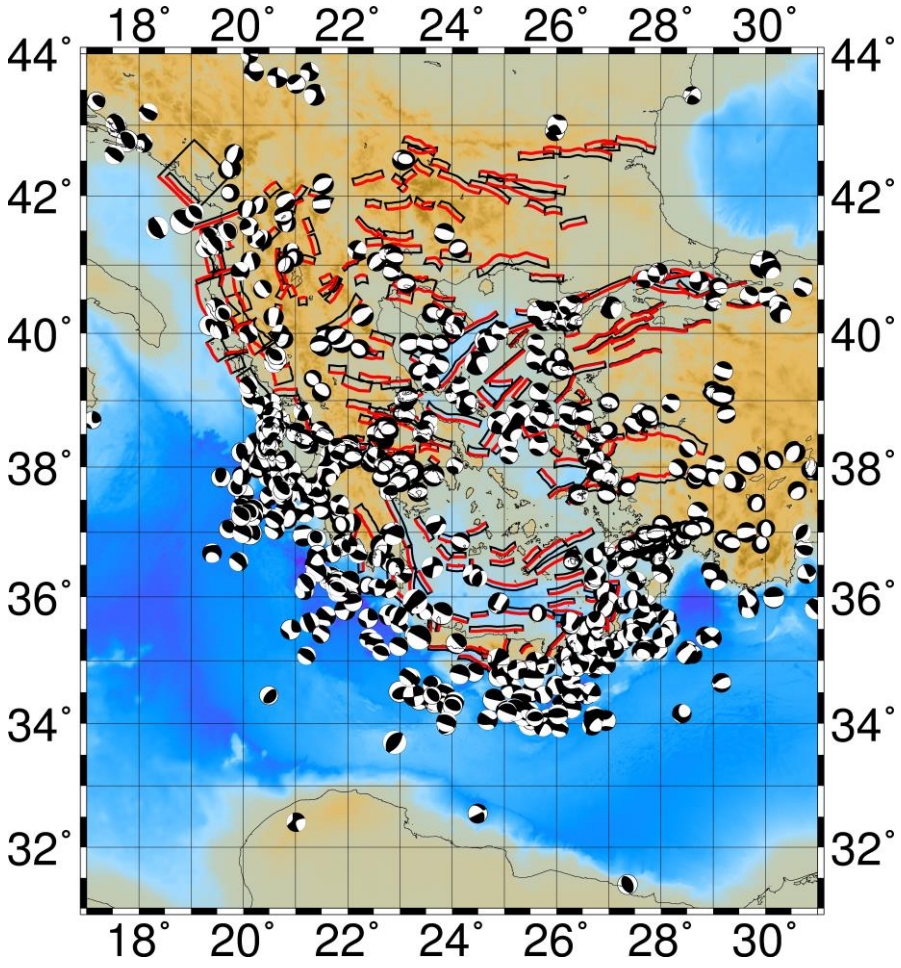

Fig. 5.2 – Focal mechanisms for the Aegean Region taken from the CMT Harvard catalogue.

Given these premises, as a general rule I will use for all the selected test sites the CMT Harvard focal mechanisms in the seismic strain rate calculations and when available or necessary I will take into account additional (local) moment tensors catalogues. The comparison with the depth distribution of seismicity has first been applied to 1D selected test sites, also as an independent tool

to verify the goodness of the obtained rheological modelling and layering. Given the aforementioned great uncertainty associated with standard localization procedure for seismic events by NOA, I first tried to realize EDH (earthquake depth histograms, *sensu* Hauksson and Meier, 2019), for each selected test site, from the standard NOA catalog (1964-2019) and then, when available, also for relocated seismic sequences occurred in the region of the corresponding test site.

For the aim of seismic depth distribution analysis, I generally selected the depth within which the 95% percent of the total number of events occurred (hereinafter referred to as 95TNE depth) to be compared with the depth of the brittle-ductile transition. EDHs have actually been realized both for background seismicity and for specific seismic sequences, always using the NOA standard catalog. The background seismicity has been obtained by declustering the catalog from the main seismic sequence occurred in the considered period, while for the seismic sequences a limited amount of time, going from one month prior to the mainshock to 5 months after it, has been taken into account.

These two different kinds of seismicity, the background one and the seismic sequence-related one, even though taken from the same (NOA standard) catalog, already provide different results in terms of 95TNE depth, with difference up to 10 km. Such a result could be somehow justified by the different time span considered in each case, though I deem it to be more indicative of potential biases in the procedure of depth attribution and of different availability of instrumental equipment through time. Indeed, in particular for the background seismicity, a significant number of events is attributed with a pre-fixed depth in order to invert for the localization and this leads to artificial and misleading alignments and clustering of seismicity at pre-determined depth values (usually standard values used for the inversion are 5, 10, 20 and 30 km).

For the seismic sequences instead, in some cases, even the standard catalog could provide more precise hypocentral depths (with respect to background seismicity), thanks to the potential temporal installation of supplementary seismic stations, which greatly improve the localization, or simply because the abundance and vicinity of the events could allow to reconstruct the extent of the seismogenic zone with a reasonably decreased uncertainty. Nonetheless, relocated seismicity from a certain seismic sequence, whose hypocentral depths have been obtained using local velocity models and specific relocation algorithms and procedures, is still much more reliable and useful for comparison with rheological modelling results and to derive any seismotectonic inference, with respect to the seismic data referred to the same sequence but taken from the standard catalog. In fact, for some of the test sites, a clear misfit between the earthquake depth distributions as obtained from the standard catalog and the relocated seismicity ones has also been observed.

Furthermore, in most cases, a general better fit of the modelled rheological layering to the (depth of the) seismic events has been obtained when just considering the relocated seismicity rather than standardly localized one. The comparison between the brittle-ductile transition and the 95TNE depth allows assessing the potential correspondence of the rheological long-term behaviour with

the short-term seismic deformation. A further parameter used for such an assessment is the depth corresponding to the 95% percent of the total released energy (95TRE) during a certain seismic sequence (given a pre-determined amount of time, which temporally defines the duration of the sequence itself), which could be even more appropriate and indicative for comparing interseismic (long-term) BDTs and seismicity depth distributions.

As concerns the relocated seismicity catalogues, different sources have been collected and taken into account (fig. 5.3). For some preliminary test sites, corresponding to the regions around Kefallinia and Kallidromo (central Greece), the catalogues from Karastathis *et al.* (2015) and Ganas *et al.* (2014) have been used, respectively. They considered and relocated the seismicity of two moderate-magnitude seismic sequences, occurred in January-February 2014 in Kefallinia and August 2013 in Kallidromo.

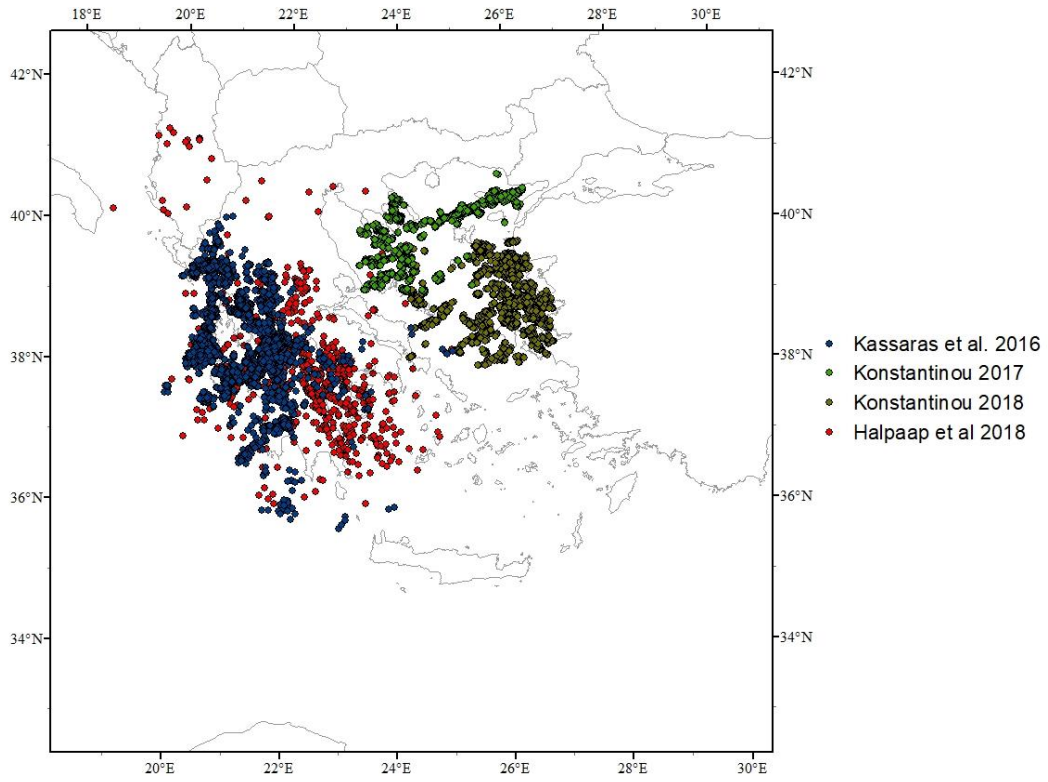

Fig. 5.3 – Relocated seismicity catalogues used in this study.

An important and very useful catalogue is the one published by Kassaras *et al.* (2016), which focuses on western Greece seismicity. They relocated a considerable number (~7500) of seismic events in the time span 1989-2012, covering an area extending from Ioannina to Kalamata and offshore southwestern Peloponnesus, by applying relocation techniques such as HypoDD and taking into account, when available, local velocities models. For the northeastern Aegean Region, the relocated seismicity catalogues by Konstantinou (Konstantinou, 2017; 2018) have been taken into account. They are focused on the seismicity occurring along the North-Aegean Trough area

and in the region comprised between the islands of Lemnos, Lesvos, Chios and Skyros. The catalogs cover a time span of ca. 7 years, going from 2011 to 2017, and the collected seismicity has been relocated using the HypoDD algorithm.

Furthermore, the catalogue by Halpaap *et al* (2018), which focuses on the seismicity of the Hellenic subduction zone, has also been taken into account, in order to obtain a better representation of the Wadati-Benioff plane and of the Hellenic slab seismic behaviour. Such a catalogue collects events going from 1995 to 2015 and also in this case the HypoDD tool has been applied in order to relocate the considered seismicity.

Finally, additional works on specific seismic sequences and/or focused on selected locations were also considered. In particular, studies by Hatzfeld *et al.* (1995, 1997, 1999, 2000) have been taken into account in order to add high-quality seismic data information in regions such as Epirus, Thessaly, Evia, western Macedonia and the Corinth Rift. They focus on selected locations and used temporarily deployed, closely-interspaced seismological stations in order to obtain precise data of the recorded seismicity, with uncertainties in the hypocentres depths values being as low as 2 km, thus providing small but accurate catalogues, useful for comparisons with and applications to seismotectonics and rheological modelling.

Additional studies by Kiratzi *et al.* (2008, 2016) and Kiratzi and Svigkas (2013) have also been considered, since they focus on regions not always well covered by other relocated seismicity catalogues. Their main contributions regard regions such as Aitoloakarnania (Lake Trichonis), NE Aegean Sea (Samothraki and Lemnos islands) and northern Macedonia, where they relocated events from moderate magnitude seismic sequences, mainly using Hypoinverse (Klein, 2002) and HypoDD algorithms and local travel-time tomographies, in order to invert for the determination of more precise, local sub-surface velocity models.

Other works collected and taken into account for the comparison with the rheological modelling are those from Sokos *et al.* (2012; 2015) and Mesimeri *et al.* (2017; 2018). The former working group, in order to relocate the routinely located events, made use of codes such as HypoDD, HypoInverse, FastHypo (Herrmann, 1979) and Hypo71PC (Lee and Valdes, 1985) and also recorderd high-quality seismic data by deploying local temporary seismic networks (*e.g.* in Trichonis region), focusing on areas such as the Corinth Rift, Kefallinia Island and Trichonis Lake. Mesimeri *et al.* (2017) also used temporary local seismic stations to localize microseismic events with high hypocentral precision in the area around Florina (Northern Greece, Western Macedonia region). They also provide a catalog of recent relocated seismicity obtained by applying the HypoDD algorithm for the Corinth Rift region, covering a time span of seven years (2008-2014). Usually the comparison with the seismicity is based firstly and solely on the correlation of the BDT depth with the depth distribution of the seismicity, so that the maximum depth of seismogenesis is determined and confirmed by both data (seismological) and models (rheological) (fig. 5.4).

However, additional comparisons could be made between the rheologically determined depth of the BDT and other seismological data. In particular as mentioned above, the bottom of the brittle and potentially seismogenic layer can be compared with the depth corresponding to the 90 or 95% (according to the data and the rheological characteristics of the sample and/or study area) of the total seismically released energy within the same volume (see fig. 4.9).

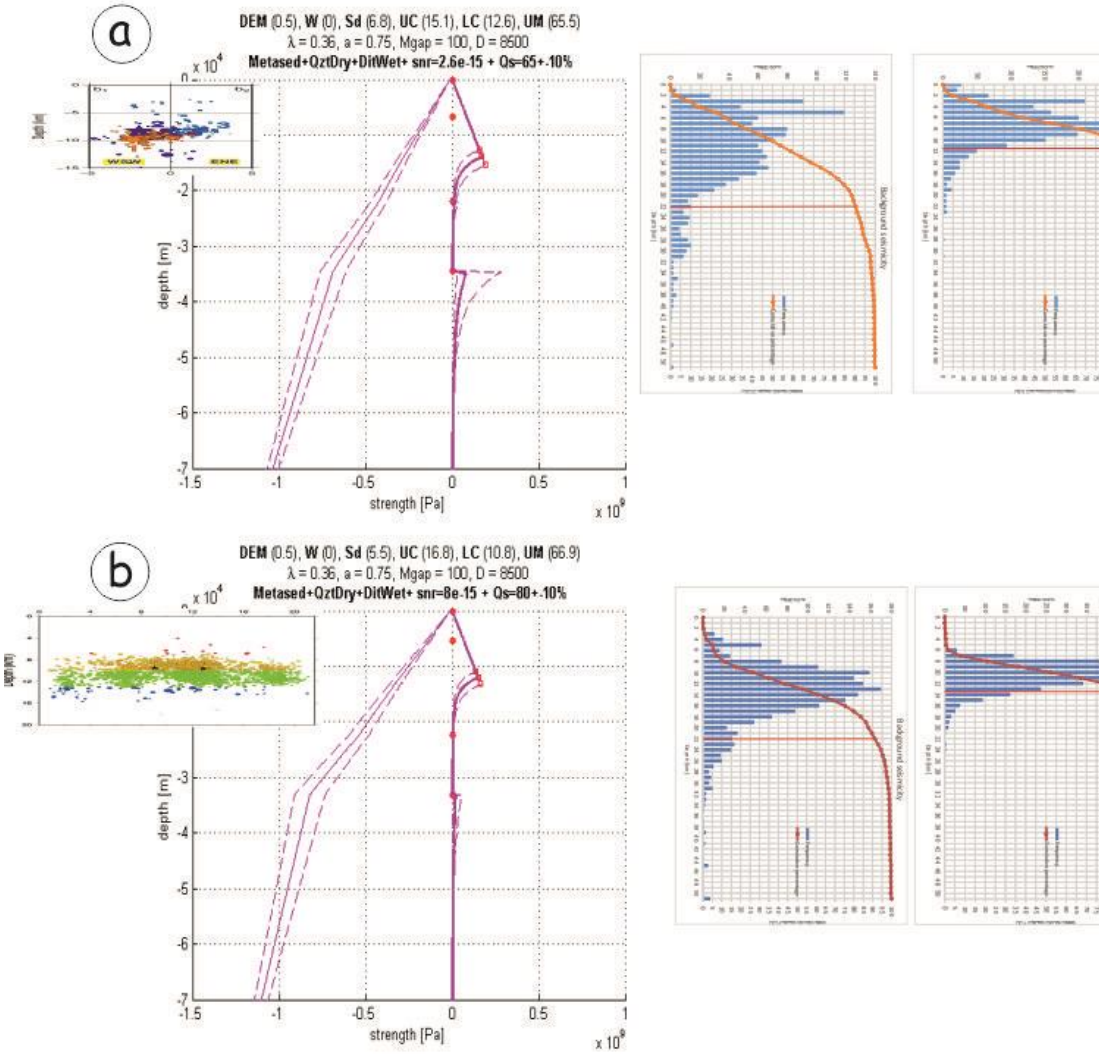

Fig. 5.4 – Comparison between the rheological BDT (red square along the strength envelope) and the cutoff depth of seismicity (90%) as indicated by cumulative distributions in the histograms. The dashed curves are obtained by varying of a ±10% the input value of the heat flow. The left histogram represents the routinely recorded seismicity, with the red solid line indicating the 90% cutoff depth. A clear misfit can be observed, while the cutoff depth shown by the right histogram, which only takes into account relocated seismicity, is in good agreement with the depth BDT and also with the depth distribution of recent seismic sequences events, as shown in the sections on the left. a – Oichalia (S. Peloponnesus; seismicity from Ganas et al.*, 2012); b – Kallidromon (C. Greece; Ganas* et al.*, 2014).*

Indeed, the bottom of the seismogenic layer is typically associated with the maximum magnitude earthquakes for that region (see *e.g.* Scholz, 1988) and since those events are the ones representing the great majority of the total energy released through seismic deformation, the BDT depth is also expected to contain a considerable portion of such energy (where for energy, by a

seismic point of view, the seismic moment is considered). Accordingly, especially for some test sites, where well-located hypocentres of recent energetic seismic sequences are available, both the comparisons, the one with the simple vertical depth distribution of the seismicity and the one with the vertical distribution of the seismic energy, have been realized in order to be analyzed and to test the reliability of the rheological modelling results.

For instance, in the regions of the Ionian Islands like Lefkada and Kefallinia, which have been struck by moderate-high intensity seismicity even in recent years, the calculated BDT depth seems to fit quite well the distribution along depth of the seismic moment release. In particular, the most energetic events corresponding to the mainshocks of the sequences tend to occur within the brittle seismogenic layer as indicated by the BDT depth and to focus towards its bottom, in agreement with the synoptic models of the seismogenic faults proposed by Scholz (1988; 1989).

5.1.3 Test sites and associated strength envelopes

Several test sites in the whole Aegean Region have been selected for the realization of 1D rheological profiles (see fig. 5.5). The test sites have been chosen on the basis of several factors, mainly taking into account: i) the availability of different kinds of data (from seismics, gravimetry, surface geology) on the crustal structure and other input parameters, such as heat flow and strain rate; ii) the occurrence and recording of quality seismological data, especially as regards the hypocentral depth determination; iii) the tectonic setting, in such a way that as many different tectonic regimes as possible, characterizing the Aegean Region, are taken into account.

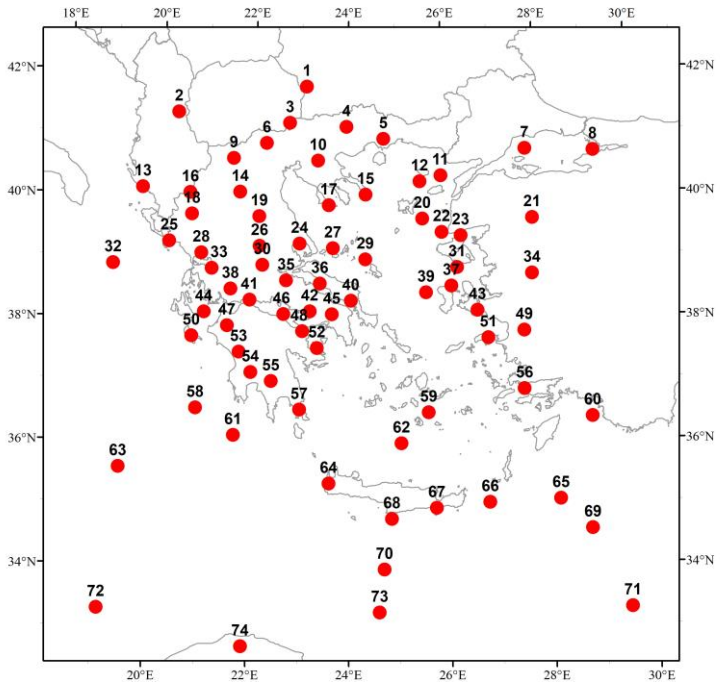

Fig. 5.5 – Geographical distribution of the 1D test sites across the study area. See the text for the associations between numbers and locations.

For the last point, test sites both from extensional (*e.g.* Xylokastro n. 46, Kaparelli n. 42, Mygdonian basin n. 10, Sperchios n. 30), transcurrent (*e.g.* Kefallinia n. 44, Andravida n. 47), transtensional (*e.g.* Samothraki n. 12, Saros Gulf n. 11) and transpressional (*e.g.* Zakynthos n. 50) regimes have been selected. For the purely compressional tectonic regime, only a few test sites are available, due to the difficulty in meeting all the above-mentioned criteria for their selection, with particular reference to the scarcity of quality seismological recordings and geophysical data for the crustal structure. Such a paucity of geophysical and seismic data, for the compressional regime regions, is due to the fact that most of them are located in the offshore region around the Hellenic trenches and therefore azimuthal coverage for the seismic data recordings is seriously limited and the acquisition of reliable geophysical data is also difficult and expensive.

Accordingly, I preferred to focus on the 'internal' Aegean Region and the great majority of the test sites belong to extensional and strike-slip, with all the intermediate cases, regimes. The selected test sites cover quite well the entire Aegean Region, spanning from Epirus (Konitsa n. 16, Ioannina n. 18) to Aitoloakarnania (Arta n. 28, Trichonis n. 38), the Corinth rift region (Efpalio n. 41, Xylokastro n. 46, Kaparelli n. 42), the Ionian islands (Kefallinia n. 44, Zakynthos n. 50), Peloponnesus (Pyrgos n. 53, Oichalia n. 54, Sparta n. 55), Attica (Fili n. 45), Evia island (n. 36 and n. 40), Thessaly (Volos n. 24)), Macedonia (Kozani n. 14, Mygdonian basin n. 10), Thrace (Kavala n. 5), northern Aegean Sea (Samothraki n. 12, Lemnos n. 20, Saros Gulf n. 11), central Aegean Sea (Skyros n. 29, Psara n. 39), southern Aegean Sea (Christiani basin n. 62, Kos n. 56) and Crete island (Gramvousa n. 64).

Moreover, many of these test sites actually correspond to the location of relevant seismic sequences ($M \geq 6$) occurred in recent and/or historical times (*e.g.* Athens 1999, Thessaloniki 1978, Kozani 1995, Volos 1980, Lefkada 2003, Kaparelli 1981, Kefallinia 2014), while others are associated with clear morphological evidences of post-LGM – Holocene activity (*e.g.* Sparta, Xylokastro).

In any case, such test sites have been selected also because they represent regions particularly subject to seismic risk and therefore an additional element for their seismotectonic characterization, obtained in this case through the rheological modelling and in particular with the knowledge of the BDT depth, could help refining the seismic hazard assessment and contribute to the risk reduction. Many of the test sites also correspond to some specific individual and/or composite seismogenic source of the GreDaSS database (Caputo and Pavlides, 2013), which represents a first source of information for the seismotectonics of the selected test sites. On the other hand, the rheological modelling and the comparison with seismicity for these test sites could also help improving and completing the GreDaSS database with missing data and additional information, based on the results of the modelling.

As it will be shown later, the test sites will be used in a first stage as direct indicators of the 1D rheological properties of the crust and lithosphere of the corresponding locations, spread all

over the study area of the broader Aegean Region. In the following phase then, the 1D test sites, after having been compared and verified with the seismicity data, will be employed as control points and constraints for the realization of the 3D rheological model of the whole Aegean Region.

Overall, the majority of the test sites show a much better fit of the rheologically-modelled BDT depth with the relocated seismicity data (when available) rather than with the routinely-localized seismic events. Indeed, the latter tend to present a corresponding 90% depth deeper than the BDT, in many cases because of concentration of events at the 30 km depth mark. As hinted above, some test sites, in particular those around the Ionian islands (Kefallinia n. 44), the Corinth Gulf area (Efpalio n. 41, Kaparelli n. 42) and southern Peloponnesus (Oichalia n. 54) show a very good agreement between the depth of the rheological transition and the statistical data on the vertical distribution of the relocated seismicity.

Other test sites, especially those from regions such as Thessaly, Thrace and the southern Aegean Sea, where recent seismological quality data are not abundant or almost totally absent, could not have been compared with relocated seismicity and a misfit with the standard localized seismicity is observed. Such a misfit has been interpreted as due to the scarce quality of the seismic data (in particular for what concerns the depth determination) rather than being attributable to errors and/or oversimplifications in the rheological modelling, even though some local unmodelled heterogeneities such as local pore fluid pressure increase, or friction coefficient variations, could occur at a very small (spacely-limited) scale and therefore not being effectively detectable and reproducible in model proposed by this research.

In any case, the above-mentioned parameters variations and uncertainties, as well as those of the heat flow and of the strain rate (see also Chapter 4), are considered to represent the most likely causes for BDT depth lateral variations. On the contrary, multiple and sudden changes of the lithologies of the various stratigraphic-mechanical layers are deemed to be much less probable and realistic as the reasons for the BDT-(routine) seismicity misfit.

Accordingly, the realization of test sites (and their comparison with the seismicity) has also demonstrated to be a useful and additional tool to help confirming the main lithological characteristics of the crustal layers in the Aegean Region, as deduced from geophysical and geological surveys, as well as from general geodynamic and tectonic considerations.

The 1D modelling, testing and comparison also suggest, from this point of view, a prevailing quartzitic upper crust in the Aegean microplate and a dioritic composition for the lower crust. The 1D test sites show different typologies of associated strength envelopes all over the Aegean domain, according to and depending on the local tectonic regime, the mechanical-lithological stratification and above all the geothermal gradient. I will now show here some examples from the different tectonothermal domains of the study area. All the other 1D envelopes can be found in the Appendix A, together with their respective number and name.

In northern- and central-western Greece (*e.g.* Konitsa, Ioannina, Arta, Trichonis, Andravida, respectively test sites n. 16, 18, 28, 38 and 47 in fig. 5.5) the majority of the test sites share a jelly sandwich typology of rheological profile (fig. 5.6), with an interposed ductile layer, usually in the lower crust or in the upper mantle, according to the local layering. In general, this area is characterized by a complex tectonic setting, ranging from a compressional regime along the coastal sectors to strike slip and extensional tectonics moving landward. Furthermore, besides the lateral juxtaposition of different tectonic regimes, the stress ratio also varies vertically, so that, especially landwards, shallow extensional tectonics overlies deep compression. Accordingly, the depth of the interposed ductile layer may vary substantially, even though its occurrence remains a common point for north- and central-western Greece. In this region, the presence of a deeper brittle layer typical of the jelly sandwich profile can be mainly explained by the low heat flow values characterizing the area.

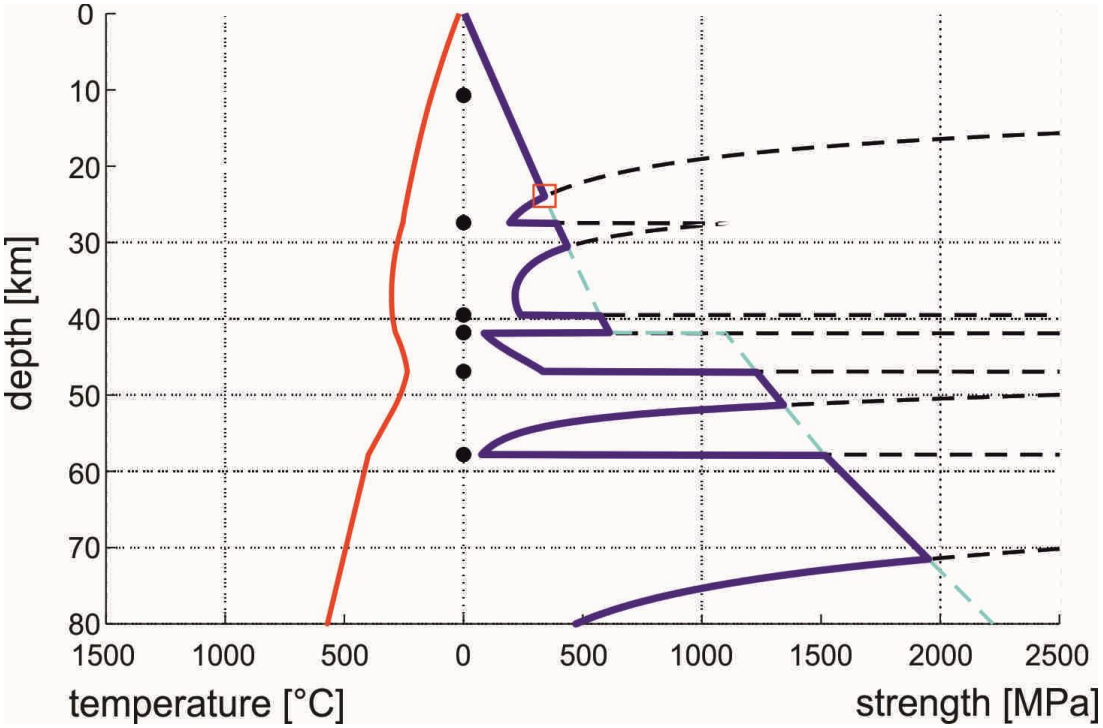

Fig. 5.6 – 1D strength envelope (solid blue curve) for the test site n. 18 - Ioannina (Epirus, Northern Greece). Note the jelly sandwich *typology, with the ductile behavior mainly characterizing the lower crust layer and the low geothermal gradient (solid red curve), resulting into the occurrence of multiple deeper brittle layers. The red square indicates the position of the BDT, while the cyan and the black dashed lines represent, respectively, the continuation of the brittle and the ductile strengths.*

However, in other sectors of the Aegean Region, the jelly sandwich shape of the strength envelope is also observed for some specific test sites, and in those cases, the reasons for such a rheological layering are different from the above-mentioned ones. For instance, the Christiani basin test site (n. 62) in the Cretan Sea is associated to a jelly sandwich envelope because of the very thin (continental) crust (around 20 km) that characterizes such region. Indeed, a limited thickness of the crustal layers reduces the amount of radiogenic heat production and above all decreases the

temperature at the Moho with respect to a geological setting characterized by a thickened crust. Accordingly, conditions for ductile flow may be met in the lower crust, also depending on additional factors (heat flow, strain rate, etc.), but the very mafic and resistant lithologies of the upper mantle at moderate depths of 20-25 km are much likely to behave in a brittle fashion, thus leading to the occurrence of a second deeper brittle layer, typical of the jelly sandwich envelope.

Additional test sites associated with the jelly-sandwich type of rheological profile occur in the region around the Evia and Skyros islands, mainly because of the lower surface heat flow in this region with respect to the surrounding areas. In central Greece instead, and especially in the regions of the Corinth and Sperchios rifts (*e.g.* Kaparelli, Xylokastro, Kenchreai, Kallidromo, Volos, respectively test sites n. 42, 46, 52, 35, 24 in fig. 5.5), the strength envelopes are characterized by a single shallow brittle layer, below which deformation takes place mainly through ductile processes down to the mantle, or alternartively to the lower plate, where rheological behaviour may locally change. Such rheological profiles are the so-called "crème brulée" ones, and result from a very high geothermal gradient (fig. 5.7).

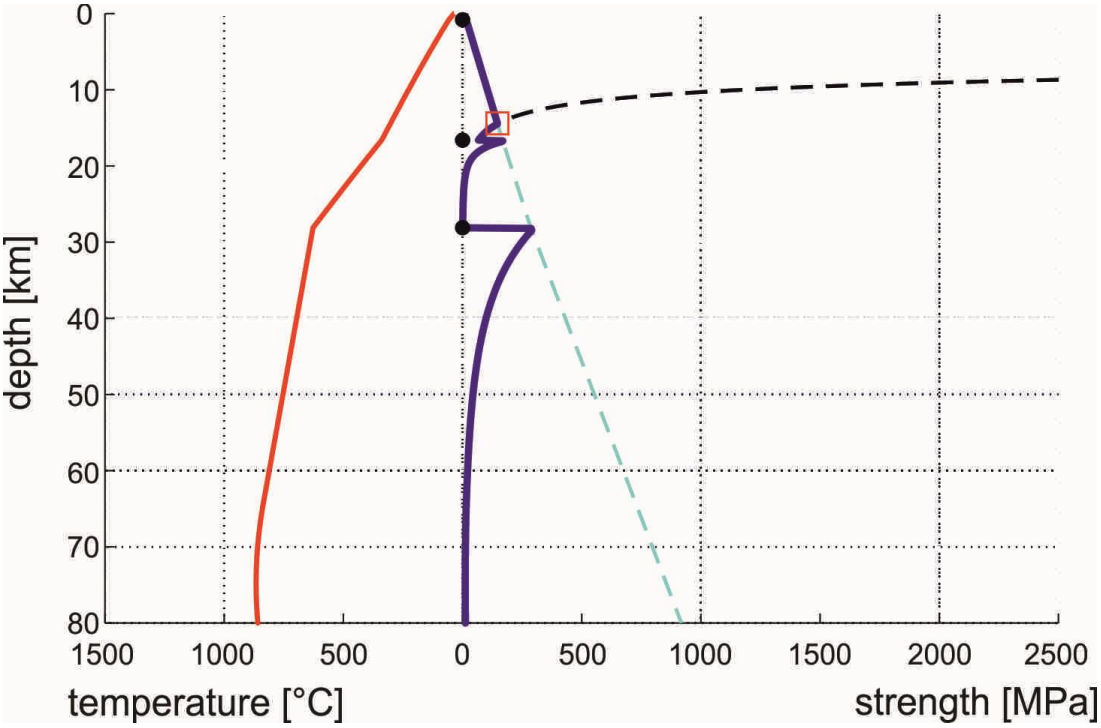

Fig. 5.7 – 1D strength envelope (solid blue curve) for the test site n. 42 - Kaparelli (Central Greece). Note the crème brulée *typology, with a single brittle layer located within the upper crust.*

Indeed, a good correlation of the geographical distribution of the above-mentioned test sites with high values of surface heat flow can be observed (see figure 3.2). The elevated geothermal gradient, which is partly related to the remarkable extension rates (see figure 3.4) characterizing Central Greece, leading also to a rising of the isotherms at depth, is also responsible for the lack of seismicity at depths greater than 15-20 km in those regions, in agreement with the "crème brulée"

style of strength envelope. Similarly, the Aegean Sea region (from north to south and also in the eastern sector at the border with the Anatolian region) is characterized by "crème brulée" rheological profiles, mainly because of the very high geothermal gradient resulting from the long-lasting crustal stretching since Miocene times, due to the back-arc extension as the Hellenic slab progressively sinked and rolled-back.

Accordingly, the test sites of Samothraki, Lemnos, Psara, Sigacik and Bodrum (respectively n. 12, 20, 39, 43, 56 in fig. 5.5.) are all associated with shallow BDTs, lying at depths comprised between 10 and 15 km. In northeastern continental Greece (test sites of Mygdonian basin, Drama and Kavala in the Thrace region, respectively n. 10, 4 and 5 in fig.5.5), the strength envelopes take the form of the "crème brulée" profile with the BDT depths occurring at ca. 13-15 km (fig. 5.8).

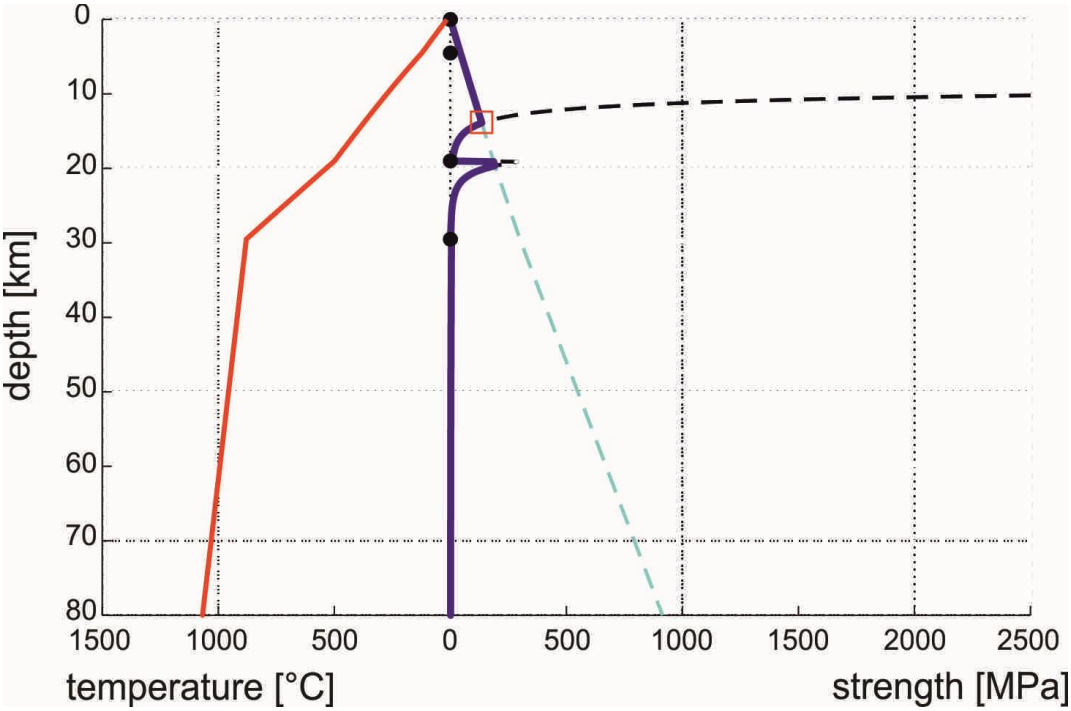

Fig. 5.8 – 1D strength envelope (solid blue curve) for the test site n. 5 - Kavala (southwestern Thrace). Note the crème brulée *typology, with a single brittle layer located within the upper crust. The BDT shallowing effect related to the very high geothermal gradient (see the red curve) is partially balanced by the greater resistance of the granodiorite lithology, selected for the upper crust, so that the resulting BDT lies at ca. 14 km.*

Here the shallowing effects of the elevated surface heat flow (and consequently high geothermal gradient) and of the low/moderate strain rates are partially counterbalanced by the higher resistance of the upper crust lithology selected for this region, corresponding to a granodioritic composition, with respect to the quartzitic lithology selected for almost the totality of the remaining portion of the Aegean Region.

As regards the lower African/Nubian plate, in the sectors not directly involved in the subduction process, the associated 1D strength envelopes (*e.g.* test sites of Libyan Sea and Eastern Mediterranean) show a single thick brittle layer, extending down to depths of ca. 40 km (fig. 5.9).

Such rheological profiles, characterized by a deep BDT occurring in the lithospheric mantle, correspond to the typology termed as "caramel slab" and in the study area are typical of the cold and resistant oceanic plate. Similar strength envelopes and BDT depths are also observed for the test sites belonging to the geological context of the external accretionary wedge (*e.g.* test sites of Offshore SW Peloponnesus-External accretionary wedge, Eastern Mediterranean-External accretionary wedge, and Offshore Cyrenaica-External accretionary wedge, respectively n. 63, 69 and 73 in fig. 5.5).

For such zones, the thickness of the sediments in the accretionary wedge of the overriding plate, limited to less than 5-6 km, is not sufficient to cause substantial variations in the resulting rheological profiles, and therefore, also given the low geothermal gradients characterizing these regions, the main rheological features and stratification remain chiefly dependent on the litho-mechanical properties of the oceanic lithosphere.

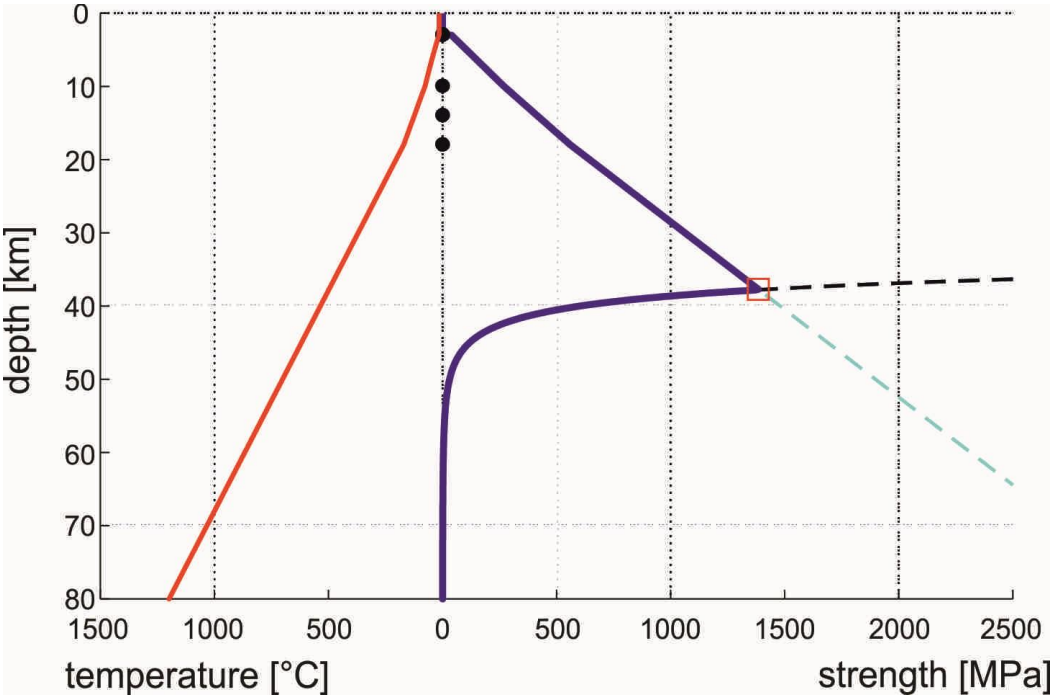

Fig. 5.9 – 1D strength envelope (solid purple curve) for the test site n. 71 – Eastern Mediterranean Sea (oceanic crust). Note the caramel slab *typology, with a single thick brittle layer extending down into the upper mantle, also because of the very low geothermal gradient.*

Indeed, the upper plate sedimentary layer (corresponding to the accretionary wedge), given its reduced thickness, is not able to produce a thermal blanketing effect relevant enough to determine a considerable increase of the temperature in the deeper crustal layer, so that the conditions for ductile flow are only met in the mantle and the depth of the BDT remains unchanged.

When moving towards the internal sectors of the accretionary wedge (*e.g.* test sites of Eastern_Mediterranean-Internal accretionary wedge and Offshore S. Crete- Internal accretionary wedge, respectively n. 65 and 70 in fig. 5.5), the thickness of the sedimentary layer increases to ca.

8-10 km and at times also a limited portion of the upper crustal layer of the overriding plate lies above the subducting slab.

However, mainly because of the low geothermal gradient and the compressional tectonic regime, the BDT does not occur within the upper plate, but it is again confined within the mantle of the lower plate, depending on its rheology. Furthermore, the old and cold subducting oceanic lithosphere causes a thermal perturbation, which results into a cooling effect at depth (see section §3.2.2), so that the temperature conditions for the onset of ductile deformation are met at even greater depths than those associated to the unsubducted oceanic plate sectors.

Accordingly, the BDTs of the test sites lying in the geological context of the internal accretionary wedge occur at depths between ca. 45 and 50 km (fig. 5.10), with the associated rheological profiles representing further examples of the "caramel slab" typology and BDTs strengths attaining even greater values than those observed in the external accretionary wedge and unsubducted oceanic lithosphere contexts.

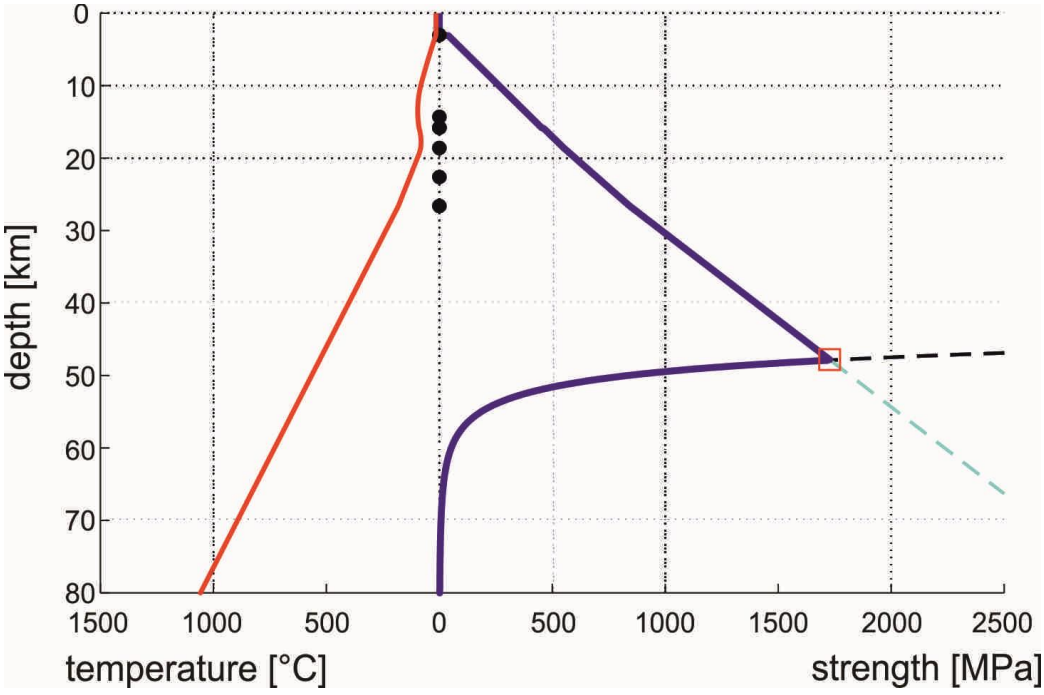

Fig. 5.10 – 1D strength envelope (solid blue curve) for the test site n. 70 - Offshore S. Crete (internal accretionary wedge above an oceanic crust setting). Note the caramel slab *typology, with a single thick brittle layer extending down into the upper mantle, also because of the very low geothermal gradient, resulting from the thermal perturbation due to the cooling effect of the subducting slab.*

In the continental collision setting that characterizes the northwestern corner of the study area (Ionian-Apulian region), the crust of the lower plate has a continental nature. Accordingly, the rheological properties for the test sites lying in the sectors of the Apulian platform that have not been directly involved in the collisional process yet, mainly depend on the mechanical characteristics of the intermediate-felsic lithologies of the continental crust. The test site of Offshore

Apulia-Corfu (n. 32 in fig. 5.5) indicates that the BDT occurs at depths just greater than 30 km, within the lower crust layer corresponding to a felsic granulite lithology (fig. 5.11).

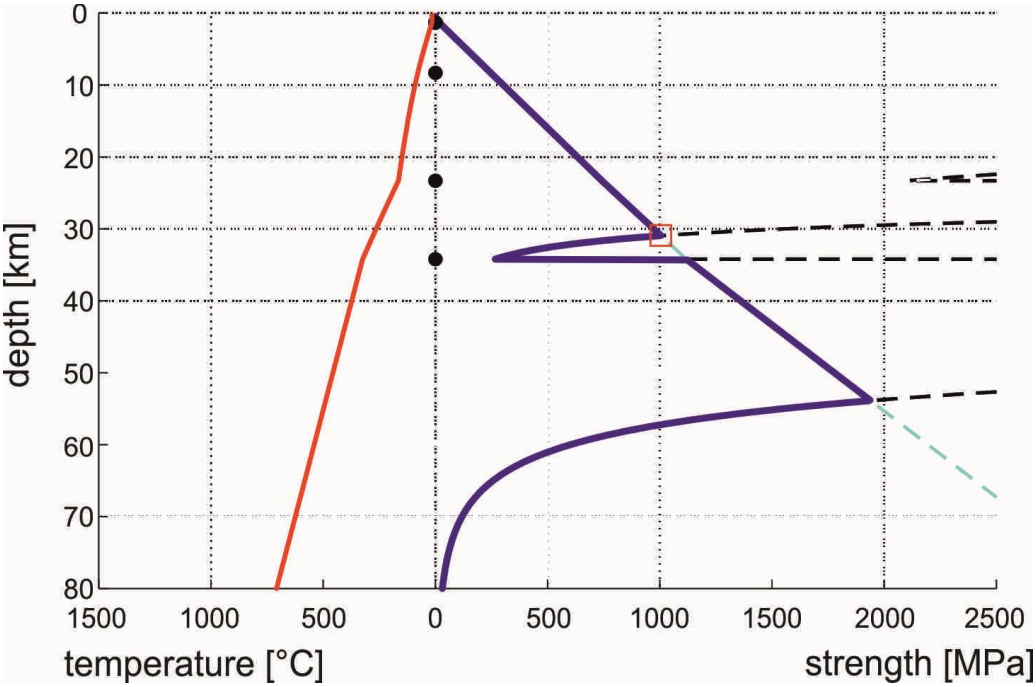

Fig. 5.11 – 1D strength envelope (solid blue curve) for the test site n. 32 - Offshore Apulia-Corfu (continental collision setting).

The shape of the strength envelope almost perfectly reproduces the jelly sandwich typology typical of the continental crust, with the lower crust behaving in a ductile fashion and embedded within two brittle layers. The BDT tends to occur close to the base of the lower crust rather than at its top or at the bottom of the upper crust (as occurs, instead, in the back-arc extending region), because of the compressional tectonic regime and, above all, because of the low geothermal gradient that makes all the layers and lithologies much more resistant and hinders ductile deformation processes.

5.2 - 2D transects

Several rheological 2D transects have been realized across the Aegean Region, with the aim of comparing the behaviour in collisional versus subducting settings. Closely spaced 1D strength envelopes, realized through a dedicated Matlab script, have been interpolated for determining the lithospheric distribution of brittle and ductile layers. Literature data and geodynamic considerations have been mainly used to fix the parameters for the rheological modelling and a particular care was spent in reproducing reliable thermal models.

The results of the mechanical-rheological model highlighted the following features and differences between the northern continental collision and the southern oceanic subduction settings:

i) a slightly shallower BDT in the western sectors of the northern transects (~30-33 km) with respect to the southern ones (~40 km); ii) on the contrary, in the central-eastern sectors of the investigated area, corresponding to an extensional tectonic regime, the northern transects have a relatively deeper BDT (around 20-25 km) if compared with the southern ones (around 15 km); iii) the occurrence of a thick, deeper brittle layer below the shallowest brittle-ductile transition, in the central-eastern sectors of the northern transects.

I suggest that such regional differences are mainly related and attributable to the surface heat flow distribution (which directly affects the geothermal gradient) and to the tectonic and geodynamic context. The results of the rheological modelling in terms of depth extent of the brittle layer(s) have been then compared with the depth distribution of available relocated seismicity, showing a good agreement with the rheological layering here proposed (see figures 5.18 and 5.20).

More specifically, for the aims of this study, I realized a total of eight transects in the Aegean Region. The first three cross the northern continental collision setting, from western offshore Corfu island (western Greece) to Thessaloniki (Central Macedonia, Greece). A second set of three transects is almost parallel but south of the first one and intersects the active western Hellenic subduction zone of the oceanic Nubian/Ionian lithosphere below the Aegean microplate, that is to say, from offshore Peloponnesus to Attica. The last two transects cross the former two sets, as they lie parallel to the axis of the Hellenides fold-and-thrust belt, the first being in an offshore external position and the other in an internal position (fig. 5.12).

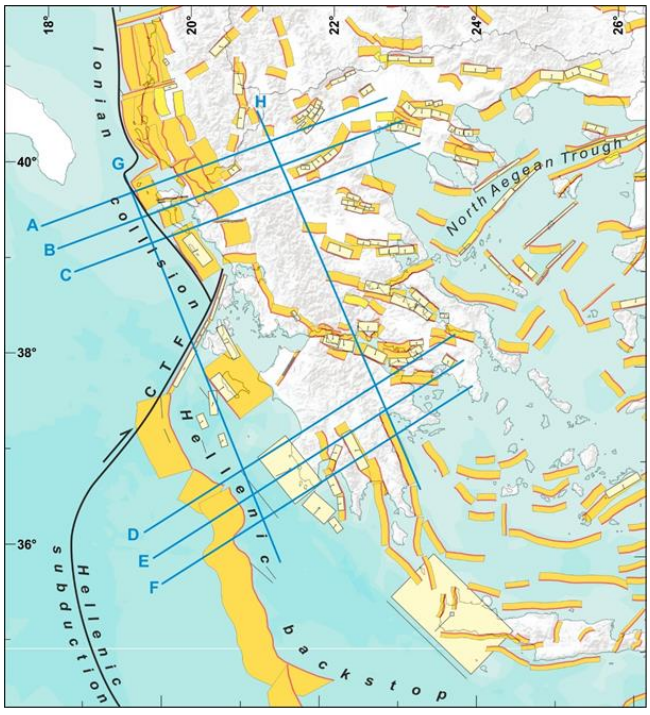

Fig. 5.12 – Geodynamic sketch map of the broader Aegean Region. Both composite and individual seismogenic sources (CSS and ISS, respectively) from GreDaSS (Caputo et al., 2012) are represented, as well as the traces of the transects generated by interpolation of densely spaced 1D rheological profiles. CTF indicates the Cephalonia Transform Fault.

The crosscutting geometry of the transects grid allows to use the intersections as both control points and 3D-view insights on the thermo-rheological characteristics of the Hellenides region. The transversal and longitudinal transects have a total length of ~430 and 450 km, respectively, and result from the projection along the traces of well-calibrated 1D strength logs with a mean distance of ~10 km. By interpolating such closely-spaced strength profiles the distribution at depth of the BDT could be obtained as well as its strength and temperature; it is worth to note that in the present study I am focused on the first 50 km of the analyzed profiles.

In order to realize the rheological transects, as many as possible literature data from different studies, methods and sources for defining the values of the input parameters in the constitutive rheological equations have been collected. I will now briefly present the literature data used for each input parameter. I tried, when possible, to consider data from more than one author or working group and from different scale studies.

The crustal structure and the thicknesses of the lithospheric layers (sedimentary cover, upper crust, lower crust, upper mantle) have been retrieved mainly from regional-scale studies based on different and integrated geophysical data and methods, such as gravimetry, seismic reflection and refraction profiles, tomographic inversions based on P and S seismic waves arrival times, etc. (Makris *et al*., 2013; Grigoriadis *et al*., 2016; Sodoudi *et al*., 2006; Zelt *et al*., 2005; Tiberi *et al*., 2001, Tirel *et al*., 2004, among others).

From the analysis of such studies it can be observed that the deepest Moho discontinuity occurs in the axial zone of the Hellenides fold-and-thrust belt, with maximum values reaching 40-45 km of depth. On the contrary, the stretched lithosphere of Northern Aegean and the Hellenic volcanic arc are characterized by a noticeably thinned continental crust, with the Moho being as shallow as 18-20 km in correspondence of the Cycladic core complex.

The lithologies for the different crustal and lithospheric layers have been selected on the basis of the long-lasting tectonic and structural evolution of the Aegean Region. I also took into account dedicated palaeogeographic reconstructions from Mountrakis (2006), Ring *et al*. (2010) and Papanikolaou (2013) and continental-scale works on lithospheric lithologies such as those of Tesauro (2009) and Tesauro *et al*. (2008).

Limestone and metasediments have been selected as the representative lithologies for the sedimentary cover layer; the upper crust of the Aegean plate corresponds to a quartzite lithology, while the one of the Nubian plate is considered to be more realistically represented by a diabase lithology.

The lower crust in the Aegean plate has been associated with a diorite lithology and the upper mantle, for both Aegean and Nubian plates, with a peridotite. Some exceptions to these choices occur in the region east of Thessaloniki, around the Mygdonia Graben, where granitoid intrusions have been mapped and granodiorite has therefore been selected as the most proper representative lithology for the upper crust.

All the values for the thermo-rheological parameters (power-law parameter, power-law exponent, activation energy, thermal conductivity and radiogenic heat production) of the corresponding lithology are reported in Table 3.1. The values used in this research are mainly literature data obtained from experimental, analogue, modelling and review works and papers from many authors.

The strain rate values have been selected and averaged from a wealth of geodetic-based works (Kreemer *et al.*, 2014; Hollenstein *et al.*, 2008; Floyd *et al.*, 2010; Muller *et al.*, 2013). Strain rates are derived from velocity fields obtained with mostly continuous displacement measurements realized with GNSS systems.

The highest deformation rates are observed around the Kefallinia Transform Fault, in the Corinth Rift, along the North Aegean Trough and the North Anatolian Fault and finally along the Hellenic Trench in the central sector south of Crete, with maximum values being up to ~2.0-2.5·10^{-14} s^{-1}. Lower values, in the order of 10^{-16} s^{-1}, characterize the central and southern Aegean Sea regions, while continental Greece and Peloponnesus are deforming at intermediate rates, with values being between 1.0·10^{-15} and 5·10^{-15} s^{-1}.

Regarding the surface heat flow values, both local and regional scale studies based on point observations and areal interpolation have been considered. The main sources used in this work come from the investigations of Fytikas and Kolios (1979), Cloetingh *et al.* (2010), Hurter and Haenel (2002).

Special care was dedicated to the averaging and smoothing of the different heat flow maps, given its primary influence on the resulting thermal regime and related rheological modelling. All the literature sources indicate that the highest heat flow values occur along the Hellenic volcanic arc and in the central Aegean-western Anatolia. On the contrary, low values characterize the outer portion with respect to the Hellenic subduction zone and western continental Greece.

For the friction coefficient parameter, a reference value of 0.6 has been selected, which is consistent with the classic experiments and reviews of Byerlee (1968; 1978) and it lies in the interval (0.5-0.8) of the most common values also proposed by Ranalli (1995).

In order to account for a lower coupling along major active faults, slightly lower values, down to 0.5, have been assigned in correspondence of the main seismogenic sources crossed by the transects (from GreDaSS database; Caputo *et al.*, 2012; Caputo and Pavlides, 2013). Such a choice is based on the higher wearing, comminution, abrasion and mineralogical-related weakening, which occur on seismic shear zones and faults, as documented by *e.g.* Collettini and Holdsworth (2004), Middleton and Copley (2014), Chiaraluce *et al.* (2007).

Regarding the pore fluid factor, a standard value of 0.4 of the Skempton coefficient has been assumed. This value approximately corresponds to a hydrostatic pore fluid pressure. For peculiar tectonic and geodynamic settings, such as the accretionary prism in the western portion of the area (fig. 5.12) and the region of the volcanic arc, slightly higher values up to 0.5 have been selected.

These geological scenarios are justified due to fluid migrations along preferential pathways such as detachment and flat-ramp thrusts, sediments compaction, limited seepage and fluid overpressure in the accretionary wedge, water release through mineralogical reactions in the mantle wedge beneath the volcanic arc region, etc.

Once assigned numerical values to all parameters, I followed a systematic methodological workflow. Firstly, closely spaced (mean inter-distance around 10 km) 1D rheological profiles have been reconstructed along each transect. The production in a first stage of 1D profiles allows to better take into account and model the peculiarities of each location, especially in terms of local lithological vertical stratification, pore fluid pressure conditions and tectonic setting.

To realize the 1D strength envelopes, a purposely developed Matlab code has been implemented. The code is based on equations [2.7], [2.9] and [2.12], which are used to calculate the thermal gradient (along with absolute temperature) and the brittle and ductile strengths along depth.

The frictional and the creep strengths are compared all along the vertical axis and the smaller value among the two, at each depth, determines the shape of the envelope and the value of the maximum shear strength rocks could theoretically support. The vertical step for the iteration of the calculations is 100 m, while the total depth covered for each profile is 100 km. These two values represent a reasonable compromise between a useful vertical resolution and computer running time. As a matter of fact, the intersection between the brittle and the ductile curves determines the BDT depth.

As previously discussed, in case of occurrence of a second deeper brittle layer, the interposed ductile layer is considered to be effective in seismically decoupling the two layers only if it attains a minimum thickness of 0.5 km. Such a value is comparable to that suggested in previous studies.

In particular, Rolandone *et al.* (2004), using seismological observations, indicate a possible post-seismic deepening of the brittle zone in the order of 2 km, while Beeler *et al.* (2018) propose a value ~1 km obtained from numerical rheological modelling. It is worth to note that for both the overriding and the undergoing plates four lithological/mechanical layers have been considered, consisting in: sedimentary cover, upper crust, lower crust and upper mantle.

From a thermal point of view, when approaching in the model the Wadati-Benioff zone, a perturbation of the geothermal gradient, resulting from the cooling effect of the downgoing lithospheric slab, has been also included in the Matlab code.

Obviously, for profiles occurring in the marine environment an additional shallow layer of water is considered. In figure 5.13, schematic geological sections of the lithospheric structure and internal subdivision into different layers are shown for selected transects.

I am now going to focus first on the northern set of transects (A, B, and C; continental collision geodynamic setting), then on the southern one (D, E and F; oceanic subduction setting) and finally on the two orthogonal transects (G and H), by describing the prominent features and lateral

variations of the main thermo-rheological parameters, namely the BDT depth and associated strength and temperature.

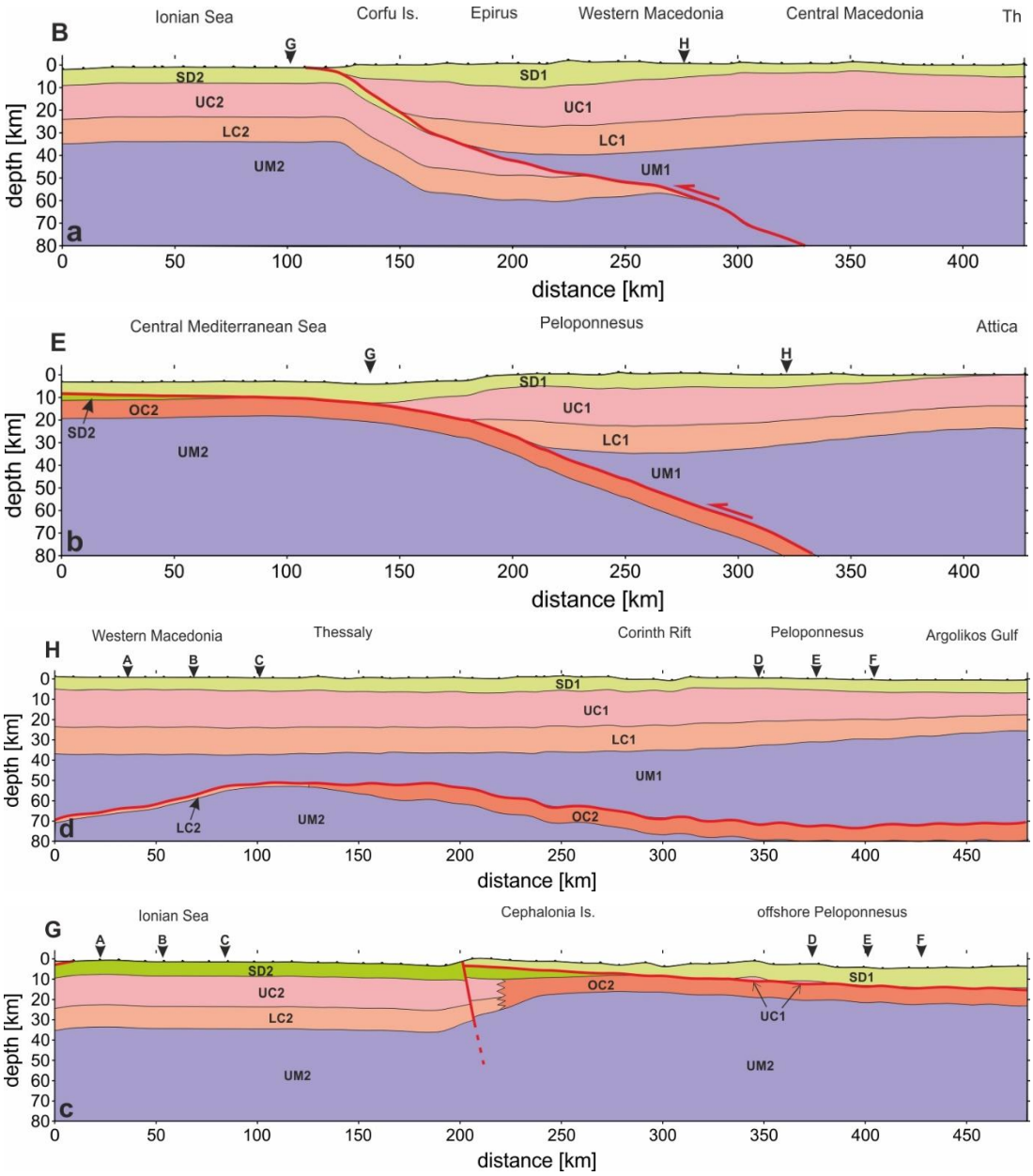

Fig. 5.13 – Lithospheric stratigraphy used for the rheological modelling of transects B, E, G and H (see Fig. 5.12 for locations). Layers labelling: SD = sedimentary rocks; UC = continental upper crust; LC = continental lower crust; OC = oceanic crust; UM = upper mantle; index "1" and "2" refer to the Aegean microplate and Ionian/Nubian plate, respectively.

In terms of BDT depth, the three northern transects (Fig. 5.14) are characterized by comparable trends. For each of them, in the westernmost 100-120 km, corresponding to the area offshore Corfu Island, the BDTs are at depths between 30 and 33 km, thus occurring within the lowermost portion of the Apulian microplate crust. Further east, closer to Corfu Island and along the coastal sector at the border between Greece and Albania, the BDTs progressively deepen to maximum depths of ca. 53 km, due to the overall bending of the lower colliding plate, as a consequence of the recent and

persisting underthrusting process. Although such rheological transition continues further deep in the lower plate, in correspondence of Epirus, at approximatively 170-200 km from the western end of the transects, a shallow BDT appears in the crust of the upper plate characterizing the transects up to their eastern termination. It occurs at depths varying from 25-30 km, to the west, shallowing eastwards up to 20 km in correspondence of Western Macedonia and reaching 15-18 km in the easternmost sector of the transects close to Thessaloniki.

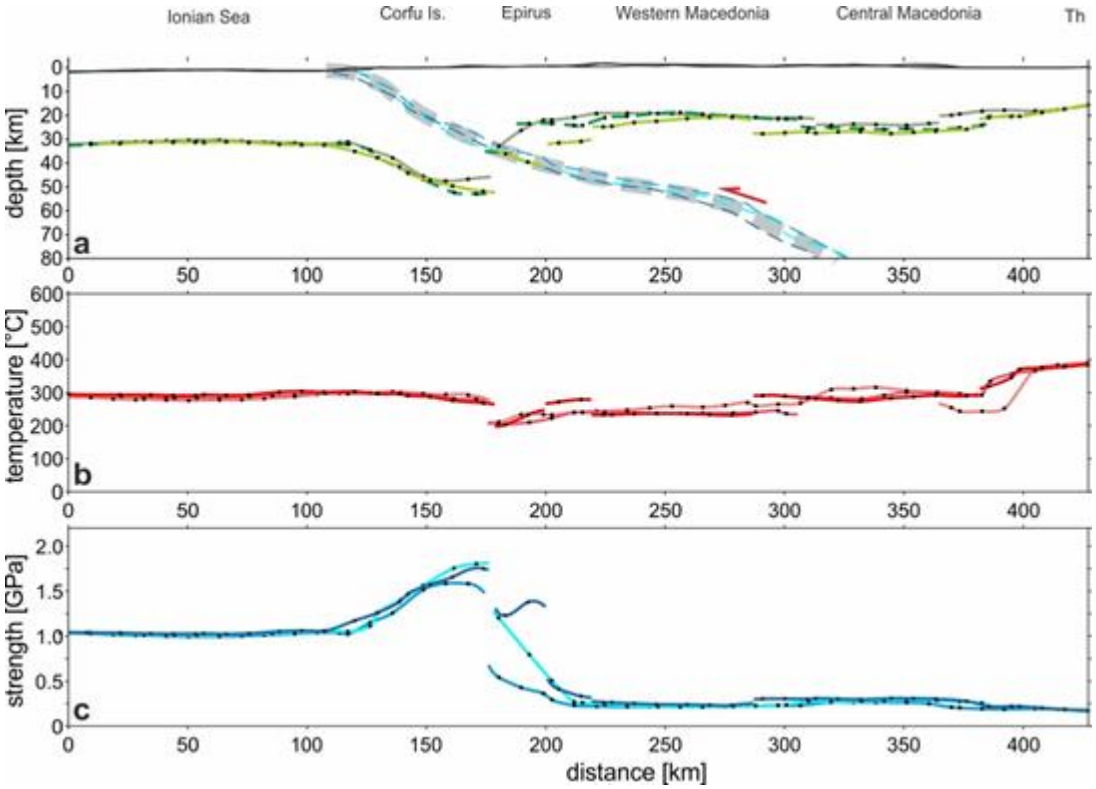

Fig. 5.14 – Northern set of transects: a) BDT depth; b) temperature at the BDT depth; c) strength at the BDT depth.

It should be noted that in a region between km 300 and 370 of the transects, the shallow BDTs are at slightly greater depths (ca. 25 km). This deepening is mainly associated to a decrease in heat flow and, as a consequence, of the geothermal gradient in that area. Indeed, lower temperatures at comparable depths cause an increase of the ductile strength and therefore the BDT is locally shifted downwards. Since the area with a relatively low heat flow has an oblique trend with respect to the transects, the BDT deepening actually appears at the km 270 in transect A, and only at km 330 in transect C. The influence of the heat flow variations on the resulting BDT depths is also confirmed by a swath-like profile that has been realized by selecting a 50 km-wide buffer zone on both sides along the transect.

As regards the strength at the BDT, a very similar trend to the one observed for the BDT depths is followed (Fig. 5.14c). Indeed, the strengths for the three profiles tend to be steadily comprised between 1000 and 1050 MPa in the western sector within the Apulian platform, progressively

increasing as the BDTs deepen eastwards, reaching maximum values of ca. 1800 MPa within the subducted plate. In the Macedonian sector of the transects where the BDTs are shifted to the upper plate, the relative strengths are always between ~200 and ~300 MPa, with the higher values attained in correspondence of the depressed BDTs sector where the heat flow and the geothermal gradient are relatively lower (as above discussed).

As for the temperatures reached at the BDT, they are clearly dependent on the thermal distribution and on the depth at which the BDTs occur (Fig. 5.14b). For example, although the BDTs in the Apulian plate are relatively deep (ca. 30 km), the very low geothermal gradients cause the BDT temperatures to remain, in the western sector of the transects, just below 300 °C. On the other hand, in the central and eastern sectors, the combined effect of generally much shallower BDTs with much higher geothermal gradients leads to comparable BDT temperatures ranging between 210 and 300 °C. The only exception is represented by the easternmost sector in the area around Thessaloniki, where the increase in geothermal gradient is exceeding the effect of the BDTs shallowing, thus increasing the temperatures up to ca. 380 °C.

The transects of the southern set (D, E and F) are also very similar among them in terms of BDT depths (Fig. 5.15a).

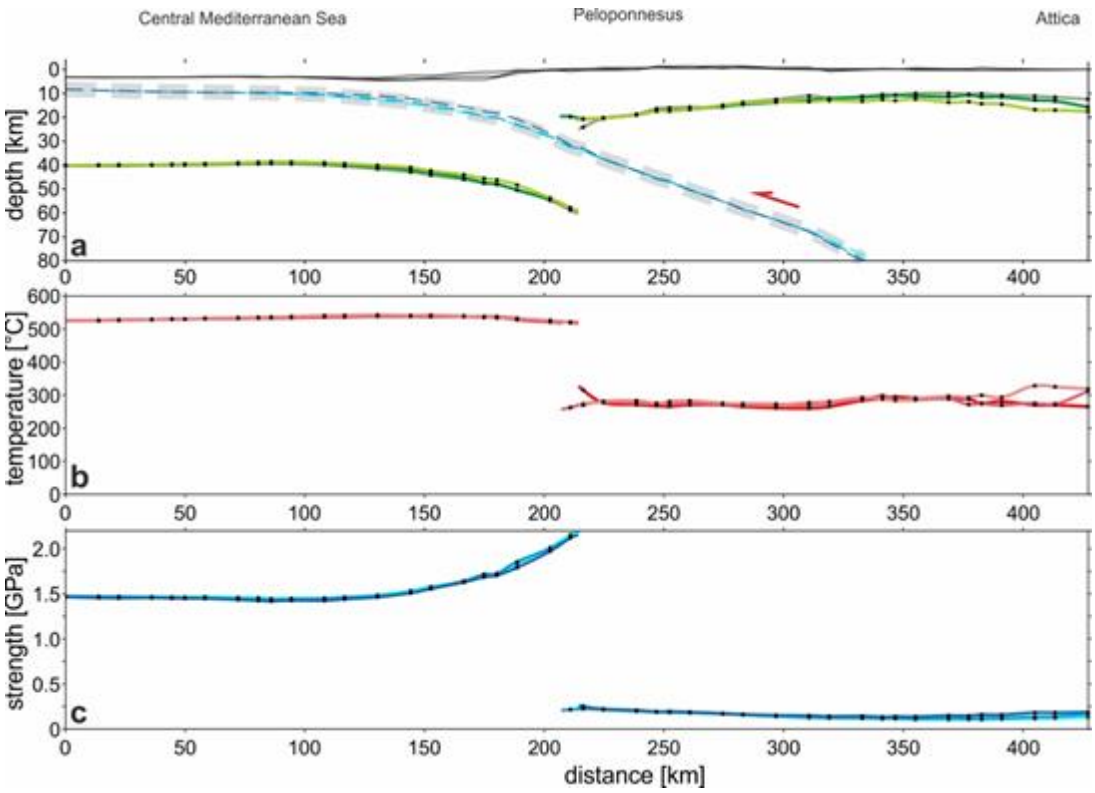

Fig. 5.15 – Southern set of transects: a) BDT depth; b) temperature at the BDT depth; c) strength at the BDT depth.

Indeed, in the westernmost sector offshore Peloponnesus, the BDTs smoothly lie at ca. 40 km, thus occurring within the mantle of the oceanic crust in the lower plate. Moving closer to the coastal

area, as the African/Ionian oceanic lithosphere subducts and bends, the BDTs follow a deepening trend. Similar to the collisional setting, the upper plate is characterized by a shallow BDT in correspondence of the Peloponnesus peninsula, where the transition occurs in the upper crust at depths between 15 and 20 km. A shallowing trend could be observed to the northeast up to minimum depths of ca. 10 km in the Saronic Gulf and southwestern Attica, before a final deepening at the easternmost sector of the transects (eastern Attica), with depths of 12-17 km. For this set of transects too, the role of the heat flow and geothermal gradient on the BDT depth is of primary relevance and greatly evident. Indeed, apart from the lithological differences with respect to the northern collisional setting, the deep BDTs in the oceanic crust are also related to the very low temperatures characterizing the cold and old oceanic lithosphere at depth, while the progressive shallowing observed in the upper Aegean microplate is correlated to, and caused by, an increase in the heat flow, as the Hellenic volcanic arc is crossed by the transects where the Aegean crust is thinned due to extension in the back-arc region.

As concerns the strengths at the BDT along the southern transects (Fig. 5.15c), the relative values are comprised between ca. 1.4 and 1.5 GPa in the western offshore sector, where the BDTs lie in the oceanic lithosphere, and tend to increase up to maximum values of almost 2.2 GPa, as the BDTs deepen along the subduction zone. In contrast, where the BDTs occur in the upper plate crust, the corresponding strength values are one order of magnitude lower (100-200 MPa), with the minimum values observed in the sector characterized by the shallowest BDT depths (western Attica and Saronic Gulf).

As for the temperatures distribution at the BDT (Fig. 5.15b), the highest values are reached in the western sector within the oceanic lithosphere, where they range between 520 and 530 °C, while within the crust of the Aegean microplate, the BDTs temperatures are systematically lower and comprised between 260 and 300 °C, with a local peak of ca. 310 °C attained in the easternmost points. Such low values in the BDT temperatures of the upper plate are mainly attributable to the generally shallow occurrence of the BDTs and their lateral variations.

Along the orthogonal profiles G and H the BDT depths clearly follow markedly distinct trends (Figs. 5.16a and 5.17a). Transect G, lying entirely in a compressional tectonic setting, is characterized by BDT depths of 30-35 km in the northern sector offshore the Corfu and Paxos islands, where the transition occurs in the deepest crustal layers of the upper continental plate.

To the south the transect crosses the Kefallinia Transform Fault, which is associated to an important forward (i.e. SW-wards) jump of the plate boundary with two further consequences: a sharp deepening (along the transect) of the Wadati-Benioff plane and an abrupt geological change, as far as the lower plate is represented by the Ionian/Nubian oceanic lithosphere.

Accordingly, at the Kefallinia Transform Fault, the BDT lies at depths greater than 50 km, rapidly shallowing southwards to depths around 38 km before slightly deepening again to ca. 45 km. Along the H profile, which entirely crosses the extensional realm of the internal Aegean

Region, the BDT always occurs in the upper plate at depths between 11 and 28 km, following a shallowing trend from the northwestern end value of ca. 28 km, at the border between Albania, FYROM and Epirus, to the southeastern termination value of ca. 12 km in the Argolikos Gulf.

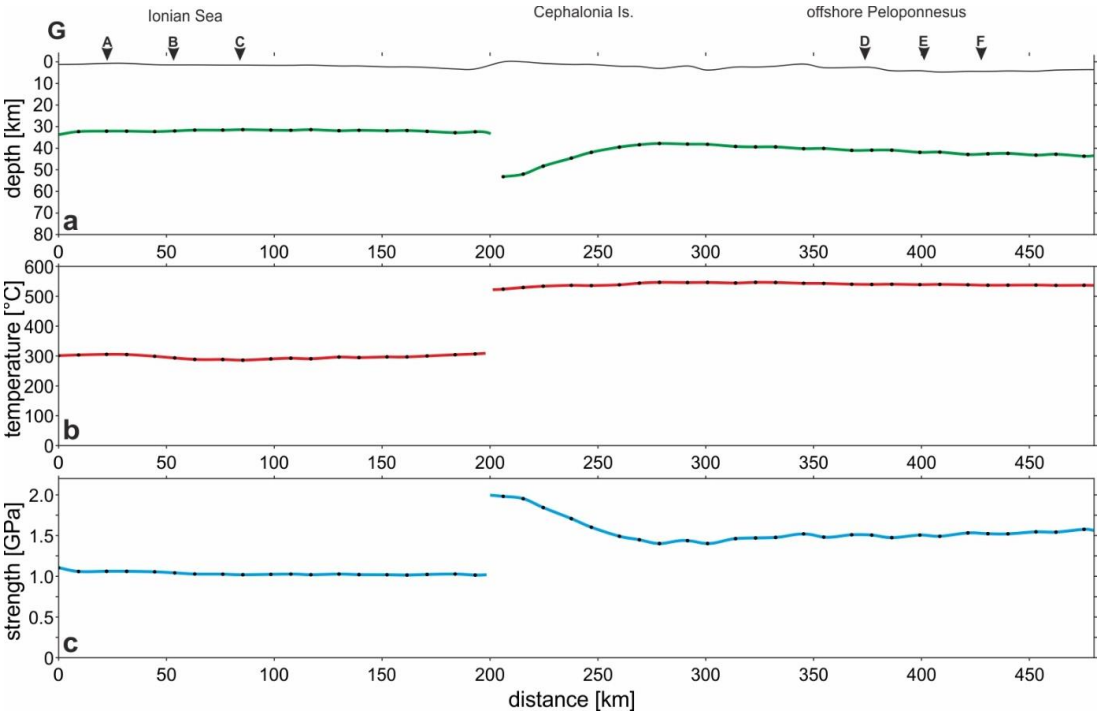

Fig. 5.16 – Transect G: a) BDT depth; b) temperature at the BDT depth; c) strength at the BDT depth.

In the central sector just south of the Corinth Gulf, a local deepening to values of ca. 18 km is observed; the BDT depth variations for the H transect are mainly related to heat flow changes, as it decreases from the northern end to the southern one, with some local (positive) oscillations, as it occurs at the southern border of the Corinth rift.

As regards the associated BDT strengths (Figs. 5.16c and 5.17c), for the G profile, they are around 1 GPa in the continental crust north of the KTF, while values of almost 2 GPa are attained in conjunction with the deepest BDT located within the subducting oceanic lithosphere, followed by slightly lower values comprised between 1.4 and 1.5 GPa in the southern sector of the transect.

In contrast, along the H profile the values of the strength are always much lower, mostly because of the different tectonic regime.

Indeed, it is well known since the findings of Sibson in the seventies (*e.g.* Sibson, 1974) that the shear strength in compressional regimes is much higher than in extensional ones. In addition, the generally higher heat flows of the eastern transect obviously contribute to this effect. Accordingly, the strength at the BDT in H ranges between ca. 300 MPa (at the northern end) and ca. 120 MPa (at the southern one) with only lateral slight variations.

The trend of the BDT temperatures for the transect G (Fig. 5.16b) is characterized by values around 300 °C in the continental crust of the Apulian block in the northern sector, sharply jumping to steady values of ca. 520-530 °C in the oceanic lithosphere south of the Kefallinia Transform Fault. The latter trend, which at least in the central-southern sector (km 210-260) seems to be uncorrelated with that of the BDT depths (Fig. 5.16a), highlights once again the great influence that the geothermal gradient has on the resulting rheological behaviour and particularly on the ductile one. Indeed, given a fixed lithological and tectonic setting, which could be considered relatively homogeneous south of the Kefallinia Transform Fault, the main factor controlling the depth of the transition is temperature.

Indeed, comparing figures 5.16a and 5.16b, the temperature at the BDT is always around 520-530 °C, but the BDT depth is much greater at the Kefallinia Transform Fault because those temperatures are only reached at greater depths due to the subduction process itself. Finally, along transect H, the BDT temperatures show only small variations between ca. 230 and 300 °C (Fig. 5.17b), and also in this case no clear correlation with the BDT depth could be observed at first glance, because of the interplay between lower/higher geothermal gradient and deeper/shallower BDT depths (Fig. 5.17a).

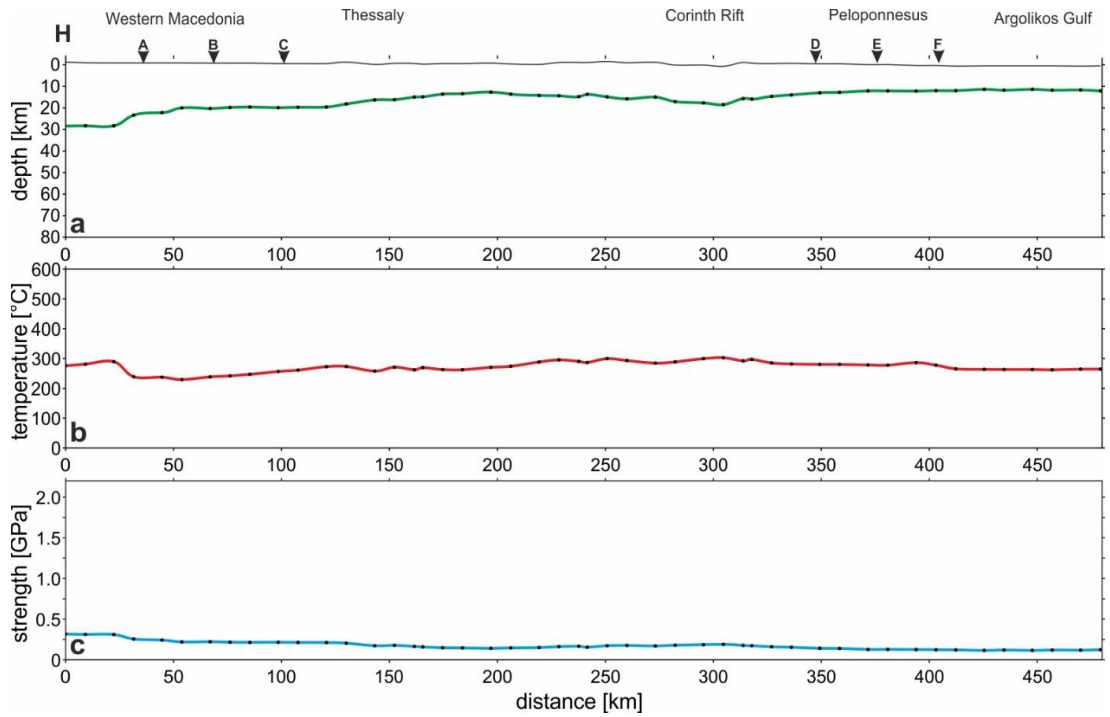

Fig. 5.17 – Transect H: a) BDT depth; b) temperature at the BDT depth; c) strength at the BDT depth.

Those two factors, indeed, tend to compensate each other and as a result the BDT temperatures remain almost constant without following any precise trend, despite the BDT depth lateral changes.

In the following, I discuss the results presented above and I compare them, especially those relative to the BDT depth, with the vertical distribution of well-recorded and possibly relocated seismicity. For the sake of simplicity, I am going to focus on profiles B (continental collision), E (oceanic subduction), G and H (orthogonal transects, respectively belonging to the compressional and extensional tectonic settings). Along these profiles, the correlation with the seismicity depth distribution is generally in good agreement with the rheological layering and in particular with the depth of the BDT, as obtained in this research (Fig. 5.18).

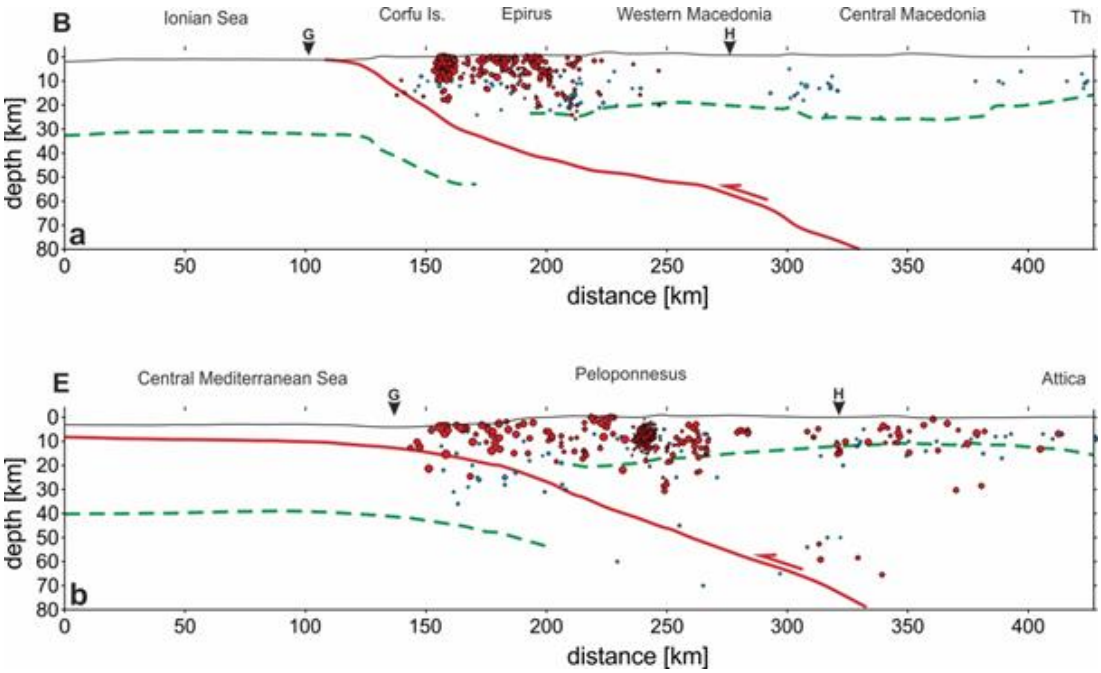

Fig. 5.18 – Comparison between the shallowest BDT (green dashed line) with the hypocentral distribution of well-located seismicity, along transects B (a) and E (b), respectively.

As regards the seismicity data used in the comparison, two different catalogs have been considered: the first one, from Kassaras *et al.* (2016), consists of relocated seismicity and the second one mainly consists of events with M > 3, for which moment tensors have been calculated by the National Kapodistrian University of Athens. In the catalogue of Kassaras and co-workers, covering a time span of 24 years (1989-2012), the seismicity is relocated through the application of relative relocation techniques such as HypoDD, which allows to substantially reduce the error of the hypocentral depth. In the NKUA catalogue of focal mechanisms (covered period 1995-2019) the good hypocentral depth resolution is guaranteed by the inversion procedures followed to determine the moment tensor solution for each event.

In the northern transect (B; Fig. 5.14) and particularly in the western offshore sector, the BDT is never deeper than 33 km, though it tends to rapidly deepen once entered the collisional zone in correspondence of the coastal region, east of Corfu Island. This behaviour is related to the continental nature of the crust of the undergoing plate and the associated intermediate/felsic typical lithologies (I selected quartzite and granulite for the upper and lower crust, respectively), which

tend to yield at lower shear stresses (and therefore at minor confining pressure and depth) with respect to mafic lithotypes. In this brittle volume, however, no seismicity is recorded in neither of the two used catalogues (Fig. 5.18a).

As previously described, in mainland Greece and eastwards, the BDT ranges between 15 and 25 km and it is entirely within the crust of the Aegean microplate, slightly deeper than what observed for the corresponding central-eastern sectors of the southern profiles. This difference is basically due to the lower heat flow characterizing Epirus and western Albania with respect to, for example, Attica and northeastern Peloponnesus. The comparison between the BDT depth and the distribution at depth of the relocated seismicity (Fig. 5.18a) shows a very good agreement (Hatzfeld *et al.*, 1995; Kassaras *et al.*, 2016). The shallower BDT in the eastern sectors is also nicely consistent with the depth distribution of the Kozani-Grevena seismic sequence (mainshock and aftershocks), occurred in 1995 (Resor *et al.*, 2005).

Regarding the southern transect (E; Fig. 5.15), the relatively deep transition in the western 180-200 km is due to the oceanic nature of the crust and particularly its old age (possibly Triassic; van Hinsbergen *et al.*, 2005; Ring *et al.*, 2010 and references therein); it is therefore cold and characterized by a low geothermal gradient. Together with the resistant mafic lithologies, this can account for such a deep transition (almost 40 km), that conversely is not necessarily mirrored by a similarly deep seismicity, since the oceanic plate also retains a very high strength (Fig. 5.15b).

Accordingly, the almost absent seismicity in the considered catalogues (Fig. 5.18b) might be also explained by the lack of, or very poor, tectonic loading (i.e. not able to overcome the critical differential stress), rather than by the prevalence of a ductile behaviour, especially in the western plate sectors not directly involved in the subduction process yet. Whatever the case, seismicity data from the NKUA catalogue show some events as deep as 35 km offshore southwestern Peloponnesus (Fig. 5.18b), which are compatible with the results on the BDT depth given in this work.

Also the shallow BDT (15-20 km-deep) east of Oichalia and Kalamata regions, which is related to the upward jump of the rheological transition from the downgoing Ionian-African plate to the overriding Aegean plate, is in good agreement with the seismicity distribution relocated by Kassaras *et al.* (2016: Fig. 5.18b). In the back-arc region corresponding to the central-eastern sector of the southern transects some deeper events are recorded at ca 30 km-depth. These few and minor events ($M \leq 4$) occurring where ductile deformation is expected according to the modelling, is likely due to a local increase in pore fluid pressure leading to a remarkable decrease in brittle strength (equation [2.7]), allowing brittle and potentially seismogenic behaviour to occur.

This hypothesis is also supported by the fact that the difference between brittle and ductile behaviour (with the latter being theoretically greater than the former), at those depths in the back-arc region along the transect, is actually quite small (Fig. 5.19b). Therefore, even a relatively limited decrease in brittle strength would be sufficient to exceed frictional resistance instead of keep deforming in a plastic and aseismic behaviour. The increase of pore fluid pressure in back-arc

regions is effectively a common event, because of the continuous release of fluids produced by the slab dehydration, within the context of the subduction process. It should be noted, however, that such variations in fluid pressure likely occur at a small scale, making them not easily detectable and hence not reproducible in the modelling due to the coarser scale of observation. Additionally, such variations may be related to temporal fluctuations of the pore fluid pressure, and since I do not consider the time variable in the model, it cannot be included in the modelling.

I would like to emphasize that some recorded seismicity deeper than the shallow BDT considered in this research (Fig. 5.18b) may be associated with a second deeper brittle (and hence seismogenic) layer, for example in the intermediate-lower crust or in the uppermost mantle. At this regard, it may be useful to observe the distribution at depth of the rheological behaviour (brittle versus ductile) within the two sections (Fig. 5.19).

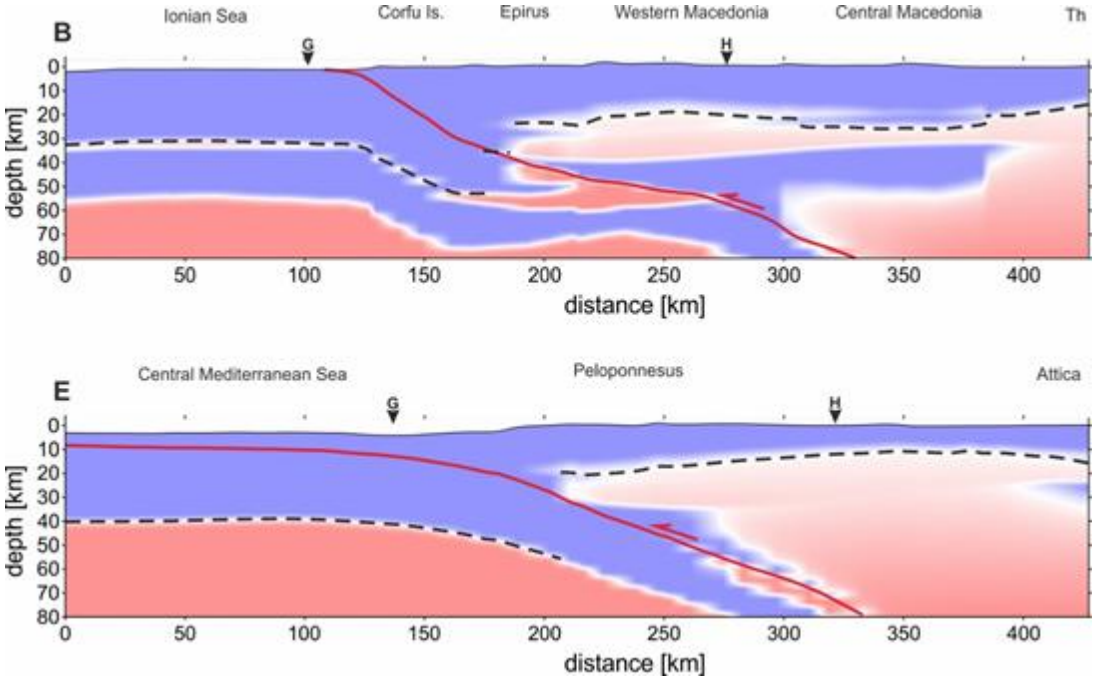

Fig. 5.19 – Distribution of brittle and ductile volumes and layers along transects B (a) and E (b), as indicated by the differential strength (brittle minus ductile strength). Blue and red correspond to dominantly brittle and ductile behaviour, respectively, while the whitish colour corresponds to differential strength values close to 0, therefore emphasizing the occurrence of a brittle-ductile transition. The shallowest BDT is marked as a dashed black line.

Both in the collisional and subduction settings (Fig. 5.19a and 5.19b, respectively), deeper brittle layers/volumes could be indeed recognized in the central-eastern sectors of the transects at variable depths from 30 to >80 km. Accordingly, these rock volumes may be potentially seismogenic as well, thus representing the source for the 'deeper' seismicity observed in Kassaras *et al.* (2016; Fig. 5.18). Relative to this issue, the comparison between northern and southern transects allow to emphasize the following differences and peculiarities.

Firstly, the upper plate in the northern transect (Fig. 5.19a) is systematically characterized by a thicker 'shallow' brittle layer with respect to the oceanic subduction setting (southern transect; Fig. 5.19b).

Secondly, in the northern transect a second continuous, 10-20 km-thick brittle layer is observed at 30-40 km-depth within the upper mantle of the Aegean microplate underlying the shallow BDT. With the exception of a small volume underlying Attica there is no evidence in the southern profile.

Thirdly, in both settings just above the Wadati-Benioff plane, rock volumes characterized by brittle behaviour are obtained in the rheological modelling. They are likely the combined effect of the strong thermal cooling induced by the subducting slab, the confining pressure and lithology. Differences in the latter parameter among the two profiles (Fig. 5.13) explain the different location of these volumes.

Fourthly, in the western sector within the lower plate, while in the collisional setting (northern transect) a second 20-25 km-thick continuous brittle layer exists, separated from the shallow one by a few km-thick ductile layer, in the southern profiles only a unique thick brittle layer occurs.

As further discussed in the following section, it is worth mentioning that I did not modelled the lithological variations (due to the intense rock fracturing and mixing up), nor the pore fluid pressure increase and hence the local mechanical weakening, likely occurring within the shear zone associated to the basal detachment delimiting the accretionary wedge. This could potentially represent an additional rheological transition characterizing the western plate.

Also as concerns the longitudinal profiles G and H, a generally good consistency between the model outputs and the seismicity data could be observed (Fig. 5.20).

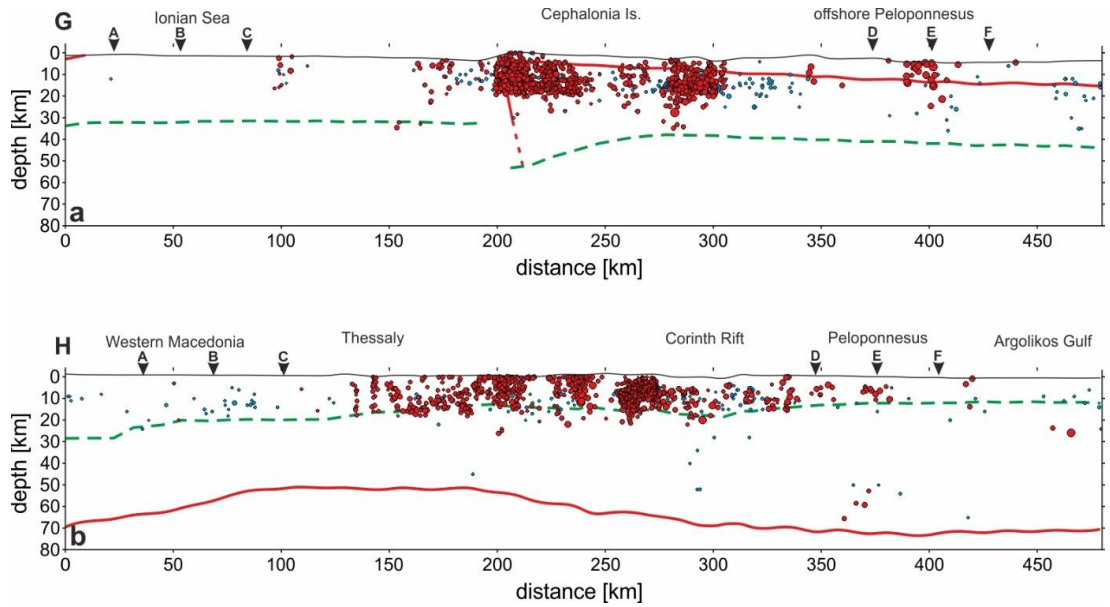

Fig. 5.20 – Comparison of the shallowest BDT (green dashed line) with the hypocentral distribution of well-located seismicity along transects G (a) and H (b), respectively.

In particular, the profile G all along seems to perfectly fit the projected seismicity from NKUA moment tensors catalogue and Kassaras *et al.* (2016) relocated seismicity. Only some minor discrepancies occur along the longitudinal transect H (Fig. 5.20b). The latter is in a geodynamically more internal position, closer to the volcanic arc and with higher heat flow, and it is therefore characterized by a thinner brittle layer with a SSE-wards shallowing BDT, which is nicely mimicked by the seismicity distributions of Kassaras *et al.* (2016), Ganas *et al.* (2012), Hatzfeld *et al.* (1995), Mesimeri and Karakostas. (2018) and NKUA moment tensors catalogue.

Actually, some discrepancies with the modelling results are represented by few events occurring down to ~30 km in the region around the Corinth Rift and in Peloponnesus (transect H), as reported in Kassaras *et al.* (2016). As above suggested, these events might be related to local increases in pore fluid pressure or very small-scale rheological heterogeneities, which may therefore not be represented in the model. Furthermore, it should be always kept in mind that the projected seismicity in the present work occurs within a buffer zone of 50 km from the analyzed transect, on each side, and therefore some misfits and differences could be possibly due to lateral out-of-plane variations.

5.3 - 3D model

The last step in the modelling workflow followed in this study has been the realization of a complete 3D model of the rheological stratification and properties of the Aegean Region lithosphere(s). In order to take into account for the intrinsic variability and uncertainties in the attribution of the values, more than one model has been reconstructed, with different values for the input parameters of the constitutive rheological equations. For each model both the map of the *rheological* BDT depth, the ones of the BDT strength and temperature and the map of the total integrated lithospheric strength have been produced (see also Chapter 7). Moreover, a map of the *seismotectonic* BDT depth, which takes into account the role of the plate interface along the subduction zone in delimiting the independent seismogenic volumes, has also been produced for the purposes of the seismotectonic applications, as it will be better described in Chapter 6.

Some minor discrepancies have been detected between the 1D rheological profiles obtained in the first stage of the modelling and the final 3D models, mainly because of the constant and progressive improvement and updating of the adopted modelling methods (*e.g.* Matlab scripts, reconstruction of the geometry of the structures, implementation of the subduction zone thermal model). Nonetheless, an overall very good agreement between the results of the 1D strength envelopes, 2D transects and 3D models has been observed, especially in delineating the main large-scale rheological features of the Aegean Region.

The Matlab script through which the models have been realized allows to obtain as an output a 3D figure, for each of the above-mentioned variables, which can be manually rotated and observed

according to the desired point of view (fig. 5.21). Moreover such figures can be stored and saved in the most suitable file format, for instance as a geotiff that can be uploaded and viewed in a GIS software, or as a SVG/PDF file that can be further modified in a dedicated vector graphics editor software. The Matlab code, furthermore, also produces matrix-ordered ASCII files of any desired variable, which can be easily georeferenced in a GIS software and then observed and analyzed as a 2D layer (*e.g.* the BDT depth areal layer).

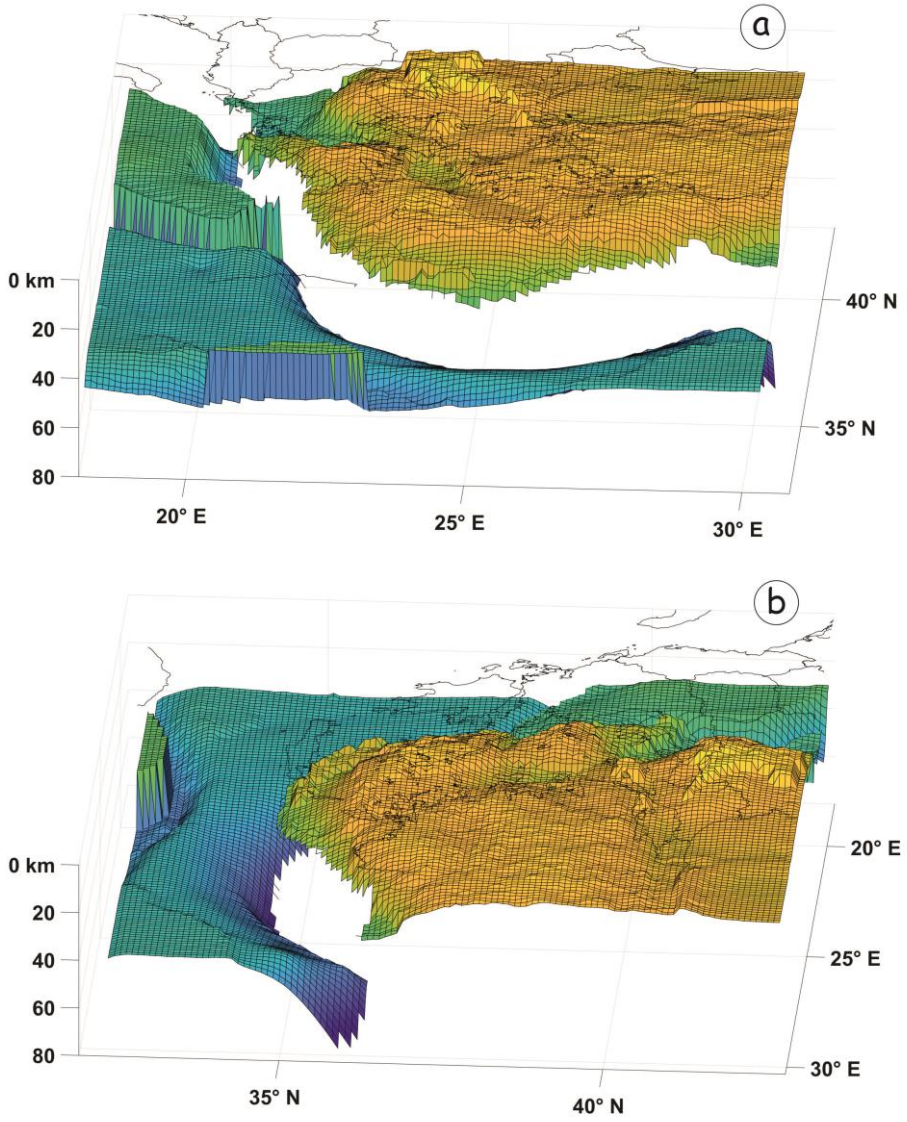

Fig. 5.21 – 3D model of the BDT depth for the study area. The deep BDTs occurring in the lower plate and the shallow ones in the upper (Aegean) plate have been graphically separated in order to help visualizing them. Note the progressive deepening of the depth in the lower plate moving towards the Hellenic subduction zone as the slab progressively deepens. The maximum values are in the order of 75 km while the minimum ones are around 6-7 km. a) view from SSE; b) view from ENE.

The starting reference model has been reconstructed by adopting a constant value of 0.4 for the pore fluid pressure ratio corresponding to a hydrostatic pore pressure (see also section §3.1.9 in Chapter 3). For the friction coefficient, the value of 0.6 has been selected, except for the surface

projections of the seismogenic sources, where a slightly lower value of 0.5 has been attributed (see also section §3.1.7 in Chapter 3).

A particular care has been devoted to the realization of the thermal model, through the selection of the most appropriate values of the surface heat flow and a thorough vertical reconstruction of the geothermal gradient. As for the surface heat flow values, the raster obtained by calculating a weighted average with a ratio of 3:1 with the source data of Fytikas and Kolios (1979) and Cloetingh *et al.* (2010) has been adopted.

This first model, in terms of *rheological* BDT depth (fig. 5.22), is characterized by deep values in the external portion south of the Hellenic trenches, generally comprised between 35 and 75 km.

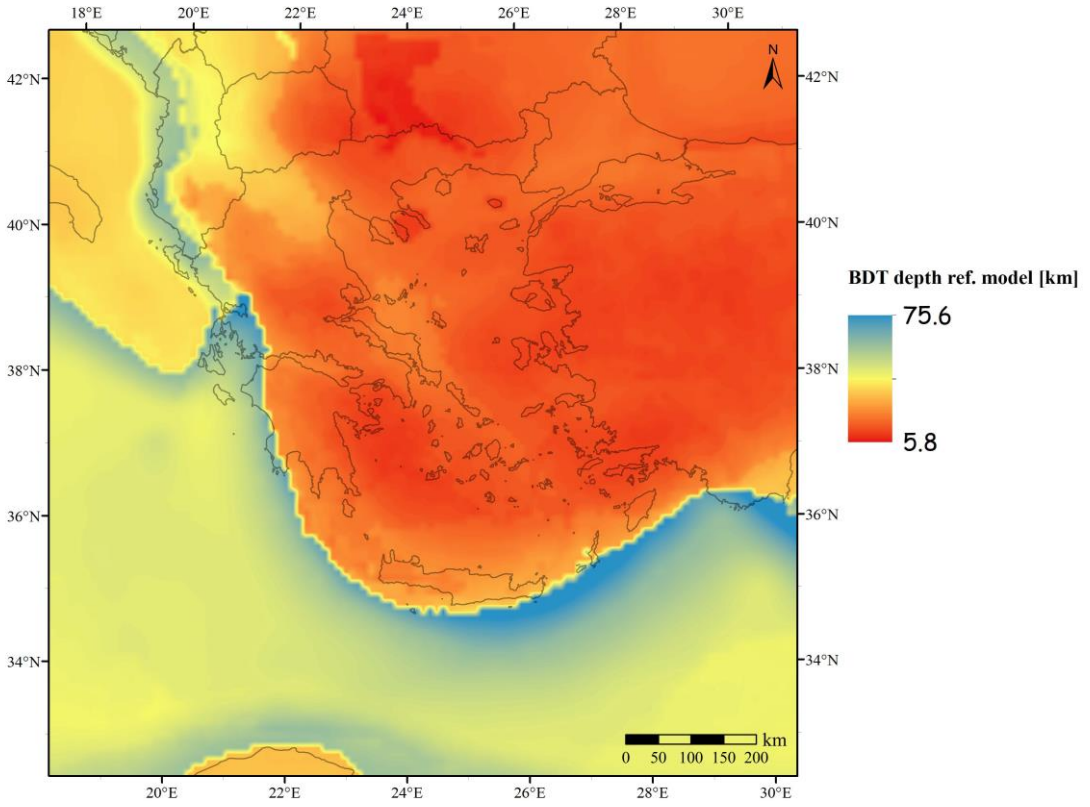

Fig. 5.22 – Map of the BDT depth for the reference model.

The deepest values are reached almost in correspondence of the trenches, because of the BDT deepening, which follows the geometry of the subducting slab. Accordingly, almost in the whole southern sector of the study area the BDT lies within the mantle layer of the downgoing oceanic plate. This is attributable to a combination of factors, *i.e.*: i) the low geothermal gradients characterizing the Mediterranean ridge accretionary wedge and the Ionian/Nubian oceanic lithosphere in general; ii) the prevalently compressional tectonic regime and iii) the mafic composition of the oceanic lithosphere lithologies, which makes them much more resistant than the corresponding continental ones.

Where the lower plate is characterized by continental crust, *i.e.* in the Apulian platform and in the Cyrenaica peninsula, the BDT depths are respectively around ca. 32 and 26 km, thus occurring

at relatively shallower depths than what observed for the oceanic portions. The contact between the two different lithospheric suites in the lower plate is quite evident from the analysis of the BDT depths at the borders of the Apulian platform and in particular along the Kefallinia Transform Fault, which effectively acts as a lateral ramp of the Hellenic subduction zone, connecting the northern continental collision zone with the southern oceanic subduction setting. Indeed, here the BDT, moving southwards across the KTF, shifts its position quite abruptly from the lower continental crust in the Apulian region at depths around 30 km to the upper oceanic mantle, where it lies at ca. 50 km of depth, as above mentioned.

In continental Greece the BDT is always shallower than 30 km, except for the western coastal region close to the islands of Corfu and Lefkada, where the deeper transitions are mostly due to the compressional tectonic setting and, above all, to the low geothermal gradient. Moving towards the central and eastern sectors of continental Greece, the BDT is generally between 10 and 20 km, with the only exception being represented by the area between northwestern Greece, North Macedonia and Albania, where once again the local deepening is associated to the low surface heat flow values and geothermal gradients. The shallowest values of the BDT in continental Greece are attained in Attica (~11 km), Thessaly (11-12 km), Chalkidiki (9-11 km) and Thrace (10-11 km).

The general shallowing of the BDT in continental Greece area is mainly related to the less resistant sialic composition of the crust with respect to the oceanic one and above all, to the increase of the geothermal gradient, which in turn is the result of the remarkable stretching that has affected the Aegean Region since Miocene times. Indeed, the crustal stretching likely related to the slab roll-back has led to a considerable thinning of the Aegean crust causing a marked rising of the isotherms, that is particularly evident and remarkable in the Aegean Sea region where even metamorphic core complexes have developed. In the central and southern Aegean Sea the BDT is quite shallow, generally between 9 and 11 km, also because of the high surface heat flow values (around 110-120 $mW \cdot m^2$), in the proximities of the Hellenic volcanic arc and around the Cycladic core complex.

Towards the Cretan Sea and the island of Crete the values of the BDT are in the range 17-25 km, and the general deepening is a direct consequence of lower heat flow values (in the order of 50-60 $mW \cdot m^2$ around Crete). A relative increase in the BDT depths with respect to the central Aegean is also observed in the northern Aegean Sea, with average values around 14 km.

However, towards both terminations of the North Aegean Trough, i.e. to the southwest (north of Evia and Skyros islands) and to the northeast of it (Gulf of Saros), a further deepening to values of ca 17-19 km occurs. In this case, the main cause of such downwards shifts of the rheological transition may be attributed to very high strain rates that characterize all the area around the North Aegean Trough and the North Anatolian Fault.

Indeed, as I already mentioned in Chapter 2 and 3, an increase in the strain rate value tends to deepen the BDT, because of the positive dependence of the ductile strength on the deformation rates, which substantially promotes brittle processes over ductile ones. Finally, the western

Anatolian Region, also included in this research, is associated with high surface heat flow values and geothermal gradients, as well as with a thinned and stretched crust. Accordingly, it is basically characterized by a shallow BDT (10-13 km).

The map of the BDT strength (fig. 5.23), expressed in terms of the differential stress at which the transition from brittle to ductile deformation occurs, emphasizes the good correlation with the BDT depth. In general, the deeper is the BDT and the greater is the value of the corresponding strength, even though additional roles are played by the tectonic regime, the pore fluid pressure and the nature of the considered crust (oceanic or continental). Indeed, a very good correspondence between high strength values and BDT depth occurring in the oceanic lithosphere, within a compressional tectonic setting, is observed in the study area.

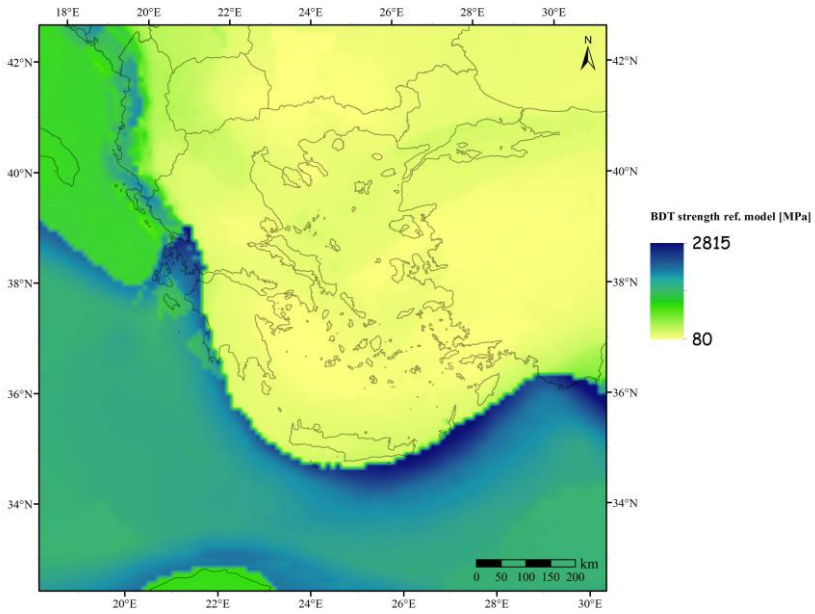

Fig. 5.23 – Map of the BDT strength for the reference model.

The strengths at the deep BDT in the oceanic crust are in the range 1300-2500 MPa, while for the continental crust portion of the lower plate (Apulian platform) the values are much smaller, generally around or lesser than 1000 MPa, despite the tectonic regime being similarly compressional. This sharp change in the mechanical properties of the lithosphere, as a function of its continental or oceanic nature, evidences how such a feature represents the effective differential factor for the strength values, whenever the tectonic regime is constant (in this case, compressional) throughout the considered area.

The tectonic regime, instead, represents the most influential factor for the BDT strength when the nature of the investigated crust is common through the selected area. Such an observation is corroborated by the strength values distribution in the extensional regions of the Aegean Sea and continental Greece, where the BDT strength is even one order of magnitude smaller (generally between 90 and 300 MPa) than what observed in the compressional region affecting the continental crust of the Apulian Platform.

More specifically, the lowest BDT strength occurs in the Central Aegean Sea, Attica and in general around the Cycladic core complex, where the formation of the metamorphic core complex has led to the exhumation of the lower crust and above all to a general rising of the isotherms, which is responsible for the very high geothermal gradients and consequently for the reduced strength. The distribution of the BDT strength all over the Aegean Region and the corresponding strength envelopes for the different tectonic settings throughout the study area are consistent with the results of other thermo-rheological numerical modellings for subduction and continental collision (*e.g.* Burov *et al.*, 2014; Francois *et al.*, 2014). In particular, a good correspondence is observed for the expected typologies of strength envelopes, which are the *caramel slab* for the oceanic lithosphere unsubducted sectors, the *jelly sandwich* for continental lithosphere regions associated to a moderate surface heat flow and the *crème bruleé* for the extending continental regions characterized by a very high geothermal gradient ("very hot lithosphere" in Burov *et al.*, 2014), as confirmed by the model proposed in this research.

A further parameter that has been analyzed and for which an output map has been produced is the temperature at the BDT depth. Such a parameter provides insights into the litho-mineralogical composition of the layers within which the BDT lies. The map of the temperature at the BDT (fig. 5.24) suggests a close correlation with the depth of the transition.

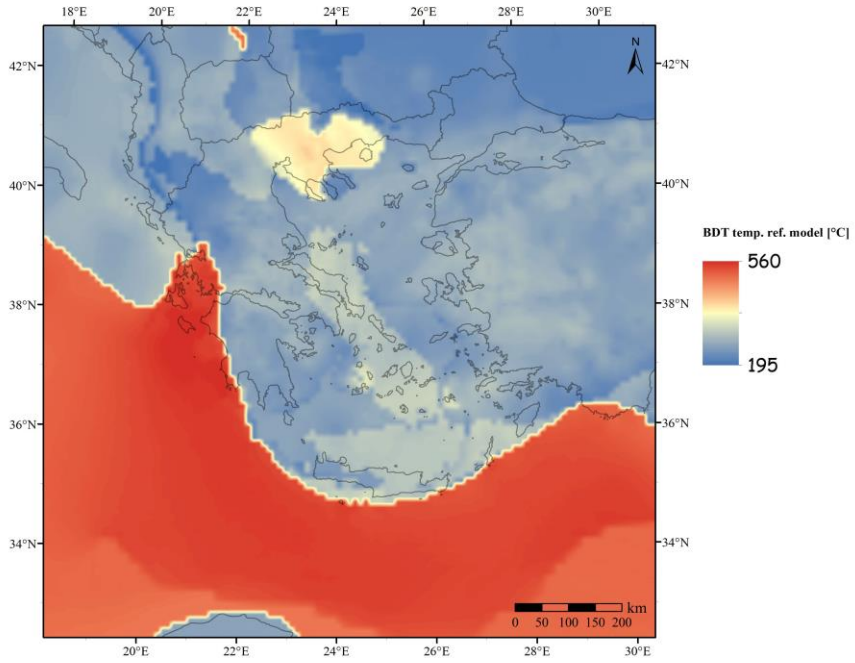

Fig. 5.24 – Map of the BDT temperature for the reference model.

However, additional factors such as the nature of the investigated lithosphere (oceanic, continental, extended), the lithological composition of the layer where the BDT occurs and, to a minor extent, the local geothermal gradient, appear to be strictly related to the distribution of the BDT temperatures. Indeed values between ca. 500 and ca. 540 °C characterize the BDT temperatures in the oceanic lithosphere (mantle) of the downgoing plate.

The continental sectors of the lower plate, even though associated to similar heat flow values, show much lower BDT temperatures, in the range 280-300 °C. These distinguished features and ambient conditions for the BDT in the two domains, - oceanic and continental – are thus attributable, at first, to the different depths of the BDT, being respectively around 40-45 km and ~30-33 km. However, it should be reminded that the varying BDT depths are due, primarily, to the different mechanical-lithological stratifications in the two lithospheric end-members. Furthermore, the more sialic lithologies of the continental crust are generally associated with lower temperatures for the onset of ductility (~200-300 °C, see *e.g.* Kohlstedt *et al.*, 1995; Scholz, 1989) with respect to the mafic oceanic ones.

In the back-arc Aegean Region, corresponding to the Aegean Sea and the majority of continental Greece, the BDT temperatures are basically between 220 and 300 °C. The variations within the above-mentioned range mainly result from the interplay and the opposite effects of the BDT depth and the surface heat flow, while the lithological characteristics are substantially common for the whole area, with some exceptions that will be discussed later.

In general, the deeper is the BDT and the greater would be the corresponding temperature; at the same time, the higher is the surface heat flow and the greater will be the geothermal gradient and the temperatures at depth. However, the two factors tend to counter-balance each other because of the shallowing effect that an elevated surface heat flow exerts on the BDT position. Accordingly, in the Aegean back-arc extensional domain, the very high surface heat flow (80 and 120 $mW \cdot m^2$) is compensated by the shallow occurrence of the BDTs, always lying in the range 10-15 km. In this way, the resulting BDT temperatures fall in the above-mentioned range of 200-300 °C, in agreement with literature data (*e.g.* Scholz, 1989; Kohlstedt *et al.*, 1995) on the onset of plasticity for typical quartz- and feldspars-rich lithologies of the continental crust.

The exception in this framework is represented by the granodioritic composition of the crust in Eastern Macedonia and in Chalkidiki (see figure 5.24). Such areas, even though characterized by remarkably high heat flow values (>90 $mW \cdot m^2$, fig. 3.2), are associated with BDTs always deeper than 12 km (fig. 5.22). This apparent inconsistency is actually explained by the mechanical-rheological characteristics of the granodiorite lithology (see also Chapter 3), which exhibits a greater strength with respect to the quartzitic ones, thus requiring higher temperatures, and hence greater depths, for the onset of the plastic/ductile deformation.

Some additional 3D models have been produced, where the values of selected input parameters have been varied on the basis of specific geological and geodynamic considerations, taking into account their potential and reasonable uncertainties and variations. In the next paragraphs I will therefore present two of these models, where the pore fluid pressure ratio and surface heat flow values have been respectively changed with respect to the reference ones. In order to assess the improvements and drawbacks of each model, I will focus on their comparison with the reference one, and especially on the BDT depth and strength variations.

In the 3D "*model 2*" all the input parameters values have been kept unaltered with respect to the reference one, with the exception of the pore fluid pressure ratio (λ_e). The latter, instead of being assigned a constant value equal to hydrostatic pressure as in the reference model, here is characterized by varying values, which define an overpressured region in correspondence of the Hellenic subduction zone and in particular along the accretionary wedge of the Mediterranean Ridge. The map of the λ_e values for the whole study area is shown in figure 3.14 as an areal layer georeferenced in a GIS environment.

As can be observed from figure 3.14, λ_e maintains values (~0.4) indicating almost hydrostatic pressures in the external zones with respect to the active front of deformation, both in the continental collisional setting and in the oceanic subduction one. In the accretionary wedge just internal with respect to the Hellenic subduction zone front, the maximum values of λ_e close to 0.8 are attained. These values are associated with highly overpressured shallow sedimentary layers, as the downgoing oceanic slab, which is particularly rich in fluids and water, is subject to increasing pressure due to load exerted by the overriding and advancing accretionary wedge. Since fluids do not easily find escape pathways across some of the low-permeability layers of the accretionary wedge, a remarkable pore pressure build-up is assumed in this region (see also the review by Saffer and Tobin, 2011, for the pore pressure increase and general features of the subduction zones).

The pore fluid pressure ratio is then slightly reduced in more internal areas, such as the back-arc region. However, especially around the volcanic arc, a slight overpressure might still be present in the overriding plate crust, because of the dewatering processes occurring within the downgoing slab, associated to mechanical reasons and, above all, mineralogical reactions. Indeed, mildly overpressured volcanic arcs and more internal regions have been also proposed for several subduction zones in the world (*e.g.* Papazachos *et al.*, 2005; Xia *et al.*, 2008; Peacock *et al.*, 2011) and the fluid pressure increase might represent a distinctive trait of the mantle wedge and the overriding plate crust above the subducting slab.

In this geodynamic setting, the fluid overpressure might be explained by dehydration phenomena and fluids expulsion occurring at different depths for several minerals within the crust of the sinking slab (see *e.g.* Schmidt and Poli, 1998). Accordingly, values of λ_e around 0.5, indicating slightly suprahydrostatic conditions, characterize the Hellenic volcanic arc, while almost the totality of the remaining sectors of the study area are associated with close-to hydrostatic pressure λ_e values.

The increase in λ_e values in the accretionary wedge around the Mediterranean Ridge causes a maximum BDT deepening in the order of 3-4 km with respect to the corresponding BDT depths of the reference model. Some isolated pixels located close to the belt where the BDT shift from the lower plate to the upper one (fig. 5.25, shown in black), actually present considerable variations in the order of tens of km. However, such variations are only a local effect due to the corresponding

BDT occurrence, jumping from one plate in the first model to the other plate in the alternative model. In other words, these variations are only induced by border effects related to the geometry of the model itself. Indeed, such pixels correspond to the zone left in blank between the two plates and their relative BDT surfaces in figure 5.21.

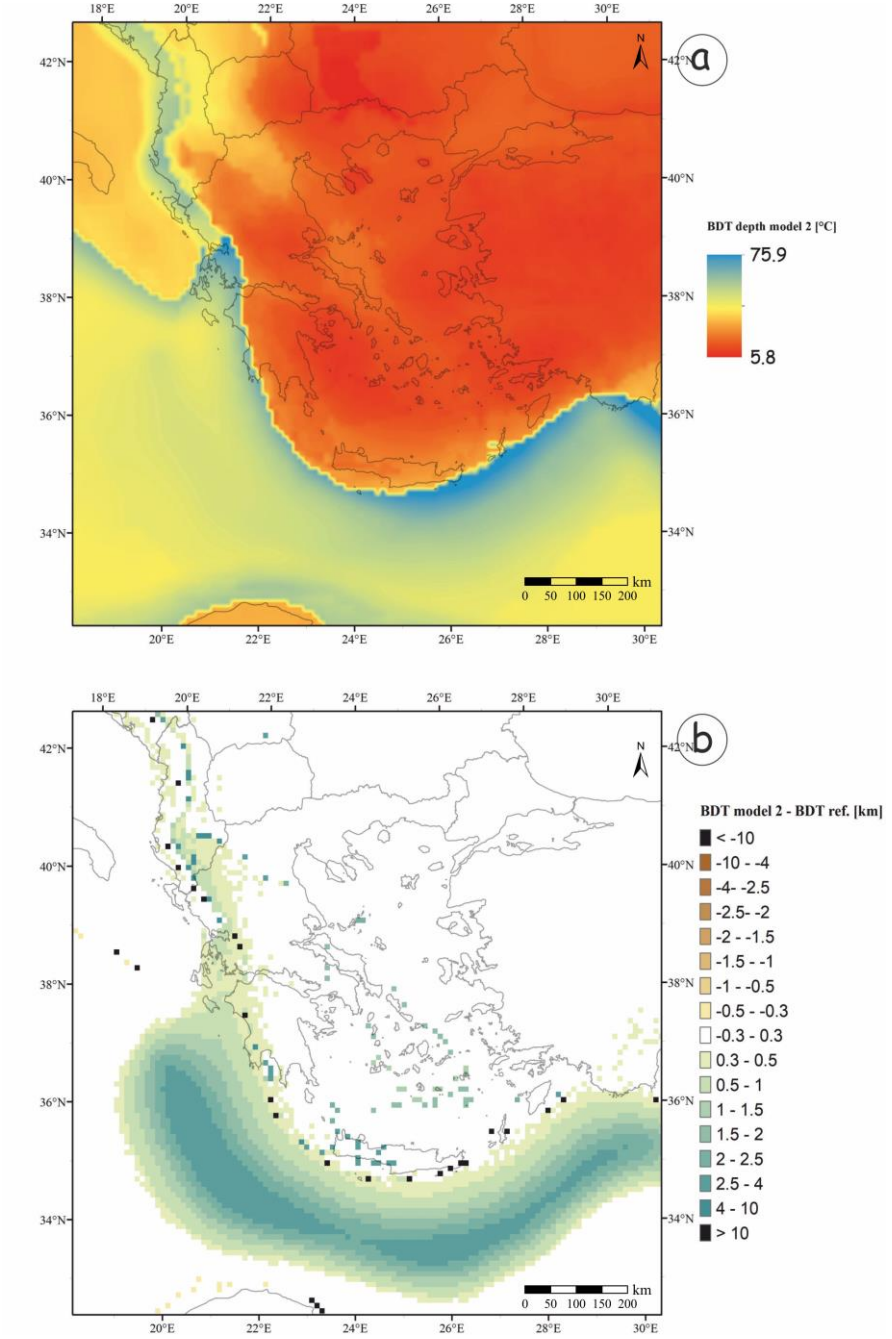

Fig. 5.25 – a) map of the BDT depth for model 2; b) difference between the BDT depth in model 2 and the reference model. The pixels in white indicate negligible differences between the two models, while the pixels in black are those related to the "jump" of the BDT from one plate to the other and are therefore not considered in this analysis (see text for further explanations).

Given these premises, such variations have not been taken into account as representative of the real variability associated to the different models and, accordingly, will not be described and dealt with. The same reasoning is also valid for the difference between strength and temperature values

and the respective ones in the various models, since the pixels showing such variations are always associated to jumps of the BDT from one plate to the other, exclusively along the subduction zone.

As concerns the Hellenic volcanic arc region, the BDT locally deepens only of ~0.5-1 km, since the increases in λ_e values, with respect to the reference model ones, are much more limited when compared to the increases in the accretionary wedge region. In western continental Greece, BDT deepenings of ca. 0.5-1 km are also observed, while the remaining sectors of the study area do not display any significant variation in terms of the BDT depth.

A further relevant effect of λ_e values increase in the Hellenic subduction zone is the remarkable decrease of the corresponding BDT strengths (fig. 5.26), where negative variations up to ca. 1 GPa, with respect to the reference model values, have been calculated, while the BDT strengths decrease in the back-arc region is limited to values around 10 MPa.

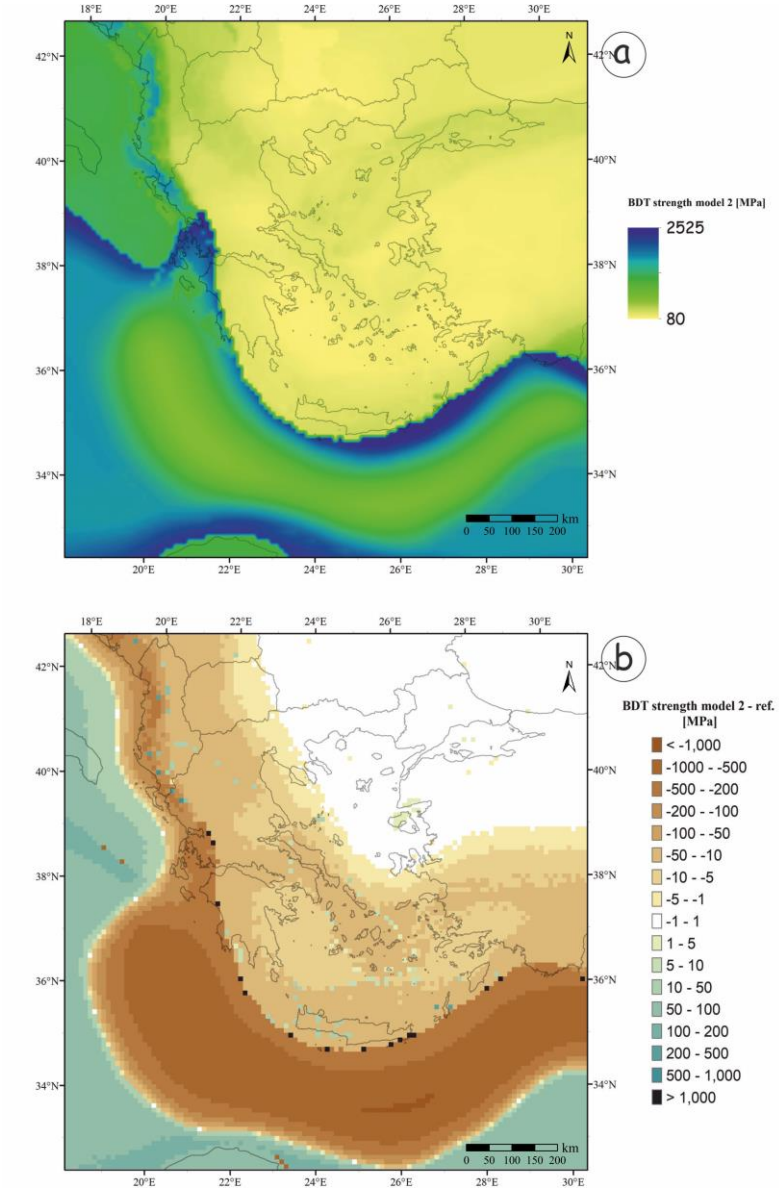

Fig. 5.26 – a) map of the BDT strength for model 2; b) difference between the BDT strength in model 2 and the reference model.

Finally, moderate increases of the BDT strength in the external and unsubducted sectors of the lower plate are recorded (respectively around 30 and 80 MPa for the continental and oceanic domains), following the slight decrease of λ_e values from 0.4 in the reference model to 0.36 in model 2.

For what concerns the BDT temperature (fig. 5.27), the changes in the λ_e values do not affect the geothermal gradient and therefore the associated BDT temperatures variations are only related to the upward or downward movement of the BDT position, thus not being particularly significant or indicative of ambient and physical conditions variations.

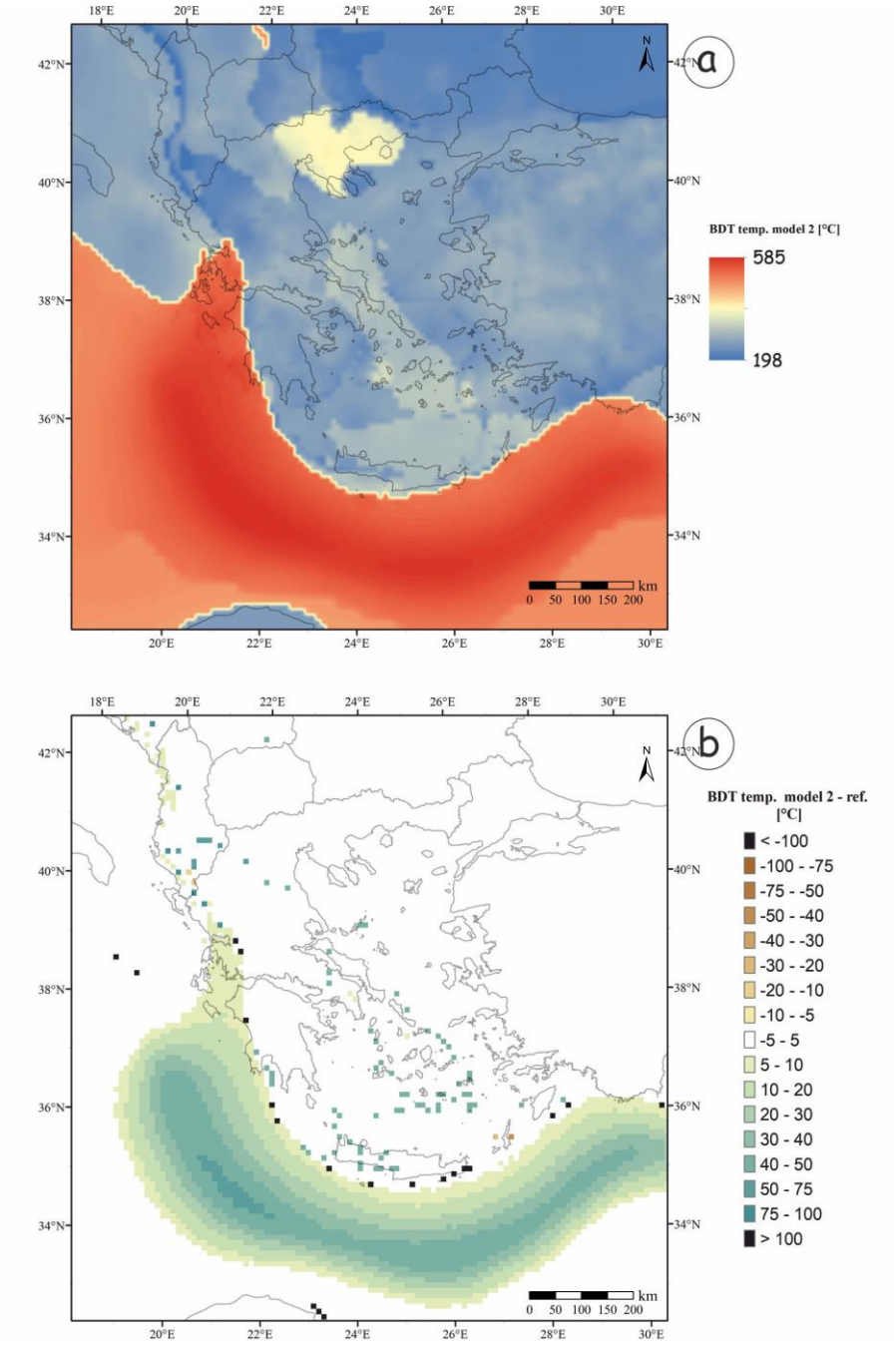

Fig. 5.27 – a) map of the BDT temperature for model 2; b) difference between the BDT temperature in model 2 and the reference model. The pixels in white indicate no differences between the two models.

Since the surface heat flow is the thermal parameter that mostly affects the geothermal gradient and consequently the resulting rheological modelling (see Chapter 4), an additional 3D model, termed as "*model 3*", has been realized on the basis of an alternative surface heat flow distribution, with respect to the reference one (fig. 5.28).

In particular, a different weighting of the local- and continental-scale data has been applied in the realization of the surface heat flow map, assigning a relatively higher weight (33% with respect to 25% in the reference model) to the large-scale data, in order to obtain a slightly more smoothed 3D model, in terms of lateral variations of BDT depth, strength and temperature distributions. Clearly, such a choice has its main drawbacks in the potential loss of some local features and in the general decrease of the areal resolution for identifying small-scale variations.

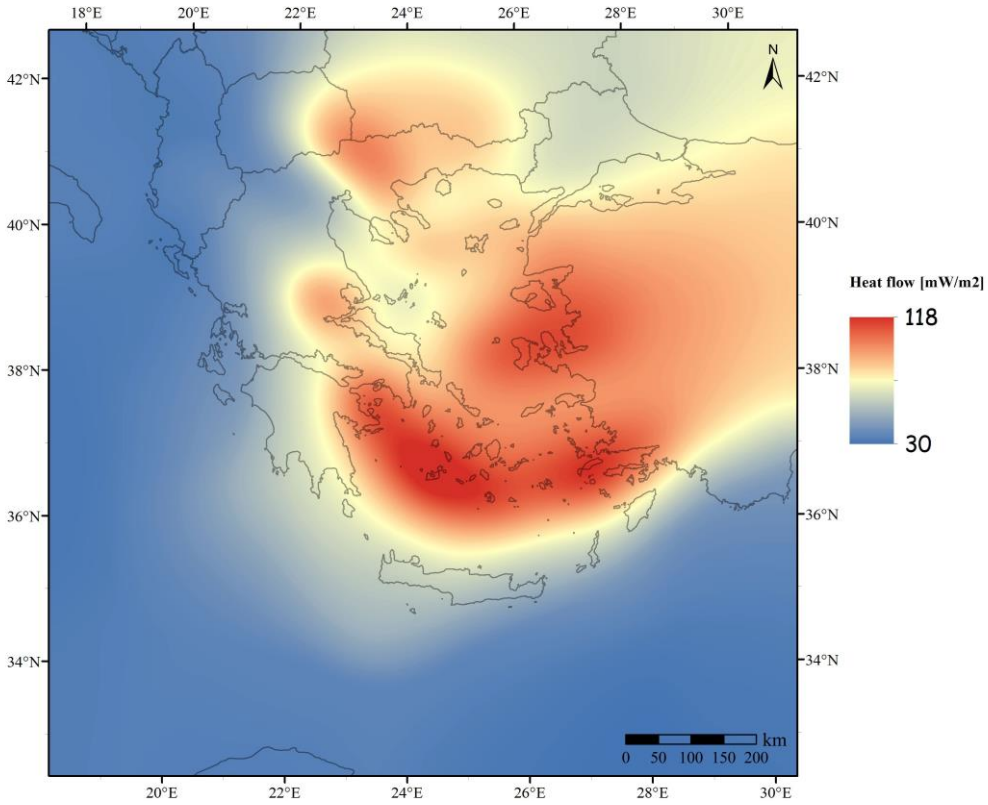

Fig. 5.28 - Map of the heat flow values adopted in model 3.

The surface heat flow map in *model 3* is generally characterized by moderately higher values than in the reference model. Accordingly, the resulting BDTs (fig. 5.29) tend to occur at slightly shallower depths with respect to the reference model, almost across the entire study area, with the only exception being represented by southeastern Albania and northeastern Macedonia (Greece) regions, where the new BDT depths are equivalent or some hundreds of metres deeper than the original ones.

The greatest BDT shallowings are instead observed in North Macedonia and at the border region between Thessaly and Central Macedonia (~4 km), while other relevant differences

characterize the northern Cylades islands, with values around 2.5 km, the Sporades islands (~3 km) and the Cretan Sea, offshore northwestern Crete (~3 km).

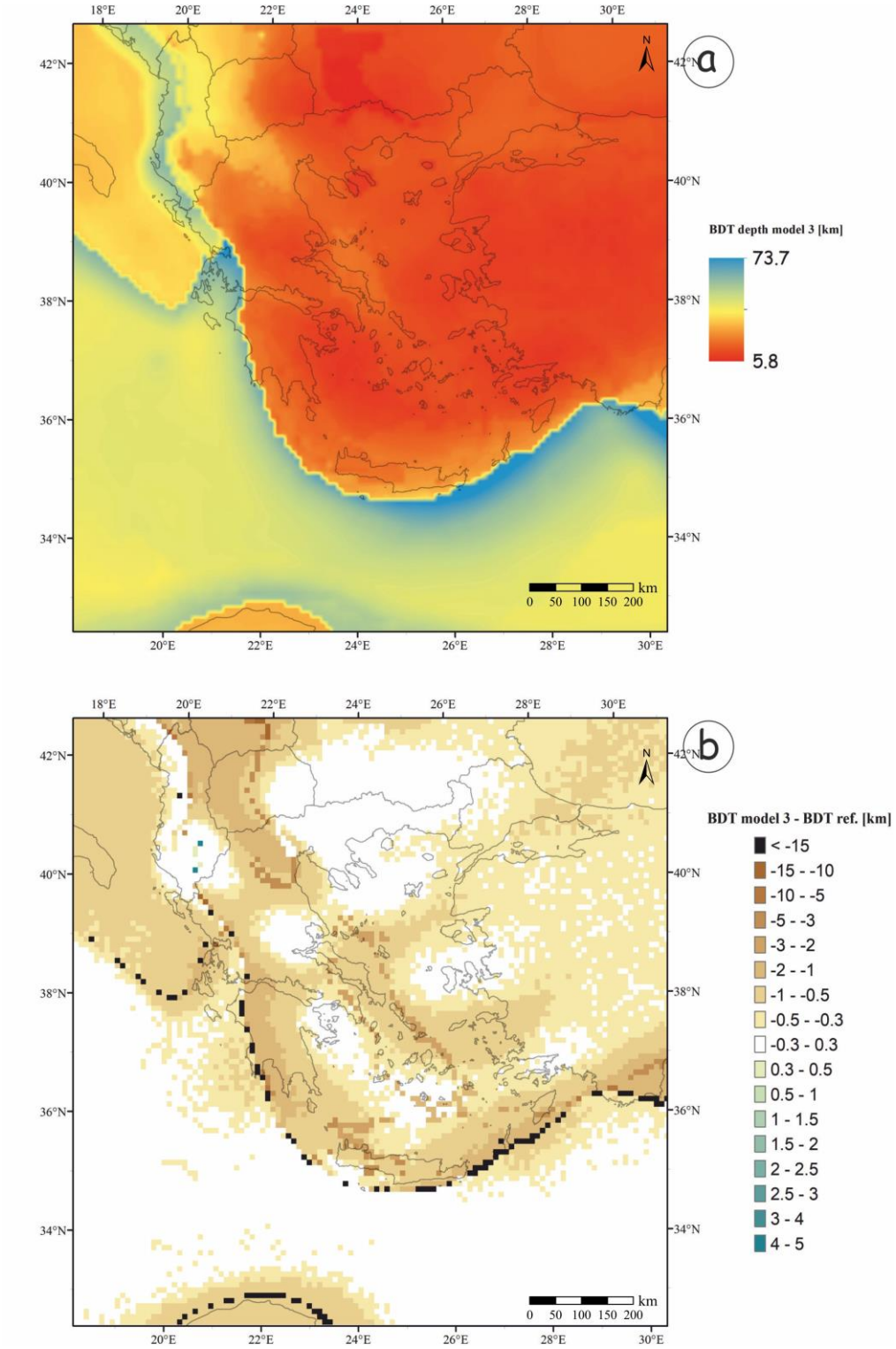

Fig. 5.29 – a) map of the BDT depth for model 3; b) difference between the BDT depth in model 3 and the reference model.

All these moderate variations are likely attributable to the shift of the BDT from one layer to another (for example from the upper crust in the former reference model to the lower crust in *model*

3, though always occurring within the same plate). Thus, they can be considered as the results of the variability and intrinsic uncertainties related to the input parameters values and to the reconstruction of the model itself.

Because of the increase in the geothermal gradient, the same areas described above (Northern and Central Aegean and Cretan Sea, northern continental Greece) are also associated with generally lower BDT strengths than in the reference model, with reductions in the range 20-50 MPa (fig. 5.30).

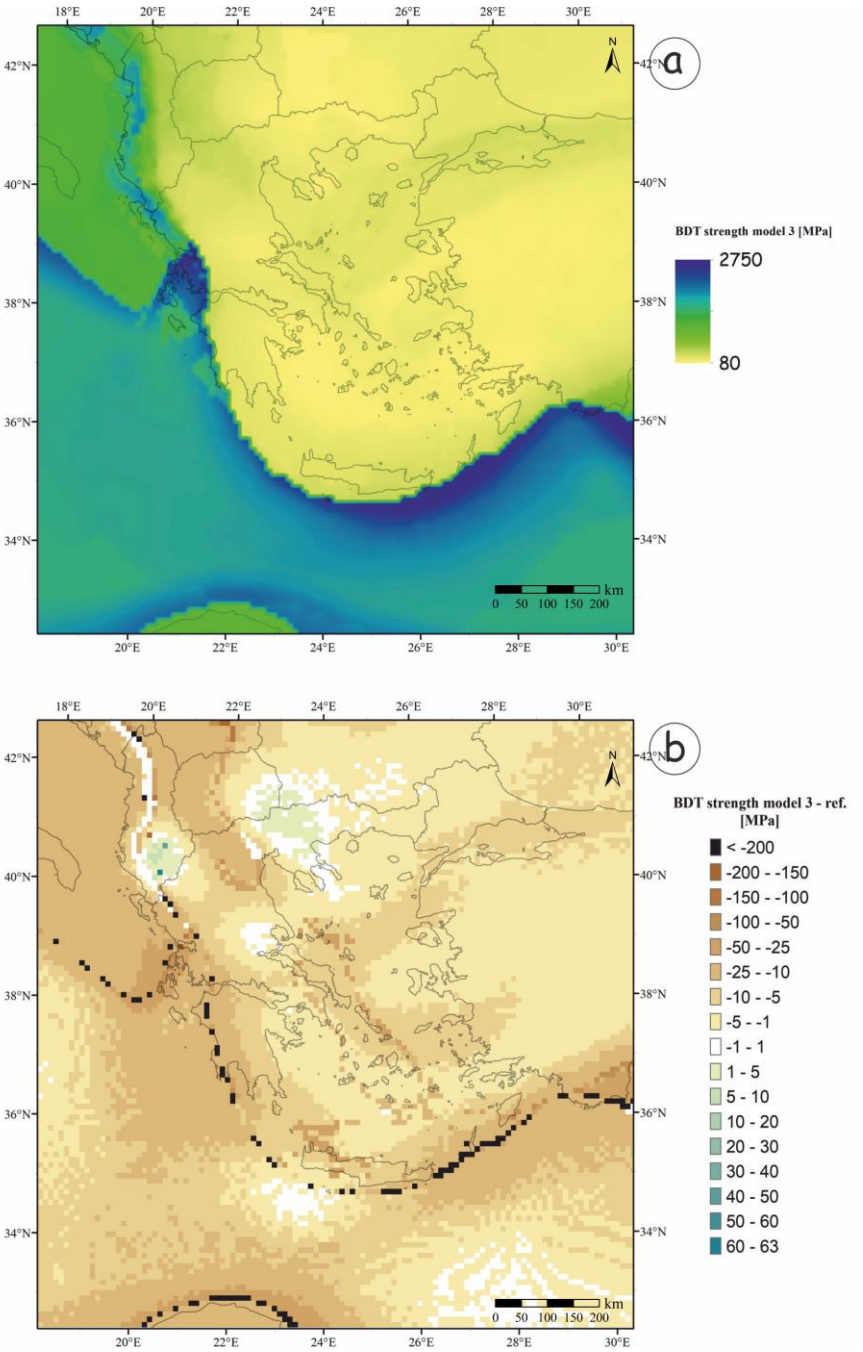

Fig. 5.30 – a) map of the BDT strength for model 3; b) difference between the BDT strength in model 3 and the reference model.

All the remaining sectors of the study area, with the exception of the "border" pixels along the subduction zone, show only minor variations of ±5-10 MPa, relative to the reference model.

The BDT temperature variations in *model 3* (fig. 5.31) represent the results of the combination of two main contrasting effects, *i.e.* the general shallowing of the BDTs and the increase in geothermal gradient, which translates into higher temperatures at depth.

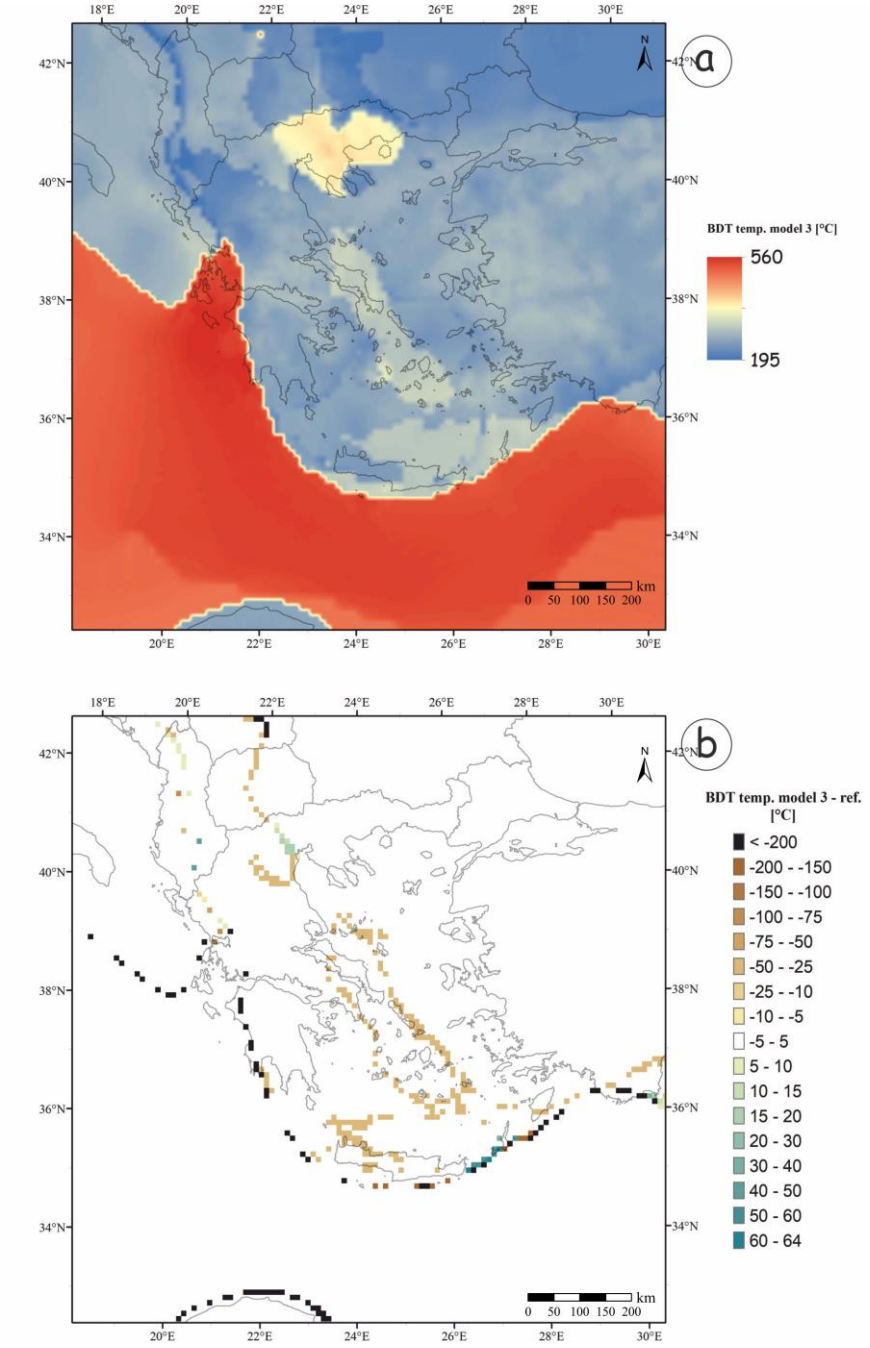

Fig. 5.31 – a) map of the BDT temperature for model 3; b) difference between the BDT temperature in model 3 and the reference model.

Once again, significant variations (greater than ±5 °C) are only observed in the above-mentioned regions, where also the BDT shallowing and the strength decrease are observed. From the analysis of the BDT temperature variations map, it can be observed and inferred that the BDT

shallowing is a more efficient factor than the geothermal gradient increase in determining the variations of the BDT temperatures.

Indeed a general decrease of such temperatures is observed, with maximum differences being around 45-50 °C close to the Sporades, in Central Aegean and western Cretan Seas, and also in the continental areas of North Macedonia and Central Macedonia.

To sum up, the two additional models with respect to the reference one, as it has just been described, present locally significant variations in BDT depth, strength and temperature, even though in a general similar framework where the large-scale features and trends always remain clearly recognizable. This stability of the results confirms the robustness of the rheological modelling and its ability to describe the main rheological features of the study area.

Chapter 6: Applications

Brief summary

In this chapter the results of the rheological modelling are applied to other fields of the geosciences, such as seismotectonics and geodynamics of the Aegean Region. I will first present the contributions and constraints that rheology can bring in for the refinement of the geometry and seismic potential of the seismogenic sources, with the final aim of improving the seismic hazard assessment.

In this sense, the results of the modelling, especially in terms of the BDT depth, will be applied for deriving inferences on seismotectonic issues, such as the definition of the seismogenic layer thickness, the width of the major seismogenic sources and the estimation of the relative maximum expected magnitude, always taking into account the intrinsic uncertainties related to the input rheological parameters necessary for the modelling. Accordingly, the results of such applications and in particular the estimates of the maximum expected magnitudes will be given within a certain range of variability, depending on the initial constraint of the BDT and also on the empirical relationships used for obtaining such estimates (a more detailed discussion on this issue is given in the next section).

Subsequently, I will focus on the determination of the seismic strain rates, for which the BDT depth can help defining the seismogenic volumes, where the deformation rates related to the seismic processes should be effectively and more precisely calculated. The calculation of the seismic strain rates has been realized for some selected seismogenic areas, following already available seismic zonations of the Aegean Region. The seismic strain rates obtained here are then compared with the ones proposed in previous literature works, where the seismogenic thickness is usually considered as a constant.

Accordingly, I will focus on assessing whether and how much a variable thickness of the seismically deforming volumes can affect the strain rates estimates. After this stage, the seismic strain rates will be also compared with the geodetically-derived ones, in order to determine how much of the currently measured deformation in the Aegean Region is taken up seismically, rather than through aseismic processes (e.g. creep, slow earthquakes, etc).

Finally, some conclusive considerations on the total integrated strength, as obtained from the 3D model, will be made, in order to evaluate the long-term and large-scale features and behaviours of the lithosphere(s) in the study area, in response to the applied tectonic stresses.

6.1 Seismotectonic applications

6.1.1 Maximum depth of GreDaSS seismogenic sources

In order to link the rheological information about the BDT depth to each seismogenic source in the GreDaSS database, I determined for each source the coordinates of the midpoint along the bottom line of the source itself. Indeed, the BDT depth is related to the bottom of the potential seismogenic layer, where faults terminate at depth. Successively, the values of the BDT depth for each source were extracted from the rheological model (layer of the BDT depth), obtained with the RheolMod3D code. The value of the BDT depth has been calculated through a bilinear interpolation around the pixel where the coordinates fall, in order to take into account the potential variability of the BDT depth, also considering the lateral extent of the source itself.

An alternative procedure for determining the corresponding BDT modelled depth, for each seismogenic source, consists in taking into account the whole area of the surface projection of each source and averaging the BDT depth values among the pixels falling within such considered area. However, this method, even though apparently taking into account the whole potential range of values assumed by the BDT for each source, may ultimately result into misleading BDT depths.

Indeed, the actual depth extent of each fault-source, rather than being represented by an areally averaged value, is determined by the BDT depth in correspondence of the presumed fault downward termination, which depends on the source geometry and in particular on its dip direction and angle. Accordingly, the first method described here, for the association of each source with its corresponding BDT depth, has been adopted in this study for the successive seismotectonic calculations and inferences.

For the purposes of seismotectonic applications, in addition to the *rheological* BDT depth map (shown in section §5.3), also a *seismotectonic* BDT has been determined and the relative depth distribution is shown in figures 6.1 and 6.2 (respectively, the 3D and the map view).

The term *seismotectonic* refers to the fact that such a map has been produced specifically for being applied to seismotectonics and in the studies on the seismogenic process depth extent and confinement. Accordingly, starting from the modelled *rheological* BDT, some modifications have been implemented in order to consider, in particular, the compartmentalization of the seismogenic volumes, related to the occurrence of the plate interface (Wadati-Benioff plane) in the subduction zone.

Indeed, the plate interface can effectively be considered as a discontinuity surface, along which the major fault zones of the upper plate are expected to terminate. In other words, in terms of seismogenic potential related to the geometrical dimensions of the sources, the plate interface acts as a boundary delimiting and restricting the seismogenic volumes solely to the upper plate. Accordingly, in the case of occurrence of the shallowest rheological BDT in the lower plate, if the

upper plate has a sufficient thickness (that is here fixed to at least 10 km) to represent an effective seismogenic volume, the seismotectonic BDT is set to correspond to the depth of the Wadati-Benioff plane. The minimum thickness of the upper plate above the Wadati-Benioff plane, for being considered as an effective seismogenic layer, is set to 10 km, because the first kilometres (generally around 5) of the accretionary wedge are characterized by an aseismic behaviour (*e.g.* Marone and Scholz, 1988; Byrne *et al.*, 1988; Olskevich *et al.*, 1999). Accordingly, the shallowest sedimentary layers, down to depths of ca. 4-5 km, are not able to host the nucleation and possibly also the propagation of the seismogenic process and therefore, only if a greater thickness (here ≥ 10 km) is selected, can significant events occur in the upper plate above the subduction zone.

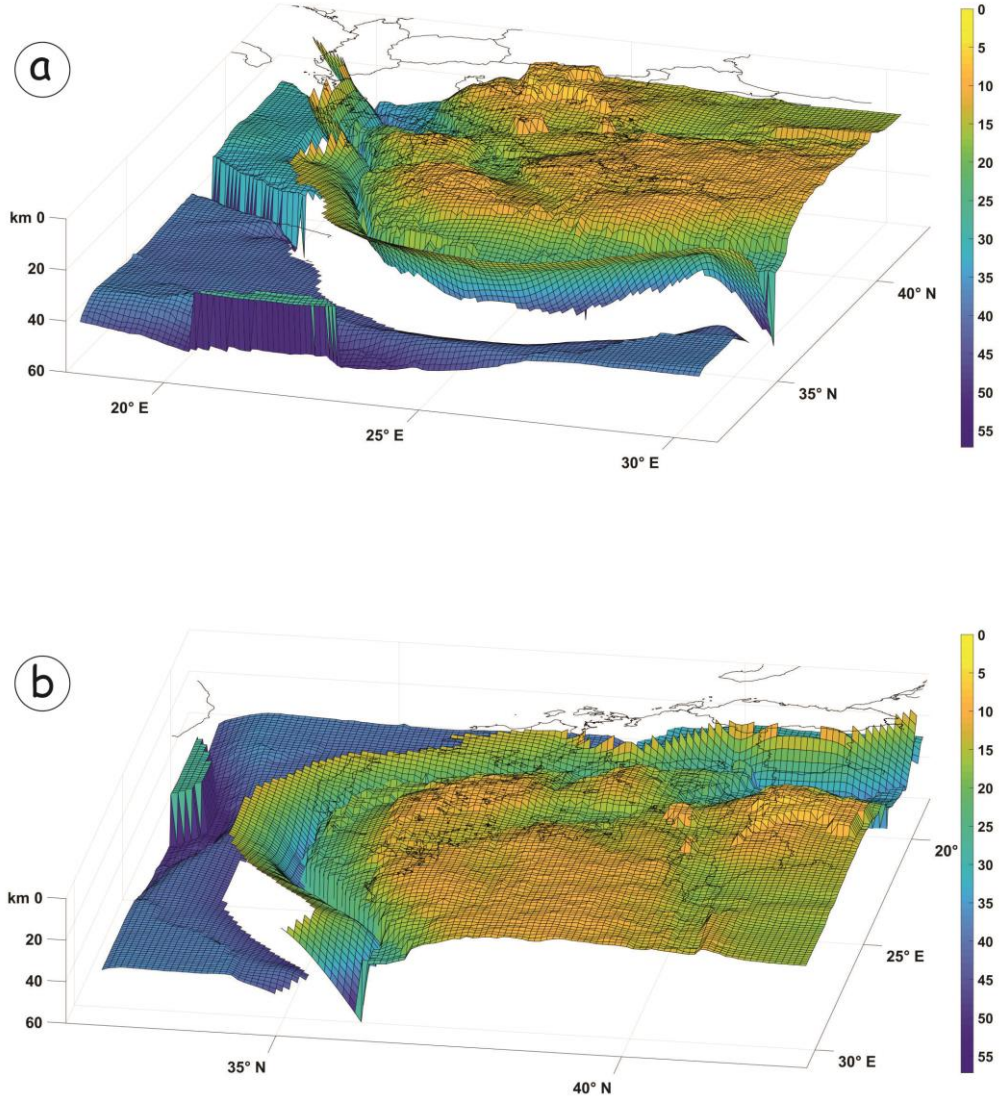

Fig. 6.1 – 3D model of the "seismotectonic" BDT depth for the study area. The deep BDTs occurring in the lower plate and the shallow ones in the upper (Aegean) plate have been graphically separated in order to help visualize them. The maximum values are in the order of 60 km while the minimum ones are around 6-7 km. a) view from SSE;b) view from ENE.

The map obtained with the conditions described above shows some differences with respect to the *rheological* BDT depth map. Especially along the external sectors of the subduction zone, a sensible shallowing of the BDT is thus observed, while in all the others sectors the *rheological* and the *seismotectonic* BDTs remain coincident.

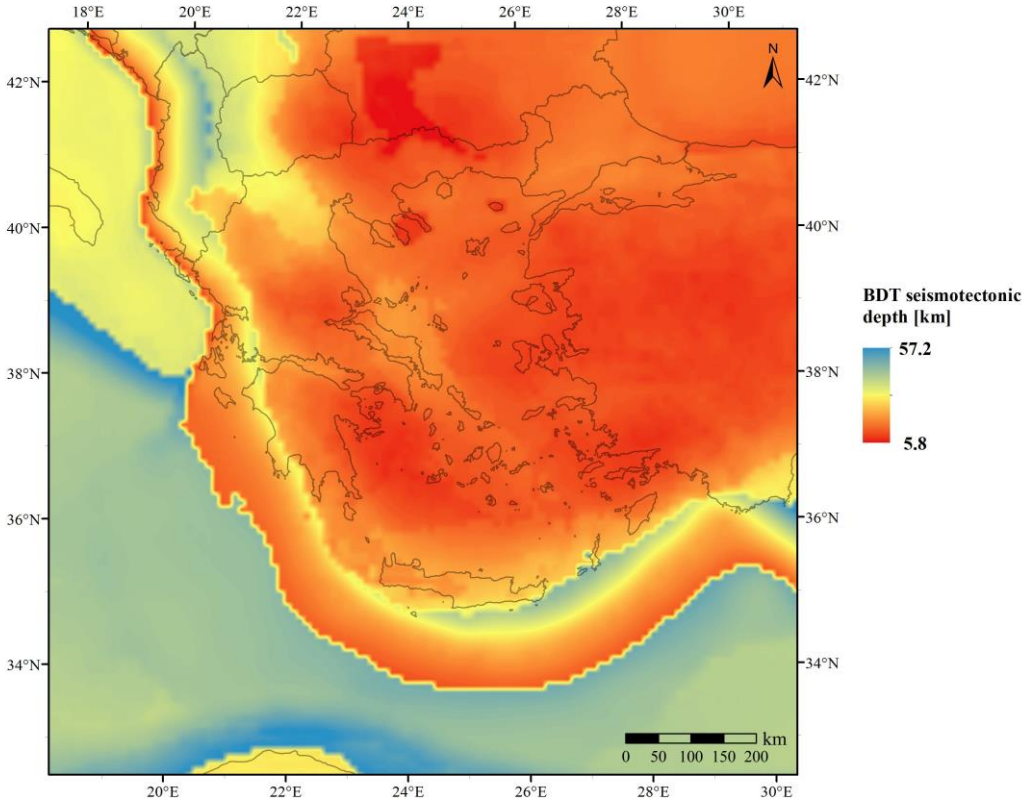

Fig. 6.2 – Map view of the "seismotectonic" BDT depth.

Once obtained the corresponding values of the *seismotectonic* BDT depth for each seismogenic source, the discrepancy (or similarity) with the maximum depth estimated in GreDaSS has been checked. The main aim was to compare the two independent information on the depth extent of the sources and, in case of relevant differences between the two, analyze the possible causes and also update the calculation on the seismogenic potential, taking into account the new geometrical characteristics.

The values of the BDT depth obtained from the reference model tend to be systematically greater than those of the maximum depth of the composite sources in GreDaSS (hereinafter MDG) for the Western Hellenic arc region, both in continental and oceanic subduction settings (fig. 6.3). Here BDTs are up to ~20-25 km deeper than the estimated maximum potential depth extent of faulting in GreDaSS. Such a discrepancy may be attributed to multiple factors, among which the most relevant can be tentatively identified in: i) the very low heat flow values used in the rheological modelling for this region, leading to a remarkable deepening of the BDT; ii) the lithological

composition of the upper crust in the dowgoing plate, corresponding to a (wet) diabase, which is clearly an approximation of the actual oceanic crust composition.

Nonetheless, no other mafic lithology for the oceanic crust are available in terms of knowledge of the corresponding rheological parameters and therefore this choice still represents the best option, even though with the awareness that potential errors should be taken into account. However, it should be also noted that a deeper BDT with respect to MDG could be consistent with geologically recent faults, which may have not entered yet their final evolutionary stage and, accordingly, also not reached yet their maximum potential dimension, in terms of both length and width.

The only exception in the Western Hellenic arc region is represented by the Zakynthos Thrust, which is characterized by a shallower *seismotectonic* BDT (~22 km deep) with respect to the corresponding MDG. Such a difference is possibly a result of the conditions applied for determining the *seismotectonic* BDT, starting from the *rheological* one. However, it should also be reminded that, since the brittle behaviour in this area is predominant down to greater depths (~35-40 km, see also Appendix A1, test site n. 50), deeper seismicity might occur, as suggested by seismological evidences (*e.g.* Papadimitriou *et al.*, 2012).

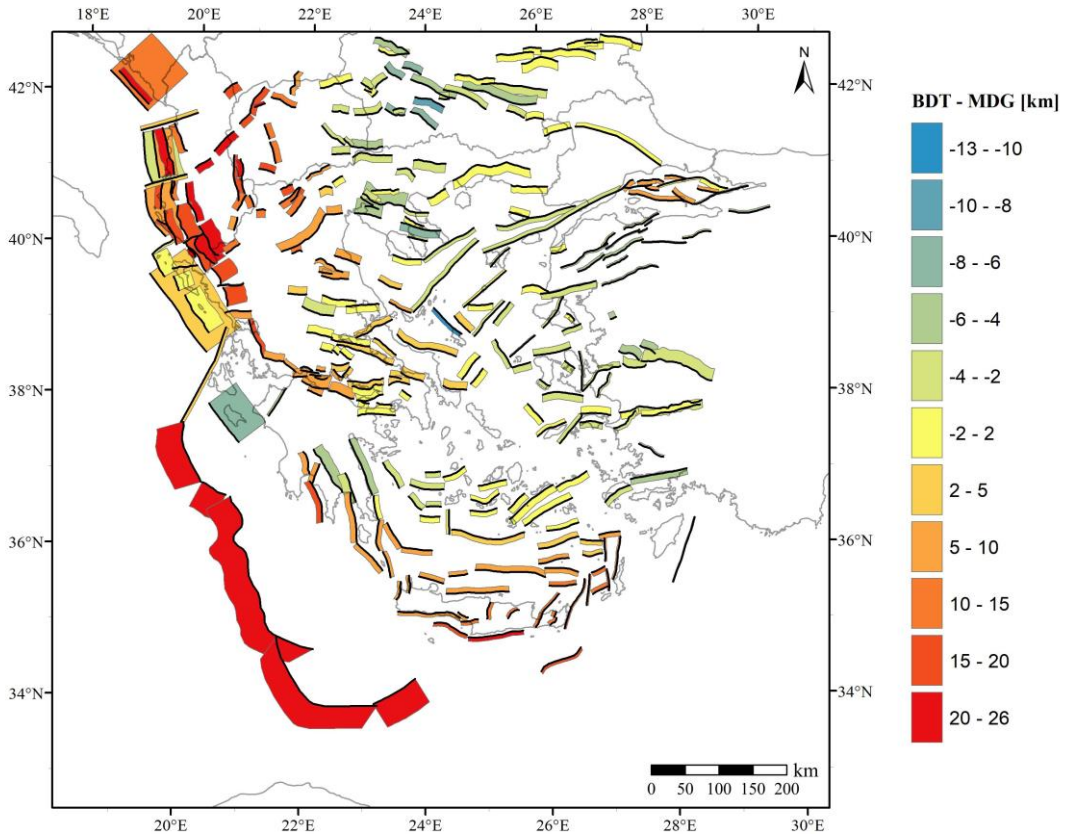

Fig. 6.3 – Map showing the difference between the "seismotectonic" BDT depth and the Maximum Depth indicated in GreDaSS (MDG) (Caputo and Pavlides, 2013), for the seismogenic sources in the study area.

In the central and southern Aegean Sea regions, around the Hellenic volcanic arc, a general good agreement between the BDTs and the MDGs is observed, except for some sources at the western and eastern tips, where the BDT tends to be slightly shallower, mainly because of the effect of the high heat flow characterizing the area. Differences are generally lower than or around 4-5 km and may be indicative of an effective overestimation of sources width in GreDaSS or might also result from a locally oversimplified rheological modelling, with small-scale variations and peculiar conditions not resolved at the resolution of this research.

In the remaining sectors of the eastern Aegean Region, in the back-arc extensional area, a tendency to moderately shallower BDTs with respect to MDGs is observed in the Northern Aegean Sea, Central-Eastern Macedonia and Thrace regions. Here the majority of the sources is actually characterized by a good fit between BDTs and MDGs, with differences lower than 3 km. Slightly greater discrepancies are observed in the Chalkidiki peninsula (~5 km) and above all in southern Bulgaria, where the BDTs are locally up to 7-8 km shallower than the corresponding MDGs. That is probably due to the very elevated surface heat flow, whose estimates might not be very accurate for this region, since the latter is located at the border of the study area, where the heat flow values have been mostly obtained through interpolation, rather than being the results of direct measurements.

In general, throughout Northern Aegean and northeastern Greece, the shallower BDTs are again attributable to the major role played by the relatively high heat flow (even though not as high as in the Central-Southern Aegean), even though the different lithological compositions (*e.g.* granite or granodiorite instead of quartzite for the upper crust layer) may also exert a relevant influence on the resulting BDT depth and its sharp lateral variations.

In central continental Greece (southern Thessaly, Central Greece and Attica) an overall consistency between BDT depths and MDGs is observed, with some local deeper BDTs for the seismogenic sources in the western Corinth Rift, mainly due to the very high strain rates characterizing the area. In northwestern continental Greece (northern Thessaly, Epirus, Western Macedonia), North Macedonia and Albania, the BDTs are generally deeper than the MDGs, with the differences going from ca. 5-8 km in Thessaly/Macedonia to even 15 km in Albania. The greatest discrepancies (on average around ~30 km) are observed along the coastal sectors of Montenegro, Albania, northwestern Greece and the Ionian Islands, possibly because of the very low heat flow values and the high strengths associated with the compressional tectonic regime that characterizes the area.

To sum up, when comparing the BDT depths from the reference model with MDG from GreDaSS, an overall good fit can be observed in the central domain of the study area and in particular in central continental Greece, Thrace and almost the entire Aegean Sea region. The greater discrepancies are instead registered in the peripheral sectors, with generally shallower BDTs in Bulgaria and Northern Greece and deeper BDTs, always with respect to the MDGs of the

seismogenic sources in GreDaSS, in the western and southern external sectors corresponding to coastal areas of Albania, western Greece and along the Hellenic subduction zone. The reasons for such differences, which in many cases are minor in terms of absolute values and may represent an improvement and contribution of the rheological modelling realized in this study to the seismotectonic characterization proposed in GreDaSS, are mainly related to heat flow and strain rate values anomalies, while local lithological variations may play a secondary role.

Differences between the modelled BDTs depths and the MDGs from GreDaSS have also been tested for the alternative models 2 and 3. In model 2, where the main variations in the BDT depths with respect to the reference one only occur in correspondence of the Mediterranean Ridge accretionary wedge and around the Hellenic Volcanic Arc, the differences between BDTs and MDGs are generally similar to what described above for the reference model.

An appreciable improvement in the fit between BDTs and MDGs is observed for some sources in the western sector of the Hellenic volcanic arc, where the increase in pore fluid pressure ratio with respect to the reference model led to slightly deeper BDTs, thus matching the depth estimates in GreDaSS. At the same time, however, the λ_e increase has also caused a moderate deepening of the BDTs in external thrusts of Hellenic subduction zone, thus leading to a further slight worsening of the fit for such sources (even though the explanations provided above are still valid).

Model 3 is characterized by slightly higher heat flow values almost throughout the whole study area and consequently by moderately shallower BDTs with respect to the reference model (see the dedicated section §5.3 in Chapter 5). Accordingly, an improvement in the BDT-MDG fit is observed for some sources where the reference model BDTs were deeper than the MDG.

In particular, with model 3, smaller differences characterize several sources around the Corinth Rift and also in the area comprised between northern Thessaly and southwestern Macedonia. On the other hand, however, for some sources in the Aegean Sea, associated with an elevated heat flow, the model 3 BDTs shallowings result into a moderate worsening of the fit.

To sum up, every rheological model realized in this work presents both its own advantages and drawbacks. Therefore, the reference 'preferred' model, with the modified, "seismotectonic" approach, will be mainly adopted in the following applications, inferences and calculations, even though also the alternative ones could be taken into account in peculiar cases and conditions.

6.1.2 Maximum expected magnitudes

Once compared the BDTs obtained from the rheological modelling with the maximum depths in GreDaSS, the results have been applied to calculate the maximum expected magnitudes for the same seismogenic sources. The BDTs depths, indeed, provide new geometrical constraints and may represent an independent tool and data source to implement such calculations. The BDT is here considered as an approximate indicator of the seismic-aseismic transition (*e.g.* Scholz, 1988;

Sibson, 1984) and therefore theoretically corresponds to the maximum depth of the faulting (coseismic) process. In other words, the BDT depth is equal to the distance from the earth surface to the bottom of the seismogenic source volume, *i.e.* the base of the seismogenic layer.

If such a distance is determined based on the rheological modelling, and information about the average dip angle of the investigated fault or seismogenic source is also available, simple trigonometric equations can provide the value of the fault width (fig. 6.4). For the dip angle of the seismogenic sources, the data have been extracted from the GreDaSS database, which usually provides an indication of both minimum and maximum potential dip angle values.

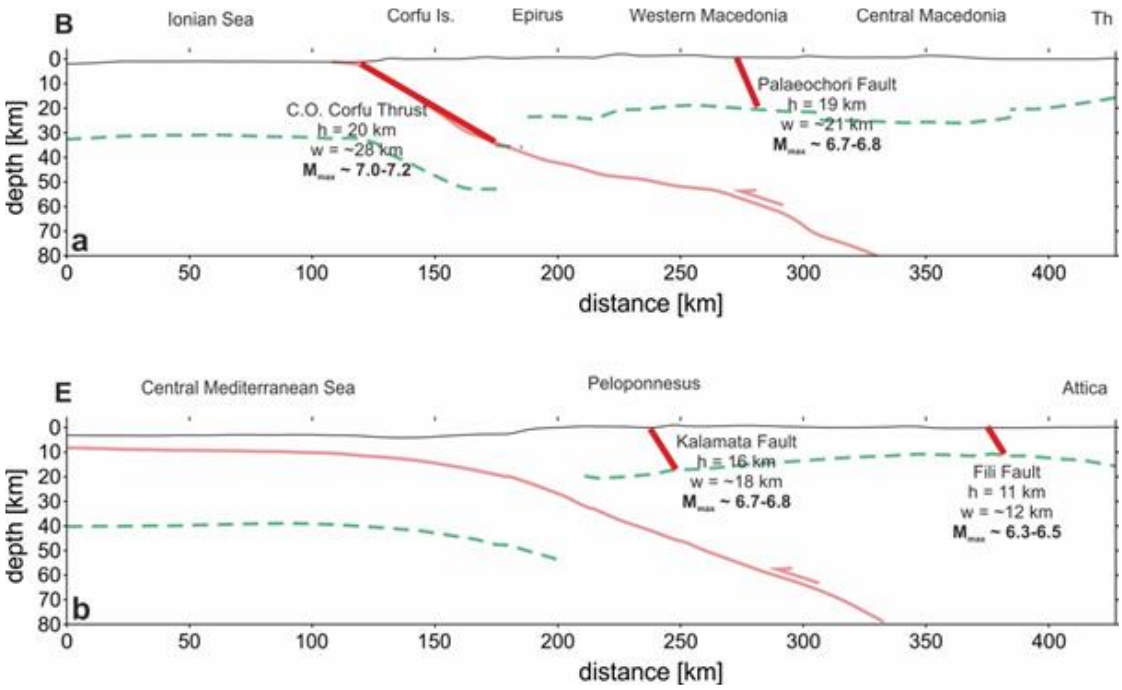

Fig. 6.4 – Examples of width-based calculations of the maximum expected magnitudes (through the application of empirical relationships) for some selected seismogenic sources along two of the transects presented and discussed in chapter 5. The width (solid thick red line) is constrained by the depth of BDT (dashed green line) and by the dip angle (known from GreDaSS; Caputo and Pavlides, 2013).

Accordingly, as a first step, a single average dip angle value for each seismogenic source has been calculated, though it must be taken into account that, especially for the composite sources of greater dimensions, the dip angle may differ along strike from the average value. The following estimates are therefore affected by such uncertainties and deviations in the geometrical input data. In order to fix this potential source of error, in a secondary phase, I also performed calculations with both the minimum and the maximum dip angle and finally compared (by a statistical point of view) all the obtained results.

The width of the seismogenic sources, constrained by the BDT depth, has thus been used to calculate the maximum expected magnitude for each source, by mainly applying the empirical relationships of Wells and Coppersmith (1994), which relate the geometrical features of the source with the moment magnitude of the corresponding earthquake. Both the width-moment magnitude,

the length-moment magnitude and the rupture area-moment magnitude relationships have been applied. This choice is motivated by the need to not overestimate and overweigh the width (which is the feature directly constrained by the rheological modelling)-moment magnitude relationship, since it is the least robustly determined one among the above-mentioned three empirical equations. Accordingly, the length has been derived by assuming it to be twice the width. Finally, also the rupture area relationship has been applied, where the rupture area is obtained from the multiplication of length times width. The three above-mentioned empirical relationships are actually separated and yield different results, for the three main tectonic regimes (compressional, extensional and transcurrent).

It follows that the maximum expected magnitude, for each seismogenic source (fig. 6.5), has been calculated by applying the relationship according to the corresponding tectonic regime that characterizes the investigated structure.

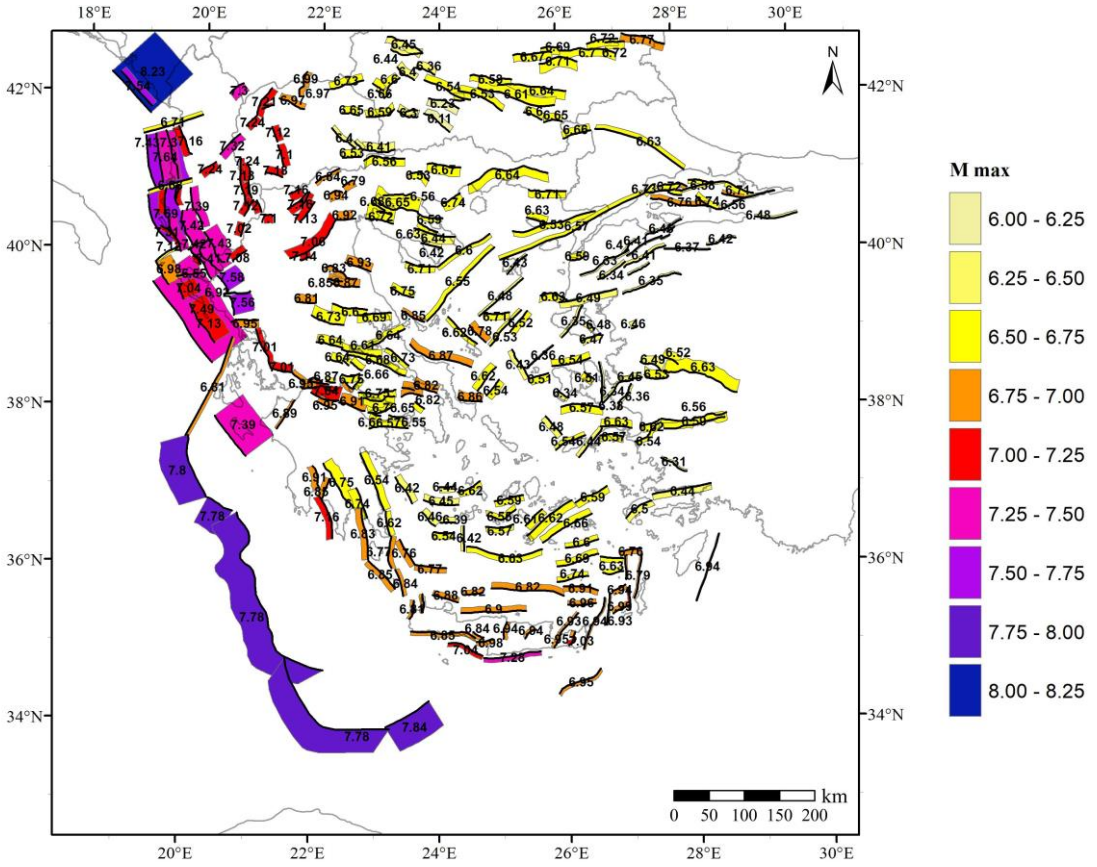

Fig. 6.5 – Maximum expected magnitudes for each composite seismogenic source in the study area. The magnitudes have been calculated by constraining the width of the sources with the BDT depth and applying a length/width ratio equal to 2.

In order to determine the corresponding tectonic regime for each source, the rake of the source, as indicated in GreDaSS, has been used. Also for the rake, both minimum and maximum values are commonly available in GreDaSS, and the average values have been calculated and used. However, similarly to what described for the dip angle, composite sources may be subject to tectonic style

changes along strike and therefore possible errors may arise. Calculations have been therefore made, also in this case, using both the minimum and the maximum rake. Given the fact that empirical relationships are only available for the three main tectonic regimes, the seismogenic sources have been categorized as follows: 45° <rake < 135° - compression and therefore the relationship for thrust fault regimes has been used; 0° ≤rake≤45° and 315°≤rake≤360° and 135°≤rake≤225° – strike-slip regime and relative relationship; 225°<rake<315° – extensional regime and relative relationship. The maximum expected magnitudes calculated as above described for the seismogenic sources in the study area are shown in fig. 6.5.

The majority of the sources in continental Greece and in the Aegean Sea, characterized by extensional tectonics, are associated to maximum expected magnitudes in the range 6.4 – 7.1. Greater values, generally comprised between 7.0 and 8.0, have been obtained, instead, for the compressional sources along the Western Hellenic arc. Such elevated maximum magnitudes, on one hand, effectively represent the high seismic hazard characterizing this region. On the other hand, a partial overestimate might have been obtained, since a complete rupture of the seismogenic layer up to the topo/bathymetric surface has been considered in the magnitude calculations, while the effective rupture process may actually arrest some kilometres below the surface, in correspondence of the updip aseismic transition, as observed along subduction zones (see also discussion and references in section §6.1.1).

All numerical results, obtained using the BDT from the reference model, the average dip and rake values and applying the rupture area-moment magnitude relationship, are shown in table 6.1.

ID source	Dip Avg	Rake Avg	BDT	Mmax_RA	Mmax_W	Mmax_L
ALCS001	45	90	32.2	7.59	7.60	7.41
ALCS016	50	85	25.7	7.35	7.35	7.21
ALCS020	45	90	33.0	7.60	7.62	7.42
ALCS070	45	90	33.2	7.61	7.63	7.43
ALCS085	82	182.5	30.8	7.33	7.67	7.00
ALCS090	79.5	182.5	14.3	6.66	6.81	6.51
ALCS201	22.5	90	26.7	7.92	7.96	7.69
ALCS210	55	90	23.9	7.24	7.23	7.12
ALCS215	47.5	90	28.9	7.47	7.48	7.31
ALCS220	45	90	23.8	7.35	7.35	7.21
ALCS230	50	90	24.9	7.32	7.32	7.19
ALCS235	60	90	21.1	7.10	7.08	7.01
ALCS240	50	90	33.8	7.56	7.58	7.39

ALCS250	45	90	32.7	7.60	7.62	7.42
ALCS290	72.5	182.5	18.0	6.89	7.10	6.68
ALCS301	22.5	90	25.0	7.87	7.91	7.64
ALCS315	35	90	22.1	7.45	7.46	7.30
ALCS325	42.5	90	31.6	7.61	7.63	7.43
ALCS335	47.5	90	22.9	7.29	7.28	7.16
ALCS390	72.5	187.5	18.9	6.93	7.16	6.71
ALCS500	72.5	265	33.1	7.38	7.29	7.18
ALCS505	60	270	29.5	7.36	7.27	7.16
ALCS510	60	270	30.6	7.40	7.31	7.19
ALCS515	60	270	27.5	7.30	7.21	7.12
ALCS520	60	270	26.4	7.26	7.17	7.09
ALCS550	60	270	24.0	7.18	7.08	7.02
ALCS600	57.5	305	36.4	7.57	7.49	7.32
ALCS610	57.5	335	37.8	7.66	8.08	7.24
ALCS850	55	285	34.1	7.54	7.46	7.30
BGCS001	55	270	9.1	6.37	6.24	6.41
BGCS010	60	255	12.5	6.60	6.49	6.59
BGCS015	60	280	8.1	6.21	6.08	6.30
BGCS020	60	270	7.7	6.18	6.05	6.27
BGCS025	60	265	13.3	6.66	6.54	6.63
BGCS028	60	270	13.6	6.68	6.57	6.65
BGCS030	60	270	13.9	6.69	6.58	6.66
BGCS035	60	270	12.6	6.61	6.49	6.60
BGCS080	60	270	15.4	6.78	6.67	6.73
BGCS100	55	270	12.8	6.67	6.56	6.64
BGCS110	57.5	270	12.5	6.63	6.51	6.61
BGCS120	65	270	11.9	6.52	6.40	6.53
BGCS130	62.5	270	12.0	6.54	6.42	6.54
BGCS150	60	270	12.4	6.60	6.48	6.58
BGCS160	60	270	8.8	6.29	6.17	6.36
BGCS170	60	285	9.4	6.35	6.22	6.40
BGCS180	60	270	10.1	6.41	6.29	6.44
BGCS190	60	270	10.2	6.42	6.30	6.45
BGCS200	60	270	13.8	6.69	6.57	6.65

BGCS210	60	270	12.6	6.61	6.49	6.60
BGCS275	60	270	12.2	6.58	6.46	6.57
BGCS280	60	290	7.3	6.12	5.99	6.23
BGCS290	65	315	7.1	6.11	6.11	6.11
BGCS400	60	270	14.8	6.75	6.64	6.70
BGCS420	60	270	14.4	6.73	6.62	6.69
BGCS440	60	270	14.1	6.71	6.59	6.67
BGCS480	55	270	14.1	6.76	6.65	6.71
BGCS510	60	270	16.4	6.84	6.74	6.77
BGCS520	60	270	15.1	6.77	6.66	6.72
BGCS530	60	270	15.1	6.77	6.66	6.72
GRCS001	62.5	270	19.1	6.95	6.85	6.85
GRCS002	65	275	18.7	6.92	6.81	6.83
GRCS004	55	270	18.1	6.98	6.88	6.87
GRCS010	55	251	13.7	6.73	6.62	6.69
GRCS015	57.5	270	12.3	6.61	6.50	6.60
GRCS020	50	275	13.7	6.79	6.68	6.73
GRCS025	57.5	270	17.0	6.90	6.79	6.81
GRCS040	55	270	19.8	7.06	6.96	6.93
GRCS048	50	270	25.1	7.33	7.24	7.14
GRCS050	60	265	25.3	7.23	7.13	7.06
GRCS058	60	270	20.4	7.04	6.94	6.92
GRCS060	72.5	260	20.0	6.93	6.83	6.84
GRCS068	57.5	255	20.7	7.07	6.97	6.94
GRCS069	60	260	16.9	6.87	6.76	6.79
GRCS070	57.5	260	28.7	7.36	7.27	7.16
GRCS072	57.5	260	28.4	7.35	7.26	7.16
GRCS077	62.5	260	28.7	7.32	7.23	7.13
GRCS080	60	270	29.2	7.35	7.26	7.16
GRCS090	57.5	285	26.0	7.27	7.18	7.10
GRCS100	55	282.5	12.9	6.68	6.57	6.65
GRCS110	75	280	13.9	6.60	6.48	6.59
GRCS120	72.5	270	13.3	6.57	6.45	6.56
GRCS130	57.5	265	11.7	6.57	6.45	6.56
GRCS140	52.5	272.5	12.9	6.70	6.59	6.67

GRCS145	65	270	12.0	6.53	6.41	6.53
GRCS150	55	245	12.7	6.66	6.55	6.64
GRCS155	55	255	14.8	6.80	6.69	6.74
GRCS160	60	255	15.0	6.76	6.65	6.71
GRCS170	62.5	255	14.3	6.70	6.59	6.66
GRCS240	52.5	270	14.3	6.80	6.69	6.74
GRCS245	57.5	285	14.0	6.73	6.61	6.68
GRCS250	58.5	275	14.9	6.77	6.66	6.72
GRCS260	72.5	312.5	14.6	6.65	6.54	6.63
GRCS265	65	260	10.2	6.38	6.26	6.42
GRCS270	60	300	10.0	6.40	6.28	6.44
GRCS280	75	227.5	14.1	6.61	6.50	6.60
GRCS285	65	227.5	15.7	6.76	6.65	6.71
GRCS288	60	255	13.3	6.66	6.54	6.63
GRCS290	74.5	202.5	14.4	6.68	6.84	6.53
GRCS300	60	265	26.2	7.26	7.16	7.08
GRCS310	84.5	335	27.1	7.21	7.51	6.92
GRCS330	57.5	270	20.9	7.08	6.98	6.95
GRCS350	70	337.5	29.5	7.34	7.68	7.01
GRCS355	60	275	23.3	7.15	7.06	7.01
GRCS357	70	315	20.0	6.99	7.24	6.76
GRCS370	30	90	29.6	7.79	7.83	7.58
GRCS377	30	90	28.7	7.77	7.80	7.56
GRCS390	75	225	14.9	6.71	6.88	6.55
GRCS400	55	270	12.8	6.67	6.56	6.64
GRCS405	57.5	270	12.5	6.62	6.51	6.61
GRCS410	62.5	275	14.8	6.73	6.62	6.68
GRCS415	60	275	17.6	6.91	6.80	6.82
GRCS418	57.5	275	17.8	6.94	6.84	6.84
GRCS420	60	270	17.6	6.91	6.80	6.82
GRCS425	55	270	15.1	6.82	6.71	6.75
GRCS430	57.5	270	15.5	6.82	6.71	6.75
GRCS432	57.5	270	13.2	6.67	6.56	6.64
GRCS433	62.5	270	13.7	6.66	6.55	6.63
GRCS434	62.5	285	14.2	6.69	6.58	6.66

GRCS436	65	265	16.1	6.79	6.68	6.73
GRCS438	65	275	17.1	6.84	6.73	6.77
GRCS440	65	252.5	15.3	6.74	6.63	6.69
GRCS441	65	270	19.8	6.97	6.87	6.87
GRCS442	65	270	20.1	6.98	6.88	6.87
GRCS443	67.5	265	19.3	6.93	6.83	6.84
GRCS444	70	270	18.8	6.89	6.79	6.81
GRCS450	62.5	280	13.7	6.66	6.55	6.64
GRCS453	60	270	11.8	6.55	6.44	6.55
GRCS470	62.5	260	13.9	6.68	6.56	6.64
GRCS473	67.5	275	16.5	6.79	6.68	6.73
GRCS480	60	277.5	18.9	6.97	6.87	6.87
GRCS488	55	270	17.7	6.96	6.86	6.86
GRCS500	40	270	18.2	7.20	7.11	7.04
GRCS505	55	265	20.4	7.08	6.98	6.95
GRCS510	47.5	272.5	17.1	7.02	6.92	6.91
GRCS518	57.5	262.5	14.3	6.75	6.63	6.70
GRCS520	60	270	13.7	6.69	6.57	6.65
GRCS522	60	270	12.8	6.62	6.51	6.60
GRCS524	50	270	18.9	7.08	6.98	6.95
GRCS525	84	172.5	25.9	7.18	7.47	6.89
GRCS540	60	265	12.2	6.58	6.47	6.57
GRCS555	57.5	270	15.5	6.82	6.71	6.75
GRCS558	60	265	15.6	6.80	6.69	6.74
GRCS560	57.5	270	19.5	7.02	6.92	6.91
GRCS562	60	280	18.3	6.94	6.84	6.85
GRCS564	57.5	265	28.8	7.36	7.27	7.16
GRCS575	60	270	11.6	6.53	6.41	6.54
GRCS580	60	270	13.0	6.64	6.53	6.62
GRCS582	62.5	270	16.8	6.84	6.74	6.77
GRCS583	65	270	19.0	6.93	6.83	6.84
GRCS584	57.5	270	17.5	6.92	6.82	6.83
GRCS586	60	260	18.4	6.94	6.84	6.85
GRCS600	25	90	21.8	7.68	7.71	7.49
GRCS605	35	90	13.5	7.07	7.05	6.98

GRCS610	35	90	14.7	7.14	7.12	7.04
GRCS615	35	90	17.0	7.25	7.24	7.13
GRCS620	77.5	175	22.5	7.07	7.33	6.81
GRCS660	30	90	22.1	7.56	7.58	7.39
GRCS670	30	90	41.8	8.06	8.12	7.80
GRCS677	30	90	40.3	8.03	8.09	7.78
GRCS680	30	90	40.4	8.03	8.09	7.78
GRCS690	30	90	40.6	8.04	8.09	7.78
GRCS698	30	90	44.2	8.10	8.16	7.84
GRCS700	70	270	19.0	6.90	6.80	6.81
GRCS705	70	270	20.6	6.97	6.87	6.87
GRCS708	57.5	270	18.9	6.99	6.89	6.88
GRCS710	57.5	270	19.3	7.01	6.91	6.90
GRCS715	67.5	265	19.6	6.94	6.84	6.85
GRCS720	67.5	275	19.5	6.94	6.83	6.84
GRCS722	67.5	265	23.8	7.11	7.02	6.98
GRCS725	65	280	25.7	7.20	7.11	7.04
GRCS730	62.5	270	35.8	7.51	7.43	7.28
GRCS740	67.5	262.5	22.5	7.07	6.97	6.94
GRCS743	70	277.5	22.9	7.07	6.97	6.94
GRCS745	70	270	23.2	7.08	6.98	6.95
GRCS748	75	275	23.2	7.05	6.95	6.93
GRCS750	60	290	21.6	7.09	6.99	6.96
GRCS752	67.5	270	25.7	7.18	7.09	7.03
GRCS755	67.5	270	24.2	7.13	7.03	6.99
GRCS760	79.5	250	23.9	7.06	6.96	6.94
GRCS770	62.5	280	23.2	7.13	7.03	6.99
GRCS772	62.5	280	21.8	7.07	6.97	6.94
GRCS774	79.5	250	23.5	7.05	6.95	6.93
GRCS776	79.5	250	29.3	7.24	7.15	7.07
GRCS778	79.5	250	18.7	6.85	6.74	6.77
GRCS779	60	270	16.1	6.83	6.72	6.76
GRCS780	79.5	250	19.2	6.87	6.76	6.79
GRCS798	82	180	28.0	7.25	7.56	6.94
GRCS799	65	330	26.1	7.26	7.58	6.95

GRCS800	77	207.5	15.5	6.74	6.91	6.57
GRCS810	72.5	180	14.7	6.71	6.88	6.55
GRCS815	65	290	16.7	6.82	6.71	6.75
GRCS820	70	285	19.9	6.94	6.84	6.85
GRCS825	82	197.5	12.8	6.55	6.68	6.43
GRCS831	79.5	178	13.7	6.62	6.76	6.48
GRCS835	82	185	17.1	6.81	7.01	6.62
GRCS837	57.5	295	16.3	6.86	6.75	6.78
GRCS838	62.5	250	15.4	6.76	6.65	6.71
GRCS840	79.5	200	14.8	6.69	6.85	6.53
GRCS845	70	195	13.9	6.67	6.83	6.52
GRCS850	79.5	195	11.2	6.45	6.54	6.35
GRCS853	84.5	190	11.5	6.45	6.55	6.36
GRCS855	67.5	265	11.2	6.45	6.33	6.47
GRCS857	67.5	285	11.3	6.45	6.33	6.48
GRCS865	67.5	345	11.8	6.54	6.66	6.43
GRCS868	60	270	11.2	6.50	6.38	6.51
GRCS870	57.5	200	14.6	6.81	7.01	6.62
GRCS873	57.5	200	12.8	6.70	6.86	6.54
GRCS880	60	252.5	11.7	6.54	6.42	6.54
GRCS885	70	345	10.5	6.43	6.52	6.34
GRCS900	57.5	270	11.9	6.58	6.46	6.57
GRCS905	62.5	335	12.3	6.61	6.75	6.48
GRCS907	72.5	235	12.8	6.54	6.42	6.54
GRCS910	72.5	225	12.4	6.56	6.68	6.44
GRCS912	57.5	270	13.0	6.66	6.55	6.63
GRCS915	62.5	265	12.5	6.58	6.46	6.57
GRCS937	60	270	12.5	6.60	6.49	6.59
GRCS938	60	270	13.0	6.64	6.52	6.62
GRCS939	60	270	10.0	6.41	6.29	6.44
GRCS940	60	275	9.7	6.38	6.25	6.42
GRCS943	57.5	247.5	9.9	6.42	6.29	6.45
GRCS947	60	275	10.3	6.43	6.31	6.46
GRCS950	62.5	270	9.5	6.33	6.21	6.39
GRCS952	62.5	280	12.2	6.56	6.44	6.55

GRCS954	60	270	12.1	6.58	6.46	6.57
GRCS956	60	270	12.9	6.63	6.51	6.61
GRCS958	62.5	255	13.4	6.64	6.53	6.62
GRCS960	60	270	12.6	6.61	6.49	6.59
GRCS962	60	270	13.9	6.70	6.58	6.66
GRCS965	65	270	11.4	6.48	6.36	6.50
GRCS970	55	270	11.0	6.54	6.42	6.54
GRCS972	72.5	270	10.7	6.38	6.25	6.42
GRCS974	55	270	12.5	6.65	6.54	6.63
GRCS976	62.5	270	13.0	6.61	6.50	6.60
GRCS978	57.5	270	14.2	6.74	6.63	6.69
GRCS979	60	270	15.7	6.80	6.70	6.74
GRCS980	65	270	14.7	6.70	6.59	6.67
GRCS981	62.5	287.5	13.7	6.66	6.55	6.63
GRCS983	60	285	16.2	6.83	6.72	6.76
GRCS985	57.5	260	15.8	6.84	6.73	6.77
GRCS990	60	270	17.6	6.90	6.80	6.82
GRCS991	52.5	270	16.2	6.91	6.80	6.82
GRCS996	57.5	270	19.5	7.02	6.92	6.91
MECS001	12	90	33.4	8.57	8.67	8.23
MECS005	35	90	32.1	7.75	7.78	7.54
MKCS001	57.5	270	11.1	6.52	6.40	6.53
MKCS010	72.5	167.5	10.6	6.42	6.51	6.34
MKCS020	72.5	167.5	11.7	6.50	6.62	6.40
MKCS100	60	270	30.2	7.38	7.29	7.18
MKCS150	60	265	33.3	7.47	7.38	7.24
MKCS500	60	265	27.7	7.31	7.21	7.12
MKCS520	60	270	26.7	7.27	7.18	7.10
MKCS600	60	270	13.6	6.68	6.56	6.65
MKCS800	60	295	32.9	7.46	7.37	7.24
MKCS810	60	275	31.6	7.42	7.33	7.21
MKCS815	75	340	32.1	7.39	7.74	7.04
MKCS850	60	335	25.5	7.28	7.60	6.97
MKCS900	65	270	23.1	7.11	7.01	6.97
RSCS001	65	270	23.8	7.13	7.04	6.99

TRCS001	70	165	16.5	6.83	7.03	6.63
TRCS020	87	180	17.5	6.82	7.02	6.63
TRCS022	82	180	16.1	6.76	6.94	6.58
TRCS024	70	255	16.3	6.76	6.65	6.71
TRCS026	84.5	180	15.7	6.73	6.90	6.56
TRCS028	60	255	16.3	6.84	6.73	6.77
TRCS030	57.5	255	15.3	6.80	6.70	6.74
TRCS032	60	250	16.1	6.83	6.72	6.76
TRCS035	57.5	150	17.3	6.96	7.20	6.73
TRCS037	60	212.5	17.5	6.95	7.18	6.72
TRCS038	60	255	17.6	6.90	6.80	6.82
TRCS039	62.5	230	16.3	6.82	6.71	6.75
TRCS040	62.5	210	17.0	6.90	7.12	6.69
TRCS090	82	180	13.7	6.62	6.76	6.48
TRCS100	65	270	13.2	6.61	6.49	6.59
TRCS120	82	200	10.8	6.41	6.49	6.33
TRCS125	84.5	180	12.3	6.52	6.63	6.41
TRCS128	84.5	180	13.0	6.56	6.69	6.44
TRCS130	82	180	12.1	6.51	6.62	6.40
TRCS134	82	180	13.3	6.59	6.72	6.46
TRCS140	84.5	180	13.2	6.58	6.71	6.45
TRCS170	79.5	180	10.9	6.42	6.51	6.34
TRCS173	77.5	200	12.1	6.52	6.63	6.41
TRCS175	84.5	180	11.7	6.47	6.57	6.37
TRCS180	82	185	12.6	6.54	6.66	6.42
TRCS190	82	185	11.6	6.47	6.57	6.37
TRCS200	62.5	255	13.7	6.66	6.55	6.63
TRCS203	65	237.5	11.3	6.47	6.35	6.49
TRCS210	82	180	11.2	6.44	6.53	6.35
TRCS250	60	270	10.3	6.43	6.31	6.46
TRCS300	57.5	270	10.8	6.49	6.37	6.51
TRCS310	80	175	10.9	6.42	6.51	6.34
TRCS313	77.5	190	11.6	6.48	6.58	6.38
TRCS315	65	265	10.6	6.41	6.29	6.45
TRCS320	79.5	195	11.3	6.45	6.55	6.36

TRCS330	55	270	10.8	6.52	6.40	6.53
TRCS335	60	265	10.8	6.47	6.35	6.49
TRCS345	57.5	275	10.9	6.51	6.39	6.52
TRCS350	47.5	265	11.3	6.66	6.54	6.63
TRCS370	60	267.5	13.1	6.64	6.53	6.62
TRCS373	75	235	13.0	6.54	6.42	6.54
TRCS380	57.5	270	12.1	6.60	6.48	6.59
TRCS400	62.5	270	12.2	6.56	6.44	6.56
TRCS430	82	180	10.6	6.39	6.46	6.31
TRCS500	62.5	275	10.3	6.41	6.28	6.44

Table 6.1 *– Values of geometrical features (dip and rake), mechanical ones (BDT depth) and corresponding maximum expected magnitudes calculated applying rupture area-, width-, and length-based empirical relationships (Wells and Coppersmith, 1994), for each seismogenic source, identified by the code on the first column.*

6.2 Seismic strain rates

A second application of the rheological modelling results is devoted to the estimation of seismic strain rates in selected areas of the Aegean region. In particular, the BDT depth, based on the rheological model, has been used as a constraint to determine a more realistic seismogenic volume, which is one of the parameters required for the calculation of the seismic strain rate, based on Kostrov (1974) method. Seismic strain rates represent a useful indicator for estimating how much of the total deformation of a selected body or volume is accommodated through seismic processes.

In particular, the comparison between seismic strain rates, long term deformation rates as indicated by geology and geodynamic considerations and geodetic strain rates allows to estimate the relative weight and relevance of the seismic processes on the total amount of deformation (see *e.g.* Jackson and McKenzie, 1988; Jenny *et al*., 2004). At the same time, such a comparison could also help inferring the potential role and contribution of other processes, such as aseismic creep, slow earthquakes and other ductile or semi-ductile phenomena to the total deformation rates.

Furthermore, if the seismic strain rates, which are usually referred to as short-term deformation indicators, present remarkable deviations from the long-term geologically-derived ones, inferences can be made on potential temporal and recent variations in the deformation rates. Potential discrepancies between seismic strain rates and the geodetically-derived ones would instead help identifying, for instance, regions characterized by an increased probability of occurrence of a significant seismic event. That would be the case of a rapidly deforming region associated with high geodetic strain rates, though characterized by lower seismic ones. This could possibly indicate

the future occurrence of seismic deformation through earthquakes, in order to reduce such an imbalance, especially if no evidences for other ductile deformation mechanisms are available and, given the last known relevant earthquake data, the seismic cycle could be close to its end.

The calculations of seismic strain rates have already been tentatively carried out for the Aegean Region by several research groups (*e.g.* Jackson and McKenzie, 1988; Ekstrom and England, 1989; Papazachos *et al.* 1992; Jackson *et al.*, 1994; Papazachos and Kiratzi, 1996; Jenny *et al.*, 2004; Rontogianni, 2010; Chousianitis *et al.*, 2015). However, in all of these studies, the width of the seismogenic layer is assumed to be equal to a constant value for the whole Aegean Region (typically 10 or 15 km), neglecting the uncertainties and differences that could occur between a particular volume and the surrounding ones. Furthermore, selecting an approximated value of the seismogenic layer thickness may also result into inaccurate calculations of the seismic strain rates. Therefore, since the BDT depth, used as a proxy for the bottom depth of the seismogenic layer, is a direct product of the rheological modelling carried out in this work, it has been applied and used for a more realistic calculation of the strain rates, thus allowing to consider the differences in seismogenic layer thickness between different blocks.

As I will also show later, given the linear inverse dependence of the seismic strain rates values on the considered volume and therefore also on the maximum depth of the seismogenic layer, a potential decrease of 50% in the BDT depth, with respect to a standard value, results into a corresponding 50% increase of the calculated seismic strain rates. In other words, selecting a seismogenic layer thickness of 10 km instead of the standard value of 15 km associated, for instance, to a $4 \cdot 10^{-15}$ s^{-1} strain rate value, would lead to an increased strain rate of $6 \cdot 10^{-15}$ s^{-1}. The decrease in the strain rate, when a thicker seismogenic layer is considered, has to attributed to the fact that, if all the other parameters remain constant, the same amount of deformation is spread over a greater volume. In other words, the considered block is associated to smaller strain rates because a greater volume is supposed to be mainly deforming by seismic processes, while the total amount of seismic moment, *i.e.* of seismic deformation, which has not changed, has to be diffused over a wider and deeper region.

The seismic strain rates calculations have initially been performed for selected test sites, corresponding to regions such as the Corinth Rift, the area around Thessaloniki in Macedonia, the North Aegean Trough and the South-East Aegean (see fig. 6.7). The selected regions all share some necessary requirements for performing the calculations, which are the occurrence of recent and instrumental seismicity and the tectonic regime and setting coherence all over the selected volume. A good number of seismic events, and possibly of high quality recording, is fundamental for extracting estimates on the seismicity rates, which are then used to quantify the deformation rates and in particular to define the magnitudes of the strain rate tensor components. A reliable catalogue of moment tensors, for each block, is instead necessary to obtain the principal axes directions of the strain rate tensor and moreover the focal mechanisms analysis allows establishing whether the

selected block is effectively characterized by a common tectonic regime and kinematics throughout the volume.

The Corinth Rift has been selected as the first test site area because of its very high seismicity rates and also because it represents one of the most rapidly deforming rifts all over the world, with values up to ca. 15 mm/yr (*e.g.* Briole *et al.*, 2000). Moreover, the Corinth Rift region is very well monitored by a geodetic point of view, with a highly developed GPS network and frequent dedicated campaigns of measurements (see *e.g.* Avallone *et al.*, 2004; Bernard *et al.*, 2006). Finally, a wealth of different strain rate maps, mainly obtained from GPS measurements-derived velocity gradient fields, is available for this area (*e.g.* Hollenstein *et al.*, 2008; Floyd *et al.*, 2010; Kreemer *et al.*, 2014), thus allowing for a precise comparison between seismic deformation and GPS-measured one. Also, the Mygdonian basin and the region around Thessaloniki have been selected as the second test site because of the relatively high seismicity rate characterizing this area and the availability of a good number of focal mechanisms. Indeed, this region has been struck by some moderate/strong magnitude events in the instrumental era (*e.g.* the 1978 Thessaloniki earthquake) and the geology, together with the sub-surface structure determined by geophysical surveys, have been very well studied. Also, reliable strain rate data are available for this region and these, together with the above-mentioned implications for its (high) seismic risk, make it a good case for representing an additional test site for the calculation of the seismic strain rates.

The seismic strain rates are generally calculated using Kostrov's formula (Kostrov, 1974). Such an equation takes into account the seismic deformation, in the form of annual seismic scalar moment release, for the magnitude, and the seismic moment tensors, for the directions. The considered seismicity occurs within a pre-determined volume, during a selected time interval, and therefore the resulting deformation rates could substantially change and also be misleading if the seismic events recordings are not continuous throughout the whole period. Accordingly, some important constraints for the seismic database are the completeness level and the temporal continuity and stability, in terms of registrations and recorded data quality.

As concerns the considered volume, the use of a well-defined vertical dimension corresponding to the bottom depth of the seismogenic layer, as indicated by the BDT depth obtained through rheological modelling, could help reducing the uncertainty and possible errors due to spatial and volumetric misselections, which may ultimately lead to overestimates or underestimates of the seismic deformation rates.

Kostrov's formula reads as follows:

$$\dot{\varepsilon}_{ij} = \frac{\dot{M}_0}{2\mu V} \sum_k m_{ij}^{(k)} \qquad [6.1]$$

where $\dot{\varepsilon}_{ij}$ are the components of the strain rate tensor, $\dot{M}_0$ is the annual release rate of seismic scalar moment, μ is the shear modulus, V is the volume of the deforming zone where earthquakes occurred and $m_{ij}^{(k)}$ are the components of the seismic moment tensor for the k-th earthquake. When applying Kostrov's formula, two main assumptions are made: i) deformation takes place within the selected volume and ii) deformation style and tectonic regime are similar and consistent throughout the entire volume. The shear, or rigidity modulus, is assumed to be equal to 30 GPa, following the most common values used in the literature.

The volume V is obtained by multiplying the seismogenic layer thickness of each sub-area (on which I will focus shortly after) of the Aegean Region with the corresponding surface extension. For the areal subdivision of the Aegean Region into internally homogenous blocks from a tectonic regime point of view, the seismic zonation of Sboras *et al.* (2012) has been adopted (fig. 6.6).

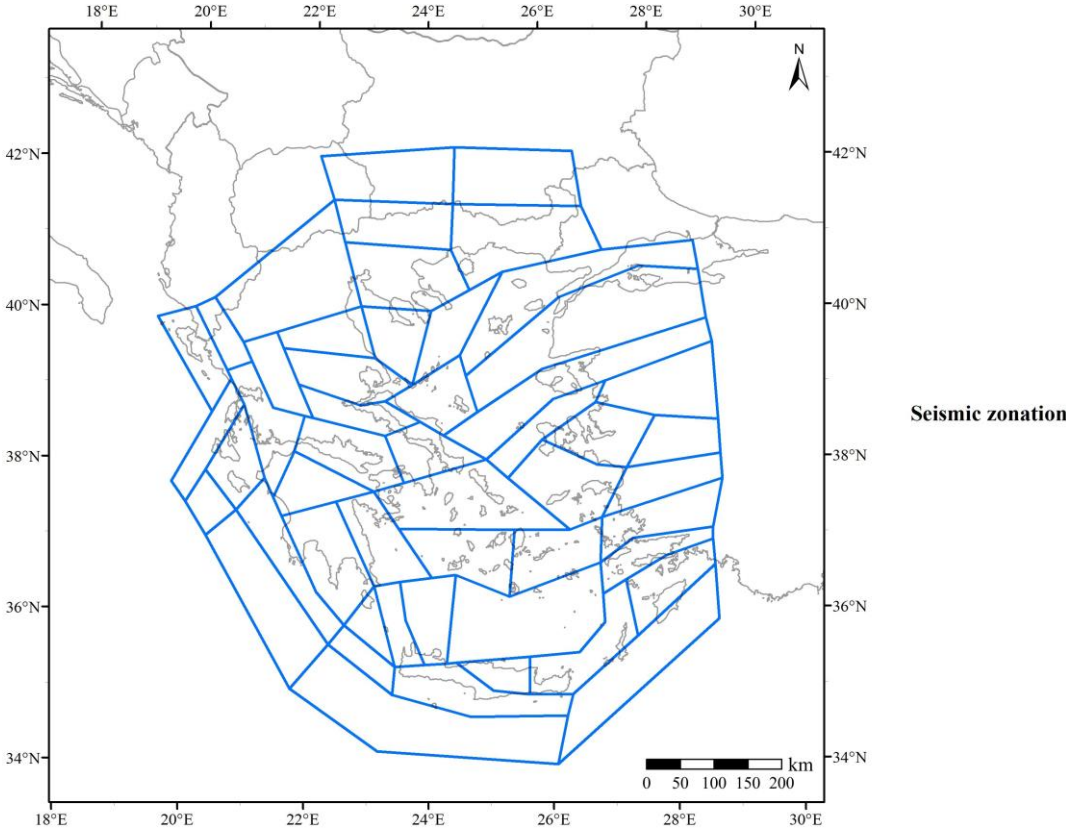

Fig. 6.6 – Seismic zonation (from Sboras et al.*, 2012) of the Aegean Region adopted for the calculation of the seismic strain rates in selected blocks (see next figure).*

Such a zonation, in addition to the typical seismological and historical seismicity data, takes into account also geological and structural information, in the form of the main active seismogenic sources of the region, as identified in the GreDaSS database (Caputo and Pavlides, 2013).

The same authors, indeed, argued that the seismic zonation of Papaioannou and Papazachos (2000) was incompatible with the geological characteristics of the main active fault and shear zones

of the Aegean Region (Sboras *et al.*, 2014) and therefore proposed a new seismic zonation (hereinafter termed as SPC2012), based on the seismogenic sources geometries, so that the latter do not crosscut any of the zone boundaries. This last feature also answers one of the specific requisites needed for applying Kostrov's formula, that is, all the (seismic) deformation must occur within the selected block(s).

As concerns the vertical dimension of the seismic zonation blocks, *i.e.* the bottom of the seismogenic layer delimiting at depth the seismically deforming volumes, the BDT depth obtained from the rheological modelling has been used. More specifically, each zone has been associated with the corresponding value of BDT depth, so that a laterally varying thickness of the seismogenic layer has been taken into account following the rheological modelling.

The procedure for the assignment of the BDT value to each seismic zone has been carried out through a GIS software. To this purpose, the mean value of the BDT depth from all the pixels belonging to each block has been calculated by applying the 'zonal statistics' tool in the GIS software, where the raster, from which the pixels values are extracted, is the one of the BDT depth and the blocks are defined on the basis of the SPC2012 seismic zonation polygons.

In order to take into account also the possible errors and the lateral variability of the BDT depth resulting from the rheological modelling, actually, in the calculation of the annual seismic scalar moment release rate, earthquakes occurring within a +5 km depth range below the selected BDT, for each block, have also been considered.

The BDT depths have therefore been associated with every polygon of the seismic zonation, by first assigning them to the corresponding centroid with the 'Extract raster values to points' tool. After that, a join has been created between the centroids and the relative respective polygon, so that each polygon was finally associated with its areally averaged BDT depth value.

The value of the BDT depth is thus stored in a dedicated field of the attribute table of the seismic zonation polygons. In this way, both the area and the vertical thickness of each seismogenic block are readily available and the seismogenic volumes can be easily and directly derived (from them), in order to be inserted and implemented into the formula for the calculation of the seismic strain rates.

As regards the seismicity catalogues, the NOA (National Observatory of Athens) one, covering the period 1964-2016, has been adopted for calculating the annual seismic moment rate, while the NKUA (National Kapodistrian University of Athens) focal mechanisms catalogue has been used for determining the representative strike, dip and rake for each seismic zone.

The seismic strain rates have been calculated for five selected zones: Corinth, Chalkidiki, North Aegean Trough (NAT), Kozani and Kos (fig. 6.7). The selected zones are characterized by different seismicity rates, tectonic regimes and strength envelopes, so that the effect of BDT depth

variations could be evaluated and the variability in the estimates of the strain rates could be representative for the various tectonic domains of the Aegean Region.

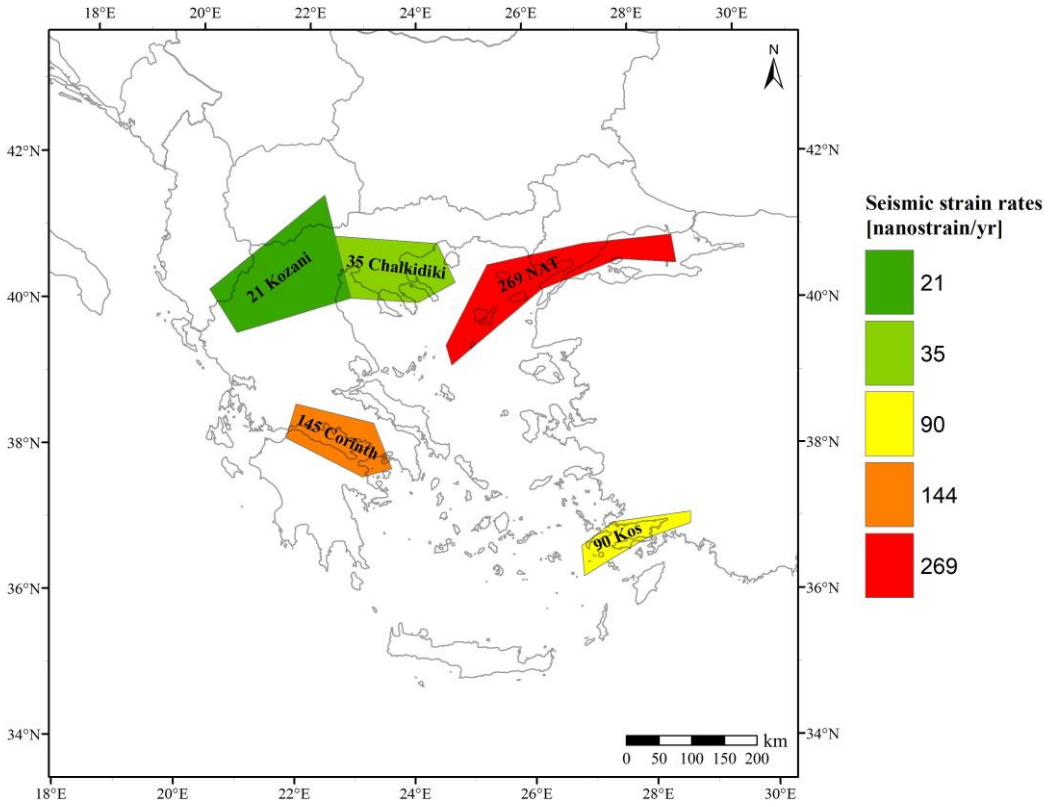

Fig. 6.7 – Values of the second invariant of the seismic strain rate tensor for the selected seismic zones in the Aegean Region.

I focused on the determination of the second invariant of the strain rate tensor (which represents its magnitude), rather than on the orientation of the axes, since the variable BDT depth only influences the absolute values (eigenvalues) of the strain rate tensor (equation [3.2]; see the description in Chapter 3 for details on the second invariant calculation). The parameters needed for applying Kostrov's formula, together with the obtained second invariant values, are shown in table 6.2, for each selected seismic zone.

Seismic zone	***μ [Pa]***	**Area** ***[km²]***	**BDT depth** ***[km]***	**M_0 rate** ***[Nm/yr]***	**2nd Invariant strain rate** ***[nanostrain/yr]***
Corinth	$3 \cdot 10^{10}$	10376.4	15.5	$2.91 \cdot 10^{16}$	144.9
Chalkidiki	$3 \cdot 10^{10}$	14126.9	14.2	$4.55 \cdot 10^{16}$	35.2
Kos	$3 \cdot 10^{10}$	9756.4	10.7	$1.52 \cdot 10^{17}$	90.4
Kozani	$3 \cdot 10^{10}$	23625.4	22.8	$2.62 \cdot 10^{16}$	21.4
North Aegean Trough	$3 \cdot 10^{10}$	19518.9	14.8	$1.25 \cdot 10^{17}$	269.3

Table 6.2 *– Values of the Kostrov's formula parameters for the calculation of the seismic strain rates.*

The obtained distribution of the seismic strain rate second invariants, for the selected seismic zones (fig. 6.7), is in good agreement with the general picture of the deformation rates in the Aegean

Region, with the highest values characterizing the North Aegean Trough and the Corinth Rift zones (*e.g.* Jenny *et al.*, 2004). The obtained values have been compared with the estimates of Papazachos and Kiratzi (1996), who calculated the seismic strain rates on the basis of a slightly different seismic zonation and assuming a constant seismogenic layer thickness of 15 km. Accordingly, the comparison had to be performed for similar, but not coinciding, zones and some differences between the results are therefore expected.

A good fit is found for the zones of Corinth, North Aegean Trough and Kos, with the values obtained in this work being slightly greater than the ones of Papazachos and Kiratzi, possibly because of the different annual seismic moment rates and the varying BDT depths (*i.e.* different thicknesses of the seismogenic layer). A more significant discrepancy is observed for the Chalkidiki zone, mainly because of the different catalogues used for the determination of the seismic moment rates and also because of the different shape of the selected zone in this work with respect to Papazachos and Kiratzi (1996). Some of the misfit may be due to the temporally reduced catalogue used here for the determination of the seismic moment rate, which may result into the lack of an adequate representation of the long-term seismicity rates (see *e.g.* discussion by Rontogianni, 2010).

However, when comparing the seismic strain rates calculated in this study with the geodetic ones used here for the rheological modelling (Kreemer *et al.*, 2014), a general good agreement is found for all the selected zones. The obtained values are indeed always of the same order of magnitude with respect to the geodetic ones, and the minor discrepancies might be attributed to the factors described above (mainly related to the adopted seismic catalogue). Moreover, if the comparison is performed with geodetic strain rates, it should be also taken into account that smaller seismic values with respect to the geodetic ones, as it is observed for the Corinth Rift (see also Chousianitis *et al.*, 2015), might be due to the occurrence of aseismic deformation processes, such as aseismic creep, which contribute only to the geodetically-measured deformation rates.

6.3 Total integrated strength

The total strength, integrated over the lithospheric thickness, can represent a valid tool for determining the long-term resistance of the investigated plate. The Matlab script realized for the rheological modelling also allowed to obtain maps of the total strength for the study area. The main features of the latter, together with the related geodynamic implications, will be discussed in this section.

The map of the total strength for the upper plate (fig. 6.8), measured in $N \cdot m^{-1}$, shows that the highest values, of ca. 30-40 $TN \cdot m^{-1}$, are attained in the Cretan Sea region, and along the border area between Albania, Greece and FYROM, at the transition between the Albanides and Hellenides. In the continental region, the elevated total strength value is mainly due to the low geothermal gradient

characterizing the area. Indeed, reduced temperatures at depth may lead to a very resistant lithosphere, where the majority of the crust behaves in a brittle fashion and also the mantle, even though deforming in a ductile way at greater depths, would retain a considerable long-term strength.

In the case of the high total strength region in the Cretan Sea, the surface heat flow, even though lower than in the close central Aegean Sea and around the Cyclades islands, indicates a moderate geothermal gradient, which would not be sufficient to explain high strength values down to the mantle. The cause for such a resistant mechanical behaviour, then, should be also looked for in the occurrence at intermediate depths (around 60-70 km) of the lower oceanic plate.

Indeed, according to the thermal subduction model discussed in Chapter 3 (section §3.2.2), the old and cold oceanic subducting lithosphere would cause a thermal perturbation also in the lowest part of the upper plate, thus resulting locally in a temperature decrease with depth. Such a decrease would allow the mantle layer of the overriding plate to retain some mechanical strength even when the original undisturbed gradient (as indicated by the surface heat flow) would imply, at the same considered depths, temperature conditions high enough for approaching a zero strength value.

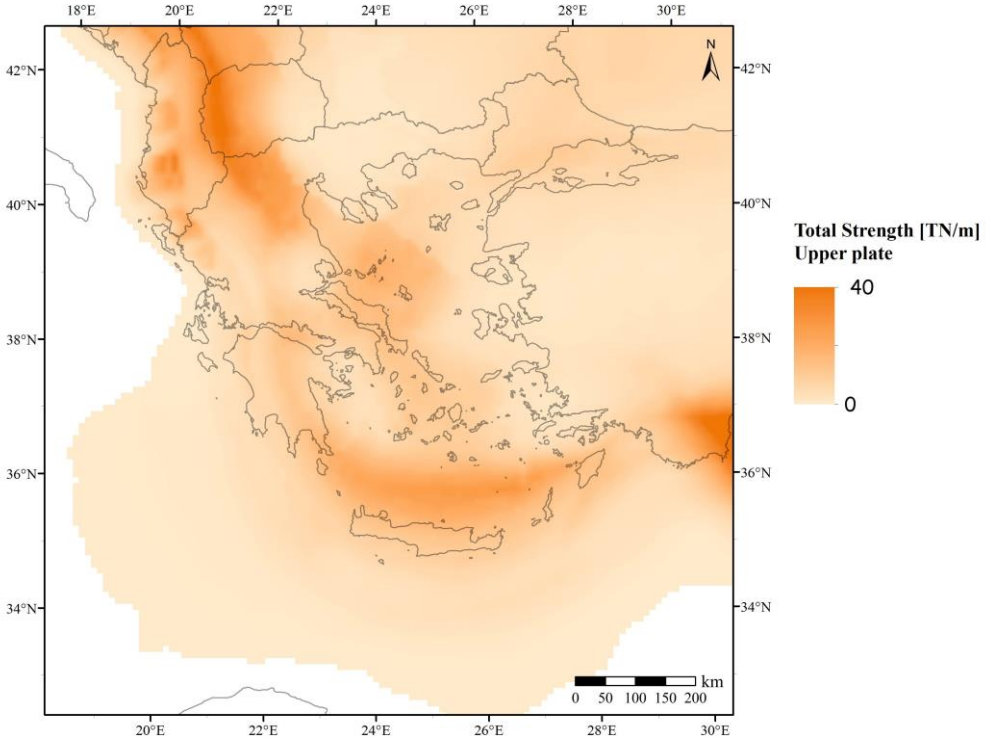

Fig. 6.8 – Map showing the distribution of the total strength of the upper plate over the study area

Clearly, when the surface heat flow (see fig. 3.2) presents very high values (above ca. 80-90 $mW \cdot m^{-2}$), its effect on the geothermal gradient is predominant and the integrated strength resides almost solely in the upper brittle layers, as it is the case of the Saronic Gulf, Attica and southern Thessaly regions, where the total strength values are in the order of 3-10 $TN \cdot m^{-1}$. In the remaining sectors of the study area (central and northern Aegean Sea, Macedonia, Thrace), which are located

in more internal positions with respect to the Hellenic subduction zone, the subducting slab is generally too deep to cause any thermo-rheological effect on the total strength of the upper plate.

Accordingly, in these regions, the variations of the integrated strength values, which anyway always remain quite low or moderate (generally in the range 1-20 $TN \cdot m^{-1}$), are mainly dependent on the upper plate geothermal gradient and therefore a good correlation of the total strength values can be observed with the surface heat flow values distribution. For instance, in the northern Aegean Sea, the westernmost sector northwest of Skyros, which is associated with relatively lower (~65 $mW \cdot m^{-2}$) heat flow values (with respect to the adjacent regions), is also characterized by a moderate integrated strength, with maximum values up to ca 20 $TN \cdot m^{-1}$.

On the contrary, the high heat flow (values around 100 $mW \cdot m^{-2}$) areas of central-eastern Aegean Sea, Western Anatolia, Chalkidiki and Central-Eastern Macedonia are associated with average/low values of total strength, being ~1.5-2 $TN \cdot m^{-1}$, with the minimum value attained in Eastern Macedonia, equal to ~0.6 $TN \cdot m^{-1}$.

The map in fig. 6.8 also allows to propose some speculations about the relationsphis between total strength and observed kinematics and current geodynamic processes. Indeed, it can be observed that the majority of the upper plate is associated with moderate-to-low total strength values, which may explain the distributed style of deformation characterizing the Aegean Region, with diffuse and frequent seismicity spread all over continental Greece and northern Aegean. The area with higher integrated strength values in the central-southern Aegean Sea is instead associated with much lower seismicity rates and also, by a kinematic point of view, tends to translate and rotate as a coherent block, rather than internally deform, thus possibly indicating and confirming the role of the high total strength in hindering internal deformation.

The map of the total strength of the lower plate (fig. 6.9), calculated down to the depth of the LAB (lithosphere-astenosphere boundary), indicates that generally lower values characterize the oceanic lithosphere, being around 25-30 $TN \cdot m^{-1}$, with respect to the integrated strength of the continental sectors of the lower plate corresponding to the regions of Apulia and Cyrenaica. In the latter regions indeed, the total strength values fall in the range 50-60 $TN \cdot m^{-1}$, even greater than what observed for the upper plate.

The reasons for this greater integrated strength of the continental lithosphere of the lower plate with respect to the upper one are mainly explained by the low geothermal gradient characterizing the lower plate and by its compressional tectonic regime (as counterposed to the mainly extensional and transtensional ones of the overriding plate), which allows greater strength to be stored especially in the brittle portion of the lithosphere.

As for the total strength discrepancy between the oceanic and continental sectors of the lower plate, the lesser values of the former with respect to the latter, given the similar tectonic and geothermal conditions, are mainly due to the reduced thickness of the oceanic lithosphere (~ 65-70

km) as compared to the continental one (being around 100-130 km). Indeed, a smaller lithospheric thickness is intuitively reflected in a lesser ability of the considered plate of sustaining applied tectonic stresses and loads, especially in terms of long-term resistance to permanent deformation.

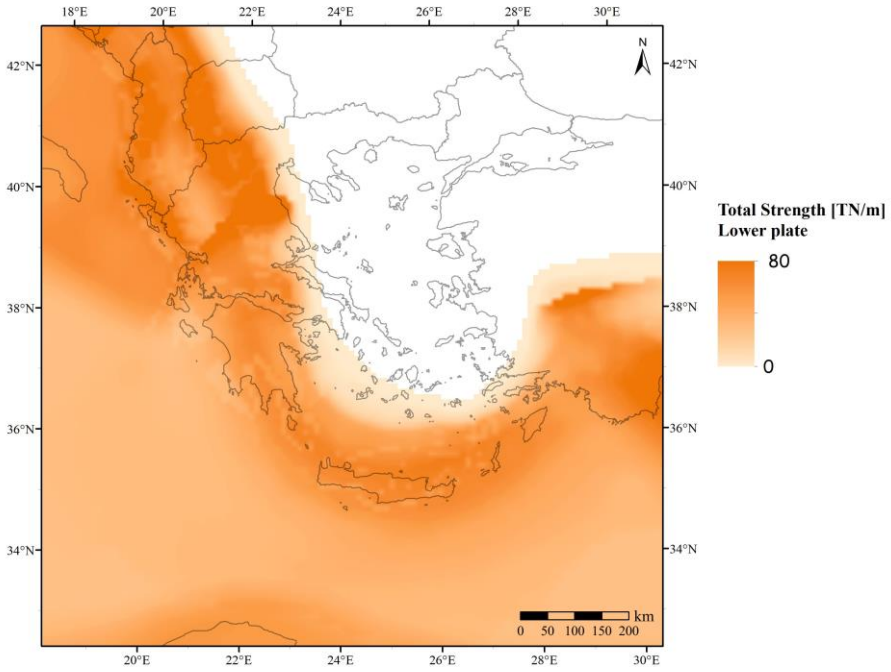

Fig. 6.9 – Map showing the distribution of the total strength of the lower plate over the study area

Additional maps representing the combined total strength of the crustal layers have been also realized for both the upper and the lower plates and are shown in figures 6.10 and 6.11. The crustal total strength can be compared with the total strength, in order to assess the amount of contribution and the relative weight of the mantle strength to the total lithospheric ability of sustaining tectonic stresses and loads.

In this view, such a comparison constitutes a further tool and method that can be applied to determine the mechanical behaviour of the different lithospheric layers and to tentatively assign a representative typology of strength envelope (*jelly sandwich, crème bruleé, caramel slab*, etc.) to each different lithospheric domain (continental, oceanic, transitional).

The total crustal strength in the upper plate shows its maxima along the coastal and close hinterland sectors of Albania and northwestern Greece, with values up to ca 25 $TN \cdot m^{-1}$. Such elevated values result from the low geothermal gradient and the compressional tectonic setting, which leads to a considerable storing of strength in the shallow brittlely deforming layers that mostly correspond to the crust. The lowest values are instead observed in the central-eastern Aegean Sea region, closely mirroring the distribution of the upper plate total strength values (see fig. 6.8).

In the lower plate instead, when considering exclusively the unsubducted sectors, the total crustal strength maximum values are found in the continental platform of Apulia, being around 18-20 $TN \cdot m^{-1}$. On the contrary, the minimum values are observed in the oceanic lithosphere sectors, with values comprised in the range 4-5 $TN \cdot m^{-1}$. Such a distribution of crustal strength values for

the lower plate is a direct consequence of the crustal thickness, which is almost double for the continental Apulian region with respect to the oceanic one.

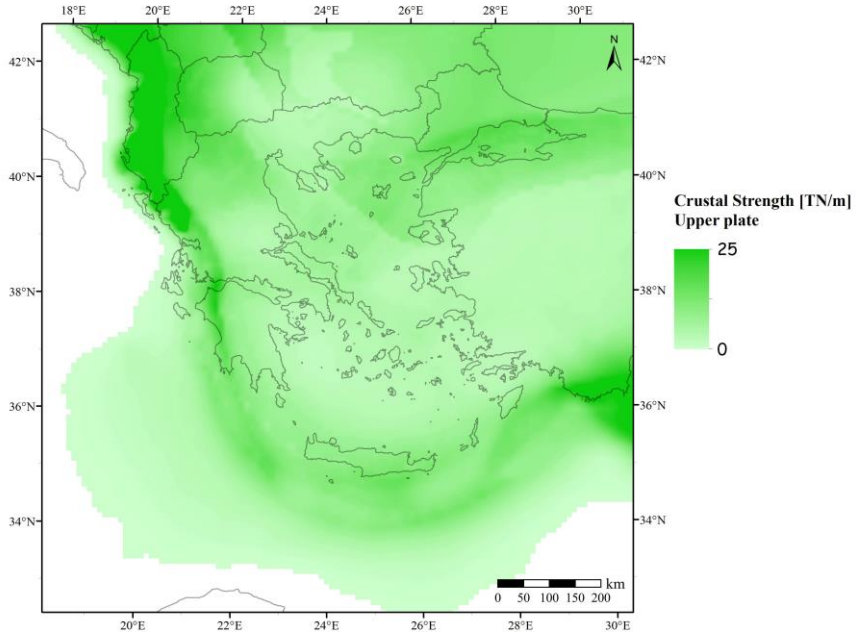

Fig. 6.10–Map showing the distribution of the total crustal strength of the upper plate over the study area.

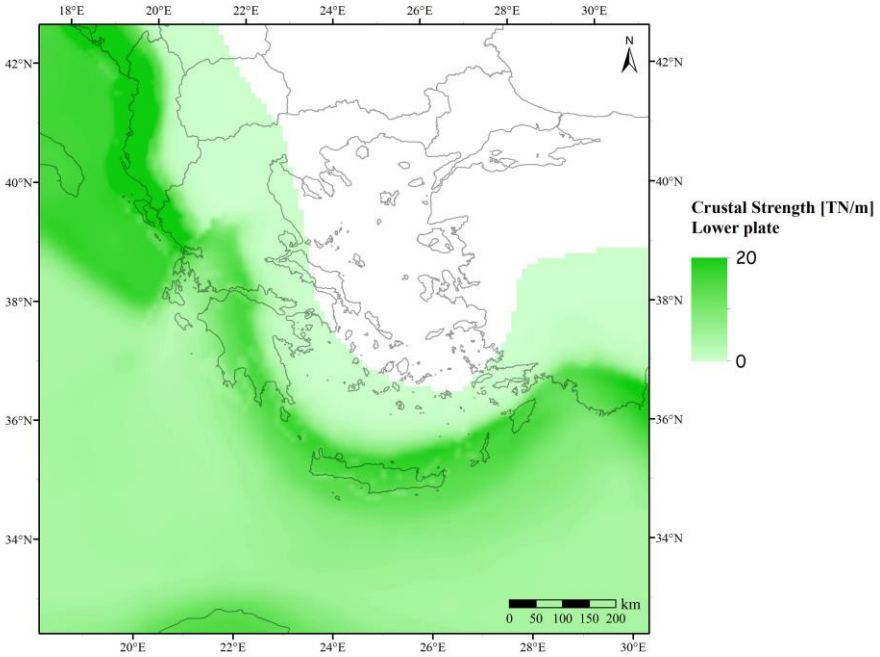

Fig. 6.11–Map showing the distribution of the total crustal strength of the lower plate over the study area.

Finally, the contribution of the mantle to the total integrated strength, expressed in terms of percentage, has been calculated by subtracting the crustal integrated strength to the total one and then by normalizing the results. The resulting map (fig. 6.12) indicates that a large percentage, comprised between 80 and 95%, of the total strength actually resides within the mantle layer for

the majority of the Aegean Sea, and also in the eastern sectors of Peloponnesus and in Attica, Thessaly and Macedonia regions.

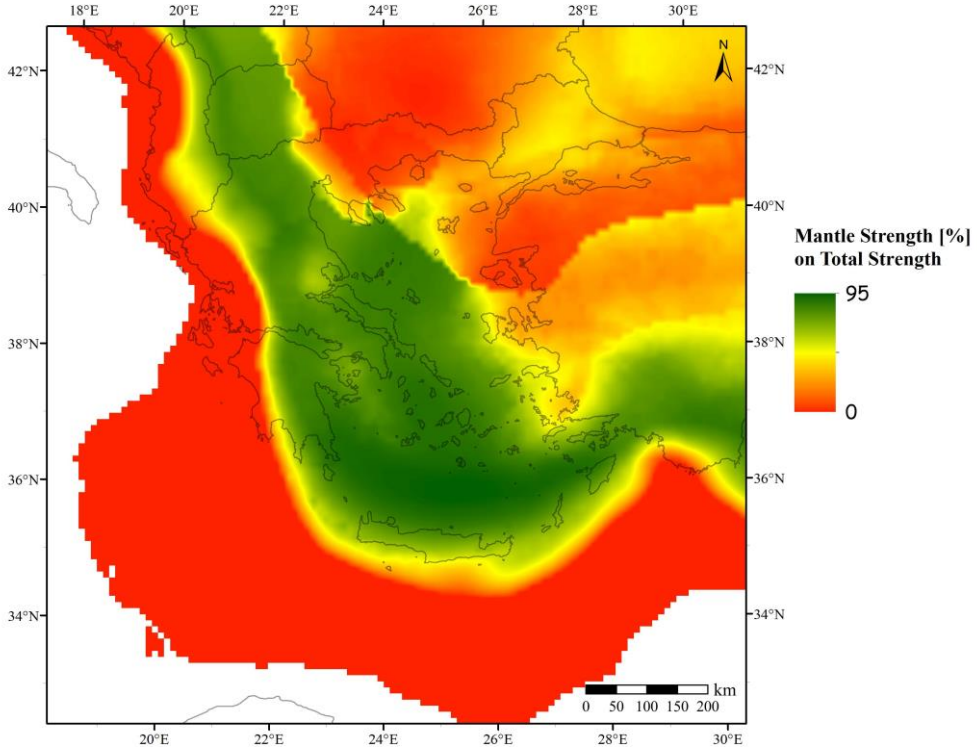

Fig. 6.12– Map showing the distribution of the mantle strength as a percentage with respect to the total integrated strength, over the study area.

It should be noted, however, that such a deep contribution of the mantle layer to the total strength does not necessarily imply that brittle processes occur at those depths. Indeed, such a contribution is expected to result, at least in part, from ductile strength accumulation.

Indeed, the latter does not approach the zero value at depth, but on the contrary tends to increase because of the presence of the old and cold oceanic slab at depth, which decreases the geothermal gradient and consequently increases the ductile strength.

Chapter 7: Conclusions

7.1 Summary and concluding remarks

The present research allowed developing and proposing a new comprehensive 3D thermo-rheological model of the Aegean Region. Literature data, together with tectonic and geodynamic considerations (Chapters 1, 2 and 3) and, to a minor extent, field observations, have been used to reconstruct the mechanical-rheological stratification of the lithosphere(s) in the investigated area. The two prevailing deformation styles (brittle and ductile), associated to the frictional sliding and power law creep behaviours (Chapter 2), have been considered and applied in order to generate 1D rheological profiles for selected test sites. In a second phase, 2D transects have been realized, which allowed to compare the rheological properties of the Aegean Region in its different tectonic domains, such as continental collision, oceanic subduction and back-arc extensional setting, thus taking into account the lateral variability of lithologies and thermophysical properties.

The last step in the modelling process corresponded to the reconstruction of the three-dimensional model, providing maps of the BDT depth, strength and temperature. The 3D model allowed also to estimate the integrated strengths (total, crustal, mantle, brittle and ductile) of the upper and lower plates. The rheological models realized for this study confirmed that, following a careful selection of the input parameters values of the constitutive equations and of the deformation processes, rheological modelling can represent a useful tool for defining and constraining the depth of the potentially seismogenic layer. In particular, in a very seismically active region as it is the broader Aegean Region, the map of the modelled BDT depth can be applied as a constraint to determine the width of the seismogenic layer and its lateral variations, thus contributing to define the maximum expected magnitudes of the main seismogenic sources.

I will now proceed with a brief recall of the main results of this research and their possible important applications to the fields of seismotectonics and geodynamics. First of all, it may be useful to recall the main outcomes of the sensitivity tests (Chapter 4) that have been performed on the various input parameters of the constitutive rheological equations, in order to determine their relative weight on the resulting deformation processes. The sensitivity analysis regarded both the rheological parameters (power-law creep equation parameters, thermal activation energy, strain rate, pore fluid pressure ratio, density, friction coefficient, tectonic parameter) and the thermal ones (surface heat flow, thermal conductivity and radiogenic heat production). The tests have been performed by varying the values of the input parameters within their uncertainty range, in order to verify how much those variations may impact on the resulting rheological model. The sensitivity analysis has been carried out, firstly, by testing each parameter singularly and then also by combining their variations to investigate their potential synergistic effects. The results indicate that

the thermal parameters, and in particular the surface heat flow and thermal conductivity, together with the thermal activation energy from the power-law creep equation, are the most influential ones, especially for what concerns the BDT depth. When considering the effects on the BDT strength, additional parameters should be taken into account, such as those related to the frictional sliding equation, like the pore fluid pressure, the friction coefficient and the tectonic regime parameter.

The analysis of the sensitivity has been performed on two selected test sites of the Aegean Region (Kallidromo and Kefallinia), belonging to different tectonic domains (respectively extensional and transpressional) and geodynamic settings. The results of the sensitivity analysis at the two test sites confirmed the reliability and stability of the values of the main thermo-rheological modelling indicators (namely BDT depth, strength and temperature), when varying the input parameters values within their relative uncertainties. Such a result indicate that, notwithstanding the intrinsic uncertainties and potential errors associated with rheological modelling, the latter, when performed after a careful selection of the input parameters values, can effectively and reliably describe the mechanical features of the investigated site, also in terms of potential seismogenic behaviour. Indeed, in the two selected sites, also a comparison of the obtained rheological models, especially in terms of brittle layer thickness, with the depth distribution of local seismicity has been carried out, showing a good fit.

After having tested the variability of the input parameters and their role and weight on the resulting rheological modelling, 1D strength envelopes have been realized for numerous test sites all over the Aegean Region (see the dedicated section in Chapter 5 and Appendix A). The strength envelopes that have been reconstructed represent different typologies of rheological profiles, in agreement with the diverse geodynamic and tectonic settings. Accordingly, the test sites in the offshore region belonging to the African/Nubian oceanic lithosphere of the lower plate are associated with deep BDTs and a *caramel slab* shape of rheological profiles. On the contrary, the strength envelopes of the test sites in continental Greece and Aegean Sea regions, characterized by extensional tectonics and continental lithosphere, generally mimic the *crème bruleé* type of profile. One relevant conclusion that can be drawn from the analysis of these 1D strength envelopes, and especially from their comparison with the distribution at depth of seismicity, is the observation of a good fit when well-relocated seismic events distribution is taken into account. Accordingly, this study suggests that routinely located seismic events may not be suitable for precise analysis of the corresponding rheological behaviour, in terms of the depth of seismogenesis and seismic rupture process propagation. On the contrary, relocated seismicity and in particular the depth within which 90% or 95% of the events occurred can be used for a direct comparison with the depth of the BDT indicating the bottom of the seismogenic layer.

The realization of several 2D rheological transects (Chapter 5, section §5.2), across various geodynamic and tectonic domains, allowed to distinguish the typical and representative mechanical-rheological features and also to analyze the lateral variability and/or continuity of the

BDT depth, strength and temperature. In particular, the 2D transects highlight the different rheological stratification in the continental collision with respect to the oceanic subduction domains (fig. 5.19). The former is indeed characterized, especially in its hinterland sectors, by a second deeper brittle layer, which is instead absent in the back-arc regions of the latter. A further observation and general rule that can be drawn from the realization of the 2D models is the possibility to recognize the main role played by the surface heat flow and the tectonic regime parameter in determining, respectively, the depth of the BDT, regardless of any other factor, and the associated strength.

In particular, the transects crossing the oceanic subduction zone and the accretionary wedge are characterized by a very deep BDT (around 40 km) in the external southwestern sectors and, on the contrary, by a shallow transition and very low strength in the northeastern sectors, where the extensional tectonics (back-arc region) prevails and an elevated geothermal gradient affects the area. Furthermore, from the analysis of the realized transects, it can be observed that the values of the main thermo-rheological parameters (BDT depth, strength and temperature) change abruptly when, moving from west to east (*i.e.* from the external sectors to the internal back-arc regions), the BDT shifts from the lower plate to the upper one (figures 5.14 and 5.15). Moving from the northwest to the southeast, across the Kefallinia Transform Fault, even though a quite sharp boundary in terms of the lithospheric nature (from continental to oceanic) and the crustal structure is crossed, the variations in the BDT depth and associated strength and temperature are not as relevant as along the transects orthogonal to the Hellenides, mainly because of an almost uniform thermal regime (fig. 5.16). Accordingly, these 2D features evidence once again the crucial role played by geothermal gradient variations in determining the resulting rheological characteristics and lateral differences.

The 3D rheological model of the study area (Chapter 5, section §5.3) has been obtained after a careful selection of the data sources, for the construction of the areal layers of the input parameters values. Particular care has been devoted to the creation of a weighted and averaged heat flow map for the Aegean Region (Chapter 3, figures 3.1 and 3.2), also taking into account the importance of such data for the geothermal gradient and the resulting rheological structure, as found out from the 1D tests and 2D transects. Also, the geometry of the crustal and lithospheric structures, in particular around the Hellenic subduction zone, has been thoroughly reconstructed by considering different sources of data (Chapter 3). Moreover, a specific section of the Matlab script used for the 3D model realization has been implemented in order to describe the thermal perturbation associated to the slab subduction process (Chapter 3, fig. 3.16).

The 3D model allowed reconstructing several maps, such as the BDT depth (fig. 5.22), strength (5.23) and temperature (5.24) and also the total integrated strength (fig. 6.8 and followings). Based on different distributions of pore fluid pressure, friction coefficient and surface heat flow, several 3D models have been realized. Although some differences do occur, all the models show similar

large-scale characteristics and comparable features for the main rheological indicators. In general, the BDT depth over the study area has a maximum depth of ca. 60-70 km close to the Hellenic subduction zone, within the downgoing slab, while in the unsubducted sectors the lower plate is characterized by BDT depths of ca. 40 km for the oceanic lithosphere and around 35 km in the continental one. Analyzing the 3D BDT depth map (fig. 5.22), the rheological transition is observed to shallow up within the upper plate in the back-arc Aegean Sea region and in most of continental Greece, at depths generally between 10 and 15 km. The main variations in the BDT depth are once again related to local changes in the geothermal gradient and in the dominant tectonic regime. The latter also represents an influential factor for the BDT strength values, whose distribution (fig. 5.23) emphasizes the occurrence of the largest values in regions affected by compressional tectonics (and associated to oceanic lithosphere).

Furthermore, and taking into account the assumed simplifications necessary for the modelling procedure, the 3D rheological models of the Aegean Region realized during this reasearch document a good correspondence between the reconstructed rheological stratification and the occurrence of seismic activity. This is confirmed by comparing the extent at depth of the brittle layer with the depth distribution of seismicity in the Aegean Region. Clearly, some detail is lost in the large-scale modelling, as some data lack the necessary resolution for perfectly describing the lateral variations in such a wide area; nonetheless, the general picture offered by the 3D thermo-rheological modelling and its results fit quite well with the main kinematic, tectonic and geodynamic features of the Aegean Region.

Moreover, the realization of the 3D model highlighted how the availability of a broader general picture of the rheological properties, over a certain region, can help avoiding the misinterpretation of local-scale 1D models, which are subjected to potential errors and uncertainties. Indeed, as shown in figures 5.25-5.27 and 5.29-5.31, if only a single 1D modelled profile is considered for a rheological study over a wider area, for particular combinations of the input parameters values, remarkably different results could be obtained within the investigated area. The added value brought by the 3D model is, then, to provide a broader view and framework on the local and large scale trends of the main rheological properties, thus enabling to better interpret and evaluate the plausibility and reliability of the modelling results.

The outputs of the 3D model have been applied: i) to obtain seismotectonic inferences on the main seismogenic sources of the study area; ii) for the calculation of seismic strain rates and iii) also for considerations on the large-scale, long-term lithospheric behaviour in terms of deformation processes related to the evolution of the kinematic and tectonic setting of the broader Aegean Region (Chapter 6).

In particular, the BDT depth has been adopted as a constraint for determining the width of the main seismogenic sources in the study area (*e.g.* Caputo and Pavlides, 2013) and, using different

empirical relationships, new independent values of the maximum expected magnitude for each source have been estimated.

The depth extent of the brittle layer, as determined by the 3D rheological modelling, also allowed to better define the volumes for calculating the strain rates, based on the Kostrov method. Such an approach has been applied to selected seismically deforming zones in the Aegean Region. (fig. 6.7).

Finally, the distribution of the total integrated strength over the investigated area has been estimated and it could be adopted as a tool to determine the long-term strength of the lithospheric plates (Aegean microplate and Nubian/African plate) and the related implications for the geodynamic processes, occurring over the Aegean Region.

7.2 Future developments

The rheological models realized in this work could find applications in other fields, such as, for instance, the study of the relationship between total integrated strength of the lithosphere and its elastic thickness. Such models could also lead to speculations on their significance for the long-term ability of the lithosphere to support tectonic and/or non-tectonic loads. However, such themes are far beyond the primary scopes of this work, which sets its focus mainly on the rheology of the crust and its relationship with seismogenesis.

From a methodological point of view, the procedure followed together with the methods and, above all, the Matlab code purposely developed during this research, could be applied also to other study areas. The code indeed, given its rationale and structure, could be easily modified in order to cover a wider region or a smaller one. To this point, if there is a need to zoom into one limited and specific area and enhance the resolution grid for the rheological modelling, the code can also readily provide the tools for decreasing the grid size and obtaining much higher resolution models.

The code itself, however, could also be enhanced in the future by including, for example, the vertical variations of the pore fluid pressure ratio or the tectonic regime parameter. Indeed, the former, in the current version of the code, is only allowed to vary areally for computational time reasons, even though variations at depth could be implemented if necessary and that may be worth in peculiar settings, especially where the fluid pressure is expected to vary substantially along the vertical direction. The tectonic regime, instead, currently varies along the vertical dimension, only from the upper plate to the lower plate. Provided that enough high-resolution information about the stress state and the prevailing tectonic regime are available, a more detailed vertical variation of the tectonic-related parameter could be possibly included in a future version of the code.

References

Abers G. A. (2009): Slip on shallow-dipping normal faults. *Geology*, **37**(8), 767-768.

Afonso J.C. and Ranalli G. (2004): Crustal and mantle strengths in continental lithosphere: is the jelly sandwich model obsolete? *Tectonophys.*, **394**(3-4), 221-232.

Akın U., Ulugergerli E. U. and Kutlu S. (2014): The assessment of geothermal potential of Turkey by means of heat flow estimatıon. *Bull. Mineral Res. Explor.*, **149**, 201-10.

Allen J. L. and Shaw C. A. (2011): Seismogenic structure of a crystalline thrust fault: Fabric anisotropy and coeval pseudotachylyte–mylonitic pseudotachylyte in the Grizzly Creek shear zone, Colorado. *Geol. Soc. London, Spec. Publ.*, **359**(1), 135-151.

Altinok Y., Alpar B., Özer N. and Gazioglu C. (2005): 1881 and 1949 earthquakes at the Chios-Cesme Strait (Aegean Sea) and their relation to tsunamis. *Nat. Hazard. Earth Sys.*, **5**(5), 717-725.

Amato A., Bianchi I. and Agostinetti N. P. (2014): Apulian crust: Top to bottom. *J. Geodyn.*, **82**, 125-137.

Ambraseys N. (2009): *Earthquakes in the Mediterranean and Middle East: A Multidisciplinary Study of Seismicity up to 1900*. Cambridge University Press, pp. 968.

Angelier J., Lyberis N., Le Pichon X., Barrier E. and Huchon P. (1982): The tectonic development of the Hellenic arc and the Sea of Crete: a synthesis. *Tectonophys.*, **86**(1-3), 159-196.

Armijo R., Meyer B., King G.C.P., Rigo A. and Papanastassiou D. (1996): Quaternary evolution of the Corinth Rift and its implications for the Late Cenozoic evolution of the Aegean. *Geophys. J. Int.*, **126**, 11-53.

Artemieva, I. (2011). *Lithosphere: an interdisciplinary approach*. Cambridge University Press, pp. 773.

Artemieva I. M., Thybo H., and Kaban M. K. (2006): Deep Europe today: geophysical synthesis of the upper mantle structure and lithospheric processes over 3.5 Ga. *Memoirs Geol. Soc. London*, **32**, 11-41.

Aubouin J. (1959): Contribution à l'étude géologique de la Grèce septentrionale: Les confines de l'Épire et de la Théssalie. *Ann. Géol. Pays Hell.*, **10**, 1-525.

Audet P. and Bürgmann R. (2014): Possible control of subduction zone slow-earthquake periodicity by silica enrichment. *Nature*, **510**(7505), 389-392.

Avallone A., Briole P., Agatza-Balodimou A. M., Billiris H., Charade O., Mitsakaki C., Nercessian A., Papazissi K., Paradissis D. and Veis G. (2004): Analysis of eleven years of deformation measured by GPS in the Corinth Rift Laboratory area. *Comptes Rendus Geoscience*, 336(4-5), 301-311.

Barr S. R., Temperley S. and Tarney J. (1999): Lateral growth of the continental crust through deep level subduction–accretion: a re-evaluation of central Greek Rhodope. *Lithos*, **46**(1), 69-94.

Beardsmore G.R. and Cull J.P. (2001): *Crustal heat flow: a guide to measurement and modelling*. Cambridge University Press, 413 pp.

Becker J.J., Sandwell D.T., Smith W.H.F., Braud J., Binder B., Depner J., Fabre D., Factor J., Ingalls S., Kim S.-H., Ladner R., Marks K., Nelson S., Pharaoh A., Trimmer R., Von Rosenberg J., Wallace G. and Weatherall P. (2009): Global bathymetry and elevation data at 30 arc seconds resolution: SRTM30_PLUS. *Marine Geodesy*, **32**(4), 355-371.

Beeler N. M., Hirth G., Tullis T. E. and Webb C. H. (2018): On the depth extent of coseismic rupture. *Bull. Seismol. Soc. Am.*, **108**(2), 761-780.

Bell R. E., McNeill L. C., Bull J. M., Henstock T. J., Collier R. L. and Leeder M. R. (2009): Fault architecture, basin structure and evolution of the Gulf of Corinth Rift, central Greece. *Basin Res*., **21**(6), 824-855.

Benedetti L., Finkel R., Papanastassiou D., King G., Armijo R., Ryerson F., Farber D. And Flerit F. (2002): Post-glacial slip history of the Sparta fault (Greece) determined by 36Cl cosmogenic dating: evidence for non-periodic earthquakes. *Geophys. Res. Lett.*, **29**(8), 87-1/87-4.

Benetatos C., Roumelioti Z., Kiratzi A. and Melis N. (2002): Source parameters of the M 6.5 Skyros island (North Aegean Sea) earthquake of July 26, 2001. *Ann. Geophys*., **45**(3-4).

Bernard P., Lyon-Caen H., Briole P., Deschamps A., Boudin F., Makropoulos K., Papadimitriou P., Lemeille F., Patau G., Birillis H., Paradissis D., Papazissi K., Castarede H., Charade O., Nercessian A., Avallone A., Pacchiani F., Zahradnik J., Sacks S. and Linde A. (2006): Seismicity, deformation and seismic hazard in the western rift of Corinth: New insights from the Corinth Rift Laboratory (CRL). *Tectonophys.*, **426**(1-2), 7-30.

Billiris H., Paradissis D., Veis G., England P., Featherstone W., Parsons B., Cross P., Rands P., Rayson M., Sellers P., Ashkenazi V., Davison M., Jackson J. and Ambraseys N. (1991): Geodetic determination of tectonic deformation in central Greece from 1900 to 1988. *Nature*, **350**(6314), 124.

Birch F. and Clark H. (1940): The thermal conductivity of rocks and its dependence upon temperature and composition. *Am. J. Sci.*, **238**(8), 529-558.

Bocchini G. M., Brüstle A., Becker D., Meier T., van Keken P. E., Ruscic M., Papadopoulos G.A:, Rische M and Friederich W. (2018): Tearing, segmentation, and backstepping of subduction in the Aegean: New insights from seismicity. *Tectonophys*., **734**, 96-118.

Boncio P. (2008): Deep-crust strike-slip earthquake faulting in southern Italy aided by high fluid pressure: insights from rheological analysis. *Geol. Soc. London, Spec. Publ.*, **299**(1), 195-210.

Boncio P., Mancini T., Lavecchia G. and Selvaggi G. (2007): Seismotectonics of strike–slip earthquakes within the deep crust of southern Italy: Geometry, kinematics, stress field and crustal rheology of the Potenza 1990–1991 seismic sequences (Mmax 5.7). *Tectonophys.*, **445**(3-4), 281-300.

Bonneau M. (1973): Sur les affinités ioniennes des calcaires en plaquettes épimetamorphiques de la Crete, le charriage de la série de Gavrovo-Tripolitza et la structure de l'arc égéen. *C.R. Acad. Sci*., **277**, 2453-2456.

Bos B. and Spiers C.J. (2002): Frictional-viscous flow of phyllosilicate-bearing fault rock: Microphysical model and implications for crustal strength profiles. *J. Geophys. Res*., **107**(B2), doi:10.1029/2001JB000301.

Bozkurt E. (2000): Timing of extension on the Büyük Menderes Graben, western Turkey, and its tectonic implications. *Geol. Soc. London, Spec. Publ.,* **173**(1), 385-403.

Bozkurt E. (2001): Neotectonics of Turkey–a synthesis. *Geodin. Acta*, **14**(1-3), 3-30.

Brace W.F. and Byerlee J.D. (1966): Stick-slip as a mechanism for earthquakes. *Science*, **153**, 990-992.

Brace W.F. and Kohlstedt D.L. (1980): Limits on lithospheric stress imposed by laboratory experiments. *J. Geophys. Res*., **85**(B11), 6248-6252.

Briole P., Rigo A., Lyon-Caen H., Ruegg J. C., Papazissi K., Mitsakaki C., Balodimou A., Veis G., Hatzfeld D. and Deschamps A. (2000): Active deformation of the Corinth rift, Greece: results from repeated Global Positioning System surveys between 1990 and 1995. *J. Geophys. Res*., **105**(B11), 25605-25625.

Brunn J.H. (1956): Contribution à l'étude géologique du Pinde septentrional et d'une partie de la Macédoine occidentale. *Ann. Géol. Pays Héll*., 1, **VII**, 1-358.

Burchfiel B. C., Royden L. H., Papanikolaou D. and Pearce F. D. (2018): Crustal development within a retreating subduction system: The Hellenides. *Geosphere*, **14**(3), 1119-1130.

Bürgmann R. and Dresen G. (2008): Rheology of the lower crust and upper mantle: Evidence from rock mechanics, geodesy, and field observations. *Annu. Rev. Earth Planet. Sci*., **36**, 531-567.

Burov E. B. (2011): Rheology and strength of the lithosphere. *Mar. Petrol. Geol.*, **28**(8), 1402-1443.

Burov E.B. and Diament M. (1995): The effective elastic thickness (T e) of continental lithosphere: what does it really mean?. *J. Geophys. Res.*, **100**(B3), 3905-3927.

Burov E., François T., Agard P., Le Pourhiet L., Meyer B., Tirel C., Lebedev S., Yamato P. and Brun J. P. (2014): Rheological and geodynamic controls on the mechanisms of subduction and HP/UHP exhumation of crustal rocks during continental collision: Insights from numerical models. *Tectonophys*., **631**, 212-250.

Byerlee J.D. (1968): Brittle-ductile transition in rocks. *J. Geophys. Res.*, **73**(14), 4741-4750.

Byerlee J.D. (1978): Friction of rocks. In: EDITORS, *Rock friction and earthquake prediction*, 615-626, Birkhäuser, Basel.

Byrne D.E., Davis D.M. and Sykes L.R. (1988): Loci and maximum size of thrust earthquakes and the mechanics of the shallow region of subduction zones. *Tectonics*, **7**(4), 833-857.

Caputo M., Panza G. F. and Postpischl D. (1970): Deep structure of the Mediterranean basin. *J. Geophys. Res*., **75**(26), 4919-4923.

Caputo R. (1996): The active Nea Anchialos Fault System (Central Greece): comparison of geological, morphotectonic, archaeological and seismological data. *Ann. Geofisica*, **39**(3), 557-574.

Caputo R. (2005): Stress variability and brittle tectonic structures. *Earth-Science Reviews*, **70**(1-2), 103-127.

Caputo R. and Pavlides S. (1993): Late Cainozoic geodynamic evolution of Thessaly and surroundings (central-northern Greece). *Tectonophys.*, **223**(3-4), 339-362.

Caputo R. and Pavlides S. (2013): *The Greek Database of Seismogenic Sources (GreDaSS), version 2.0.0: A compilation of potential seismogenic sources (Mw > 5.5) in the Aegean Region.* http://gredass.unife.it/, doi: 10.15160/unife/gredass/0200.

Caputo R., Catalano S., Monaco C., Romagnoli G., Tortorici G. and Tortorici L. (2010): Active faulting on the island of Crete (Greece). *Geophys. J. Int.*, **183**, 111-126.

Caputo R., Chatzipetros A., Pavlides S. and Sboras S. (2012): The Greek Database of Seismogenic Sources (GreDaSS): state-of-the-art for northern Greece. *Ann. Geophys.*, **55**(5), 859-894, doi: 10.4401/ag-5168.

Carpenter B.M., Marone C. and Saffer D.M. (2011): Weakness of the San Andreas Fault revealed by samples from the active fault zone. *Nature Geoscience*, **4**(4), 251-254, doi: 10.1038/ngeo1089.

Carter N. L., Christie J. M. and Griggs D. T. (1964): Experimental deformation and recrystallization of quartz. *The Journal of Geology*, **72**(6), 687-733.

Carter N. L., Anderson D. A., Hansen F. D. and Kranz R. L. (1981): Creep and creep rupture of granitic rocks. *Geoph. Monog.*, **24**, 61-82.

Carter N.L. and Tsenn M.C. (1987): Flow properties of continental lithosphere. *Tectonophys.*, **136**, 27-63.

Čermák V. (1982): Crustal temperature and mantle heat flow in Europe. *Tectonophys.*, **83**, 123-142.

Čermak V. and Rybach L. (1982): *Thermal properties: thermal conductivity and specific heat of minerals and rocks*. Physical Properties of Rocks, 305–343, ed. Angenheister G., Springer.

Chapman D. S. (1986): Thermal gradients in the continental crust. *Geol. Soc. London Spec. Publ.*, **24**(1), 63-70.

Chatzipetros A., Pavlides S. and Mourouzidou O. (2004): Re-evaluation of Holocene earthquake activity in Mygdonia basin, Greece, based on new paleoseismological results. 5th Intern. Symp. Eastern Mediterranean Geology, April 14-20, 2004, Thessaloniki, Greece. *Proceedings*, **2**, 920-925.

Chatzipetros A., Kiratzi A., Sboras S., Zouros N. and Pavlides S. (2013): Active faulting in the north-eastern Aegean Sea Islands. *Tectonophys.*, **597**, 106-122.

Chen W. P. and Molnar P. (1983): Focal depths of intracontinental and intraplate earthquakes and their implications for the thermal and mechanical properties of the lithosphere. *J. Geophys. Res.*, **88**(B5), 4183-4214.

Chen W. P., Hung S. H., Tseng T. L., Brudzinski M., Yang Z. and Nowack R. L. (2012): Rheology of the continental lithosphere: progress and new perspectives. *Gondwana Res.*, **21**(1), 4-18.

Chen W. P., Yu C. Q., Tseng T. L., Yang Z., Wang C. Y., Ning J., and Leonard T. (2013): Moho, seismogenesis, and rheology of the lithosphere. *Tectonophys*., **609**, 491-503.

Chiaraluce L., Chiarabba C., Collettini C., Piccinini D. and Cocco M. (2007): Architecture and mechanics of an active low-angle normal fault: Alto Tiberina fault, northern Apennines, Italy. *J. Geophys. Res*., **112**(B10310), doi: 10.1029/2007JB005015.

Chopra P.N. and Paterson M.S. (1981): The experimental deformation of dunite. *Tectonophys.*, **78**, 453-473.

Chopra P. N. and Paterson M. S. (1984): The role of water in the deformation of dunite. *J. Geophys. Res.*, **89**(B9), 7861-7876.

Chousianitis K., Ganas A. and Evangelidis C. P. (2015): Strain and rotation rate patterns of mainland Greece from continuous GPS data and comparison between seismic and geodetic moment release. *J. Geophys. Res.*, **120**(5), 3909-3931.

Christensen N. I. and Mooney W. D. (1995): Seismic velocity structure and composition of the continental crust: A global view. *J. Geophys. Res.*, **100**(B6), 9761-9788.

Clarke P.J., Davies R.R., England P.C., Parsons B., Billiris H., Paradissis D., Veis G., Cross P.A., Denys P.H., Ashkenazi V., Bingley R., Kahle H.-G., Muller M.-V. and Briole P. (1998): Crustal strain in central Greece from repeated GPS measurements in the interval 1989-1997. *Geophys. J. Int.*, **135**, 195-214.

Cloetingh S. and Burov E. B. (1996): Thermomechanical structure of European continental lithosphere: constraints from rheological profiles and EET estimates. *Geophys. J. Int.,* **24**(3), 695-723.

Cloetingh S.A.P.L., Van Wees J.D., Ziegler P.A., Lenkey L., Beekman F., Tesauro M., Forster A., Norden B., Kaban M., Hardebol N., Bonté D., Genter A., Guillou-Frottier L., Ter Voorde M., Sokoutis D., Willingshofer E., Cornu T. and Worum G. (2010): Lithosphere tectonics and thermo-mechanical properties: an integrated modelling approach for Enhanced Geothermal Systems exploration in Europe. *Earth Science Reviews,* **102**(3-4), 159-206.

Collettini C. and Holdsworth R.E. (2004): Fault zone weakening and character of slip along low-angle normal faults: insights from the Zuccale fault, Elba, Italy. *J. Geol. Soc. London*, **161**(6), 1039-1051.

Collettini C., Tesei T., Scuderi M. M., Carpenter B. M. and Viti C. (2019): Beyond Byerlee friction, weak faults and implications for slip behavior. *Earth Planet. Sc. Lett.*, **519**, 245-263.

Copley A., Grützner C., Howell A., Jackson J., Penney C., and Wimpenny S. (2018): Unexpected earthquake hazard revealed by Holocene rupture on the Kenchreai Fault (central Greece): Implications for weak sub-fault shear zones. *Earth and Planet. Sci. Lett.*, **486**, 141-154.

Craig T. J., Jackson J. A., Priestley K. and McKenzie D. (2011): Earthquake distribution patterns in Africa: their relationship to variations in lithospheric and geological structure, and their rheological implications. *Geophys. J. Int.*, **185**(1), 403-434.

Currie C. A. and Hyndman R. D. (2006): The thermal structure of subduction zone back arcs. *J. Geophys. Res.*, **111**(B8).

D'Alessandro A., Papanastassiou D. and Baskoutas I. (2011): Hellenic Unified Seismological Network: an evaluation of its performance through SNES method. *Geophys. J.l Int.*, **185**(3), 1417-1430.

Devoti R. Esposito A., Pietrantonio G., Pisani A.R. and Riguzzi F. (2011): Evidence of large scale deformation patterns from GPS data in the Italian subduction boundary. *Earth Planet. Sci. Lett.*, **311**, 230-241, doi: 10.1016/j.epsl.2011.09.034

Dewey J.F. and Sengör A.M.C. (1979): Aegean and surrounding regions: Complex multiplate and continuum tectonics in a convergent zone, *Geol. Soc. Am. Bull.*, **90**, 84-92.

Di Toro G., Goldsby D. L. and Tullis T. E. (2004): Friction falls towards zero in quartz rock as slip velocity approaches seismic rates. *Nature*, **427**(6973), 436.

Di Toro G., Han R., Hirose T., De Paola N., Nielsen S., Mizoguchi K., Ferri F., Cocco M. and Shimamoto T. (2011): Fault lubrication during earthquakes. *Nature*, **471**(7339), 494.

Dieterich J. H. (1978). Time-dependent friction and the mechanics of stick-slip. *Rock Friction and Earthquake Prediction*, 790-806. Birkhäuser, Basel.

Dieterich J. H. (1979): Modeling of rock friction: 1. Experimental results and constitutive equations. *J. Geophys. Res.*, **84**(B5), 2161-2168.

Doglioni C., Barba S., Carminati E. and Riguzzi F. (2015): Fault on-off versus strain rate and earthquakes energy. *Geosci. Front.*, **6**(2), 265-276.

Doser D. I. and Kanamori, H. (1986): Depth of seismicity in the Imperial Valley region (1977–1983) and its relationship to heat flow, crustal structure and the October 15, 1979, earthquake. *J. Geophys. Res.*, **91**(B1), 675-688.

Doutsos T. and Koukouvelas I. (1998): Fractal analysis of normal faults in northwestern Aegean area, Greece. *J. Geodyn.*, **26**(2-4), 197-216.

Doutsos T., Pe-Piper G., Boronkay K. T. and Koukouvelas I. (1993): Kinematics of the central Hellenides. *Tectonics*, **12**(4), 936-953.

Doutsos T., Koukouvelas I., Zelilidis A. and Kontopoulos N. (1994): Intracontinental wedging and post-orogenic collapse in the Mesohellenic Trough. *Geol. Rundsch.*, **83**, 257-275.

Doutsos T., Koukouvelas I. K., and Xypolias P. (2006): A new orogenic model for the External Hellenides. *Geol. Soc. London Spec. Publ.*, **260**(1), 507-520.

Drury M. J. (1986): *Thermal conductivity, thermal diffusivity, density and porosity of crystalline rocks*. Energy, Mines and Resources Canada, Earth Physics Branch.

Ekström G. and England P. (1989): Seismic strain rates in regions of distributed continental deformation. *J. Geophys. Res.*, **94**(B8), 10231-10257.

Ekström G., Nettles M. and Dziewonski A. M. (2012): The global CMT project 2004-2010: Centroid-moment tensors for 13,017 earthquakes. *Phys. Earth Planet. Inter.*, **200-201**, 1-9, 2012. doi:10.1016/j.pepi.2012.04.002

Engdahl E. R., van der Hilst R. and Buland R. (1998): Global teleseismic earthquake relocation with improved travel times and procedures for depth determination. *Bull. Seismol.l Soc.Am.*, **88**(3), 722-743.

England P. and Jackson J. (1989): Active deformation of the continents. *Annual Review of Earth and Planetary Sciences*, **17**(1), 197-226.

England P., Houseman G. and Nocquet J.M. (2016): Constraints from GPS measurements on the dynamics of deformation in Anatolia and the Aegean. *J. Geophys. Res*., **121**(12), 8888-8916.

Erickson A. J. (1970): *The measurement and interpretation of heat flow in the Mediterranean and Black Seas*. Doctoral dissertation, Massachusetts Institute of Technology.

Evangelidis C. P. (2015): Imaging supershear rupture for the 2014 Mw 6.9 Northern Aegean earthquake by backprojection of strong motion waveforms. *Geophys. Res. Lett.*, **42**(2), 307-315.

Fagereng Å. and Den Hartog S. A. (2017): Subduction megathrust creep governed by pressure solution and frictional–viscous flow. *Nat. Geosci.*, **10**(1), 51.

Fagereng Å. and Toy V. G. (2011): Geology of the earthquake source: an introduction. *Geol. Soc. London, Spec. Publ.*, **359**(1), 1-16.

Fernandez M. and Ranalli, G. (1997): The role of rheology in extensional basin formation modelling. T*ectonophys.*, **282**(1-4), 129-145.

Floyd M.A., Billiris H., Paradissis D., Veis G., Avallone A., Briole P., McClusky S., Nocquet J. M., Palamartchouk K., Parsons B. and England P.C. (2010): A new velocity field for Greece: Implications for the kinematics and dynamics of the Aegean. *J. Geophys. Res*., **115**(B10).

Fossen H. (2010). *Structural geology*. Cambridge University Press, pp. 463.

Fossen H. and Cavalcante G. C. G. (2017): Shear zones–A review. *Earth-Sci Rev.*, **171**, 434-455.

François T., Burov E., Agard P. and Meyer B. (2014): Buildup of a dynamically supported orogenic plateau: Numerical modeling of the Zagros/Central Iran case study. *Geochem. Geophy. Geosy*., **15**(6), 2632-2654.

Fytikas M.D. and Kolios N.P. (1979): Preliminary heat flow map of Greece. In *Terrestrial heat flow in Europe*, 197-205. Springer, Berlin, Heidelberg.

Gallais F., Graindorge D., Gutscher M. A. and Klaeschen, D. (2013): Propagation of a lithospheric tear fault (STEP) through the western boundary of the Calabrian accretionary wedge offshore eastern Sicily (Southern Italy). *Tectonophys.*, **602**, 141-152.

Ganas A. and Parsons T. (2009): Three-dimensional model of Hellenic Arc deformation and origin of the Cretan uplift. *J. Geophys. Res.*, **114**, doi: 10.1029/2008JB005599.

Ganas A., Roberts G.P. and Memou T. (1998): Segment boundaries, the 1894 ruptures and strain patterns along the Atalanti fault, Central Greece. *J. Geodyn.*, **26**, 2-4, 461-486.

Ganas A., Drakatos G., Pavlides S. B., Stavrakakis G. N., Ziazia M., Sokos E. and Karastathis V. K. (2005): The 2001 Mw= 6.4 Skyros earthquake, conjugate strike-slip faulting and spatial variation in stress within the central Aegean Sea. *J. Geodyn.*, **39**(1), 61-77.

Ganas A., Lekkas E., Kolligri M., Moshou A. and Makropoulos K. (2012): The 2011 Oichalia (SW Peloponnese, Greece) seismic swarm: geological and seismological evidence for EW extension and reactivation of the NNW-SSE striking Siamo fault. *Bulletin of the Geological Society of Greece*, **46**, 81-94.

Ganas A., Karastathis V., Moshou A., Valkaniotis S., Mouzakiotis E., and Papathanassiou, G. (2014): Aftershock relocation and frequency–size distribution, stress inversion and seismotectonic setting of the 7 August 2013 M= 5.4 earthquake in Kallidromon Mountain, central Greece. *Tectonophys*., **617**, 101-113.

Ganas A., Elias P., Bozionelos G., Papathanassiou G., Avallone A., Papastergios A., Valkaniotis S., Parcharidis I. and Briole P. (2016): Coseismic deformation, field observations and seismic fault of the 17 November 2015 M = 6.5, Lefkada Island, Greece earthquake. *Tectonophys.*, **687**, 210-222, doi: 10.1016/j.tecto.2016.08.012.

Gaucher E., Schoenball M., Heidbach O., Zang A., Fokker P. A., van Wees J. D. and Kohl T. (2015): Induced seismicity in geothermal reservoirs: A review of forecasting approaches. *Renewable and Sustainable Energy Reviews*, **52**, 1473-1490.

Gautier P., Brun J. P. and Jolivet L. (1993): Structure and kinematics of upper Cenozoic extensional detachment on Naxos and Paros (Cyclades Islands, Greece). *Tectonics*, **12**(5), 1180-1194.

Gerya T. V. and Meilick F. I. (2011): Geodynamic regimes of subduction under an active margin: effects of rheological weakening by fluids and melts. *J. Metamorph. Geol*., **29**(1), 7-31.

Gerya T. V., Stöckhert B. and Perchuk A. L. (2002): Exhumation of high-pressure metamorphic rocks in a subduction channel: A numerical simulation. *Tectonics*, **21**(6), 6-1.

Goetze C. and Evans B. (1979): Stress and temperature in the bending lithosphere as constrained by experimental rock mechanics. *Geophys. J. Int*., **59**(3), 463-478.

Govers R. and Wortel M. J. R. (2005). Lithosphere tearing at STEP faults: Response to edges of subduction zones. *Earth and Planet. Sci. Lett.*, **236**(1-2), 505-523.

Gratier J. P., Dysthe D. K. and Renard F. (2013): The role of pressure solution creep in the ductility of the Earth's upper crust. *Adv. Geophys*., **54**, 47-179.

Gressier J.B., Mourgues R., Bodet L., Matthieu J.Y., Galland O. and Cobbold P. (2010): Control of pore fluid pressure on depth of emplacement of magmatic sills: An experimental approach. *Tectonophys*., **489**(1-4), 1-13.

Grigoriadis V.N., Tziavos I.N., Tsokas G.N. and Stampolidis A. (2016): Gravity data inversion for Moho depth modeling in the Hellenic area. *Pure Appl. Geophys*., **173**(4), 1223-1241.

Gung Y., Panning M. and Romanowicz B. (2003): Global anisotropy and the thickness of continents. *Nature*, **422**, 707-711.

Guzmán O., Mugnier J. L., Vassallo R., Koçi R. and Jouanne F. (2013): Vertical slip rates of active faults of southern Albania inferred from river terraces. *Ann. Geophys.*, **56**(6).

Haenel R., Rybach L. and Stegena L. (1988): Fundamentals of geothermics. *Handbook of terrestrial heat-flow density determination.* Springer, Dordrecht.

Haines A. J. and Holt W. E. (1993): A procedure for obtaining the complete horizontal motions within zones of distributed deformation from the inversion of strain rate data. *J. Geophys. Res.*, **98**(B7), 12057-12082.

Haines S., Marone C. and Saffer D. (2014): Frictional properties of low-angle normal fault gouges and implications for low-angle normal fault slip. *Earth Planet. Sci. Lett.*, **408**, 57-65, doi: 10.1016/j.epsl.2014.09.034.

Halpaap F., Rondenay S. and Ottemöller L. (2018): Seismicity, deformation, and metamorphism in the Western Hellenic subduction zone: New constraints from tomography. *J. Geophys. Res.* **123**(4), 3000-3026.

Handy M. R., Wissing S. B. and Streit L. E. (1999): Frictional–viscous flow in mylonite with varied bimineralic composition and its effect on lithospheric strength. *Tectonophys.,* **303**(1-4), 175-191.

Hansen F.D. and Carter N.L. (1982): Creep of selected crustal rocks at 1000 MPa. *Trans. Amer. Geophys. Union,* **63**, 437.

Hatzfeld D., Kassaras I., Panagiotopoulos D., Amorese D., Makropoulos K., Karakaisis G. and Coutant O. (1995): Microseimicity and strain pattern in northwestern Greece. *Tectonics*, **14**(4), 773-785.

Hatzfeld D., Nord J., Paul A., Guiguet R., Briole P., Ruegg J.C., Cattin R., Armijo R., Meyer B., Hubert A., Bernard P., Makropoulos K., Karakostas V., Papaioannou C., Papanastassiou D. and Veis G. (1997): The Kozani-Grevena (Greece) earthquake of May 13, 1995, Ms=6.6 Preliminary results of a field pluridisciplinary survey. *Seism. Res. Lett.*, **66**, 61-70.

Hatzfeld D., Ziazia M., Kementzetzidou D., Hatzidimitriou P., Panagiotopoulos D., Makropoulos K., Papadimitriou P. and Deschamps A. (1999): Microseismicity and focal mechanisms at the western termination of the North Anatolian Fault and their implications for continental tectonics. *Geophys. J. Int.*, **137**, 891, doi: 10.1046/j.1365-246x.1999.00851.x.

Hatzfeld D., Karakostas V., Ziazia M., Kassaras I., Papadimitriou E., Makropoulos K., Voulgaris N. and Papaioannou C. (2000): Microseismicity and faulting geometry in the Gulf of Corinth (Greece). *Geophys. J. Int.*, **141**, 438-456.

Hauksson E. and Meier M. A. (2019): Applying Depth Distribution of Seismicity to Determine Thermo-Mechanical Properties of the Seismogenic Crust in Southern California: Comparing Lithotectonic Blocks. *Pure Appl. Geophys.,* **176**(3), 1061-1081.

Heard H. C. (1976): A Discussion on natural strain and geological structure-Comparison of the flow properties of rocks at crustal conditions. *Philosophical Transactions of the Royal Society of London. Series A, Mathematical and Physical Sciences*, **283**(1312), 173-186.

Herrmann R. B. (1979): FASTHYPO—a hypocenter location program. *Earthquake Notes*, **50**(2), 25-38.

Himmerkus F., Reischmann T., and Kostopoulos D. (2009): Serbo-Macedonian revisited: a Silurian basement terrane from northern Gondwana in the Internal Hellenides, Greece. *Tectonophys.* **473**(1-2), 20-35.

Hirth G. and Kohlstedt D. L. (1996): Water in the oceanic upper mantle: implications for rheology, melt extraction and the evolution of the lithosphere. *Earth Planet. Sci. Lett.*, **144**(1-2), 93-108.

Hirth G., Teyssier C. and Dunlap J. W. (2001): An evaluation of quartzite flow laws based on comparisons between experimentally and naturally deformed rocks. *Int. J. Earth Sci.*, **90**(1), 77-87.

Holbrook W.S., Mooney W.D. and Christensen N.I. (1992): The seismic velocity structure of the deep continental crust. In Fountain, D., Arculus, R., and Kay, R.W. (1992), *Continental lower crust*, Elsevier Science Ltd, **23**, 1-43.

Hollenstein C., Müller M.D., Geiger A. and Kahle H.G. (2008): Crustal motion and deformation in Greece from a decade of GPS measurements, 1993–2003. *Tectonophys.*, **449**(1-4), 17-40.

Hooft E. E., Nomikou P., Toomey D. R., Lampridou D., Getz C., Christopoulou M. E., O'Hara D., Arnoux G.M., Bodmer M., Gray M., Heath B. A. and VanderBeek B.P. (2017): Backarc tectonism, volcanism, and mass wasting shape seafloor morphology in the Santorini-Christiana-Amorgos region of the Hellenic Volcanic Arc. *Tectonophys.*, **712**, 396-414.

Howell A., Jackson J., England P., Higham T. and Synolakis C. (2015): Late Holocene uplift of Rhodes, Greece: evidence for a large tsunamigenic earthquake and the implications for the tectonics of the eastern Hellenic Trench System. *Geophys. J. Int.*, **203**(1), 459-474.

Howell A., Palamartchouk K., Papanikolaou X., Paradissis D., Raptakis C., Copley A., England E. and Jackson J. (2017): The 2008 Methoni earthquake sequence: the relationship between the earthquake cycle on the subduction interface and coastal uplift in SW Greece. *Geophys. J. Int.*, **208**(3), 1592-1610.

Hsü K. J., Montadert L., Garrison R. E., Fabricius F. H., Bernoulli D., Melieres F., Kidd R. B., Muller C., Cita M., Bizon G., Wright R. and Erickson A. (1975): Glomar challenger returns to the Mediterranean Sea. *Geotimes*, **20**(8), 16-19.

Huet B., Le Pourhiet L., Labrousse L., Burov E. and Jolivet L. (2011): Post-orogenic extension and metamorphic core complexes in a heterogeneous crust: the role of crustal layering inherited from collision. Application to the Cyclades (Aegean domain). *Geophys. J. Int.*, **184**(2), 611-625.

Hurter S. and Haenel R. (2002): *Atlas of Geothermal Resources in Europe*. Commission of the European Communities, Publication Nr. 1781 1.

Hurtig E., Cermak V., Haenel R. and Zui V. (1992): *Geothermal atlas of Europe*. Hermann Haack, Potsdam (1992), p. 156.

Ikari M. J., Marone C. and Saffer D. M. (2011): On the relation between fault strength and frictional stability. *Geology*, **39**(1), 83-86.

Jackson J. (1994): Active tectonics of the Aegean region: *Annual Review of Earth and Planetary Sciences*, **22**, 239-271, doi: 10.1146/annurev.ea.22.050194.001323.

Jackson J.A. (2002): Strength of the continental lithosphere: time to abandon the jelly sandwich? *GSA today*, **12**, 4-10.

Jackson J. and McKenzie D. (1988): The relationships between plate motions and seismic moment tensors, and the rates of active deformation in the Mediterranean and Middle East. *Geophys. J.*, **93**(1), 45-73, doi: 10.1111/j.1365-246X.1988.tb01387.x

Jackson J., Haines J. and Holt W. (1994): A comparison of satellite laser ranging and seismicity data in the Aegean region. *Geophys. Res. Lett.*, **21**(25), 2849-2852.

Jackson J., McKenzie D., Priestley K. and Emmerson B. (2008): New views on the structure and rheology of the lithosphere. *J. Geol. Soc. London*, **165**(2), 453-465.

Jacobshagen V. (ed) (1986): Geologie von Griechenland. Borntraeger, Berlin Stuttgart, 363 pp.

Jenny S., Goes S., Giardini D. and Kahle H.G. (2004): Earthquake recurrence parameters from seismic and geodetic strain rates in the eastern Mediterranean. *Geophys. J. Int.*, **157**, 1331-1347.

Jolivet L. and Brun J.-B. (2010): Cenozoic geodynamic evolution of the Aegean. *Int. J. Earth Sci.*, **99**(1), 109-138.

Jongsma D. (1974): Heat flow in the Aegean Sea. *Geophys. J. R. astron. Soc.*, **37**, 337-346.

Kahle H.-G., Straub C., Reilinger R., McClusky S., King R.W., Hurst K., Veis G., Kastens K. and Cross P. (1998): The strain rate field in the eastern Mediterranean region, estimated by repeated GPS measurements. *Tectonophys.*, **294**, 237-252.

Kahle H.-G., Cocard M., Peter Y., Geiger A., Reilinger R., Barka A. and Veis G. (2000): GPS-derived strain rate field within the boundary zones of the Eurasian, Africa, and Arabian Plates. *J. Geophys. Res.*, **195**(B10), 23,353-23,370.

Kanamori H. (1983): Magnitude scale and quantification of earthquakes. *Tectonophys.*, **93**(3-4), 185-199.

Karabulut H., Roumelioti Z., Benetatos C., Mutlu A.K., Özalaybey S., Aktar M. and Kiratzi A. (2006): A source study of the 6 July 2003 (Mw 5.7) earthquake sequence in the Gulf of Saros (Northern Aegean Sea): Seismological evidence for the western continuation of the Ganos fault. *Tectonophys.*, **412**, 195-216.

Karasözen E., Nissen E., Büyükakpınar P., Cambaz M. D., Kahraman M., Kalkan Ertan E., Abgarmi B., Bergman E., Ghods A. and Özacar, A. A. (2018): The 2017 July 20 M w 6.6 Bodrum–Kos earthquake illuminates active faulting in the Gulf of Gökova, SW Turkey. *Geophys. J. Int.,* **214**(1), 185-199.

Karastathis V. K., Mouzakiotis E., Ganas A., and Papadopoulos G. A. (2015): High-precision relocation of seismic sequences above a dipping Moho: the case of the January-February 2014 seismic sequence on Cephalonia island (Greece). *Solid Earth*, **6**(1), 173, doi:10.5194/se-6-173-2015.

Karato S. I. (1989): Plasticity-crystal structure systematics in dense oxides and its implications for the creep strength of the Earth's deep interior: a preliminary result. *Phys. Earth Planet. In.*, **55**(3-4), 234-240.

Karato S. I. (2003): Mapping water content in upper mantle. *Geophys. Monogr. Am. Geophys Union*, **138**, 135-152.

Karato S. I. and Wu P. (1993): Rheology of the upper mantle: A synthesis. *Science*, **260**(5109), 771-778.

Kassaras I., Kapetanidis V., Karakonstantis A., Kaviris G., Papadimitriou P., Voulgaris N., Makropoulos K., Popandopoulos G. and Moshou A. (2014): The April–June 2007 Trichonis Lake earthquake swarm (W. Greece): New implications toward the causative fault zone. *J. Geodyn.*, **73**, 60-80.

Kassaras I., Kapetanidis V., Karakonstantis A., Kouskouna V., Ganas A., Chouliaras G., Drakatos G., Moshou A., Mitropoulou V., Argyrakis P., Lekkas E. and Makropoulos K. (2014): Constraints on the dynamics and spatio-temporal evolution of the 2011 Oichalia seismic swarm (SW Peloponnesus, Greece). *Tectonophys*., **614**, 100-127.

Kassaras I., Kapetanidis V. and Karakonstantis A. (2016): On the spatial distribution of seismicity and the 3D tectonic stress field in western Greece. *Phys. Chem. Earth*, **95**, 50-72.

Keay S. (1998): The Geological Evolution of the Cyclades, Greece: Constraints from SHRIMP U-Pb Geochronology. *Unpublished PhD Thesis. Australian National University*, Canberra.

Kementzetzidou D. (1996): *Étude sismotectonique du système Thessalie-îles Sporades (Grèce centrale)*. Ph.D. thesis, Université J. Fourier-Grenoble I, 151 pp., Grenoble.

Kiratzi A. (2013): The January 2012 earthquake sequence in the Cretan Basin, south of the Hellenic Volcanic Arc: Focal mechanisms, rupture directivity and slip models. *Tectonophys.*, **586**, 160-172.

Kiratzi A. (2018): The 12 June 2017 Mw 6.3 Lesvos Island (Aegean Sea) earthquake: Slip model and directivity estimated with finite-fault inversion. *Tectonophys.*, **724**, 1-10.

Kiratzi A. and Louvari E. (2003): Focal mechanisms of shallow earthquakes in the Aegean Sea and the surrounding lands determined by waveform modelling: a new database. *J. Geodyn,*, **36**(1-2), 251-274.

Kiratzi A. and Svigkas N. (2013): A study of the 8 January 2013 Mw5. 8 earthquake sequence (Lemnos Island, East Aegean Sea). *Tectonophys.*, **608**, 452-460.

Kiratzi A., Sokos E., Ganas A., Tselentis A., Benetatos C., Roumelioti Z., Serpetsidaki A., Andriopoulos G., Galanis O and Petrou P. (2008): The April 2007 earthquake swarm near Lake Trichonis and implications for active tectonics in western Greece. *Tectonophys.*, **452**(1-4), 51-65.

Kiratzi A., Tsakiroudi E., Benetatos C. and Karakaisis G. (2016): The 24 May 2014 (M_w6. 8) earthquake (North Aegean Trough): spatiotemporal evolution, source and slip model from teleseismic data. *Phys. Chem. Earth,* **95**, 85-100.

Kirby S.H. (1985): Rock mechanics observations pertinent to the rheology of the continental lithosphere and the localization of strain along shear zones. *Tectonophys.*, **119**(1-4), 1-27.

Kirby S.H. and Kronenberg A.K. (1987): Rheology of the lithosphere: Selected topics. *Rev. Geophys.*, **25**(6), 1219–1244.

Kissling E., Ellsworth W. L., Eberhart-Phillips D. and Kradolfer U. (1994): Initial reference models in local earthquake tomography. *J. Geophys. Res.*, **99**(B10), 19635-19646.

Klein, F. W. (1989). *User's guide to HYPOINVERSE, a program for VAX computers to solve for earthquake locations and magnitudes*, No. 89-314. US Geological Survey.

Klein F. W. (2002): *User's guide to HYPOINVERSE-2000, a Fortran program to solve for earthquake locations and magnitudes*, No. 2002-171. US Geological Survey.

Koch N. and Masch L. (1992): Formation of Alpine mylonites and pseudotachylytes at the base of the Silvretta nappe, Eastern Alps. *Tectonophys.*, **204**(3-4), 289-306.

Kohlstedt D.L., Evans B. and Mackwell S.J. (1995): Strength of the lithosphere: Constraints imposed by laboratory experiments. *J. Geophys. Res.*, **100**(B9), 17587-17602.

Kokkalas S., Xypolias P., Koukouvelas I. and Doutsos T. (2006): Postcollisional contractional and extensional deformation in the Aegean region. In*:* Dilek Y. and Pavlides S. (Eds.), *Postcollisional tectonics and magmatism in the Mediterranean region and Asia*. Geol. Soc. Am., Spec. Paper, **409**, 97-123.

Konstantinou K. I. (2010): Crustal rheology of the Santorini–Amorgos zone: Implications for the nucleation depth and rupture extent of the 9 July 1956 Amorgos earthquake, southern Aegean. *J. Geodyn.*, **50**(5), 400-409.

Konstantinou K. I. (2017): Accurate relocation of seismicity along the North Aegean Trough and its relation to active tectonics. *Tectonophys.*, **717**, 372-382.

Konstantinou K. I., Kalogeras I. S., Melis N. S., Kourouzidis M. C. and Stavrakakis G. N. (2006): The 8 January 2006 earthquake (Mw 6.7) offshore Kythira Island, Southern Greece: seismological, strong-motion, and macroseismic observations of an intermediate-depth event. *Seismol. Res. Lett.*, **77**(5), 544-553.

Konstantinou K. I., Lee S. J., Evangelidis C. P. and Melis N. S. (2009): Source process and tectonic implications of the 8 January 2006 (Mw 6.7) Kythira earthquake, southern Greece. *Phys. Earth Planet. In.*, **175**(3-4), 167-182.

Kontogianni V. A., Tsoulos N. and Stiros S. C. (2002): Coastal uplift, earthquakes and active faulting of Rhodes Island (Aegean Arc): modeling based on geodetic inversion. *Mar. Geol.*, **186**(3-4), 299-317.

Kostrov V. V. (1974): Seismic moment and energy of earthquakes, and seismic flow of rock. *Izv. Acad. Sci. USSR Phys. Solid Earth*, **1**, 23-44.

Koukouvelas I.K. and Aydin A. (2002): Fault structure and related basins of the North Aegean Sea and its surroundings. *Tectonics*, **21**, 1046, doi: 10.1029/2001TC901037.

Koukouvelas I.K., Katsonopoulou D., Soter S. and Xypolias P. (2005): Slip rates on the Helike Fault, Gulf of Corinth, Greece: new evidence from geoarchaeology. *Terra Nova*, **17**, 158-164.

Kreemer C., Blewitt G. and Klein E.C. (2014): A geodetic plate motion and Global Strain Rate Model. *Geochem. Geophys*., **15**(10), 3849-3889.

Kufner S. K., Hüpers A. and Kopf A. J. (2014): Constraints on fluid flow processes in the Hellenic Accretionary Complex (eastern Mediterranean Sea) from numerical modeling. *J. Geophys. Res*., **119**(4), 3601-3626.

Lachenbruch A.H. (1968): Preliminary geothermal model of the Sierra Nevada. *J. Geophys. Res*., **73**(22), 6977-6989.

Lachenbruch A. H. and Sass J. H. (1977): Heat flow in the United States and the thermal regime of the crust. *The Earth's crust*, **20**, 626-675.

Lachenbruch A.H. and Sass J.H. (1980): Heat flow and energetics of the San Andreas fault zone. *J. Geophys. Res*., **85**(B11), 6185-6222.

Laigle M., Sachpazi M. and Hirn A. (2004): Variation of seismic coupling with slab detachment and upper plate structure along the western Hellenic subduction zone. *Tectonophys*., **391**(1-4), 85-95.

Lamontagne M. and Ranalli G. (1996): Thermal and rheological constraints on the earthquake depth distribution in the Charlevoix, Canada, intraplate seismic zone. *Tectonophys*., **257**(1), 55-69.

Le Pichon X., and Angelier J. (1979): The Hellenic arc and trench system: a key to the neotectonic evolution of the eastern Mediterranean area. *Tectonophys*., **60**(1-2), 1-42.

Lee W. H. and Valdes C. M. (1985). *HYPO71PC; a personal computer version of the HYPO71 earthquake location program*, No. 85-749. US Geological Survey.

Lin A., Maruyama T., Aaron S., Michibayashi K., Camacho A. and Kano K. I. (2005): Propagation of seismic slip from brittle to ductile crust: Evidence from pseudotachylyte of the Woodroffe thrust, central Australia. *Tectonophys*., **402**(1-4), 21-35.

Liotta D., Ruggieri G., Brogi A., Fulignati P., Dini A. and Nardini I. (2010): Migration of geothermal fluids in extensional terrains: the ore deposits of the Boccheggiano-Montieri area (southern Tuscany, Italy). *Int. J. Earth Sci*., **99**(3), 623-644.

Lips A. L., White S. H. and Wijbrans J. R. (2000): Middle-late Alpine thermotectonic evolution of the southern Rhodope Massif, Greece. *Geodin. Acta*, **13**(5), 281-292.

Lockner D.A., Morrow C., Moore D. and Hickman S. (2011): Low strength of deep San Andreas fault gouge from SAFOD core. *Nature*, **472**(7341), 82.

Louvari E., Kiratzi A.A. and Papazachos B.C. (1999): The Cephalonia transform fault and its extension to western Lefkada Island (Greece). *Tectonophys*., **308**(1-2), 223-236.

Lucazeau F. and Le Douaran S. (1985): The blanketing effect of sediments in basins formed by extension: a numerical model. Application to the Gulf of Lion and Viking graben. *Earth and Planet. Sci. Lett*., **74**(1), 92-102.

Lyberis N., Angelier J., Barrier E. and Lallemant S. (1982): Active deformation of a segment of arc: the strait of Kythira, Hellenic arc, Greece. *J. Struct. Geol.*, **4**, 299-311, Oxford.

Maggi A., Jackson J.A., McKenzie D. and Priestley K. (2000): Earthquake focal depths, effective elastic thickness, and the strength of the continental lithosphere. *Geology,* **28**(6), 495-498.

Makris J., Papoulia J., Papanikolaou D. and Stavrakakis G. (2001): Thinned continental crust below northern Evoikos Gulf, central Greece, detected from deep seismic soundings. *Tectonophys.*, **341**(1-4), 225-236.

Makris J., Papoulia J. and Yegorova T. (2013): A 3-D density model of Greece constrained by gravity and seismic data. *Geophys. J. Int.*, **194**(1), 1-17.

Makropoulos K. and Burton P. (1984): Greek tectonics and seismicity. *Tectonophys.*, **106**, 275-304.

Makropoulos K., Kaviris G. and Kouskouna V. (2012): An updated and extended earthquake catalogue for Greece and adjacent areas since 1900. *Natural Hazards and Earth System Sciences*, **12**(5), 1425-1430.

Mareschal J. C. and Jaupart C. (2013): Radiogenic heat production, thermal regime and evolution of continental crust. *Tectonophys.*, **609**, 524-534.

Mariani E., Mecklenburgh J. and Faulkner D. R. (2015): Towards an improved understanding of the mechanical properties and rheology of the lithosphere: an introductory article to 'Rock Deformation from Field, Experiments and Theory: A Volume in Honour of Ernie Rutter'. *Geol. Soc. London, Spec. Publ.*, **409**(1), 1-18.

Marone C. and Scholz C.H. (1988): The depth of seismic faulting and the upper transition from stable to unstable slip regimes. *Geophys. Res. Lett.*, **15**(6), 621-624.

Marotta A.M., Splendore R. and Barzaghi R. (2015): An application of model uncertainty statistical assessment: A case study of tectonic deformation in the Mediterranean. *J. Geodyn.*, **85**, 24-31.

Mascle J. and Martin L. (1990): Shallow structure and recent evolution of the Aegean Sea: A synthesis based on continuous reflection profiles. *Mar. Geol.*, **94**, 271-299.

Mastrolembo B. and Caporali A. (2017): Stress and strain rate fields: a comparative analysis for the Italian territory. *B. Geofis. Teor. Appl.*, **58**(4).

McClusky S., Balassanian S., Barka A., Demir C., Ergintav S., Georgiev I., Gurkan O., Hamburger M., Hurst K., Kahle H.-G., Kastens K., Kekelidze G., King R.W., Kotzev V., Lenk O., Mahmoud S., Mishin A., Nadariya M., Ouzounis A., Paradissis D., Peter Y., Prilepin M., Reilinger R., Sanli I., Seeger H., Tealeb A., Tokzöz M. and Veis G. (2000): Global Positioning System constraints on plate kinematics and dynamics in the eastern Mediterranean and Caucasus. *J. Geophys. Res.*, **105**(B3), 5695-5719.

McGuire A. V. and Stern R. J. (1993): Granulite xenoliths from western Saudi Arabia: the lower crust of the late Precambrian Arbian-Nubian Shield. *Contrib. Mineral. Petrol.*, **114**(3), 395-408.

McKenzie D. (1972): Active Tectonics of the Mediterranean Region. *Geophys. J. R. Astr. Soc.*, **30**, 109-185.

McKenzie D. (1978): Active tectonics of the Alpine—Himalayan belt: the Aegean Sea and surrounding regions. *Geophys. J. Int.*, **55**(1), 217-254.

McKenzie D. and Jackson J. (1983): The relationship between strain rates, crustal thickening, palaeomagnetism, finite strain and fault movements within a deforming zone. *Earth Planet. Sci. Lett.*, **65**(1), 182-202.

McKenzie D., Jackson J. and Priestley K. (2005): Thermal structure of oceanic and continental lithosphere. *Earth Planet. Sci. Lett.*, **233**(3-4), 337-349.

McNeill L.C., Mille A., Minshull T.A., Bull J.M., Kenyon N.H. and Ivanov M. (2004): Extension of the North Anatolian Fault into the North Aegean Trough: Evidence for transtension, strain partitioning, and analogues for Sea of Marmara basin models, *Tectonics*, **23**, TC2016.

McQuarrie N., Stock J. M. Verdel C. and Wernicke B. P. (2003): Cenozoic evolution of Neotethys and implications for the causes of plate motions. *Geophys. Res. Lett.*, **30**(20).

Mercier J.-L. (1976): La neotectonique. Ses methodes et ses buts. Un exemple: I'Arc Egéen (Méditerranée orientale). *Rev. Géogr. Phys. Géol. Dyn.*, **18**(4), 323-346.

Mercier J.-L., Delibasis N., Gauthier A., Jarrige J., Lemeille F., Philip H., Sebrier M. and Sorel D. (1979a): La néotectonique de I'Arc Egéen. *Rev. Géogr. Phys. Géol. Dyn.*, **21**, 67-92.

Mercier J.-L., Mouyaris N., Simeakis C., Roundoyannis T. and Angelidhis C. (1979b): Intraplate tectonics: a quantitative study of the faults activated by the 1978 Thessaloniki earthquakes, *Nature*, **278**, 45-48, doi: 10.1038/278045a0.

Mercier J.-L., Sorel D. and Simeakis K. (1987): Changes in the state of stress in the overriding plate of a subduction zone: the Aegean Arc from the Pliocene to the Present. *Annales Tectonicae*, **1**, 20-39.

Mercier J.-L., Sorel D., Vergely P. and Simeakis K. (1989): Extensional tectonic regimes in the Aegean basins during the Cenozoic. *Basin Res.*, **2**(1), 49-71.

Mesimeri M. and Karakostas V. (2018): Repeating earthquakes in western Corinth Gulf (Greece): implications for aseismic slip near locked faults. *Geophys. J. Int.*, **215**(1), 659-676.

Mesimeri M., Karakostas V., Papadimitriou E., Tsaklidis G. and Jacobs K. (2017): Relocation of recent seismicity and seismotectonic properties in the Gulf of Corinth (Greece). *Geophys. J. Int.* **212**(2), 1123-1142.

Middleton T.A and Copley A. (2014): Constraining fault friction by re-examining earthquake nodal plane dips. *Geophys. J. Int.*, **196**(2), 671-680, doi: 10.1093/gji/ggt427.

Mountrakis D. (1986): The Pelagonian Zone in Greece: a polyphase-deformed fragment of the Kimmerian continent and its role in the geotectonic evolution of the eastern Mediterranean. *J. Geology*, **94**, 335-347.

Mountrakis D. (2006): Tertiary and Quaternary tectonics of Greece. In: Dilek Y. and Pavlides S. (Eds.): *Postcollisional tectonics and magmatism in the Mediterranean region and Asia*, *Geol. Soc. Am. Spec. Paper*, **409**, 125-136.

Mountrakis D.M. and Tranos M.D. (2004): The Kavala-Xanthi-Komotini fault (KXKF): a complicated active fault zone in Eastern Macedonia-Thrace (Northern Greece). 5th International Symposium on Eastern Mediterranean Geology, Thessaloniki, Greece, 14-20 April 2004, Thessaloniki, Greece, *Proceedings*, Ref.: S1-19.

Mposkos E. D. and Kostopoulos D. K. (2001): Diamond, former coesite and supersilicic garnet in metasedimentary rocks from the Greek Rhodope: a new ultrahigh-pressure metamorphic province established. *Earth and Planet. Sci. Lett.*, **192**(4), 497-506.

Müller M. D., Geiger A., Kahle H. G., Veis G., Billiris H., Paradissis D. and Felekis S. (2013): Velocity and deformation fields in the North Aegean domain, Greece, and implications for fault kinematics, derived from GPS data 1993–2009. *Tectonophys*., **597**, 34-49.

Niemeijer A. R., Spiers C. J. and Bos B. (2002) : Compaction creep of quartz sand at 400–600 C: Experimental evidence for dissolution-controlled pressure solution. *Earth Planet. Sci. Lett*., **195**(3-4), 261-275.

North R.G. (1977): Seismic moment, source dimensions, and stress associated with earthquakes in the Mediterranean and Middle East. *Geophys. J. R. astr. Soc.*, **48**, 137-161.

Numelin T., Marone C. and Kirby E. (2007): Frictional properties of natural fault gouge from a low-angle normal fault, Panamint Valley, California. *Tectonics*, **26**, TC2004, doi: 10.1029/2005TC001916.

Ocakoğlu F., Açıkalın S., Güneş G., Özkes S., Dirik K. and Özsayın E. (2013): Was the 1899 Menderes Valley Earthquake a double earthquake? Historical and paleosismological constraints. *J. Asian Earth Sci.*, **67**, 187-198.

Oleskevich D.A., Hyndman R.D. and Wang K. (1999): The updip and downdip limits to great subduction earthquakes: Thermal and structural models of Cascadia, south Alaska, SW Japan, and Chile. *J. Geophys. Res.*, **104**(B7), 14965-14991.

Olhoeft G.R. and Johnson G.R. (1989): Densities of rocks and minerals. *Practical Handbook of Physical Properties of Rocks and Minerals*, **2**, 1-38.

Palyvos N., Pavlopoulos K., Froussou E., Kranis H., Pustovoytov K., Forman S.L. and Minos-Minopoulos D. (2010): Paleoseismological investigation of the oblique-normal Ekkara ground rupture zone accompanying the M 6.7-7.0 earthquake on 30 April 1954 in Thessaly, Greece: Archaeological and geochronological constraints on ground rupture recurrence. *J. Geophys. Res.*, **115**, B06301, doi:10.1029/2009JB006374.

Pantosti D., De Martini P.M., Papanastassiou D., Palyvos N., Lemeille F. and Stavrakakis C. (2001): A reappraisal of the 1894 Atalanti earthquake surface ruptures (central Greece). *Bull. Seism. Soc. Am.*, **91**(4), 760-780.

Papadimitriou E. (2002): Mode of strong earthquake recurrence in the central Ionian Islands (Greece): possible triggering due to Coulomb stress changes generated by the occurrence of previous strong shocks. *Bull. Seismol. Soc. Am.,* **92**(8), 3293-3308.

Papadimitriou E. and Sykes L. (2001): Evolution of the stress field in the northern Aegean (Greece). *Geoph. J. Int.*, **146**, 747-759, doi: 10.1046/j.0956-540x.2001.01486.x.

Papadimitriou E. E., Evison F. F., Rhoades D. A., Karakostas V. G., Console R. and Murru M. R. (2006): Long-term seismogenesis in Greece: Comparison of the evolving stress field and precursory scale increase approaches. *J. Geophys. Res.*, **111**(B5).

Papadimitriou P., Kaviris G., Karakonstantis A. and Makropoulos K. (2010): The Cornet seismological network: 10 years of operation, recorded seismicity and significant applications. *Ann. Geol. Pays Hell.*, **45**, 193-208.

Papadimitriou P., Chousianitis K., Agalos A., Moshou A., Lagios E. and Makropoulos K. (2012): The spatially extended 2006 April Zakynthos (Ionian Islands, Greece) seismic sequence and evidence for stress transfer. *Geophys. J. Int.*, **190**(2), 1025-1040.

Papadopoulos C. and Kilias, A. (1985): Altersbeziehungen zwischen Metamorphose und Deformation im zentralen Teil des Serbomazedonischen Massivs (Vertiskos Gebirge, Nord-Griechenland). *Geol. Rundsch.*, **74**(1), 77-85.

Papadopoulos G. A. and Pavlides S. B. (1992): The large 1956 earthquake in the South Aegean: Macroseismic field configuration, faulting, and neotectonics of Amorgos Island. *Earth Planet. Sc. Lett.,* **113**(3), 383-396.

Papadopoulos G.A., Karastathis V.K., Koukouvelas I., Sachpazi M., Baskoutas I., Chouliaras G., Agalos A., Dashalaki E., Minadakis G., Moshou A., Mouziakiotis A., Orfanogiannaki K., Papageorgiou A,. Spanos D. and Triantafyllou I. (2014): The Cephalonia, Ionian Sea (Greece), sequence of strong earthquakes of January-February 2014: a first report. *Research in Geophysics*, **4**(1), 5441, 19-30, doi: 10.4081/rg.2014.5441.

Papadopoulos G., Agalos A., Charalampakis M., Kontoes C., Papoutsis I., Atzori S., Svigkas N. and Triantafyllou I. (2019): Fault models for the Bodrum–Kos tsunamigenic earthquake (Mw6. 6) of 20 July 2017 in the east Aegean Sea. *J. Geodyn.*, **131**, 101646.

Papaioannou C.A. and Papazachos B.C. (2000): Time-Independent and Time-Dependent Seismic Hazard in Greece Based on Seismogenic Sources. *Bull. Seism. Soc. Am.*, **90**(1), 22-33.

Papanastassiou D. (2001): The Konitsa, Epirus-NW Greece, July 26 (Ms = 5.4) and August 5, 1996, (Ms = 5.7) earthquakes sequence. *Bull. Geol. Soc. Greece*, **34**(4), 1555-1562.

Papanikolaou, D. (1986). Geology of Greece. *Heptalofos, Athens*, 1-240.

Papanikolaou D. (2013): Tectonostratigraphic models of the Alpine terranes and subduction history of the Hellenides. *Tectonophys.*, **595**, 1-24.

Papanikolaou I. D., Roberts G. P., Deligiannakis G., Sakellariou A. and Vassilakis E. (2013): The Sparta Fault, Southern Greece: from segmentation and tectonic geomorphology to seismic hazard mapping and time dependent probabilities. *Tectonophys.*, **597**, 85-105.

Papastamatiou D. and Mouyiaris N. (1986): The Sophadhes earthquake occurred on April 30th 1954 - field observations by Yannis Papastamatiou. *Geol. & Geoph. Res., Sp. Issue,* 341-362.

Papazachos B.C. (1990): Seismicity of the Aegean and surrounding area. *Tectonophys.*, **178**, 287-308.

Papazachos B. and Papazachou C. (1997): *The earthquakes of Greece.* Second edition, Editions ZITI, Thessaloniki, 304 pp.

Papazachos B.C., Panagiotopoulos D.G., Tsapanos T.M., Mountrakis D.M. and Dimopoulos G.Ch. (1983): A study of the 1980 summer seismic sequence in the Magnesia region of Central Greece. *Geophys. J. Royal astron. Soc.,* **75**, 155-168.

Papazachos B.C., Kiratzi A., Karacostas B., Panagiotopoulos D., Scordilis E. and Mountrakis D. (1988): Surface fault traces, fault plane solution and spatial distribution of the aftershocks of the September 13, 1986 earthquake of Kalamata (south Greece). *Pageoph.*, **126**, 55-68.

Papazachos B.C., Comninakis P.E., Karakaisis G. F., Karakostas B.G., Papaioannou C.A., Papazachos C.B. and Scordilis E.M. (2000): A catalogue of earthquakes in Greece and surrounding area for the period 550 BC-1999. *Geophys. Lab. Univ. Thessaloniki, Greece*, **1**, 333 pp.

Papazachos B. C., Dimitriadis S. T., Panagiotopoulos D. G., Papazachos C. B. and Papadimitriou E. E. (2005): Deep structure and active tectonics of the southern Aegean volcanic arc. In *Developments in Volcanology* (Vol. 7, pp. 47-64). Elsevier.

Papazachos C.B. and Kiratzi A. (1996): A detailed study of the active crustal deformation in the Aegean and surrounding area: *Tectonophys.*, **253**, 129-153.

Papazachos C. B., Kiratzi A. A. and Papazachos B. C. (1992): Rates of active crustal deformation in the Aegean and the surrounding area. *J. Geodyn.,* **16**(3), 147-179.

Paradisopoulou P. M., Papadimitriou E. E., Karakostas V. G., Taymaz T., Kilias A. and Yolsal S. (2010): Seismic hazard evaluation in western Turkey as revealed by stress transfer and time-dependent probability calculations. *Pure Appl. Geophys.*, **167**(8-9), 1013-1048.

Passchier C.W. (1982): Pseudotachylite and the development of ultramylonite bands in the Saint-Barthelemy Massif, French Pyrenees. *J. Struct. Geol.*, **4**, 69-79.

Pauselli C., Ranalli G. and Federico C. (2010): Rheology of the Northern Apennines: Lateral variations of lithospheric strength. *Tectonophys.,* **484**(1-4), 27-35.

Pauselli C. and Ranalli G. (2017): Effects of lateral variations of crustal rheology on the occurrence of post-orogenic normal faults: The Alto Tiberina Fault (Northern Apennines, Central Italy). *Tectonophys.*, **721**, 45-55.

Pavlides S. and Caputo R. (1994): The North Aegean Region: a Tectonic Paradox? *Terra Nova*, **6**(1), 37-44, Oxford.

Pavlides S. and Caputo R. (2004): Magnitude *versus* faults' surface parameters: quantitative relationships from the Aegean *Tectonophys.*, **380**, 159-188, doi: 10.1016/j.tecto.2003.09.019.

Pavlides S.B. and Tranos M.D. (1991): Structural characteristic of two strong earthquakes in the North Aegean: Ierissos (1932): and Agios Efstratios (1968). *J. Struct. Geol.*, **13**(2), 205-214.

Pavlides S.B, Zouros N.C, Chatzipetros A.A., Kostopoulos D.S. and Mountrakis D.M. (1995): The 13 May 1995 western Macedonia, Greece (Kozani Grevena) earthquake; preliminary results, *Terra Nova*, **7**, 544-549.

Peacock S.M., Christensen N.I., Bostock M.G. and Audet P. (2011): High pore pressures and porosity at 35 km depth in the Cascadia subduction zone. *Geology*, **39**(5), 471-474.

Pec M., Stünitz H. and Heilbronner R. (2012): Semi-brittle deformation of granitoid gouges in shear experiments at elevated pressures and temperatures. *J. Struct. Geol.,* **38**, 200-221.

Pérouse E., Sébrier M., Braucher R., Chamot-Rooke N., Bourlès D., Briole P., Sorel D., Dimitrov D. and Arsenikos, S. (2017): Transition from collision to subduction in Western Greece: the Katouna–Stamna active fault system and regional kinematics. *Int. J. Earth Sci.*, **106**(3), 967-989.

Peslier A. H., Woodland A. B., Bell D. R. and Lazarov M. (2010): Olivine water contents in the continental lithosphere and the longevity of cratons. *Nature*, **467**(7311), 78.

Pollack H.N. and Chapman D.S. (1977): On the regional variation of heat flow, geotherms, and lithospheric thickness. *Tectonophys*., **38**(3-4), 279-296.

Ranalli G. (1995): *Rheology of the Earth.* Springer Science & Business Media, 413 pp.

Ranalli G. and Murphy D.C. (1987): Rheological stratification of the lithosphere. *Tectonophys*., **132**(4), 281-295.

Raykova R. and Nikolova S. (2007): Tomography and velocity structure of the crust and uppermost mantle in southeastern Europe obtained from surface wave analysis. *Stud. Geophys. Geod.*, **51**, 165-184.

Reilinger R., McClusky S., Vernant P., Lawrence S., Ergintav S., Cakmak R., Ozener H., Kadirov F., Guliev I., Stepanyan R., Nadariya M., Hahubia G., Mahmoud S., Sakr K., ArRajehi A., Paradissis, D., Al-Aydrus A., Prilepin M., Guseva T., Evren E., Dmitrotsa A., Filikov S.V., Gomez F., Al-Ghazzi R. and Karam G. (2006): GPS constraints on continental deformation in the Africa–Arabia–Eurasia continental collision zone and implications for the dynamics of plate interactions. *J. Geophys. Res.*, **111**(B5), B05411.

Remitti F., Smith S.A.F., Mittempergher S., Gualtieri A.F., and Di Toro G. (2015): Frictional properties of fault zone gougesfrom the J-FAST drilling project (Mw9.02011 Tohoku-Oki earthquake). *Geophys.Res. Lett.*, **42**, 2691-2699, doi: 10.1002/2015GL063507.

Resor P.G., Pollard D.D., Wright T.J. and Beroza G.C. (2005): Integrating high-precision aftershock locations and geodetic observations to model coseismic deformation associated with the 1995 Kozani-Grevena earthquake, Greece. *J. Geophys. Res.*, **110**, B09402.

Rigo A., de Chabalier J.-B., Meyer B. and Armijo R. (2004): The 1995 Kozani-Grevena (northern Greece) earthquake revisited: An improved faulting model from synthetic aperture radar interferometry. *Geophys. J. Int.*, **157**, 727-736.

Ring U., Glodny J., Will T. and Thomson S. (2010): The Hellenic subduction system: high-pressure metamorphism, exhumation, normal faulting, and large-scale extension. *Annual Rev. Earth and Planet. Sci*., **38**, 45-76.

Roberts G. P., Houghton S. L., Underwood C., Papanikolaou I., Cowie P. A., van Calsteren P., Wigley T., Cooper F.J. and McArthur J. M. (2009): Localization of Quaternary slip rates in an active rift in 105 years: An example from central Greece constrained by 234U-230Th coral dates from uplifted paleoshorelines. *J. Geophys. Res.*, **114**(B10).

Robertson A. H. (2008): Late Palaeozoic–Early Mesozoic metasedimentary and metavolcanic rocks of the Phyllite-Quartzite Unit, eastern Crete (Greece): an extensional, rift-related setting for the southern margin of Tethys in the Eastern Mediterranean region [Spätpaläozoisch-frühmesozoische Metasedimente und-vulkanite der Phyllit-Quarzit-Serie von Ostkreta (Griechenland): ein extensionales, riftbezogenes Setting für den südlichen Rand der Tethys im östlichen Mittelmeerraum.]. *Z. Dtsch. Ges. Geowiss*., **159**(3), 351-374.

Robertson A.H.F. and Dixon J.F. (1984): Introduction: aspects of the geological evolution of the Eastern Mediterranean. *In:* Dixon J.E. and Robertson A.H.F. (Eds.): The Geological Evolution of the Eastern Mediterranean. *Geol. Soc. London Spec. Publ.*, **17**, 1-74.

Robertson A.H.F., Clift P.D., Degnan P.J. and Jones G. (1991): Palaeogeographic and palaeotectonic evolution of the Eastern Mediterranean Neotethys. *Palaeogeogr., Palaeoclimatol., Palaeoecol.*, **87**, 289-343.

Rolandone F., Bürgmann R. and Nadeau R.M. (2004): The evolution of the seismic-aseismic transition during the earthquake cycle: Constraints from the time-dependent depth distribution of aftershocks. *Geophys. Res. Letts.*, **31**, L23610, doi: 10.1029/2004GL021379.

Rontogianni S. (2010): Comparison of geodetic and seismic strain rates in Greece by using a uniform processing approach to campaign GPS measurements over the interval 1994–2000. *J. Geodyn.*, **50**(5), 381-399.

Roumelioti Z., Benetatos C. and Kiratzi A. (2009): The 14 February 2008 earthquake (M6.7) sequence offshore south Peloponnese (Greece): Source models of the three strongest events. *Tectonophys.*, **471**, 272-284, doi: 10.1016/j.tecto.2009.02.028

Roy R. F., Beck A. E. and Touloukian Y. S. (1981): *Thermophysical properties of rocks*. Physical properties of rocks and minerals: McGraw-Hill Book Co., New York, pp. 409-502.

Royden L.H. and Papanikolaou D.J. (2011): Slab segmentation and late Cenozoic disruption of the Hellenic arc. *Geochem. Geophys.*, **12**(3).

Rudnick R.L. and Fountain D.M. (1995): Nature and composition of the continental crust: a lower crustal perspective. *Rev. Geophys*., **33**(3), 267-309.

Rudnick R.L. and Gao S. (2003): Composition of the continental crust. *Treatise on geochemistry,* **3**, 659.

Rutter E. H. (1976): A discussion on natural strain and geological structure-the kinetics of rock deformation by pressure solution. *Philosophical Transactions of the Royal Society of London. Series A, Mathematical and Physical Sciences*, **283**(1312), 203-219.

Rutter E. H. (1986): On the nomenclature of mode of failure transitions in rocks. *Tectonophys.*, **122**(3-4), 381-387.

Saffer D. M. and Tobin H. J. (2011): Hydrogeology and mechanics of subduction zone forearcs: Fluid flow and pore pressure. *Annual Review of Earth and Planetary Sciences*, **39**, 157-186.

Sakkas V. and Lagios E. (2015): Fault modelling of the early-2014~ M6 Earthquakes in Cephalonia Island (W. Greece) based on GPS measurements. *Tectonophys.*, **644**, 184-196, doi:10.1016/j.tecto.2015.01.010.

Savage J. C. (1983): A dislocation model of strain accumulation and release at a subduction zone. *J. Geophys. Res.*, **88**(B6), 4984-4996.

Sboras S., Caputo R., Pavlides S., Tsapanos T. and Kalogirou E. (2012): Seismic zonation in Greece: the contribution of earthquake geology. *International Earth Science Colloquium on the Aegean Region, IESCA-2012*, 1-5 October 2012, Izmir, Turkey. Abstract book, p. 119.

Sboras S., Pavlides S., Caputo R., Chatzipetros A., Michailidou A., Valkaniotis S. and Papathanassiou G. (2014): The use of geological data to improve SHA estimates in Greece. *B. Geofis. Teor. Appl.*, **55**(1).

Schettino A. (2014): *Quantitative plate tectonics*: *Physics of the Earth–Plate Kinematics–Geodynamics*. New York, NY: Springer.

Schmid S. M., Boland J. N. and Paterson M. S. (1977): Superplastic flow in finegrained limestone. *Tectonophys.*, **43**(3-4), 257-291.

Schmidt M. W. and Poli S. (1998): Experimentally based water budgets for dehydrating slabs and consequences for arc magma generation. *Earth Planet. Sci. Lett.*, **163**(1-4), 361-379.

Scholz C.H. (1988): The brittle-plastic transition and the depth of seismic faulting. *Geol. Rundsch.*, **77**(1), 319-328.

Scholz C.H. (1989): *The mechanics of earthquakes and faulting*. Cambridge University Press., 471 pp.

Scholz C. H. (1998): Earthquakes and friction laws. *Nature*, **391**(6662), 37.

Scordilis E.M., Karakaisis G.F., Karacostas B.G., Panagiotopoulos D.G., Comninakis P.E. and Papazachos B.C. (1985): Evidence for transform faulting in the Ionian Sea: The Cephalonia Island earthquake sequence of 1983. *Pure Appl. Geophys.*, **123**(3), 388-397.

Şengör A.M.C. (1985): The story of Tethys: How many wives did Okeanos have? *Episodes*, 8, 3-12.

Şengör A.M.C. and Yilmaz Y. (1981): Tethyan evolution of Turkey: a plate tectonic approach. *Tectonophys.*, **75**(3-4), 181-241.

Serpelloni E., Anzidei M., Baldi P., Casula G. and Galvani A. (2005): Crustal velocity and strain rate fileds in Italy and surrounding regions: new results from the analysis of perrmanent and non-permanent GPS networks. *Geophys. J. Int.*, **161**, 861-880, doi: 10.1111/j.1365-246X.2005.02618.x.

Serpetsidaki A., Sokos E., Tselentis G.A. and Zahradnik J. (2010): Seismic sequence near Zakynthos Island, Greece, April 2006: identification of the activated fault plane. *Tectonophys.*, **480**(1-4), 23-32.

Shaw B. and Jackson J. (2010): Earthquake mechanisms and active tectonics of the Hellenic subduction zone. *Geophys.l J.l Int.,* **181**(2), 966-984.

Shelton G. and Tullis J.A. (1981): Experimental flow laws for crustal rocks, *Trans. Amer. Geophys. Union,* **62**, 396.

Sibson R.H. (1974): Frictional constraints on thrust, wrench and normal faults. *Nature*, **249**(5457), 542.

Sibson R. H. (1975): Generation of pseudotachylyte by ancient seismic faulting. *Geophys. J. R. astron. Soc.*, **43**(3), 775-794.

Sibson R.H. (1977): Fault rocks and fault mechanisms. *J. Geol. Soc. London*, **133**(3), 191-213.

Sibson R.H. (1980): Transient discontinuities in ductile shear zones. *J. Struct. Geol.*, **2**(1-2), 165-171.

Sibson R.H. (1982): Fault zone models, heat flow, and the depth distribution of earthquakes in the continental crust of the United States. *B. Seismol. Soc. Am.* **72**(1), 151-163.

Sibson R.H. (1983): Continental fault structure and the shallow earthquake source. *J. Geol. Soc. London*, **140**, 741-767.

Sibson R.H. (1984): Roughness at the Base of the Seismogenic Zone: Contributing Factors. *J. Geophys. Res.*, **89**(B7), 5791-5799.

Sibson, R. H. (1985). A note on fault reactivation. *J. Struct. Geol.*, **7**(6), 751-754.

Sibson, R.H. (1986): Earthquakes and rock deformation in crustal fault zones. *Annual Review of Earth and Planetary Sciences*, **14**(1), 149-175.

Sleep N. H. and Blanpied M. L. (1992): Creep, compaction and the weak rheology of major faults. *Nature*, **359**(6397), 687.

Smith A.G. and Moores E.M. (1974): Hellenides. *Geol Soc London Spec. Publ.*, **4**(1), 159-185.

Sodoudi F., Kind R., Hatzfeld D., Priestley K., Hanka W., Wylegalla K., Stavrakakis G., Vafidis A., Harjes H.-P. and Bohnhoff M. (2006): Lithospheric structure of the Aegean obtained from P and S receiver functions. *J. Geophys. Res*. **111**(B12).

Sokos E., Zahradník J., Kiratzi A., Janský J., Gallovič F., Novotny O., Kostelecky J., Serpetsidaki A. and Tselentis G. A. (2012): The January 2010 Efpalio earthquake sequence in the western Corinth gulf (Greece). *Tectonophys.*, **530**, 299-309.

Sokos E., Kiratzi A., Gallovič F., Zahradník J., Serpetsidaki A., Plicka V., Jansky J., Kostelecky J. and Tselentis G. A. (2015): Rupture process of the 2014 Cephalonia, Greece, earthquake doublet (Mw6) as inferred from regional and local seismic data. *Tectonophys.*, **656**, 131-141, doi:10.1016/j.tecto.2015.06.013.

Sorel D. (2000): A Pleistocene and still-active detachment fault and the origin of the Corinth-Patras rift, Greece. *Geology*, **28**, 83-86.

Soto J. I., Fernández-Ibáñez F., Fernandez M. and García-Casco A. (2008): Thermal structure of the crust in the Gibraltar Arc: Influence on active tectonics in the western Mediterranean. *Geochem. Geophys.,* **9**(10).

Stiros S. C. (1991): *Heat flow and thermal structure of the Aegean Sea and the Southern Balkans*. Terrestrial Heat Flow and the Lithosphere Structure, 395-416. Springer, Berlin, Heidelberg.

Stiros S. C., Marangou L. and Arnold M. (1994): Quaternary uplift and tilting of Amorgos Island (southern Aegean) and the 1956 earthquake. *Earth Planet. Sc. Lett.*, **128**(3-4), 65-76.

Sulstarova E. and Koçiaj S. (1980): The Dibra (Albania) earthquake of November 30 1967. *Tectonophys.*, **67**, 333-344.

Sulstarova E., Peçi V. and Shuteriqi P. (2000): Vlora-Elbasani-Dibra (Albania) transversal fault zone and its seismic activity. *J. Seismol.*, **4**(2), 117-131.

Suppe J. (2014): Fluid overpressures and strength of the sedimentary upper crust. *J. Struct. Geol.*, **69**, 481-492, doi: 10.1016/j.jsg.2014.07.009.

Taktikos S. (2001): *Heat flow – Underground temperatures of Greece* (in Greek). 2 volumes and 12 maps set, Institute of Geology and Mineral Exploration, Athens, 72 pp.

Taymaz T., Jackson J. and McKenzie D.P. (1991): Active tectonics of the north and central Aegean Sea. *Geophys. J. Int.*, **106**, 433- 490.

Tesauro M. (2009): *An integrated study of the structure and thermomechanical properties of the European lithosphere*. PhD Thesis, Vrije Universiteit, Netherlands, 178 pp.

Tesauro, M., Kaban, M.K. and Cloetingh, S.A. (2008): EuCRUST-07: A new reference model for the European crust. *Geophys. Res. Lett.* **35**(5).

Tesauro M., Kaban M.K. and Cloetingh S.A. (2013): Global model for the lithospheric strength and effective elastic thickness. *Tectonophys*., **602**, 78-86.

Tezcan A. K. and Turgay I. (1989): *Heat flow map of Turkey*. General Directorate of Mineral Research and Exploration (MTA), Department of Geophysics Research, Ankara (in Turkish, unpublished).

Thomson S. N., Stöckhert B. and Brix M. R. (1998): Thermochronology of the high-pressure metamorphic rocks of Crete, Greece: implications for the speed of tectonic processes. *Geology*, **26**(3), 259-262.

Tiberi C., Diament M., Lyon Caen H. and King T. (2001): Moho topography beneath the Corinth Rift area (Greece) from inversion of gravity data. *Geophys. J. Int*. **145**(3), 797-808.

Tirel C., Gueydan F., Tiberi C. and Brun J. P. (2004): Aegean crustal thickness inferred from gravity inversion. Geodynamical implications. *Earth Planet. Sci. Lett.*, **228**(3-4), 267-280.

Tiryakioğlu İ., Aktuğ B., Yiğit C. Ö., Yavaşoğlu H. H., Sözbilir H., Özkaymak Ç., Poyraz F., Taneli E., Bulut F., Dogru A. and Özener H. (2018): Slip distribution and source parameters of the 20 July 2017 Bodrum-Kos earthquake (Mw6. 6) from GPS observations. *Geodin. Acta*, **30**(1), 1-14.

Tranos M., Papadimitriou E. and Kilias A. (2003): Thessaloniki-Gerakarou Fault Zone (TGFZ): the western extension of the 1978 Thessaloniki earthquake fault (Northern Greece) and seismic hazard assessment. *J. Struct. Geol.*, **25**, 2109-2123.

Truffert C., Chamot-Rooke N., Lallemant S., De Voogd B., Huchon P. and Le Pichon X. (1993): The crust of the Western Mediterranean Ridge from deep seismic data and gravity modelling. *Geophys. J. Int.*, **114**(2), 360-372.

Tse S.T. and Rice J.R. (1986): Crustal earthquake instability in relation to the depth variation of frictional slip properties. *J. Geophys. Res.* **91**(B9), 9452-9472.

Tselentis G.-A., Sokos E., Martakis N. and Serpetsidaki A. (2006): Seismicity and Seismotectonics in Epirus, Western Greece: Results from a Microearthquake Survey, *Bull. Seism. Soc. Am.*, **96**(5), 1706-1717.

Tsenn M. C. and Carter N. L. (1987): Upper limits of power law creep of rocks. *Tectonophys.*, **136**(1-2), 1-26.

Tullis J. and Yund R. A. (1980): Hydrolytic weakening of experimentally deformed Westerly granite and Hale albite rock. *J. Struct. Geol.*, **2**(4), 439-451.

Tullis J., Christie J. M. and Griggs D. T. (1973): Microstructures and preferred orientations of experimentally deformed quartzites. *Geol. Soc. Am. Bull.*, **84**(1), 297-314.

Turcotte D. and Schubert G. (2014): *Geodynamics*. Cambridge University Press, Cambridge, 626 pp.

van Hinsbergen D.J.J., Hafkenscheid E., Spakman W., Meulenkamp J.E. and Wortel R. (2005): Nappe stacking resulting from subduction of oceanic and continental lithosphere below Greece. *Geology*, **33**(4), 325-328.

Vassilakis E., Royden L. and Papanikolaou D. (2011): Kinematic links between subduction along the Hellenic trench and extension in the Gulf of Corinth, Greece: a multidisciplinary analysis. *Earth Planet. Sc. Lett.*, **303**(1-2), 108-120.

Vernant P., Reilinger R. and McClusky S. (2014): Geodetic evidence for low coupling on the Hellenic subduction plate interface. *Earth Planet. Sci. Lett.*, **385**, 122-129.

Vilà M., Fernández M. and Jiménez-Munt I. (2010): Radiogenic heat production variability of some common lithological groups and its significance to lithospheric thermal modeling. *Tectonophys.*, **490**(3-4), 152-164.

Voulgaris N., Pirli M., Papadimitriou P., Kassaras J. and Makropoulos K. (2001): Seismotectonic characteristics of the area of western Attica derived from the study of the September 7, 1999 Athens earthquake aftershock sequence. *Bulletin of the Geological Society of Greece*, **34**(4), 1645-1651.

Waldhauser F. and Ellsworth W. L. (2000): A double-difference earthquake location algorithm: Method and application to the northern Hayward fault, California. *Bull. Seismol. Soc. Am.*, **90**(6), 1353-1368.

Wassmann S. and Stoeckhert B. (2013): Rheology of the plate interface—dissolution precipitation creep in high pressure metamorphic rocks. *Tectonophys.*, **608**, 1-29.

Watts A.B. and Burov E.B. (2003): Lithospheric strength and its relationship to the elastic and seismogenic layer thickness. *Earth Planet. Sci. Lett.*, **213**(1-2), 113-131.

Wei R.Q. and Zang S.X. (2006): Effects of temperature and strain rate on fracture strength of rocks and their influence on rheological structure of the lithosphere. *Chinese J. Geophys.*, **49**(6), 1576-1584.

Wells D.L. and Coppersmith J.K. (1994): New empirical Relationships among Magnitude, Rupture Length, Rupture Width, Rupture Area, and Surface Displacement. *Bull. Seism. Soc. Am.*, **84**, 974-1002.

Wessel P. and Smith W.H. (1991): Free software helps map and display data. *Eos, Transactions American Geophysical Union*, **72**(41), 441-446.

White R. S., McKenzie D. and O'Nions R. K. (1992): Oceanic crustal thickness from seismic measurements and rare earth element inversions. *J. Geophys. Res.*, **97**(B13), 19683-19715.

Williams C. F. (1996): Temperature and the seismic/aseismic transition: Observations from the 1992 Landers earthquake. *Geophys. Res. Lett.*, **23**(16), 2029-2032.

Xia S., Zhao D. and Qiu X. (2008): The 2007 Niigata earthquake: Effect of arc magma and fluids. *Phys. Earth Planet. In.*, **166**(3-4), 153-166.

Xypolias P. and Doutsos T. (2000): Kinematics of rock flow in a crustal-scale shear zone: implication for the orogenic evolution of the southwestern Hellenides. *Geol. Mag.*, **137**(1), 81-96. doi:10.1017/S0016756800003496.

Xypolias P., Iliopoulos I., Chatzaras V. and Kokkalas S. (2012): Subduction-and exhumation-related structures in the Cycladic Blueschists: Insights from south Evia Island (Aegean region, Greece). *Tectonics*, **31**(2), TC2001, doi:10.1029/2011TC002946.

Zang S.X., Wei R.Q. and Ning J.Y. (2007): Effect of brittle fracture on the rheological structure of the lithosphere and its application in the Ordos. *Tectonophys.*, **429**(3-4), 267-285.

Zelt B.C., Taylor B., Sachpazi M. and Hirn A. (2005): Crustal velocity and Moho structure beneath the Gulf of Corinth, Greece. *Geophys. J. Int.,* **162**(1), 257-268.

Zoback M.D., Zoback M.L., Mount V.S., Suppe J., Eaton J.P., Healy J.H., Oppenheimer D., Reasenberg P., Jones L., Barry Rayleigh G., Scotti O., Wentworth C. and Wong I.G. (1987): New evidence on the state of stress of the San Andreas fault system. *Science*, **238**(4830), 1105-1111.

Zulauf G., Klein T., Kowalczyk G., Krahl J. and Romano S. S. (2008): The Mirsini Syncline of eastern Crete, Greece: a key area for understanding pre-Alpine and Alpine orogeny in the eastern Mediterranean [Die Mulde von Mirsini in Ostkreta, Griechenland: ein Schlüsselgebiet zum Verständnis präalpiner und alpiner Orogenese im östlichen Mittelmeerraum.]. *Z. Dtsch Ges. Geowiss*, **159**(3), 399-414.

Zulauf G., Dörr W., Fisher-Spurlock S. C., Gerdes A., Chatzaras V. and Xypolias P. (2015): Closure of the Paleotethys in the External Hellenides: constraints from U–Pb ages of magmatic and detrital zircons (Crete). *Gond. Res.*, **28**(2), 642-667.

Appendix A

1D strength envelopes for selected test sites in the Aegean Region

This appendix contains all the rheological profiles for the test sites present in fig. 5.5, which have not been shown yet in the text (see Chapter 4 and Chapter 5). Figure 5.5 is also reported here in a modified version (fig. A1), where the rheological profiles contained in the Appendix are shown in red and all the others, already reported in the text, are in black.

The strength envelopes are grouped into 11 figures (A2-A12), with 6 (5 in the last one) profiles each. The envelopes are grouped according to their progressive corresponding number (which increases from north to south).The 1D rheological profile for each test site is representative of an area of 10 km × 10 km and is shown in figure down to a depth of 80 km. The strength envelope is always shown in solid blue, with the BDT being indicated by a red square. The associated geothermal gradient is represented by the red solid curve. The dashed cyan and black curves represent, respectively, the continuation of the brittle and ductile behaviours. The black dots indicate the depth of the interface between the litho-mechanical layers (sedimentary cover, upper crust, lower crust, upper mantle, for the upper and the lower plate). On top of each profile, the corresponding number and toponym are indicated.

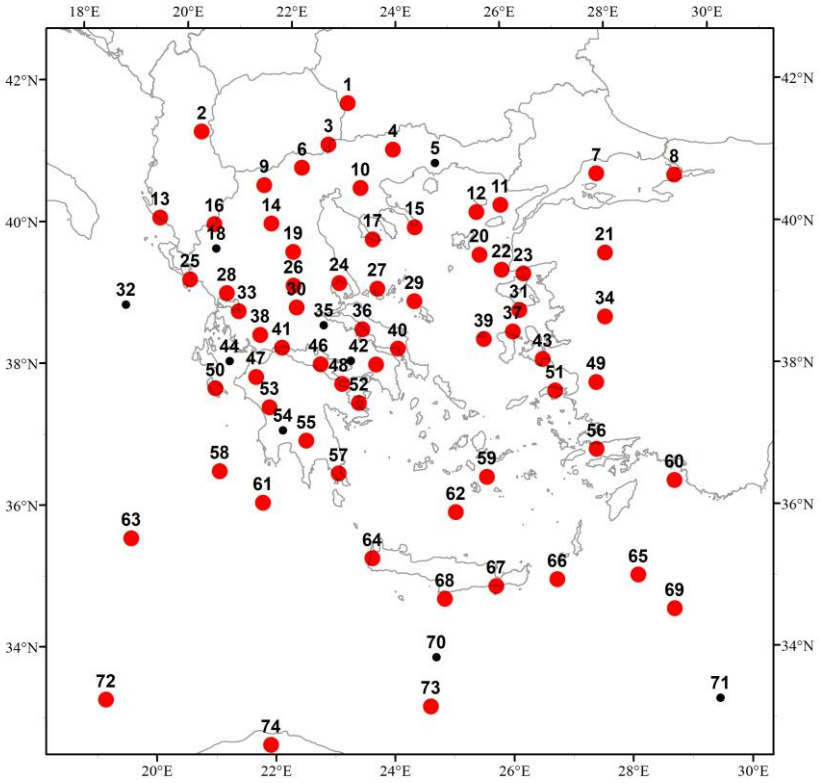

Fig. A1 – Distrubtion of the test sites (in red) whose rheological profiles are shown in the Appendix.

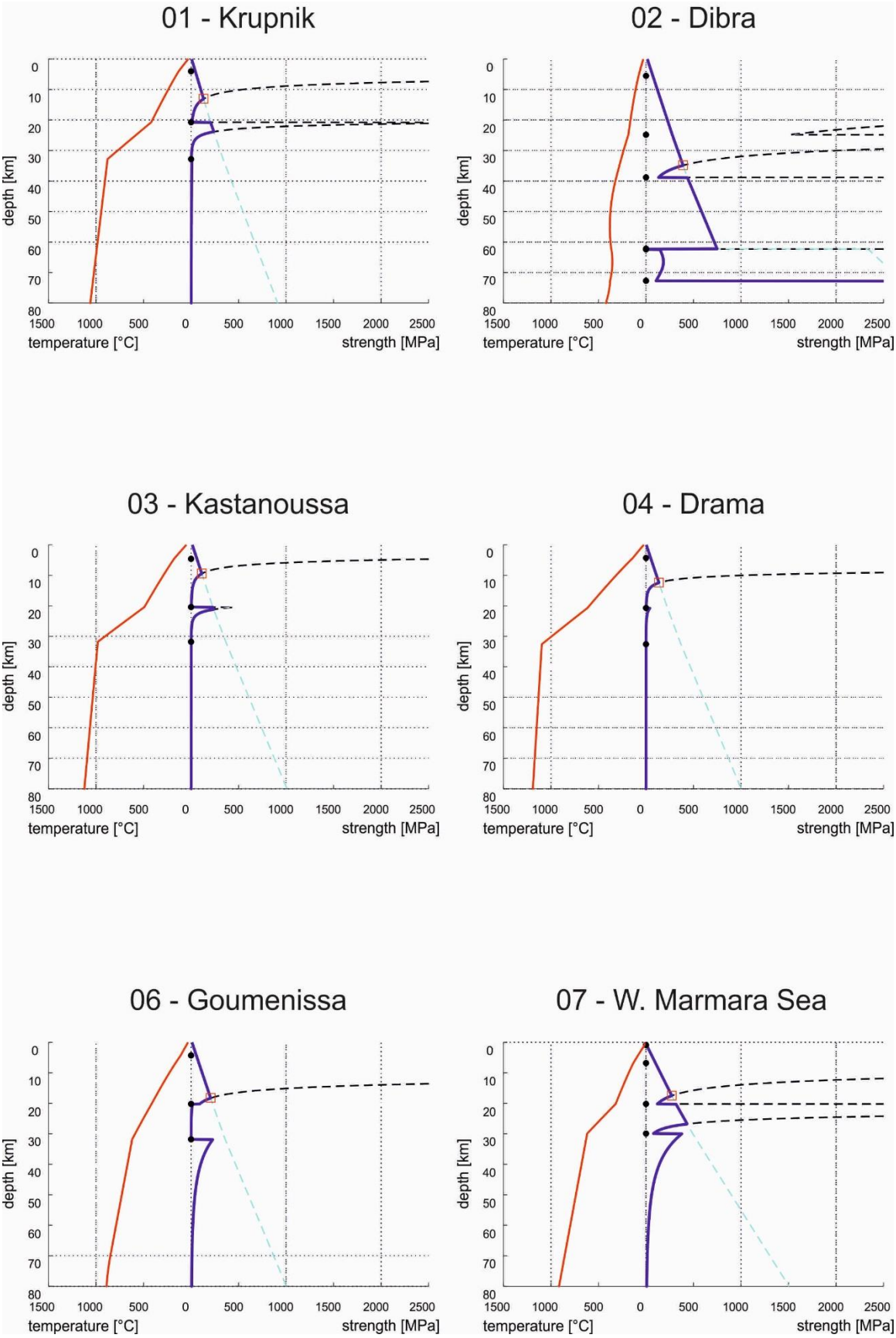
01 - Krupnik
02 - Dibra
03 - Kastanoussa
04 - Drama
06 - Goumenissa
07 - W. Marmara Sea
depth [km]
0
10
20
30
40
50
60
70
80
1500
1000
500
0
500
1000
1500
2000
2500
temperature [°C]
strength [MPa]

Fig. A2

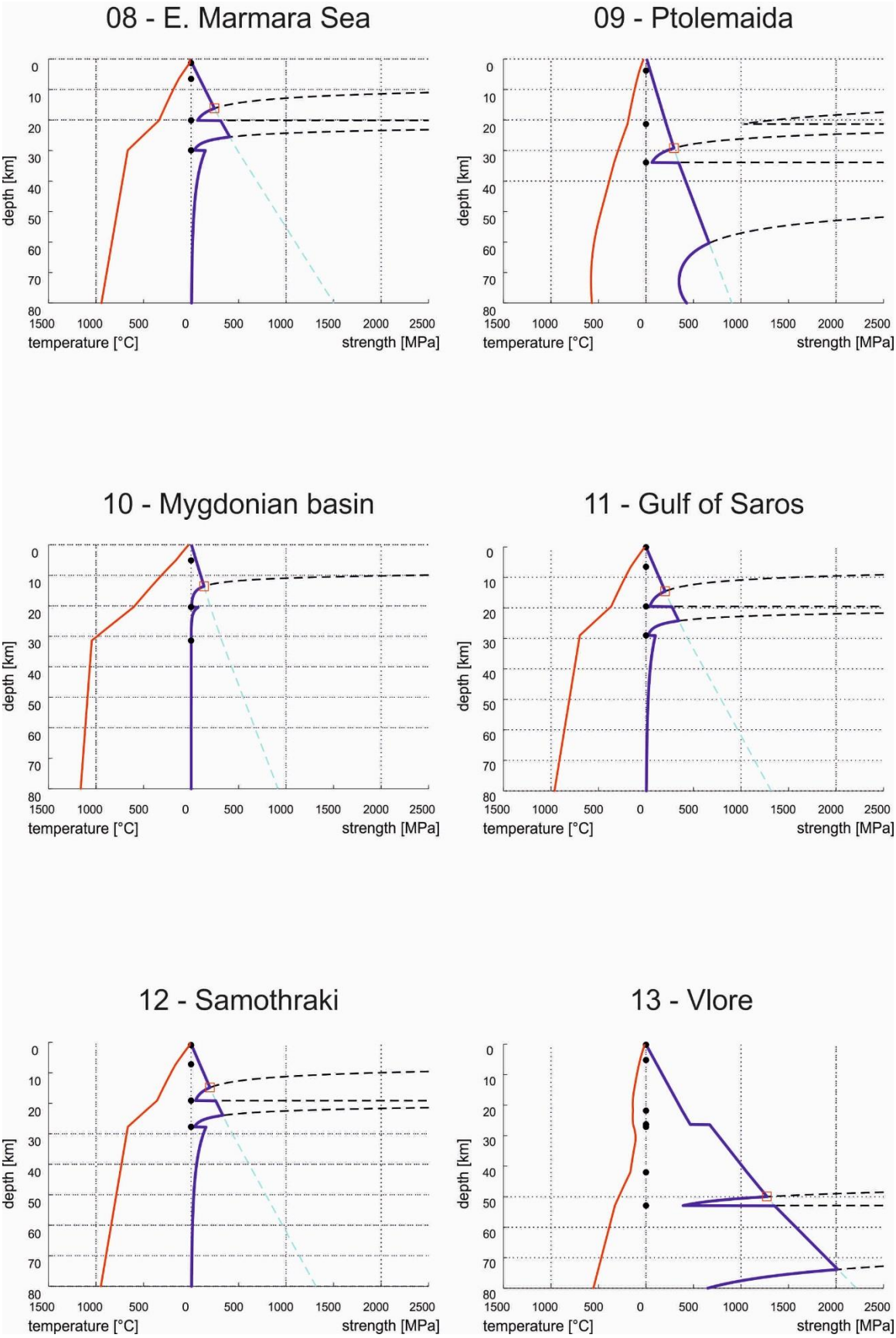
08 - E. Marmara Sea
09 - Ptolemaida
10 - Mygdonian basin
11 - Gulf of Saros
12 - Samothraki
13 - Vlore
depth [km]
temperature [°C]
strength [MPa]

Fig. A3

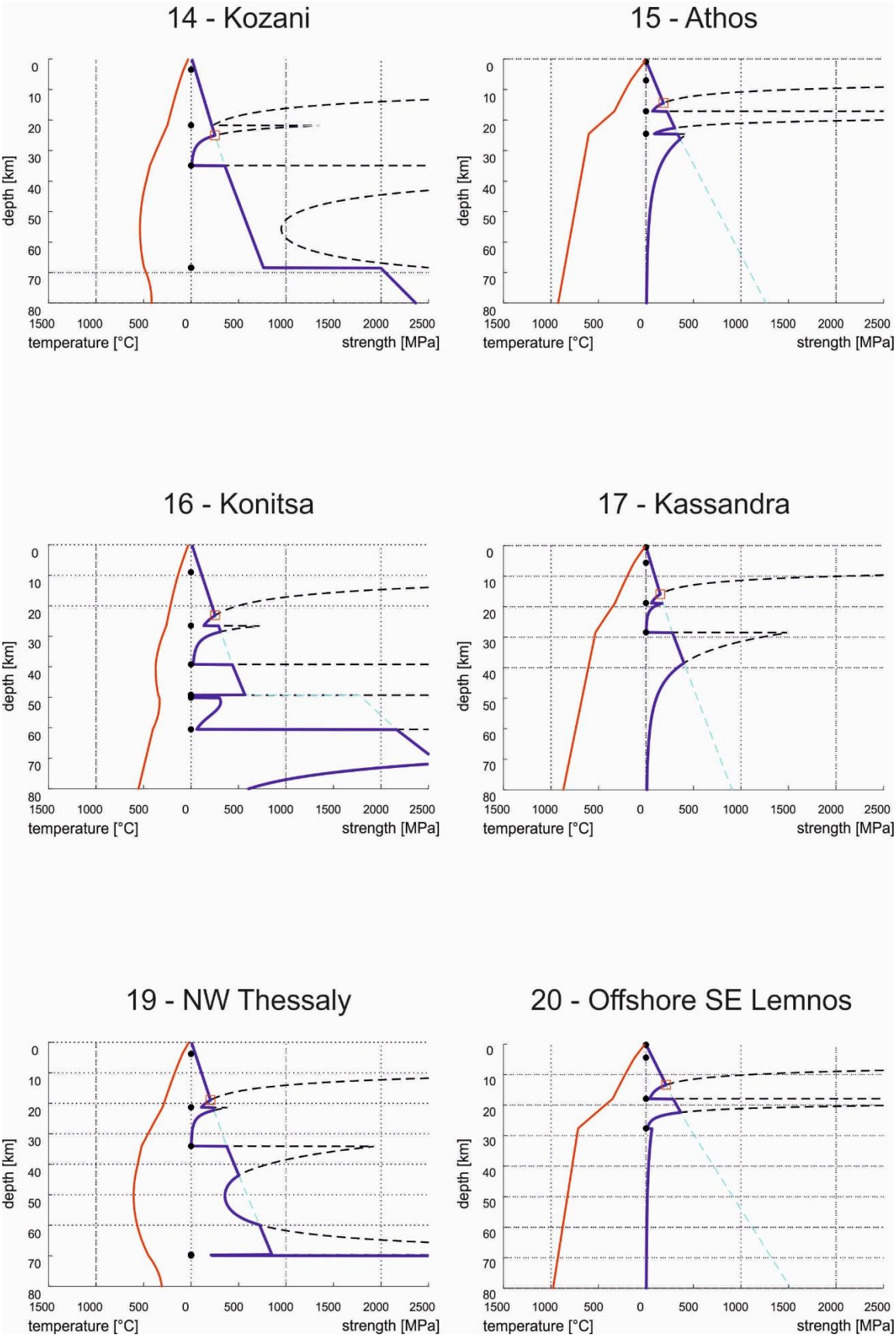
14 - Kozani
15 - Athos
16 - Konitsa
17 - Kassandra
19 - NW Thessaly
20 - Offshore SE Lemnos
depth [km]
0
10
20
30
40
50
60
70
80
1500
1000
500
0
500
1000
1500
2000
2500
temperature [°C]
strength [MPa]

Fig. A4

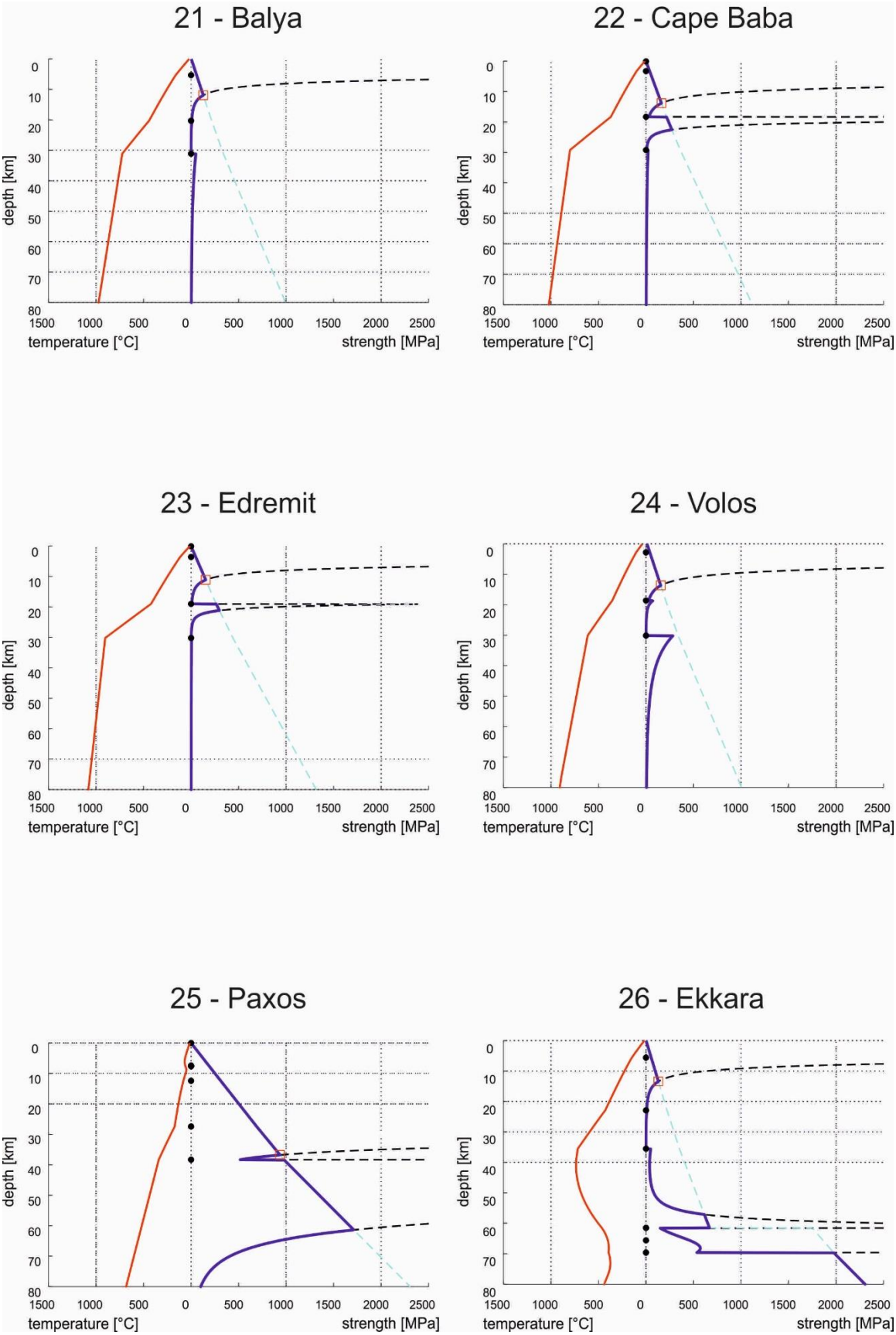
21 - Balya
22 - Cape Baba
23 - Edremit
24 - Volos
25 - Paxos
26 - Ekkara
depth [km]
0
10
20
30
40
50
60
70
80
1500
1000
500
0
500
1000
1500
2000
2500
temperature [°C]
strength [MPa]

Fig. A5

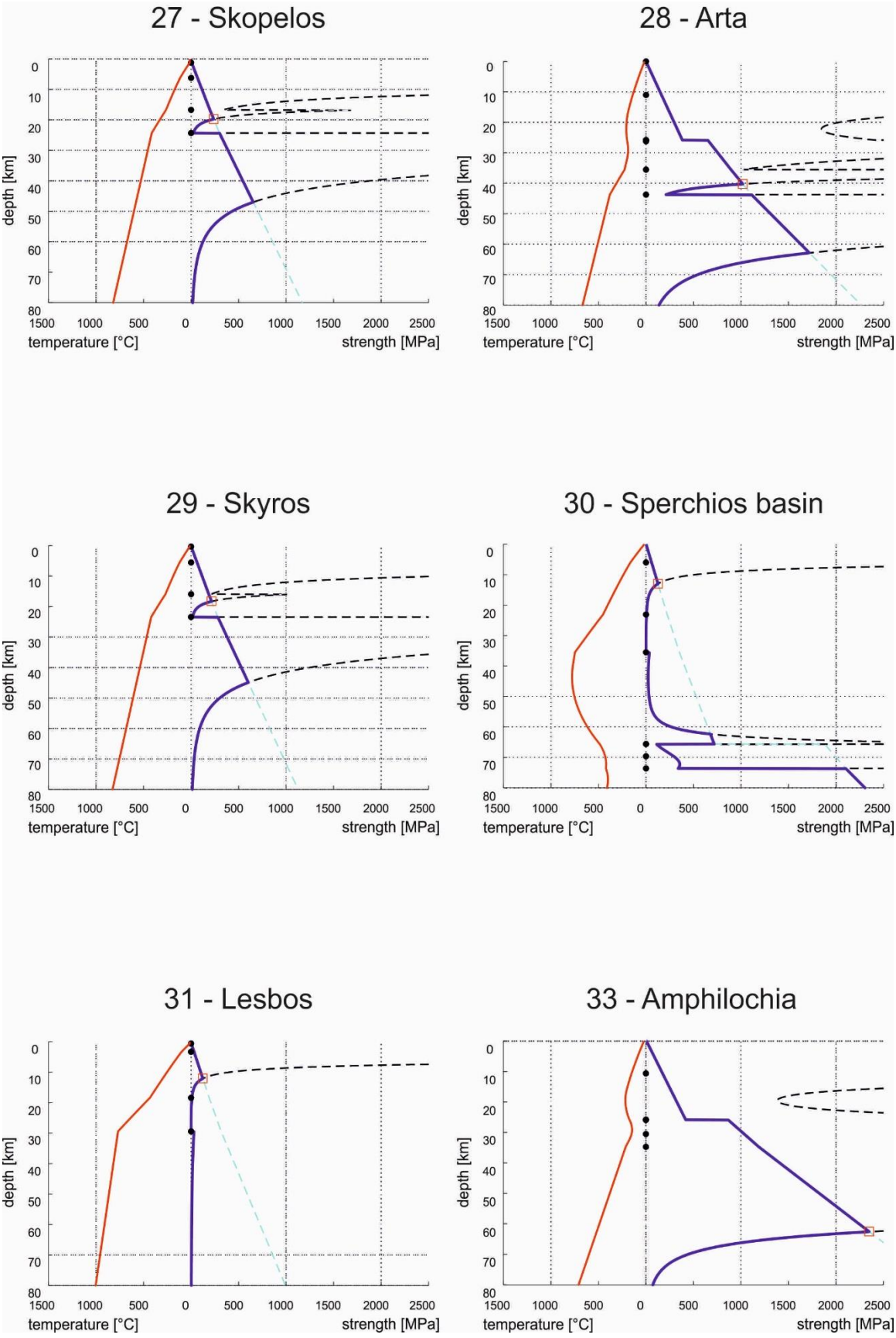
27 - Skopelos
28 - Arta
29 - Skyros
30 - Sperchios basin
31 - Lesbos
33 - Amphilochia
depth [km]
temperature [°C]
strength [MPa]

Fig. A6

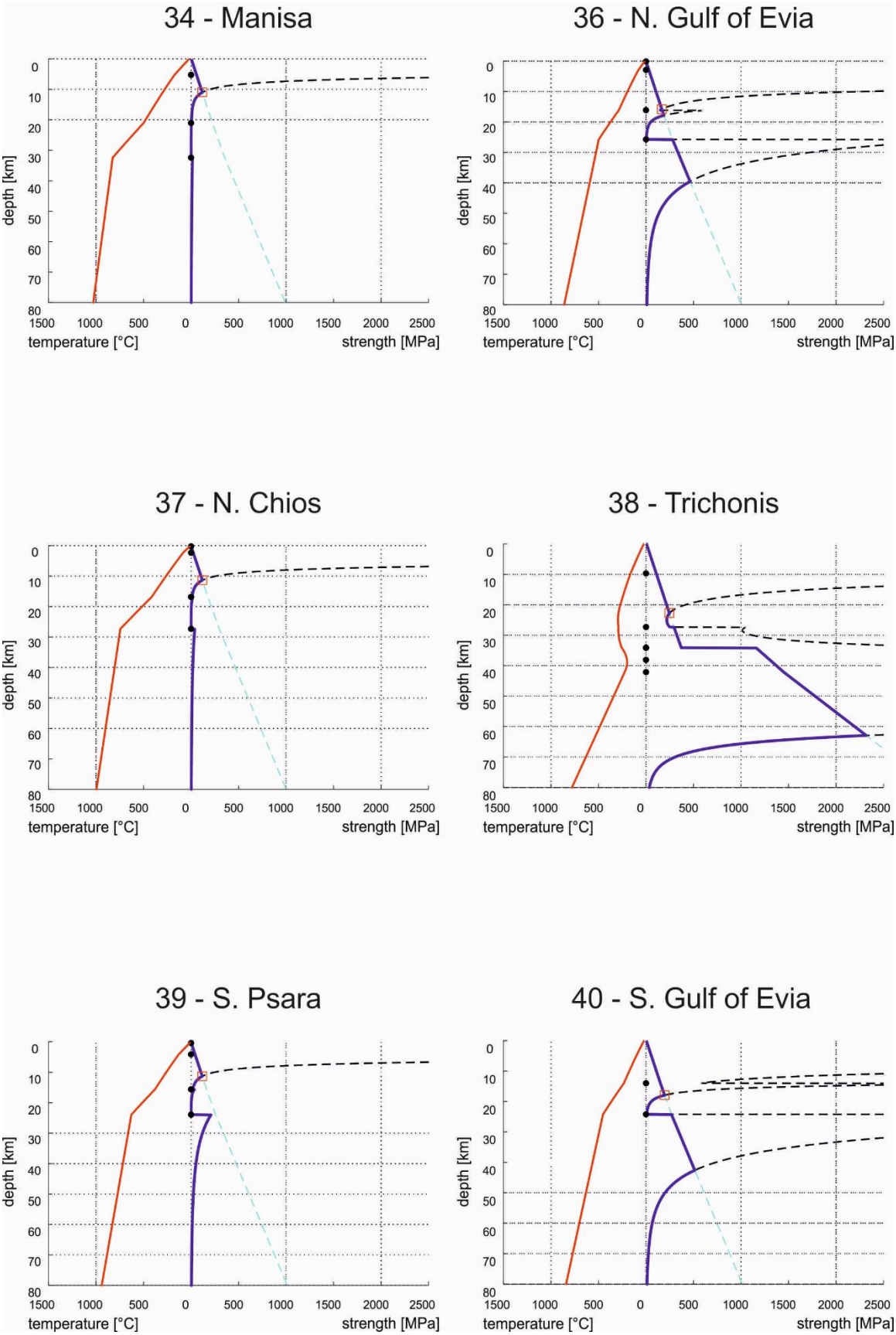
34 - Manisa
36 - N. Gulf of Evia
37 - N. Chios
38 - Trichonis
39 - S. Psara
40 - S. Gulf of Evia
depth [km]
0
10
20
30
40
50
60
70
80
1500
1000
500
0
500
1000
1500
2000
2500
temperature [°C]
strength [MPa]

Fig. A7

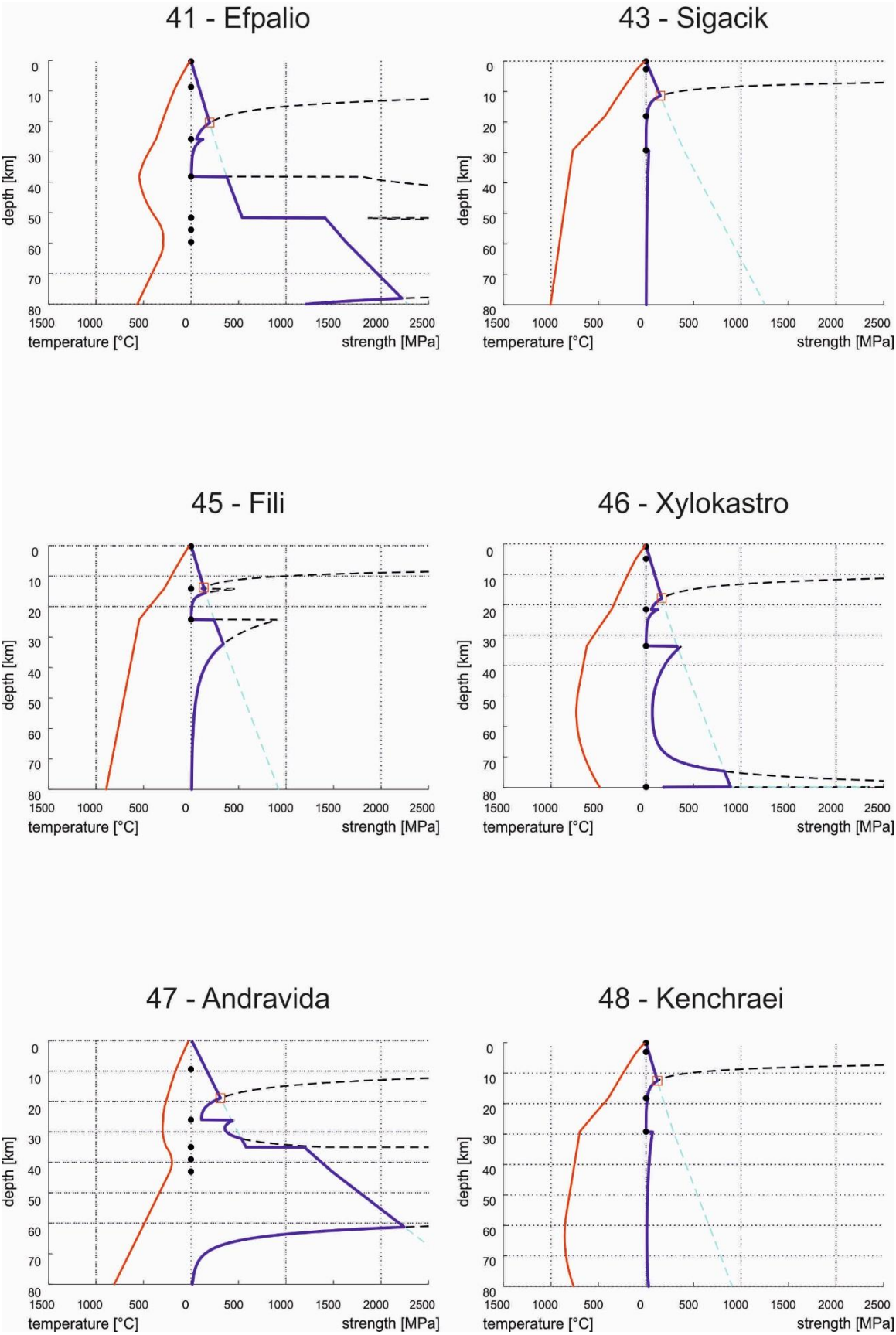
41 - Efpalio
43 - Sigacik
45 - Fili
46 - Xylokastro
47 - Andravida
48 - Kenchraei
depth [km]
0
10
20
30
40
50
60
70
80
1500
1000
500
0
500
1000
1500
2000
2500
temperature [°C]
strength [MPa]

Fig. A8

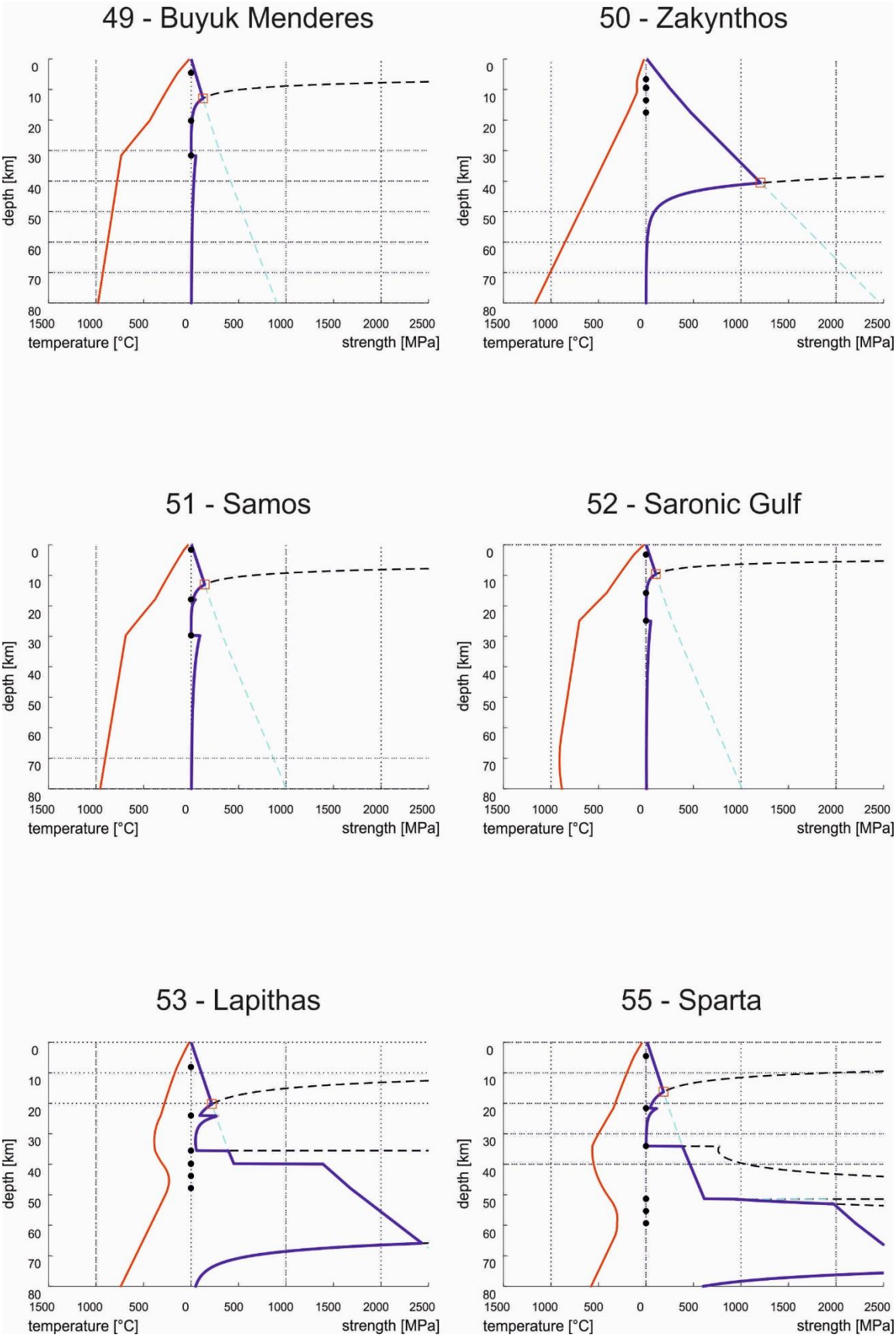
49 - Buyuk Menderes
50 - Zakynthos
51 - Samos
52 - Saronic Gulf
53 - Lapithas
55 - Sparta
depth [km]
temperature [°C]
strength [MPa]

Fig. A9

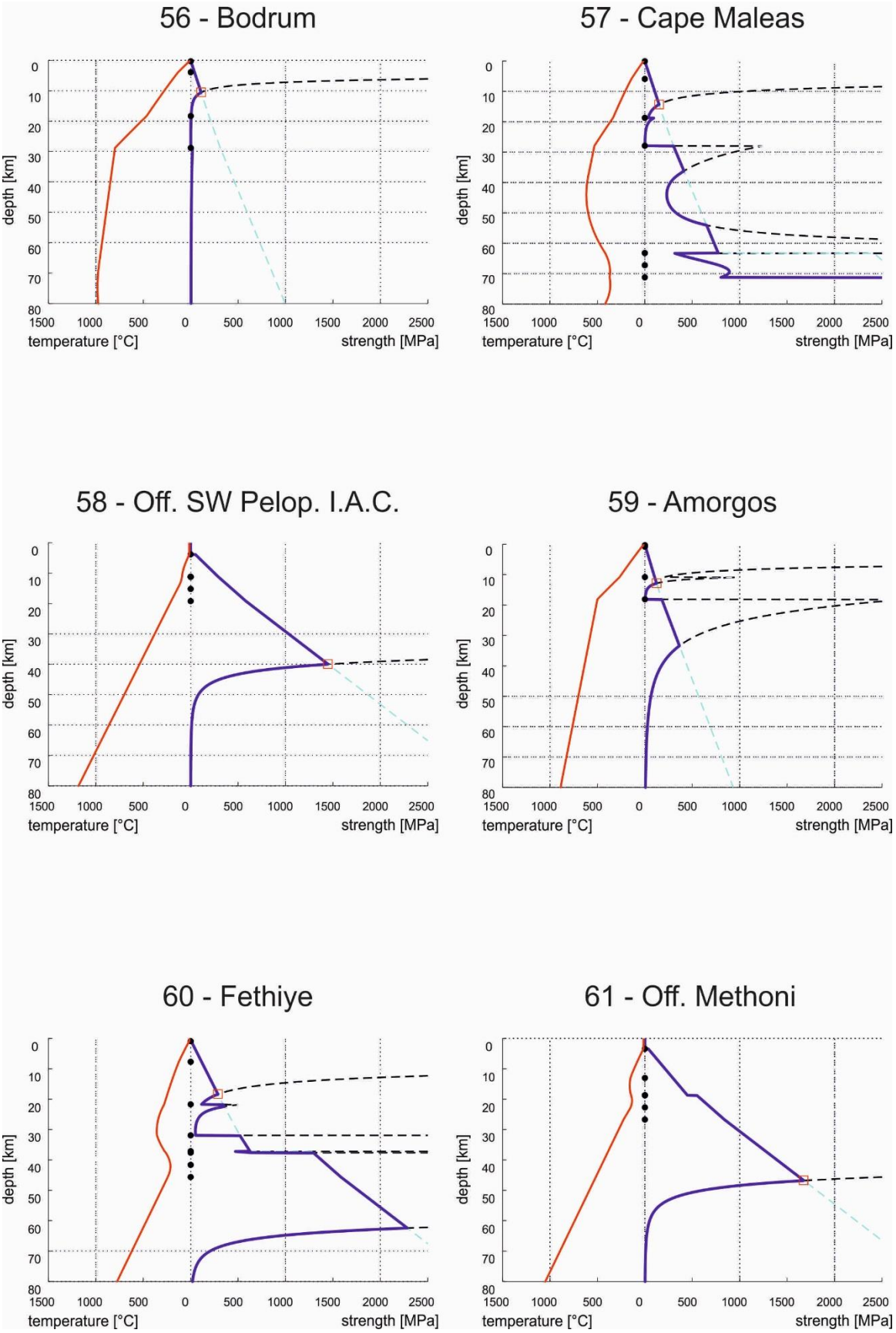
56 - Bodrum
57 - Cape Maleas
58 - Off. SW Pelop. I.A.C.
59 - Amorgos
60 - Fethiye
61 - Off. Methoni
depth [km]
temperature [°C]
strength [MPa]

Fig. A10

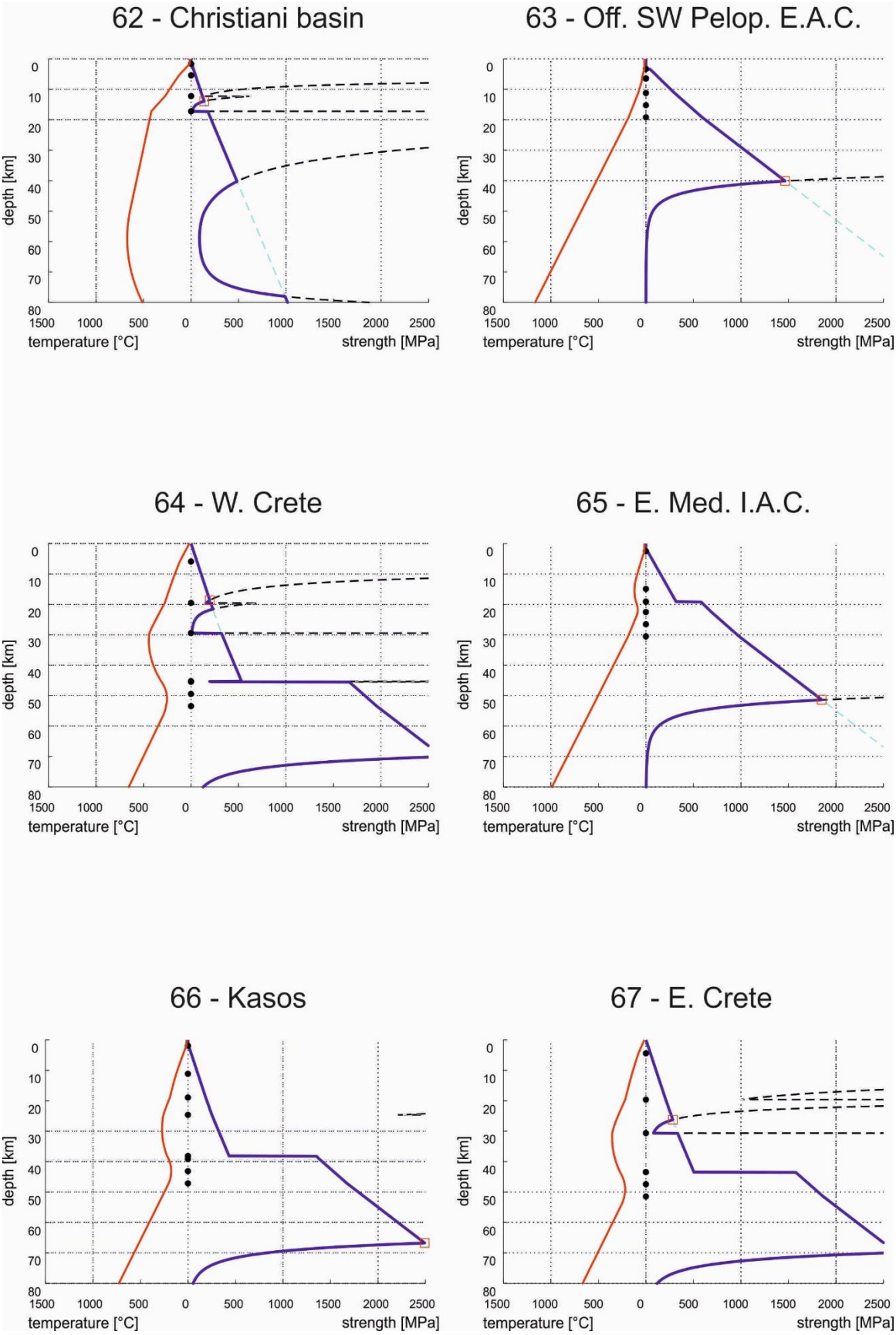
62 - Christiani basin
63 - Off. SW Pelop. E.A.C.
64 - W. Crete
65 - E. Med. I.A.C.
66 - Kasos
67 - E. Crete
depth [km]
temperature [°C]
strength [MPa]

Fig. A11

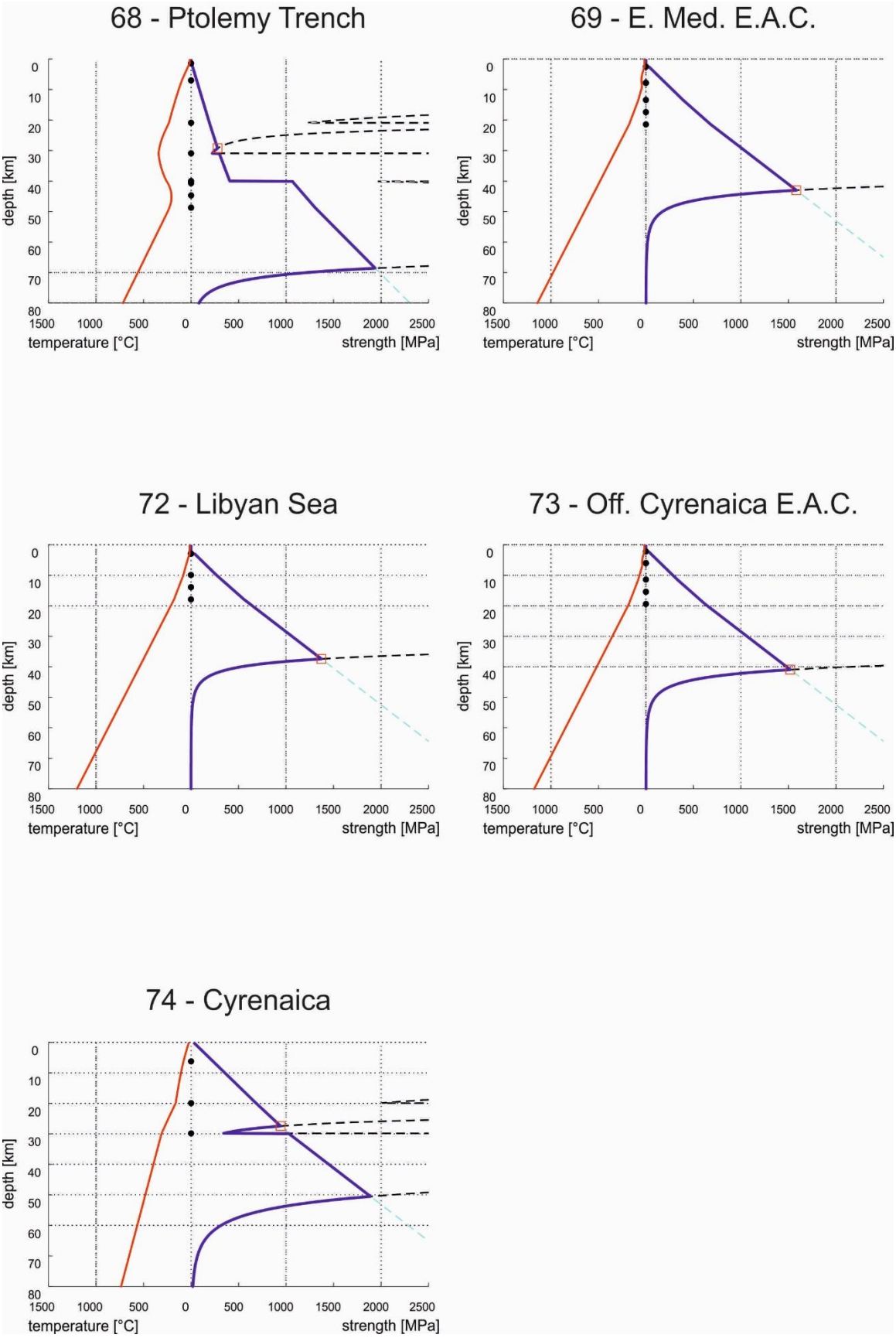
68 - Ptolemy Trench
69 - E. Med. E.A.C.
72 - Libyan Sea
73 - Off. Cyrenaica E.A.C.
74 - Cyrenaica
depth [km]
0
10
20
30
40
50
60
70
80
1500
1000
500
0
500
1000
1500
2000
2500
temperature [°C]
strength [MPa]

Fig. A12